

# Multicellular defense against phage infection in *Streptomyces* – impact of secondary metabolites and mycelial development

Larissa Kever

Schlüsseltechnologien / Key Technologies

Band / Volume 274

ISBN 978-3-95806-724-0







Forschungszentrum Jülich GmbH  
Institut für Bio-und Geowissenschaften  
Biotechnologie (IBG-1)

# **Multicellular defense against phage infection in *Streptomyces* – impact of secondary metabolites and mycelial development**

Larissa Kever

Schriften des Forschungszentrums Jülich  
Reihe Schlüsseltechnologien / Key Technologies

Band / Volume 274

ISSN 1866-1807

ISBN 978-3-95806-724-0

Bibliografische Information der Deutschen Nationalbibliothek.  
Die Deutsche Nationalbibliothek verzeichnet diese Publikation in der  
Deutschen Nationalbibliografie; detaillierte Bibliografische Daten  
sind im Internet über <http://dnb.d-nb.de> abrufbar.

Herausgeber  
und Vertrieb:           Forschungszentrum Jülich GmbH  
                                Zentralbibliothek, Verlag  
                                52425 Jülich  
                                Tel.: +49 2461 61-5368  
                                Fax: +49 2461 61-6103  
                                zb-publikation@fz-juelich.de  
                                www.fz-juelich.de/zb

Umschlaggestaltung:   Grafische Medien, Forschungszentrum Jülich GmbH

Druck:                    Grafische Medien, Forschungszentrum Jülich GmbH

Copyright:              Forschungszentrum Jülich 2023

Schriften des Forschungszentrums Jülich  
Reihe Schlüsseltechnologien / Key Technologies, Band / Volume 274

D 61 (Diss. Düsseldorf, Univ., 2023)

ISSN 1866-1807  
ISBN 978-3-95806-724-0

Vollständig frei verfügbar über das Publikationsportal des Forschungszentrums Jülich (JuSER)  
unter [www.fz-juelich.de/zb/openaccess](http://www.fz-juelich.de/zb/openaccess).



This is an Open Access publication distributed under the terms of the [Creative Commons Attribution License 4.0](https://creativecommons.org/licenses/by/4.0/),  
which permits unrestricted use, distribution, and reproduction in any medium, provided the original work is properly cited.

The thesis has been conducted at the Institute of Bio- and Geosciences, IBG-1: Biotechnology, Forschungszentrum Jülich GmbH, from March 2019 until October 2022 under the supervision of Prof. Dr. Julia Frunzke.

Published by permission of the  
Faculty of Mathematics and Natural Sciences at  
Heinrich-Heine-University Düsseldorf

**Supervisor:** Prof. Dr. Julia Frunzke  
Institute of Bio- and Geosciences, IBG-1: Biotechnology  
Forschungszentrum Jülich GmbH  
Jülich

**Co-supervisor:** Prof. Dr. Ilka Maria Axmann  
Institute for Synthetic Microbiology  
Heinrich-Heine-University Düsseldorf  
Düsseldorf

Date of oral examination: 29th March 2023





“There is something fascinating about science. One gets such wholesale returns of conjecture out of such a trifling investment of fact.”

Mark Twain (1835-1910)



**The research presented in this dissertation has been published in the following manuscripts:**

Hardy, A., Sharma, V., **Kever, L.** & Frunzke, J. (2020). Genome sequence and characterization of five bacteriophages infecting *Streptomyces coelicolor* and *Streptomyces venezuelae*: Alderaan, Coruscant, Dagobah, Endor1 and Endor2. *Viruses*, 12(10), 1065. doi:10.3390/v12101065

**Kever, L.**, Hünnefeld, M., Brehm, J., Heermann, R. & Frunzke, J. (2021). Identification of Gip as a novel phage-encoded gyrase inhibitor protein of *Corynebacterium glutamicum*. *Mol Microbiol*, 116(5), 1268-1280. doi:10.1111/mmi.14813

**Kever, L.\***, Hardy, A.\*, Luthe, T., Hünnefeld, M., Gätgens, C., Milke, L., Wiechert, J., Wittmann, J., Moraru, C., Marienhagen, J. & Frunzke, J. (2022). Aminoglycoside Antibiotics Inhibit Phage Infection by Blocking an Early Step of the Infection Cycle. *mBio*, 13(3). doi:10.1128/mbio.00783-22

\*These authors contributed equally to this work.

Hardy, A., **Kever, L.** & Frunzke, J. (2023). Antiphage small molecules produced by bacteria - beyond protein-mediated defenses. *Trends Microbiol*. 31(1). doi:10.1016/j.tim.2022.08.001

**To be submitted:**

**Kever, L.** & Frunzke, J. (2022). Inactivation of phage particles in the extracellular space of *Streptomyces* populations.

**Further contributions not included in this dissertation:**

Luthe, T., **Kever, L.**, Hänsch, S., Hardy, A., Tschowri, N., Weidtkamp-Peters, S. & Frunzke, J. (2023). *Streptomyces* development is involved in the efficient containment of viral infections. *microLife*, 4, uqad002. doi:10.1093/femsml/uqad002

Forschungszentrum Jülich GmbH. Protein-basierter Wachstumsinhibitor in Bakterien. German patent application published as DE102021004449A1 (2022). (Inventors: Frunzke, J., **Kever, L.** & Hünnefeld, M.)



## Abbreviations

16S-RMTase	16S ribosomal RNA methyltransferases
AAC	Aminoglycoside acetyltransferase
Abi	Abortive infection
AME	Aminoglycoside-modifying enzyme
ATCC	American Type Culture Collection
Cas	CRISPR-associated protein
CBASS	Cyclic oligonucleotide-based antiphage signaling systems
cf.	confer
CGP3	<i>Corynebacterium glutamicum</i> prophage 3
CgpS	<i>C. glutamicum</i> prophage silencer
CRISPR	Clustered regularly interspaced short palindromic repeats
DNA	Deoxyribonucleic acid
dsDNA	Double-stranded DNA
dsRNA	Double-stranded RNA
e.g.	exempli gratia
et al.	et alii
FISH	Fluorescence in situ hybridization
Gip	Gyrase-inhibiting protein
HGT	Horizontal gene transfer
LC-MS	Liquid chromatography – mass spectrometry
PCR	Polymerase chain reaction
PFU	Plaque-forming units
pVip	Prokaryotic viperins
R-M	Restriction-modification
RNA	Ribonucleic acid
RNA-seq	RNA-sequencing
SEM	Scanning electron microscopy
SM	Spent medium
ssDNA	Single-stranded DNA
ssRNA	Single-stranded RNA
XS	Xenogeneic silencing

Further abbreviations not included in this section can exemplarily be found in the JCB abbreviation list under the following hyperlink: [Standard Abbreviations | Journal of Cell Biology | Rockefeller University Press \(rupress.org\)](https://www.jcb.org/standard-abbreviations/)





## Table of contents

<b>1. Summary.....</b>	<b>1</b>
<b>2. Scientific context and key results.....</b>	<b>3</b>
2.1. Bacteriophages: Ubiquitous bacterial viruses shaping bacterial evolution .....	3
2.1.1. Discovery, classification and life style.....	3
2.1.2. (Pro-)phage proteins affecting bacterial hosts.....	6
2.1.3. Bacterial antiphage defense systems .....	8
2.2. <i>Streptomyces</i> , a filamentous soil bacterium as major producer of bioactive compounds .....	12
2.2.1. Multicellular development and its hierarchical regulatory network .....	12
2.2.2. Complex secondary metabolism as hallmark of <i>Streptomyces</i> .....	14
2.3. Multicellular antiphage defense systems of <i>Streptomyces</i> .....	17
2.3.1. Phage infection of <i>Streptomyces</i> : Initial observations .....	17
2.3.2. Chemical defense via aminoglycoside antibiotics .....	19
2.3.3. Inactivation of infectious phage particles in the extracellular space.....	28
2.3.4. Community-wide protection against phage infection .....	37
2.4. Conclusion and perspectives .....	41
2.5. References.....	43
<b>3. Publications and manuscripts .....</b>	<b>59</b>
3.1. Identification of Gip as a novel phage-encoded gyrase inhibitor protein of <i>Corynebacterium glutamicum</i> .....	60
3.2. Aminoglycoside antibiotics inhibit phage infection by blocking an early step of the infection cycle.....	74
3.3. Inactivation of phage particles in the extracellular space of <i>Streptomyces</i> populations ..	91
3.4. Genome sequence and characterization of five bacteriophages infecting <i>Streptomyces coelicolor</i> and <i>Streptomyces venezuelae</i> : Alderaan, Coruscant, Dagobah, Endor1 and Endor2 .....	108
3.5. Antiphage small molecules produced by bacteria – beyond protein-mediated defenses .....	124

<b>4. Appendix.....</b>	<b>140</b>
4.1. Appendix to 3.1. Identification of Gip as a novel phage-encoded gyrase inhibitor protein of <i>Corynebacterium glutamicum</i> .....	140
4.2. Appendix to 3.2: Aminoglycoside antibiotics inhibit phage infection by blocking an early step of the infection cycle.....	202
4.3. Appendix to 3.3: Inactivation of phage particles in the extracellular space of <i>Streptomyces</i> populations.....	227
4.4. Appendix to 3.4: Genome sequence and characterization of five bacteriophages infecting <i>Streptomyces coelicolor</i> and <i>Streptomyces venezuelae</i> : Alderaan, Coruscant, Dagobah, Endor1 and Endor2 .....	239
 <b>Acknowledgements .....</b>	 <b>243</b>
 <b>Erklärung .....</b>	 <b>245</b>

## 1. Summary

In almost every habitat, bacteria are challenged with persistent attacks of bacterial viruses, so-called bacteriophages (or phages). Upon infection, phages can target key cellular processes in their host cell to optimize reproduction conditions making them a promising source for identification of novel antimicrobial proteins. This was exemplified by the identification of the gyrase-inhibiting protein Cg1978, termed Gip, encoded by the CGP3 prophage of *Corynebacterium glutamicum*. In vitro studies confirmed a direct interaction of Gip with gyrase subunit A of its host *C. glutamicum* leading to an inhibition of the gyrase supercoiling activity.

The evolutionary pressure exerted by phages forced bacteria to evolve multiple lines of defense. However, our current knowledge of antiphage defense is dominated by systems acting at a cellular level, but there is an increasing evidence that bacterial communities also employ several strategies specifically protecting multiple cells from phage predation at the same time. By using the filamentous soil bacterium *Streptomyces* as a model, this doctoral thesis focused on the contribution of bacterial small molecule production and multicellular development to antiphage defense.

To this end, five newly isolated *Streptomyces* phages were comprehensively characterized to establish a set of model phages for further investigations. Next, we focused on the chemical defense against phages via aminoglycosides, which are naturally derived, bactericidal antibiotics produced by *Streptomyces*. Using bacterial strains producing aminoglycoside-modifying enzymes as resistance mechanism, a significant inhibition of phage infection by structurally divergent aminoglycosides in Gram-negative as well as Gram-positive bacterial hosts was observed. The interference with phage infection occurred at an early step of phage life cycle between injection and replication with potential differences between individual host organisms. As exemplified with the aminoglycoside apramycin, in vitro modification of the aminoglycoside scaffold via acetylation prevented the antibacterial mode of action, but had no impact on the antiphage properties, suggesting different molecular targets underlying this dual functionality. Moreover, culture supernatant of the natural apramycin producer *S. tenebrarius* was shown to mimic the effect of the pure compound, hinting towards the physiological relevance of aminoglycoside antibiotics as chemical defense against phages in the environment.

As a further part of this work, we analysed the inactivation of phages in the extracellular space of *Streptomyces* populations. In contrast to prototypical infections with unicellular-growing bacteria, infectious phage titers dropped again at later stages of *Streptomyces* infection, which coincided with re-growth of phage-resistant mycelium. When considering different parameters underlying this inactivation, we observed a potential influence of medium acidification, production of antiphage metabolites and proteins as well as mycelial growth. Mature mycelium revealed a reduced susceptibility to phage infection hinting towards an important contribution of multicellular development to antiphage defense. A decline in phage titer was further observed upon incubation of *Streptomyces* mycelium with different non-host phages, which coincided with the phase of hyphae-spore transition. This led to the hypothesis that mycelium might efficiently adsorb phages from the environment with important implications for community interactions.

Overall, the work presented in this thesis expands our knowledge about bacterial immune systems by unravelling the antiphage properties of aminoglycoside antibiotics and the important impact of cellular development, thereby adding further layers of antiviral defense acting at the multicellular level.





## 2. Scientific context and key results

### 2.1. Bacteriophages: Ubiquitous bacterial viruses shaping bacterial evolution

#### 2.1.1. Discovery, classification and life style

Bacteriophages, or shortly known as phages, are ubiquitous viruses infecting bacteria. With an estimated number of  $\sim 10^{31}$  phage particles in the biosphere, they represent the most abundant biological entity distributed over all natural habitats (Clokier et al., 2011; Hendrix et al., 1999; Mushegian, 2020).

Phage research finds its origin in the early twentieth century with the independent discovery of bacteriophages through the pioneering work of Frederick Twort (1915) and Félix d'Herelle (1917), the latter coining the name "bacteriophage" meaning bacteria-eater (d'Herelle, 2007; Twort, 1915). At that time, phages were mainly studied for their potential to treat bacterial infections in clinics. This initial motivation was quickly faded in western countries as the antibiotic era dawned (Salmond & Fineran, 2015; Summers, 2001). However, a general interest in phage research persisted, which led to the first visualization of phages by electron microscopy and the identification of DNA as the carrier of the genetic information (Hershey & Chase, 1952; Ruska et al., 1939). Over the years, the increasing understanding of phage biology has contributed significantly to our current knowledge of fundamental, biological principles (Salmond & Fineran, 2015). This has been accompanied by the establishment of diverse molecular tools for biotechnological applications, including exemplarily the T7 expression system of the *Enterobacteria* phage T7 (Studier & Moffatt, 1986) as well as restriction-modification systems (Roberts, 2005). More recently, the discovery of CRISPR-Cas systems as adaptive bacterial immune system against phages initiated a new era of genetic and genome engineering (Barrangou et al., 2007; Doudna & Charpentier, 2014). Additionally, emerging antibiotic resistance as major health issue led to the resurgence of phage therapy approaches as alternative antimicrobials (Kortright et al., 2019).

Bacteriophages are necessarily dependent on the metabolic machinery of their bacterial host for their propagation – regardless of whether they follow a lytic, a lysogenic or a chronic life style (Roucourt & Lavigne, 2009). Infection starts with a receptor-based attachment of the phage to the bacterial host cell and subsequent injection of the viral genome (Rakhuba et al., 2010). Afterwards, temperate phages can choose either the lytic or the lysogenic life cycle (Figure 1), while virulent phages are strictly lytic (Bertani, 1953).

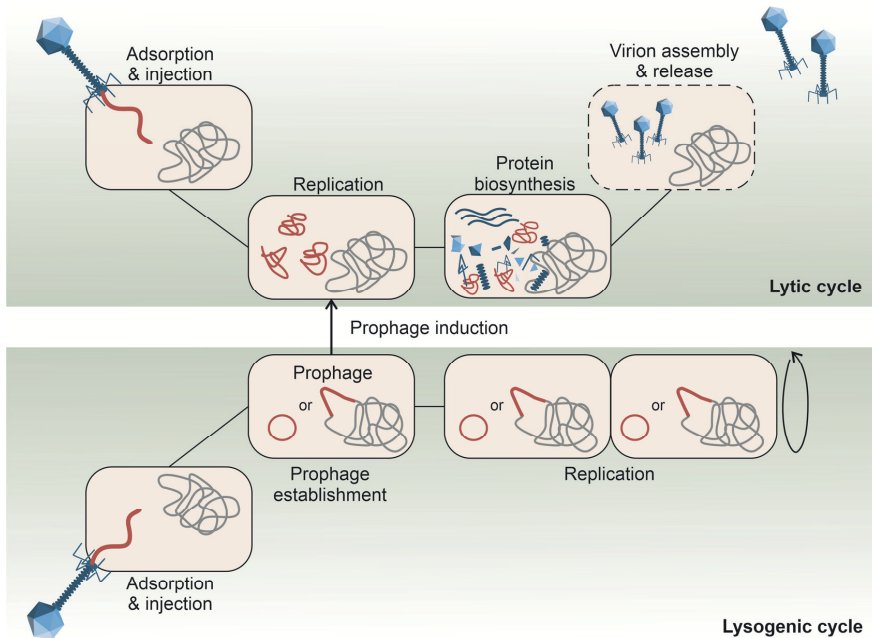


**Figure 1: Lytic and lysogenic life cycle of bacteriophages.** Phages following the lytic life cycle use the bacterial host for production of new phage progenies, which are released by subsequent cell lysis. Temperate phages can alternatively follow a lysogenic life cycle by integrating their DNA into the bacterial chromosome or establishing as an episome. Unfavorable conditions can trigger induction of the prophage to allow reproduction via the lytic life cycle. In addition, some phages propagate via chronic infection or transitionally establish a pseudolysogenic state, which is not included in this schematic illustration (Clokic et al., 2011).

By entering the **lysogenic life cycle**, the phage establishes itself as an episome (e.g. phage P1) or integrates its DNA into the bacterial chromosome via specific attachment sites (e.g. phage  $\lambda$ ) (Ikeda & Tomizawa, 1968; Landy & Ross, 1977). This so-called prophage is replicated in conjunction with the bacterial DNA and typically a phage repressor protein is involved in the maintenance of the lysogenic state. Upon certain, usually DNA-damaging conditions (e.g. UV radiation or DNA-damaging agents), the prophage leaves its dormant state and excises itself out of the bacterial chromosome to switch to the lytic life cycle, a process called prophage induction. In response to spontaneous DNA damage events, this induction can even occur in the absence of an external trigger (Helfrich et al., 2015; Nanda et al., 2015; Oppenheim et al., 2005).

A special case of lysogeny is represented by a **pseudolysogenic state**, which describes the establishment of a circular, non-replicating pre-prophage. This unstable state can occur upon infection under nutrient deficiency and is maintained until conditions are improved and the lytic or lysogenic life cycle is entered (Feiner et al., 2015). In the **lytic cycle**, the bacterial cell machinery is harnessed for phage DNA replication and phage protein synthesis, which allows the assembly of

new phage progenies and their subsequent release via cell lysis (Salmond & Fineran, 2015). An exception of phage release without disintegration of the host cell was observed for filamentous phages like M13, some archaeal viruses and for plasmaviruses infecting *Mycoplasma*. This lifestyle is called **chronic infection** (Clokier et al., 2011).

In addition to their life style, phages differ in gene content, genome type and virion morphology (Dion et al., 2020). The latter two have been used in the past for phage classification. According to this decades-old taxonomy, the vast majority of phages belonged to the order of *Caudovirales* unifying phages with a tailed morphology and double-stranded DNA (dsDNA) genome. Based on their tail contractility and length, these phages were further grouped into the three families of *Siphoviridae*, *Myoviridae* and *Podoviridae* (Ackermann, 2009). Contrary to this tailed morphotypes, other virions exhibit a cubic, pleomorphic and filamentous nature with their genomes being single-stranded (ss) or double-stranded DNA or RNA. Additionally, some phages have lipid constituents, which all in all defined the further phage families as illustrated in Figure 2 (Ackermann, 2009).

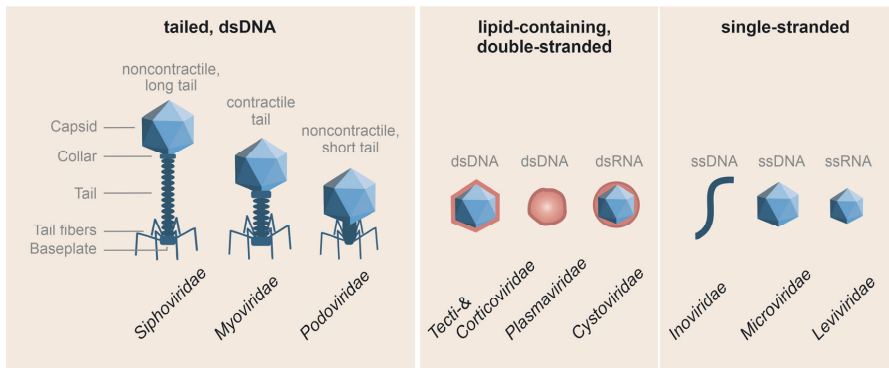


**Figure 2: Phage taxa based on genome types and morphology.** Phage families are grouped by tailed, dsDNA phages, lipid-containing phages with double-stranded genomes and phages with a single-stranded genome. The figure was designed based on Ofir and Sorek (2018) and Hyman and Abedon (2012).

In recent years, the discovery of the mosaic-like architecture of phage genomes exposed a hitherto unexpected genetic diversity, which could be attributed to a high rate of horizontal gene transfer (HGT) during phage evolution (Hatfull, 2008). With the increasing availability of genomic and metagenomic data, it became apparent that the caudoviral families of *Sipho*-, *Myo*-, and *Podoviridae* are not monophyletic. The need of considering their evolutionary origin initiated a comprehensive re-classification towards a genome-based megataxonomy (Koonin et al., 2020; Turner et al., 2021). However, distinguishing phages based on their morphotypes can still be useful to get a first overview of phage diversity.

### 2.1.2. (Pro-)phage proteins affecting bacterial hosts

Upon infection, phages are able to subvert and control key cellular processes to create favorable conditions for their own reproduction (De Smet et al., 2017). For this host-takeover, phage proteins expressed in the early stages of infection appear to be of primary importance. For instance, in direct competition for the transcription machinery, they can redirect the host RNA polymerase to viral gene expression or even temporarily inhibit it if the phage encodes its own RNA polymerase (De Smet et al., 2017; Drulis-Kawa et al., 2012; Lammens et al., 2020). Furthermore, they can shut down host DNA replication and degrade the bacterial chromosome to increase the pool of precursors for viral DNA replication (Drulis-Kawa et al., 2012). In addition, further studies revealed that phage proteins can amongst others also directly target translation-related processes and cell division (De Smet et al., 2017; Lammens et al., 2020). Deciphering the underlying mechanisms of these host-interfering processes is not only essential to deepen our knowledge of phage-host interactions, but may also be harnessed for the development of new antimicrobial agents (De Smet et al., 2017; Roach & Donovan, 2015).

However, recent advances in viral genomics exposed a high number of open reading frames in phage genomes whose function remains to be elucidated (Yin & Fischer, 2008). Of particular interest are previously overlooked small phage genes, as their gene products are known to frequently exert regulatory functions by activating, inhibiting or redirecting target proteins (De Smet et al., 2017; Fremin et al., 2022; Orr et al., 2020; Storz et al., 2014). For example, the early small protein Mip of *Pseudomonas aeruginosa* podovirus LUZ24 prevents silencing of phage DNA by inhibiting the activity of the host-encoded xenogeneic silencer MvaT (Wagemans et al., 2015). Another example is the protein Gp2 from *E. coli* phage T7, which inhibits the host RNA polymerase to prevent interference with its own faster T7 RNA polymerase (Nechaev & Severinov, 1999).

Besides directly targeting regulatory hubs to optimize reproduction conditions, phage proteins can also improve fitness of their bacterial host, which may partly explain the frequency of long-term relationships between phages and bacteria (Bondy-Denomy & Davidson, 2014). Almost half of all sequenced bacterial genomes harbor at least one, but frequently even more prophages (Touchon et al., 2016). These prophages can increase bacterial pathogenicity or contribute to defense against other phages, a process called lysogenic conversion (Bondy-Denomy & Davidson, 2014; Davies et al., 2016). However, many prophages appear to be cryptic as rapid inactivation of these ‘molecular time bombs’ is under tough selection, which let them suffer from mutations preventing completion of the lytic life cycle. This domestication process allows the bacterial host to keep beneficial prophage elements while limiting the risk of phage-induced cell lysis (Bobay et al., 2014; Ramisetty & Sudhakari, 2019; Wang et al., 2010).

In search of phage-derived proteins affecting their bacterial host, we focused on the prophage CGP3 (~219 kb, including CGP4), which is one of overall four cryptic prophages (CGP1-4) found in the genome of the actinobacterial strain *Corynebacterium glutamicum* ATCC 13032 (Ikeda & Nakagawa, 2003). Upon induction, CGP3 can excise itself out of the bacterial chromosome and replicate as a circular genome, but it appears to be unable to cause cell lysis or produce active phage progenies (Donovan et al., 2015; Frunzke et al., 2008). The lysogenic state of CGP3 is maintained by the prophage-encoded nucleoid-associated protein CgpS, which silences phage gene expression (Pfeifer et al., 2016). During a screening of several small proteins encoded by the CGP3 prophage, the protein Cg1978 (6.8 kDa) was identified as a novel **gyrase-inhibiting protein**, therefore termed Gip. In vitro pull-down assays and surface plasmon resonance spectroscopy exposed a highly specific interaction of Gip with DNA gyrase subunit A of its bacterial host *C. glutamicum*, which was proven to inhibit the gyrase supercoiling activity in vitro (Figure 3). In addition, overproduction of Gip was found to severely impair bacterial growth and lead to an activation of the host SOS response. On a transcriptome level, Gip-mediated gyrase inhibition was compensated with an upregulation of the gyrase-encoding genes *gyrAB* and a downregulation of *topA* coding for topoisomerase I (Kever et al., 2021).

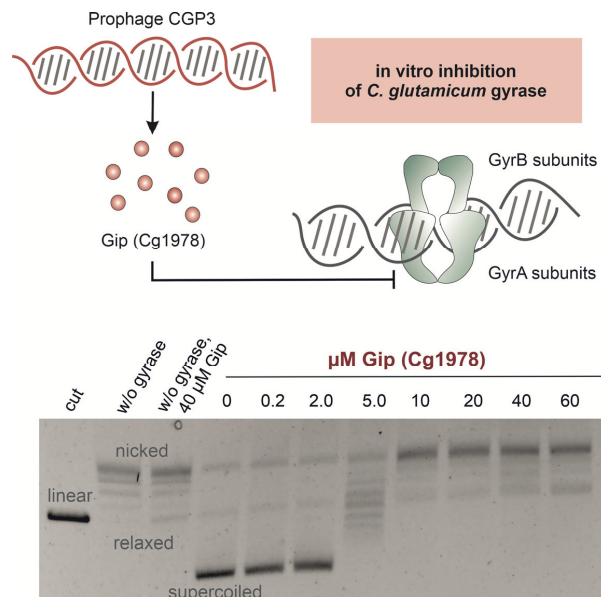


**Figure 3: Supercoiling inhibition assays showing the Gip-mediated inhibition of the DNA gyrase.** Increasing concentrations of the GyrA-targeting protein Gip (Cg1978) inhibit the DNA supercoiling activity of the *C. glutamicum* DNA gyrase, which leads to an accumulation of nicked/relaxed DNA (adapted and modified from Kever et al. (2021)).



Being crucial for DNA metabolism and absent in mammalian cells, the bacterial DNA gyrase is one of the most prominent targets of proteinaceous and chemical toxins (Khan et al., 2018). This heterotetrameric enzyme (GyrA<sub>2</sub>GyrB<sub>2</sub>, type IIA topoisomerase) catalyzes the ATP-dependent introduction of negative supercoils into double-stranded DNA. Gyrase subunit A cleaves and rejoins the DNA, while subunit B is responsible for ATP hydrolysis (N. G. Bush et al., 2015; McKie et al., 2021; Vanden Broeck et al., 2019). Based on what is currently known from already characterized gyrase-inhibiting small molecules and proteins, inhibition of this enzyme can be mediated by i) stabilization of the gyrase-DNA cleavage intermediate (Bernard et al., 1993; Drlica & Malik, 2003; Pierrat & Maxwell, 2003), ii) inhibition of ATP hydrolysis (Maxwell & Lawson, 2003) or iii) DNA mimicry (Shah & Heddle, 2014). However, while clearly showing that Gip targets the gyrase subunit A, the underlying molecular basis of this inhibition still needs to be elucidated. Mimicking the mechanism of gyrase inhibition applied by phages could open up new directions for antibacterial drug design.

From a physiological point of view, the question arises to what extent the coding of such an inhibitor could benefit phages. The existence of further phage-derived proteins targeting topology modulators such as the small peptide Igy (5.6 kDa) encoded by phage LUZ24 of *Pseudomonas aeruginosa* (De Smet et al., 2021) or gp55.2 encoded by the T4 phage of *E. coli* (Mattenberger et al., 2015) suggests that DNA supercoiling and relaxation plays a crucial role during the phage life cycle. Consistent with the hypothesis of Mattenberger and colleagues, we propose that the production of such inhibitory proteins might allow a modulation of topoisomerase activity to enable an optimal phage DNA replication (Mattenberger et al., 2015). Even though CGP3 is a cryptic prophage, it can be assumed that Gip originally had a comparable function for the active phage.

### **2.1.3. Bacterial antiphage defense systems**

The omnipresence of phages in almost all ecosystems and the persistent threat of viral predation has led to a competitive co-evolution of bacteria and phages. Bacteria were forced to evolve an impressive arsenal of antiphage defense systems, while phages co-evolve to overcome these barriers (Hampton et al., 2020; Shabbir et al., 2016; Stern & Sorek, 2011). New antiphage defense systems can be acquired through horizontal gene transfer from closely related strains (Koonin et al., 2017; van Houte et al., 2016). Accordingly, the antiphage defense repertoire of a single strain is subjected to high fluctuation, making defense genes a rather shared community resource as recently described with the term ‘pan-immune system’ (Bernheim & Sorek, 2020).

Escaping phage infection can already be mediated by **blocking adsorption** of the phage to its specific receptor on the bacterial surface. Typical receptors like surface proteins or lipopolysaccharides can exemplarily be mutated (Clément et al., 1983), modified by post-translational glycosylation (Harvey et al., 2018) or masked by proteins or extracellular polymers (Nordström & Forsgren, 1974; Scholl et al., 2005). Besides, a simultaneous protection of several cells against phage adsorption is mediated by release of outer membrane vesicles (OMV) sequestering phages (Manning & Kuehn, 2011) and formation of biofilms shielding interior cells (Hansen et al., 2019). Such multicellular defense strategies will be addressed in further detail in chapter 2.3.4.

Once attached, injection of phage DNA can be blocked by **superinfection exclusion** mechanisms. These protein-based defense systems are encoded by pre-existing phages and serve as protection against specific secondary infections by e.g. inhibiting phage DNA translocation into the cytoplasm through conformational changes or blocking the lysozyme-based degradation of the peptidoglycan layer (Labrie et al., 2010; Lu & Henning, 1994).

After passing these two potential barriers of adsorption and injection, a plethora of intracellular defense mechanisms come into play, among them systems targeting viral nucleic acids, most prominently **R-M (restriction-modification)** and **CRISPR-Cas (Clustered Regularly Interspaced Palindromic Repeats/CRISPR-associated protein)** (Figure 4). R-M systems are based on the enzymatic activity of a restriction endonuclease digesting DNA as well as a methyltransferase modifying DNA. Methylation of host DNA enables the discrimination between host and foreign genetic material and avoids sequence-specific binding and cutting by the restriction endonuclease, whereas incoming, non-methylated phage DNA is digested (Raleigh & Brooks, 1998; Tock & Dryden, 2005). In contrast to innate R-M systems, antiphage defense via CRISPR-Cas entails a prior infection with the same phage to acquire short foreign DNA sequences, called spacers. These spacers are incorporated into a CRISPR array, which enables a subsequent sequence-specific cleavage of identical or similar invader DNA (Barrangou et al., 2007; Hille et al., 2018).

In addition to these destructive mechanisms, **xenogeneic silencer (XS)** proteins could potentially contribute to bacterial antiphage defense as well. With their C-terminal DNA-binding domain and their N-terminal oligomerization domain, xenogeneic silencers preferentially bind to AT-rich sequences thereby silencing viral gene expression through formation of dense nucleoprotein complexes (Duan et al., 2018; Gordon et al., 2010; Navarre, 2016). However, at least in case of the prophage-encoded xenogeneic silencer CgpS in *C. glutamicum*, which maintains the lysogenic state of the CGP3 prophage, a direct contribution to phage defense was not yet confirmed (Hünnefeld et al., 2021; Pfeifer et al., 2019; Pfeifer et al., 2016).

**Abortive infection (Abi)**, a further strategy to combat viral predation, implies sensing of infection by an individual cell and subsequent cell suicide to prevent phage spread into the surrounding community (Lopatina et al., 2020) (Figure 4). Phage infection is typically recognized through phage replication intermediates, phage proteins or altered expression profiles. This in turn activates an effector module causing e.g. cell death by increasing membrane permeability, inhibiting protein biosynthesis, cleaving nucleic acids or phosphorylating multiple host proteins. The mechanistic diversity is further expanded by toxin-antitoxin mediated Abi systems relying on a phage-induced, missing neutralization of a toxin by its corresponding anti-toxin (Lopatina et al., 2020). Another principle is utilized by CBASS (cyclic oligonucleotide-based antiphage signaling system), where the communication between the sensing module and the killing module is mediated by production of cyclic nucleotide molecules as secondary messengers (Cohen et al., 2019).

In recent years, bioinformatics screenings and the discovery that defense genes are clustered in so-called ‘defense islands’, significantly extended the known repertoire of antiphage defense mechanisms to more than 100 systems, which together form the prokaryotic ‘immune system’. However, most of them still need to be mechanistically described (Bernheim & Sorek, 2020; Doron et al., 2018; Makarova et al., 2011; Tesson et al., 2022). Although the last years have revealed new defense systems at unprecedented speed, the step of phage sensing is still a major blind spot for a multitude of systems. A current study started to shed light on this by defining the phage replication machinery, host take over mechanisms and structural phage proteins as unified key determinants for phage sensing (Stokar-Avihail et al., 2023). This may open the door for further mechanistic elucidations.

Two already well-characterized examples of newly discovered antiphage defense systems are **prokaryotic viperins (pVip)** and **nucleotide depletion** (Figure 4). The antiviral activity of viperins against various DNA and RNA viruses was initially detected in humans (Helbig & Beard, 2014; Rivera-Serrano et al., 2020). Like their eukaryotic homologues, prokaryotic viperins can modify nucleotides to ddh-(didehydro)-nucleotides, which act as chain terminators during viral polymerase-dependent transcription (Bernheim et al., 2021; Gizzi et al., 2018). Nucleotide depletion as antiviral defense was also already known from the human immune system (Ayinde et al., 2012; Goldstone et al., 2011). Bacterial dGTPases or dCTP deaminases manipulate the dNTP pool by depleting dGTP or dCTP, respectively, which halts phage DNA replication (Tal et al., 2022). Interestingly, several other recently described antiviral defense strategies are conserved between eukaryotes and prokaryotes, suggesting a bacterial origin of several central eukaryotic immune mechanisms (Wein & Sorek, 2022).

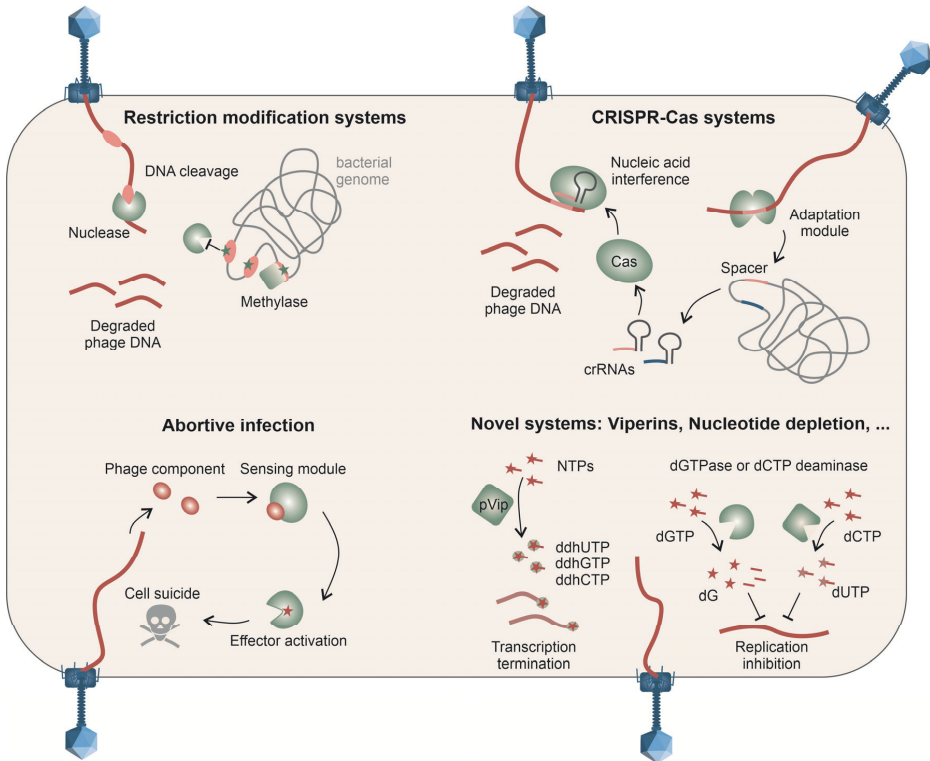


**Figure 4: Selected bacterial antiphage defense systems.** After successful injection of phage DNA, different mechanisms can interfere with the phage life cycle. Restriction modification systems as well as CRISPR-Cas systems directly target and cleave intracellular phage DNA. Abortive infection mechanisms are highly diverse, but have in common that they consist of a module sensing the infection and a module initiating cell suicide to prevent phage spread. The repertoire of defense system was recently supplemented with the discovery of diverse new systems, including exemplarily prokaryotic viperins inhibiting transcription of viral DNA or mechanisms of nucleotide depletion halting viral DNA replication. The figure was designed based on Tal and Sorek (2022).

## 2.2. *Streptomyces*, a filamentous soil bacterium as major producer of bioactive compounds

### 2.2.1. Multicellular development and its hierarchical regulatory network

*Streptomyces* is a Gram-positive, filamentous-growing actinobacterium, which is highly abundant in soil habitats (Anderson & Wellington, 2001; Janssen, 2006). As all soil-dwelling organisms, it has to deal with a high level of microbial competition and constant fluctuations in nutrient availability (Fierer, 2017). To survive in this challenging environment, *Streptomyces* can initiate the formation of dormant exospores as part of its multicellular life cycle, allowing its dispersal into new environments as well as the protection of its genetic material throughout various environmental stresses (Bobek et al., 2017).

The multicellular development of *Streptomyces* has parallels to the one of filamentous fungi, but is rather a peculiarity among prokaryotes (Elliot & Talbot, 2004). Favorable conditions initiate germination of spores to build up a network of vegetative hyphae, which grow by branching and tip extension. Upon stressful conditions like nutrient deficiency, parts of this vegetative mycelium are self-degraded via programmed cell death to provide a nutrient source for the morphological differentiation into apical-growing, aerial hyphae (Flärdh & Buttner, 2009; Manteca et al., 2007). This developmental transition to reproductive growth usually coincides with the onset of antibiotic production, probably to protect released nutrients from other soil-living competitors in the same ecological niche (van der Meij et al., 2017). During sporogenesis, the multigenomic aerial hyphae differentiate into chains of unigenomic pre-spores via synchronized septation and chromosome segregation. After subsequent spore maturation, dormant exospores are released into the environment, which can outlast various environmental insults, until germination is triggered again (Flärdh & Buttner, 2009) (Figure 5a).

This life cycle is used for the general description of surface-grown cultures. However, many *Streptomyces* species including the historical model *Streptomyces coelicolor* are arrested in a pre-sporulation state when growing in submerged cultures (Manteca et al., 2008). Therefore, more recent studies have tended to focus on *Streptomyces venezuelae* as new model species due to its ability to undergo sporulation even in submerged cultures (Glazebrook et al., 1990). This facilitated the elucidation of the development-specific regulatory network by allowing the application of established "omics" methods (M. J. Bush et al., 2015).

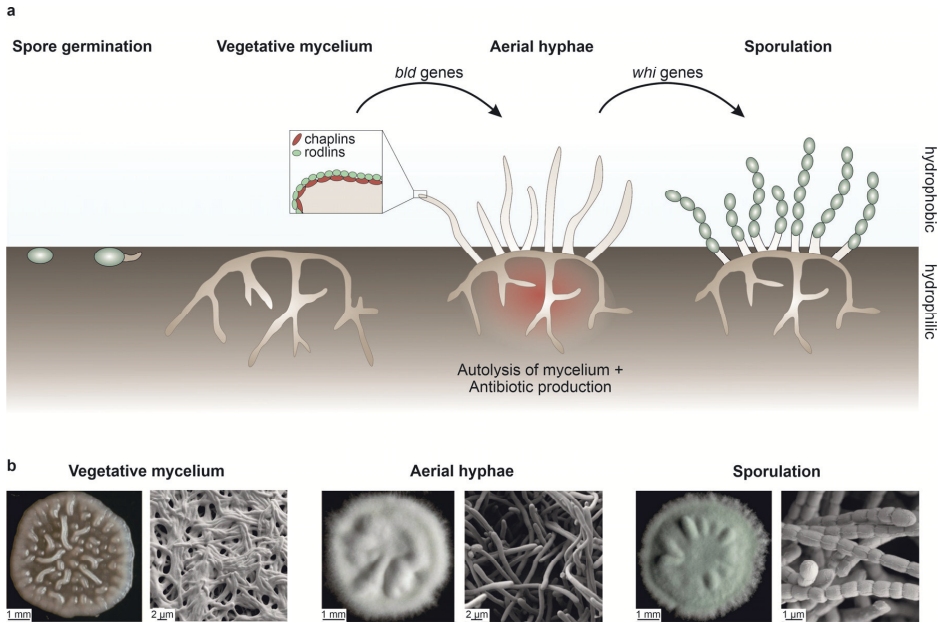


**Figure 5: Multicellular life cycle of surface-grown *Streptomyces* cultures.** a) The life cycle starts with the germination of spores, which leads to the formation of a branched network of vegetative hyphae. Upon nutrient starvation, parts of the vegetative mycelium are self-degraded to supply nutrients for the morphological differentiation into aerial hyphae. This transition is mediated by Bld regulators. The accompanied production of antibiotics is proposed to protect released nutrients from other competitors in close proximity. Unlike vegetative hyphae, aerial hyphae are characterized by a hydrophobic surface, which is based on a coating layer of rodlin and chaplin proteins. The regulatory activity of the Whi proteins mediate further differentiation from aerial hyphae to mature exospores. The figure was designed based on Jones and Elliot (2017) and Urem et al. (2016). b) Morphology of *S. venezuelae* colonies in different developmental stages with corresponding scanning electron micrographs (images taken from Tschowri (2016)).

Hyphae-spore transition is orchestrated by two classes of developmental regulators, Bld and Whi regulators. Their names were coined by the phenotypic appearance of corresponding developmental mutants: Deletion of *bld* genes prevents transition from vegetative growth to aerial hyphae and hence shows up in a bald and shiny phenotype, whereas *whi* mutants are unable to differentiate from aerial hyphae to mature spores and thus have a white, fuzzy appearance (Figure 5b) (McCormick & Flärdh, 2012). These regulators are part of a complex hierarchical network, which is controlled by the c-di-GMP-dependent activity of the master regulator BldD. BldD inhibits the expression of most key developmental genes delaying the onset of differentiation (M. J. Bush et al., 2015; den Hengst et al., 2010; Tschowri et al., 2014). Roughly summarized, relieving repression by BldD initiates the first developmental transition from vegetative mycelium to aerial hyphae. In contrast to the hydrophilic vegetative hyphae in the moist soil, aerial hyphae are highly hydrophobic, which is dependent on the sigma-factor BldN ( $\sigma^{\text{BldN}}$ )-regulated transcription of rodlin and chaplin genes (Bibb et al., 2012). Their gene products assemble to build up a hydrophobic

sheath covering the surface of aerial hyphae, which – on certain media together with surfactant protein SapB lowering surface tension – enables the escape from the aqueous environment into the air (Claessen et al., 2003; Claessen et al., 2002; Elliot et al., 2003; Elliot & Talbot, 2004; Willey & Losick, 1991). Besides regulating expression of rodlin and chaplin genes,  $\sigma^{\text{BldN}}$  activates transcription of *bldM*, which in turn allows the expression of sporulation genes, including *whiB* (Al-Bassam et al., 2014). The heterodimer formed of WhiAB was shown to stop aerial growth and activates genes for chromosome segregation and cell division (Bush et al., 2013; Bush et al., 2016). Finally, spore maturation is initiated via the regulatory activity of  $\sigma^{\text{WhiG}}$  and its downstream cascade (M. J. Bush et al., 2015).

Interestingly, recent studies discovered an alternative mode of growth, termed exploration, which is initiated in response to fungal competitors or glucose depletion. During exploratory growth, unbranched, vegetative hyphae rapidly outgrow and move across solid surfaces, which allows a sporulation-independent colonization of new environments. Accordingly, exploration might represent a further strategy to promote survival in this challenging soil environment by facilitating nutrient access (Jones & Elliot, 2017; Jones et al., 2017; Jones et al., 2019).

### **2.2.2. Complex secondary metabolism as hallmark of *Streptomyces***

In addition to its multicellular life cycle, *Streptomyces* is well studied for its rich source of secondary metabolites (Donald et al., 2022), whose secretion can sometimes even be observed with the naked eye (Figure 6a). In contrast to primary metabolites, secondary metabolites are not essential for growth and development, but instead can confer producers an adaptive benefit in ecological interactions (Challis & Hopwood, 2003; Seyedsayamdost, 2019). With their antibacterial, antifungal and antitumor activity, these compounds find applications in medical, biotechnological and agricultural sectors (Barka et al., 2016). The ability of *Streptomyces* to produce bioactive compounds was initially recognized by Waksman and colleagues almost 80 years ago (Waksman & Woodruff, 1940; Waksman & Woodruff, 1942). The inspiring discovery of penicillin by Alexander Fleming was soon followed by the isolation of the first *Streptomyces*-derived antibiotics, among them also streptomycin, which served as the first successful treatment against tuberculosis (Fleming, 1929; Schatz & Waksman, 1944). The finding that *Streptomyces*, but also fungi produce a variety of bioactive compounds, revolutionized medicine drastically. About 2/3 of all natural-derived antibiotics are produced by *Streptomyces*, while the potential for the discovery of new antibiotics has not yet been exhausted (Bibb, 2013; Kieser et al., 2000). According to an estimation of Watve and colleagues, just 3% of natural products encoded by *Streptomyces* species have been reported until 2001 (Watve et al., 2001). However, the fact that most of the corresponding

biosynthetic gene clusters are silent under laboratory conditions, hampers their isolation and functional characterization (Liu et al., 2021).

Production and release of secondary metabolites is not just frequently linked to the developmental transition into aerial hyphae, but is probably also influenced by a broad variety of biotic and abiotic environmental triggers indicative for their host demands (Bibb, 2005; van der Meij et al., 2017). For instance, antibiotic production and secretion can be activated when competition-related stress such as nutrient deficiency or cell damage is sensed (Cornforth & Foster, 2013). Because producers are resistant to their own substances, they can outcompete other sensitive soil organisms in close proximity (Fajardo et al., 2009; van der Meij et al., 2017). However, the traditional image of antibiotics as chemical weapons has been challenged by the fact that despite local extremes the overall concentration of antibiotics found in soil is generally subinhibitory (Fajardo et al., 2009). This shaped the current assumption that antibiotics exhibit rather a concentration-dependent functionality (Figure 6b). At high concentrations, they can serve as direct weapons against microbial competitors, while at subinhibitory concentrations they may be used as signaling molecules between interacting microbes (Hashem & Van Impe, 2022; Linares et al., 2006; Spagnolo et al., 2021; Vaz Jauri et al., 2013). Nonetheless, the biochemical diversity and the ecological role of most secondary metabolites is far from being entirely understood (Tyc et al., 2017).

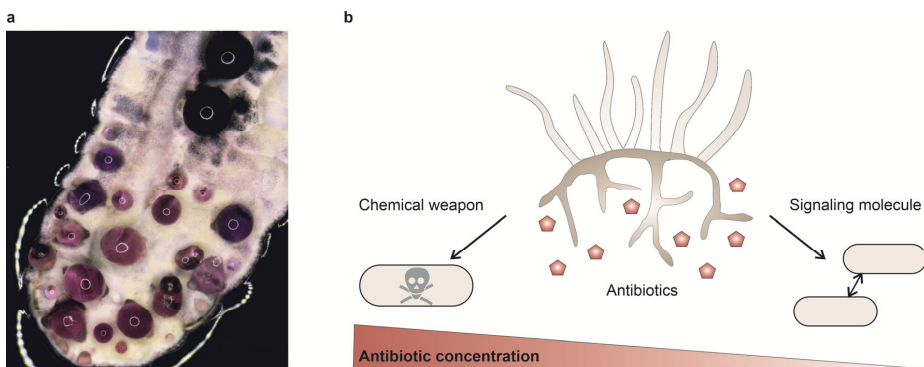


**Figure 6: Secondary metabolite production in *Streptomyces*.** a) Stereomicroscopic image showing the production of the pigmented antibiotic actinorhodin as droplets on the colony surface of *S. coelicolor* M145. b) Current hypothesis on the concentration-dependent function of antibiotics as chemical weapons or signaling molecules.

Interestingly, biosynthetic gene clusters encoding secondary metabolites are enriched in the flanking arms of the linear *Streptomyces* chromosome (Aigle et al., 2014; Bentley et al., 2002). In contrast to the core genome harboring essential genes for replication, protein biosynthesis and central metabolism, the arm regions containing conditionally adaptive genes are more frequently affected by genetic rearrangement leading to amplifications and deletions under laboratory



conditions (Bentley et al., 2002; Thibessard & Leblond, 2014; Volff & Altenbuchner, 1998). This arm plasticity is proposed to possibly confer an adaptive benefit on a population level by facilitating the differentiation into social subpopulations, which may produce an extended pool of ‘public goods’ (Lorenzi et al., 2021). Such concept was recently exemplified for the antibiotic production in *S. coelicolor*, which was shown to be organized by a division of labor. The terminal differentiation led to genetically heterogeneous *S. coelicolor* colonies containing antibiotic hyper-producing mutant strains with massive genomic deletions. Although this enhanced antibiotic production came at the expense of individual fitness, colony-wide reproduction was not affected when combining mutant and parental strains (Zhang et al., 2020). However, after their emergence these mutant cells further accumulate genetic deletions and mutations leading to their cell death via mutational meltdown over time (Zhang et al., 2022).

## 2.3. Multicellular antiphage defense systems of *Streptomyces*

### 2.3.1. Phage infection of *Streptomyces*: Initial observations

Like other bacteria, *Streptomyces* is continuously challenged by phage attacks. Over the years, *Streptomyces* phages were primarily studied for their source of genetic tools to manipulate the host genome, enabling for instance the construction of phage-based integration vectors (Baltz, 2012; Bierman et al., 1992; Gregory et al., 2003). In the last decade, vast efforts were spent on the isolation and characterization of new phages infecting actinobacterial species, including *Streptomyces*. This was mainly driven by the Science Education Alliance Phage Hunters Advancing Genomics and Evolutionary Sciences (SEA-PHAGES) program, which markedly expanded the collection of sequenced actinobacteriophages (Jordan et al., 2014). To date, more than 21,000 actinobacteriophages have been isolated and more than 4,000 sequenced genomes are deposited in 'The Actinobacteriophage Database' (phagesdb.org, (Russell & Hatfull, 2016)), including ~300 sequenced *Streptomyces* phages (as of October 2022). However, the amount of experimentally studied phages infecting this genus remained comparable low. Furthermore, little is known about the extent to which the extensive chemical repertoire and the multicellular life cycle of *Streptomyces* might contribute to antiphage defense. This topic has just recently gained significant interest and is the focus of this doctoral thesis.

To establish a set of model phages in our laboratory for studying phage-host interactions, pioneering work started with the isolation and characterization of five novel *Streptomyces* phages, preying on either *S. venezuelae* or *S. coelicolor*. In contrast to the majority of known *Streptomyces* phages, these new phage isolates were comprehensively characterized with regard to plaque and virion morphology, genome sequence, phylogeny and infection dynamics (Hardy et al., 2020). All newly isolated phages are siphophages as they possess a long-tailed morphology and a dsDNA genome (Figure 7a). In terms of their life cycle, the two phages infecting *S. venezuelae*, named Alderaan and Coruscant, were shown to be virulent phages, while all three phages infecting *S. coelicolor*, named Dagobah, Endor1 and Endor2, were predicted to be temperate.

Strikingly, for all *S. coelicolor* phages, plaque formation was accompanied by secretion of pigmented secondary metabolites at the infection interface ((Hardy et al., 2020), Figure 7b). Although it is still under investigation whether this formation of colored halos is a specific response to phage infection or rather a general stress response triggered by cell lysis (Hardy et al., ongoing work), it served as an inspiration to actively search for *Streptomyces*-derived secondary metabolites harboring an antiphage activity as chemical defense mechanism (cf. chapter 2.3.2). In addition to the increased secondary metabolite production, *Streptomyces* frequently responded

to phage infection with a ring of enhanced morphological differentiation surrounding the plaques, which was especially the case for Alderaan infecting *S. venezuelae* and Dagobah infecting *S. coelicolor* (Figure 7b). Further examination revealed that this formation of aerial hyphae was essential for the emergence of transiently phage-resistant mycelium and hence for the containment of phage infection (Luthe et al., 2023a). Another interesting observation was made when performing infection assays in submerged cultures. The extent of culture lysis and phage proliferation showed significant differences, ranging from complete culture collapse during Alderaan infection to only minor effects on bacterial growth upon infection with Dagobah (Hardy et al., 2020). However, it was notable that for all phages, a successful initial phage propagation was often followed by a decrease in extracellular infectious phage particles at later stages of the infection experiment (Figure 7c). Such time course of phage titers was not obtained for infection of unicellular bacteria recently performed in our laboratory (Erdrich et al., 2022; Hünnefeld et al., 2021), which gave rise to further investigate the molecular basis of this phenomenon (chapter 2.3.3).

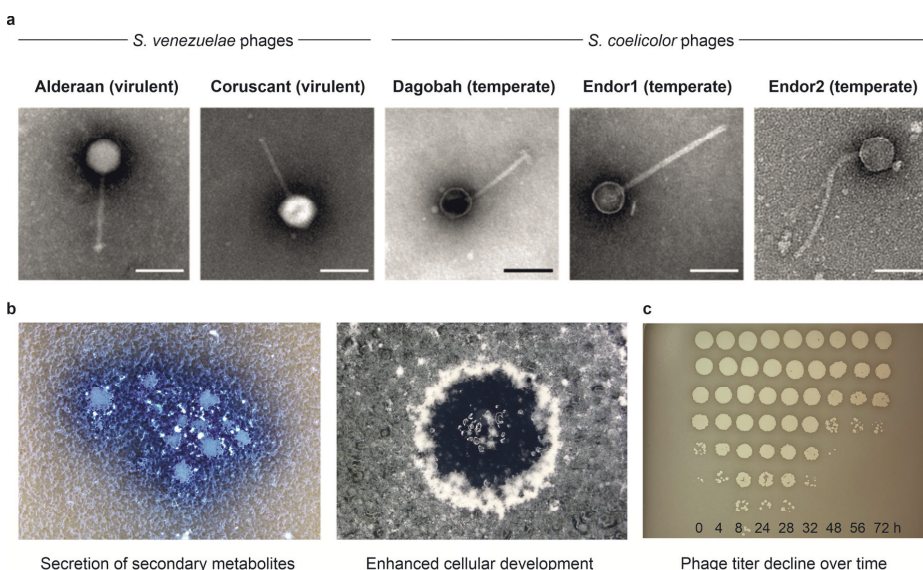


**Figure 7: Particle morphology of novel *Streptomyces* phages and phenotypic observations upon infection.** a) Transmission electron microscopy identifies all phages as siphophages (scale bar: 150 nm, images taken from Hardy et al. (2020)). b) Stereomicroscopic images showing the production of the blue-pigmented compound actinorhodin (left) as well as enhanced sporulation at the plaque interface (right) in response to infection of *S. coelicolor* M145 with phage Dagobah. c) Development of phage titers upon infection of *S. venezuelae* NRRL B-65442 with phage Alderaan.

### 2.3.2. Chemical defense via aminoglycoside antibiotics

#### Aminoglycosides – a case of molecular multitasking

In search for secondary metabolites featuring an antiphage activity, we observed that phage infection was significantly impaired in presence of the aminoglycoside apramycin, which was the cornerstone for studying the antiphage properties of these well-studied antibacterial compounds (Kever et al., 2022). Actually, antiphage activity of aminoglycosides was already described in reports published in the middle of the last century, which showed an inhibitory effect of streptomycin on various phages (Brock et al., 1963; Brock & Wooley, 1963). However, the biological relevance of these molecules as part of the bacterial immune system was not investigated and the mode of action remained controversial.

Aminoglycosides are naturally derived, bactericidal antibiotics, which interfere with protein biosynthesis in several aerobic Gram-positive, but particularly Gram-negative bacteria (Krause et al., 2016). Structurally, they are characterized by an amino sugar core structure, which is glycosidically linked to a dibasic aminocyclitol, mostly 2-deoxystreptamin, whose presence and substitutions define four different subclasses (Magnet & Blanchard, 2005; Mingeot-Leclercq et al., 1999). The uptake of these polycationic antibiotics starts with their binding to the negatively charged surface of the bacterial membrane. This electrostatic interaction causes the dissociation of divalent cations and thus a permeabilization of the bacterial membrane, which promotes initial aminoglycoside uptake into the cytoplasm in an energy-dependent process (Ramirez & Tolmasky, 2010). Once taken up, they inhibit bacterial protein translation by a high-affinity binding to the aminoacyl site (A-site) on the 16S rRNA of the 30S ribosomal subunit (Kotra et al., 2000; Magnet & Blanchard, 2005). The induced conformational changes cause an error-prone translation through misreading or a direct blocking of translation initiation or elongation. Incorporation of mistranslated proteins into the membrane further enhances aminoglycoside uptake, finally resulting in cell death (Krause et al., 2016).

Resistance towards these antibiotics is mediated by enzymatic modifications of the aminoglycoside scaffold or the ribosomal target site, active export via efflux pumps or modifications of the cell membrane (Garneau-Tsodikova & Labby, 2016). Among these resistance mechanisms, antibiotic modification is the most common one, which relies on the catalytic activity of aminoglycoside-modifying enzymes (AME), subdivided into aminoglycoside O-phosphotransferases (APHs), aminoglycoside N-acetyltransferases (AACs) and aminoglycoside O-nucleotidyltransferases (ANTs). According to their functional categorization, these enzymes can modify various positions of the aminoglycoside scaffold via phosphorylation, acetylation or adenylation, which prevents the

efficient binding of the antibiotic to the 16S rRNA (Ramirez & Tolmasky, 2010). In contrast to this rather specific resistance mechanism towards single aminoglycosides, enzymatic modification of the primary target site via 16S rRNA methyltransferases (RMTase) offers a broader resistance profile. By methylating distinct nucleotides of the 16S rRNA, namely G1405 or A1408, RMTases prevent binding of various structurally related aminoglycosides at the same time (Garneau-Tsodikova & Labby, 2016; Krause et al., 2016).

Following the natural resistance of producers to their own compounds, the project was started with the construction of aminoglycoside-resistant strains carrying a plasmid-borne gene coding for an AME. This step was considered essential for a systematic screening of the antiphage properties of aminoglycoside antibiotics, since the strong antibacterial effect of these compounds would markedly hamper the recognition of an additional antiphage effect. As a screening platform, double-agar overlays with increasing antibiotic concentrations were used to correlate reduced plaque formation with increased aminoglycoside pressure. To keep the spectrum of this tripartite interaction between phages, hosts and aminoglycosides quite broad, structurally divergent aminoglycosides were combined with phages of different morphotypes (sipho-, myo-, podo-, ino- and levivirus) and specific for different host organisms (*S. venezuelae*, *S. coelicolor*, *C. glutamicum* and *E.coli*).

Substantial differences were perceived for the individual phage-host pairs and aminoglycosides, ranging from complete inhibition of plaque formation to no noticeable changes. When trying to find an underlying pattern for this aminoglycoside-mediated inhibition, the only statement that can currently be made is that all affected phages are siphophages, which are characterized by a dsDNA genome and a tailed morphology. Among them, the strongest effect of aminoglycoside addition was observed for phage Alderaan infecting *S. venezuelae* in presence of apramycin and hygromycin, but also infection of *E. coli* model phage  $\lambda$  was significantly impaired in presence of apramycin and kanamycin. Interestingly, all phages infecting *S. coelicolor* revealed no inhibition upon aminoglycoside treatment, potentially suggesting that differences in cell envelope structures and aminoglycoside uptake by the host strain might contribute to the observed cluster as well (Figure 8). Therefore, ongoing studies are currently expanding the diversity of screened phages including also a *Streptomyces* phage with a broad host range, which may allow a more precise distinction between host-specific and phage-specific differences in aminoglycoside-mediated inhibition of phage infection. However, based on this screening, follow-up studies focused mainly on the inhibitory effect of apramycin on the virulent phage Alderaan infecting *S. venezuelae* and the temperate phage  $\lambda$  infecting *E. coli*.

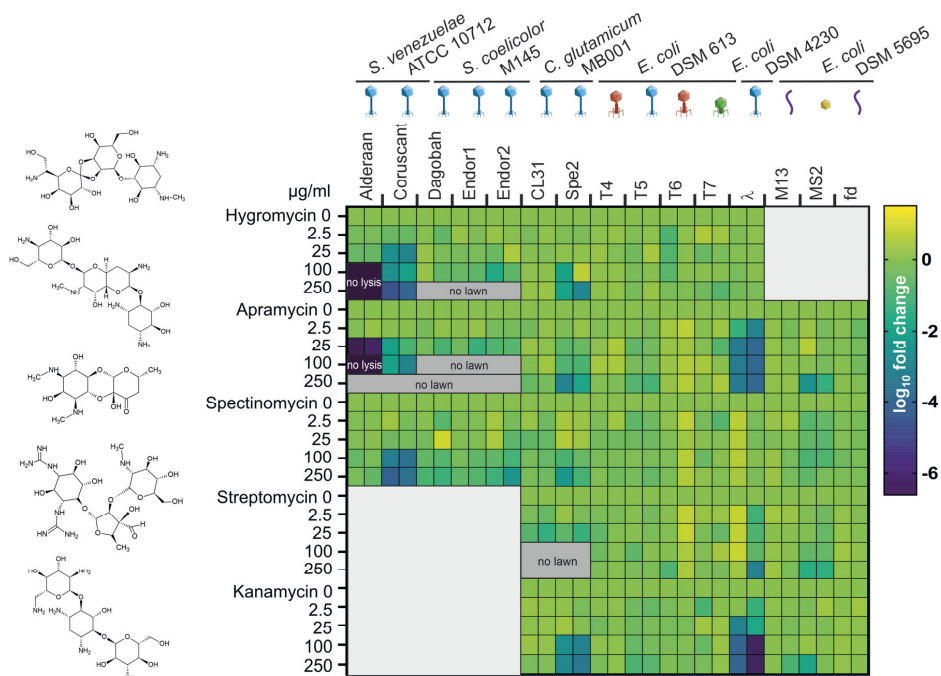


**Figure 8: Aminoglycosides are potent inhibitors of phage infection.** This heat map shows the screening results as log<sub>10</sub> fold change comparing plaque formation under aminoglycoside pressure to antibiotic-free conditions. If aminoglycoside treatment completely prevented plaque formation by the phage or bacterial growth, it was stated as ‘no lysis’ or ‘no lawn’, respectively (n = 2 independent biological replicates). The corresponding molecular structures of the tested aminoglycosides are provided on the left. The different phage morphologies are schematically shown with icons according to the following color scheme: blue, siphovirus; red, myovirus; green, podovirus; purple, inovirus; yellow, levivirus (adapted and modified from Kever et al. (2022)).

### Mechanism of antiphage activity: Interference with an early step of the phage life cycle

To investigate the mechanism of action, infection experiments with aminoglycoside-resistant strains were performed in submerged cultures to benefit from a larger number of established methods (Figure 9a). While infection of *S. venezuelae* with Alderaan usually results in a culture collapse, addition of apramycin (10 µg/ml) completely prevented phage amplification and phage-mediated cell lysis (Figure 9b). This inhibitory effect of apramycin could also be observed to a similar extent during infection assays with phage λ. Interestingly, infection with both phages was completely restored when adding simultaneously high concentrations of MgCl<sub>2</sub>, which was in line with previous reports describing the antagonistic effect of MgCl<sub>2</sub> on aminoglycoside-mediated phage inhibition (Brock & Wooley, 1963). This could potentially be attributed to the known interference of enhanced Mg<sup>2+</sup> levels with aminoglycoside uptake (Hancock et al., 1981) and hence already gave a first hint that interference most likely occurs on an intracellular level. In line with this, pre-incubation of Alderaan particles with physiologically relevant apramycin concentrations

of  $<50 \mu\text{g/ml}$  and subsequent spotting on a bacterial lawn showed no influence on phage infectivity.

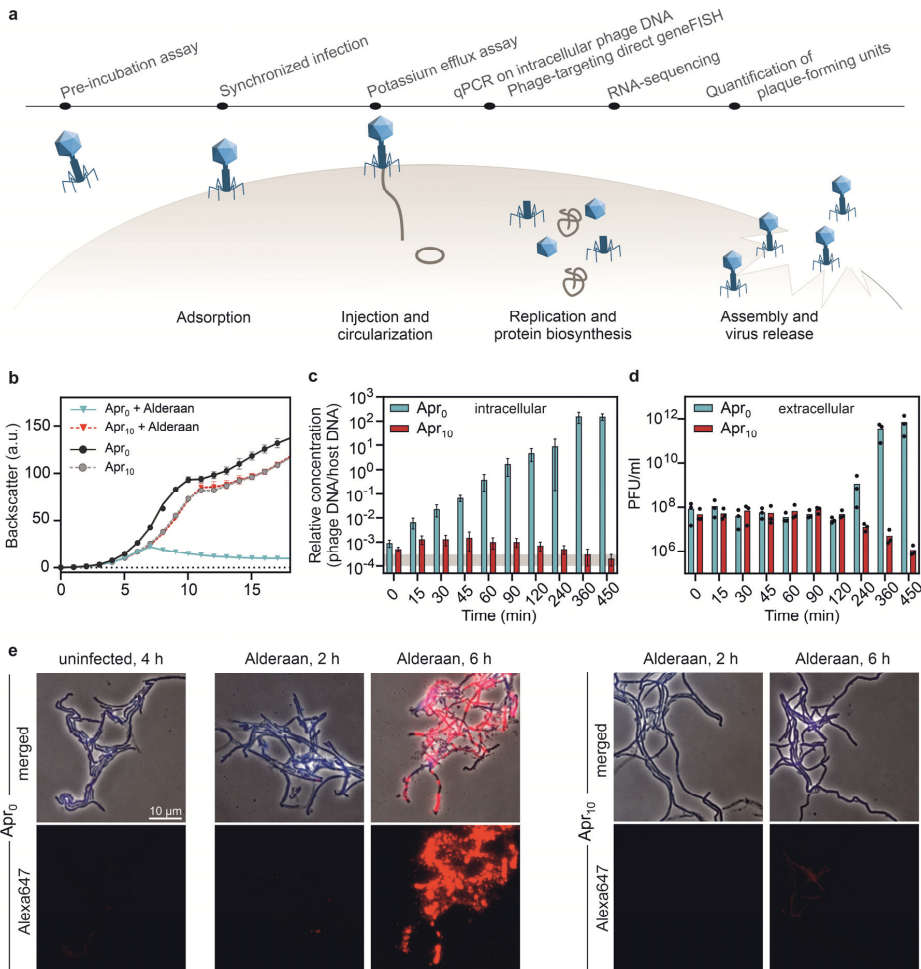


**Figure 9: Apramycin inhibits an early step of phage life cycle.** a) Schematic representation of the different steps of the lytic life cycle and respective experiments, which were performed to study the effect of apramycin. b) Alderaan infection assays of the apramycin-resistant strain *S. venezuelae* ATCC 10712 producing the aminoglycoside acetyltransferase AAC(3)IV as resistance mechanism. Infection was performed in presence and absence of  $10 \mu\text{g/ml}$  apramycin ( $n = 3$  independent biological replicates). c) Relative concentration of phage DNA to host DNA calculated via quantitative PCR during the time course of Alderaan infection in presence and absence of  $10 \mu\text{g/ml}$  apramycin. Data represent means of three independent biological replicates measured as technical duplicates. The range of relative phage DNA concentrations measured for an uninfected control is highlighted in gray. d) Corresponding time-resolved measurement of extracellular phage titers via double-agar overlay assays ( $n = 3$  independent biological replicates). e) Visualization of intracellular Alderaan DNA during infection by phage-targeting direct geneFISH. Fluorescence signals from phage DNA (Alexa647, red) are once shown separately (second row) and once as merged images with phase-contrast and fluorescence signal from bacterial DNA (DAPI, blue) (first row) (adapted and modified from Kever et al. (2022)).

To identify the step that is inhibited in the presence of apramycin, each step of the phage life cycle was systematically addressed by appropriate techniques (Figure 9a). The influence of apramycin on phage adsorption as the first step of the phage life cycle was examined with a synchronized infection assay. After an initial incubation phase of *Streptomyces* mycelium with phage Alderaan in presence of apramycin, free and reversible-attached phage particles as well as extracellular apramycin were removed. A successful following phage amplification suggested no obvious effect of the aminoglycoside on irreversible phage adsorption. In accordance with this, when apramycin was not added to the pre-incubation step, but instead thereafter, no phage propagation was possible (cf. chapter 4.2, Figure S3).

To assess phage DNA injection and replication upon apramycin treatment, the relative amount of intracellular Alderaan DNA to host DNA was calculated via quantitative PCR, while simultaneously quantifying extracellular phage titers via double-agar overlays (Figure 9c and d). Under normal infection conditions, an exponential increase of relative phage DNA levels and a concomitant increase in extracellular phage titers was detected, indicating the successful release of newly amplified phage progenies. In contrast, intracellular phage DNA levels increased only slightly in the presence of apramycin, which was even followed by a decrease until the detection limit. Together with the decline of extracellular phage titers, these data hinted on a successful phage adsorption, but a blockage of subsequent replication.

A further visual proof of this inhibited replication in presence of apramycin was gained when performing a fluorescence in situ hybridization (FISH) assay with fluorescently labelled gene probes specifically targeting the phage genome (phage-targeting direct geneFISH). Focusing on  $\lambda$  infection first, distinct fluorescent foci were detected in the early stages of infection independent of the presence of apramycin, which indicated a successful phage DNA delivery. This was in line with an apramycin-independent efflux of potassium ions as indicator for successful injection of the  $\lambda$  genome (Boulanger & Letellier, 1992). However, a further increase in fluorescence revealing an ongoing phage DNA replication was just observed for apramycin-free conditions. Also for *Streptomyces* phage Alderaan, the intensity and amount of fluorescent foci progressively increased over time under normal infection conditions. Conversely, just a more diffuse signal without distinct fluorescent foci could be detected during infection under apramycin pressure (Figure 9e). This could be either traced back to i) technical limitation in detecting single injected phage DNA genomes, as they may be obscured by *S. venezuelae* autofluorescence ii) delayed sampling time points or iii) an interference of apramycin at the level of phage DNA injection. To conclude, quantification of phage DNA via qPCR and phage-targeting geneFISH suggested an inhibition of phage infection at an early step of phage life cycle, most likely between phage DNA injection and



replication. Thereby, it cannot be excluded that the mechanism of inhibition might further be dependent on the phage-host pair, since results obtained for  $\lambda$  and Alderaan showed potential differences in the influence of apramycin on the DNA injection step.

Finally, we examined the step of phage DNA transcription by performing RNA-sequencing. Whereas normal infection conditions exhibited an increasing amount of phage DNA transcripts, almost no viral DNA transcription seemed to have taken place in presence of apramycin (cf. chapter 3.2., Figure 4d).

### **Targeting of injected phage DNA as potential mechanism of antiphage activity**

While the obtained data indicated an inhibition of phage infection at an early step in the life cycle prior to DNA replication and transcription, the underlying mechanism of action remains to be elucidated. A comparable point of attack, namely a blocking of phage DNA replication, was also proposed in a parallel conducted study describing the inhibition of two mycobacteriophages by hygromycin, kanamycin, and streptomycin (Jiang et al., 2020). Worth mentioning, a comparatively low phage-inhibiting activity was detected for tetracycline as another ribosome-targeting antibiotic. This comparison suggests that inhibition of phage infection by aminoglycosides is not just a general trait of blocked protein translation, but might be rather dependent on the mechanism of translation inhibition (Zuo et al., 2021). Remarkably, antagonistic effects of translation inhibitors and phage infection were also demonstrated in two recent studies: Bacteriostatic translation inhibitors can impair phage infection by decelerating phage reproduction, which extends the time for the acquisition of adaptive CRISPR immunity (Dimitriu et al., 2022). In addition, subinhibitory concentrations of chloramphenicol, tetracycline and erythromycin were shown to hinder amplification of phages encoding anti-CRISPR proteins in a CRISPR-immune bacterial host, probably by impeding translation of the phage-encoded counter-defense proteins. Contrary to this, the bactericidal aminoglycoside gentamicin had no impact on the immunosuppression via anti-CRISPR proteins, but instead impaired phage infection independent of the presence of CRISPR-Cas and anti-CRISPR proteins, suggesting a distinct mode of antiviral activity of aminoglycoside antibiotics (Pons et al., 2023).

Interestingly, DNA-intercalating anthracyclines, which represent a further class of antiphage secondary metabolites produced by *Streptomyces*, were proposed to interfere with phage infection on a similar stage of phage life cycle as aminoglycosides (Kronheim et al., 2018). Taken together, it can be hypothesized that these antiphage molecules may target injected but not yet replicated DNA, since the linear and relaxed conformation and a missing protection by DNA-binding proteins makes injected phage DNA possibly sensitive to DNA-binding molecules. A direct

interaction could inhibit either DNA circularization or protein-DNA interaction mandatory for replication and transcription (Casjens & Gilcrease, 2009; Kronheim et al., 2018). The general ability of aminoglycosides to target nucleic acids is already demonstrated by their inhibitory binding to the 16S rRNA as their antibacterial mode of action. A first evidence for a potential, direct binding to phage DNA was given by in vitro studies with purified  $\lambda$  DNA, proposing formation of a clamp around the phage DNA causing structural deformations (Kopaczynska et al., 2004; Kopaczynska et al., 2016).

To further examine this early phase of phage life cycle, phage DNA injection and a potential apramycin-phage DNA interaction in vivo could be analysed via **super resolution microscopy (SRM)**. Therefore, phage DNA could be labeled by the incorporation of 5-ethynyl-2'-deoxyuridine (EdU), a thymidine analogue, which can be detected through reaction with a fluorescent azide ("click" chemistry) (Ohno et al., 2012; Salic & Mitchison, 2008). At the same time, the aminoglycoside could potentially be conjugated to a cyanine fluorophore as it was recently described for the labeling of a neomycin derivative with sulfonated Cy3 or Cy5 (Sabeti Azad et al., 2020). Additionally, further efforts should focus on **phage DNA circularization** as step between DNA injection and replication. To do so, total intracellular DNA in the early stages of infection in presence and absence of apramycin could be isolated and analysed in terms of DNA topology via **pulsed field gel electrophoresis**, either followed by a phage DNA-targeting southern-blot hybridization or in case of a previous Edu-labeling of phage DNA by visualization via click chemistry as described above. Alternatively, one could attempt to use a **restriction mapping** to discriminate between circular and linear phage DNA based on different DNA fingerprints. Due to the used packaging mechanisms, phage  $\lambda$  would be more suitable for this approach. The  $\lambda$  DNA circularizes via pairing of cohesive ends with following ligation (Wu & Kaiser, 1968). After rolling circle replication and translocation, each capsid contains exactly one genome with cohesive ends leading to identical phage progenies (Merrill et al., 2016). In contrast, Alderaan DNA is circularized by homologous recombination of the genomes ends and subsequent ligation. After replication, translocation of single phage genomes into the capsid happens via the headful packaging mechanisms (Hardy et al., 2020). As the name says, DNA is packed into the phage head until it is completely filled, which usually corresponds to a bit more than genome length leading to heterogeneous progenies with terminal redundancy and cyclic permutations (Merrill et al., 2016).

**Coordinating molecular multitasking of aminoglycoside antibiotics**

A striking feature of aminoglycoside antibiotics is that they can function as antibacterial and – at the same time - antiphage molecules. In all assays, aminoglycoside resistant strains were used to circumvent the antibacterial effect on the host during infection. In case of apramycin, this bacterial resistance mechanism relied on the acetylation of the 3-amino group of the deoxystreptamine ring via aminoglycoside N(3)-acetyltransferase (AAC(3)IV) preventing efficient binding to the 16S rRNA (Magalhaes & Blanchard, 2005). To examine the influence of this modification on the antiviral activity, in vitro acetylated apramycin (Ac-Apr) was supplemented to infection assays with the non-resistant wild type strain. Since this modification is known to abolish the antibacterial effect, no impact of acetylated apramycin on bacterial growth was detected. Conversely, the antiphage activity of apramycin appeared to be unaffected by this modification as indicated by the complete inhibition of phage infection (Figure 10a), which was in line with the results gained for unmodified apramycin during infection of the resistant strain carrying a plasmid-borne AAC(3)IV.

To further screen for the antiphage activity of the unmodified compound, the rRNA methyltransferase KamB from the natural apramycin producer *Streptoalloteichus tenebrarius* (formerly known as *Streptomyces tenebrarius*) was harnessed as alternative resistance mechanism (Holmes et al., 1991; Tamura et al., 2008). This enzyme catalyzes the N1-methylation of the 16S rRNA at position A1408 conferring resistance to the *Streptomyces*-derived aminoglycosides kanamycin, apramycin and tobramycin (Koscinski et al., 2007). Comparable to the results obtained for acetylated apramycin, methylation of the target site almost completely abolished the antibacterial effect of apramycin, but still allowed a strong inhibition of phage infection (Figure 10b). Altogether, acetylation appeared to neither impair nor be essential for the antiphage activity of apramycin. At the same time, drug modification and target site modification prevented the antibacterial mode of action, which is a further indication for the different target sites of this dual functionality. However, whether such uncoupling of antiphage and antibacterial properties via modification of the aminoglycoside scaffold can be generalized to other AMEs and aminoglycosides as well, needs to be determined in future experiments.

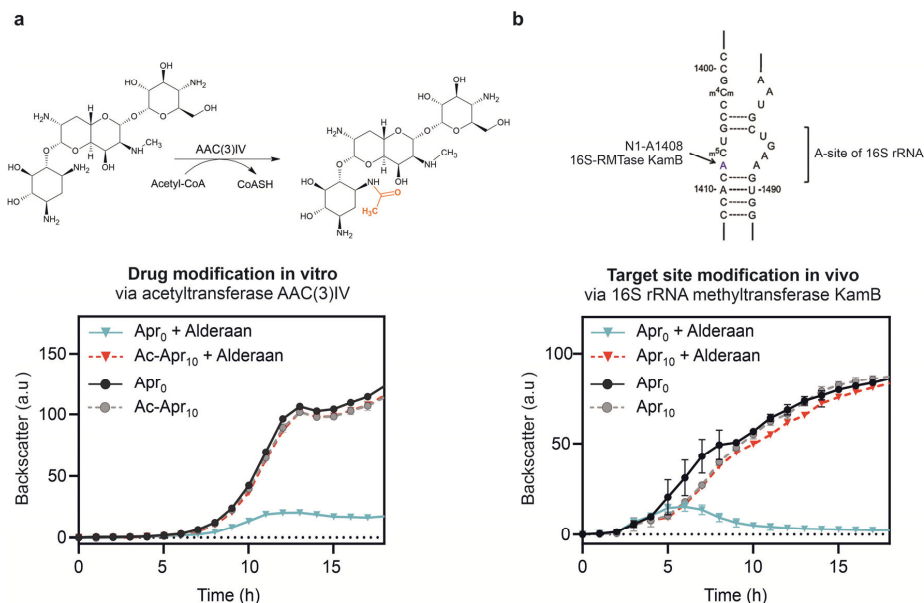


**Figure 10: Aminoglycoside resistance mechanisms uncouple antibacterial and antiviral properties of apramycin.** a) Alderaan infection assays of the *S. venezuelae* ATCC 10712 wild type strain using in vitro acetylated apramycin (Ac-Apr, 10  $\mu\text{g}/\text{ml}$ ). The acetylation reaction via acetyltransferase AAC(3)IV is shown above ( $n = 3$  independent biological replicates, adapted and modified from Kever et al. (2022)). b) Alderaan infection assays of the apramycin-resistant strain *S. venezuelae* NRRL B-65442 producing the 16S rRNA methyltransferase KamB as resistance mechanism. Infection was performed in presence and absence of 10  $\mu\text{g}/\text{ml}$  apramycin ( $n = 3$  independent biological replicates) (cf. chapter 4.2, Part B). A schematic illustration of the methylation position A1408 in the A-site of the 16S rRNA was adapted and modified from Wachino and Arakawa (2012).

### Spent medium from natural apramycin producer showed antiphage activity

Since aminoglycosides are naturally secreted small molecules, their antiphage activity could potentially be relevant in natural settings as well. To take a first step towards answering this question, culture supernatants (= spent media) of the natural apramycin producer *S. tenebrarius* were collected at two different time points after inoculation and analysed for apramycin production via liquid chromatography-mass spectrometry (LC-MS). When adding these spent media to infection assays, a strong correlation between the antiphage effect and the contained apramycin concentration was detected. This means that spent medium collected from natural producer strains after apramycin production was able to mimic the antiphage effect of the pure compound by completely preventing cell lysis and phage amplification, whereas apramycin-free spent medium showed no impact on phage infection (cf. chapter 3.2, Figure 3). Although the production of further antiphage molecules by *S. tenebrarius* could not be ruled out at this stage, these data already gave a first indication of a possible ecological relevance of chemical defense by aminoglycosides, which will be further addressed in chapter 2.3.4. However, to finally determine

whether the antiphage effect of the tested spent medium is mainly caused by apramycin, ongoing studies are focusing on the antiphage activity of spent medium from *S. tenebrarius* mutants lacking different genes of the biosynthetic pathway for apramycin production. In addition, this could shed light on the biosynthetic step and thus on the chemical groups or structural features leading to an antiphage activity, which is crucial to decipher the structure-function relationship of aminoglycosides.

Moreover, to address the physiological relevance of the antiphage effect of aminoglycosides, it would be of special interest to directly study phage infection in a bacterial host capable of aminoglycoside production. Therefore, current efforts are focusing on the isolation of corresponding phages, which would allow us to examine whether phage infection even triggers the production of these antiphage compounds.

### 2.3.3. Inactivation of infectious phage particles in the extracellular space

#### Dropping phage titer temporally coincides with re-growth of mycelium

The characterization of several novel phage isolates in our group exposed that *Streptomyces* phage infection appears to differ from prototypical infections in terms of phage titer development, which piqued our interest with respect to a potential, further layer of *Streptomyces* phage defense (Hardy et al., 2020). The observation of dropping phage titers during *Streptomyces* phage infection was taken up in our recent study by focusing on the phage Alderaan infecting *S. venezuelae* as a model system (Kever & Frunzke, 2022, to be submitted). To directly compare the development of infectious extracellular phage titers at later stages of *Streptomyces* infection with the one of unicellular-growing bacteria, long-term infection assays were performed for phage Alderaan infecting *S. venezuelae* NRRL B-65442, phage CL31 infecting *C. glutamicum* MB001 and phage  $\lambda$  infecting *E. coli* LE392. For all phage-host pairs, the impact on bacterial growth strongly correlated with the applied initial phage titer, resulting in a significant growth defect at a high phage pressure. Consistent with the previous observations, accompanying quantification of phage titers revealed an initial phage amplification and a subsequent drop in plaque-forming units (PFU) for infection of *S. venezuelae* with phage Alderaan (Hardy et al., 2020). This decline in titer started ~48 h after infection and temporally coincided with the emergence and re-growth of mycelium (Figure 11a-b), which appeared to be resistant towards re-infection with the same phage (cf. chapter 4.3, Figure S1a). Contrary to this, infection of *C. glutamicum* MB001 with CL31 and *E. coli* with phage  $\lambda$  resulted in progressive phage amplification and a subsequent plateau in titer despite renewed bacterial growth for an intermediate phage pressure (Figure 11a-b).

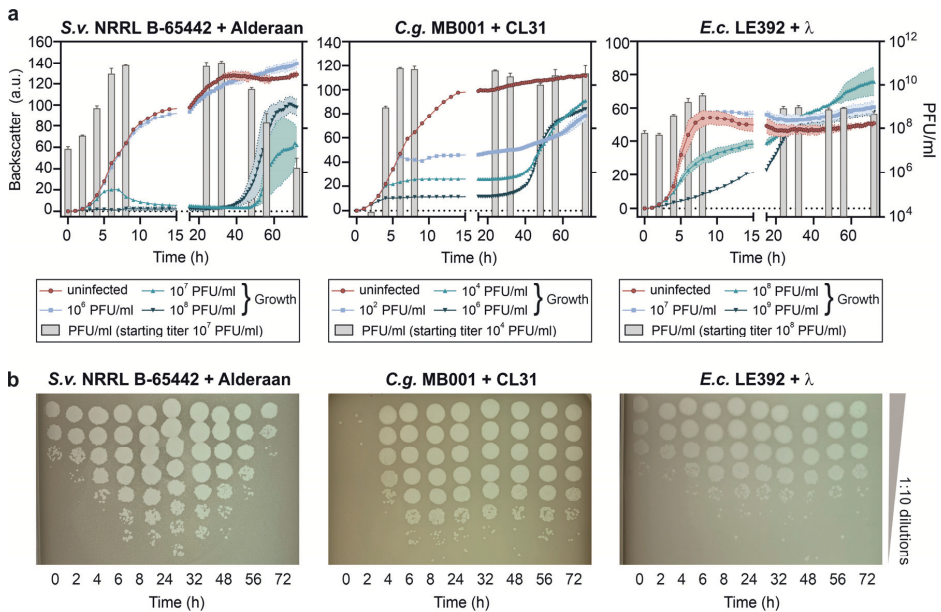


**Figure 11: Emergence of phage-resistant *Streptomyces* mycelium results in a decrease in extracellular infectious phage particles.** a) Growth curves of *S. venezuelae* NRRL B-65442 infected by Alderaan, *C. glutamicum* MB001 infected by CL31 and *E. coli* LE392 infected by  $\lambda$ . Phage titers were calculated over time via double-agar overlays for infection with an intermediate phage pressure (see PFU/ml values in brackets; grey bars) ( $n = 3$  independent biological replicates). b) Representative double-agar overlay assays of three independent biological replicates (adapted from Kever and Frunzke (2022, to be submitted)).

To study this dropping titer during *Streptomyces* phage infection in more detail, we compared the amount of plaque-forming units counted on double-agar overlay assays with total extracellular phage DNA levels quantified via qPCR (Figure 12a). Calculating the percent decrease of remaining phages ( $t = 72$  h post infection) to the maximum titer reached ( $t = 8$  h post infection) exposed a stronger reduction in infectious phage particles than in phage DNA levels. This suggested that dropping phage titers at later stages of infection were synergistically caused by a high proportion of completely removed/degraded phages ( $\sim 92\text{--}96\%$  decrease in DNA levels) and an additional proportion of inactivated/partially destroyed phages ( $>99.9\%$  overall decrease in PFU/ml) (Figure 12b). However, it should be noted that this ratio might be biased by an unknown amount of non-encapsulated phage DNA deriving from lysed cells. In the following, the term ‘phage inactivation’ refers to the overall decrease of infectious phage particles in the extracellular space.

To approach the molecular basis of this phage inactivation, several factors were considered that might contribute to the decline in infectious phage particles: i) instability of phage particles due to acidification of the culture supernatant, ii) production and secretion of antiphage metabolites or proteins as well as iii) adsorption of phages to mycelial structures (Figure 12b).

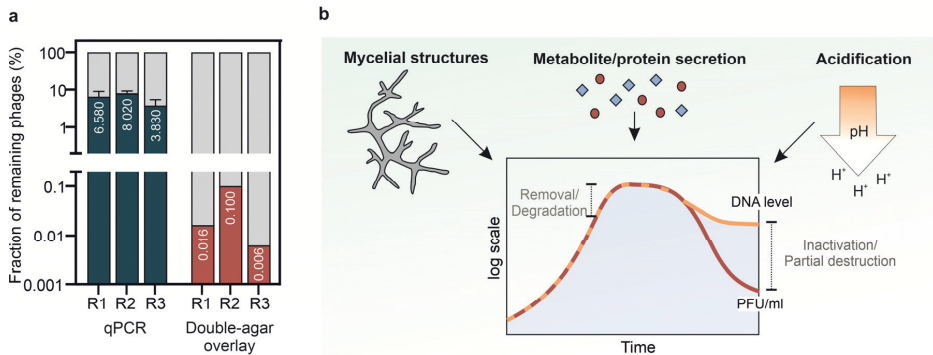


**Figure 12: Synergistic effects on phage titer decline.** a) Comparison of remaining Alderaan phages ( $t_{72}/t_8$ ) based on quantification of Alderaan genome equivalents via qPCR (biological replicates R1-R3 measured as technical triplicates) and quantification of plaque-forming units via double-agar overlay assays. b) Schematic illustration of different influencing factors possibly contributing to the observed decrease in extracellular phage titers (adapted and modified from Kever and Frunzke (2022, to be submitted)).

Growth of *S. venezuelae* in complex medium can be accompanied by acidification of the medium, reaching pH values of  $\sim 4.5$ -5.0. This is presumably due to secretion of organic acids, as it has been described previously for *S. venezuelae* and other *Streptomyces* strains (Ahmed et al., 1984; Hobbs et al., 1992; Madden & Ison, 1996). Accordingly, infectious extracellular phage titers were tracked during incubation of phage Alderaan in medium adjusted to different pH values for 24 h. While a high pH stability was observed for pH 5.0-9.0, incubation of phages at pH 4.0 led to a  $\sim 100$ -fold reduction in infectious phage particles (cf. chapter 4.3, Figure S1e). Interestingly, during further long-term infection studies under buffered conditions, an earlier re-growth of mycelium and a less pronounced, but still distinct drop in infectious phage particles ( $\sim 92\%$ ) could be detected (cf. chapter 3.3, Figure 2c). However, whether this reduced drop is due to the eliminated influence of medium acidification or rather due to downstream effects of buffered cultivation conditions, e.g. an altered morphology or exo-metabolome, needs to be addressed by future experiments.

Moreover, a possible effect of secreted metabolites and proteins on infectious phage particles was investigated, even though *S. venezuelae* is, for instance, unable to produce aminoglycosides and anthracyclines as the two main classes of antiphage metabolites currently known (Kever et al., 2022; Kronheim et al., 2018). For that purpose, supernatants (= spent media) of uninfected *S. venezuelae* cultures were harvested and filtrated at different time points after inoculation (8, 24 and 48 h). After subsequent incubation of phage Alderaan in these cell-free spent media for 48 h, infectious phage particles were quantified via double-agar overlay assays. The highest impact on the number of infectious phage particles was observed upon incubation in spent medium, which was harvested after 24 h of *Streptomyces* cultivation in unbuffered conditions (pH 6.9), showing a  $\sim 60$ -73% reduction in infectious phage titers (cf. chapter 3.3, Figure 2d). In contrast, the number

of infectious Alderaan particles stayed almost constant upon incubation with all other tested spent media, overall hinting on the transient production of phage-inactivating metabolites or proteins. Moreover, examining plaque formation on double-agar overlay assays containing increasing chloramphenicol concentrations as a well-known antibiotic produced by *S. venezuelae* (Vining & Stuttard, 1995) revealed no impact on phage infectivity as well. However, it is important to emphasize that this experimental setup used for studying the effect of spent medium did not consider potential intracellular effects of small molecule production on phage amplification as well as a phage-triggered production of some antiphage metabolites or enzymes, which highlights the need to include spent medium of infected cultures in follow-up studies.

### **Mature mycelium showed enhanced phage tolerance**

In addition to medium acidification and secretion of antiphage molecules, further efforts focused on the impact of mycelial structures on the phage titer decline. Therefore, pre-cultures of different developmental stages of *S. venezuelae* mycelium were used for inoculation of infection assays. The highest susceptibility towards Alderaan infection was observed for stationary pre-cultures comprising already a high amount of spore chains. Upon inoculation of a fresh culture, infection of germinating spores led to a substantial growth defect and a significant increase in extracellular phage titers already at an intermediate initial phage pressure of  $10^7$  PFU/ml. A comparable outcome of phage infection was gained for young, vegetative mycelium deriving from pre-cultures in the early exponential growth phase. Contrary to this, infection of dense mycelium from mid exponential pre-cultures with  $10^7$  PFU/ml of Alderaan exposed no impact on bacterial growth and even a decrease in extracellular phage titers over time (Figure 13a-c). These data revealed that mature and densely branched *Streptomyces* mycelium features a significantly reduced susceptibility to phage infection. This could be due to several reasons. On the one hand, the phages could adsorb directly to the mycelium, but productive infection is prevented. On the other hand, shielding of phage receptors and thereby prevention of phage adsorption could lead to prolonged retention of phages in the extracellular space, where phages are inactivated over time by secretion of antiphage molecules or lowering of pH.

In the case of *Streptomyces albus*, a study of the 1980's described the enhanced adsorption capacity of actinophage Pal6 to mature mycelium compared to germinated spores. This effect also led to a decline in extracellular phage titers over time (Rosner & Gutstein, 1981). Conversely, adsorption studies with phage  $\Phi$ A7 infecting *Streptomyces antibioticus* revealed that phage adsorption was restricted to germ tubes and not observed during incubation of phages with spores or mycelium (Diaz et al., 1991). Further evidence for an influence of the developmental stage on



phage susceptibility was recently described by Luthe et al. (2023a), who demonstrated a decrease in plaque diameter up to a complete prevention of plaque formation by phage Alderaan with increasing age of the surface-grown mycelium used as bacterial lawn. Interestingly, a decrease in extracellular phage density after initial amplification was also observed at later stages of *Streptomyces lividans* infection with phage KC301 in soil microcosms, which was presumed to be caused by a high adsorption rate of phages to vegetative mycelium of mature colonies (Burroughs et al., 2000; Marsh & Wellington, 1992).

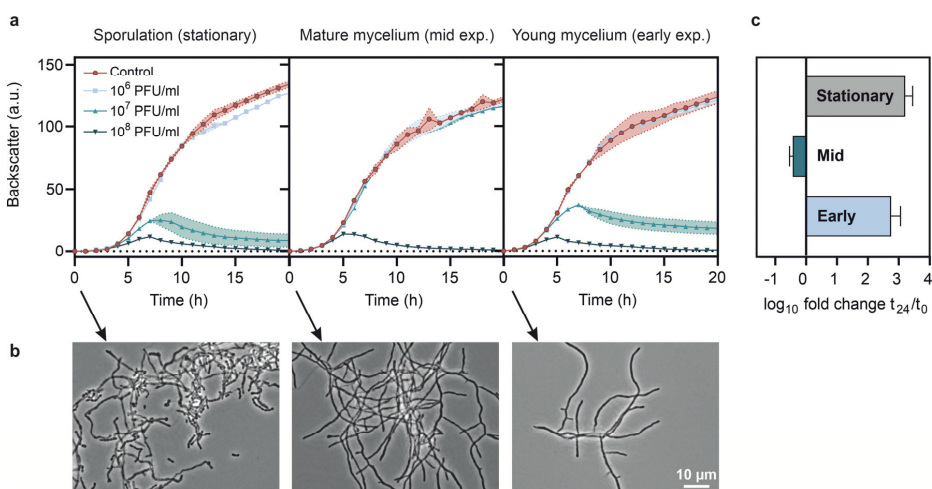


**Figure 13: Influence of *S. venezuelae* developmental stage on phage susceptibility** a) Infection curves of *S. venezuelae* NRRL B-65442 infected by phage Alderaan ( $n = 3$  independent biological replicates). Pre-cultures of different developmental stages were used to inoculate main cultures for conducting infection assays (early exp.: 16 h pre-cultivation, mid exp.: 20 h pre-cultivation, stationary: 30 h pre-cultivation). (b) Microscopic analysis of *S. venezuelae* pre-cultures (scale bar = 10  $\mu$ m, exposure time = 120 ms). (c)  $\log_{10}$  fold change of extracellular infectious phage particles based on plaque-forming units quantified via double-agar overlay assays, which indicates the level of phage amplification for an initial phage pressure of  $10^7$  PFU/ml over 24 h of infection ( $n = 3$  independent biological replicates) (adapted from Kever and Frunzke (2022, to be submitted)).

### Inactivation of a non-host phage coincides with the hyphae-spore transition phase

To further analyse general abilities of mature mycelium to inactivate phages non-specifically in the extracellular space, titers of diverse non-host phages (referring to phages unable to infect *S. venezuelae*) with different morphotypes and host specificities were tracked during incubation with *S. venezuelae* mycelium under buffered conditions in submerged cultures. Among overall twelve tested phages, the *C. glutamicum* phage CL31 and the two *E. coli* phages T4 and MS2 exhibited a decrease in extracellular phage titers upon incubation with mycelium - listed in descending order. Using CL31 as a model phage for a time-resolved quantification revealed a simultaneous decline in infectious phage particles and extracellular phage DNA levels suggesting a

complete removal of the phages from the extracellular space (Figure 14a). Interestingly, this decline in phage titer coincided with the phase of hyphae-spore transition, as indicated by the concomitant microscopic analysis of mycelium (Figure 14b). Moreover, incubation of new CL31 particles in *S. venezuelae* spent medium harvested during the drop in CL31 titers had no effect on phage infectivity giving a first indication that this decline was probably not caused by a CL31-triggered production of previously unknown antiphage metabolites or proteins in *S. venezuelae*.

As already explained in chapter 2.2.1, the developmental transition to spores is regulated by a complex hierarchical network. The master regulator BldD represses key developmental genes, amongst them *bldN*. Unfavorable conditions like nutrient starvation relieve repression by BldD and initiate the morphological differentiation to spores (M. J. Bush et al., 2015). In surface grown cultures, this transition includes the formation of aerial hyphae, which are coated by a hydrophobic surface layer based on the  $\sigma^{\text{BldN}}$ -dependent transcription of rodlin and chaplin genes. Although the growth of aerial mycelium is not relevant in submerged cultures, hyphae-spore transition was proven to be still accompanied by expression of rodlin and chaplin genes (Bibb et al., 2012). To analyse the importance of this morphological differentiation for the phage titer decline, the incubation assay was repeated with two developmental mutant strains: i) *S. venezuelae*  $\Delta\text{bldD}::\text{apr}$ , which is characterized by a hypersporulation phenotype forming premature spores from vegetative mycelium (Tschowri et al., 2014) and ii) *S. venezuelae*  $\Delta\text{bldN}::\text{apr}$ , which can only grow vegetatively and is lacking hydrophobic rodlin and chaplin proteins (Bibb et al., 2012). For both mutant strains, incubation with CL31 led to a lower decline in phage titer in comparison to the wild type strain (Figure 14c). Consistent with this, overexpression of *bldN* markedly accelerated the reduction in CL31 particles, possibly due to higher expression levels of rodlin and chaplin genes (cf. chapter 3.3, Figure 4e). Moreover, a substantially less pronounced reduction in CL31 titers was observed for incubation with *S. coelicolor* and *S. olivaceus* (Figure 14c). In contrast to *S. venezuelae*, both strains were unable to form spores during the entire cultivation under the applied conditions, which – at least for *S. coelicolor* – is already sufficiently described in literature (Glazebrook et al., 1990; Manteca et al., 2008). In addition, incubation of CL31 with other bacteria dividing by binary fission, namely *E. coli*, *B. subtilis* and *P. putida*, exhibited no decline in extracellular CL31 titers as well (Figure 14c). Overall, this led to the assumption that hyphae-spore transformation with a switch from hydrophilic to hydrophobic surface properties may substantially contribute to declining extracellular titers of the non-host phage CL31, possibly by allowing adsorption of phage particles to the mycelial surface via hydrophobic interactions. However, the levels of hydrophobic sheath proteins actually produced under the applied conditions still needs to be determined. Apart from that, a transient production of antiphage metabolites or proteases leading to phage

inactivation cannot be definitively excluded by the single time point measurements conducted in our studies.

The hydrophobic surface proteins of *Streptomyces* are functionally related to the hydrophobins of filamentous-growing fungi. These fungal hydrophobins have several functions like for instance conferring hydrophobicity to aerial hyphae and allowing their attachment to hydrophobic surfaces (Elliot & Talbot, 2004; Wösten, 2001). Assumed, that the decrease in CL31 titers upon incubation with *S. venezuelae* mycelium could be attributed to hydrophobic interactions, incubation with fungal mycelium might lead to a comparable phenotype. Just recently, Ghanem and colleagues described such a hydrophobicity-dependent phage retention by fungal mycelium in a microfluidic chip platform (Ghanem et al., 2019). Unfortunately, our access to appropriate fungal strains was limited to haploid, yeast-like cells of *Ustilago cynodontis*, which revealed no effect on CL31 titers (Figure 14c). It should be noted, that this basidiomycete is a dimorphic fungi, which just exhibit filamentous, pathogenic growth upon fusion of two haploid cells with different mating types (Bölker, 2001). As shown for *Ustilago maydis*, in these fungal strains hydrophobins appear to be functionally substituted by small amphipathic peptides called repellents. Their production is associated with filamentous growth and required for aerial hyphae formation (Teertstra et al., 2006; Teertstra et al., 2009; Wösten et al., 1996). Accordingly, it is reasonable to assume that a reduced or even lacking production of hydrophobicity-mediating proteins during yeast-like growth of *U. cynodontis* could be an explanation for the lack of decline in CL31 titers. Apart from that, several studies already described a certain influence of surface hydrophobicity on phage adhesion to various solid materials like aluminum oxide-coated sand or polypropylene (Attinti et al., 2010; Dika et al., 2013; Farkas et al., 2015; Richter et al., 2021). Finally yet importantly, the phage T4, which showed a strong reduction upon incubation with *S. venezuelae* mycelium as well, is referred to as hydrophobic phage (Ghanem et al., 2019), whereas the degree of surface hydrophobicity of the less affected phage MS2 is controversially described in the literature (Farkas et al., 2015; Sautrey et al., 2018; Vodolazkaya et al., 2022). Altogether, this supported the hypothesis of a potential influence of hydrophobic interactions on the phage titer decline.

However, attempts to visualize CL31 phages on the mycelial surface via scanning electron microscopy (SEM) failed by now. Additionally, repeated efforts to detach phages from the mycelial fraction were not yet successful as well, which may account for a high affinity, irreversible binding of phages to hyphae or degradation of the phage particles by alternative mechanisms.

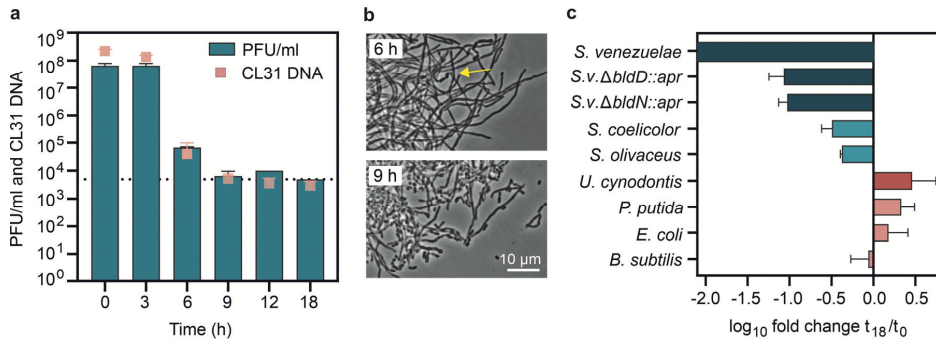


**Figure 14: Influence of *Streptomyces* mycelium on extracellular phage titers of the non-host phage CL31.** a) Time-resolved quantification of extracellular CL31 phage particles during incubation with *S. venezuelae* NRRL B-65442 mycelium via double-agar overlay assays (PFU/ml, cyan bars, three biological replicates) and via qPCR (CL31 genome equivalents, reddish dots, means of three biological replicates measured as technical duplicates). The detection limit for double-agar overlay assays is indicated by the dotted line; for qPCR, measurement points minimally outside of the standards are marked by increased transparency ( $t_9, t_{12}, t_{18}$ ). b) Microscopic images of *S. venezuelae* mycelium during declining CL31 titers at 6 h and 9 h post inoculation (scale bar: 10  $\mu$ m, exposure time = 200 ms). The yellow arrow points to the first spore chains detected after 6 h of incubation. c) Reduction in extracellular infectious CL31 particles during cultivation with different microorganism calculated via double-agar overlay assays, shown as  $\log_{10}$  fold change  $t_{18}/t_0$ . In case of incubation with *S. venezuelae* wild type, one replicate showed a  $\log_{10}$  fold change of  $\sim -4$ , while two out of three replicates showed no more plaque formation after 18 h of incubation ( $\log_{10}$  fold change not determinable) (adapted and modified from Kever and Frunzke (2022, to be submitted)).

### The interplay of many factors shapes *Streptomyces* multicellular defense

Based on our current results, development of phage titers during infection of *S. venezuelae* with phage Alderaan cannot be attributed to a single parameter, but may instead be conditioned by an interplay of several factors likely influencing each other. So far, only a vague guess can be made on how the different dissected parameters could contribute to the phage titer decline: The reduction in extracellular infectious phage titers temporally correlates with the re-growth of phage-resistant mycelium. One could envision, that phages are removed from the extracellular space via direct **adsorption to mycelium**. Here, one could further discriminate between i) receptor-specific attachment without following phage amplification and ii) a rather unspecific entrapment in the mycelial network, e.g. via interaction with the hydrophobic sheath proteins as suggested for the non-host phages (CL31, MS2, T4). However, the fact that a drop in phage titer after a successful initial phage amplification was previously also observed during infection of *S. coelicolor* with its host phages Dagobah, Endor1 and Endor2 (Hardy et al., 2020), but incubation of the non-host phage CL31 with *S. coelicolor* mycelium caused a comparatively low reduction in extracellular phage titers might rather hint at two different mechanisms of phage inactivation for host- and non-host phages in presence of *Streptomyces* mycelium. Moreover, incubation of Alderaan particles with *S. venezuelae* spent medium of uninfected cultures harvested after 24 h of cultivation resulted

in a reduction in infectious phage particles. This refers to a transient production and secretion of **phage-inactivating metabolites or proteases**, which might be even enhanced under infection conditions. These antiphage molecules or proteins could either directly target phages in the extracellular space or interfere with phage amplification on an intracellular level after successful phage adsorption. Apart from that, Alderaan particles showed a high **pH instability** in acidic conditions at  $\text{pH} < 5.0$ , which can be reached during *Streptomyces* growth. However, since a substantial, but less pronounced reduction in infectious particles was observed even under buffered conditions, an influence of medium acidification on declining phage titers cannot be excluded, but might be rather minor. Another factor, which was not considered yet, is a potential phage neutralization through binding to **extracellular vesicles**. These vesicles are released from hyphal tips of *S. venezuelae* upon cell-wall stress, but their extrusion in response to phage infection was not investigated so far (Fröjd & Flärdh, 2019).

To further shed light on the molecular mechanism of dropping phage titers, a variety of different experiments could be performed, some of which are listed below. First, **visualization of a potential phage attachment** to mycelial structures could be re-attempted by using fluorescently labeled phages. Moreover, performing **phage adsorptions assays** with mycelium of the wild type and respective developmental mutant strains in buffer would allow to analyse the impact of the current developmental stage on phage adsorption. To further examine the involvement of hydrophobic interactions, in vitro analysis of **phage adhesion to purified rodlin and chaplin filaments** might be a useful experimental addition as well. Moreover, **omics-analysis of re-grown mycelium** might provide further insights into the molecular basis of phage resistance, which could emerge through cell surface alterations, e.g. shielding of phage receptors, or activation of further antiphage defense systems. In this context, determining the composition of spent medium under infection conditions and testing its effects on infection dynamics is crucial to elaborate on a potential **release of antiphage molecules**.

Altogether, the current results emphasize an important impact of *Streptomyces* development on phage susceptibility. Furthermore, we can deduce that *Streptomyces* has evolved a complex antiphage defense with several components acting at the multicellular level that may provide a community-wide protection against phage predation – as further discussed in chapter 2.3.4.

#### 2.3.4. Community-wide protection against phage infection

Our current knowledge of antiphage defense is very much dominated by systems that act at the cellular level. Such mechanisms protect an individual bacterium from phage infection and hence the surrounding community by preventing phage spread (cf. chapter 2.1.3).

However, in their natural environment, bacteria preferentially reside in complex, multispecies microbial communities (Stubbendieck et al., 2016). Numerous studies already indicated that these communities have also evolved various antiphage strategies, which are extracellularly available to allow protection of multiple cells at the same time (Figure 15). For instance, bacterial **biofilm formation** serves as an efficient protection against various abiotic and biotic environmental insults, among them also bacteriophages. The antiphage defense mechanisms of biofilms are multifaceted including shielding of susceptible bacteria by resistant cells, reducing phage amplification through metabolically inactive cells, limiting phage diffusion and trapping phages in the self-produced polymer matrix as recently reviewed by Visnapuu et al. (2022). A matrix-mediated protection against T5 and T7 phage predation was exemplarily described for curli amyloid fibers as a proteinaceous component of the *E. coli* biofilm matrix. These amyloid fibers allow a collective antiphage defense by preventing phage diffusion as well as an individual cell protection by entrapping phages in the cell surface-covering fibers, hence inhibiting cell-phage attachment (Vidakovic et al., 2018). Though, curli-trapped phages can remain infectious and kill biofilm-invading cells (Bond et al., 2021). Moreover, the release of **outer membrane vesicles** provides another adsorption trap. Due to comparable surface structures as the bacterial cell, these vesicles serve as cellular decoys and enable irreversible phage neutralization (Manning & Kuehn, 2011; Reyes-Robles et al., 2018). In addition, **quorum sensing-regulated activation of antiphage defense systems** via release of extracellular signaling molecules represents another mechanism of multicellular protection against phage predation. Accumulation of these signaling molecules at high cell densities can alter the gene expression profile on a population scale leading e.g. to the downregulation of phage receptors (Høyland-Kroghsbo et al., 2013; Tan et al., 2015), activation of CRISPR-Cas immunity (Høyland-Kroghsbo et al., 2017; Patterson et al., 2016) or production of phage-inactivating proteases as it was shown for the haemagglutinin protease in *Vibrio cholera* (Hoque et al., 2016). Besides extracellular signaling molecules, especially actinobacterial strains like *Streptomyces* produce and secrete an impressive diversity of bioactive molecules, which can be harnessed as chemical weapons in competitive or predatory microbial interactions (Donald et al., 2022; Tyc et al., 2017). Their potential contribution to prokaryotic antiphage defense was just recognized recently. Kronheim and colleagues discovered that *Streptomyces*-derived **anthracyclines**, namely doxorubicin and daunorubicin, exhibit a broad antiphage activity. These

DNA-intercalating agents were shown to block replication of various dsDNA phages. Accordingly, their secretion could provide a chemical shield allowing protection against phage predation at the community level (Kronheim et al., 2018).

With the description of the antiviral properties of **aminoglycosides**, this doctoral thesis provides a further example for a chemical antiphage defense mechanism. Aminoglycoside antibiotics were shown to inhibit phage infection in widely divergent bacterial hosts by blocking an early step of phage life cycle. The fact, that aminoglycoside, but also anthracycline secretion by a natural producer was sufficient to inhibit phage infection opens the door for discussing the ecological significance of such chemical antiphage defense mechanisms, which was also outlined in our recent review about phage inhibition via bacterial small molecules (Hardy et al., 2023). *Streptomyces* as main producer of aminoglycosides predominantly lives in the soil, which is a highly challenging environment in terms of microbial density and diversity (Fierer, 2017). In this context, the dual functionality of aminoglycosides might provide an outstanding benefit. Their secretion could create an antibacterial and antiviral microenvironment, which would allow producers as well as resistant strains in the surrounding community to be chemically protected against various phages and competing bacteria at the same time. However, most bacteria are naturally sensitive to aminoglycosides. Here, the high mobility of genes coding for aminoglycoside-modifying enzymes (AME) might come into play, which increases the probability of acquiring resistance through horizontal gene transfer from producer strains (Ramirez & Tolmasky, 2010). Assuming that a decoupling of antibacterial and antiphage properties by aminoglycoside modification can be generalized, acquisition of AMEs might allow neighboring cells to benefit from the antiphage properties upon aminoglycoside uptake, without suffering from the antibacterial effect. Overall, one could imagine a division of labor, where secretion of aminoglycosides as ‘public goods’ provide protection from phages on a community level, while the producers themselves could in turn profit from complementary tasks carried out by other members of the cooperating community (Smith & Schuster, 2019; Zhang et al., 2016). Interestingly, sublethal aminoglycoside concentration were just recently shown to be still sufficient to impair phage infection (Zuo et al., 2021), which – dependent on the locally achieved concentration – potentially opens up the protective effect against phages to aminoglycoside-sensitive bacteria in the cooperating community as well. It could be argued that the broad antiphage activity may also favor the growth of non-cooperating bacteria, which would be controversial from a sociomicrobiological perspective. However, one could envision that such social cheating could be limited by spatial structuring, e.g. biofilm formation, that enables to set up a local pool of public goods (Hardy et al., 2023; Smith & Schuster, 2019).

In addition to the antiviral properties of aminoglycosides, this doctoral thesis further examined the **phage inactivation in the extracellular space** of *Streptomyces* populations, which was specifically observed at later stages of infections. Such inactivation could especially be relevant on a community level, where resistant or tolerant fractions might inactivate phages in the surroundings to protect susceptible cells from viral predation. Related to that, we observed that mature mycelium exhibits a transient tolerance towards phage infection, which was consistent with other studies (Diaz et al., 1991; Rosner & Gutstein, 1981). Based on the present data, we hypothesize that mycelial growth contributes to the observed decline in extracellular phage titers and thereby to antiphage defense, possibly by allowing an efficient adsorption of phages from the environment without producing phage progenies. A comparable scenario was proposed when studying phage-host interactions in *Streptomyces* using soil microcosms, which imitate natural conditions with the physical separation of vegetative and aerial mycelium more properly than submerged cultures. By showing a reduction of free phages in the soil with raising mycelial density, the authors suggested that vegetative mycelium adsorbs the majority of phages, thereby protecting young, susceptible hyphae from phage predation (Burroughs et al., 2000; Marsh & Wellington, 1992). Apart from that, another study from our group recently pointed out that sensing of phage infection seems to trigger the formation of aerial hyphae and spores in surface-grown cultures leading to a transient phage resistance. In this context, *Streptomyces* development was shown to be crucial for limiting phage spread (Luthe et al., 2023a). Overall, it can be inferred that a cooperative behavior of mycelial structures of different ages could contribute essentially to antiphage defense at the community level, although the molecular basis of the increased phage tolerance of mature mycelium requires further investigations.

Interestingly, phage inactivation in presence of *Streptomyces* mycelium was also detected for specific non-host phages, which could possibly open up this antiphage defense to some interspecies communities as well. Under the assumption, that a reduced extracellular phage density could, at least for non-host phages, be attributed to interaction with the hydrophobic sheath during hyphae-spore transition (cf. chapter 2.3.3), it appears to be debatable to what extent this could contribute to community-wide antiphage defense in the natural soil habitat. Susceptible members of the community are likely located in the moist soil and hence spatially separated from the hydrophobic aerial mycelium in surface-grown cultures. This suggests that hydrophobic mycelial surface structures have a limited ability to protect the surrounding community from infection by adsorbing phages from the subsurface. A similar assumption was also made in a previous study by Burroughs et al. (2000). Nonetheless, it can be hypothesized that aerial mycelium could interfere with the water-based phage transport at the water-air interface by retaining phages



via hydrophobic interactions and impacting the infiltration properties of the soil, which was already discussed in a comparable manner for fungal mycelium (Ghanem et al., 2019; Ritz & Young, 2004).

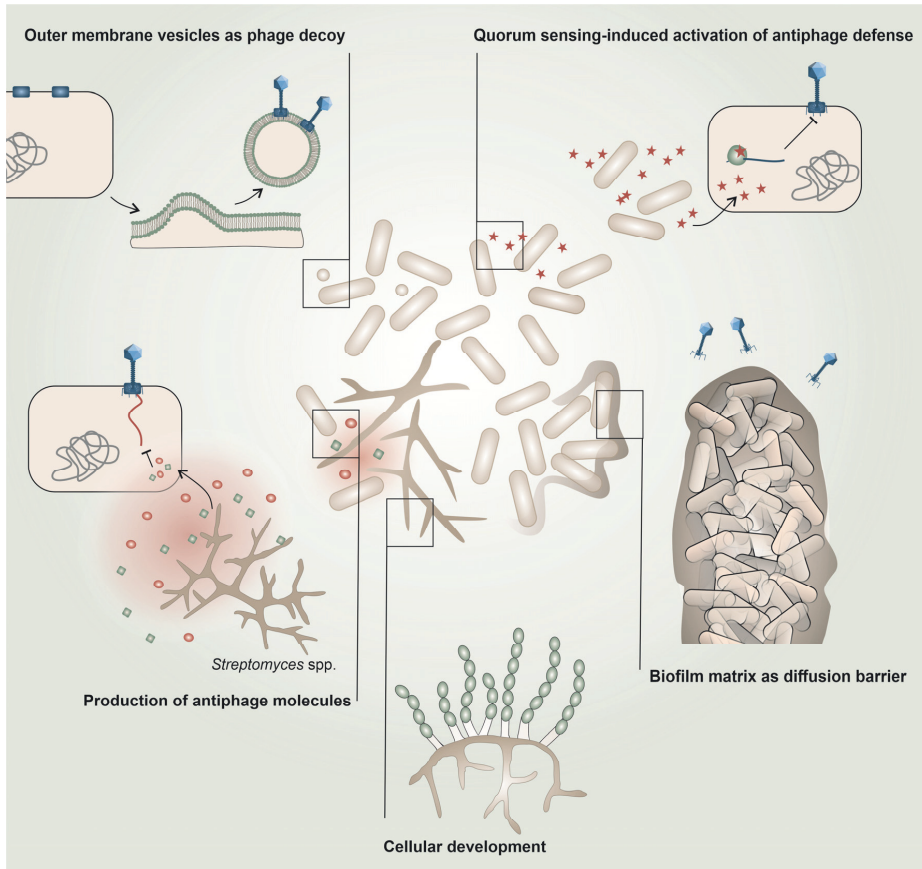


**Figure 15: Overview of multicellular antiphage defense strategies.** Protection against phages on a multicellular level can be mediated by i) extrusion of outer membrane vesicles sequestering phages, which prevents attachment to susceptible cells, ii) quorum sensing-mediated activation of antiphage defense systems, iii) biofilm formation and trapping of phages via interaction with components of the extracellular matrix, iv) production of antiphage molecules as chemical defense and v) cellular development allowing emergence of transient phage tolerance. A modified version of this figure was after submission of this thesis published in Luthe et al. (2023b).

## 2.4. Conclusion and perspectives

The abundance of phages in almost all ecosystems leads to an ongoing arms race between bacteria and phages (Hampton et al., 2020). Phages encode unique proteins that interfere with key cellular processes to create favorable reproduction conditions (De Smet et al., 2017). With the description of the gyrase-inhibiting protein Gip encoded by the CGP3 prophage of *C. glutamicum*, this doctoral thesis represents a further example of a host-affecting protein, whose mechanistic elucidation might open up new directions for antimicrobial drug design (Kever et al., 2021).

To counteract viral attacks, bacteria have evolved numerous antiphage defense mechanisms, which collectively build up the bacterial immune system (Tal & Sorek, 2022). This doctoral thesis provides novel insights into the contribution of bacterial secondary metabolite production and multicellular development to the antiphage arsenal of *Streptomyces*, both having the potential for a community-wide antiphage defense. To provide the basis for studying phage host interactions, we started with the characterization of five newly isolated *Streptomyces* phages preying on the model species *S. coelicolor* and *S. venezuelae* (Hardy et al., 2020). Inspired by the striking observation of enhanced secondary metabolite production at the infection interface and the description of the antiviral properties of anthracyclines (Kronheim et al., 2018), we studied the antiphage properties of another class of small molecules produced by *Streptomyces*, namely aminoglycoside antibiotics (Kever et al., 2022). The interference of aminoglycosides with phage infection could be narrowed down to an early step of phage life cycle between injection and replication. Moreover, aminoglycoside-mediated inhibition of phage infection could be reproduced with culture supernatant of the natural producer, hinting on an ecological relevance of the antiphage activity of aminoglycoside antibiotics, which was discussed in further detail in our recent review article (Hardy et al., 2023). Although the underlying mechanism of action for the two main classes of currently known antiphage molecules – aminoglycoside and anthracyclines – remains to be elucidated, these studies represent a cornerstone for further establishing chemical defense as part of the bacterial immune system. The identification of further antiphage molecules and their mechanism of action will expand our knowledge about this previously unappreciated facet of bacterial immunity and may also fuel the discovery line for novel antiviral drugs with important medical and biotechnological applications.

In addition to the role of aminoglycosides in antiphage defense, we examined the observation of dropping infectious phage titers in the extracellular space of *Streptomyces* populations upon re-growing of mycelium with an emphasis on cellular development as a potential further layer of antiphage defense. By showing the potential contribution of secreted antiphage molecules and

proteins, medium acidification and mycelial growth to phage inactivation, we point to the complexity of the multicellular antiphage defense employed by *Streptomyces* (Kever & Frunzke, 2022, to be submitted). Such phage inactivation could have its significance on a community-level, where phage-tolerant mycelial structures could protect susceptible cells from viral predation. This could be further analysed in future studies by deciphering the underlying mechanism of inactivation and performing co-cultivation experiments with tolerant and susceptible cells.

Currently, defense strategies against phages are primarily examined as isolated systems, but the efficiency of antiphage defense depends rather on the interaction and complementation of different systems acting at a cellular and multicellular level. The integration of these different lines of defense into the bacterial immune system and their temporal coordination is an exciting aspect for future studies, which could be addressed by spatiotemporal visualization of defense system activity via reporter assays or transcriptomic profiling. Since it is already known that antibiotic production is frequently linked to morphological differentiation (Bibb, 2005), it might be of particular interest to investigate a possible connection between production of antiphage metabolites and cellular development of phage-tolerant phenotypes. One could imagine that released antiphage compounds are not just used as chemical weapon against viral predation, but may serve as a warning molecule for adjacent cells, which might trigger the emergence of phage tolerance in the surrounding community.

## 2.5. References

- Ackermann, H.-W. (2009). Phage Classification and Characterization. In M. R. J. Clokie & A. M. Kropinski (Eds.), *Bacteriophages: Methods and Protocols, Volume 1: Isolation, Characterization, and Interactions* (pp. 127-140). Humana Press. [https://doi.org/10.1007/978-1-60327-164-6\\_13](https://doi.org/10.1007/978-1-60327-164-6_13)
- Ahmed, Z. U., Shapiro, S., & Vining, L. C. (1984). Excretion of  $\alpha$ -keto acids by strains of *Streptomyces venezuelae*. *Can. J. Microbiol.*, 30(8), 1014-1021. <https://doi.org/10.1139/m84-158>
- Aigle, B., Lautru, S., Spitteller, D., Dickschat, J. S., Challis, G. L., Leblond, P., & Pernodet, J. L. (2014). Genome mining of *Streptomyces ambofaciens*. *J. Ind. Microbiol. Biotechnol.*, 41(2), 251-263. <https://doi.org/10.1007/s10295-013-1379-y>
- Al-Bassam, M. M., Bibb, M. J., Bush, M. J., Chandra, G., & Buttner, M. J. (2014). Response regulator heterodimer formation controls a key stage in *Streptomyces* development. *PLoS Genet.*, 10(8), e1004554. <https://doi.org/10.1371/journal.pgen.1004554>
- Anderson, A. S., & Wellington, E. M. (2001). The taxonomy of *Streptomyces* and related genera. *Int. J. Syst. Evol. Microbiol.*, 51(Pt 3), 797-814. <https://doi.org/10.1099/00207713-51-3-797>
- Attinti, R., Wei, J., Kniel, K., Sims, J. T., & Jin, Y. (2010). Virus' (MS2, phiX174, and Aichi) Attachment on Sand Measured by Atomic Force Microscopy and Their Transport through Sand Columns. *Environ. Sci. Technol.*, 44(7), 2426-2432. <https://doi.org/10.1021/es903221p>
- Ayinde, D., Casartelli, N., & Schwartz, O. (2012). Restricting HIV the SAMHD1 way: through nucleotide starvation. *Nat Rev Microbiol*, 10(10), 675-680. <https://doi.org/10.1038/nrmicro2862>
- Baltz, R. H. (2012). *Streptomyces* temperate bacteriophage integration systems for stable genetic engineering of actinomycetes (and other organisms). *J. Ind. Microbiol. Biotechnol.*, 39(5), 661-672. <https://doi.org/10.1007/s10295-011-1069-6>
- Barka, E. A., Vatsa, P., Sanchez, L., Gaveau-Vaillant, N., Jacquard, C., Meier-Kolthoff, J. P., Klenk, H. P., Clement, C., Ouhdouch, Y., & van Wezel, G. P. (2016). Taxonomy, Physiology, and Natural Products of Actinobacteria. *Microbiol Mol Biol Rev*, 80(1), 1-43. <https://doi.org/10.1128/MMBR.00019-15>
- Barrangou, R., Fremaux, C., Deveau, H., Richards, M., Boyaval, P., Moineau, S., Romero, D. A., & Horvath, P. (2007). CRISPR Provides Acquired Resistance Against Viruses in Prokaryotes. *Science*, 315(5819), 1709-1712. <https://doi.org/10.1126/science.1138140>
- Bentley, S. D., Chater, K. F., Cerdeño-Tárraga, A. M., Challis, G. L., Thomson, N. R., James, K. D., Harris, D. E., Quail, M. A., Kieser, H., Harper, D., Bateman, A., Brown, S., Chandra, G., Chen, C. W., Collins, M., Cronin, A., Fraser, A., Goble, A., Hidalgo, J., Hornsby, T., Howarth, S., Huang, C. H., Kieser, T., Larke, L., Murphy, L., Oliver, K., O'Neil, S., Rabinowitsch, E., Rajandream, M. A., Rutherford, K., Rutter, S., Seeger, K., Saunders, D., Sharp, S., Squares, R., Squares, S., Taylor, K., Warren, T., Wietzorrek, A., Woodward, J., Barrell, B. G., Parkhill, J., & Hopwood, D. A. (2002). Complete genome sequence of the model actinomycete *Streptomyces coelicolor* A3(2). *Nature*, 417(6885), 141-147. <https://doi.org/10.1038/417141a>
- Bernard, P., Kézdy, K. E., Van Melderden, L., Steyaert, J., Wyns, L., Pato, M. L., Higgins, P. N., & Couturier, M. (1993). The F Plasmid CcdB Protein Induces Efficient ATP-dependent DNA Cleavage by Gyrase. *J. Mol. Biol.*, 234(3), 534-541. <https://doi.org/10.1006/jmbi.1993.1609>

- Bernheim, A., Millman, A., Ofir, G., Meitav, G., Avraham, C., Shomar, H., Rosenberg, M. M., Tal, N., Melamed, S., Amitai, G., & Sorek, R. (2021). Prokaryotic viperins produce diverse antiviral molecules. *Nature*, 589(7840), 120-124. <https://doi.org/10.1038/s41586-020-2762-2>
- Bernheim, A., & Sorek, R. (2020). The pan-immune system of bacteria: antiviral defence as a community resource. *Nat Rev Microbiol*, 18(2), 113-119. <https://doi.org/10.1038/s41579-019-0278-2>
- Bertani, G. (1953). LYSOGENIC VERSUS LYTIC CYCLE OF PHAGE MULTIPLICATION. *Cold Spring Harb. Symp. Quant. Biol.*, 18, 65-70. <https://doi.org/10.1101/sqb.1953.018.01.014>
- Bibb, M. J. (2005). Regulation of secondary metabolism in streptomycetes. *Curr Opin Microbiol*, 8(2), 208-215. <https://doi.org/10.1016/j.mib.2005.02.016>
- Bibb, M. J. (2013). Understanding and manipulating antibiotic production in actinomycetes. *Biochem. Soc. Trans.*, 41(6), 1355-1364. <https://doi.org/10.1042/BST20130214>
- Bibb, M. J., Domonkos, A., Chandra, G., & Buttner, M. J. (2012). Expression of the chaplin and rodlin hydrophobic sheath proteins in *Streptomyces venezuelae* is controlled by  $\sigma^{BldN}$  and a cognate anti-sigma factor, RsbN. *Mol Microbiol*, 84(6), 1033-1049. <https://doi.org/10.1111/j.1365-2958.2012.08070.x>
- Bierman, M., Logan, R., O'Brien, K., Seno, E. T., Nagaraja Rao, R., & Schoner, B. E. (1992). Plasmid cloning vectors for the conjugal transfer of DNA from *Escherichia coli* to *Streptomyces* spp. *Gene*, 116(1), 43-49. [https://doi.org/10.1016/0378-1119\(92\)90627-2](https://doi.org/10.1016/0378-1119(92)90627-2)
- Bobay, L. M., Touchon, M., & Rocha, E. P. (2014). Pervasive domestication of defective prophages by bacteria. *PNAS*, 111(33), 12127-12132. <https://doi.org/10.1073/pnas.1405336111>
- Bobek, J., Smidova, K., & Cihak, M. (2017). A Waking Review: Old and Novel Insights into the Spore Germination in *Streptomyces*. *Front Microbiol*, 8, 2205. <https://doi.org/10.3389/fmicb.2017.02205>
- Bölker, M. (2001). *Ustilago maydis* – a valuable model system for the study of fungal dimorphism and virulence. *Microbiology*, 147(Pt6), 1395-1401. <https://doi.org/10.1099/00221287-147-6-1395>
- Bond, M. C., Vidakovic, L., Singh, P. K., Drescher, K., & Nadell, C. D. (2021). Matrix-trapped viruses can prevent invasion of bacterial biofilms by colonizing cells. *Elife*, 10, e65355. <https://doi.org/10.7554/eLife.65355>
- Bondy-Denomy, J., & Davidson, A. R. (2014). When a virus is not a parasite: the beneficial effects of prophages on bacterial fitness. *J Microbiol.*, 52(3), 235-242. <https://doi.org/10.1007/s12275-014-4083-3>
- Boulanger, P., & Letellier, L. (1992). Ion channels are likely to be involved in the two steps of phage T5 DNA penetration into *Escherichia coli* cells. *J. Biol. Chem.*, 267(5), 3168-3172. [https://doi.org/10.1016/s0021-9258\(19\)50710-4](https://doi.org/10.1016/s0021-9258(19)50710-4)
- Brock, T. D., Mosser, J., & Peacher, B. (1963). The Inhibition by Streptomycin of Certain *Streptococcus* Bacteriophages, using Host Bacteria Resistant to the Antibiotic. *J. Gen. Microbiol.*, 33(1), 9-22. <https://doi.org/10.1099/00221287-33-1-9>
- Brock, T. D., & Wooley, S. O. (1963). Streptomycin as an Antiviral Agent: Mode of Action. *Science*, 141(3585), 1065-1067. <https://doi.org/10.1126/science.141.3585.1065>
- Burroughs, N. J., Marsh, P., & Wellington, E. M. H. (2000). Mathematical Analysis of Growth and Interaction Dynamics of Streptomycetes and a Bacteriophage in Soil. *Appl. Environ. Microbiol.*, 66(9), 3868-3877. <https://doi.org/10.1128/AEM.66.9.3868-3877.2000>

- Bush, M. J., Bibb, M. J., Chandra, G., Findlay, K. C., & Buttner, M. J. (2013). Genes required for aerial growth, cell division, and chromosome segregation are targets of WhiA before sporulation in *Streptomyces venezuelae*. *mBio*, 4(5), e00684-00613. <https://doi.org/10.1128/mBio.00684-13>
- Bush, M. J., Chandra, G., Bibb, M. J., Findlay, K. C., & Buttner, M. J. (2016). Genome-Wide Chromatin Immunoprecipitation Sequencing Analysis Shows that WhiB Is a Transcription Factor That Cocontrols Its Regulon with WhiA To Initiate Developmental Cell Division in *Streptomyces*. *mBio*, 7(2), e00523-00516. <https://doi.org/10.1128/mBio.00523-16>
- Bush, M. J., Tschowri, N., Schlimpert, S., Flärdh, K., & Buttner, M. J. (2015). c-di-GMP signalling and the regulation of developmental transitions in streptomycetes. *Nat Rev Microbiol*, 13(12), 749-760. <https://doi.org/10.1038/nrmicro3546>
- Bush, N. G., Evans-Roberts, K., & Maxwell, A. (2015). DNA Topoisomerases. *EcoSal Plus*, 6(2). <https://doi.org/10.1128/ecosalplus.ESP-0010-2014>
- Casjens, S. R., & Gilcrease, E. B. (2009). Determining DNA packaging strategy by analysis of the termini of the chromosomes in tailed-bacteriophage virions. *Methods Mol Biol*, 502, 91-111. [https://doi.org/10.1007/978-1-60327-565-1\\_7](https://doi.org/10.1007/978-1-60327-565-1_7)
- Challis, G. L., & Hopwood, D. A. (2003). Synergy and contingency as driving forces for the evolution of multiple secondary metabolite production by *Streptomyces* species. *PNAS*, 100(suppl\_2), 14555-14561. <https://doi.org/10.1073/pnas.1934677100>
- Claessen, D., Rink, R., de Jong, W., Siebring, J., de Vreugd, P., Boersma, F. G., Dijkhuizen, L., & Wösten, H. A. (2003). A novel class of secreted hydrophobic proteins is involved in aerial hyphae formation in *Streptomyces coelicolor* by forming amyloid-like fibrils. *Genes Dev*, 17(14), 1714-1726. <https://doi.org/10.1101/gad.264303>
- Claessen, D., Wösten, H. A. B., van Keulen, G., Faber, O. G., Alves, A. M. C. R., Meijer, W. G., & Dijkhuizen, L. (2002). Two novel homologous proteins of *Streptomyces coelicolor* and *Streptomyces lividans* are involved in the formation of the rodlet layer and mediate attachment to a hydrophobic surface. *Mol. Microbiol.*, 44(6), 1483-1492. <https://doi.org/10.1046/j.1365-2958.2002.02980.x>
- Clément, J. M., Lepouce, E., Marchal, C., & Hofnung, M. (1983). Genetic study of a membrane protein: DNA sequence alterations due to 17 *lamB* point mutations affecting adsorption of phage lambda. *EMBO J.*, 2(1), 77-80. <https://doi.org/10.1002/j.1460-2075.1983.tb01384.x>
- Clokic, M. R., Millard, A. D., Letarov, A. V., & Heaphy, S. (2011). Phages in nature. *Bacteriophage*, 1(1), 31-45. <https://doi.org/10.4161/bact.1.1.14942>
- Cohen, D., Melamed, S., Millman, A., Shulman, G., Oppenheimer-Shaanan, Y., Kacen, A., Doron, S., Amitai, G., & Sorek, R. (2019). Cyclic GMP-AMP signalling protects bacteria against viral infection. *Nature*, 574(7780), 691-695. <https://doi.org/10.1038/s41586-019-1605-5>
- Cornforth, D. M., & Foster, K. R. (2013). Competition sensing: the social side of bacterial stress responses. *Nat Rev Microbiol*, 11(4), 285-293. <https://doi.org/10.1038/nrmicro2977>
- d'Herelle, F. (2007). On an invisible microbe antagonistic toward dysenteric bacilli: brief note by Mr. F. D'Herelle, presented by Mr. Roux 1917. *Res. Microbiol.*, 158(7), 553-554. <https://doi.org/10.1016/j.resmic.2007.07.005>
- Davies, E. V., Winstanley, C., Fothergill, J. L., & James, C. E. (2016). The role of temperate bacteriophages in bacterial infection. *FEMS Microbiol. Lett.*, 363(5), fnw015. <https://doi.org/10.1093/femsle/fnw015>

- De Smet, J., Hendrix, H., Blasdel, B. G., Danis-Wlodarczyk, K., & Lavigne, R. (2017). *Pseudomonas* predators: understanding and exploiting phage-host interactions. *Nat. Rev. Microbiol.*, 15(9), 517-530. <https://doi.org/10.1038/nrmicro.2017.61>
- De Smet, J., Wagemans, J., Boon, M., Ceyssens, P. J., Voet, M., Noben, J. P., Andreeva, J., Ghilarov, D., Severinov, K., & Lavigne, R. (2021). The bacteriophage LUZ24 "Igy" peptide inhibits the *Pseudomonas* DNA gyrase. *Cell Rep.*, 36(8), 109567. <https://doi.org/10.1016/j.celrep.2021.109567>
- den Hengst, C. D., Tran, N. T., Bibb, M. J., Chandra, G., Leskiw, B. K., & Buttner, M. J. (2010). Genes essential for morphological development and antibiotic production in *Streptomyces coelicolor* are targets of BldD during vegetative growth. *Mol Microbiol.*, 78(2), 361-379. <https://doi.org/10.1111/j.1365-2958.2010.07338.x>
- Diaz, L. A., Gomez, P., Hardisson, C., & Rodicio, M. R. (1991). Biological characterization of the lytic cycle of actinophage ΦA7 in *Streptomyces antibioticus*. *FEMS Microbiol. Lett.*, 83(1), 65-68. <https://doi.org/10.1111/j.1574-6968.1991.tb04390.x>
- Dika, C., Ly-Chatain, M. H., Francius, G., Duval, J. F. L., & Gantzer, C. (2013). Non-DLVO adhesion of F-specific RNA bacteriophages to abiotic surfaces: Importance of surface roughness, hydrophobic and electrostatic interactions. *Colloids Surf. A Physicochem. Eng.*, 435, 178-187. <https://doi.org/10.1016/j.colsurfa.2013.02.045>
- Dimitriu, T., Kurilovich, E., Łapińska, U., Severinov, K., Pagliara, S., Szczelkun, M. D., & Westra, E. R. (2022). Bacteriostatic antibiotics promote CRISPR-Cas adaptive immunity by enabling increased spacer acquisition. *Cell Host Microbe*, 30(1), 31-40 e35. <https://doi.org/10.1016/j.chom.2021.11.014>
- Dion, M. B., Oechslin, F., & Moineau, S. (2020). Phage diversity, genomics and phylogeny. *Nat Rev Microbiol*, 18(3), 125-138. <https://doi.org/10.1038/s41579-019-0311-5>
- Donald, L., Pipite, A., Subramani, R., Owen, J., Keyzers, R. A., & Taufa, T. (2022). *Streptomyces*: Still the Biggest Producer of New Natural Secondary Metabolites, a Current Perspective. *Microbiol. Res.*, 13(3), 418-465. <https://doi.org/10.3390/microbiolres13030031>
- Donovan, C., Heyer, A., Pfeifer, E., Polen, T., Wittmann, A., Kramer, R., Frunzke, J., & Bramkamp, M. (2015). A prophage-encoded actin-like protein required for efficient viral DNA replication in bacteria. *Nucleic Acids Res.*, 43(10), 5002-5016. <https://doi.org/10.1093/nar/gkv374>
- Doron, S., Melamed, S., Ofir, G., Leavitt, A., Lopatina, A., Keren, M., Amitai, G., & Sorek, R. (2018). Systematic discovery of antiphage defense systems in the microbial pangenome. *Science*, 359(6379), eaar4120. <https://doi.org/10.1126/science.aar4120>
- Doudna, J. A., & Charpentier, E. (2014). The new frontier of genome engineering with CRISPR-Cas9. *Science*, 346(6213), 1258096. <https://doi.org/10.1126/science.1258096>
- Drlica, K., & Malik, M. (2003). Fluoroquinolones: Action and Resistance. *Curr Top Med Chem*, 3(249), 249-282. <https://doi.org/10.2174/1568026033452537>
- Drulis-Kawa, Z., Majkowska-Skrobek, G., Maciejewska, B., Delattre, A., & Lavigne, R. (2012). Learning from bacteriophages - advantages and limitations of phage and phage-encoded protein applications. *Curr Protein Pept Sci.*, 13(8), 699-722. <https://doi.org/10.2174/138920312804871193>
- Duan, B., Ding, P., Hughes, T. R., Navarre, W. W., Liu, J., & Xia, B. (2018). How bacterial xenogeneic silencer rok distinguishes foreign from self DNA in its resident genome. *Nucleic Acids Res.*, 46(19), 10514 - 10529. <https://doi.org/10.1093/nar/gky836>

- Elliot, M. A., Karoonuthaisiri, N., Huang, J., Bibb, M. J., Cohen, S. N., Kao, C. M., & Buttner, M. J. (2003). The chaplins: a family of hydrophobic cell-surface proteins involved in aerial mycelium formation in *Streptomyces coelicolor*. *Genes Dev*, 17(14), 1727-1740. <https://doi.org/10.1101/gad.264403>
- Elliot, M. A., & Talbot, N. J. (2004). Building filaments in the air: aerial morphogenesis in bacteria and fungi. *Curr Opin Microbiol*, 7(6), 594-601. <https://doi.org/10.1016/j.mib.2004.10.013>
- Erdrich, S. H., Sharma, V., Schurr, U., Arsova, B., & Frunzke, J. (2022). Isolation of Novel *Xanthomonas* Phages Infecting the Plant Pathogens *X. translucens* and *X. campestris*. *Viruses*, 14(7). <https://doi.org/10.3390/v14071449>
- Fajardo, A., Linares, J. F., & Martinez, J. L. (2009). Towards an ecological approach to antibiotics and antibiotic resistance genes. *Clin Microbiol Infect*, 15 (Suppl 1), 14-16. <https://doi.org/10.1111/j.1469-0691.2008.02688.x>
- Farkas, K., Varsani, A., & Pang, L. (2015). Adsorption of Rotavirus, MS2 Bacteriophage and Surface-Modified Silica Nanoparticles to Hydrophobic Matter. *Food Environ Virol*, 7(3), 261-268. <https://doi.org/10.1007/s12560-014-9171-3>
- Feiner, R., Argov, T., Rabinovich, L., Sigal, N., Borovok, I., & Herskovits, A. A. (2015). A new perspective on lysogeny: prophages as active regulatory switches of bacteria. *Nat Rev Microbiol*, 13(10), 641-650. <https://doi.org/10.1038/nrmicro3527>
- Fierer, N. (2017). Embracing the unknown: disentangling the complexities of the soil microbiome. *Nat Rev Microbiol*, 15(10), 579-590. <https://doi.org/10.1038/nrmicro.2017.87>
- Flärdh, K., & Buttner, M. J. (2009). *Streptomyces* morphogenetics: dissecting differentiation in a filamentous bacterium. *Nat Rev Microbiol*, 7(1), 36-49. <https://doi.org/10.1038/nrmicro1968>
- Fleming, A. (1929). On the Antibacterial Action of Cultures of a Penicillium, with Special Reference to their Use in the Isolation of *B. influenzae*. *Br. J. Exp. Pathol.*, 10(3), 226-236.
- Fremin, B. J., Bhatt, A. S., Kypides, N. C., & Global Phage Small Open Reading Frame (GP-SmORF) Consortium. (2022). Thousands of small, novel genes predicted in global phage genomes. *Cell Rep*, 39(12), 110984. <https://doi.org/10.1016/j.celrep.2022.110984>
- Fröjd, M. J., & Flärdh, K. (2019). Extrusion of extracellular membrane vesicles from hyphal tips of *Streptomyces venezuelae* coupled to cell-wall stress. *Microbiology* 165(12), 1295-1305. <https://doi.org/10.1099/mic.0.000836>
- Frunzke, J., Bramkamp, M., Schweitzer, J. E., & Bott, M. (2008). Population Heterogeneity in *Corynebacterium glutamicum* ATCC 13032 caused by prophage CGP3. *J. Bacteriol.*, 190(14), 5111-5119. <https://doi.org/10.1128/JB.00310-08>
- Garneau-Tsodikova, S., & Labby, K. J. (2016). Mechanisms of Resistance to Aminoglycoside Antibiotics: Overview and Perspectives. *Medchemcomm*, 7(1), 11-27. <https://doi.org/10.1039/C5MD00344J>
- Ghanem, N., Stanley, C. E., Harms, H., Chatzinotas, A., & Wick, L. Y. (2019). Mycelial Effects on Phage Retention during Transport in a Microfluidic Platform. *Environ Sci Technol*, 53(20), 11755-11763. <https://doi.org/10.1021/acs.est.9b03502>
- Gizzi, A. S., Grove, T. L., Arnold, J. J., Jose, J., Jangra, R. K., Garforth, S. J., Du, Q., Cahill, S. M., Dulyaninova, N. G., Love, J. D., Chandran, K., Bresnick, A. R., Cameron, C. E., & Almo, S. C. (2018). A naturally occurring antiviral ribonucleotide encoded by the human genome. *Nature*, 558(7711), 610-614. <https://doi.org/10.1038/s41586-018-0238-4>



- Glazebrook, M. A., Doull, J. L., Stuttard, C., & Vining, L. C. (1990). Sporulation of *Streptomyces venezuelae* in submerged cultures. *J Gen Microbiol*, 136(3), 581-588. <https://doi.org/10.1099/00221287-136-3-581>
- Goldstone, D. C., Ennis-Adeniran, V., Hedden, J. J., Groom, H. C., Rice, G. I., Christodoulou, E., Walker, P. A., Kelly, G., Haire, L. F., Yap, M. W., de Carvalho, L. P., Stoye, J. P., Crow, Y. J., Taylor, I. A., & Webb, M. (2011). HIV-1 restriction factor SAMHD1 is a deoxynucleoside triphosphate triphosphohydrolase. *Nature*, 480(7377), 379-382. <https://doi.org/10.1038/nature10623>
- Gordon, B. R. G., Li, Y., Wang, L., Sintsova, A., van Bakel, H., Tian, S., Navarre, W. W., Xia, B., & Liu, J. (2010). Lsr2 is a nucleoid-associated protein that targets AT-rich sequences and virulence genes in *Mycobacterium tuberculosis*. *PNAS*, 107(11), 5154-5159. <https://doi.org/10.1073/pnas.0913551107>
- Gregory, M. A., Till, R., & Smith, M. C. (2003). Integration site for *Streptomyces* phage phiBT1 and development of site-specific integrating vectors. *J Bacteriol*, 185(17), 5320-5323. <https://doi.org/10.1128/JB.185.17.5320-5323.2003>
- Hampton, H. G., Watson, B. N. J., & Fineran, P. C. (2020). The arms race between bacteria and their phage foes. *Nature*, 577(7790), 327-336. <https://doi.org/10.1038/s41586-019-1894-8>
- Hancock, R. E., Raffle, V. J., & Nicas, T. I. (1981). Involvement of the outer membrane in gentamicin and streptomycin uptake and killing in *Pseudomonas aeruginosa*. *J. Antimicrob.*, 19(5), 777-785. <https://doi.org/10.1128/AAC.19.5.777>.
- Hansen, M. F., Svenningsen, S. L., Roder, H. L., Middelboe, M., & Burmolle, M. (2019). Big Impact of the Tiny: Bacteriophage-Bacteria Interactions in Biofilms. *Trends Microbiol.*, 27(9), 739-752. <https://doi.org/10.1016/j.tim.2019.04.006>
- Hardy, A., Kever, L., & Frunzke, J. (2023). Antiphage small molecules produced by bacteria - beyond protein-mediated defenses. *Trends Microbiol.*, 31(1), 92-106. <https://doi.org/10.1016/j.tim.2022.08.001>
- Hardy, A., Sharma, V., Kever, L., & Frunzke, J. (2020). Genome sequence and characterization of five bacteriophages infecting *Streptomyces coelicolor* and *Streptomyces venezuelae*: Alderaan, Coruscant, Dagobah, Endor1 and Endor2. *Viruses*, 12(10), 1065. <https://doi.org/10.3390/v12101065>
- Harvey, H., Bondy-Denomy, J., Marquis, H., Sztanko, K. M., Davidson, A. R., & Burrows, L. L. (2018). *Pseudomonas aeruginosa* defends against phages through type IV pilus glycosylation. *Nat. Microbiol.*, 3(1), 47-52. <https://doi.org/10.1038/s41564-017-0061-y>
- Hashem, I., & Van Impe, J. F. M. (2022). A Game Theoretic Analysis of the Dual Function of Antibiotics. *Front Microbiol*, 12, 812788. <https://doi.org/10.3389/fmicb.2021.812788>
- Hatfull, G. F. (2008). Bacteriophage genomics. *Curr Opin Microbiol*, 11(5), 447-453. <https://doi.org/10.1016/j.mib.2008.09.004>
- Helbig, K. J., & Beard, M. R. (2014). The role of viperin in the innate antiviral response. *J. Mol. Biol*, 426(6), 1210-1219. <https://doi.org/10.1016/j.jmb.2013.10.019>
- Helfrich, S., Pfeifer, E., Krämer, C., Sachs, C. C., Wiechert, W., Kohlheyer, D., Noh, K., & Frunzke, J. (2015). Live cell imaging of SOS and prophage dynamics in isogenic bacterial populations. *Mol. Microbiol.*, 98(4), 636-650. <https://doi.org/10.1111/mmi.13147>
- Hendrix, R. W., Smith, M. C. M., Burns, R. N., Ford, M. E., & Hatfull, G. F. (1999). Evolutionary relationships among diverse bacteriophages and prophages: All the world's a phage. *PNAS*, 96(5), 2192-2197. <https://doi.org/10.1073/pnas.96.5.2192>

- Hershey, A. D., & Chase, M. (1952). Independent functions of viral protein and nucleic acid in growth of bacteriophage. *J Gen Physiol.*, 36(1), 39-56. <https://doi.org/10.1085/jgp.36.1.39>
- Hille, F., Richter, H., Wong, S. P., Bratovic, M., Ressel, S., & Charpentier, E. (2018). The Biology of CRISPR-Cas: Backward and Forward. *Cell*, 172(6), 1239-1259. <https://doi.org/10.1016/j.cell.2017.11.032>
- Hobbs, G., Obanye, A. I. C., Petty, J., Mason, J. C., Barratt, E. M., Gardner, D. C. J., Flett, F. J., Smith, C. P., Broda, P. M. A., & Oliver, S. G. (1992). An integrated approach to studying regulation of production of the antibiotic methylenomycin by *Streptomyces coelicolor* A3(2). *J. Bacteriol.*, 174(5), 1487 - 1494. <https://doi.org/10.1128/jb.174.5.1487-1494.1992>
- Holmes, D. J., Drocourt, D., Tiraby, G., & Cundliffe, E. (1991). Cloning of an aminoglycoside-resistance-encoding gene, *kamC*, from *Saccharopolyspora hirsuta*: comparison with *kamB* from *Streptomyces tenebrarius*. *Gene*, 102 (1), 19-26. [https://doi.org/10.1016/0378-1119\(91\)90532-G](https://doi.org/10.1016/0378-1119(91)90532-G)
- Hoque, M. M., Naser, I. B., Bari, S. M. N., Zhu, J., Mekalanos, J. J., & Faruque, S. M. (2016). Quorum Regulated Resistance of *Vibrio cholerae* against Environmental Bacteriophages. *Sci Rep*, 6(1), 37956. <https://doi.org/10.1038/srep37956>
- Høyland-Kroghsbo, N. M., Maerkedahl, R. B., & Svenningsen, S. L. (2013). A quorum-sensing-induced bacteriophage defense mechanism. *mBio*, 4(1), e00362-00312. <https://doi.org/10.1128/mbio.00362-12>
- Høyland-Kroghsbo, N. M., Paczkowski, J., Mukherjee, S., Broniewski, J., Westra, E., Bondy-Denomy, J., & Bassler, B. L. (2017). Quorum sensing controls the *Pseudomonas aeruginosa* CRISPR-Cas adaptive immune system. *PNAS*, 114(1), 131-135. <https://doi.org/10.1073/pnas.1617415113>
- Hünnefeld, M., Viets, U., Sharma, V., Wirtz, A., Hardy, A., & Frunzke, J. (2021). Genome Sequence of the Bacteriophage CL31 and Interaction with the Host Strain *Corynebacterium glutamicum* ATCC 13032. *Viruses*, 13(3), 495. <https://doi.org/10.3390/v13030495>
- Hyman, P., & Abedon, S. T. (2012). Smaller fleas: viruses of microorganisms. *Scientifica* 2012(4814), 734023. <https://doi.org/10.6064/2012/734023>
- Ikeda, H., & Tomizawa, J.-i. (1968). Prophage P1, an Extrachromosomal Replication Unit. *Cold Spring Harb. Symp. Quant. Biol.*, 33, 791-798. <https://doi.org/10.1101/sqb.1968.033.01.091>
- Ikeda, M., & Nakagawa, S. (2003). The *Corynebacterium glutamicum* genome: features and impacts on biotechnological processes. *Appl. Microbiol. Biotechnol.*, 62(2-3), 99-109. <https://doi.org/10.1007/s00253-003-1328-1>
- Janssen, P. H. (2006). Identifying the dominant soil bacterial taxa in libraries of 16S rRNA and 16S rRNA genes. *Appl. Environ. Microbiol.*, 72(3), 1719-1728. <https://doi.org/10.1128/AEM.72.3.1719-1728.2006>
- Jiang, Z., Wei, J., Liang, Y., Peng, N., & Li, Y. (2020). Aminoglycoside Antibiotics Inhibit Mycobacteriophage Infection. *Antibiotics*, 9(10), 714. <https://doi.org/10.3390/antibiotics9100714>
- Jones, S. E., & Elliot, M. A. (2017). *Streptomyces* Exploration: Competition, Volatile Communication and New Bacterial Behaviours. *Trends Microbiol.*, 25(7), 522-531. <https://doi.org/10.1016/j.tim.2017.02.001>
- Jones, S. E., Ho, L., Rees, C. A., Hill, J. E., Nodwell, J. R., & Elliot, M. A. (2017). *Streptomyces* exploration is triggered by fungal interactions and volatile signals. *Elife*, 6, e21738. <https://doi.org/10.7554/eLife.21738>

- Jones, S. E., Pham, C. A., Zambri, M. P., McKillip, J., Carlson, E. E., & Elliot, M. A. (2019). *Streptomyces* Volatile Compounds Influence Exploration and Microbial Community Dynamics by Altering Iron Availability. *mBio*, 10(2), e00171-00119. <https://doi.org/10.1128/mBio.00171-19>.
- Jordan, T. C., Burnett, S. H., Carson, S., Caruso, S. M., Clase, K., DeJong, R. J., Dennehy, J. J., Denver, D. R., Dunbar, D., Elgin, S. C., Findley, A. M., Gissendanner, C. R., Golebiewska, U. P., Guild, N., Hartzog, G. A., Grillo, W. H., Hollowell, G. P., Hughes, L. E., Johnson, A., King, R. A., Lewis, L. O., Li, W., Rosenzweig, F., Rubin, M. R., Saha, M. S., Sandoz, J., Shaffer, C. D., Taylor, B., Temple, L., Vazquez, E., Ware, V. C., Barker, L. P., Bradley, K. W., Jacobs-Sera, D., Pope, W. H., Russell, D. A., Cresawn, S. G., Lopatto, D., Bailey, C. P., & Hatfull, G. F. (2014). A broadly implementable research course in phage discovery and genomics for first-year undergraduate students. *mBio*, 5(1), e01051-01013. <https://doi.org/10.1128/mBio.01051-13>
- Kever, L., & Frunzke, J. (2022). Inactivation of phage particles in the extracellular space of *Streptomyces* populations. *Inside this thesis. To be submitted*.
- Kever, L., Hardy, A., Luthe, T., Hünnefeld, M., Gätgens, C., Milke, L., Wiechert, J., Wittmann, J., Moraru, C., Marienhagen, J., & Frunzke, J. (2022). Aminoglycoside Antibiotics Inhibit Phage Infection by Blocking an Early Step of the Infection Cycle. *mBio*, 13(3). <https://doi.org/10.1128/mbio.00783-22>
- Kever, L., Hünnefeld, M., Brehm, J., Heermann, R., & Frunzke, J. (2021). Identification of Gip as a novel phage-encoded gyrase inhibitor protein of *Corynebacterium glutamicum*. *Mol Microbiol*, 116(5), 1268-1280. <https://doi.org/10.1111/mmi.14813>
- Khan, T., Sankhe, K., Suvarna, V., Sherje, A., Patel, K., & Dravyakar, B. (2018). DNA gyrase inhibitors: Progress and synthesis of potent compounds as antibacterial agents. *Biomed Pharmacother*, 103, 923-938. <https://doi.org/10.1016/j.biopha.2018.04.021>
- Kieser, T., Bibb, M., Chater, K., Butter, M., Hopwood, D., Bittner, M., & Buttner, M. (2000). *Practical Streptomyces Genetics: A Laboratory Manual*.
- Koonin, E. V., Dolja, V. V., Krupovic, M., Varsani, A., Wolf, Y. I., Yutin, N., Zerbini, F. M., & Kuhn, J. H. (2020). Global Organization and Proposed Megataxonomy of the Virus World. *Microbiol. Mol. Biol. Rev.*, 84(2), e00061-00019. <https://doi.org/10.1128/MMBR.00061-19>
- Koonin, E. V., Makarova, K. S., & Wolf, Y. I. (2017). Evolutionary Genomics of Defense Systems in Archaea and Bacteria. *Annu. Rev. Microbiol.*, 71, 233-261. <https://doi.org/10.1146/annurev-micro-090816-093830>
- Kopaczynska, M., Lauer, M., Schulz, A., Wang, T., Schaefer, A., & Fuhrhop, J.-H. (2004). Aminoglycoside antibiotics aggregate to form starch-like fibers on negatively charged surfaces and on phage λ-DNA. *Langmuir*, 20(21), 9270-9275. <https://doi.org/10.1021/la049207m>
- Kopaczynska, M., Schulz, A., Fraczowska, K., Kraszewski, S., Podbielska, H., & Fuhrhop, J. H. (2016). Selective condensation of DNA by aminoglycoside antibiotics. *Eur Biophys J*, 45(4), 287-299. <https://doi.org/10.1007/s00249-015-1095-9>
- Kortright, K. E., Chan, B. K., Koff, J. L., & Turner, P. E. (2019). Phage Therapy: A Renewed Approach to Combat Antibiotic-Resistant Bacteria. *Cell Host Microbe*, 25(2), 219-232. <https://doi.org/10.1016/j.chom.2019.01.014>
- Koscinski, L., Feder, M., & Bujnicki, J. M. (2007). Identification of a Missing Sequence and Functionally Important Residues of 16S rRNA:m1A1408 Methyltransferase KamB that Causes Bacterial Resistance to Aminoglycoside Antibiotics. *Cell Cycle*, 6(10), 1268-1271. <https://doi.org/10.4161/cc.6.10.4231>

- Kotra, L. P., Haddad, J., & Mobashery, S. (2000). Aminoglycosides: Perspectives on Mechanisms of Action and Resistance and Strategies to Counter Resistance. *Antimicrob. Agents Chemother.*, 44(12), 3249-3256. <https://doi.org/10.1128/aac.44.12.3249-3256.2000>
- Krause, K. M., Serio, A. W., Kane, T. R., & Connolly, L. E. (2016). Aminoglycosides: An Overview. *Cold Spring Harb. Perspect. Med.*, 6(6), a027029. <https://doi.org/10.1101/cshperspect.a027029>
- Kronheim, S., Daniel-Ivad, M., Duan, Z., Hwang, S., Wong, A. I., Mantel, I., Nodwell, J. R., & Maxwell, K. L. (2018). A chemical defence against phage infection. *Nature*, 564(7735), 283-286. <https://doi.org/10.1038/s41586-018-0767-x>
- Labrie, S. J., Samson, J. E., & Moineau, S. (2010). Bacteriophage resistance mechanisms. *Nat Rev Microbiol*, 8(5), 317-327. <https://doi.org/10.1038/nrmicro2315>
- Lammens, E. M., Nikel, P. I., & Lavigne, R. (2020). Exploring the synthetic biology potential of bacteriophages for engineering non-model bacteria. *Nat Commun*, 11(1), 5294. <https://doi.org/10.1038/s41467-020-19124-x>
- Landy, A., & Ross, W. (1977). Viral Integration and Excision: Structure of the Lambda att Sites. *Science*, 197(4309), 1147-1160. <https://doi.org/10.1126/science.331474>
- Linares, J. F., Gustafsson, I., Baquero, F., & Martinez, J. L. (2006). Antibiotics as intermicrobial signaling agents instead of weapons. *PNAS*, 103(51), 19484-19489. <https://doi.org/10.1073/pnas.0608949103>
- Liu, Z., Zhao, Y., Huang, C., & Luo, Y. (2021). Recent Advances in Silent Gene Cluster Activation in *Streptomyces*. *Front Bioeng Biotechnol*, 9, 632230. <https://doi.org/10.3389/fbioe.2021.632230>
- Lopatina, A., Tal, N., & Sorek, R. (2020). Abortive Infection: Bacterial Suicide as an Antiviral Immune Strategy. *Annu. Rev. Virol.*, 7(1), 371-384. <https://doi.org/10.1146/annurev-virology-011620-040628>
- Lorenzi, J. N., Lespinet, O., Leblond, P., & Thibessard, A. (2021). Subtelomeres are fast-evolving regions of the *Streptomyces* linear chromosome. *Microb Genom*, 7(6), 000525. <https://doi.org/10.1099/mgen.0.000525>
- Lu, M.-J., & Henning, U. (1994). Superinfection exclusion by T-even-type coliphages. *Trends Microbiol.*, 2(4), 137-139. [https://doi.org/10.1016/0966-842X\(94\)90601-7](https://doi.org/10.1016/0966-842X(94)90601-7)
- Luthe, T., Kever, L., Hänsch, S., Hardy, A., Tschowri, N., Weidtkamp-Peters, S., & Frunzke, J. (2023a). *Streptomyces* development is involved in the efficient containment of viral infections. *microLife*, 4, uqad002. <https://doi.org/10.1093/femsml/uqad002>
- Luthe, T., Kever, L., Thormann, K., & Frunzke, J. (2023b). Bacterial multicellular behavior in antiviral defense. *Current Opinion in Microbiology*, 74, 102314. <https://doi.org/10.1016/j.mib.2023.102314>
- Madden, T., & Ison, J. M. W. A. P. (1996). Organic acid excretion by *Streptomyces lividans* TK24 during growth on defined carbon and nitrogen sources. *Microbiology*, 142((Pt11)), 3181-3185. <https://doi.org/10.1099/13500872-142-11-3181>
- Magalhaes, M. L., & Blanchard, J. S. (2005). The kinetic mechanism of AAC3-IV aminoglycoside acetyltransferase from *Escherichia coli*. *Biochemistry*, 44(49), 16275-16283. <https://doi.org/10.1021/bi051777d>
- Magnet, S., & Blanchard, J. S. (2005). Molecular Insights into Aminoglycoside Action and Resistance. *Chem. Rev.*, 105(2), 477-498. <https://doi.org/10.1021/cr0301088>

- Makarova, K. S., Wolf, Y. I., Snir, S., & Koonin, E. V. (2011). Defense islands in bacterial and archaeal genomes and prediction of novel defense systems. *J Bacteriol*, 193(21), 6039-6056. <https://doi.org/10.1128/JB.05535-11>
- Manning, A. J., & Kuehn, M. J. (2011). Contribution of bacterial outer membrane vesicles to innate bacterial defense. *BMC Microbiology*, 11(258). <https://doi.org/10.1186/1471-2180-11-258>
- Manteca, A., Alvarez, R., Salazar, N., Yagüe, P., & Sanchez, J. (2008). Mycelium differentiation and antibiotic production in submerged cultures of *Streptomyces coelicolor*. *Appl Environ Microbiol*, 74(12), 3877-3886. <https://doi.org/10.1128/AEM.02715-07>
- Manteca, A., Claessen, D., Lopez-Iglesias, C., & Sanchez, J. (2007). Aerial hyphae in surface cultures of *Streptomyces lividans* and *Streptomyces coelicolor* originate from viable segments surviving an early programmed cell death event. *FEMS Microbiol Lett*, 274(1), 118-125. <https://doi.org/10.1111/j.1574-6968.2007.00825.x>
- Marsh, P., & Wellington, E. M. H. (1992). Interactions between Actinophage and their Streptomyces Hosts in Soil and the Fate of Phage Borne Genes. In M. J. Gauthier (Ed.), *Gene Transfers and Environment* (pp. 135-142). Springer Berlin Heidelberg. [https://doi.org/10.1007/978-3-642-77450-8\\_15](https://doi.org/10.1007/978-3-642-77450-8_15)
- Mattenberger, Y., Silva, F., & Belin, D. (2015). 55.2, a phage T4 ORFan gene, encodes an inhibitor of *Escherichia coli* topoisomerase I and increases phage fitness. *PLoS One*, 10(4), e0124309. <https://doi.org/10.1371/journal.pone.0124309>
- Maxwell, A., & Lawson, D. M. (2003). The ATP-Binding Site of Type II Topoisomerases as a Target for Antibacterial Drugs. *Curr Top Med Chem*, 3(3), 283-303. <https://doi.org/10.2174/1568026033452500>
- McCormick, J. R., & Flärdh, K. (2012). Signals and regulators that govern *Streptomyces* development. *FEMS Microbiology Reviews*, 36(1), 206-231. <https://doi.org/10.1111/j.1574-6976.2011.00317.x>
- McKie, S. J., Neuman, K. C., & Maxwell, A. (2021). DNA topoisomerases: Advances in understanding of cellular roles and multi-protein complexes via structure-function analysis. *Bioessays*, 43(4), e2000286. <https://doi.org/10.1002/bies.202000286>
- Merrill, B. D., Ward, A. T., Grose, J. H., & Hope, S. (2016). Software-based analysis of bacteriophage genomes, physical ends, and packaging strategies. *BMC Genomics*, 17, 679. <https://doi.org/10.1186/s12864-016-3018-2>
- Mingeot-Leclercq, M.-P., Glupczynski, Y., & Tulkens, P. M. (1999). Aminoglycosides: Activity and Resistance. *Antimicrob. Agents Chemother.*, 43(4). <https://doi.org/10.1128/AAC.43.4.727>
- Mushegian, A. R. (2020). Are There 10<sup>31</sup> Virus Particles on Earth, or More, or Fewer? *J. Bacteriol.*, 202(9), e00052-00020. <https://doi.org/10.1128/JB.00052-20>
- Nanda, A. M., Thormann, K., & Frunzke, J. (2015). Impact of spontaneous prophage induction on the fitness of bacterial populations and host-microbe interactions. *J Bacteriol*, 197(3), 410-419. <https://doi.org/10.1128/JB.02230-14>
- Navarre, W. W. (2016). The Impact of Gene Silencing on Horizontal Gene Transfer and Bacterial Evolution. *Adv. Microb. Physiol.*, 69, 157-186. <https://doi.org/10.1016/bs.ampbs.2016.07.004>
- Nechaev, S., & Severinov, K. (1999). Inhibition of *Escherichia coli* RNA Polymerase by Bacteriophage T7 Gene 2 Protein. *J. Mol. Biol.*, 289(4), 815-826. <https://doi.org/10.1006/jmbi.1999.2782>

- Nordström, K., & Forsgren, A. (1974). Effect of protein A on adsorption of bacteriophages to *Staphylococcus aureus*. *J. Virol.*, 14(2), 198-202. <https://doi.org/10.1128/JVI.14.2.198-202.1974>
- Ofir, G., & Sorek, R. (2018). Contemporary Phage Biology: From Classic Models to New Insights. *Cell*, 172(6), 1260-1270. <https://doi.org/10.1016/j.cell.2017.10.045>
- Ohno, S., Okano, H., Tanji, Y., Ohashi, A., Watanabe, K., Takai, K., & Imachi, H. (2012). A method for evaluating the host range of bacteriophages using phages fluorescently labeled with 5-ethynyl-2'-deoxyuridine (EdU). *Appl. Microbiol. Biotechnol.*, 95(3), 777-788. <https://doi.org/10.1007/s00253-012-4174-1>
- Oppenheim, A. B., Kobilier, O., Stavans, J., Court, D. L., & Adhya, S. (2005). Switches in bacteriophage lambda development. *Annu. Rev. Genet.*, 39, 409-429. <https://doi.org/10.1146/annurev.genet.39.073003.113656>
- Orr, M. W., Mao, Y., Storz, G., & Qian, S. B. (2020). Alternative ORFs and small ORFs: shedding light on the dark proteome. *Nucleic Acids Res.*, 48(3), 1029-1042. <https://doi.org/10.1093/nar/gkz734>
- Patterson, A. G., Jackson, S. A., Taylor, C., Evans, G. B., Salmond, G. P. C., Przybilski, R., Staals, R. H. J., & Fineran, P. C. (2016). Quorum Sensing Controls Adaptive Immunity through the Regulation of Multiple CRISPR-Cas Systems. *Mol Cell*, 64(6), 1102-1108. <https://doi.org/10.1016/j.molcel.2016.11.012>
- Pfeifer, E., Hünnefeld, M., Popa, O., & Frunzke, J. (2019). Impact of Xenogeneic Silencing on Phage-Host Interactions. *J. Mol. Biol.*, 431(23), 4670-4683. <https://doi.org/10.1016/j.jmb.2019.02.011>
- Pfeifer, E., Hünnefeld, M., Popa, O., Polen, T., Kohlheyer, D., Baumgart, M., & Frunzke, J. (2016). Silencing of cryptic prophages in *Corynebacterium glutamicum*. *Nucleic Acids Res.*, 44(21), 10117-10131. <https://doi.org/10.1093/nar/gkw692>
- Pierrat, O. A., & Maxwell, A. (2003). The action of the bacterial toxin microcin B17. *J. Biol. Chem.*, 278(37), 35016-35023. <https://doi.org/10.1074/jbc.M304516200>
- Pons, B. J., Dimitriu, T., Westra, E. R., & van Houte, S. (2023). Antibiotics that affect translation can antagonize phage infectivity by interfering with the deployment of counter-defences. *PNAS*, 120(4), e2216084120. <https://doi.org/10.1073/pnas.2216084120>
- Rakhuba, D. V., Kolomiets, E. I., Szwajcer Dey, E., & Novik, G. I. (2010). Bacteriophage receptors, mechanisms of phage adsorption and penetration into host cell. *Pol J Microbiol.*, 59(3), 145-155.
- Raleigh, E. A., & Brooks, J. E. (1998). Restriction Modification Systems: Where They Are and What They Do. In F. J. de Bruijn, J. R. Lupski, & G. M. Weinstock (Eds.), *Bacterial Genomes: Physical Structure and Analysis* (pp. 78-92). Springer US. [https://doi.org/10.1007/978-1-4615-6369-3\\_8](https://doi.org/10.1007/978-1-4615-6369-3_8)
- Ramirez, M. S., & Tolmasky, M. E. (2010). Aminoglycoside modifying enzymes. *Drug Resist Updat*, 13(6), 151-171. <https://doi.org/10.1016/j.drup.2010.08.003>
- Ramisetty, B. C. M., & Sudhakari, P. A. (2019). Bacterial 'Grounded' Prophages: Hotspots for Genetic Renovation and Innovation. *Front Genet*, 10, Article 65. <https://doi.org/10.3389/fgene.2019.00065>
- Reyes-Robles, T., Dillard, R. S., Cairns, L. S., Silva-Valenzuela, C. A., Housman, M., Ali, A., Wright, E. R., & Camilli, A. (2018). *Vibrio cholerae* Outer Membrane Vesicles Inhibit Bacteriophage Infection. *J. Bacteriol.*, 200(15), e00792-00717. <https://doi.org/10.1128/JB.00792-17>

- Richter, L., Ksiezarczyk, K., Paszkowska, K., Janczuk-Richter, M., Niedziolka-Jonsson, J., Gapinski, J., Los, M., Holyst, R., & Paczesny, J. (2021). Adsorption of bacteriophages on polypropylene labware affects the reproducibility of phage research. *Sci Rep*, 11(1), 7387. <https://doi.org/10.1038/s41598-021-86571-x>
- Ritz, K., & Young, I. M. (2004). Interactions between soil structure and fungi. *Mycologist*, 18(2), 52-59. [https://doi.org/10.1017/S0269-915X\(04\)00201-0](https://doi.org/10.1017/S0269-915X(04)00201-0)
- Rivera-Serrano, E. E., Gizzi, A. S., Arnold, J. J., Grove, T. L., Almo, S. C., & Cameron, C. E. (2020). Viperin Reveals Its True Function. *Annu. Rev. Virol.*, 7(1), 421-446. <https://doi.org/10.1146/annurev-virology-011720-095930>
- Roach, D. R., & Donovan, D. M. (2015). Antimicrobial bacteriophage-derived proteins and therapeutic applications. *Bacteriophage*, 5(3), e1062590. <https://doi.org/10.1080/21597081.2015.1062590>
- Roberts, R. J. (2005). How restriction enzymes became the workhorses of molecular biology. *PNAS*, 102(17), 5905-5908. <https://doi.org/10.1073/pnas.0500923102>
- Rosner, A., & Gutstein, R. (1981). Adsorption of actinophage Pal6 to developing mycelium of *Streptomyces albus*. *Can. J. Microbiol.*, 27(2), 254-257. <https://doi.org/10.1139/m81-039>
- Roucourt, B., & Lavigne, R. (2009). The role of interactions between phage and bacterial proteins within the infected cell: a diverse and puzzling interactome. *Environ Microbiol*, 11(11), 2789-2805. <https://doi.org/10.1111/j.1462-2920.2009.02029.x>
- Ruska, H., Borries, B. v., & Ruska, E. (1939). Die Bedeutung der Übermikroskopie für die Virusforschung. *Archiv f Virusforschung*, 1, 155-169. <https://doi.org/10.1007/BF01243399>
- Russell, D. A., & Hatfull, G. F. (2016). PhagesDB: the actinobacteriophage database. *Bioinformatics*, 33(5), 784-786. <https://doi.org/10.1093/bioinformatics/btw711>
- Sabeti Azad, M., Okuda, M., Cyrenne, M., Bourge, M., Heck, M. P., Yoshizawa, S., & Fourmy, D. (2020). Fluorescent Aminoglycoside Antibiotics and Methods for Accurately Monitoring Uptake by Bacteria. *ACS Infect. Dis.*, 6(5), 1008-1017. <https://doi.org/10.1021/acsinfecdis.9b00421>
- Salic, A., & Mitchison, T. J. (2008). A chemical method for fast and sensitive detection of DNA synthesis *in vivo*. *PNAS*, 105(7), 2415-2420. <https://doi.org/10.1073/pnas.0712168105>
- Salmond, G. P., & Fineran, P. C. (2015). A century of the phage: past, present and future. *Nat Rev Microbiol*, 13(12), 777-786. <https://doi.org/10.1038/nrmicro3564>
- Sautrey, G., Brie, A., Gantzer, C., & Walcarius, A. (2018). MS2 and Q $\beta$  bacteriophages reveal the contribution of surface hydrophobicity on the mobility of non-enveloped icosahedral viruses in SDS-based capillary zone electrophoresis. *Electrophoresis*, 39(2), 377-385. <https://doi.org/10.1002/elps.201700352>
- Schatz, A., & Waksman, S. A. (1944). Effect of Streptomycin and Other Antibiotic Substances upon *Mycobacterium tuberculosis* and Related Organisms. *Proc. Soc. Exp. Biol. Med.*, 57(2), 244-248. <https://doi.org/10.3181/00379727-57-14769>
- Scholl, D., Adhya, S., & Merrill, C. (2005). *Escherichia coli* K1's capsule is a barrier to bacteriophage T7. *Appl. Environ. Microbiol.*, 71(8), 4872-4874. <https://doi.org/10.1128/AEM.71.8.4872-4874.2005>
- Seyedsayamdost, M. R. (2019). Toward a global picture of bacterial secondary metabolism. *J. Ind. Microbiol. Biotechnol*, 46(3-4), 301-311. <https://doi.org/10.1007/s10295-019-02136-y>



- Shabbir, M. A., Hao, H., Shabbir, M. Z., Wu, Q., Sattar, A., & Yuan, Z. (2016). Bacteria vs. Bacteriophages: Parallel Evolution of Immune Arsenal. *Front Microbiol*, 7, 1292. <https://doi.org/10.3389/fmicb.2016.01292>
- Shah, S., & Heddle, J. G. (2014). Squaring up to DNA: pentapeptide repeat proteins and DNA mimicry. *Appl. Microbiol. Biotechnol.*, 98(23), 9545-9560. <https://doi.org/10.1007/s00253-014-6151-3>
- Smith, P., & Schuster, M. (2019). Public goods and cheating in microbes. *Curr Biol*, 29(11), R442-R447. <https://doi.org/10.1016/j.cub.2019.03.001>
- Spagnolo, F., Trujillo, M., & Dennehy, J. J. (2021). Why Do Antibiotics Exist? *mBio*, 12(6), e01966-01921. <https://doi.org/10.1128/mBio.01966-21>
- Stern, A., & Sorek, R. (2011). The phage-host arms race: shaping the evolution of microbes. *Bioessays*, 33(1), 43-51. <https://doi.org/10.1002/bies.201000071>
- Stokar-Avihail, A., Fedorenko, T., Hör, J., Garb, J., Leavitt, A., Millman, A., Shulman, G., Wojtania, N., Melamed, S., Amitai, G., & Sorek, R. (2023). Discovery of phage determinants that confer sensitivity to bacterial immune systems. *Cell*, 186(9), 1863-1876.e1816. <https://doi.org/10.1016/j.cell.2023.02.029>
- Storz, G., Wolf, Y. I., & Ramamurthi, K. S. (2014). Small proteins can no longer be ignored. *Annu. Rev. Biochem.*, 83, 753-777. <https://doi.org/10.1146/annurev-biochem-070611-102400>
- Stubbendieck, R. M., Vargas-Bautista, C., & Straight, P. D. (2016). Bacterial Communities: Interactions to Scale. *Front Microbiol*, 7, 1234. <https://doi.org/10.3389/fmicb.2016.01234>
- Studier, F. W., & Moffatt, B. A. (1986). Use of bacteriophage T7 RNA polymerase to direct selective high-level expression of cloned genes. *J. Mol. Biol.*, 189(1), 113-130. [https://doi.org/10.1016/0022-2836\(86\)90385-2](https://doi.org/10.1016/0022-2836(86)90385-2)
- Summers, W. C. (2001). Bacteriophage Therapy. *Annu. Rev. Microbiol.*, 55, 437-451. <https://doi.org/10.1146/annurev.micro.55.1.437>
- Tal, N., Millman, A., Stokar-Avihail, A., Fedorenko, T., Leavitt, A., Melamed, S., Yirmiya, E., Avraham, C., Brandis, A., Mehlman, T., Amitai, G., & Sorek, R. (2022). Bacteria deplete deoxynucleotides to defend against bacteriophage infection. *Nat Microbiol*, 7(8), 1200-1209. <https://doi.org/10.1038/s41564-022-01158-0>
- Tal, N., & Sorek, R. (2022). SnapShot: Bacterial immunity. *Cell*, 185(3), 578-578.e571. <https://doi.org/10.1016/j.cell.2021.12.029>
- Tamura, T., Ishida, Y., Otoguro, M., Hatano, K., & Suzuki, K.-i. (2008). Classification of 'Streptomyces tenebrarius' Higgins and Kastner as *Streptoalloteichus tenebrarius* nom. rev., comb. nov., and emended description of the genus *Streptoalloteichus*. *Int. J. Syst. Evol. Microbiol.*, 58(3), 688-691. <https://doi.org/10.1099/ijs.0.65272-0>
- Tan, D., Svenningsen, S. L., & Middelboe, M. (2015). Quorum Sensing Determines the Choice of Antiphage Defense Strategy in *Vibrio anguillarum*. *mBio*, 6(3), e00627-00615. <https://doi.org/10.1128/mBio.00627-15>
- Teertstra, W. R., Deelstra, H. J., Vranes, M., Bohlmann, R., Kahmann, R., Kämper, J., & Wösten, H. A. B. (2006). Repellents have functionally replaced hydrophobins in mediating attachment to a hydrophobic surface and in formation of hydrophobic aerial hyphae in *Ustilago maydis*. *Microbiology*, 152(12), 3607-3612. <https://doi.org/10.1099/mic.0.29034-0>
- Teertstra, W. R., van der Velden, G. J., de Jong, J. F., Kruijtz, J. A., Liskamp, R. M., Kroon-Batenburg, L. M., Muller, W. H., Gebbink, M. F., & Wösten, H. A. (2009). The filament-specific Rep1-1 repellent of the phytopathogen *Ustilago maydis* forms functional surface-



- p active amyloid-like fibrils.
- J Biol Chem*
- , 284(14), 9153-9159.
- <https://doi.org/10.1074/jbc.M900095200>
- Tesson, F., Herve, A., Mordret, E., Touchon, M., d'Humieres, C., Cury, J., & Bernheim, A. (2022). Systematic and quantitative view of the antiviral arsenal of prokaryotes. *Nat Commun*, 13(1), 2561. <https://doi.org/10.1038/s41467-022-30269-9>
- Thibessard, A., & Leblond, P. (2014). Subtelomere Plasticity in the Bacterium *Streptomyces*. In E. J. Louis & M. M. Becker (Eds.), *Subtelomeres* (pp. 243-258). Springer Berlin Heidelberg. [https://doi.org/10.1007/978-3-642-41566-1\\_14](https://doi.org/10.1007/978-3-642-41566-1_14)
- Tock, M. R., & Dryden, D. T. F. (2005). The biology of restriction and anti-restriction. *Current Opinion in Microbiology*, 8(4), 466-472. <https://doi.org/10.1016/j.mib.2005.06.003>
- Touchon, M., Bernheim, A., & Rocha, E. P. (2016). Genetic and life-history traits associated with the distribution of prophages in bacteria. *ISME J*, 10(11), 2744-2754. <https://doi.org/10.1038/ismej.2016.47>
- Tschowri, N. (2016). Cyclic Dinucleotide-Controlled Regulatory Pathways in *Streptomyces* Species. *J Bacteriol*, 198(1), 47-54. <https://doi.org/10.1128/JB.00423-15>
- Tschowri, N., Schumacher, M. A., Schlimpert, S., Chinnam, N. B., Findlay, K. C., Brennan, R. G., & Buttner, M. J. (2014). Tetrameric c-di-GMP mediates effective transcription factor dimerization to control *Streptomyces* development. *Cell*, 158(5), 1136-1147. <https://doi.org/10.1016/j.cell.2014.07.022>
- Turner, D., Kropinski, A. M., & Adriaenssens, E. M. (2021). A Roadmap for Genome-Based Phage Taxonomy. *Viruses*, 13(3). <https://doi.org/10.3390/v13030506>
- Twort, F. W. (1915). An investigation on the nature of ultramicroscopic viruses. *The Lancet*, 186(4814), 1241-1243. [https://doi.org/10.1016/S0140-6736\(01\)20383-3](https://doi.org/10.1016/S0140-6736(01)20383-3)
- Tyc, O., Song, C., Dickschat, J. S., Vos, M., & Garbeva, P. (2017). The Ecological Role of Volatile and Soluble Secondary Metabolites Produced by Soil Bacteria. *Trends Microbiol.*, 25(4), 280-292. <https://doi.org/10.1016/j.tim.2016.12.002>
- Urem, M., van Rossum, T., Bucca, G., Moolenaar, G. F., Laing, E., Swiatek-Polatynska, M. A., Willemse, J., Tenconi, E., Rigali, S., Goosen, N., Smith, C. P., & van Wezel, G. P. (2016). OsdR of *Streptomyces coelicolor* and the Dormancy Regulator DevR of *Mycobacterium tuberculosis* Control Overlapping Regulons. *mSystems*, 1(3). <https://doi.org/10.1128/mSystems.00014-16>
- van der Meij, A., Worsley, S. F., Hutchings, M. I., & van Wezel, G. P. (2017). Chemical ecology of antibiotic production by actinomycetes. *FEMS Microbiol Rev*, 41(3), 392-416. <https://doi.org/10.1093/femsre/fox005>
- van Houte, S., Buckling, A., & Westra, E. R. (2016). Evolutionary Ecology of Prokaryotic Immune Mechanisms. *Microbiol Mol Biol Rev*, 80(3), 745-763. <https://doi.org/10.1128/MMBR.00011-16>
- Vanden Broeck, A., Lotz, C., Ortiz, J., & Lamour, V. (2019). Cryo-EM structure of the complete *E. coli* DNA gyrase nucleoprotein complex. *Nat. Commun.*, 10(1), 4935. <https://doi.org/10.1038/s41467-019-12914-y>
- Vaz Jauri, P., Bakker, M. G., Salomon, C. E., & Kinkel, L. L. (2013). Subinhibitory antibiotic concentrations mediate nutrient use and competition among soil *Streptomyces*. *PLoS One*, 8(12), e81064. <https://doi.org/10.1371/journal.pone.0081064>
- Vidakovic, L., Singh, P. K., Hartmann, R., Nadell, C. D., & Drescher, K. (2018). Dynamic biofilm architecture confers individual and collective mechanisms of viral protection. *Nat Microbiol*, 3(1), 26-31. <https://doi.org/10.1038/s41564-017-0050-1>

- Vining, L. C., & Stuttard, C. (1995). CHAPTER 18 - Chloramphenicol. In L. C. Vining & C. Stuttard (Eds.), *Genetics and Biochemistry of Antibiotic Production* (pp. 505-530). Butterworth-Heinemann. <https://doi.org/10.1016/B978-0-7506-9095-9.50028-9>
- Visnapuu, A., Van der Gucht, M., Wagemans, J., & Lavigne, R. (2022). Deconstructing the Phage-Bacterial Biofilm Interaction as a Basis to Establish New Antibiofilm Strategies. *Viruses*, 14(5). <https://doi.org/10.3390/v14051057>
- Vodolazkaya, N., Nikolskaya, M., Laguta, A., Farafonov, V., Balklava, Z., Stich, M., McHedlov-Petrosyan, N., & Nerukh, D. (2022). Estimation of Nanoparticle's Surface Electrostatic Potential in Solution Using Acid-Base Molecular Probes. III. Experimental Hydrophobicity/Hydrophilicity and Charge Distribution of MS2 Virus Surface. *J Phys Chem B*, 126(41), 8166-8176. <https://doi.org/10.1021/acs.jpcb.2c04491>
- Volff, J.-N., & Altenbuchner, J. (1998). Genetic instability of the *Streptomyces* chromosome. *Mol. Microbiol.*, 27(2), 239-246. <https://doi.org/10.1046/j.1365-2958.1998.00652.x>
- Wachino, J., & Arakawa, Y. (2012). Exogenously acquired 16S rRNA methyltransferases found in aminoglycoside-resistant pathogenic Gram-negative bacteria: an update. *Drug Resist Updat*, 15(3), 133-148. <https://doi.org/10.1016/j.drug.2012.05.001>
- Wagemans, J., Delattre, A. S., Uytterhoeven, B., De Smet, J., Cenens, W., Aertsens, A., Ceyssens, P. J., & Lavigne, R. (2015). Antibacterial phage ORFans of *Pseudomonas aeruginosa* phage LUZ24 reveal a novel MvaT inhibiting protein. *Front Microbiol*, 6, 1242. <https://doi.org/10.3389/fmicb.2015.01242>
- Waksman, S. A., & Woodruff, H. B. (1940). Bacteriostatic and Bactericidal Substances Produced by a Soil Actinomyces. *Proc. Soc. Exp. Biol. Med.*, 45(2), 609-614. <https://doi.org/10.3181/00379727-45-11768>
- Waksman, S. A., & Woodruff, H. B. (1942). Selective Antibiotic Action of Various Substances of Microbial Origin. *J. Bacteriol.*, 44(3), 373-384. <https://doi.org/10.1128/jb.44.3.373-384.1942>
- Wang, X., Kim, Y., Ma, Q., Hong, S. H., Pokusaeva, K., Sturino, J. M., & Wood, T. K. (2010). Cryptic prophages help bacteria cope with adverse environments. *Nat Commun*, 1, 147. <https://doi.org/10.1038/ncomms1146>
- Watve, M. G., Tickoo, R., Jog, M. M., & Bhole, B. D. (2001). How many antibiotics are produced by the genus *Streptomyces*? *Arch Microbiol*, 176(5), 386-390. <https://doi.org/10.1007/s002030100345>
- Wein, T., & Sorek, R. (2022). Bacterial origins of human cell-autonomous innate immune mechanisms. *Nat Rev Immunol*, 22(10), 629-638. <https://doi.org/10.1038/s41577-022-00705-4>
- Willey, J., Santamaria, R., Guijarro, J., Geistlich, M., & Losick, R. (1991). Extracellular complementation of a developmental mutation implicates a small sporulation protein in aerial mycelium formation by *S. coelicolor*. *Cell*, 65, 641-650. [https://doi.org/10.1016/0092-8674\(91\)90096-h](https://doi.org/10.1016/0092-8674(91)90096-h)
- Wösten, H. A., Bohlmann, R., Eckerskorn, C., Lottspeich, F., Bölker, M., & Kahmann, R. (1996). A novel class of small amphipathic peptides affect aerial hyphal growth and surface hydrophobicity in *Ustilago maydis*. *The EMBO Journal*, 15(16), 4274-4281. <https://doi.org/10.1002/j.1460-2075.1996.tb00802.x>
- Wösten, H. A. B. (2001). Hydrophobins: Multipurpose Proteins. *Mol Microbiol*, 55, 625-646. <https://doi.org/10.1146/annurev.micro.55.1.625>

- Wu, R., & Kaiser, A. D. (1968). Structure and Base Sequence in the Cohesive Ends of Bacteriophage Lambda DNA. *J. Mol. Biol.*, 35(3), 523-537. [https://doi.org/10.1016/S0022-2836\(68\)80012-9](https://doi.org/10.1016/S0022-2836(68)80012-9)
- Yin, Y., & Fischer, D. (2008). Identification and investigation of ORFans in the viral world. *BMC Genomics*, 9, 24. <https://doi.org/10.1186/1471-2164-9-24>
- Zhang, Z., Claessen, D., & Rozen, D. E. (2016). Understanding Microbial Divisions of Labor. *Front. Microbiol.*, 7, 2070. <https://doi.org/10.3389/fmicb.2016.02070>
- Zhang, Z., Du, C., de Barsy, F., Liem, M., Liakopoulos, A., van Wezel, G. P., Choi, Y. H., Claessen, D., & Rozen, D. E. (2020). Antibiotic production in *Streptomyces* is organized by a division of labor through terminal genomic differentiation. *Sci Adv.*, 6(3), eaay5781. <https://doi.org/10.1126/sciadv.aay5781>
- Zhang, Z., Shitut, S., Claushuis, B., Claessen, D., & Rozen, D. E. (2022). Mutational meltdown of putative microbial altruists in *Streptomyces coelicolor* colonies. *Nat Commun*, 13(1), 2266. <https://doi.org/10.1038/s41467-022-29924-y>
- Zuo, P., Yu, P., & Alvarez, P. J. J. (2021). Aminoglycosides Antagonize Bacteriophage Proliferation, Attenuating Phage Suppression of Bacterial Growth, Biofilm Formation, and Antibiotic Resistance. *Appl. Environ. Microbiol.*, 87(15), e0046821. <https://doi.org/10.1128/aem.00468-21>

### 3. Publications and manuscripts

Contributions of the listed authors to the manuscripts were described using the 'Contributor Roles Taxonomy (CRediT)' ([CRediT – Contributor Roles Taxonomy \(niso.org\)](https://niso.org/CRediT-Contributor-Roles-Taxonomy)):

Contributor role	Definition
<b>Conceptualization</b>	Ideas; formulation or evolution of overarching research goals and aims
<b>Data curation</b>	Management activities to annotate (produce metadata), scrub data and maintain research data (including software code, where it is necessary for interpreting the data itself) for initial use and later re-use
<b>Formal analysis</b>	Application of statistical, mathematical, computational, or other formal techniques to analyse or synthesize study data
<b>Funding acquisition</b>	Acquisition of the financial support for the project leading to this publication
<b>Investigation</b>	Conducting a research and investigation process, specifically performing the experiments, or data/evidence collection
<b>Methodology</b>	Development or design of methodology; creation of models
<b>Project administration</b>	Management and coordination responsibility for the research activity planning and execution
<b>Resources</b>	Provision of study materials, reagents, materials, patients, laboratory samples, animals, instrumentation, computing resources, or other analysis tools
<b>Software</b>	Programming, software development; designing computer programs; implementation of the computer code and supporting algorithms; testing of existing code components
<b>Supervision</b>	Oversight and leadership responsibility for the research activity planning and execution, including mentorship external to the core team
<b>Validation</b>	Verification, whether as a part of the activity or separate, of the overall replication/reproducibility of results/experiments and other research outputs
<b>Visualization</b>	Preparation, creation and/or presentation of the published work, specifically visualization/data presentation
<b>Writing – original draft</b>	Preparation, creation and/or presentation of the published work, specifically writing the initial draft (including substantive translation)
<b>Writing – review and editing</b>	Preparation, creation and/or presentation of the published work by those from the original research group, specifically critical review, commentary or revision – including pre- or post-publication stages

### 3.1. Identification of Gip as a novel phage-encoded gyrase inhibitor protein of *Corynebacterium glutamicum*

Keuer, L., Hünnefeld, M., Brehm, J., Heermann, R. and Frunzke, J.

Published in Molecular Microbiology, 2021

Contributor role	Contributor
Conceptualization	LK (50%), MH (20%), JF (30%)
Data curation	LK (80%), MH (10%), JB (10%)
Formal analysis	LK (65%), MH (25%), JB (10%)
Funding acquisition	JF (95%), RH (5%)
Investigation	LK (80%), MH (10%), JB (10%)
Methodology	LK (60%), MH (30%), JB (10%)
Project administration	LK (50%), MH (30%), JF (20%)
Resources	-
Software	-
Supervision	JF (50%), LK (25%) MH (15%), JB (7.5%), RH (2.5%)
Validation	LK (65%), MH (25%), JB (10%)
Visualization	LK (100%)
Writing – original draft	LK (70%), JF (30%)
Writing – review and editing	LK (40%), JF (40%), MH (10%), JB (5%), RH (5%)

#### Overall contribution: 80%

Most of the presented experimental work and data analysis was done by LK except the pull-down assay done in cooperation Rebecca Lukaschewsky during her bachelor thesis (Figure 3a), the SPR spectroscopy done by JB (Figure 3b), MALDI-TOF-MS done in cooperation with Christina Mack from the research group of Prof. Dr. Michael Bott and Dr. Meike Baumgart from the Forschungszentrum Jülich GmbH, LC-MS/MS analysis done in cooperation with Astrid Wirtz from the research group of Dr. Tino Polen from the Forschungszentrum Jülich GmbH as well as initial screenings (Figure 1 and S1) and analysis of DNA microarrays (Table 1 and S4) done in cooperation with MH. The visualization of the obtained data was performed by LK. The original draft was mainly prepared by LK and LK was significantly involved in the revision and editing process.

Received: 9 April 2021 | Revised: 14 September 2021 | Accepted: 14 September 2021

DOI: 10.1111/mmi.14813

## RESEARCH ARTICLE

WILEY

# Identification of Gip as a novel phage-encoded gyrase inhibitor protein of *Corynebacterium glutamicum*

Larissa Kever<sup>1</sup> | Max Hünnefeld<sup>1</sup> | Jannis Brehm<sup>2</sup> | Ralf Heermann<sup>2</sup> | Julia Frunzke<sup>1</sup> <sup>1</sup>Institute of Bio- und Geosciences, IBG-1: Biotechnology, Forschungszentrum Jülich, Jülich, Germany<sup>2</sup>Institut für Molekulare Physiologie, Biozentrum II, Mikrobiologie und Weinforschung, Johannes-Gutenberg-Universität Mainz, Mainz, Germany**Correspondence**Julia Frunzke, Institute of Bio- und Geosciences, IBG-1: Biotechnology, Forschungszentrum Jülich, 52425 Jülich, Germany.  
Email: j.frunzke@fz-juelich.de**Funding information**

H2020 European Research Council, Grant/Award Number: 757563; Helmholtz-Gemeinschaft, Grant/Award Number: W2/W3-096

**Abstract**

By targeting key regulatory hubs of their host, bacteriophages represent a powerful source for the identification of novel antimicrobial proteins. Here, a screening of small cytoplasmic proteins encoded by the CGP3 prophage of *Corynebacterium glutamicum* resulted in the identification of the gyrase-inhibiting protein Cg1978, termed Gip. Pull-down assays and surface plasmon resonance revealed a direct interaction of Gip with the gyrase subunit A (GyrA). The inhibitory activity of Gip was shown to be specific to the DNA gyrase of its bacterial host *C. glutamicum*. Overproduction of Gip in *C. glutamicum* resulted in a severe growth defect as well as an induction of the SOS response. Furthermore, reporter assays revealed an RecA-independent induction of the cryptic CGP3 prophage, most likely caused by topological alterations. Overexpression of *gip* was counteracted by an increased expression of *gyrAB* and a reduction of *topA* expression at the same time, reflecting the homeostatic control of DNA topology. We postulate that the prophage-encoded Gip protein plays a role in modulating gyrase activity to enable efficient phage DNA replication. A detailed elucidation of the mechanism of action will provide novel directions for the design of drugs targeting DNA gyrase.

**KEYWORDS**

bacteriophages, DNA gyrase, gyrase inhibitors, prophage induction, topoisomerase II inhibitors

## 1 | INTRODUCTION

Bacteriophages represent the "dark matter" of the biological world (Hatfull, 2015; Ofir & Sorek, 2018; Rohwer & Youle, 2011). With the recent massive expansion of the genomic sequence space, the number of functionally unknown open reading frames (ORFs) in phage genomes is continuously increasing (Yin & Fischer, 2008). By targeting diverse cellular processes and regulatory hubs in their host cell, bacteriophages represent a rich source for the identification of novel antibacterial proteins as well as for the establishment of highly

efficient molecular tools (De Smet et al., 2017; Nobrega et al., 2018; Roach & Donovan, 2015; Schroven et al., 2021). Especially, small cytoplasmic phage proteins have been shown to influence and reprogram a variety of key cellular processes, including transcription, translation, cell division, and central metabolism (De Smet et al., 2017; Orr et al., 2020; Storz et al., 2014).

DNA gyrase represents a type IIA topoisomerase present in all bacteria and plays a crucial role in the homeostatic control of DNA topology. Because of its unique ability to introduce negative supercoils into covalently linked double-stranded DNA (dsDNA), the

This is an open access article under the terms of the Creative Commons Attribution-NonCommercial License, which permits use, distribution and reproduction in any medium, provided the original work is properly cited and is not used for commercial purposes.  
© 2021 The Authors. *Molecular Microbiology* published by John Wiley & Sons Ltd.

activity of DNA gyrase is indispensable for bacterial growth and a key target of antibacterial agents. The heterotetrameric enzyme consists of two GyrA and two GyrB subunits (GyrA<sub>2</sub>GyrB<sub>2</sub>). While the GyrA subunit of the enzyme catalyzes the breakage and resealing of dsDNA, the GyrB subunit exhibits ATPase activity (Bush et al., 2015; McKie et al., 2021; Vanden Broeck et al., 2019). Currently, two major classes of small molecule drugs targeting the bacterial gyrase are known: the aminocoumarins and the quinolones (Collin et al., 2011). Besides a range of small molecules, also some proteinaceous, bacterial toxins were found to inhibit the activity of the gyrase, including Microcin B17 (Pierrat & Maxwell, 2003), a glycine-rich peptide found in *Escherichia coli* strains carrying the *mcb* operon as well as the CcdB toxin as part of the *ccd* toxin-antitoxin system encoded by the *F*-plasmid (Dao-Thi et al., 2005; Miki et al., 1992).

*Corynebacterium glutamicum*—a member of the phylum Actinobacteria—is an important industrial platform organism used for the industrial production of a wide range of value-added compounds, including amino acids, organic acids, and proteins (Wendisch et al., 2016). The genome of the model organism *C. glutamicum* ATCC 13032 contains four cryptic prophages (CGP1-4) (Frunzke et al., 2008; Ikeda & Nakagawa, 2003). The largest prophage CGP3 (~219 kb, containing also prophage CGP4) was shown to be inducible in an SOS-dependent manner as well as in an SOS-independent manner (Helfrich et al., 2015; Nanda et al., 2014; Pfeifer et al., 2016). Recently, the Lsr2-type protein CgpS was identified as a prophage-encoded nucleoid-associated protein involved in the silencing of phage gene expression maintaining the lysogenic state of the large CGP3 prophage (Pfeifer et al., 2016). Interference with CgpS binding was shown to result in prophage activation and consequently cell death.

In this study, a systematic screening of small cytoplasmic proteins encoded by the CGP3 prophage of *C. glutamicum* resulted in the identification of phage proteins causing severe growth defects and prophage induction. The small phagic protein Cg1978 was further shown to directly target the DNA gyrase enzyme by interacting with the GyrA subunit and inhibiting the supercoiling activity of the *C. glutamicum* DNA gyrase *in vitro*. Cg1978 was therefore termed Gip for gyrase inhibiting protein. A detailed elucidation of the mechanism of action may point to novel directions for the design of drugs targeting DNA gyrase.

## 2 | RESULTS

### 2.1 | Systematic screening of small CGP3-encoded proteins influencing growth and prophage induction

Most of the proteins encoded by the cryptic CGP3 prophage are of unknown function. Phage proteins were shown to frequently target key regulatory hubs to shut down bacterial metabolism (Roach & Donovan, 2015). In this study, we screened the impact of overall 11 small (<75 amino acids), cytoplasmic phage-encoded proteins on cellular growth and prophage induction. For this purpose, plasmid-based overexpression (pAN6-GOI) of the selected genes of interest

was performed in the prophage reporter strain *C. glutamicum* ATCC 13032::P<sub>lys</sub>-*eyfp*. In previous studies, this chromosomal reporter (P<sub>lys</sub>-*eyfp*) was successfully established to translate prophage activation into a fluorescent output (Helfrich et al., 2015). During cultivation, biomass was measured as a function of backscattered light intensity with an excitation wavelength of 620 nm. Following this approach, the overproduction of 9 out of 11 phage proteins (Cg1902, Cg1910, Cg1924, Cg1925, Cg1971, Cg2026, Cg2035, Cg2045, and Cg2046) displayed comparable phenotypes as the empty vector control regarding backscatter signal and fluorescence output measured via flow cytometry (Figure 1c and Figure S1a,b). By contrast, overproduction of Cg1914 and Cg1978 showed a significant effect on growth and prophage induction in the presence of 50 μM IPTG. Cg1914 overproduction resulted in a reduced growth rate ( $\mu = 0.23 \pm 0.01 \text{ hr}^{-1}$ ) and a reduced final backscatter (Figure 1a, blue line) compared with the empty vector control pAN6 ( $\mu = 0.38 \pm 0.01 \text{ hr}^{-1}$ ). In the case of Cg1978, overproduction led to an elongated lag-phase, but the final backscatter as well as the growth rate in the exponential phase ( $\mu = 0.36 \pm 0.01 \text{ hr}^{-1}$ ) (Figure 1a, red line) were comparable with those of the empty vector control.

A comparable impact on cell growth due to cg1914 or cg1978 overexpression was also detected in the prophage-free strain MB001, indicating that the observed growth defect was independent of the presence and/or activity of the CGP3 island (Figure 1b).

For both target proteins, Cg1914 and Cg1978, overproduction resulted in an increased fluorescence signal after 24 hr of cultivation (cg1914:  $7.4 \pm 2.6\%$  induced cells, cg1978:  $3.5 \pm 0.2\%$  induced cells) indicating CGP3 prophage induction in the respective subpopulation (Figure 1c). As a positive control, we expressed an N-terminally truncated variant of the prophage silencer CgpS (CgpS-N), which was previously shown to trigger prophage induction (Pfeifer et al., 2016).

Since overproduction of Cg1914 and Cg1978 showed a high impact on prophage induction, we tested the inducibility of the CGP3 prophage in mutants lacking the respective genes using a plasmid-based prophage reporter (P<sub>lys</sub>-*lys*-*venus*). Remarkably, the corresponding strains *C. glutamicum* ATCC 13032 Δcg1914 and Δcg1978 featured no difference—neither in cell growth nor in prophage inducibility—upon treatment with the DNA-damaging antibiotic mitomycin C (Tomasz, 1995), which was used to trigger SOS-dependent prophage induction (Figure S2). These results indicated that both proteins are not essentially involved in SOS-dependent CGP3 induction. Prophage induction, therefore, appeared to be an indirect effect of Cg1914 or Cg1978 overproduction. Based on further results described in the following, we focused on the role and cellular target of the small phage protein Cg1978.

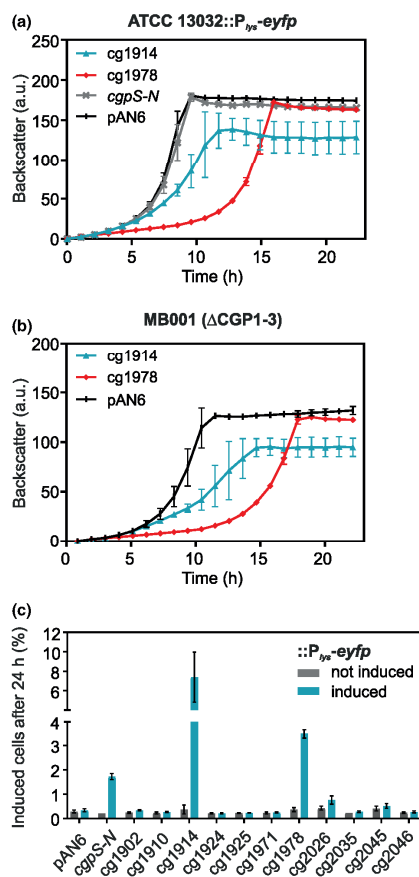
### 2.2 | Overproduction of Cg1978 triggers the activation of SOS response and RecA-independent prophage induction

As the CGP3 prophage was already characterized to be inducible in an SOS-dependent manner as well as in an SOS-independent

manner (Helfrich et al., 2015; Nanda et al., 2014; Pfeifer et al., 2016), we determined the SOS dependency of Cg1978-mediated prophage induction. To this end, the fluorescent outputs of different reporter strains were measured via flow cytometry in a time-resolved manner during cg1978 overexpression. Besides the prophage reporter strain (C.g. ATCC 13032::P<sub>lys</sub>-eyfp), an SOS reporter strain (C.g. ATCC 13032::P<sub>recA</sub>-venus) as well as an SOS-deficient prophage reporter strain (C.g. ATCC 13032 ΔrecA::P<sub>lys</sub>-eyfp) lacking the coprotease RecA—required for the induction of the host SOS response (Janion, 2008)—were used.

As described above, overexpression of cg1978 resulted in a similar growth phenotype of all reporter strains characterized by an elongated lag-phase (marked in gray) with subsequent wild type-like growth (Figure 2a). The impaired cell growth under cg1978 overexpression conditions was confirmed by time-lapse fluorescent

**FIGURE 1** Screening of small phagic proteins regarding their impact on cellular growth and CGP3 induction in *Corynebacterium glutamicum*. The cultivation of the prophage-reporter strain *C. glutamicum* ATCC 13032::P<sub>lys</sub>-eyfp and the prophage-free strain MB001 carrying the corresponding gene sequences of the small proteins on the pAN6 vector (under control of P<sub>tac</sub>) was performed in CGXII-Kan<sub>25</sub> medium with 2% (w/v) glucose and 50 μM IPTG for 24 hr. All data represent mean values with standard deviations from three independent biological replicates (*n* = 3). (a) Growth curves of the prophage reporter strain (*C. glutamicum* ATCC 13032::P<sub>lys</sub>-eyfp) upon small protein overproduction are based on the backscatter measurements in the BioLector® microcultivation system. (b) Growth curves of the prophage-free strain MB001 upon small protein overproduction are based on the backscatter measurements in the BioLector® microcultivation system. (c) Percentage of induced cells after 24 hr cultivation without and with 50 μM IPTG based on the flow cytometric measurements of the prophage reporter strain *C. glutamicum* ATCC 13032::P<sub>lys</sub>-eyfp



microscopy of a *C. glutamicum* microcolony of the prophage reporter strain, which was grown in a microfluidic chamber. Increased levels of Cg1978 led to elongated cell morphology and a small fraction of cells featuring a strongly increased output of the prophage reporter (Figure 2c and Videos S1 and S2).

Measurement of the reporter output over time not only confirmed CGP3 induction but also revealed an induction of the cellular SOS response (Figure 2b). Interestingly, the wild type-like and the RecA-deficient prophage reporter strain showed nearly the same percentage of induced cells upon cg1978 overexpression throughout the entire measurement, reaching a peak value after 9.5 hr of cultivation (ΔrecA::P<sub>lys</sub>-eyfp:  $4.6 \pm 0.7$ , P<sub>lys</sub>-eyfp:  $4.8 \pm 0.9$ ). These results emphasize RecA-independent CGP3 induction as an indirect effect of cg1978 overexpression.

Remarkably, all reporter strains revealed an increasing fluorescence during the lag-phase, which decreased again upon transition into the exponential growth phase (Figure 2b), suggesting the growth of a subpopulation resistant to Cg1978 overproduction effects.

### 2.3 | Cg1978 directly interacts with gyrase subunit A (GyrA)

To identify the direct cellular target of Cg1978, we performed an in vitro pull-down assay. For this purpose, the small protein Cg1978 containing a C-terminal Strep-tag was overproduced in *E. coli* BL21 (DE3) and purified via affinity purification. The purified target protein was incubated with *C. glutamicum* cell extract and this sample was again passed over a Strep-Tactin column to identify proteins copurifying with Cg1978. SDS PAGE analysis of proteins coeluting with Cg1978 revealed an additional protein band at ~100 kDa (Figure 3a). Analysis of the copurified protein via MALDI-TOF as well as LC-MS/MS analysis of the whole elution fraction indicated the copurification of Cg1978 with *C. glutamicum* (C.g.) DNA gyrase subunit A (~95 kDa), a subunit of the heterotetrameric ATP-dependent DNA gyrase complex (A<sub>2</sub>B<sub>2</sub>). The DNA gyrase belongs



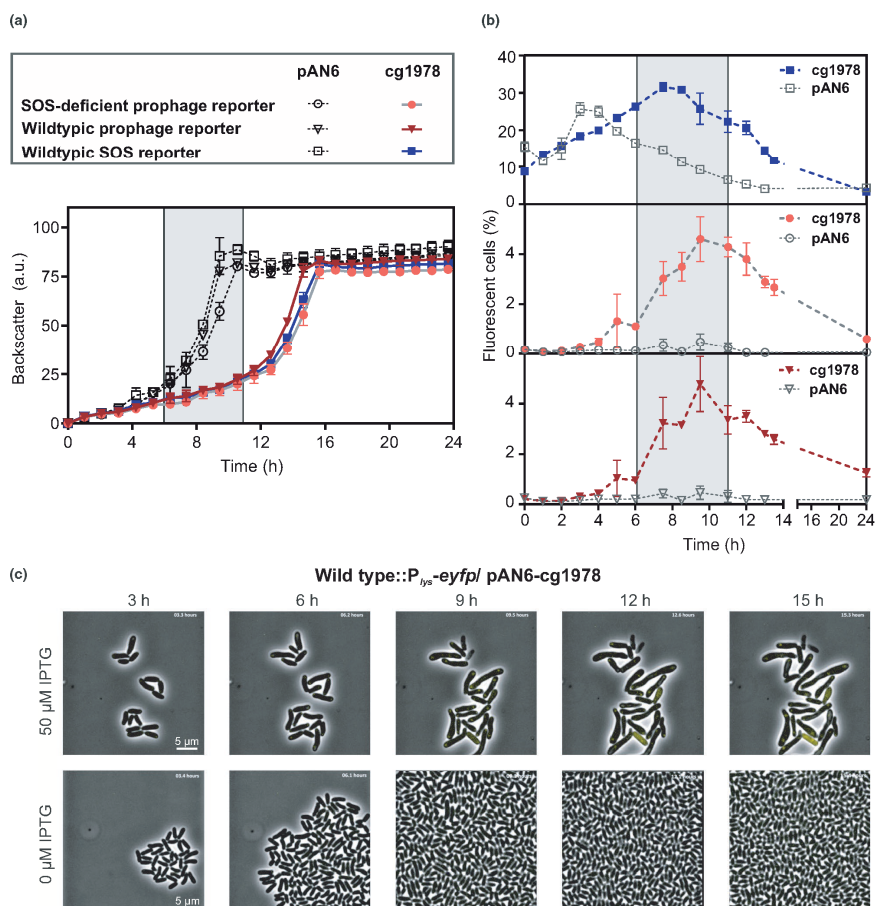


**FIGURE 2** Time-resolved measurement of reporter outputs upon Cg1978 overproduction in *Corynebacterium glutamicum* showed activation of SOS response and RecA-independent prophage induction. Cultivation of an SOS reporter strain ATCC 13032::P<sub>recA</sub>-venus, a prophage reporter strain ATCC 13032::P<sub>lys</sub>-eyfp and an SOS-deficient prophage reporter strain ATCC 13032  $\Delta$ recA::P<sub>lys</sub>-eyfp carrying the plasmids pAN6 or pAN6-cg1978 was performed in the BioLector<sup>®</sup> microcultivation system in CGXII-Kan<sub>25</sub> medium with 2% (w/v) glucose and 50  $\mu$ M IPTG. All data represent mean values with SDs from three independent biological replicates ( $n = 3$ ). (a) Growth curves based on the backscatter measurements in the BioLector<sup>®</sup> microcultivation system. The elongated lag-phase of the Cg1978 overproducing strain is marked in gray. (b) Percentage of induced cells based on the flow cytometric measurements of eYFP or Venus fluorescence of the reporter strains. (c) Time-lapse fluorescence imaging of the *C. glutamicum* prophage reporter strain ATCC 13032::P<sub>lys</sub>-eyfp carrying the pAN6-cg1978 plasmid. Cells were cultivated in PDMS-based microfluidic chip devices (Grünberger et al., 2015) using CGXII-Kan<sub>25</sub> medium with 2% (w/v) glucose. The medium was continuously supplied with a flow rate of 300 nL/min. Overexpression of cg1978 was induced by the addition of 50  $\mu$ M IPTG. Fluorescent images represent cutouts from Videos S1 and S2

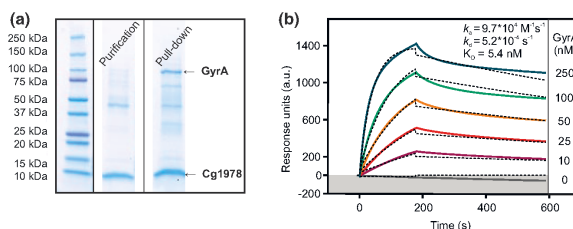


**FIGURE 3** Cg1978 directly interacts with the gyrase subunit A (GyrA) in vitro. (a) The small protein Cg1978 containing a C-terminal Strep-tag was overproduced in *Escherichia coli* BL21 (DE3) and purified via affinity purification. For the pull-down assay, the *Corynebacterium glutamicum* wild-type strain was cultivated in BHI medium until  $OD_{600}$  of 6. The purified target protein was incubated with *C. glutamicum* cell extract and again passed over a Strep-Tactin column aiming at the copurification of Cg1978 with possible interaction partners. Proteins in the elution fractions were analyzed via SDS-PAGE using the Precision Plus Protein™ Dual protein marker as a standard and further identified using LC-MS/MS and MALDI-TOF. Gels were spliced for labeling purposes. (b) Surface plasmon resonance spectroscopy of GyrA-N-Strep binding to Cg1978-C-His ( $k_a$ , association constant;  $k_d$ , dissociation constant,  $K_D$ , equilibrium dissociation constant). The colored lines represent the experimental data, the dotted lines represent the fitted data using a 1:1 binding algorithm that was the basis for the binding kinetics calculation

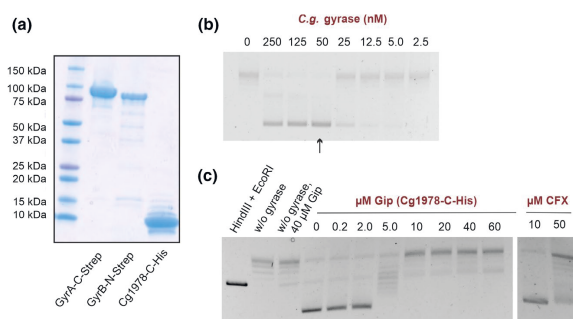


**FIGURE 4** Cg1978 inhibits gyrase supercoiling activity in vitro. The assay was conducted according to the manual of the *Mycobacterium tuberculosis* Gyrase (HIS) Supercoiling Assay Kit from Inspiralis (Norwich, UK). (a) Cg1978 containing a C-terminal His-tag as well as gyrase subunit A containing a C-terminal and subunit B containing an N-terminal Strep-tag were separately overproduced in *Escherichia coli* BL21 (DE3) and purified via affinity purification. (b) After formation of the heterotetrameric gyrase complex, the activity assay of the purified DNA gyrase from *Corynebacterium glutamicum* ATCC 13032 was performed to identify the gyrase concentration required for maximal supercoiling of 0.5 μg relaxed plasmid DNA, which was defined as 1 U. (c) Supercoiling inhibition assay to test the inhibitory effect of Cg1978 on 1 U of the DNA gyrase from *C. glutamicum* ATCC 13032. Incubation of relaxed plasmid DNA with Cg1978 in the absence of DNA gyrase was used as a negative control to screen for any nuclease activity. The known gyrase inhibitor Ciprofloxacin (CFX) served as a positive control for efficient gyrase inhibition. Two agarose gels were compiled as indicated by the boundaries

to the subclass of type II topoisomerases and plays a key role in DNA metabolism as it is able to introduce negative supercoiling to double-stranded DNA in an ATP-dependent manner. Gyrase subunit B was also detected in the elution fraction, but in a significantly lower amount compared to GyrA rather suggesting unspecific copurification.

As a next step, surface plasmon resonance spectroscopy was used to examine the binding affinity of Cg1978 to GyrA. The sensorgram revealed a stable and specific 1:1 interaction between Cg1978 and GyrA with a high association rate ( $k_a = 9.7 \times 10^4 \text{ M}^{-1} \text{ s}^{-1}$ ) and a slow dissociation rate ( $k_d = 5.2 \times 10^{-4} \text{ s}^{-1}$ ) resulting in an overall

affinity ( $K_D$ ) of 5.4 nM (Figure 3b). Purification of Cg1978-C-His and GyrA-N-Strep for SPR analysis are shown in Figure S3.

## 2.4 | Cg1978 inhibits DNA supercoiling via interaction with the DNA gyrase in vitro

Due to its essential role for cell survival, DNA gyrase represents an important drug target of antibiotics and protein-based inhibitors (Collin et al., 2011). Based on the observed growth defect upon Cg1978 overproduction and the interaction with GyrA, we

further assessed the effect of Cg1978 on gyrase activity by performing *in vitro* supercoiling inhibition assays with the purified enzyme.

For this purpose, Cg1978-C-His, GyrA-C-Strep, and GyrB-N-Strep from *C. glutamicum* were purified separately using affinity chromatography (Figure 4a). The formation of the heterotetrameric enzyme complex was obtained by incubating equimolar amounts of both gyrase subunits on ice for 30 min. In the first step, the activity of the purified C.g. DNA gyrase was measured by incubating 0.5  $\mu$ g relaxed pBR322 plasmid DNA with different C.g. gyrase concentrations. The addition of increasing C.g. gyrase concentrations led to an increase in supercoiling of the plasmid DNA resulting in maximal supercoiling using 50 nM of C.g. gyrase. This concentration was defined as 1 U (corresponding to a specific activity of  $1.88 \times 10^3$  U/mg) and was used for testing the potential inhibitory effect of Cg1978 (Figure 4b).

As shown in Figure 4c, incubation of increasing concentrations of Cg1978 (0.2–60  $\mu$ M) with 1 U C.g. DNA gyrase and relaxed plasmid DNA resulted in a decreased supercoiling activity of the C.g. DNA gyrase. Complete inhibition of the introduction of supercoils by DNA gyrase was achieved by the addition of 10  $\mu$ M Cg1978 leading to an accumulation of the relaxed/nicked conformation. Therefore, we named the gene product of cg1978 Gip (gyrase inhibiting protein).

As a negative control, Gip was incubated with relaxed plasmid DNA in absence of DNA gyrase to visualize any potential nuclease activity in the elution fraction of Gip. A slight band reflecting linear DNA could be detected when adding 40  $\mu$ M Gip. However, incubating increasing concentrations of Gip with the C.g. DNA gyrase did not lead to an accumulation of linear DNA. As a positive control, the known fluoroquinolone-based gyrase-inhibitor ciprofloxacin (CFX) stabilizing the gyrase-DNA cleavage complex (Drlica & Malik, 2003) was used showing significant inhibition of the supercoiling activity of the C.g. gyrase at 50  $\mu$ M (16.6  $\mu$ g/ml). This was in line with already published data for the DNA gyrase of *Mycobacterium smegmatis*, which showed 50% inhibition of the supercoiling activity of 1 U gyrase by the addition of 10  $\mu$ g/ml CFX (Manjunatha et al., 2002). As for Gip, inhibition of the DNA gyrase via CFX led to an accumulation of the relaxed/nicked plasmid conformation.

To further investigate the activity profile of Gip, we determined its effect on the DNA gyrases of *Mycobacterium tuberculosis* and *E. coli*. Gyrase subunits A of the actinobacterial species *C. glutamicum* and *M. tuberculosis* (*M.tb.*) share a sequence identity of ~71%, while GyrA of *C. glutamicum* and *E. coli* (*E.c.*) only show a ~45% sequence identity (Figures S4 and S5). As described previously for the DNA gyrase of *C. glutamicum*, 1 U of the *E.c.* and *M.tb.* gyrases were used to examine supercoiling inhibition via Gip. The supercoiling assay showed no significant change in the supercoiling activity of the respective gyrases when adding increasing concentrations of Gip. In case of the *M.tb.* gyrase, a slight shift from supercoiled plasmid DNA to linear plasmid DNA could be detected by addition of 40  $\mu$ M Gip, which was even less pronounced for the *E.c.* gyrase. The corresponding assays are shown in Figure S6.

## 2.5 | Compensatory expression of *gyrAB* and *topA* as a response to gyrase inhibition via Gip

Supercoiling inhibition assays showed that Cg1978 (Gip) is a gyrase-inhibiting protein. As the activity of DNA gyrase is indispensable for bacterial growth, we investigated the impact of *gip* overexpression on the transcriptome of *C. glutamicum*. Since the *gip* overexpressing strain revealed a wild type-like growth rate after an elongated lag-phase, we were especially interested to understand how the bacterial host counteracts gyrase inhibition. For this purpose, comparative transcriptome analysis of the *C. glutamicum* ATCC 13032 strain containing the empty vector control and the strain containing the overexpression plasmid pAN6-*gip* was performed using DNA microarrays. The shown transcriptomic changes are based on mRNA levels of cells harvested at an OD<sub>600</sub> of 6 in the mid-exponential growth phase.

The *gip* overexpressing strain showed a partial upregulation of CGP3 genes due to overexpression of *gip* (Table S4), confirming the prophage induction also revealed by the above-described reporter assays. Apart from the CGP3 region, overexpression of *gip* led to upregulation of 352 genes and downregulation of 333 genes reflecting the high impact of gyrase inhibition on overall cell metabolism.

Interestingly, both gyrase subunits *gyrA* and *gyrB* were markedly upregulated showing a more than 4-fold increase in expression levels (Table 1). In contrast, *topA* coding for topoisomerase I, which catalyzes the opposing reaction of DNA gyrase by removing negative supercoils, showed a reduced expression level. Moreover, the expression of further genes involved in DNA metabolism was influenced by *gip* overexpression including for example the reduced expression of genes coding for helicases (exemplarily cg0838, cg0842, cg0843, cg0845, cg0889, and cg1498). Additionally, 10 targets of the SOS key player LexA, for example, *recN* (DNA repair) and *ftsK* (cell division and chromosome segregation), showed an increased mRNA ratio, which was in line with the high fluorescent outputs of the SOS reporter strain upon Gip overproduction (Table 1, see Table S4 for the complete list of genes with altered expression levels).

## 3 | DISCUSSION

In this study, a screening of small cytoplasmic proteins encoded by the CGP3 prophage of *C. glutamicum* resulted in the identification of the novel gyrase inhibitor protein Gip (Cg1978, 6.8 kDa). Overproduction of Gip resulted in significant growth defects and prophage induction in a subpopulation. Further characterization of this small phagic protein confirmed a specific, stable, and high-affinity interaction with the GyrA subunit and inhibition of the supercoiling activity of the DNA gyrase *in vitro*.

DNA gyrase possesses the unique ability to catalyze the ATP-dependent negative supercoiling of double-stranded DNA by cleaving and rejoining it (Bush et al., 2015). Supercoiling inhibition assays showed that Gip-mediated gyrase inhibition resulted in the accumulation of the nicked/relaxed plasmid conformation, while no more

Gene locus	Gene name	Annotation	mRNA ratio
Genes coding for proteins involved in DNA metabolism			
cg0015	<i>gyrA</i>	DNA gyrase subunit A, DNA topoisomerase II	6.23
cg0007	<i>gyrB</i>	DNA gyrase subunit B, DNA topoisomerase II	4.44
cg0373	<i>topA</i>	DNA topoisomerase I	0.40
cg0845		Putative superfamily II DNA/RNA helicase, SNF2 family	0.49
cg0889		Putative DNA helicase RecQ	0.48
cg0843		Putative helicase	0.45
cg1498		Putative RecG-like helicase	0.43
cg0842		Putative DNA helicase	0.39
cg0838		Putative helicase	0.22
LexA target genes			
cg1602	<i>recN</i>	DNA repair protein	10.96
cg1255		Putative HNH endonuclease, conserved	5.11
cg1977		Putative secreted protein	4.52
cg0470	<i>htaB</i>	Secreted heme transport-associated protein	4.41
cg0738	<i>dnaE2</i>	DNA polymerase III subunit $\alpha$	3.11
cg1288		Putative multidrug efflux permease of the major facilitator superfamily	2.83
cg1080		Putative multicopper oxidase	2.67
cg2158	<i>ftsK</i>	Cell division protein	2.46
cg0713		Hypothetical protein	2.13
cg2114	<i>lexA</i>	Transcriptional regulator, involved in SOS/stress response	2.09
cg2950	<i>radA</i>	Putative ATP-dependent protease, DNA repair	0.48
cg2381		Hypothetical protein	0.47
cg0834	<i>tusE</i>	Bacterial extracellular solute-binding protein, trehalose uptake system	0.34
cg0841		Hypothetical protein	0.31
cg1314	<i>putP</i>	Proline transport system	0.30
cg3345		Hypothetical protein	0.24

TABLE 1 Impact of *gip* (cg1978) overexpression on global expression levels

Note: A genome-wide comparison of mRNA levels of the *Corynebacterium glutamicum* ATCC 13032 strain overexpressing *gip* and the wild-type strain carrying the empty vector control was performed. The shown mRNA ratios indicate mean values from three independent biological replicates ( $n = 3$ ). The strains were cultivated in CGXII-Kan<sub>25</sub> minimal medium with 2% (w/v) glucose and 50  $\mu$ M IPTG and mRNA was prepared from cells harvested at an OD<sub>500</sub> of 6. The mRNA ratios were calculated by dividing the mRNA levels of the *gip* overexpressing strain by the mRNA levels of the strain carrying the empty vector control. The table includes selected genes from a larger set which showed a changed mRNA level in all experiments (mRNA ratio >2.0: upregulation [red] or <0.5: downregulation [green],  $p$ -value <0.05).

supercoiled plasmid DNA was detectable (Figure 4). Different molecular mechanisms of gyrase inhibition have been described so far. Fluoroquinolones and the well-characterized proteinaceous bacterial toxins Microcin B17 (MccB17, 3.1 kDa) and CcdB (11.7 kDa) poison the DNA gyrase by stabilizing the gyrase-DNA cleavage complex leading to double-strand DNA breaks (Bernard et al., 1993; Drlica & Malik, 2003; Pierrat & Maxwell, 2003). In contrast, aminocoumarins

(c.g. novobiocin) inhibit ATP hydrolysis as the binding site overlaps with the ATP-binding pocket of the GyrB subunit (Maxwell & Lawson, 2003). Further proteins targeting DNA gyrase are pentapeptide repeat proteins (PRPs) like Qnr proteins or MfpA, whose inhibitory interaction is proposed to be based on DNA mimicry (Shah & Heddle, 2014). However, no conserved domains of *Gip* with other known proteinaceous gyrase inhibitors could be identified using the

conserved domain database (CDD) with Reverse Position-Specific BLAST (RPS-BLAST) (Lu et al., 2020). Accordingly, further studies and structural analysis are required to elucidate the exact molecular mechanism of Gip-mediated gyrase inhibition.

Investigations regarding the activity profile of Gip suggested that the inhibitory activity seems to be highly specific for the DNA gyrase of its bacterial host *C. glutamicum*, as the DNA gyrase of *M. tuberculosis* and *E. coli* were not significantly affected by Gip. Similar observations were made for the proteinaceous bacterial toxins Microcin B17 (MccB17, 3.1 kDa) and CcdB (11.7 kDa), which target the DNA gyrase of their host *E. coli* in vitro, while no inhibition of the DNA gyrase of *M. smegmatis* could be detected (Chatterji et al., 2001). Even though DNA gyrase is a conserved protein among bacteria, Gram-positive and Gram-negative bacteria show substantial differences in the amino acid sequence of GyrAB (Madhusudan & Nagaraja, 1996; Manjunatha et al., 2000). Accordingly, the absence of specific target residues potentially explains the different levels of susceptibility of the DNA gyrase to proteinaceous toxins (Chatterji et al., 2001).

Reporter outputs of the RecA-dependent SOS reporter strain and transcriptomic analysis of Gip overproducing cells revealed an induction of the SOS response (Figure 2b, Table 1). These findings are in agreement with already published data describing activation of the SOS response as one of the pleiotropic effects of gyrase inhibition (Jeong et al., 2006). Stabilization of the gyrase-cleaved DNA complex results in arrested replication forks and widespread DNA damage by stimulating the formation of DNA breaks triggering the SOS response (DeMarini & Lawrence, 1992; Dwyer et al., 2007).

Gip overproduction was further shown to activate the induction of the CGP3 prophage. However, the fact that the observed growth defect of Gip overproducing cells is independent of the presence of the CGP3 prophage (Figure 1b) and that deletion of *gip* did not result in altered inducibility of CGP3 (Figure S2) emphasize prophage activation as an indirect effect of Gip overproduction. Recent studies already confirmed that CGP3 is inducible in an SOS-dependent manner as well as in an SOS-independent manner (Helfrich et al., 2015; Nanda et al., 2014; Pfeifer et al., 2016). As the wild type and the RecA-deficient prophage reporter strain revealed nearly identical fluorescent outputs, we propose that prophage induction occurred mainly in a RecA-independent manner. Here, influencing the introduction of supercoils due to gyrase inhibition might be a possible reason for CGP3 induction. The lysogenic state of CGP3 is maintained by the Lsr2-type silencer protein CgpS, which was shown to target more than 35 AT-rich regions within the CGP3 element (Pfeifer et al., 2016). The formation of this dense nucleoprotein complex was shown to be crucial for efficient CgpS-mediated silencing (Wiechert et al., 2020). Especially in the case of proteins-targeting AT-rich DNA sequences, the topologic state of DNA can affect protein–DNA interactions (Dorman & Dorman, 2016). Apart from that, different studies already demonstrated an influence of DNA supercoiling on the  $\lambda$  repressor and the lysogenic-lytic decision of phage  $\lambda$  (Ding et al., 2014; Norregaard et al., 2013, 2014).

In general, it is conceivable that the CGP3 prophage could have an advantage from encoding a gyrase inhibitor as it might allow a

more efficient phage DNA replication by modulating host gyrase activity. Similar assumptions were recently made for the topo I inhibitor protein gp55.2 encoded by the T4 phage of *E. coli*. It was hypothesized that modulating DNA relaxation activity of topo I is required for an optimal phage yield during infection (Mattenberger et al., 2015). Another example of a phage-encoded protein altering DNA topology is represented by the gyrase-inhibiting peptide Igy encoded by phage LUZ24 infecting *Pseudomonas aeruginosa* (De Smet et al., 2021). Interaction of Igy with GyrB, possibly by functioning as a DNA mimicry protein, inhibits the DNA gyrase and LUZ24 infection seems to be independent of a functioning host DNA gyrase.

Global topological alterations caused by Gip overproduction were also reflected by the transcriptome analysis revealing a marked impact on global gene expression patterns (Table 1). As DNA gyrase is indispensable for replication and transcription by changing the topological state of DNA, its inhibition was previously described to globally affect the gene expression profile (Guha et al., 2018; Jeong et al., 2006). Particularly noteworthy in this context are the significantly increased mRNA levels of *gyrA* and *gyrB* as well as the down-regulation of *topA*. The DNA topology modulatory proteins, gyrase and topoisomerase I (topo I), catalyze opposing reactions of DNA supercoiling and relaxation (McKie et al., 2021). Previous studies already revealed that expression of the *gyrAB* and *topA* is controlled in a supercoiling-sensitive manner: While increasing DNA relaxation stimulates *gyrAB* expression (Menzel & Gellert, 1983), it represses expression of *topA* allowing homeostatic maintenance of DNA topology (Ahmed et al., 2016; Tse-Dinh, 1985). As gyrase inhibition blocks the introduction of negative supercoils, increased expression levels of *gyrAB* and a decreased expression level of *topA* upon Gip overproduction are most probably used to counteract gyrase inhibition. The adaptation at the level of gene expression could then explain the resumed growth of the *gip* expressing strain—reaching almost wild type-like growth rates after a pronounced lag phase (Figure 1).

In summary, we identified Gip as a novel gyrase inhibitor protein encoded by the CGP3 prophage of *C. glutamicum*. Gip was shown to specifically inhibit the gyrase of its bacterial host *C. glutamicum*, but further studies are required to decipher its impact on the phage life cycle.

## 4 | EXPERIMENTAL PROCEDURES

### 4.1 | Bacterial strains and growth conditions

All bacterial strains and plasmids used in this study are listed in Tables S1 and S2, respectively. *Corynebacterium glutamicum* ATCC 13032 (NCBI reference: NC\_003450.3) was used as a wild type strain (Ikeda & Nakagawa, 2003). For growth studies and fluorescence measurements as well as for transcriptome analysis, *C. glutamicum* cells were precultivated in BHI (brain heart infusion, Difco BHI, BD, Heidelberg, Germany) at 30°C for 8 hr. The preculture was used to inoculate an overnight culture in CGXII minimal medium with 2% (w/v) glucose (Keilhauer et al., 1993), which was cultivated under

the same conditions. The next day, the overnight culture was used to inoculate the main culture in CGXII minimal medium with 2% (w/v) glucose to an  $OD_{600}$  of 1. All media contained kanamycin in a concentration of 25  $\mu$ g/ml. Gene expression was induced using 50  $\mu$ M IPTG (Isopropyl  $\beta$ -D-1-thiogalactopyranoside). For standard cloning applications, *E. coli* DH5 $\alpha$  was cultivated in Lysogeny Broth (Difco LB, BD, Heidelberg, Germany) medium containing 50  $\mu$ g/ml kanamycin (LB Kan<sub>50</sub>) at 37°C and 170 rpm. For protein overproduction and following purification, the *E. coli* BL21 (DE3) strain was used. Precultivation was performed in LB Kan<sub>50</sub> medium, which was incubated overnight at 37°C and 120 rpm. The main culture was inoculated in LB Kan<sub>50</sub> medium to an  $OD_{600}$  of 0.1 using the pre-culture. At an  $OD_{600}$  of 0.6 gene expression was induced using 100  $\mu$ M IPTG. Cells were harvested after additional 24 hr incubation at 16°C.

## 4.2 | Recombinant DNA work and cloning techniques

All plasmids and oligonucleotides used in this study are listed in Tables S2 and S3, respectively. Standard cloning techniques like PCR and restriction digestion were performed according to standard protocols (Sambrook & Russell, 2001). In all cases, Gibson assembly was used for plasmid construction (Gibson, 2011). DNA regions of interest were amplified via PCR using the chromosomal DNA of *C. glutamicum* ATCC 13032 as a template. The plasmid backbone was cut using the indicated restriction enzymes. Sequencing and synthesis of oligonucleotides were performed by Eurofins Genomics (Ebersberg, Germany). Genomic deletions were constructed using the pK19mobsacB plasmid and the two-step homologs recombination method (Niebisch & Bott, 2001). The 500 bp up- and downstream regions of the respective gene were amplified using the oligonucleotides listed in Table S3. Both PCR products and the digested pK19mobsacB plasmid (with HindIII, EcoRI) were assembled via Gibson assembly (Gibson, 2011). The correct deletion was verified by sequencing of the colony PCR product with the indicated oligonucleotides (Table S3).

## 4.3 | Microtiter cultivation and reporter assays

For growth experiments and fluorescence assays, the BioLector® microcultivation system of m2p-labs (Aachen, Germany) was used (Kensy et al., 2009). The main cultivation was executed in FlowerPlates (MTP-48-B, m2p-labs) at 30°C and 1,200 rpm with a starting  $OD_{600}$  of 1 using 750  $\mu$ l of CGXII minimal media with 2% (w/v) glucose containing 50  $\mu$ M IPTG and 25  $\mu$ g/ml kanamycin. During cultivation, biomass was measured as a function of backscattered light intensity with an excitation wavelength of 620 nm (filter module:  $\lambda_{Ex}/\lambda_{Em}$ : 620 nm/620 nm, gain: 15). Data for biomass measurements were baseline-corrected by subtracting the  $t_0$  value from all data points. The measurements of backscatter were taken at 15 min intervals.

## 4.4 | Protein purification via affinity tags

For heterologous protein overproduction, *E. coli* BL21 (DE3) cells containing the pET-cg1978-C-strep plasmid, the pET-gyrA-C-strep plasmid, the pET-gyrA-N-strep plasmid, the pET-gyrB-N-strep plasmid, or the pET-cg1978-C-his plasmid were cultivated as described in "Bacterial strains and growth conditions."

Cell harvesting and disruption were performed as described by Pfeifer et al. (2016). In case of Cg1978-C-Strep, buffer A (100 mM Tris-HCl, pH 8.0) with cComplete™ Protease inhibitor (Roche, Basel, Switzerland) was used for cell disruption and buffer B (100 mM Tris-HCl, 250 mM NaCl, pH 8.0) for purification. Purification of Strep-tagged Cg1978 was conducted by applying the supernatant to an equilibrated 2 ml Strep-Tactin®-Sepharose® column (IBA, Göttingen, Germany). After washing with 20 ml buffer B, the protein was eluted with 6 ml buffer B containing 15 mM d-desthiobiotin (Sigma-Aldrich, St. Louis, MO, USA). Purification of GyrA-C-Strep, GyrA-N-Strep, and GyrB-N-Strep was conducted in the same way using an adjusted buffer B<sub>gyr</sub> for cell disruption and purification (buffer B<sub>gyr</sub>: 20 mM Tris-HCl, 500 mM NaCl, 10% (w/v) glycerol, 5 mM EDTA, 1 mM DTT, pH 7.9).

For purification of Cg1978-C-His, the cell pellet was resuspended in 50 ml TN120 buffer (20 mM Tris-HCl, 300 mM NaCl, 20 mM imidazole, and pH 8.0) with cComplete™ Protease inhibitor (Roche, Basel, Switzerland), and cells were disrupted as described above. Purification of His-tagged Cg1978 was performed by applying the supernatant to an equilibrated 2 ml Ni-NTA Agarose column (Invitrogen, California, USA). After washing with 30 ml TN120 buffer, the protein was eluted with increasing imidazole concentrations using TN1 buffer (20 mM Tris-HCl, 300 mM NaCl, pH 8.0) containing 50 mM, 100 mM, 200 mM, or 400 mM imidazole.

After purification, the elution fractions with the highest protein concentration were pooled and analyzed with SDS-PAGE (Laemmli, 1970) using a 4%-20% Mini-PROTEAN® gradient gel (Bio-Rad, Munich, Germany).

## 4.5 | In vitro pull-down assay and MALDI-TOF analysis

Protein purification of Cg1978-C-Strep was conducted as described above. The elution fractions showing the highest protein concentration in a Bradford assay (Bradford, 1976) were pooled and purified with size-exclusion chromatography using PD10 desalting columns (GE Healthcare, Freiburg, Germany) and buffer B (100 mM Tris-HCl, 250 mM NaCl, pH 8.0) according to manufacturer's manual to remove excess desthiobiotin. For the detection of possible interaction partners of the target protein on a protein-protein level, *C. glutamicum* ATCC 13032 wild-type cells were cultivated in a BHI medium. At an  $OD_{600}$  of 5 to 6, the cells were harvested at 11,325 g and 4°C for 15 min and cell pellet of 100 ml cell culture was resuspended in 25 ml buffer A (100 mM Tris-HCl, pH 8.0) with cComplete™ Protease inhibitor (Roche, Basel, Switzerland). Cell disruption was performed using the French Press cell with a pressure of 172 mPa for five passages followed by a centrifugation step at 5,000 g for 50 min.



For copurification of possible protein interaction partners, the purified target protein Cg1978 was incubated with the *C. glutamicum* crude extract at RT for 1 hr. After loading the mixture to the StrepTactin column, the purification was performed as described above. The elution fractions with the highest protein concentration were precipitated by the addition of 100% (w/v) trichloroacetic acid (TCA) in a volume ratio of four units of protein to one unit TCA (Sivaraman et al., 1997). After incubation at 4°C overnight, the precipitation approach was centrifuged for 5 min at 14,000 g. The supernatant was discarded and the pellet was washed with 200  $\mu$ l cold acetone twice. Afterward, the pellet was dried for 10 min at 95°C and resuspended in 30  $\mu$ l 1.5  $\times$  SDS loading buffer for gel electrophoresis or in 30  $\mu$ l trypsin reaction buffer provided by the Trypsin Singles, Proteomics Grade kit (Sigma-Aldrich) for LC-MS/MS sample preparation. Analysis of elution fractions via SDS-PAGE (Laemmli, 1970) was performed using a 4%–20% Mini-PROTEAN® gradient gel (Bio-Rad, Munich, Germany). After staining the gel with Coomassie dye-based RAPIDstain solution (G-Biosciences, St. Louis, MO, USA) MALDI-TOF-MS measurements were performed with an Ultraflex III TOF/TOF mass spectrometer (Bruker Daltonics, Bremen, Germany) for identification of the co-purified proteins (Bussmann et al., 2010). Elution fractions were further analyzed via LC-MS/MS.

#### 4.6 | LC-MS/MS sample preparation and measurement

LC-MS/MS was performed after TCA precipitation using the Trypsin Singles, Proteomics Grade kit (Sigma-Aldrich, St. Louis, MO, USA) according to the manufacturer's instruction. The prepared tryptic peptide samples were separated chromatographically on a nanoLC Eksigent ekspert™ 425 LC system in microLC modus (Sciex) coupled with a 25 Micron ESI Electrode to a TripleTOF™ 6600 mass spectrometer (Sciex). As a trap, a YMC-Triart C18 column with the dimension 5  $\times$  0.5 mm ID, 3  $\mu$ m, 12 nm (YMC) was used, combined with a YMC-Triart C18 column with 150  $\times$  0.3 mm ID, 12 nm, S-3  $\mu$ m (YMC) as an analytical column. The column oven was set to 40°C.

For trapping, 2% acetonitrile in dd.H<sub>2</sub>O with 0.5% formic acid served as a loading solvent, whereas 0.1% formic acid was used as mobile phase A and acetonitrile with 0.1% formic acid (both LC-MS grade, ROTISOLV®, ≥99.9%, Carl Roth) as mobile phase B. First, 10  $\mu$ l of each sample containing up to 8  $\mu$ g of digested protein was loaded from the cooled autosampler onto the trap column using 100% loading solvent for 10 min at 10  $\mu$ l/min for desalting and enrichment.

For the following separation of the peptides on the analytical column, a linear gradient with increasing concentrations of mobile phase B was used starting with 7% A and 3% B and a flow rate of 5  $\mu$ l/min as an initial condition. During Information-Dependent Acquisition (IDA) and SWATH measurements, the following source and gas settings were applied: 5,500 V spray voltage, 35 psi curtain gas, 12 psi ion source gas 1, 20 psi ion source gas 2, and 150°C interface heater. Each sample was injected three times.

For shotgun measurements, the mass spectrometer was operated with a "top 50" method: Initially, a 250-ms survey scan (TOF-MS mass range  $m/z$  400–1,500, high-resolution mode) was collected from which the top 50 precursor ions were automatically selected for fragmentation, whereby each MS/MS 97 Appendix event (mass range  $m/z$  170–1,500, in high-sensitivity mode) consisted of a 40 ms fragment ion scan. For parent ion selection, the precursor ion intensity served as the main selection criterion. Ions with an intensity exceeding 100 counts/s and with a charge state of 2+ to 5+ were preferentially selected. Selected precursors were added to a dynamic exclusion list for 22 s and subsequently isolated using a quadrupole resolution of 0.7 amu and fragmented in the collision cell with a rolling collision energy (CE) of 10 eV. If <50 precursor ions fulfilling the selection criteria were detected per survey scan, the detected precursors were subjected to extended MS/MS accumulation time to maintain a constant total cycle time of 2.3 s.

For data analysis, the IDA data were processed with ProteinPilot™ (V5.01, Sciex, USA) using the Paragon™ Algorithm for peptide identification and the ProGroup™ Algorithm for protein identification.

#### 4.7 | DNA microarrays

For a comparative transcriptome analysis of *C. glutamicum* ATCC 13032 carrying the empty pAN6 vector and cells carrying the pAN6-cg1978 vector, cultivation was performed as described in "Bacterial strains and growth conditions" using CGXII-Kan<sub>25</sub> minimal media with 2% (w/v) glucose and 50  $\mu$ M IPTG. For both strains, cells were harvested at an OD<sub>600</sub> of 6 in a reaction tube filled with ice (50 ml) for 5 min at 5,000 g and 4°C. RNA purification was carried out using the "RNeasy Mini"-Kit (QIAGEN, Hilden, Germany) according to the manufacturer's manual. The preparation of labeled cDNA and DNA microarray analysis was performed as described previously (Donovan et al., 2015). The data processing was executed with in-house software according to (Polen & Wendisch, 2004). Genes with an mRNA ratio (sample/neg. control) of >2.0 ( $p$ -value <0.05) were classified as upregulated, whereas genes with an mRNA ratio of <0.5 ( $p$ -value <0.05) were classified as down-regulated. Array data were deposited in the GEO database (ncbi.nlm.nih.gov/geo) with accession number GSE151224.

#### 4.8 | Flow cytometry

Analysis of fluorescent reporter outputs at the single-cell level was performed using the BD Accuri™ C6 flow cytometer (BD biosciences, Heidelberg, Germany). The chromophore of the yellow fluorescent protein eYFP or Venus was excited with a blue laser with an excitation wavelength of 488 nm. The fluorescence emission of eYFP and Venus was measured using a 530/30 nm standard filter. Particle size was detected using the forward light scatter (FSC). The flow cytometer was started up by flushing with filtered, dd.H<sub>2</sub>O for 10 min. For preparing flow cytometry samples, cell cultures were mixed with 1 ml flow cytometric fluid (BD™ 342003

FACSCFlow™ Sheath Fluid). For every sample, 100,000 events were analyzed via BD Accuri C6 software (version 1.0.264.21).

#### 4.9 | Cultivation and perfusion in microfluidic device

Single-cell analysis of Cg1978 overexpressing cells was performed using an in-house developed microfluidic platform (Grünberger et al., 2013, 2015; Helfrich et al., 2015). Cultivation and time-lapse imaging were performed in CGXII minimal medium with 2% (w/v) glucose and 25 µg/ml kanamycin as described by (Pfeifer et al., 2016). Overexpression of Cg1978 in the prophage reporter strain ATCC 13032::P<sub>lys</sub>-*eyfp* carrying the pAN6-Cg1978 vector was induced by adding 50 µM IPTG to the medium. An uninduced control served as a reference.

#### 4.10 | Supercoiling inhibition assay

For the supercoiling inhibition assay, Cg1978 as well as both gyrase subunits (GyrA and GyrB) were purified by the means of a C-terminal His-Tag for Cg1978, a C-terminal Strep-Tag for GyrA, and an N-terminal Strep-Tag for GyrB as described above. Using PD10 desalting columns (GE Healthcare, Freiburg, Germany), the buffer of Cg1978 was exchanged to PBS (137 mM NaCl, 2.7 mM KCl, 8 mM Na<sub>2</sub>HPO<sub>4</sub>, 1.5 mM KH<sub>2</sub>PO<sub>4</sub>, pH 7.4). In case of GyrA and GyrB, the buffer was exchanged to 20 mM Tris-HCl, pH 7.9, 50% (w/v) glycerol, 0.5 M KCl, and 1 mM DTT. Formation of the heterotetrameric gyrase complex was obtained by incubating equimolar amounts of GyrA and GyrB for 30 min on ice. The activity of the purified *C. glutamicum* (C.g.) gyrase as well as its inhibition by Cg1978 were determined using the *M. tuberculosis* Gyrase (HIS) Supercoiling Assay Kit (Inspiralis, Norwich, UK) according to the manufacturer's manual. According to the assay conditions, the C.g. gyrase concentration of 50 nM resulting in full supercoiling of 0.5 µg relaxed plasmid DNA after 30 min of incubation at 37°C was determined as 1 U. Supercoiling inhibition of the C.g. gyrase was assayed by using 1 U of the C.g. gyrase with increasing concentrations of Cg1978-C-His (0.02–60.0 µM). Additionally, different concentrations of the known inhibitor ciprofloxacin (10 and 50 µM) were used as a positive control.

Moreover, the inhibitory effect of Cg1978 on the *M.tb* and *E.c.* gyrase was investigated according to the *M. tuberculosis* and *E. coli* Gyrase (HIS) Supercoiling Assay Kits (Inspiralis, Norwich, UK) using 1 U of the respective gyrases and the same Cg1978 concentrations as for the C.g. gyrase. All reactions were stopped by adding 30 µl STEB buffer (40% (w/v) sucrose, 100 mM Tris-HCl pH 8.0, 10 mM EDTA, 0.5 mg/ml Bromophenol Blue), and 30 µl chloroform/isoamyl alcohol (v:v, 24:1).

#### 4.11 | Surface Plasmon Resonance Spectroscopy (SPR)

For SPR analysis, Cg1978-C-His and GyrA-N-Strep were purified as described above. After purification, the buffer of both proteins was

exchanged to PBS (137 mM NaCl, 2.7 mM KCl, 8 mM Na<sub>2</sub>HPO<sub>4</sub>, 1.5 mM KH<sub>2</sub>PO<sub>4</sub>, pH 7.4) using PD10 Desalting columns (GE Healthcare, Freiburg, Germany). The binding of His-tagged Cg1978-C-His to GyrA-N-Strep was analyzed by SPR analysis in a Biacore 3000 device (GE Healthcare, Freiburg, Germany) using a Sensor Chip CM5 (GE Healthcare, Freiburg, Germany). As the first step, an anti-histidine antibody (GE Healthcare, Freiburg, Germany) was immobilized to the chip matrix using amino coupling chemistry. All experiments were carried out in HBS-EP buffer (0.01 M HEPES, pH 7.4, 0.15 M NaCl, 3 mM EDTA, 0.005% v/v Surfactant P20) at 25°C. Following the standard coupling protocol for antibody immobilization, the mixture of 0.05 M N-Hydroxysuccinimide (NHS) and 0.2 M 1-Ethyl-3-(3-dimethylaminopropyl) carbodiimide hydrochloride (EDC) was injected for a total contact time of 420 s to activate the matrix. Then, the anti-histidine antibody (50 µg/ml) diluted in immobilization buffer (10 mM sodium acetate, pH 4.5) was injected for 420 s. To deactivate the unbound parts of the chip matrix, 1 M ethanolamine hydrochloride-NaOH (pH 8.5) was injected for 420 s. The flow rate was set to 10 µl/min during this immobilization procedure. Approximately 8,000–10,000 response units (RU) of the anti-histidine antibody were immobilized per flow cell. For the binding analysis, 180–250 RU of Cg1978-C-His was captured via injection of 40 µl (10 nM) at a flow rate of 5 µl/min followed by 10 min of HBS-EP buffer to remove unbound protein from the chip. The binding analysis between Cg1978-C-His and GyrA-N-Strep was then performed by injecting 90 µl of GyrA-N-Strep (10–250 nM) followed by a dissociation time of 300 s at a flow rate of 30 µl/min. After each cycle, the surface was regenerated by injection of regeneration buffer (10 mM Glycine-HCl, pH 1.5) for 30 s, at a flow rate of 30 µl/min. After the equilibration with three start up cycles without the analyte, this was repeated for various concentrations of GyrA-N-Strep (10–250 nM). Sensorgrams were recorded using Biacore 3000 Control Software 4.1.2 and analyzed with BIAevaluation software 4.1.1 (GE Healthcare, Freiburg, Germany). The surface of flow cell 1 immobilized with the anti-histidine antibody was used to obtain blank sensorgrams for the subtraction of the bulk refractive index background. The referenced sensorgrams were normalized to a baseline of 0. Peaks in the sensorgrams at the beginning and the end of the injection are due to the run-time difference between the flow cells for the chip.

#### ACKNOWLEDGMENTS

We thank the European Research Council (ERC Starting Grant, grant number 757563) and the Helmholtz Association (grant number W2/W3-096) for financial support. We thank Astrid Wirtz for technical assistance with respect to the LC-MS/MS measurement. We thank Rebecca Lukaschewsky for constructing the gyrase overexpression plasmids. SPR analyses were performed in the Bioanalytics service unit of the JGU Biocenter. We very much thank the reviewers of this manuscript for their critical but constructive comments during the review process. Open access funding enabled and organized by ProjektDEAL.

#### CONFLICT OF INTEREST

The authors declare no conflict of interest.



## AUTHOR CONTRIBUTIONS

LK, MH, and JF conceived the study; LK and JB performed the experiments; LK, MH, JB, RH, and JF analyzed the data; LK and JF wrote the manuscript. All authors reviewed and edited the manuscript.

## DATA AVAILABILITY STATEMENT

The data that support the findings of this study are available in the supplementary material of this article. Microarray data were deposited in the GEO database (ncbi.nlm.nih.gov/geo) with accession number GSE151224.

## ORCID

Julia Frunzke  <https://orcid.org/0000-0001-6209-7950>

## REFERENCES

- Ahmed, W., Menon, S., Karthik, P.V., & Nagaraja, V. (2016) Autoregulation of topoisomerase I expression by supercoiling sensitive transcription. *Nucleic Acids Research*, 44(4), 1541–1552. <https://doi.org/10.1093/nar/gkv1088>
- Bernard, P., Kézdy, K.E., Van Melderden, L., Steyaert, J., Wyns, L., Pato, M.L. et al. (1993) The F plasmid CcdB protein induces efficient ATP-dependent DNA cleavage by gyrase. *Journal of Molecular Biology*, 234(3), 534–541. <https://doi.org/10.1006/jmbi.1993.1609>
- Bradford, M.M. (1976) A rapid and sensitive method for the quantitation of microgram quantities of protein utilizing the principle of protein-dye binding. *Analytical Biochemistry*, 72, 248–254. <https://doi.org/10.1006/abio.1976.9999>
- Bush, N.G., Evans-Roberts, K., & Maxwell, A. (2015) DNA topoisomerases. *EcoSal Plus*, 6(2). <https://doi.org/10.1128/ecosalplus.ESP-0010-2014>
- Bussmann, M., Baumgart, M., & Bott, M. (2010) RosR (Cg1324), a hydrogen peroxide-sensitive MarR-type transcriptional regulator of *Corynebacterium glutamicum*. *Journal of Biological Chemistry*, 285(38), 29305–29318. <https://doi.org/10.1074/jbc.M110.156372>
- Chatterji, M., Unniraman, S., Mahadevan, S., & Nagaraja, V. (2001) Effect of different classes of inhibitors on DNA gyrase from *Mycobacterium smegmatis*. *Journal of Antimicrobial Chemotherapy*, 48(4), 479–485. <https://doi.org/10.1093/jac/48.4.479>
- Collin, F., Karkare, S., & Maxwell, A. (2011) Exploiting bacterial DNA gyrase as a drug target: current state and perspectives. *Applied Microbiology and Biotechnology*, 92(3), 479–497. <https://doi.org/10.1007/s00253-011-3557-z>
- Dao-Thi, M.H., Van Melderden, L., De Genst, E., Afif, H., Buts, L., Wyns, L. et al. (2005) Molecular basis of gyrase poisoning by the addiction toxin CcdB. *Journal of Molecular Biology*, 348(5), 1091–1102. <https://doi.org/10.1016/j.jmb.2005.03.049>
- De Smet, J., Hendrix, H., Blasdel, B.G., Danis-Wlodarczyk, K., & Lavigne, R. (2017) *Pseudomonas* predators: understanding and exploiting phage-host interactions. *Nature Reviews Microbiology*, 15(9), 517–530. <https://doi.org/10.1038/nrmicro.2017.61>
- De Smet, J., Wagemans, J., Boon, M., Ceyssens, P.-J., Voet, M., Noben, J.-P. et al. (2021) The bacteriophage LUZ24 "lgy" peptide inhibits the *Pseudomonas* DNA gyrase. *Cell Reports*, 36(8), 109567. <https://doi.org/10.1016/j.celrep.2021.109567>
- DeMarini, D.M., & Lawrence, B.K. (1992) Prophage induction by DNA topoisomerase II poisons and reactive-oxygen species: role of DNA breaks. *Mutation Research*, 267(1), 1–17. [https://doi.org/10.1016/0027-5107\(92\)90106-C](https://doi.org/10.1016/0027-5107(92)90106-C)
- Ding, Y., Manzo, C., Fulcrand, G., Leng, F., Dunlap, D., & Finzi, L. (2014) DNA supercoiling: a regulatory signal for the  $\lambda$  repressor. *Proceedings of the National Academy of Sciences of the United States of America*, 111(43), 15402–15407. <https://doi.org/10.1073/pnas.1320644111>
- Donovan, C., Heyer, A., Pfeifer, E., Polen, T., Wittmann, A., Krämer, R. et al. (2015) A prophage-encoded actin-like protein required for efficient viral DNA replication in bacteria. *Nucleic Acids Research*, 43(10), 5002–5016. <https://doi.org/10.1093/nar/gkv374>
- Dorman, C.J., & Dorman, M.J. (2016) DNA supercoiling is a fundamental regulatory principle in the control of bacterial gene expression. *Biophysical Reviews*, 8(3), 209–220. <https://doi.org/10.1007/s12551-016-0205-y>
- Drlica, K., & Malik, M. (2003) Fluoroquinolones: action and resistance. *Current Topics in Medicinal Chemistry*, 3(3), 249–282. <https://doi.org/10.2174/1568026033452537>
- Dwyer, D.J., Kohanski, M.A., Hayete, B., & Collins, J.J. (2007) Gyrase inhibitors induce an oxidative damage cellular death pathway in *Escherichia coli*. *Molecular Systems Biology*, 3, 91. <https://doi.org/10.1038/msb4100135>
- Frunzke, J., Brankamp, M., Schweitzer, J.E., & Bott, M. (2008) Population Heterogeneity in *Corynebacterium glutamicum* ATCC 13032 caused by prophage CGP3. *Journal of Bacteriology*, 190(14), 5111–5119. <https://doi.org/10.1128/JB.00310-08>
- Gibson, D.G. (2011) Enzymatic assembly of overlapping DNA fragments. *Methods in Enzymology*, 498, 349–361. <https://doi.org/10.1016/B978-0-12-385120-8.00015-2>
- Grünberger, A., Probst, C., Helfrich, S., Nanda, A., Stute, B., Wiechert, W. et al. (2015) Spatiotemporal microbial single-cell analysis using a high-throughput microfluidics cultivation platform. *Cytometry Part A*, 87(12), 1101–1115. <https://doi.org/10.1002/cyto.a.22779>
- Grünberger, A., van Ooyen, J., Paczia, N., Rohe, P., Schiendzielorz, G., Eggeling, L. et al. (2013) Beyond growth rate 0.6: *Corynebacterium glutamicum* cultivated in highly diluted environments. *Biotechnology and Bioengineering*, 110(1), 220–228. <https://doi.org/10.1002/bit.24616>
- Guha, S., Udupa, S., Ahmed, W., & Nagaraja, V. (2018) Rewired down-regulation of DNA gyrase impacts cell division, expression of topology modulators, and transcription in *Mycobacterium smegmatis*. *Journal of Molecular Biology*, 430(24), 4986–5001. <https://doi.org/10.1016/j.jmb.2018.10.001>
- Hatfull, G.F. (2015) Dark matter of the biosphere: the amazing world of bacteriophage diversity. *Journal of Virology*, 89(16), 8107–8110. <https://doi.org/10.1128/jvi.01340-15>
- Helfrich, S., Pfeifer, E., Krämer, C., Sachs, C.C., Wiechert, W., Kohlheyer, D. et al. (2015) Live cell imaging of SOS and prophage dynamics in isogenic bacterial populations. *Molecular Microbiology*, 98(4), 636–650. <https://doi.org/10.1111/mmi.13147>
- Ikeda, M., & Nakagawa, S. (2003) The *Corynebacterium glutamicum* genome: features and impacts on biotechnological processes. *Applied Microbiology and Biotechnology*, 62(2–3), 99–109. <https://doi.org/10.1007/s00253-003-1328-1>
- Janion, C. (2008) Inducible SOS response system of DNA repair and mutagenesis in *Escherichia coli*. *International Journal of Biological Sciences*, 4(6), 338–344. <https://doi.org/10.7150/ijbs.4.338>
- Jeong, K.S., Xie, Y., Hiasa, H., & Khodursky, A.B. (2006) Analysis of pleiotropic transcriptional profiles: a case study of DNA gyrase inhibition. *PLoS Genetics*, 2(9), e152. <https://doi.org/10.1371/journal.pgen.0020152>
- Keilhauer, C., Eggeling, L., & Sahm, H. (1993) Isoleucine synthesis in *Corynebacterium glutamicum*: molecular analysis of the *ilvB-ilvN-ilvC* operon. *Journal of Bacteriology*, 175(17), 5595–5603. <https://doi.org/10.1128/jb.175.17.5595-5603.1993>
- Kensy, F., Zang, E., Faulhammer, C., Tan, R.K., & Büchs, J. (2009) Validation of a high-throughput fermentation system based on online monitoring of biomass and fluorescence in continuously shaken microtiter plates. *Microbial Cell Factories*, 8, 31. <https://doi.org/10.1186/1475-2859-8-31>
- Laemmli, U.K. (1970) Cleavage of structural proteins during assembly of head of bacteriophage T4. *Nature*, 227(5259), 680–685. <https://doi.org/10.1038/227680a0>

- Lu, S., Wang, J., Chitsaz, F., Derbyshire, M.K., Geer, R.C., Gonzales, N.R. et al. (2020) CDD/SPARCLE: the conserved domain database in 2020. *Nucleic Acids Research*, 48(D1), D265–D268. <https://doi.org/10.1093/nar/gkz991>
- Madhusudan, K. & Nagaraja, V. (1996) Alignment and phylogenetic analysis of type II DNA topoisomerases. *Journal of Biosciences*, 21, 613–629. <https://doi.org/10.1007/BF02703140>
- Manjunatha, U.H., Dalal, M., Chatterji, M., Radha, D.R., Visweswariah, S.S. & Nagaraja, V. (2002) Functional characterisation of mycobacterial DNA gyrase: an efficient decatenase. *Nucleic Acids Research*, 30(10), 2144–2153. <https://doi.org/10.1093/nar/30.10.2144>
- Manjunatha, U.H., Madhusudan, K., Visweswariah, S. & Nagaraja, V. (2000) Structural heterogeneity in DNA gyrases in Gram-positive and Gram-negative bacteria. *Current Science*, 79(7), 968–974.
- Mattenberger, Y., Silva, F. & Belin, D. (2015) 55.2, a phage T4 ORFan gene, encodes an inhibitor of *Escherichia coli* topoisomerase I and increases phage fitness. *PLoS One*, 10(4), e0124309. <https://doi.org/10.1371/journal.pone.0124309>
- Maxwell, A. & Lawson, D.M. (2003) The ATP-binding site of type II topoisomerases as a target for antibacterial drugs. *Current Topics in Medicinal Chemistry*, 3(3), 283–303. <https://doi.org/10.2174/1568026033452500>
- McKie, S.J., Neuman, K.C. & Maxwell, A. (2021) DNA topoisomerases: advances in understanding of cellular roles and multi-protein complexes via structure-function analysis. *BioEssays*, 43(4), e2000286. <https://doi.org/10.1002/bies.202000286>
- Menzel, R. & Gellert, M. (1983) Regulation of the genes for *E. coli* DNA gyrase: homeostatic control of DNA supercoiling. *Cell*, 34, 105–113. [https://doi.org/10.1016/0092-8674\(83\)90140-X](https://doi.org/10.1016/0092-8674(83)90140-X)
- Miki, T., Park, J.A., Nagao, K., Murayama, N. & Horiuchi, T. (1992) Control of segregation of chromosomal DNA by sex factor F in *Escherichia coli*. Mutants of DNA gyrase subunit A suppress *letD* (*ccdB*) product growth inhibition. *Journal of Molecular Biology*, 225(1), 39–52. [https://doi.org/10.1016/0022-2836\(92\)91024-j](https://doi.org/10.1016/0022-2836(92)91024-j)
- Nanda, A.M., Heyer, A., Krämer, C., Grünberger, A., Kohlheyer, D. & Frunzke, J. (2014) Analysis of SOS-induced spontaneous prophage induction in *Corynebacterium glutamicum* at the single-cell level. *Journal of Bacteriology*, 196(1), 180–188. <https://doi.org/10.1128/JB.01018-13>
- Niebisch, A. & Bott, M. (2001) Molecular analysis of the cytochrome *bc<sub>1</sub>-aa<sub>3</sub>* branch of the *Corynebacterium glutamicum* respiratory chain containing an unusual dihem cytochrome *c<sub>1</sub>*. *Archives of Microbiology*, 175(4), 282–294. <https://doi.org/10.1007/s002030100262>
- Nobrega, F.L., Vlot, M., de Jonge, P.A., Dreesens, L.L., Beaumont, H.J.E., Lavigne, R. et al. (2018) Targeting mechanisms of tailed bacteriophages. *Nature Reviews Microbiology*, 16(12), 760–773. <https://doi.org/10.1038/s41579-018-0070-8>
- Norregaard, K., Andersson, M., Snekpen, K., Nielsen, P.E., Brown, S. & Oddershede, L.B. (2013) DNA supercoiling enhances cooperativity and efficiency of an epigenetic switch. *Proceedings of the National Academy of Sciences of the United States of America*, 110(43), 17386–17391. <https://doi.org/10.1073/pnas.1215907110>
- Norregaard, K., Andersson, M., Snekpen, K., Nielsen, P.E., Brown, S. & Oddershede, L.B. (2014) Effect of supercoiling on the  $\lambda$  switch. *Bacteriophage*, 4(1), e27517. <https://doi.org/10.4161/bact.27517>
- Ofir, G. & Sorek, R. (2018) Contemporary phage biology: from classic models to new insights. *Cell*, 172(6), 1260–1270. <https://doi.org/10.1016/j.cell.2017.10.045>
- Orr, M.W., Mao, Y., Storz, G. & Qian, S.B. (2020) Alternative ORFs and small ORFs: shedding light on the dark proteome. *Nucleic Acids Research*, 48(3), 1029–1042. <https://doi.org/10.1093/nar/gkz734>
- Pfeifer, E., Hünnefeld, M., Popa, O., Polen, T., Kohlheyer, D., Baumgart, M. et al. (2016) Silencing of cryptic prophages in *Corynebacterium glutamicum*. *Nucleic Acids Research*, 44(21), 10117–10131. <https://doi.org/10.1093/nar/gkw692>
- Pierrat, O.A. & Maxwell, A. (2003) The action of the bacterial toxin microcin B17. *Journal of Biological Chemistry*, 278(37), 35016–35023. <https://doi.org/10.1074/jbc.M304516200>
- Polen, T. & Wendisch, V.F. (2004) Genomewide expression analysis in amino acid-producing bacteria using DNA microarrays. *Applied Biochemistry and Biotechnology*, 118, 215–232. <https://doi.org/10.1385/ABAB:118:1-3:215>
- Roach, D.R. & Donovan, D.M. (2015) Antimicrobial bacteriophage-derived proteins and therapeutic applications. *Bacteriophage*, 5(3), e1062590. <https://doi.org/10.1080/21597081.2015.1062590>
- Rohwer, F. & Youle, M. (2011) Consider something viral in your search. *Nature Reviews Microbiology*, 9(5), 308–309. <https://doi.org/10.1038/nrmicro2563>
- Sambrook, J. & Russell, D.W. (2001) *Molecular cloning: a laboratory manual*, 3rd edition. Cold Spring Harbor Laboratory Press.
- Schroven, K., Aertsen, A. & Lavigne, R. (2021) Bacteriophages as drivers of bacterial virulence and their potential for biotechnological exploitation. *FEMS Microbiology Reviews*, 45(1), fuad041. <https://doi.org/10.1093/femsre/fuaa041>
- Shah, S. & Hedde, J.G. (2014) Squaring up to DNA: pentapeptide repeat proteins and DNA mimicry. *Applied Microbiology and Biotechnology*, 98(23), 9545–9560. <https://doi.org/10.1007/s00253-014-6151-3>
- Sivaraman, T., Kumar, T.K.S., Jayaraman, G. & Yu, C. (1997) The mechanism of 2,2,2-trichloroacetic acid-induced protein precipitation. *Journal of Protein Chemistry*, 16(4), 291–297. <https://doi.org/10.1023/A:1026357009886>
- Storz, G., Wolf, Y.I. & Ramamurthi, K.S. (2014) Small proteins can no longer be ignored. *Annual Review of Biochemistry*, 83, 753–777. <https://doi.org/10.1146/annurev-biochem-070611-102400>
- Tomasz, M. (1995) Mitomycin C: small, fast and deadly (but very selective). *Chemistry and Biology*, 2(9), 575–579. [https://doi.org/10.1016/1074-5521\(95\)90120-5](https://doi.org/10.1016/1074-5521(95)90120-5)
- Tse-Dinh, Y.-C. (1985) Regulation of the *Escherichia coli* DNA topoisomerase I gene by DNA supercoiling. *Nucleic Acids Research*, 13(13), 4751–4763. <https://doi.org/10.1093/nar/13.13.4751>
- Vanden Broeck, A., Lotz, C., Ortiz, J. & Lamour, V. (2019) Cryo-EM structure of the complete *E. coli* DNA gyrase nucleoprotein complex. *Nature Communications*, 10(1), 4935. <https://doi.org/10.1038/s41467-019-12914-y>
- Wendisch, V.F., Jorge, J.M.P., Pérez-García, F. & Sgobba, E. (2016) Updates on industrial production of amino acids using *Corynebacterium glutamicum*. *World Journal of Microbiology and Biotechnology*, 32(6), 105. <https://doi.org/10.1007/s11274-016-2060-1>
- Wiechert, J., Filipchuk, A., Hünnefeld, M., Gätgens, C., Brehm, J., Heermann, R. et al. (2020). Deciphering the rules underlying xenogeneic silencing and counter-silencing of Lsr2-like proteins using CgP5 of *Corynebacterium glutamicum* as a model. *mBio*, 11(1), e02273-19. <https://doi.org/10.1128/mBio.02273-19>
- Yin, Y. & Fischer, D. (2008) Identification and investigation of ORFans in the viral world. *BMC Genomics*, 9, 24. <https://doi.org/10.1186/1471-2164-9-24>

## SUPPORTING INFORMATION

Additional supporting information may be found in the online version of the article at the publisher's website.

**How to cite this article:** Kever, L., Hünnefeld, M., Brehm, J., Heermann, R. & Frunzke, J. (2021) Identification of Gip as a novel phage-encoded gyrase inhibitor protein of *Corynebacterium glutamicum*. *Molecular Microbiology*, 116, 1268–1280. <https://doi.org/10.1111/mmi.14813>

### 3.2. Aminoglycoside antibiotics inhibit phage infection by blocking an early step of the infection cycle

**Kever, L.<sup>#</sup>, Hardy, A.<sup>#</sup>, Luthe, L., Hünnefeld, M., Gätgens, C., Milke, L, Wiechert, J., Wittmann, J., Moraru, C., Marienhagen, J. and Frunzke, J.**

<sup>#</sup> Authors contributed equally to this work.

Published in mBio, 2022

Contributor role	Contributor
<b>Conceptualization</b>	LK (30%), AH (30%), JF (25%), TL (10%), MH (5%)
<b>Data curation</b>	LK (50%), AH (30%), TL (10%), LM (5%), JWie (5%)
<b>Formal analysis</b>	LK (60%), MH (20%), AH (10%), LM (10%)
<b>Funding acquisition</b>	JF (95%), JM (5%)
<b>Investigation</b>	LK (40%), AH (30%), TL (12.5%), MH (7.5%), CG (5%), LM (2.5%), JWie (2.5%)
<b>Methodology</b>	LK (40%), AH (25%), TL (15%), MH (10%), LM (5%), CM (5%)
<b>Project administration</b>	LK (40%), AH (30%), JF (20%), CG (10%)
<b>Resources</b>	JWit (60%), CM (40%)
<b>Software</b>	MH (60%), LM (20%), TL (20%)
<b>Supervision</b>	JF (50%), LK (25%), AH (20%), MH (2.5%), JM (2.5%)
<b>Validation</b>	LK (65%), AH (25%), JF (10%)
<b>Visualization</b>	LK (55%), AH (25%), TL (10%), MH (5%), LM (5%)
<b>Writing – original draft</b>	AH (45%), LK (40%), JF (7.5%), MH (2.5%), TL (2.5%) LM (2.5%)
<b>Writing – review and editing</b>	JF (40%), AH (30%), LK (15%), TL (5%), JM (5%), JWie (2.5%), MH (2.5%)

#### Overall contribution: 35%

Planned and conducted experiments and respective data analysis performed by LK is shown in the following figures: Figure 1 (*Streptomyces* screening), Figure 2a and e, Figure 2d (in cooperation with CG), Figure 4b and c, Figure 4d (RNA was isolated by LK, RNA-seq was performed by GENEWIZ (Leipzig), data analysis was conducted by MH), Figure S1, Figure S4a and b and Figure S5. Phage-targeting geneFISH experiments (Figure 5, S6a and c) were done in cooperation with MH. LK drafted all figures based on partially pre-visualized data received from contributing authors, which were subsequently revised in collaboration with AH, TL, MH, and LM. LK was substantially involved in writing the original draft and contributes to a lesser extent to the revision and editing process.



# Aminoglycoside Antibiotics Inhibit Phage Infection by Blocking an Early Step of the Infection Cycle

Larissa Kever,<sup>a</sup> Aél Hardy,<sup>a</sup> Tom Luthe,<sup>a</sup> Max Hünnefeld,<sup>a</sup> Cornelia Gätgens,<sup>a</sup> Lars Milke,<sup>a</sup> Johanna Wiechert,<sup>a</sup> Johannes Wittmann,<sup>b</sup> Cristina Moraru,<sup>c</sup> Jan Marienhagen,<sup>a,d</sup> Julia Frunzke<sup>a</sup>

<sup>a</sup>Institute of Bio- und Geosciences, IBG-1: Biotechnology, Forschungszentrum Jülich, Jülich, Germany

<sup>b</sup>Leibniz Institute DSMZ – German Collection of Microorganisms and Cell Cultures, Braunschweig, Germany

<sup>c</sup>Institute for Chemistry and Biology of the Marine Environment, Carl von Ossietzky University Oldenburg, Oldenburg, Germany

<sup>d</sup>Institute of Biotechnology, RWTH Aachen University, Aachen, Germany

Larissa Kever and Aél Hardy contributed equally to this work. To determine the order of the two co-first authors, we flipped a coin.

**ABSTRACT** In response to viral predation, bacteria have evolved a wide range of defense mechanisms, which rely mostly on proteins acting at the cellular level. Here, we show that aminoglycosides, a well-known class of antibiotics produced by *Streptomyces*, are potent inhibitors of phage infection in widely divergent bacterial hosts. We demonstrate that aminoglycosides block an early step of the viral life cycle, prior to genome replication. Phage inhibition was also achieved using supernatants from natural aminoglycoside producers, indicating a broad physiological significance of the antiviral properties of aminoglycosides. Strikingly, we show that acetylation of the aminoglycoside antibiotic apramycin abolishes its antibacterial effect but retains its antiviral properties. Altogether, our study expands the knowledge of aminoglycoside functions, suggesting that aminoglycosides not only are used by their producers as toxic molecules against their bacterial competitors but also could provide protection against the threat of phage predation at the community level.

**IMPORTANCE** Predation by phages is a major driver of bacterial evolution. As a result, elucidating antiphage strategies is crucial from both fundamental and therapeutic standpoints. While protein-mediated defense mechanisms, like restriction-modification systems or CRISPR/Cas, have been extensively studied, much less is known about the potential antiphage activity of small molecules. Focusing on the model bacteria *Escherichia coli* and *Streptomyces venezuelae*, our findings revealed significant antiphage properties of aminoglycosides, a major class of translation-targeting antibiotics produced by *Streptomyces*. Further, we demonstrate that supernatants from natural aminoglycoside producers protect bacteria from phage propagation, highlighting the physiological relevance of this inhibition. Suppression of phage infection by aminoglycosides did not result from the indirect inhibition of bacterial translation, suggesting a direct interaction between aminoglycosides and phage components. This work highlights the molecular versatility of aminoglycosides, which have evolved to efficiently block protein synthesis in bacterial competitors and provide protection against phages.

**KEYWORDS** *Streptomyces*, aminoglycosides, antibiotics, bacteriophages, phage defense, phage-host interaction

**B**acteriophages are viruses that prey upon bacteria. Facing the existential threat posed by phage predation, prokaryotes have developed numerous lines of defense, which together form the prokaryotic “immune system” (1). In response, phages have evolved a multitude of ways to circumvent these barriers, thereby fostering the diversification of

**Editor** Gisela Storz, National Institute of Child Health and Human Development

**Copyright** © 2022 Kever et al. This is an open-access article distributed under the terms of the Creative Commons Attribution 4.0 International license.

Address correspondence to Julia Frunzke, j.frunzke@fz-juelich.de.

The authors declare no conflict of interest.

**Received** 18 March 2022

**Accepted** 1 April 2022

**Published** 4 May 2022

bacterial antiviral strategies. Recent bioinformatics-guided screenings revealed a large number of previously unknown antiviral defense systems (2, 3). However, the majority of currently known prokaryotic defense systems rely on a wide range of molecular mechanisms but are mediated mainly by protein or RNA complexes (4).

Environmental bacteria produce a wide range of small molecules, conferring producer cells a specific fitness advantage in competitive or predatory interactions. However, the potential antiphage role of this extensive chemical repertoire remains largely unexplored. Recently, new types of defense systems that rely on small molecules rather than on proteins or RNA have been discovered (5, 6). Anthracyclines are secondary metabolites naturally produced by *Streptomyces* species and were shown to inhibit infection by double-stranded-DNA (dsDNA) phages (5). These molecules act as DNA-intercalating agents and block the replication of phage—but not bacterial—DNA. Since these secondary metabolites are excreted by *Streptomyces* cells and are diffusible molecules, their production may provide broad protection against dsDNA phages at the community level.

In nature, producers of secondary metabolites are generally resistant to the molecules they synthesize (7, 8). This feature is of special importance when screening small molecules for antiviral properties, as toxic effects on bacterial growth would prevent the appreciation of any inhibition of phage infection. In this study, we leveraged this principle to look for phage inhibition by secondary metabolites, using bacterial hosts resistant to the compounds tested.

Aminoglycosides are antibiotics well known for their bactericidal effect by targeting the 30S subunit of the ribosome and thereby either directly inhibiting protein synthesis or, for most aminoglycosides, promoting mistranslation. The aminoglycoside streptomycin, discovered in 1943, was the first antibiotic active against *Mycobacterium tuberculosis* (9). Strikingly, we observed strong phage inhibition in the presence of aminoglycosides when using strains resistant to the antibiotic. In agreement with this observation, decades-old reports described the inhibition of various phages by streptomycin (10–12). However, the biological significance of these observations was not explored, and the underlying mechanism of action remains unclear. For these reasons, we focused our efforts on aminoglycosides and set out to investigate their potential antiphage properties.

In this study, we show that aminoglycoside antibiotics inhibit phages infecting the actinobacterial model species *Streptomyces venezuelae* and *Corynebacterium glutamicum* as well as the  $\lambda$  phage infecting *Escherichia coli*. Investigations of the mechanism of action point toward a blockage of phage infection occurring after DNA injection but before genome replication. Furthermore, the antiphage activity observed with the purified aminoglycoside apramycin could be reproduced with supernatants from the natural producer *Streptoalloteichus tenebrarius*, suggesting a broad physiological significance of the antiphage properties of aminoglycosides.

## RESULTS

**Aminoglycosides inhibit a broad range of phages.** To investigate a potential antiviral activity of aminoglycosides, we first constructed resistant strains carrying a plasmid-borne resistance cassette encoding an aminoglycoside-modifying enzyme (Table S1 and S2A). With respect to the aminoglycosides selected for this study, we focused on antibiotics produced by *Streptomyces* species and included the atypical aminoglycoside streptomycin, aminoglycosides containing a monosubstituted deoxystreptamine ring (apramycin and hygromycin), kanamycin (4,6-di-substituted deoxystreptamine ring), and the aminocyclitol spectinomycin (13, 14). We challenged the aminoglycoside-resistant strains with a set of different phages using double-agar overlays with increasing aminoglycoside concentrations as screening platform (Fig. 1a). In the screening, we included phages from three different viral realms (15): dsDNA viruses from the order *Caudovirales* in *Duplodnaviria* (families *Sipho*-, *Myo*-, and *Podoviridae*), single-stranded DNA (ssDNA) viruses from the family *Inoviridae* in *Monodnaviria*, and

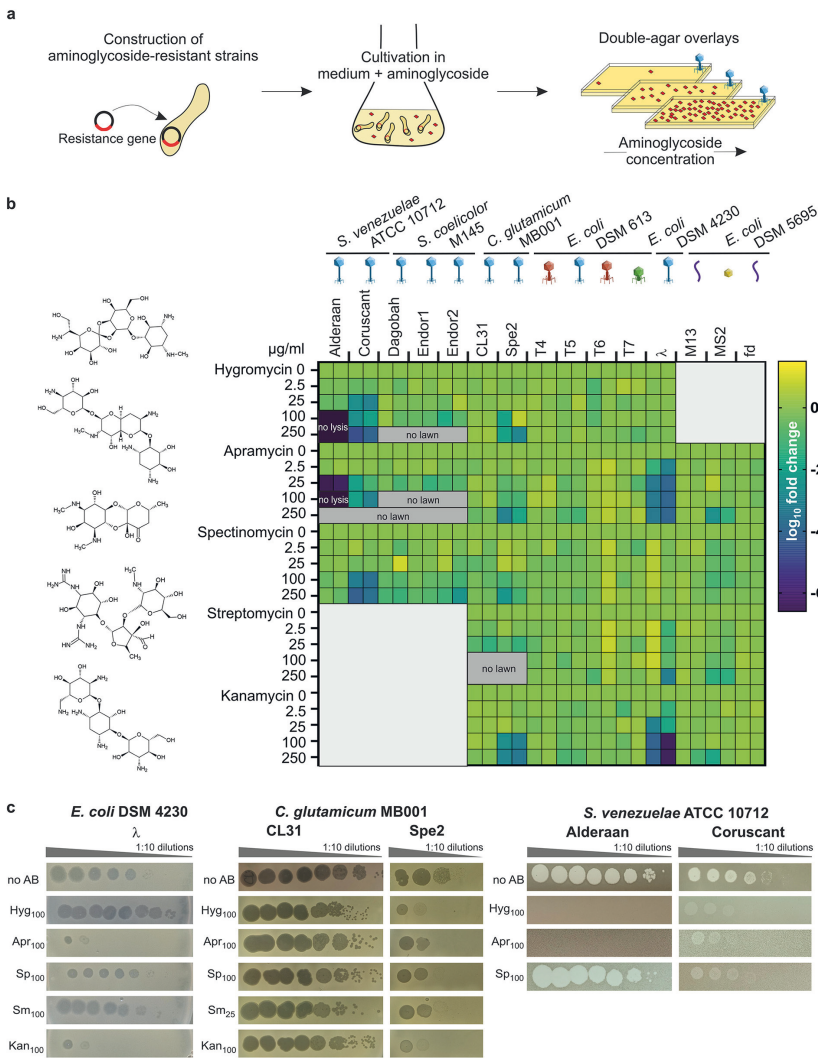


**FIG 1** Aminoglycosides inhibit a wide range of phages. (a) Schematic representation of the screening for the antiphage effect of different aminoglycosides. Strains resistant to the aminoglycosides were constructed using plasmid-borne resistance cassettes and subsequently challenged by phages in the presence of increasing aminoglycoside concentrations. (b) Overview of the screening results, showing the log<sub>10</sub> fold change in plaque formation by tested phages relative to the aminoglycoside-free control. Molecular structures of the aminoglycosides tested are indicated on the left. High concentrations of aminoglycosides prevented in some cases either the formation of plaque or lysis zone by the spotted phages ("no lysis") or bacterial growth ("no lawn"). *n* = 2 independent biological replicates. The different phage morphologies are depicted with icons according to the following color scheme: blue, *Siphoviridae*; red, *Myoviridae*; green, *Podoviridae*; purple, *Inoviridae*; yellow, *Leviviridae*. (c) Exemplary pictures from propagation assays performed in the presence of the indicated aminoglycoside concentration. Results are representative of two biological replicates.



ssRNA viruses from the family *Leviviridae* in *Riboviria* (Table S2B). The efficiency of plating comparing plaque formation under aminoglycoside pressure with aminoglycoside-free conditions was calculated for phages infecting either the actinobacterial model species *Streptomyces venezuelae*, *Streptomyces coelicolor*, and *Corynebacterium glutamicum* or the Gram-negative species *Escherichia coli* (Fig. 1b).

The extent of inhibition showed clear differences between the individual phages and aminoglycosides. Remarkably, infection with some phages, namely, the virulent phages Alderaan, Coruscant, and Spe2 as well as the temperate *E. coli* phage  $\lambda$ , was significantly impaired with increasing aminoglycoside concentrations. In contrast, all phages infecting *S. coelicolor*, CL31 infecting *C. glutamicum* MB001, and the T phages, RNA phage MS2, and filamentous phages M13 and fd infecting *E. coli* displayed no susceptibility to the tested aminoglycosides. The phages susceptible to aminoglycosides infect widely divergent hosts and possess different lifestyles and types of genome ends (Table S2B). However, they are all dsDNA phages belonging to the family *Siphoviridae*, suggesting a specificity of aminoglycosides for this phage family.

In the case of *S. venezuelae* phages, we observed the strongest inhibition with the aminocyclitol antibiotic apramycin. The *S. venezuelae* phage Alderaan showed the highest susceptibility among all tested phages, leading to  $\sim 10^6$ -fold reduction in numbers of PFU for 25  $\mu\text{g}/\text{mL}$  apramycin and a complete inhibition of cell lysis at 100  $\mu\text{g}/\text{mL}$  hygromycin or apramycin (Fig. 1b and c). This observation was in line with results from infection assays in liquid culture revealing no more culture collapse when supplementing the respective aminoglycosides (Fig. 2a). The antiviral activity was further demonstrated to be dose dependent, showing already an inhibition of infection at 1  $\mu\text{g}/\text{mL}$  apramycin (Fig. S1). In contrast, no antiviral activity was detected for spectinomycin (Fig. 2a).

To visualize the effect of apramycin on infection dynamics using live-cell imaging, *S. venezuelae* mycelium was grown from spores in a microfluidic device and infected with the phage Alderaan. Addition of apramycin almost completely inhibited phage-mediated lysis of *Streptomyces* mycelium, confirming the protective effect of apramycin against phage infection (Fig. 2b and Video S1).

Infection of *E. coli* with the model phage  $\lambda$  was also strongly impaired in the presence of aminoglycosides. Here, apramycin and kanamycin at concentrations as low as 25  $\mu\text{g}/\text{mL}$  showed a protective effect in liquid cultures (Fig. 2c and Fig. S2a) as well as an up to 1,000-fold reduction in numbers of PFU (Fig. 1b and c). Furthermore, this effect was shown to be independent of the host strain used (Fig. S2b).

In the case of temperate phages such as  $\lambda$ , an increased entry into the lysogenic cycle could explain the absence of phage amplification in the presence of aminoglycosides. To test this hypothesis, we conducted a reinfection experiment, in which cells surviving the first round of infection were washed and exposed to the same phage again. In the first infection round, cultures without apramycin showed a strongly increasing phage titer associated with extensive lysis of the culture. In contrast, infection in the presence of apramycin was completely inhibited, showing no phage amplification during  $\lambda$  infection and even an  $\sim 100$ -fold decrease in phage titers over time for Alderaan (Fig. 2d and Fig. S2c).

Interestingly, removal of the antibiotic and reinfection of cells from apramycin-treated cultures resulted in similar amplification kinetics of Alderaan and  $\lambda$  compared to an untreated control. Hence, these results do not support the selection of genetically encoded resistance traits or, in the case of  $\lambda$ , an increased formation of lysogens but rather indicate a reversible antiphage effect of apramycin.

Since elevated  $\text{Mg}^{2+}$  levels were previously shown to interfere with aminoglycoside uptake (16) and streptomycin-mediated inhibition of phage infection (12), we examined whether the antiviral effect of apramycin is alleviated in the presence of  $\text{MgCl}_2$ . As shown in Fig. 2e, phage infection was completely restored by the addition of 5 mM  $\text{MgCl}_2$ , as evidenced by the strong growth defect and the increasing phage titer during infection. Comparable results regarding the antagonistic effects of  $\text{MgCl}_2$  were also

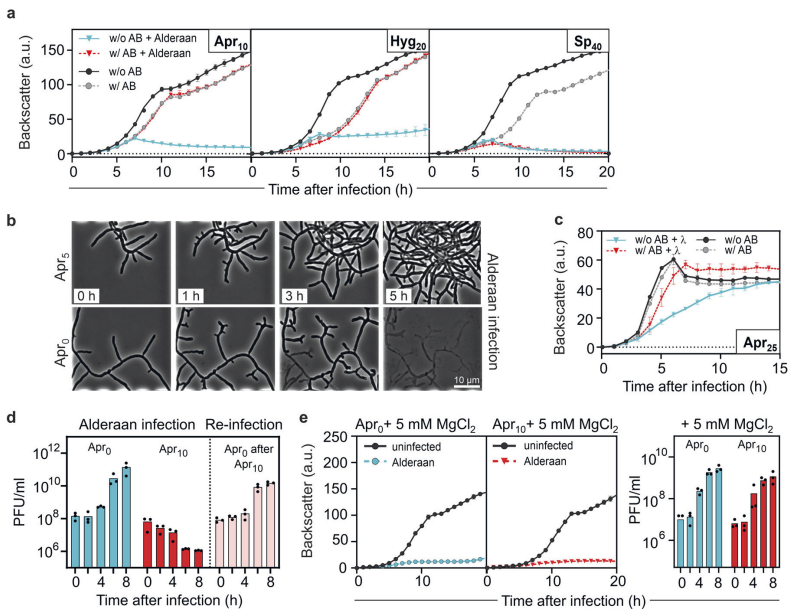


**FIG 2** Aminoglycosides strongly inhibit phage amplification in liquid cultures. (a) Infection curves for *Streptomyces venezuelae* infected by phage Alderaan in the presence of different aminoglycosides (concentrations, in  $\mu$ g/mL, are indicated with subscripts; AB, antibiotic). (b) Time-lapse micrographs of *S. venezuelae* cultivated in a microfluidics system and challenged with Alderaan (insets show time after infection). (c) Infection curves for *E. coli* DSM 4230 infected by  $\lambda$  in the presence of 25  $\mu$ g/mL apramycin. (d) Phage titers determined over two successive rounds of infection. A first infection round of *S. venezuelae* by Alderaan was performed in the presence or absence of apramycin. At the end of the cultivation, surviving cells from the apramycin-treated cultures were collected and exposed to phage Alderaan again, this time in the absence of apramycin. (e) Effect of MgCl<sub>2</sub> on infection of *S. venezuelae* by Alderaan, assessed by infection curves and determination of the corresponding phage titers over time. (a, d, and e) Alderaan was added to an initial titer of  $10^7$  PFU/mL; (c)  $\lambda$  was added to an initial titer of  $10^8$  PFU/mL. For growth curves and phage titers in panels a, c, d, and e, data are averages for three independent biological replicates ( $n = 3$ ).

obtained for  $\lambda$  (Fig. S2d). Overall, these results suggest that the antiviral effect of aminoglycosides is based on an interference with phage infection at the intracellular level, probably during or shortly after phage DNA injection.

**Spent medium of a natural aminoglycoside producer provides protection against phage predation.** As *Streptomyces* are the natural producers of aminoglycosides, we examined whether infection of *S. venezuelae* in spent medium of the apramycin producer *Streptoalloteichus tenebrarius* (formerly known as *Streptomyces tenebrarius* [17]) provides protection against phage predation. Alderaan infection was not impaired by spent medium of *S. tenebrarius* harvested after 1 day of cultivation. In contrast, cultivation in spent medium taken after 2 days completely reproduced the antiviral effect observed during experiments with supplemented purified apramycin, showing equivalent growth of infected and uninfected cultures (Fig. 3a). Endpoint quantification of extracellular phage titers confirmed this inhibition of infection, as no more infective extracellular phages were detectable in the supernatants of the infected cultures (Fig. 3b). Importantly, this protective effect of *S. tenebrarius* spent medium coincided with the presence of apramycin in cultures, as determined by liquid chromatography-mass spectrometry (LC-MS) (Fig. 3c). While the phage-inhibitory effect of the supernatants is very likely to be caused by the native levels of apramycin, we cannot exclude the possibility that this strain may produce other compounds with antiphage



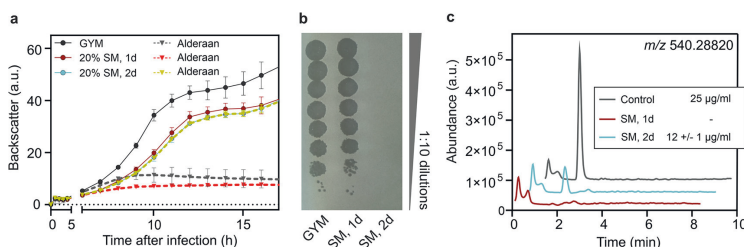


**FIG 3** Secondary metabolites produced by *Streptoalloteichus tenebrarius* inhibit phage infection. (a) Influence of spent medium from *S. tenebrarius* on infection of *S. venezuelae* by Alderaan. Data are averages for three independent biological replicates; error bars represent standard deviations. (b) Determination of the final phage titers of infected cultures shown in panel a. Results are representative of two biological replicates. (c) Extracted ion chromatogram of samples analyzed by LC-MS assessing the presence of apramycin (molecular weight, 539.58 g/mol) in spent medium (SM) of *S. tenebrarius*. The indicated concentrations of apramycin are close to the detection limit under these measuring conditions. GYM, glucose-yeast extract-malt extract medium.

properties. Taken together, these data suggest that production of aminoglycoside antibiotics in natural environments might serve as a chemical defense providing protection against phage infection on a community level.

**Aminoglycosides block an early step of phage infection.** To decipher the mechanism underlying the antiviral activity of aminoglycosides, we investigated the influence of apramycin on the different steps of the phage infection cycle (Fig. 4a).

First, we determined the impact of apramycin on the adsorption step, by following phage titers over time after performing an intense washing 15 min after phage addition to remove Alderaan phages that are only reversibly adsorbed to *Streptomyces mycelium* (Fig. S3). We confirmed that this 15-min preincubation time was sufficient to reach the stage of irreversible adsorption of phage particles, as the control without apramycin showed strongly increasing titers following washing. Importantly, the outcome of phage amplification was determined only in the presence of apramycin in the main culture, as preincubation with apramycin had no influence on later phage titers. Taken together with the adsorption assay performed in the presence of apramycin (Fig. S4a), these data suggest that apramycin does not inhibit irreversible adsorption but rather a later stage of the phage life cycle. In accordance with these findings, preincubation of phage particles with apramycin showed no impact on phage infectivity at physiologically relevant levels of 10 or 50  $\mu\text{g/mL}$  apramycin (Fig. S5). In contrast, higher concentrations ( $>500 \mu\text{g/mL}$ ) strongly impacted phage infectivity, showing a  $\sim 100$ -fold reduction in PFU/mL after 24 h of incubation.

Next, we assessed phage DNA delivery and amplification by determining the level of intracellular Alderaan DNA during infection via quantitative real-time PCR (qPCR). In the absence of apramycin, the phage DNA levels increased exponentially until 360 min post-infection, indicating active genome replication across several rounds of infection (Fig. 4b). Simultaneous measurement of extracellular phage titers showed stable titers until 120 min, followed by a strong rise indicative of the release of new phage progeny after cells lysis (Fig. 4c). Conversely, only a slight increase in intracellular DNA was obtained for infection under apramycin pressure (Fig. 4b; note that measurement in the presence of apramycin is close to the detection limit). Relative phage concentrations then declined starting at 45 min and were even similar to those measured in the uninfected controls at 360 and 450 min, hinting at degradation of intracellular phage DNA. In the meantime, extracellular phage titers of apramycin-treated cultures declined from 120 min (Fig. 4c). Overall, these results suggest an inhibition of phage genome replication but do not exclude an interference with the injection process in *S. venezuelae*.

Assuming that apramycin blocks an early step of phage infection prior to genome replication, addition of the antibiotic after the replication phase would not interfere

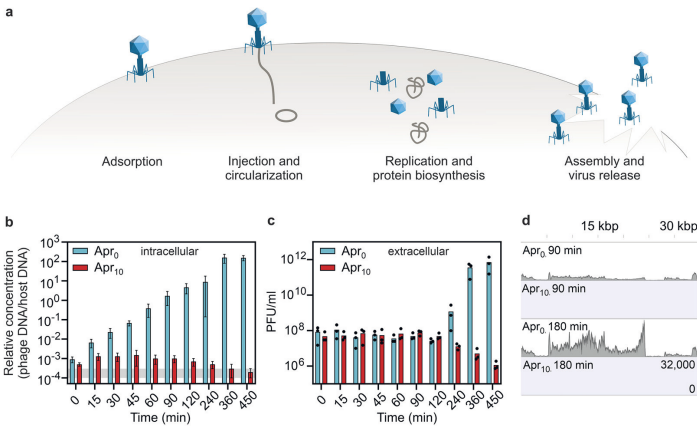


**FIG 4** Apramycin blocks the phage life cycle at an early stage—before replication and transcription of phage DNA. (a) Scheme of the phage lytic life cycle, highlighting the different steps which could be inhibited by antiphage metabolites. (b) Infection of *S. venezuelae* by Alderaan; time-resolved quantification of phage DNA by qPCR in the intracellular fraction. To quantify the relative concentration of phage DNA per host DNA, a gene coding for the minor tail protein of Alderaan (HQ601\_00028) and the housekeeping gene *atpD* of *S. venezuelae* were used. The corresponding oligonucleotide sequences are provided in Table S2D. Data are means for three independent biological replicates measured as technical duplicates. The range of relative concentrations measured for the uninfected controls (measured 120 min postinfection) is marked in gray. Note that the values measured for apramycin-treated samples are close to or even below the detection limit. (c) Time-resolved determination of Alderaan titers in the extracellular medium via double-agar overlays.  $n = 3$  independent replicates. (d) RNA-seq coverage of the Alderaan genome (39 kbp) during infection in the presence and absence of apramycin.

with the infection. This hypothesis was indeed confirmed by supplementation of the aminoglycoside at different time points post infection (Fig. S4b). Corresponding infection assays indicated that apramycin addition 30 min after infection was sufficient to prevent a reproductive Alderaan infection. The observed decrease in extracellular phage titers is probably the result of adsorption and subsequent DNA injection of a fraction of phages without release of new infective viral particles.

In contrast, no decrease in extracellular phage titers was observed when apramycin was added 1 to 2 h after infection, indicating that the first phages were able to complete their infection cycle before apramycin was added. Comparison of these results with the quantification of intracellular phage DNA (Fig. 4b) further showed that this period corresponds to the replication phase, indicating that replication is a sensitive time point for the antiviral activity of aminoglycosides. In the case of the *E. coli* system, the measurement of potassium efflux is an established approach to probe the successful delivery of phage DNA into the bacterial cell (18). Applying this method to infection of *E. coli* with phage  $\lambda$  confirmed that the injection process was not impaired by apramycin (Fig. S2e).

Next, we examined the influence of apramycin on phage DNA transcription. RNA sequencing revealed an increasing transcription of Alderaan DNA during phage infection under normal infection conditions, whereas addition of apramycin drastically hindered phage gene expression (Fig. 4d and Fig. S4c). In accordance with the previous results, these data suggest a blockage of phage infection prior to phage DNA replication and transcription, which is congruent with a recent report of inhibition of two mycobacteriophages by streptomycin, kanamycin, and hygromycin (19).

To visualize intracellular phage infections in the presence and absence of apramycin, we performed fluorescence *in situ* hybridization of phage DNA (phage-targeting direct-geneFISH) using Alexa Fluor 647-labeled probes specific for the phage genome. In this

assay, the formation of bright and distinct fluorescent foci is indicative of advanced viral infections (20). When infecting *E. coli* with  $\lambda$ , comparable amounts of injected phage DNA were detected for both infection conditions after 30 min. This result is in line with the potassium efflux assay described above, which showed similar injection kinetics in the presence of apramycin for *E. coli* (Fig. S2e). As the infection progressed, only samples without apramycin exhibited a strong increase in fluorescence intensity 90 min and 180 min post-infection, further hinting at an inhibited replication in the presence of apramycin (Fig. 5a). For Alderaan, an increase in red fluorescence and thus intracellular phage DNA could be observed 4 h after infection and was even more pronounced at 6 h, reflecting phage DNA replication. In contrast, apramycin-treated samples showed only a very weak and more diffuse red fluorescent signal in the 6-h samples (Fig. 5c), which is overall consistent with the quantification of intracellular phage DNA by qPCR (Fig. 4b). Plotting the distribution of fluorescence intensity per pixel confirmed that the massive increase in fluorescence at the last time point (180 min for  $\lambda$  and 6 h for Alderaan, respectively) was inhibited in the presence of apramycin, supporting the blockage of replication exerted by apramycin (Fig. 5b and d; Fig. S6a and c). Interestingly, determination of the percentage of  $\lambda$ -infected *E. coli* cells over time showed a peak at 30 min in apramycin-treated samples followed by a decline down to almost no infected cell at 180 min (Fig. S6b). This observation suggests that intracellular phage DNA was degraded following the halt of the phage life cycle caused by apramycin.

#### Acetylation of apramycin abolishes its antibacterial, but not antiphage properties.

Enzymatic modification of aminoglycosides is a major mechanism of bacterial resistance to these antibiotics. Aminoglycoside-modifying enzymes are categorized in three major classes: aminoglycoside *N*-acetyltransferases (AACs), aminoglycoside *O*-nucleotidyltransferases (ANTs), and aminoglycoside *O*-phosphotransferases (APHs) (13). Addition of an acetyl, adenylyl, or phosphoryl group at various positions of the aminoglycoside core scaffold decreases the binding affinity of the drug for its primary ribosomal target, leading to the loss of the antibacterial potency, with the modified aminoglycosides being described as “inactivated.”

However, the impact of these modifications on the antiphage activity of aminoglycosides is unknown. We set out to answer this question using apramycin and the acetyltransferase AAC(3)IV (21), also referred to as “Apr” in the literature. In the presence of apramycin, AAC(3)IV catalyzes the acetylation of the 3-amino group of the deoxystreptamine ring, using acetyl coenzyme A (acetyl-CoA) as a cosubstrate (Fig. 6a).

Using purified AAC(3)IV enzyme, we performed an *in vitro* acetylation reaction of apramycin. LC-MS analysis of the reaction mixtures revealed complete acetylation of apramycin, as the peak of apramycin (*m/z* 540) disappeared in favor of the one corresponding to acetylated apramycin (*m/z* 582) (Fig. 6b).

The efficiency of the acetylation reaction being confirmed, we tested the effect of acetylated apramycin on phage infection in liquid medium, using wild-type *S. venezuelae* (not carrying a plasmid-borne acetyltransferase gene) and its phage Alderaan. As expected, apramycin fully prevented growth of *S. venezuelae*, while acetylated apramycin did not show any toxicity effect. Strikingly, phage infection was completely inhibited in the presence of acetylated apramycin, suggesting that acetylation of apramycin does not interfere with its antiphage properties (Fig. 6c). Plate assays showed a comparable pattern: acetylation of apramycin suppressed its antibacterial effect but did not disrupt its ability to inhibit phage infection (Fig. 6d). Altogether, these results suggest a decoupling of the antibacterial and antiphage properties of apramycin and further highlight the distinct molecular target accounting for apramycin's antiphage properties.

## DISCUSSION

We have shown that aminoglycosides inhibit phage infection in a diverse set of bacterial hosts by blocking an early step of the phage life cycle prior to DNA replication. These findings highlight the multifunctionality of this class of antibiotics, as they possess both antibacterial and antiviral properties. The dual properties of aminoglycosides

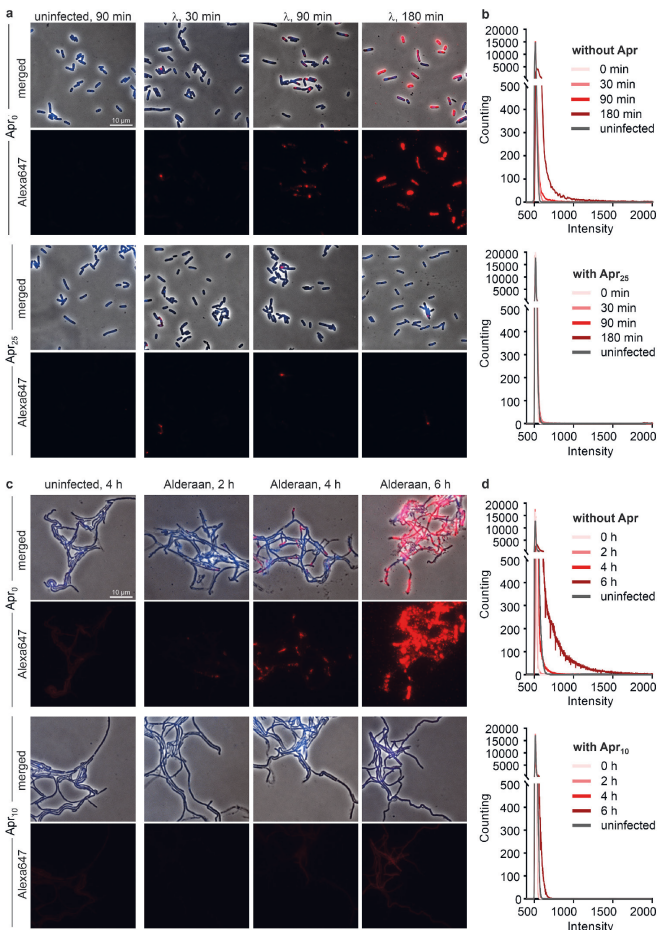


**FIG 5** Visualization of intracellular phage DNA by phage targeting direct-geneFISH. (a and c) Phage-targeting direct-geneFISH micrographs of (a) *E. coli* DSM4230 infected with  $\lambda$  and (c) *S. venezuelae* infected with Alderaan in the presence and absence of 25  $\mu$ g/mL and 10  $\mu$ g/mL apramycin, respectively. (First and third rows) Phase-contrast pictures merged with fluorescence signal from bacterial DNA (DAPI, blue) and phage DNA (Alexa647, red). (Second and fourth rows) Fluorescence signal from phage DNA only (Alexa647, red). Bar, 10  $\mu$ m. (b and d) Quantification of Alexa647 fluorescence in (b) *E. coli* cells infected with  $\lambda$  and (d) *S. venezuelae* cells infected with Alderaan, shown as density plots of pixel counts relative to their fluorescence intensity. Data are averages for biological three independent biological replicates ( $n = 3$ ); the data for all replicates are shown in Fig. S6a and b.

were first recognized in the 1950s and 1960s (10–12, 22), but mechanistic studies about their impact on phage infection differed in their conclusions. Brock and colleagues proposed a 2-fold inhibition of streptomycin on *Enterococcus faecium*, where streptomycin would be able to inhibit both genome injection and replication (12). In the same year, it was proposed that streptomycin inhibits the process of injection of

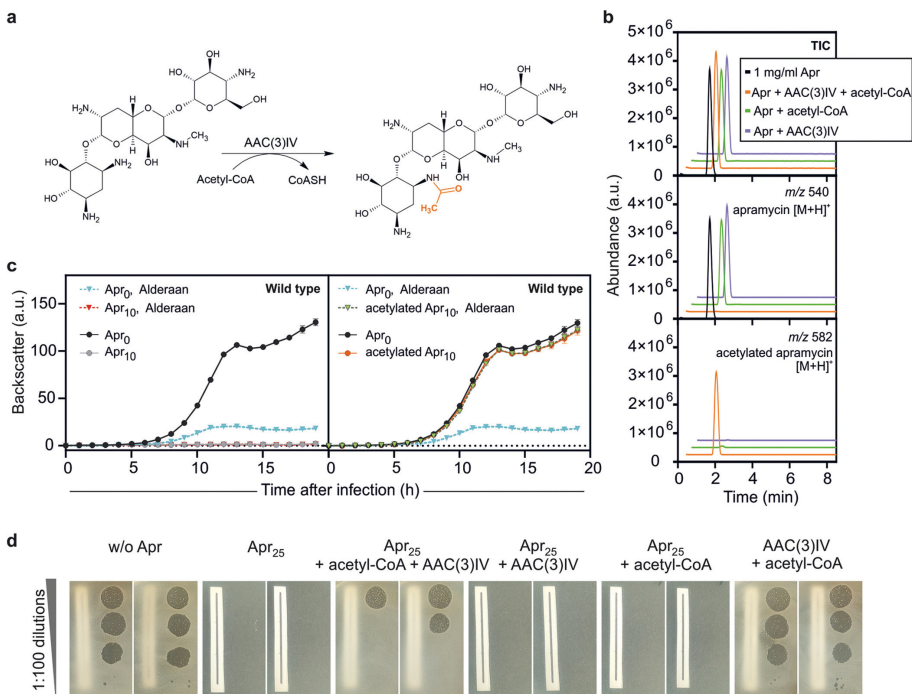


**FIG 6** Acetylated apramycin strongly inhibits phage infection, despite the loss of its antibacterial properties. (a) Acetylation reaction of apramycin catalyzed by the AAC(3)IV acetyltransferase. (b) Total ion chromatogram and extracted ion chromatograms of samples analyzed by LC-MS assessing the presence of apramycin (molecular weight, 539.58 g/mol;  $m/z$  540) and acetylated apramycin (molecular weight, 581.62 g/mol;  $m/z$  582) after *in vitro* acetylation of apramycin. (c and d) Effect of acetylated apramycin on infection of wild-type *S. venezuelae* with Alderaan, performed in liquid (c) and solid (d) media. For panel d, the reaction mixtures of the *in vitro* acetylation assays containing apramycin, acetyl-CoA, the AAC(3)IV acetyltransferase, or different combinations of these were used to supplement the plates. A piece of paper was placed below plates to facilitate assessment of bacterial growth.

these phages by preventing proper unfolding of the phage genome through cross-linking of the phage DNA (23). Recently, Jiang and colleagues reported the inhibition of two *M. tuberculosis* phages by streptomycin, kanamycin, and hygromycin (19). Following adsorption and quantifying of viral DNA, the authors proposed that the blockage caused by aminoglycosides occurs between genome circularization and replication. Our results put forward different pictures depending on the bacterial host. Infection with  $\lambda$  and Alderaan phages seems to be blocked at the genome replication stage by apramycin in both cases. However, we cannot exclude some additional interference with the injection step of phage Alderaan. This disparity presumably has its roots in the major differences in cell wall architectures between Gram-positive and -negative bacteria. Moreover, it opens the possibility that aminoglycosides exert a multilayered inhibition of phage infection in their natural producers.

More recently, sublethal aminoglycoside concentrations of aminoglycosides were shown to inhibit phage infection in *E. coli* and *Bacillus cereus* (24). Interestingly, tetracycline, another translation-inhibiting antibiotic binding to the 30S ribosome, was much less effective at suppressing phage proliferation. This difference suggests a direct

antiphage action of aminoglycosides and indicates that inhibition of phage replication is not a common trait of antibiotics blocking protein synthesis.

One crucial question is that of which structural features or chemical groups of aminoglycosides are responsible for their antiphage properties. Our screening revealed that aminoglycosides belonging to 3 of 4 subclasses showed antiphage activity, suggesting that these properties are widespread among aminoglycosides and not limited to one particular subclass. Furthermore, a potential antiviral activity is probably also strongly influenced by the uptake and cell envelope structure of a particular host species. However, thorough structure-function relationship studies are needed to address this topic.

The versatility of aminoglycosides can be attributed to their ability to bind a wide variety of molecules, including nucleic acids—DNA or RNA, biologically or nonbiologically derived. The most prominent target of aminoglycosides is the 16S rRNA, accounting for the disruption of protein translation and hence their bactericidal properties (13). Aminoglycosides have also been shown to bind to seemingly unrelated families of RNA molecules such as group I introns (25), a hammerhead ribozyme (26), the *trans*-activating response element (TAR) (27) and the Rev response element (RRE) of the human immunodeficiency virus (HIV) (28–30). Interestingly, this effect on HIV is the only report of a direct inhibition of eukaryotic viruses by aminoglycosides. Evidence of indirect influence on infection by eukaryotic viruses comprises the activation of interferon-based antiviral response following topical application of aminoglycosides (31), and the enhancement of plaque formation by coxsackieviruses via increased diffusion of virions in the extracellular matrix (32). Furthermore, *in vitro* studies showed condensation of purified phage  $\lambda$  DNA by aminoglycosides. It was proposed that the clamp formed by aminoglycosides around the DNA double helix causes a bend responsible for the formation of toroids and other structural deformations (33, 34).

Injected phage DNA is linear, in a relaxed state, and not protected by DNA-binding proteins, and it is therefore probably highly sensitive to DNA-binding molecules. Interestingly, anthracyclines—another class of secondary metabolites produced by *Streptomyces* strains with antiphage properties—inhibit phage infection at a similar stage (5). While the exact mechanism of action underlying phage inhibition by anthracyclines and aminoglycosides remains elusive, these recent results suggest that already injected but not yet replicating phage DNA is preferentially targeted by antiviral molecules. Repeated efforts to isolate Alderaan clones that developed resistance to apramycin were not successful, suggesting that phage inhibition by apramycin relies on structural properties of phage DNA that cannot be readily overcome by single-base mutations or small structural variants.

Therapeutical use of phages—known as phage therapy—is often combined with an antibiotic treatment due to the potentially synergistic effect between these two antimicrobial agents. In contrast, we describe here an antagonistic impact of a common antibiotic class on phages, which has important implications for phage-aminoglycoside combination treatment. We propose that sensitivity of the phage to aminoglycosides be assessed *in vitro* before administration of such combination therapy.

From a more fundamental perspective, these findings also shed new light on the role of aminoglycosides in natural bacterial communities. While their use as antibiotics for medical applications has been extensively documented, until now, relatively little was known about their function in the natural setting. We posit that aminoglycosides not only are used by their producers as a powerful weapon against bacterial competitors but also protect them against phage predation at the community level. In streptomycetes, antibiotic production happens mainly at later stages of development, typically during the formation of aerial hyphae (35–37), while phages preferentially attack young mycelium (38). This clear difference in chronology may make secondary-metabolite-mediated antiphage defense seem irrelevant when studied in a laboratory setting. However, this defense strategy takes its full meaning in the light of community



ecology, where older fractions of an established microbial community could ensure a protective “antiviral milieu” for their descendants.

Another key consideration to appreciate aminoglycoside antiviral properties in an ecological context concerns the importance of the resistance mechanism to these antibiotics. Using *Streptomyces venezuelae* and its phage Alderaan, we showed that acetylation of apramycin led to a loss of its antibacterial properties, while leaving its ability to block phage infection untouched. Assuming that this observation can be extended to more phages and aminoglycoside-modifying enzymes, it raises the question of whether deflecting the antibacterial effect of aminoglycosides while benefiting from their intracellular protective effect against phages would be a strategy favored over antibiotic resistance by efflux. Interestingly, unlike many antibiotic classes (39), efflux proteins reported to pump out aminoglycosides are relatively rare and conferred only partial resistance to aminoglycosides (13). In contrast, aminoglycoside-modifying enzymes are widespread and found in natural producers and clinical isolates alike (13, 40). Natural aminoglycoside producers often encode a second line of resistance represented by 16S rRNA methyltransferases, whose action makes their ribosomes insensitive to aminoglycosides without interfering with the action of the latter on phages (40).

Considering the colossal number of molecules produced by environmental bacteria whose physiological role is still unclear, we postulate that additional prokaryotic anti-phage metabolites are to be discovered in the future, further underlining the extraordinary diversity of strategies employed by bacteria against their viral predators.

## MATERIALS AND METHODS

**Bacterial strains and growth conditions.** All bacterial strains, phages, and plasmids used in this study are listed in Table S2A, B, and C, respectively. For growth studies and double-agar overlay assays, *Streptomyces* sp. cultures were inoculated from spore stocks and cultivated at 30°C and 120 rpm using glucose-yeast extract-malt extract (GYM) medium for *S. venezuelae* and *Streptoalloteichus tenebrarius* and yeast extract-malt extract (YEME) medium for *S. coelicolor* (35). *E. coli* was cultivated in lysogeny broth (LB) medium at 37°C and 170 rpm, while *C. glutamicum* was grown in brain heart infusion (BHI) medium at 30°C and 120 rpm.

For double-agar overlays, BHI agar for *C. glutamicum*, LB agar for *E. coli*, and GYM agar (pH 7.3) for all *Streptomyces* species were used, with 0.4% and 1.5% agar for the top and bottom layers, respectively. For quantification of extracellular phages, 2  $\mu$ L of the culture supernatants was spotted on a bacterial lawn propagated on a double-agar overlay inoculated at an initial optical density at 450 nm ( $OD_{450}$ ) of 0.4 for *Streptomyces* spp., an  $OD_{600}$  of 0.1 for *E. coli*, and an  $OD_{600}$  of 0.7 for *C. glutamicum*. Both agar layers were supplemented with antibiotics at the indicated concentrations.

For standard cloning applications, *E. coli* DH5 $\alpha$  was cultivated in LB medium containing the appropriate antibiotic at 37°C and 120 rpm. For conjugation between *Streptomyces* spp. and *E. coli*, the conjugative *E. coli* strain ET12567/pUZ8002 was used (41).

**Recombinant DNA work and cloning.** All plasmids and oligonucleotides used in this study are listed in Table S2C and D, respectively. Standard cloning techniques such as PCR and restriction digestion were performed according to standard protocols (42). In all cases, Gibson assembly was used for plasmid construction (43). DNA regions of interest were amplified via PCR using the indicated plasmid DNA as the template. The plasmid backbone was cut using the listed restriction enzymes. DNA sequencing and synthesis of oligonucleotides was performed by Eurofins Genomics (Ebersberg, Germany).

**Phage infection curves.** For phage infection curves, the BioLector microcultivation system of m2p-labs (Baesweiler, Germany) was used (44). Cultivations were performed as biological triplicates in FlowerPlates (m2p-labs, Germany) at 30°C and a shaking frequency of 1,200 rpm. During cultivation, biomass was measured as a function of backscattered light intensity with an excitation wavelength ( $\lambda_{ex}$ ) of 620 nm (filter module:  $\lambda_{ex}/\lambda_{em}$  620 nm/620 nm; gain, 25 or 20 in Fig. 3a) every 15 min. All growth curves are baseline corrected. Main cultures of *Streptomyces* spp. in 1 mL GYM medium containing the indicated supplements were inoculated with overnight cultures in the same medium to an initial  $OD_{450}$  of 0.15. Infection was performed by adding phages to an initial titer of  $10^7$  PFU/mL. Supernatants were collected in 2-h intervals to determine the time course of phage titer via double-agar overlays. Phage infection curves in *E. coli* were done in the same way at 37°C and 1,200 rpm using an initial  $OD_{600}$  of 0.1 in 1 mL LB medium and an initial phage titer of  $10^8$  PFU/mL, resulting in a multiplicity of infection (MOI) of 1.

Phage infection curves in shaking flasks were performed analogously to the cultivation in microbioreactors using a shaking frequency of 120 rpm. To study phage infection and the influence of aminoglycosides in *Streptomyces*, we draw attention to the importance of ion content, e.g., of water used for medium preparation.

**Cultivation and perfusion in microfluidic devices.** Single-cell analysis of *S. venezuelae* cells infected with phage Alderaan in presence and absence of apramycin was performed using an in-house-developed microfluidic platform (45–47). Cultivation and time-lapse imaging were performed in three steps. First, cultivation chambers in the microfluidic chip were inoculated with GYM medium containing an

initial spore titer of  $10^8$  PFU/mL. During the following precultivation phase, cells in all chambers were cultivated under continuous GYM medium supply supplemented with  $2.5 \mu\text{g/mL}$  apramycin (flow rate,  $300 \text{ nL/min}$ ) to allow comparable growth conditions. After 6 h of precultivation, cells were cultivated for 3 h in GYM medium containing one of the final apramycin concentrations (0, 5, or  $10 \mu\text{g/mL}$ ). Subsequently, infection was initiated by a continuous supply of GYM medium containing the final apramycin concentrations and Alderaan phages with a titer of  $10^8$  PFU/mL (flow rate,  $200 \text{ nL/min}$ ). By using disposable syringes (Omnifix-F tuberculin, 1 mL; B. Braun Melsungen AG, Melsungen, Germany) and a high-precision syringe pump system (neMESYS; Cetoni GmbH, Korbussen, Germany), continuous medium supply and waste removal were achieved. Phase-contrast images were obtained at 5-min intervals (exposure time, 100 ms) by a fully motorized inverted Nikon Eclipse Ti microscope (Nikon Europe B.V., Amsterdam, Netherlands). During the complete cultivation, the temperature was set to  $30^\circ\text{C}$  using an incubator system (PeCon GmbH, Erbach, Germany).

**Cultivation in spent medium.** For preparation of spent medium, cultures of the natural apramycin producer *Streptalloteichus tenebrarius* were prepared by inoculating 50 mL of GYM medium to an initial  $\text{OD}_{550}$  of 0.1 and were cultivated for 4 days. Spent medium of the culture was collected every day by centrifugation and subsequent filtration of the supernatant. After adjustment of the pH to 7.3, GYM medium and spent medium were mixed in a ratio of 4:1, so that spent medium accounted for 20% of the total volume. Ten-times-concentrated GYM was added to keep the concentration of C sources equal to that of fresh GYM medium. Cultivation and infection of the apramycin-resistant *S. venezuelae*/pJLK04 strain in 20% spent medium was conducted in microbioreactors as describe above by using an initial  $\text{OD}_{550}$  of 0.5 and an initial phage titer of  $10^8$  PFU/mL.

**LC-MS measurements of apramycin.** Aminoglycosides were analyzed using an Agilent ultrahigh-performance LC (UHPLC) 1290 Infinity system coupled to a 6130 Quadrupole LC-MS system (Agilent Technologies, Waldbronn, Germany). LC separation was carried out using an InfinityLab Poroshell 120 2.7- $\mu\text{m}$  EC-C<sub>18</sub> column (3.0 by 150 mm; Agilent Technologies, Waldbronn, Germany) at  $40^\circ\text{C}$ . For elution, 0.1% acetic acid (solvent A) and acetonitrile supplemented with 0.1% acetic acid (solvent B) were applied as the mobile phases at a flow rate of  $0.3 \text{ mL/min}$ . A gradient elution was used, where the amount of solvent B was increased stepwise: minutes 0 to 6, 10% to 25%; minutes 6 to 7, 25% to 50%; minutes 7 to 8, 50% to 100%; and minutes 8 to 8.5, 100% to 10%. The mass spectrometer was operated in the positive electrospray ionization (ESI) mode, and data were acquired using the selected-ion-monitoring (SIM) mode. An authentic apramycin standard was obtained from Sigma-Aldrich (Munich, Germany). Area values for  $[\text{M}+\text{H}]^+$  mass signals were linear for metabolite concentrations from 10 to  $50 \mu\text{g/mL}$ .

**Potassium efflux assays.** Cultures of *E. coli* DSM 4230/pEKEx2.d were grown in LB medium supplemented with  $50 \mu\text{g/mL}$  apramycin at  $37^\circ\text{C}$  and 170 rpm overnight. Fresh LB medium ( $50 \mu\text{g/mL}$  apramycin if needed) was inoculated 1:100 from the overnight cultures and incubated at  $37^\circ\text{C}$  and 120 rpm for 1.5 h. The cultures were centrifuged at  $5,000 \times g$  for 20 min, and the pellets were resuspended in SM buffer (0.1 M NaCl, 8 mM  $\text{MgSO}_4$ , 50 mM Tris-HCl [pH 7.5]). The  $\text{OD}_{600}$  was measured and adjusted to 2. The cultures were stored at  $4^\circ\text{C}$  and incubated at  $37^\circ\text{C}$  for 5 min directly before use. The measurements were performed using an Orion potassium ion selective electrode (Thermo Fisher Scientific, Waltham, MA, USA). Five microliters of the prepared cultures was mixed 1:50 with Orion ionic strength adjuster (ISA) (Thermo Fisher Scientific, Waltham, MA, USA), and measurements were started immediately to monitor the electric potential (in millivolts) every 5 s for a total of 60 min at room temperature with constant stirring. If apramycin was needed, it was added in the beginning to a concentration of  $100 \mu\text{g/mL}$ . After 5.5 min,  $100 \mu\text{L}$  of a polyethylene glycol (PEG)-precipitated  $\lambda$  phage lysate in SM buffer ( $10^{11}$  PFU/mL) was added to the cultures.

**Quantitative real-time PCR.** Quantification of cell-associated Alderaan phages was performed via quantitative real-time PCR. For this, infection of the apramycin-resistant strain *S. venezuelae* ATCC 10712/pJLK04 with Alderaan was performed as described in "Phage infection curves." At the indicated time points, 3 OD units of cells were harvested via centrifugation at  $5,000 \times g$  and  $4^\circ\text{C}$  for 10 min and washed twice with phosphate-buffered saline (PBS) before being stored at  $-20^\circ\text{C}$ . For quantification of intracellular phage DNA in presence and absence of apramycin, cells were resuspended in  $500 \mu\text{L}$  lysis buffer (10 mM Tris, 50 mM NaCl [pH 7.0]), and cell disruption was performed using a Precellys instrument (Bertin, Montigny Le Bretonneux, France) at  $6,000 \text{ rpm}$  three times for 40 s each. After centrifugation at  $16,000 \times g$  and  $4^\circ\text{C}$  for 10 min, DNA concentrations in the supernatants were determined via nanophotometer (Implen, Munich, Germany) and adjusted to  $1 \text{ ng}/\mu\text{L}$ . Finally,  $5 \mu\text{L}$  of the diluted supernatants as the template DNA was mixed with  $10 \mu\text{L}$   $2\times$  Luna universal qPCR master mix (New England Biolabs, Ipswich, MA, USA) and  $1 \mu\text{L}$  of each oligonucleotide (Table S2D) (final oligonucleotide concentration,  $0.5 \mu\text{M}$ ) and adjusted to a final volume of  $20 \mu\text{L}$  with double-distilled water ( $\text{ddH}_2\text{O}$ ). Measurements were performed in 96-well plates in the qTOWER 2.2 (Analytik Jena, Jena, Germany). For the determination of the relative concentration of cell-associated phages, the relative expression ratio of the phage target phage gene (HQ601\_00028, coding for the minor tail protein of Alderaan; PCR product, 144 bp) to the *S. venezuelae* housekeeping gene *atpD* (coding for the ATP synthase beta subunit; PCR product, 147 bp) was calculated via the "Relative quantification method" function of the qPCRsoft 3.1 software (Analytik Jena, Jena, Germany).

**Transcriptomics via RNA sequencing.** To compare transcription of phage and host DNA in presence and absence of apramycin, infection of the apramycin-resistant strain *S. venezuelae* ATCC 10712/pJLK04 with Alderaan was conducted as described in "Phage infection curves." Cells were harvested 90 min and 180 min after infection on ice at  $5,000 \times g$  and  $4^\circ\text{C}$  for 10 min. RNA purification was done using the Monarch total RNA miniprep kit (New England Biolabs, Ipswich, MA, USA) according to the



manufacturer's manual. Depletion of rRNA, library preparation, and sequencing were conducted by Genewiz (Leipzig, Germany).

After sequencing, all subsequent steps were conducted using CLC genomic workbench V. 20.0.4 software (Qiagen, Hilden, Germany). The initial quality check to analyze read quality and sequencing performances was followed by a trimming step. This step was used to remove read-through adapter sequences, leftover adapter sequences, low-quality reads (limit = 0.05), and ambiguous nucleotides. Subsequently, the trimmed reads were mapped against the genomes of *S. venezuelae* (accession no. NC\_018750.1) and the phage Alderaan (accession no. MT711975.1). Coverage plots were generated to show the distribution of mapped reads on both genomes. Subsequently, transcripts-per-million (TPM) values were calculated using the RNA-seq analysis tool of CLC genomics workbench (read alignment parameters: mismatch cost, 2; insertion cost, 3; deletion cost, 3; length fraction, 0.8; similarity fraction, 0.8; strand specificity, both; maximum number of hits for a read, 10). A table containing these values and an overview matrix containing all values were exported for each sample.

**Phage targeting direct-geneFISH.** Visualization and quantification of intracellular phage DNA during the time course of infection were conducted via fluorescence *in situ* hybridization (FISH), following the direct-geneFISH protocol (48), with modifications as described below.

Design of phage gene probes was done using the gene-PROBER (49). Sequences of the 200-bp polynucleotides for Alderaan and 300-bp polynucleotides for  $\lambda$  are provided in Table S3. Phage infection was performed as described in "Phage infection curves" using  $10^7$  PFU/mL as the initial phage titer for both phages. For infection of *E. coli*, the chemical labeling of polynucleotides with Alexa Fluor 647 dye (Thermo Fisher Scientific, Waltham, MA, USA) as well as the "core" direct-geneFISH protocol for microscopic slides was conducted as described previously using 0.5 mg/mL lysozyme for permeabilization and 35% (vol/vol) formamide during the hybridization step. Imaging of cells was performed with an inverted time-lapse live cell microscope (Nikon Europe B.V., Amsterdam, Netherlands) using a 100 $\times$  oil immersion objective (CFI Plan Apo Lambda DM; 100 $\times$  oil; numerical aperture [NA], 1.45; Nikon Europe B.V., Amsterdam, Netherlands) (45). Fluorescence was recorded using the optical filters DAPI (4',6-diamidino-2-phenylindole) and CY5-4040C (DAPI: excitation, 360/40 nm; dichroic, 400 nm; emission, 460/50 nm; exposure time, 500 ms; CY5: excitation, 628/40 nm; dichroic, 660 nm; emission, 692/40 nm; exposure time, 500 ms [AHF Analysentechnik AG, Tübingen, Germany]). Phase contrast was imaged with an exposure time of 500 ms.

For *S. venezuelae* infection, the protocol was adjusted as follows. Fixation of cells and phages was performed in 50% ethanol overnight at 4°C. After washing and immobilization, permeabilization was performed with 1.5 mg/mL lysozyme for 60 min at 37°C. Due to the high GC content of the phage Alderaan, the formamide concentration in the hybridization buffer and in the humidity chamber was adjusted to 60% (vol/vol) and the NaCl concentration in the washing buffer was reduced to 4 mM. After counterstaining with DAPI, imaging of cells was performed as described for *E. coli* using the optical filters DAPI and CY5-4040C with the indicated exposure times (DAPI: excitation, 360/40 nm; dichroic, 400; emission, 460/50 nm; exposure time, 800 ms; CY5: excitation, 628/40 nm; dichroic, 660; emission, 692/40 nm; exposure time, 500 ms [AHF Analysentechnik AG, Tübingen, Germany]). Phase contrast was imaged with an exposure time of 500 ms. The images for phage signal quantification were taken at the same exposure times to enable comparison; exposure times were adjusted to avoid overexposure of the signals. Preparation of image cut-outs and adjustments of lookup tables (LUTs) were performed using NIS-Elements BR 5.30.03 (64 bit).

As a quantification of the microscopic analyses, plots showing the distribution of Cy5 signal intensities for single microscopy images were generated. To this end, signal intensity of each pixel of the Cy5 channel images was determined using the software Fiji (50), and the frequency of occurrence of each intensity was calculated and plotted using R with the Rstudio interface (51, 52). Fluorescence intensity profiles of single replicates are shown in Fig. S6a and c.

**Purification of the AAC(3)IV apramycin acetyltransferase.** For heterologous protein overproduction, *E. coli* BL21(DE3) cells containing the pAN6\_aac(3)IV\_CStrep plasmid were cultivated as described in "Bacterial strains and growth conditions." Precultivation was performed in LB medium supplemented with 50  $\mu$ g/mL kanamycin (LB Kan<sub>50</sub>), which was incubated overnight at 37°C and 120 rpm. The main culture in LB Kan<sub>50</sub> medium was inoculated to an OD<sub>600</sub> of 0.1 using the preculture. At an OD<sub>600</sub> of 0.6, gene expression was induced using 100  $\mu$ M IPTG (isopropyl- $\beta$ -D-thiogalactopyranoside). Cells were harvested after additional 24 h of incubation at 20°C.

Cell harvesting and disruption were performed as described earlier (53) using buffer A (100 mM Tris-HCl [pH 8.0]) with cOmplete protease inhibitor (Roche, Basel, Switzerland) for cell disruption and buffer B (100 mM Tris-HCl, 500 mM NaCl [pH 8.0]) for purification. Purification of the Strep-tagged AAC(3)IV apramycin acetyltransferase was conducted by applying the supernatant to an equilibrated 2-mL Strep-Tactin-Sepharose column (IBA, Göttingen, Germany). After washing with 20 mL buffer B, the protein was eluted with 5 mL buffer B containing 15 mM D-thiobiotin (Sigma-Aldrich, St. Louis, MO, USA).

After purification, the purity of the elution fractions was checked by SDS-PAGE (54) using a 4 to 20% Mini-Protean gradient gel (Bio-Rad, Munich, Germany). The protein concentration of the elution fraction was determined with the Pierce bicinchoninic acid (BCA) protein assay kit (Thermo Fisher Scientific, Waltham, MA, USA), and the elution fraction with the highest protein concentration was chosen for further use.

**In vitro acetylation reaction of apramycin.** Protein purification of the AAC(3)IV apramycin acetyltransferase was conducted as described above. Acetylation of apramycin was performed using a modified version of the protocol described by Magalhaes and Blanchard (21). Assay mixtures were composed of 100  $\mu$ L 100 mM Tris-HCl–500 mM NaCl (pH 8.0) containing the AAC(3)IV at a concentration of 10  $\mu$ g/mL, as well as 10 mM apramycin (approximately 5 mg/mL) and 10 mM acetyl-CoA sodium salt (Sigma-Aldrich, St. Louis, MO, USA). The assay mixtures were incubated at 37°C for 20 min.

**Data availability.** Raw data as well as processed tables were deposited in the GEO database under the accession number [GSE171784](https://www.ncbi.nlm.nih.gov/geo/query/acc.cgi?acc=GSE171784).

## SUPPLEMENTAL MATERIAL

Supplemental material is available online only.

**VIDEO S1**, MOV file, 2 MB.

**FIG S1**, PDF file, 1.1 MB.

**FIG S2**, PDF file, 2.5 MB.

**FIG S3**, PDF file, 1.1 MB.

**FIG S4**, PDF file, 1 MB.

**FIG S5**, PDF file, 1.1 MB.

**FIG S6**, PDF file, 1.1 MB.

**TABLE S1**, DOCX file, 0.01 MB.

**TABLE S2**, DOCX file, 0.05 MB.

**TABLE S3**, DOCX file, 0.02 MB

## ACKNOWLEDGMENTS

We thank the European Research Council (ERC Starting Grant, grant number 757563), the Deutsche Forschungsgemeinschaft (SPP 2330, project 464434020), and the Helmholtz Association (grant number W2/W3-096) for financial support.

We thank Paul Ramp (Forschungszentrum Jülich) and Natalia Tschowri (University of Hannover) for providing strains and plasmids and our bachelor's degree student Lisa Helm for her contribution to this project. We furthermore thank Mark Buttner (John Innes Centre, Norwich, United Kingdom) for introducing us into *Streptomyces* biology and for many fruitful discussions.

We declare no conflict of interest.

## REFERENCES

- Hampton HG, Watson BNJ, Fineran PC. 2020. The arms race between bacteria and their phage foes. *Nature* 577:327–336. <https://doi.org/10.1038/s41586-019-1894-8>.
- Doron S, Melamed S, Ofir G, Leavitt A, Lopatina A, Keren M, Amitai G, Sorek R. 2018. Systematic discovery of antiphage defense systems in the microbial pangenome. *Science* 359:eaar4120. <https://doi.org/10.1126/science.aar4120>.
- Gao L, Altae-Tran H, Böhning F, Makarova KS, Segel M, Schmid-Burgk JL, Koob J, Wolf YI, Koonin EV, Zhang F. 2020. Diverse enzymatic activities mediate antiviral immunity in prokaryotes. *Science* 369:1077–1084. <https://doi.org/10.1126/science.aba0372>.
- Röstl JT, Marraffini L. 2019. (Ph)lighting phages: how bacteria resist their parasites. *Curr Opin Microbiol* 25:184–194. <https://doi.org/10.1016/j.crom.2019.01.009>.
- Kronheim S, Daniel-Ivad M, Duan Z, Hwang S, Wong AJ, Mantel I, Nodwell JR, Maxwell KL. 2018. A chemical defence against phage infection. *Nature* 564:283–286. <https://doi.org/10.1038/s41586-018-0767-x>.
- Bernheim A, Millman A, Ofir G, Meitav G, Avraham C, Shomar H, Rosenberg MM, Tal N, Melamed S, Amitai G, Sorek R. 2021. Prokaryotic vipers produce diverse antiviral molecules. *Nature* 589:120–124. <https://doi.org/10.1038/s41586-020-2762-2>.
- Hopwood DA. 2007. How do antibiotic-producing bacteria ensure their self-resistance before antibiotic biosynthesis incapacitates them? *Mol Microbiol* 63:937–940. <https://doi.org/10.1111/j.1365-2958.2006.05584.x>.
- Tenconi E, Rigali S. 2018. Self-resistance mechanisms to DNA-damaging antitumor antibiotics in actinobacteria. *Curr Opin Microbiol* 45:100–108. <https://doi.org/10.1016/j.mib.2018.03.003>.
- Schatz A, Bugle E, Waksman SA. 2005. The classic: streptomycin, a substance exhibiting antibiotic activity against gram-positive and gram-negative bacteria. *Clin Orthop Relat Res* 437:3–6. <https://doi.org/10.1097/01.blo.0000175887.98112.fe>.
- Schindler J. 1964. Inhibition of reproduction of the f2 bacteriophage by streptomycin. *Folia Microbiol* 9:269–276. <https://doi.org/10.1007/BF02873305>.
- Bowman BJ. 1967. Biological activity of phi-X DNA. I. Inhibition of infectivity by streptomycin. *J Mol Biol* 25:559–561. [https://doi.org/10.1016/0022-2836\(67\)90207-0](https://doi.org/10.1016/0022-2836(67)90207-0).
- Brock TD, Mosser J, Peachey B. 1963. The inhibition by streptomycin of certain *Streptococcus* bacteriophages, using host bacteria resistant to the antibiotic. *J Gen Microbiol* 33:9–22. <https://doi.org/10.1099/00221287-33-1-9>.
- Krause KM, Serio AW, Kane TR, Connolly LE. 2016. Aminoglycosides: an overview. *Cold Spring Harb Perspect Med* 6:a027029. <https://doi.org/10.1101/cshperspect.a027029>.
- Padilla IMG, Burgos L. 2010. Aminoglycoside antibiotics: structure, functions and effects on in vitro plant culture and genetic transformation protocols. *Plant Cell Rep* 29:1203–1213. <https://doi.org/10.1007/s00299-010-0900-2>.
- Koonin EV, Dolja VV, Krupovic M, Varsani A, Wolf YI, Yutin N, Zerbini FM, Kuhn JH. 2020. Global organization and proposed megataxonomy of the virus world. *Microbiol Mol Biol Rev* 84:e00061-19. <https://doi.org/10.1128/MMBR.00061-19>.
- Hancock RE, Raffle VJ, Nicas TI. 1981. Involvement of the outer membrane in gentamicin and streptomycin uptake and killing in *Pseudomonas aeruginosa*. *Antimicrob Agents Chemother* 19:777–785. <https://doi.org/10.1128/AAC.19.5.777>.
- Tamura T, Ishida Y, Otaguro M, Hatano K, Suzuki K. 2008. Classification of *Streptomyces tenebrarius* Higgins and Kastner as *Streptoalloteichus tenebrarius* nom. rev., comb. nov., and emended description of the genus *Streptoalloteichus*. *Int J Syst Evol Microbiol* 58:688–691. <https://doi.org/10.1099/ijs.0.65272-0>.
- Boulanger P, Letellier L. 1992. Ion channels are likely to be involved in the two steps of phage T5 DNA penetration into *Escherichia coli* cells. *J Biol Chem* 267:3168–3172. [https://doi.org/10.1016/0021-9258\(19\)50710-4](https://doi.org/10.1016/0021-9258(19)50710-4).
- Jiang Z, Wei J, Liang Y, Peng N, Li Y. 2020. Aminoglycoside antibiotics inhibit mycobacteriophage infection. *Antibiotics (Basel)* 9:714. <https://doi.org/10.3390/antibiotics9100714>.
- Allers E, Moraru C, Duhaime MB, Beneze E, Solonenko N, Barrero-Canosa J, Amann R, Sullivan MB. 2013. Single-cell and population level viral infection dynamics revealed by phageFISH, a method to visualize intracellular and free viruses. *Environ Microbiol* 15:2306–2318. <https://doi.org/10.1111/1462-2920.12100>.
- Magalhaes ML, Blanchard JS. 2005. The kinetic mechanism of AAC3-IV aminoglycoside acetyltransferase from *Escherichia coli*. *Biochemistry* 44:16275–16283. <https://doi.org/10.1021/bi051777d>.

22. Perlman D, Langlykke AF, Rothberg HD, Jr. 1951. Observations on the chemical inhibition of *Streptomyces griseus* bacteriophage multiplication. *J Bacteriol* 61:135–143. <https://doi.org/10.1128/jb.61.2.135-143.1951>.
23. Brock TD, Wooley SO. 1963. Streptomycin as an antiviral agent: mode of action. *Science* 141:1065–1067. <https://doi.org/10.1126/science.141.3585.1065>.
24. Zuo P, Yu P, Alvarez PJJ. 2021. Aminoglycosides antagonize bacteriophage proliferation, attenuating phage suppression of bacterial growth, biofilm formation, and antibiotic resistance. *Appl Environ Microbiol* 87:e0046821. <https://doi.org/10.1128/AEM.00468-21>.
25. Chow CS, Bogdan FM. 1997. A structural basis for RNA–ligand interactions. *Chem Rev* 97:1489–1514. <https://doi.org/10.1021/cr960415w>.
26. Tor Y, Hermann T, Westhof E. 1998. Deciphering RNA recognition: aminoglycoside binding to the hammerhead ribozyme. *Chem Biol* 5:R277–R283. [https://doi.org/10.1016/S1074-5521\(98\)90286-1](https://doi.org/10.1016/S1074-5521(98)90286-1).
27. Zapp ML, Stern S, Green MR. 1993. Small molecules that selectively block RNA binding of HIV-1 Rev protein inhibit Rev function and viral production. *Cell* 74:969–976. [https://doi.org/10.1016/0092-8674\(93\)90720-8](https://doi.org/10.1016/0092-8674(93)90720-8).
28. Litovchick A, Evdokimov AG, Lapidot A. 1999. Arginine-aminoglycoside conjugates that bind to HIV transactivation responsive element RNA in vitro. *FEBS Lett* 445:73–79. [https://doi.org/10.1016/S0014-5793\(99\)00092-7](https://doi.org/10.1016/S0014-5793(99)00092-7).
29. Litovchick A, Evdokimov AG, Lapidot A. 2000. Aminoglycoside–arginine conjugates that bind TAR RNA: synthesis, characterization, and antiviral activity. *Biochemistry* 39:2838–2852. <https://doi.org/10.1021/bi9917885>.
30. Mei H-Y, et al. 1995. Inhibition of an HIV-1 Tat-derived peptide binding to TAR RNA by aminoglycoside antibiotics. *Bioorg Med Chem Lett* 5:2755–2760. [https://doi.org/10.1016/0960-894X\(95\)00467-8](https://doi.org/10.1016/0960-894X(95)00467-8).
31. Gopinath S, Kim MV, Rakib T, Wong PW, van Zandt M, Barry NA, Kaisho T, Goodman AL, Iwasaki A. 2018. Topical application of aminoglycoside antibiotics enhances host resistance to viral infections in a microbiota-independent manner. *Nat Microbiol* 3:611–621. <https://doi.org/10.1038/s41564-018-0138-2>.
32. Acevedo MAW, Erickson AK, Pfeiffer JK, Greber UF. 2019. The antibiotic neomycin enhances coxsackievirus plaque formation. *mSphere* 4:e00632-18. <https://doi.org/10.1128/mSphere.00632-18>.
33. Kopaczynska M, Lauer M, Schulz A, Wang T, Schaefer A, Fuhrhop J-H. 2004. Aminoglycoside antibiotics aggregate to form starch-like fibers on negatively charged surfaces and on phage lambda-DNA. *Langmuir* 20:9270–9275. <https://doi.org/10.1021/la049207m>.
34. Kopaczynska M, Schulz A, Fraczekowska K, Kraszewski S, Podbielska H, Fuhrhop JH. 2016. Selective condensation of DNA by aminoglycoside antibiotics. *Eur Biophys J* 45:287–299. <https://doi.org/10.1007/s00249-015-1095-9>.
35. Kieser T, Bibb MJ, Buttner MJ, Chater KF, Hopwood DA. 2000. Practical streptomyces genetics: a laboratory manual. John Innes Foundation, Norwich, United Kingdom.
36. Bibb MJ. 2013. Understanding and manipulating antibiotic production in actinomycetes. *Biochem Soc Trans* 41:1355–1364. <https://doi.org/10.1042/BST20130214>.
37. McCormick JR, Flärdh K. 2012. Signals and regulators that govern *Streptomyces* development. *FEMS Microbiol Rev* 36:206–231. <https://doi.org/10.1111/j.1574-6976.2011.00317.x>.
38. Rosner A, Gutstein R. 1981. Adsorption of actinophage Pal 6 to developing mycelium of *Streptomyces albus*. *Can J Microbiol* 27:254–257. <https://doi.org/10.1139/m81-039>.
39. Reygaert WC. 2018. An overview of the antimicrobial resistance mechanisms of bacteria. *AIMS Microbiol* 4:482–501. <https://doi.org/10.3934/microbiol.2018.3.482>.
40. Ogawara H. 2019. Comparison of antibiotic resistance mechanisms in antibiotic-producing and pathogenic bacteria. *Molecules* 24:3430. <https://doi.org/10.3390/molecules24193430>.
41. MacNeil DJ, Gewinn KM, Ruby CL, Dezeny G, Gibbons PH, MacNeil T. 1992. Analysis of *Streptomyces avermitilis* genes required for avermectin biosynthesis utilizing a novel integration vector. *Gene* 111:61–68. [https://doi.org/10.1016/0378-1119\(92\)90603-M](https://doi.org/10.1016/0378-1119(92)90603-M).
42. Sambrook J, Russell DW. 2001. Molecular cloning: a laboratory manual, 3rd ed. Cold Spring Harbor Laboratory Press, Cold Spring Harbor, NY.
43. Gibson DG. 2011. Enzymatic assembly of overlapping DNA fragments. *Methods Enzymol* 498:349–361. <https://doi.org/10.1016/B978-0-12-385120-8.00015-2>.
44. Kensy F, Zang E, Faulhammer C, Tan RK, Buchs J. 2009. Validation of a high-throughput fermentation system based on online monitoring of biomass and fluorescence in continuously shaken microtiter plates. *Microb Cell Fact* 8:31. <https://doi.org/10.1186/1475-2859-8-31>.
45. Grünberger A, Probst C, Helfrich S, Nanda A, Stute B, Wiechert W, von Lieres E, Nöh K, Frunzke J, Kohlheyer D. 2015. Spatiotemporal microbial single-cell analysis using a high-throughput microfluidics cultivation platform. *Cytometry A* 87:1101–1115. <https://doi.org/10.1002/cyto.a.22779>.
46. Grünberger A, van Ooyen J, Paczia N, Rohe P, Schindzielorz G, Eggeling L, Wiechert W, Kohlheyer D, Noack S. 2013. Beyond growth rate 0.6: *Corynebacterium glutamicum* cultivated in highly diluted environments. *Bio-technol Bioeng* 110:220–228. <https://doi.org/10.1002/bit.24616>.
47. Helfrich S, Pfeifer E, Krämer C, Sachs CC, Wiechert W, Kohlheyer D, Nöh K, Frunzke J. 2015. Live cell imaging of SOS and prophage dynamics in isogenic bacterial populations. *Mol Microbiol* 98:636–650. <https://doi.org/10.1111/mmi.13147>.
48. Barrero-Canosa J, Moraru C. 2021. Linking microbes to their genes at single cell level with direct-geneFISH. *Methods Mol Biol* 2246:169–205. [https://doi.org/10.1007/978-1-0716-1115-9\\_12](https://doi.org/10.1007/978-1-0716-1115-9_12).
49. Moraru C. 2021. Gene-PROBER—a tool to design polynucleotide probes for targeting microbial genes. *Syst Appl Microbiol* 44:126173. <https://doi.org/10.1016/j.syapm.2020.126173>.
50. Schindelin J, Arganda-Carreras I, Frise E, Kaynig V, Longair M, Pietzsch T, Preibisch S, Rueden C, Saalfeld S, Schmid B, Tinevez J-Y, White DJ, Hartenstein V, Eliceiri K, Tomancak P, Cardona A. 2012. Fiji: an open-source platform for biological-image analysis. *Nat Methods* 9:676–682. <https://doi.org/10.1038/nmeth.2019>.
51. Allaire J. 2012. RStudio: integrated development environment for R. RStudio, Boston, MA.
52. R Core Team. 2021. R: a language and environment for statistical computing. R Foundation for Statistical Computing, Vienna, Austria.
53. Pfeifer E, Hünnefeld M, Popa O, Polen T, Kohlheyer D, Baumgart M, Frunzke J. 2016. Silencing of cryptic prophages in *Corynebacterium glutamicum*. *Nucleic Acids Res* 44:10117–10131. <https://doi.org/10.1093/nar/gkw692>.
54. Laemmli UK. 1970. Cleavage of structural proteins during the assembly of the head of bacteriophage T4. *Nature* 227:680–685. <https://doi.org/10.1038/227680a0>.

### 3.3. Inactivation of phage particles in the extracellular space of *Streptomyces* populations

Kever, L. and Frunzke, J.

Research article is part of this thesis; *to be submitted*

Contributor role	Contributor
Conceptualization	LK (65%), JF (35%)
Data curation	LK (100%)
Formal analysis	LK (100%)
Funding acquisition	JF (100%)
Investigation	LK (100%)
Methodology	LK (80%), JF (20%)
Project administration	LK (50%), JF (50%)
Resources	-
Software	-
Supervision	JF (60%), LK (40%)
Validation	LK (80%), JF (20%)
Visualization	LK (100%)
Writing – original draft	LK (70%), JF (30%)
Writing – review and editing	LK (50%), JF (50%)

**Overall contribution: 85%**

LK did all experimental work, data analysis and visualization except the scanning electron microscopy (Figure S4a) done by Dr. Mathias Müsken from the ZEIM department at Helmholtz Centre for Infection Research (HZI, Braunschweig, Germany). The original draft was mainly prepared by LK and LK took over a large part (50 %) of the revision and editing process.

# Inactivation of phage particles in the extracellular space of *Streptomyces* populations

Larissa Kever<sup>1</sup> and Julia Frunzke<sup>1\*</sup>

<sup>1</sup>Institute of Bio- und Geosciences, IBG-1: Biotechnology, Forschungszentrum Jülich, 52425 Jülich, Germany

\*Corresponding author: Julia Frunzke; Email: j.frunzke@fz-juelich.de

## Abstract

Multicellular development is one of the main characteristics of *Streptomyces*. However, its impact on the protection against phage infection remains largely unclear. In this study, we observed that *Streptomyces* phage infection significantly differs from infection of unicellular-growing bacteria. As exemplified by phage Alderaan infecting *Streptomyces venezuelae*, infection experiments revealed a successful phage amplification followed by a significant drop in infectious phage particles at later stages. This reduction in phage titer coincided with the re-growth of phage-resistant mycelium. In the following, we systematically considered bacterial molecule secretion, medium acidification and mycelial growth as potential influencing factors that could condition the reduction in infectious phage particles in the supernatant. In addition to the first two factors showing a possible contribution to the observed phenotype, the developmental state of the mycelium showed a strong impact on phage susceptibility. Besides Alderaan, we also observed a significant reduction for other non-host phages. This effect was even enhanced upon overexpression of *blaN*, which is involved in the formation of the hydrophobic protein sheath formed at later stages during mycelial development. Overall, these results suggest that the multicellular development of *Streptomyces* might represent an additional layer of the complex multicellular antiphage defense employed by these bacteria, which might have substantial ecological implications for community interactions.

**Introduction** | The Gram positive soil bacterium *Streptomyces* represents the largest genus of Actinobacteria (Anderson & Wellington, 2001). Besides being a prolific producer of bioactive molecules (Hopwood, 1999; Watve et al., 2001), *Streptomyces* spp. differ significantly from other prokaryotes dividing by binary fission as they possess a unique developmental life cycle (Chater, 2016; Flårdh & Buttner, 2009). Starting with the germination of a spore, *Streptomyces* forms a network of branching hyphae known as vegetative mycelium. Unfavorable conditions such as nutrient deficiency foster transition to reproductive growth with erection of unbranched aerial hyphae and subsequent compartmentalization into unigenomic, stress-resistant spores (Flårdh & Buttner, 2009; McCormick & Flårdh, 2012). This transition is preceded by an auto-degradation of the first substrate mycelium serving as nutrient source (Manteca et al., 2007; Miguélez et al., 1999). The production of bioactive compounds is intriguingly linked to this developmental program and is typically triggered by nutrient starvation or stress stimuli (Bibb, 2005).

The multicellular life style is regulated by a complex hierarchical network, which is controlled by the c-di-GMP-dependent activity of the master regulator BldD (Bush et al., 2015; Tschowri et al., 2014). During vegetative growth, BldD delays the onset of differentiation by repressing the key developmental *bld* and *whi* genes (Bush et al., 2015; den Hengst et al., 2010). Relieving repression by BldD initiates the first developmental transition from vegetative mycelium to aerial hyphae, which is accompanied by a change from hydrophilic to hydrophobic cell surface properties based on the  $\alpha^{BldD}$ -regulated transcription of *rodlin* and *chaplin* genes (Bibb et al., 2012; Claessen et al., 2003; Claessen et al., 2002; Elliot et al., 2003). In case of *S. venezuelae*, this so-called rodlet layer consists of three types of rodlin proteins (RdIA-C) as well as six types of chaplin proteins, two of them belonging to the group of long chaplins (ChpB and C) and four of them being short chaplins (ChpE-H) (Bibb et al., 2012). Together with the surfactant protein SapB, these proteins allow the escape of aerial hyphae from the aqueous environment into the air (Elliot & Talbot, 2004; Willey et al., 2006).

Due to the constant threat of phage attacks in almost every habitat, bacteria evolved multiple lines of

antiphage defense including the well-characterized restriction-modification systems, CRISPR-Cas systems as well as abortive infection strategies. This repertoire experienced a significant expansion by the discovery of a multitude of new defense mechanisms fostering the notion of a prokaryotic immune system (Bernheim & Sorek, 2020; Doron et al., 2018). Despite the resurgence of phage research and the increasing amount of known actinobacteriophages (Hatfull, 2020), less is actually known about the extent to which *Streptomyces* can employ its features of bioactive molecule production and multicellular development as defense against viral predators. Just recently, bacterial small molecule production was discovered as a new anti-viral strategy as exemplified by *Streptomyces*-derived anthracyclins and aminoglycoside antibiotics (Kever et al., 2022; Kronheim et al., 2018). As important contributor of soil biomass, the dense, partly hydrophobic mycelium might represent a further layer of antiphage defense by retaining phages, as it was already described for fungal mycelia-phage-interactions (Ghanem et al., 2019).

Previous studies describing one-step infection curves with *Streptomyces* revealed a distinct drop in infectious phage particles at later stages of the experiment indicating inactivation of released viruses (Hardy et al., 2020). In this study, we dissected different parameters contributing to the reduction in phage titer by considering the impact of small molecule production, medium acidification and mycelial growth as potential influencing factors using *Streptomyces venezuelae* as model strain. Besides a potential impact of secreted antiphage molecules and medium acidification, we observed a high impact of the developmental stage of mycelium on phage susceptibility as evidenced by the transient phage tolerance of mature mycelium. Interestingly, a significant decline in infectious extracellular non-host phages during incubation with *Streptomyces* mycelium was observed, which seemed to coincide with the onset of differentiation. We could envision that phages might be adsorbed by the hydrophobic bacterial surface layer during hyphae-spore transition. Overall, these findings emphasize a contribution of multicellular development to antiphage defense potentially providing a community-wide protection on an interspecies level.

### Results

Mycelial growth coincides with a significant reduction of infectious phage particles | Infection curves with different *Streptomyces* phages recently revealed a significant reduction in extracellular phage titers upon re-growth of *Streptomyces* mycelium (Hardy et al., 2020). To investigate if this phenotype can also be observed during phage infection of non-filamentous growing hosts, long-term infection was comparatively performed for phages infecting different bacterial species, including Alderaan infecting *S. venezuelae* NRRL B-65442, CL31 infecting *C. glutamicum* MB001 and  $\lambda$  infecting *E. coli* LE392. Phage titers were quantified over time for an intermediate phage pressure (Alderaan:  $10^7$  PFU/ml; CL31:  $10^4$  PFU/ml; Lambda:  $10^8$  PFU/ml).

Growth defects correlated well with applied initial phage titers, with high titers resulting in a significant culture collapse. Accompanied quantification of the corresponding

phage titers over time revealed an initial increase within the first hours of infection indicative for a successful phage amplification (Figure 1). In case of Alderaan, this ~1000-fold increase in infectious phage particles was followed by a decrease in extracellular titers starting ~48 h post infection. This temporally coincided with the re-growth of *Streptomyces* mycelium, which was later shown to be resistant towards re-infection with the same phage at an initial phage pressure of  $10^8$  PFU/ml (Figure S1a). In contrast, CL31 titers during re-growing of *C. glutamicum* stayed almost constant. A comparable time course of phage titer was also quantified during  $\lambda$  infection indicating a ~100-fold increase within the first 8 h of infection, before reaching a plateau. To conclude, this phenotypic observation of declining phage titers could not be seen for unicellular-growing bacteria as exemplified by *E. coli* and *C. glutamicum* phage infection and thus might be conditioned by the filamentous growth of *Streptomyces*.

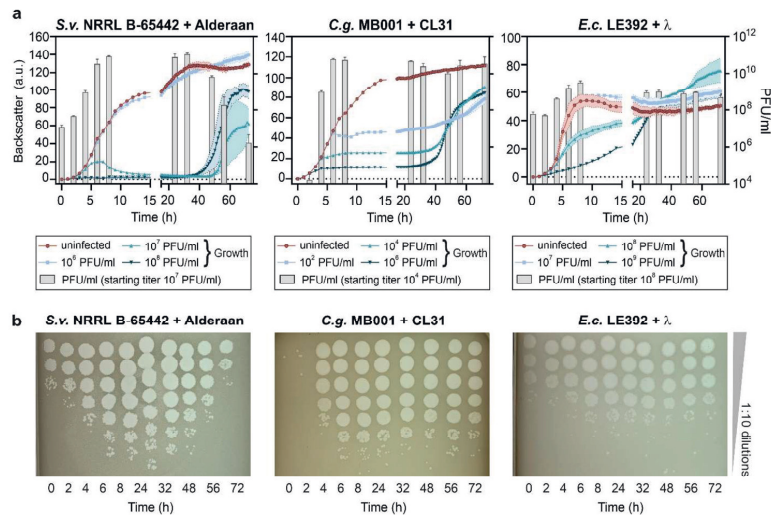


Figure 1: Emergence of phage-resistant *Streptomyces* mycelium results in a decrease in extracellular infectious phage particles. a) Infection curves of *S. venezuelae* NRRL B-65442 infected by Alderaan, *C. glutamicum* MB001 infected by CL31 and *E. coli* LE392 infected by  $\lambda$ . Cultivations were conducted in the BioLector microcultivation systems (Beckman Coulter Life Sciences, Krefeld, Germany) using three different initial phage titers as indicated ( $n=3$  independent biological replicates). Phage titers were calculated over time via double-agar overlays for infection with an intermediate phage pressure (see PFU/ml values in brackets; grey bars). b) Representative double-agar overlay assays of three independent biological replicates.



Contribution of bacterial molecule secretion and medium acidification to phage inactivation | Phage infection in *Streptomyces* spp. exemplified by Alderaan infecting *S. venezuelae* exhibits an atypical time course of phage titers showing a drop during re-growing of phage-resistant *Streptomyces* mycelium. To discriminate between a decrease in total extracellular phage particles or rather in infectious phages, double-agar overlays and qPCR were comparatively conducted during the entire infection experiment. Calculation of the end point fraction of remaining phages (72 h post infection) to the maximum titer reached (8 h post infection) showed a reduction in infectious phage particles of  $\geq 99.9\%$  for double-agar overlay quantification, whereas extracellular phage DNA-levels measured via qPCR just exposed a decline of  $\sim 92\text{--}96\%$  (Figure 2a und Figure S1b and c). This hints on combinatorial effects of factors causing a complete removal/degradation of viral particles and further factors contributing to the inactivation of remaining particles.

In the following, different factors were considered for their contribution to the decline in infectious phage particles: (i) instability of phage particles due to acidification of the culture supernatant, (ii) inactivation of phages by production and secretion of antiphage metabolites or proteins as well as (iii) adsorption of phages to mycelial structures.

Growth of *S. venezuelae* in GYM medium can result in a significant acidification of the medium reaching pH values of  $\sim 4.5\text{--}5.0$  (Figure S1d), most likely due to secretion of organic acids (Ahmed et al., 1984; Madden & Ison, 1996). Testing pH stability of phage Alderaan in GYM medium adjusted to different pH values showed a high pH stability at pH 5.0–9.0. At pH 4.0, a  $\sim 100$ -fold reduction in infectious phage particles was detected after 24 h of incubation. This was less pronounced than

the decline observed during long-term infection, even at a lower pH value than usually reached during cultivation in GYM medium (Figure S1e). Nevertheless, to eliminate any influence of acidification, long-term infection was repeated in GYM medium buffered with 100 mM MOPS (pH 7.3). Interestingly, bacteria showed significantly faster re-growth of mycelium in buffered conditions starting already at 18 h post infection, which coincided with a less pronounced, but still distinct reduction in infectious phage particles of  $\sim 10$ -fold (Figure 2c). This could be explained by either eliminating acidification itself as an influence factor or by downstream effects of buffered cultivation conditions potentially resulting in an altered morphology or exo-metabolome.

Further, we tested the impact of secreted metabolites or proteins on phage stability by incubating Alderaan in either fresh GYM medium or in phage-free spent medium (SM) of *S. venezuelae*. Additionally, the effect of chloramphenicol (Cm) as a well-known antibiotic produced by *S. venezuelae* (Vining & Stuttard, 1995) was directly tested on Alderaan plaque formation. The highest impact on infectious phage particles was observed upon incubation in spent medium harvested after 24 h of *Streptomyces* cultivation in unbuffered conditions (pH 6.9) showing a decline in phage titers of 60–73%, while all other tested conditions showed no substantial differences in infectious phage titers (Figure 2d and S1f). However, it should be noted that transient production of antiphage molecules cannot be completely ruled out and may not have been detected in this experimental setup.

Altogether, these data already gave a first hint that bacterial metabolite or protein secretion as well as medium acidification could contribute to the observed decline in infectious titers.



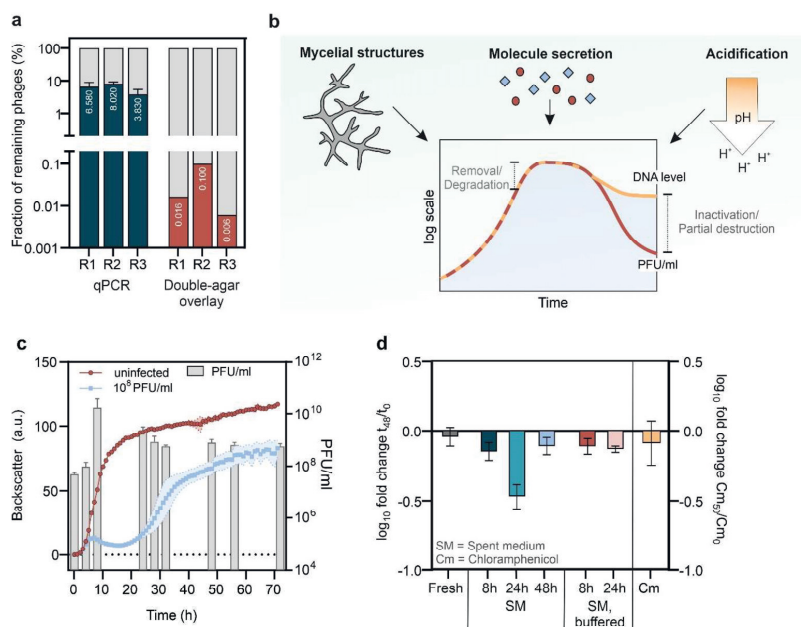


Figure 2: Influence of acidification and molecule secretion on infectious Alderaan particles. a) Fraction of remaining Alderaan phages ( $t_{72}/t_0$ ) based on quantification of Alderaan genome equivalents via qPCR (three independent biological replicates (R1-R3) measured as technical triplicates) and quantification of PFUs (three independent biological replicates R1-R3). Corresponding growth curves and time-resolved measurements of phage DNA and PFUs are shown in Figure S1b and c. b) Schematic illustration of different influencing factors potentially contributing to the observed decrease in extracellular phage titers. c) Infection *S. venezuelae* NRRL B-65442 infected by Alderaan in GYM medium buffered with 100 mM MOPS (pH 7.3). Phage titers over time were calculated via double-agar overlays (grey bars) ( $n=3$  independent biological replicates). d) Influence of spent media and chloramphenicol on Alderaan plaque formation. Phage Alderaan was incubated in different spent media of uninfected cultures under cultivation conditions for 48 h. Infectious phages were quantified via double-agar overlays directly after and in the end of incubation to calculate the  $\log_{10}$  fold change ( $t_{48}/t_0$ ) ( $n=3$  independent biological replicates). In case of chloramphenicol (Cm) assays, plaque formation was counted on plates with and without 50  $\mu\text{g}/\text{ml}$  Cm, shown as  $\log_{10}$  fold change ( $\text{Cm}_{50}/\text{Cm}_0$ ). For comparison, plaque formation at further Cm concentrations is shown Figure S1f.

Mature *Streptomyces* mycelium features a significant reduction in phage susceptibility | In addition to medium acidification and secreted bacterial molecules, a potential impact of mycelial structures on the decline in infectious phage particles was examined. Therefore, phage susceptibility of different developmental stages of *S. venezuelae* was investigated by using pre-cultures of different growth phases to inoculate main cultures for infection assays. The highest susceptibility towards Alderaan infection was observed for stationary pre-cultures containing already a high proportion of spore chains. Upon inoculation of a fresh culture, spore germination led to a significant culture collapse upon addition of  $10^7$  and  $10^8$  PFU/ml of Alderaan (Figure 3a and b). An almost equivalent extent of phage infection on bacterial growth was obtained for young, vegetative

mycelium just starting to branch, which derived from pre-cultures in the early exponential phase.

In contrast, the mature, dense mycelium from mid exponential pre-cultures showed a significantly enhanced phage tolerance as indicated by an omitted cell lysis at an intermediate phage pressure of  $10^7$  PFU/ml. Comparing phage amplification until 24 h post infection revealed a ~1000 fold increase in extracellular phage titers for stationary and early exponential pre-cultures when using an initial phage titer of  $10^7$  PFU/ml for infection. This differed significantly for mid exponential cultures revealing no substantial phage amplification and even a slight decrease in infectious Alderaan phages over time (Figure 3c and Figure S2).

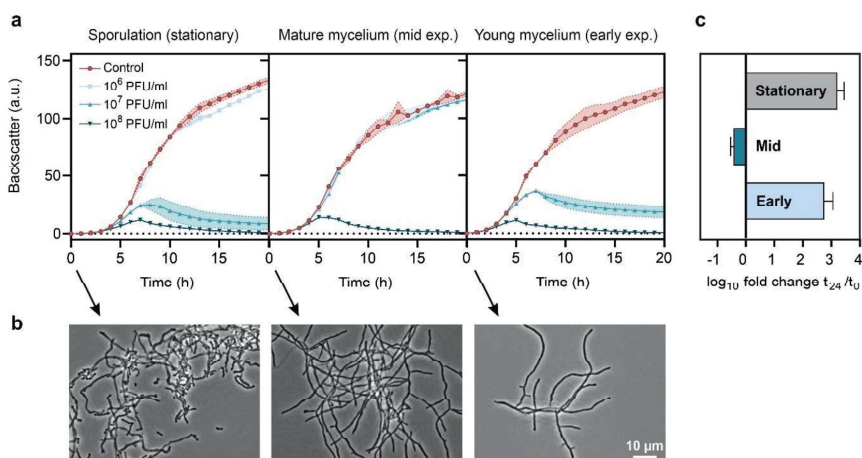


Figure 3: Influence of *S. venezuelae* developmental stage on phage susceptibility. a) Infection curves of *S. venezuelae* NRRL B-65442 infected by Alderaan. Pre-cultures of different developmental stages were used to inoculate main cultures for conducting infection assays in microtiter plates using three different initial phage titers as indicated (n=3 independent biological replicates) (early exp.: 16 h pre-cultivation, mid exp.: 20 h pre-cultivation, stationary: 30 h pre-cultivation). (b) Microscopy of *S. venezuelae* pre-cultures (scale bar = 10  $\mu$ m, exposure time = 120 ms). (c)  $\log_{10}$  fold change of phage titers indicating the level of phage amplification until 24 h post infection. Phage titers over time were calculated at an intermediate phage pressure of  $10^7$  PFU/ml via double-agar overlays (n=3 independent biological replicates). Corresponding double-agar overlay assays are shown in Figure S2.

Incubation with *Streptomyces* mycelium caused a decline in non-host phage titers | Based on the high phage tolerance of dense mycelium and the dropping phage titer upon re-growth of phage-resistant mycelium we hypothesized that the mycelial growth might contribute to the observed phenotype by efficiently adsorbing phages from the environment.

To prove this hypothesis, a broad set of phages infecting different bacterial species and belonging to different phage families was incubated with mycelium of *S. venezuelae*: Endor1,  $\lambda$ , T-phages, Langgrundblatt1, Pfeifenkraut, Athelas and CL31 as tailed dsDNA viruses from the class *Caudoviricetes*, M13 as filamentous ssDNA viruses from the class *Faserviricetes* and MS2 as ssRNA viruses from class *Leviviricetes* (Table S2). To eliminate pH effects on phage stability, GYM medium was buffered with 100 mM MOPS (pH 7.3). Calculating start and end titers of infectious phage particles in the culture supernatants via double-agar overlays revealed no substantial influence of growing *S. venezuelae* mycelium on the majority of tested phages. However, listed in descending order CL31 infecting *C. glutamicum* MB001, T4 infecting *E. coli* B and MS2 infecting *E. coli* W1485 exhibited a decrease in extracellular phage titers upon incubation with mycelium, while corresponding spent medium showed no influence on phage infectivity (Figure 4a and Figure S3a-c). In the following, the term 'non-host phage' refers to phages unable to infect *S. venezuelae*.

Focusing on the lytic siphophage CL31 as the most affected one, incubation assays were repeated in a time-resolved manner with simultaneous quantification of CL31 DNA levels via qPCR. Continuously decreasing quantities of infectious phage particles in culture supernatant were detected from 6 h post inoculation, which coincided with the simultaneous decrease in CL31 DNA levels (Figure 4b). Microscopic analysis of mycelium during this decrease exposed first spore chains at 6 h and already a high proportion of spores at 9 h post inoculation. This indicates that a reduction in infectious CL31 particles went along with a transition from hyphal growth to sporulation suggesting an impact of the developmental stage of mycelium on this decrease. In contrast, spent medium taken at these time points and addition of new phage particles to the remaining ones showed no further decrease in

infectious CL31 titers over 18 h, thereby widely excluding spent medium as main influencing factor (Figure 4c). However, attempts to get phages back in culture supernatant via extensive shaking or mechanical cell disruption as well as visualization of CL31 particles at the mycelial surface via scanning electron microscopy were not successful so far (Figure S4a and b).

To further focus on the influence of the developmental transition to spores on the decline in extracellular phage titers, incubation assays with CL31 were comparatively conducted with other microorganisms unable to sporulate as well as different *Streptomyces* species. Here, we included mycelium of *S. coelicolor* and *S. olivaceus*, the *S. venezuelae* developmental mutants  $\Delta bldD::apr$  (hypersporulation phenotype (Tschowri et al., 2014)) and  $\Delta bldN::apr$  (only vegetative growth (Bibb et al., 2012)), a couple of bacteria dividing by binary fission comprising *E. coli*, *P. putida* and *B. subtilis* as well as the haploid, yeast-like growing fungi *Ustilago cynodontis* (Table S1). Addition of CL31 phages to bacterial cultures of *E. coli*, *P. putida* and *B. subtilis* exhibited no significant decline in extracellular infectious CL31 particles (Figure 4d). The same applied to incubation of CL31 with the fungi *U. cynodontis*, which probably does not produce hydrophobicity-mediating proteins in its haploid, yeast-like state (Teertstra et al., 2006; Teertstra et al., 2009). Additionally, a reduced decline was observed for *S. coelicolor* and *S. olivaceus*, which – different from *S. venezuelae* – revealed no sporulation during the entire cultivation in submerged cultures (Glazebrook et al., 1990; Manteca et al., 2008).

While the *S. venezuelae* wild type strain showed significant effects on extracellular CL31 titers, this decline was less pronounced during incubation with the developmental mutants  $\Delta bldD::apr$  and  $\Delta bldN::apr$  (Figure 4d). Deletion of *bldD* as the master regulator repressing the key developmental genes results in a hypersporulation phenotype forming premature spores from vegetative mycelium (Bush et al., 2015; Tschowri et al., 2014). Null mutants of  $\sigma^{bldN}$  are restricted to vegetative growth as they are unable to build up the hydrophobic surface layer during aerial hyphae formation by expression of *rodlin* and *chaplin* genes. Although the formation of aerial mycelium is not

relevant in submerged cultures, hyphae-spore transition was proven to be still accompanied by expression of *rodlin* and *chaplin* genes (Bibb et al., 2012). Accordingly, results gained for these two mutants lead to the hypothesis that dense mycelial networks as well as hydrophobic surface structures during late stages of *Streptomyces* development might substantially influence extracellular titers of infectious non-host phage particles. Consistent with this,

overproduction of the mature BldN protein and expected enhanced expression of *rodlin* and *chaplin* genes (Bibb et al., 2012) accelerated the observed decline in CL31 titers in direct comparison to the wild type strain cultivated in the same batch of medium (Figure 4e). This further strengthened the assumption that the hydrophobic layer could be one factor conditioning the drop in infectious phage particles (Figure 4f).

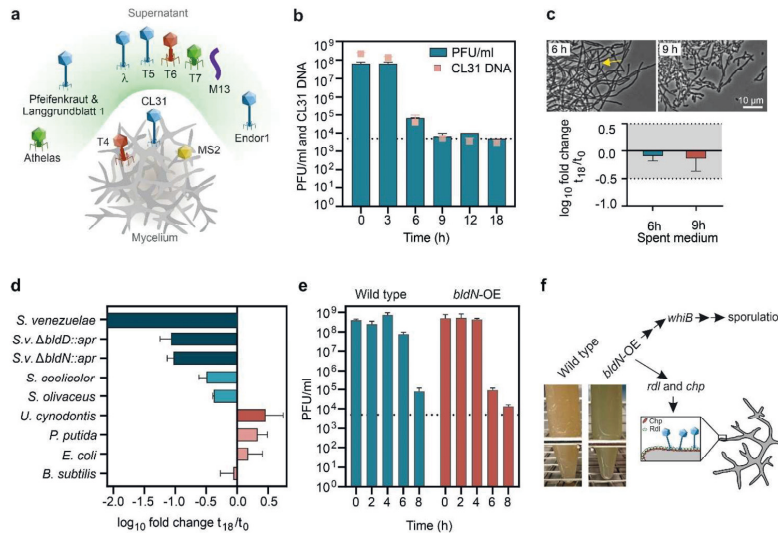


**Figure 4:** Influence of *Streptomyces* mycelium on extracellular phage titers of non-related phages. a) Schematic presentation of phages showing a reduction in titer upon incubation with *S. venezuelae* NRRL B-65442 mycelium and phages showing stable extracellular phage titers in presence of mycelium. Corresponding double-agar overlays are shown in Supplementary Figure S3b and c. The different phage morphotypes are illustrated as follows: blue - siphovirus; red - myovirus; green - podovirus; purple - inovirus; yellow – levivirus. b) Time-resolved quantification of CL31 phage particles during incubation with *S. venezuelae* NRRL B-65442 mycelium via double-agar overlays (cyan bars, n = 3 independent biological replicates) and via qPCR (reddish dots, n = 6, three independent biological replicates measured as technical duplicates). The detection limit for double-agar overlays is indicated by the dotted line; for qPCR, measurement points minimally outside of the standards are marked by increased transparency ( $t_0$ ,  $t_{12}$ ,  $t_{18}$ ). c) Microscopic images of *S. venezuelae* mycelium during declining CL31 titers at 6 h and 9 h post inoculation (scale bar: 10  $\mu$ m, exposure time = 200 ms) and influence of incubation with corresponding spent medium on extracellular CL31 titers. The yellow arrow points to the first spore chains detected after 6 h of incubation. d) Reduction in extracellular infectious CL31 particles during cultivation with different microorganism calculated via double-agar overlays, shown as  $\log_{10}$  fold change  $t_{18}/t_0$ . In case of incubation with *S. venezuelae* wild type, one replicate showed a  $\log_{10}$  fold change of  $\sim -4$ , while two out of three replicates showed no more plaque formation after 18 h of incubation. e) Time-resolved reduction in extracellular infectious CL31 particles during cultivation with the wild type *S. venezuelae* NRRL B 65442 and *S. venezuelae* overexpressing *bldN*. f) Phenotype of the *bldN* overexpression strain in comparison to the wild type – both cultivated in GYM medium supplemented with 100 mM MOPS (pH 7.3) – with schematic representation of hypothetical downstream effects of enhanced BldN levels.

**Discussion** | Phage infection of *Streptomyces* spp. was shown to exhibit a unique time course of phage titers, which is characterized by a drop in extracellular infectious phage particles upon bacterial re-growth after an initial successful phage amplification. Such behavior markedly differs from prototypical infections and was not observed for the unicellular-growing bacteria included in our assays. Accordingly, we further investigated this declining titer by focusing on the potential contribution of mycelial growth of *Streptomyces*, which could present a further layer of antiphage defense.

Even when taking into account the different measurement inaccuracies of phage quantification via double-agar overlays and qPCR, we demonstrated that extracellular levels of phage DNA remain above the level of infectious phage particles. This suggests that the observed phenotypic time course of infectious phage particles is synergistically caused by a high proportion of completely removed phages from the extracellular fraction (~92-96% decrease in DNA levels) and an additional minor proportion of inactivated/partially destroyed phages (>99.9% decrease in PFU/ml). However, it should be noted that an unknown amount of non-encapsulated phage DNA deriving from lysed cells contributes to the quantified DNA level as well, which might bias the ratio of reduced infectivity versus DNA reduction. Another recent study from our laboratory revealed comparable results when quantifying the phage load from plaques of phage Alderaan on *S. venezuelae*. Analogously to our results gained for submerged cultures, plaque diameters started to decrease again after an initial cell lysis. Upon reconquering of the lysis zone and plaque shrinkage, a high reduction in infectious phage particles was measured, which co-occurred with a less pronounced decline in phage DNA levels. Additionally, reduction in plaque size was shown to be neglectable for developmental mutants highlighting the significance of the hyphal structures for containment of phage infection (Luthe et al., 2023).

Approaching this phage inactivation in the extracellular space in more detail revealed a high impact of the developmental stage of mycelium on infection dynamics. Mature, highly branched mycelium of *S. venezuelae* exposed a transient tolerance towards

Alderaan infection leading even to a decrease in extracellular phage titers over time. However, the molecular basis of this increased phage tolerance at later stages during *Streptomyces* development was not investigated in detail thus far, but could potentially involve either a direct adsorption of phages to mycelium without following phage amplification or a shielding of phage receptors, which prevents phage adsorption and may favor the targeting of phages by extracellular phage-inactivating factors. The influence of mycelium age on phage susceptibility was also investigated in further studies. Exemplarily, mature mycelium of *Streptomyces albus* showed an enhanced adsorption capacity of actinophage Pal6 in comparison to newly germinated spores leading also to a decline in extracellular titers over time (Rosner & Gutstein, 1981). Moreover, Luthe et al. (2023) demonstrated a decrease in plaque diameter up to a complete prevention of Alderaan plaque formation with increasing age of the surface-grown mycelium used as bacterial lawn. They proposed that a reduced diffusivity upon increasing mycelial density significantly influenced spreading of infection. Comparable results regarding the influence of diffusivity were also published for *E. coli* biofilms serving as a multicellular antiphage defense by trapping phages in a curli fiber network (Bond et al., 2021; Vidakovic et al., 2018). Interestingly, a decrease in unadsorbed phages after initial phage amplification was also detected in soil microcosms at later stages of *S. lividans* infection with phage KC301. This was attributed to a high adsorption of phages to vegetative mycelium of mature colonies (Burroughs et al., 2000; Marsh & Wellington, 1992).

Apart from a potential direct influence of mycelial structures, an impact of medium acidification and secreted metabolites or proteins on extracellular infectious Alderaan particles was observed, but appeared to be rather minor. However, it should be noted that the current data just reflect the influence of spent medium from uninfected cultures. Accordingly, the transient production of antiphage molecules in response to phage infection cannot yet be ruled out and is an important aspect for further investigations, although *S. venezuelae* is not capable of producing aminoglycosides or anthracyclines as the two main classes of antiphage metabolites currently known

(Kever et al., 2022; Kronheim et al., 2018). Summarized, all considered parameters might contribute to the observed decline in infectious phage titers upon bacterial re-growth, but to a yet unknown extent. Another possible influencing factor, which requires further consideration, is the release of extracellular membrane vesicles, which has not yet been studied in the context of *Streptomyces* phage infection (Fröjd & Flärdh, 2019; Schrepf et al., 2011).

An inactivation of phages in the extracellular space by hyphal structures was further analysed by tracking extracellular titers of non-host phages during cultivation with *S. venezuelae* mycelium over time. Among the tested phages, CL31, T4 and MS2 revealed a reduction in extracellular titers with T4 described to be hydrophobic (Ghanem et al., 2019). Performing a time-resolved quantification of CL31 titers as the most affected phage revealed a simultaneous decrease in infectivity and phage DNA content, which coincided with the developmental transition to spores and thus probably with the expression of the hydrophobic sheath (Bibb et al., 2012). This sheath is composed of rodlin and chaplin proteins (Claessen et al., 2003; Claessen et al., 2002; Elliot et al., 2003), whose expression is regulated by the  $\sigma$  factor BldN and anti- $\sigma$  factor RsbN (Bibb et al., 2012). Although the levels of these hydrophobic proteins actually produced under the applied conditions were not determined so far, results gained for *bldN* overexpression and *bldN* deletion strains – showing either a faster or a less pronounced decline in infectious phage particles, respectively – refer to a direct involvement of hydrophobic interactions. The hydrophobic proteins of *Streptomyces* spp. harbor a comparable function as hydrophobins in filamentous-growing fungi (Elliot & Talbot, 2004; Wösten, 2001). Interestingly, physiochemical interactions between phages and fungal mycelium were already studied in a microfluidic platform by Ghanem et al. (2019). Combining mycelium of highly hydrophobic *Coprinopsis cinerea* or moderately hydrophobic *Pythium ultimum* with two different phages, hydrophobic T4 and more hydrophilic PSA-HS2, revealed an increasing phage retention with increasing hydrophobicity of the phage and the hyphae, the latter having the higher impact (Ghanem et al., 2019). Fitting to this, a general influence of hydrophobicity on phage

retention was described in various studies when screening for phage adhesion to different solid surfaces like aluminum oxide-coated sand or polypropylene (Attinti et al., 2010; Dika et al., 2013; Farkas et al., 2015). All in all, this supported our hypothesis that switching from a hydrophilic to a hydrophobic surface during hyphae-spore transition contributes to declining extracellular titers of a non-host phage. Unfortunately, attempts to detach phages from the mycelial fraction failed, which accounts for a high affinity, irreversible binding of phages to hyphae or degradation of the phage particles. To finally confirm the interaction between phage particles and the hydrophobic sheath further investigations are required.

Altogether, this study emphasizes an important impact of *Streptomyces* cellular development on phage susceptibility. Furthermore, we can deduce that *Streptomyces* has evolved a complex antiphage defense with several components acting at the multicellular level that may provide a community-wide protection against phage predation.

## Material and Methods

**Microbial strains and growth conditions** | All bacterial strains, fungi and phages used in this study are listed in Table S1 and S2. For growth studies and double-agar overlay assays, *Streptomyces* cultures were inoculated from spore stocks and cultivated at 30°C and 120 rpm using glucose-yeast extract-malt extract (GYM) medium containing 50% tap water, pH 7.3). For double-agar overlays and phage titer determination, 2 µl of decimal dilution series of culture supernatants in sodium chloride/magnesium sulfate (SM) buffer (10 mM Tris-HCl pH 7.3, 100 mM NaCl, 10 mM MgCl<sub>2</sub>, 2 mM CaCl<sub>2</sub>) were spotted on a bacterial lawn propagated on a double-agar overlay with the top layer inoculated at an initial optical density (OD<sub>450</sub>) of 0.3 in GYM soft-agar (0.4% agarose).

Cultivation of *Corynebacterium glutamicum* MB001 and quantification of phage CL31 was done analogously using brain heart infusion (BHI) medium and BHI soft-agar (0.4% agarose) inoculated to an OD<sub>600</sub> of 0.5. *Escherichia coli*, *Bacillus subtilis* and *Pseudomonas putida* were cultivated in lysogeny broth (LB) medium. *E. coli* infecting phages were quantified using LB soft-agar (0.4% agarose) inoculated to an OD<sub>600</sub> of 0.2. For the plant pathogens *Pseudomonas syringae* pv. *lapsa* and *Xanthomonas translucens* pv. *translucens* nutrient broth (NB) medium (pH 7.0) and NB soft-agar (0.4% agarose, OD<sub>600</sub> of 0.2) served as cultivation medium for phage titer determination. The haploid, yeast-like growing fungi *Ustilago cynodontis* NBRC 9727 was inoculated in Modified Tabuchi Medium (MTM) (Geiser et al., 2014) containing 200 g/l glucose. All cultivations were performed at 30 °C.

*E. coli* DH5a cultivated at 37°C and 120 rpm in LB medium containing the appropriate antibiotic was utilized for standard cloning application. For conjugation *E. coli* strain ET12567/pUZ8002 was used.

**Recombinant DNA work and cloning** | All plasmids and oligonucleotides used in this study are listed in Table S3. Standard cloning techniques such as PCR, restriction digestion with indicated restrictions enzymes and Gibson assembly were performed according to standard protocols (Gibson, 2011; Sambrook & Russell, 2001). For amplification via PCR, genomic DNA of

*S. venezuelae* NRRL B-65442 was used as template. DNA sequencing and synthesis of oligonucleotides was performed by Eurofins Genomics (Ebersberg, Germany).

**Phage propagation** | For amplification of phage Alderaan, *S. venezuelae* main cultures in GYM medium (pH 7.3, 50% tap water) were inoculated from overnight cultures after ~16 h of cultivation to an OD<sub>450</sub> of 0.15. Phages were added to an initial phage titer of ~5\*10<sup>7</sup> PFU/ml. Cultivation at 30 °C and 120 rpm was performed until complete lysis. After harvesting of supernatants via centrifugation at 5.000 g for 10 min and following sterile filtration, spent medium was exchanged by SM buffer using Amicon Ultra Filter falcons with a 30 kDa cutoff membrane (MerckMillipore, Burlington, MA, USA). For CL31, phage amplification in *C. glutamicum* MB001 was done as described previously by Hünnefeld et al. (2021) using a starting OD<sub>600</sub> of 0.5 and an MOI of 0.1.

**Phage infection curves in microcultivation systems** | Phage infection curves were performed in the BioLector microcultivation system (Beckman Coulter Life Sciences (formerly m2p-labs), Krefeld, Germany) (Kensy et al., 2009) using a cultivation temperature of 30°C and shaking frequency of 1200 rpm. Biomass was measured as a function of backscattered light intensity with an excitation wavelength of 620 nm (filter module: λ<sub>Ex</sub>/λ<sub>Em</sub>: 620 nm/ 620 nm, gain: 25) from three independent biological replicates. All growth curves are baseline corrected with respect to the backscatter values at time point t<sub>0</sub>.

Main cultures of *S. venezuelae* in 1 ml GYM medium (pH 7.3, 50% tap water) were inoculated with overnight cultures to an initial OD<sub>450</sub> of 0.15. Infection was performed by adding phages to the indicated initial phage titers (10<sup>6</sup> – 10<sup>8</sup> PFU/ml). Phage infection curves in *E. coli* LE392 and *C. glutamicum* MB001 were done in the same way using an initial OD<sub>600</sub> of 0.15 in 1 ml LB medium or 1 ml BHI medium, respectively, and the indicated initial phage titers. Supernatants were collected in specific time intervals to quantify plaque forming units (PFU) via double-agar overlay assays over time.



**Re-infection experiments** | To investigate, if re-grown *Streptomyces* mycelium is resistant towards re-infection with the same phage, mycelium was harvested after 72 h of infection by centrifugation at 16,000 g for 5 min and washed two times with fresh GYM medium (pH 7.3, 50% tap water) to remove residual extracellular phages. After re-suspending in fresh GYM medium again, OD<sub>450</sub> was determined and new cultures were inoculated to an initial OD<sub>450</sub> of 0.15. Cultivation was performed as described in 'Phage infection curves' as biological triplicates. Infection was conducted by adding 10<sup>8</sup> PFU/ml as initial phage titer, while uninfected samples served as a growth control. Additionally, mycelium which was not infected in the first infection cycle was re-inoculated and infected analogously serving as a control for successful infection.

**Incubation assays of phages with *Streptomyces* mycelium** | To investigate the adsorption capacity of *S. venezuelae* mycelium on phages, pre-cultures were inoculated from spore stocks and grown in GYM medium (pH 7.3, 50% tap water) to be subsequently used to inoculate main cultures in the same medium to an OD<sub>450</sub> of 1.2. To eliminate pH effects on phage stability, GYM medium was supplemented with 100 mM MOPS (pH 7.3). Finally, 20 µl of the different phage stocks were incubated with 700 µl of resuspended mycelium, which was done in biological triplicates. Cultivation was conducted in Flower plates (Beckman Coulter Life Sciences (formerly m2p-labs), Krefeld, Germany) at 900 rpm and 30°C. Extracellular phage titers were quantified via double agar overlays after 18 h, which were performed as described in 'Microbial strains and growth conditions', while pH values were measured via pH indicator stripes (Carl Roth, Karlsruhe, Germany). As control, phage titers were also tracked upon incubation in *S. venezuelae* spent medium harvested after 18 h of cultivation under the same conditions.

The same set-up was used for investigating the influence of other *Streptomyces* strains on infectious CL31 phage particles. Incubation of CL31 phages with *B. subtilis*, *P. putida* and *E. coli* was done analogously using LB medium with a starting OD<sub>600</sub> of 1.2, while incubation with *U. cynodontis* was conducted in MTM medium with 200 g/l glucose.

**Stability assays in spent medium** | To determine potential effects of spent medium (secreted metabolites and proteins) on infectious phage particles, *S. venezuelae* main cultures were inoculated in GYM medium (pH 7.3, 50% tap water) with overnight cultures to an initial OD<sub>450</sub> of 0.15 and cultivated at 30 °C and 120 rpm. Spent medium was harvested via centrifugation at 5,000 g for 10 min and subsequent sterile filtration at the indicated time points.

In case of Alderaan stability assays, spent medium of uninfected *S. venezuelae* cultures was collected at 8 h, 24 h and 48 h post inoculation in buffered and unbuffered medium and subsequently used for incubation with ~10<sup>8</sup> PFU/ml Alderaan particles at cultivation conditions at 30 °C and 900 rpm.

For CL31, spent medium of *S. venezuelae* was taken during the decrease in infectious CL31 particles 6 h and 9 h post infection. After sterile filtration, ~10<sup>9</sup> PFU/ml of fresh CL31 particles were added to the remaining ones still present in the spent medium and incubated 30 °C and 900 rpm. Extracellular phage titers of Alderaan and CL31 were tracked over time via double-agar overlay assays.

For investigating the influence of chloramphenicol on Alderaan plaque formation, a decimal dilution series of phage Alderaan in SM buffer (10 mM Tris-HCl pH 7.3, 100 mM NaCl, 10 mM MgCl<sub>2</sub>, 2 mM CaCl<sub>2</sub>) was directly spotted on a bacterial lawn propagated on double-agar overlays containing either 0, 10, 50 or 200 µg/ml chloramphenicol in both agar layers.

**pH stability assays** | To examine the pH stability of phage Alderaan, GYM medium (50% tap water) was adjusted to different pH values (pH 4.0-9.0) using HCl or NaOH. Subsequently, Alderaan particles were added to these media using an initial phage titer of 10<sup>9</sup> PFU/ml and incubated at cultivation conditions at 30 °C and 900 rpm for 24 h in DeepWell plates. Phage titers were tracked over time via double-agar overlays as described in 'Microbial strains and growth conditions'.



**Determining extracellular phage titers via quantitative PCR** | In addition to spot assays, extracellular phage titers were further quantified via quantitative PCR to discriminate between an inactivation and total removal/degradation of phage particles. To do so, 5 µl of supernatants (1:10 or 1:100 diluted in phage buffer for quantification of CL31 and Alderaan phages, respectively) as template DNA were mixed with 10 µl 2x Luna® Universal qPCR Master Mix (New England Biolabs, Ipswich, MA, USA) and 0.5 µl of each oligonucleotide (Table S3, final oligonucleotide concentration: 0.25 µM), before adjusting to a final volume of 20 µl with dd. H<sub>2</sub>O. Quantification was performed in 96-well plates in the qTOWER 2.2 (Analytik Jena, Jena, Germany).

For determining the absolute concentration of extracellular phage DNA, amplification of the phage target gene HQ601\_00028 (coding for the minor tail protein of Alderaan, PCR product: 144 bp) was calculated via the 'Absolute quantification method' of the qPCRsoft 3.1 software (Analytik Jena, Jena, Germany). A decimal dilution series of the phage stock with known phage titer was used as standard. Quantification of extracellular CL31 phages was done analogously based on the phage target phage gene clg56 (coding for the minor tail protein of CL31, PCR product: 150 bp).

In case of Alderaan, the fraction of remaining phages and the corresponding deviation was calculated as follows:

$$\Phi_{remaining} = \frac{t_{72}}{t_8} \pm \left| \left( \frac{\Delta t_{72}}{t_{72}} + \frac{\Delta t_8}{t_8} \right) * \frac{t_{72}}{t_8} \right|$$

$t_x$ : Mean concentration calculated via 'Absolute quantification method' of qPCRsoft 3.1

$\Delta_{tx}$ : Standard deviation calculated via 'Absolute quantification method' of qPCRsoft 3.1

**Microscopy** | Analysis of the developmental level of *Streptomyces* cultures was conducted via microscopic Z-stack imaging using the Axio Imager M2 phase contrast microscope (Zeiss, Germany) with the indicated exposure time (120 or 200 ms). Images were taken using the AxioVision 4.8.2 software (Zeiss, Jena, Germany) and subsequently stacked via ImageJ (Schneider et al., 2012) and the Extended Depth of Field Plugin (Forster et al., 2004).

**Scanning electron microscopy (SEM)** | Incubation of CL31 particles with *S. venezuelae* mycelium was conducted as described in 'Incubation assays of phages with *Streptomyces* mycelium' using GYM medium (50% tap water, pH 7.3) supplemented with 100 mM MOPS. At the decline in infectious phage particles at 9 h post inoculation, *S. venezuelae* mycelium was diluted with fresh medium to an OD<sub>450</sub> of ~1 in a total volume of 3.6 ml and fixed via addition of 400 µl 25% glutaraldehyde and 1 ml 25% paraformaldehyde. As control, a phage-free sample was handled in the same way. Scanning electron microscopy was conducted at the ZFIM department (Central Facility for Microscopy) in the Helmholtz center for infection research (HZI, Braunschweig, Germany).

## References

- Ahmed, Z. U., Shapiro, S., & Vining, L. C. (1984). Excretion of  $\alpha$ -keto acids by strains of *Streptomyces venezuelae*. *Can. J. Microbiol.*, 30(8), 1014-1021. <https://doi.org/10.1139/m84-158>
- Anderson, A. S., & Wellington, E. M. H. (2001). The taxonomy of *Streptomyces* and related genera. *Int. J. Syst. Evol. Microbiol.*, 51(3), 797-814. <https://doi.org/10.1099/00207713-51-3-797>
- Attinti, R., Wei, J., Kniel, K., Sims, J. T., & Jin, Y. (2010). Virus' (MS2, phiX174, and Aichi) Attachment on Sand Measured by Atomic Force Microscopy and Their Transport through Sand Columns. *Environ. Sci. Technol.*, 44(7), 2426-2432. <https://doi.org/10.1021/es903221p>
- Bernheim, A., & Sorek, R. (2020). The pan-immune system of bacteria: antiviral defence as a community resource. *Nat Rev Microbiol.*, 18(2), 113-119. <https://doi.org/10.1038/s41579-019-0278-2>
- Bibb, M. J. (2005). Regulation of secondary metabolism in streptomycetes. *Curr Opin Microbiol.*, 8(2), 208-215. <https://doi.org/10.1016/j.mib.2005.02.016>
- Bibb, M. J., Domanos, A., Chandra, G., & Buttner, M. J. (2012). Expression of the chaplin and rodlin hydrophobic sheath proteins in *Streptomyces venezuelae* is controlled by  $\sigma^{BldN}$  and a cognate anti-sigma factor, RsbN. *Mol Microbiol.*, 84(6), 1033-1049. <https://doi.org/10.1111/j.1365-2958.2012.08070.x>
- Bond, M. C., Vidakovic, L., Singh, P. K., Drescher, K., & Nadell, C. D. (2021). Matrix-trapped viruses can prevent invasion of bacterial biofilms by colonizing cells. *Elife*, 10, e65355. <https://doi.org/10.7554/eLife.65355>
- Burroughs, N. J., Marsh, P., & Wellington, E. M. H. (2000). Mathematical Analysis of Growth and Interaction Dynamics of Streptomycetes and a Bacteriophage in Soil. *Appl. Environ. Microbiol.*, 66(9), 3868-3877. <https://doi.org/10.1128/AEM.66.9.3868-3877.2000>
- Bush, M. J., Tschowri, N., Schlimpert, S., Flårdh, K., & Buttner, M. J. (2015). c-di-GMP signalling and the regulation of developmental transitions in streptomycetes. *Nat Rev Microbiol.*, 13(12), 749-760. <https://doi.org/10.1038/nrmicro3546>
- Chater, K. F. (2016). Recent advances in understanding *Streptomyces*. *F1000Res*, 5, 2795. <https://doi.org/10.12688/f1000research.9534.1>
- Claessen, D., Rink, R., de Jong, W., Siebring, J., de Vreugd, P., Boersma, F. G., Dijkhuizen, L., & Wosten, H. A. (2003). A novel class of secreted hydrophobic proteins is involved in aerial hyphae formation in *Streptomyces coelicolor* by forming amyloid-like fibrils. *Genes Dev.*, 17(14), 1714-1726. <https://doi.org/10.1101/gad.264303>
- Claessen, D., Wösten, H. A. B., Keulen, G. v., Faber, O. G., Alves, A. M. C. R., Meijer, W. G., & Dijkhuizen, L. (2002). Two novel homologous proteins of *Streptomyces coelicolor* and *Streptomyces lividans* are involved in the formation of the rodlet layer and mediate attachment to a hydrophobic surface. *Mol Microbiol.*, 44(6), 1483-1492. <https://doi.org/10.1046/j.1365-2958.2002.02980.x>
- den Hengst, C. D., Tran, N. T., Bibb, M. J., Chandra, G., Leskiw, B. K., & Buttner, M. J. (2010). Genes essential for morphological development and antibiotic production in *Streptomyces coelicolor* are targets of BldD during vegetative growth. *Mol Microbiol.*, 78(2), 361-379. <https://doi.org/10.1111/j.1365-2958.2010.07338.x>
- Dika, C., Ly-Chatain, M. H., Francius, G., Duval, J. F. L., & Gantzer, C. (2013). Non-DLVO adhesion of F-specific RNA bacteriophages to abiotic surfaces: Importance of surface roughness, hydrophobic and electrostatic interactions. *Colloids Surf. A Physicochem. Eng. Asp.*, 435, 178-187. <https://doi.org/10.1016/j.colsurfa.2013.02.045>
- Doron, S., Melamed, S., Ofir, G., Leavitt, A., Lopatina, A., Keren, M., Amitai, G., & Sorek, R. (2018). Systematic discovery of antiphage defense systems in the microbial pangenome. *Science*, 359(6379), eaar4120. <https://doi.org/10.1126/science.aar4120>
- Elliot, M. A., Karoonuthaisiri, N., Huang, J., Bibb, M. J., Cohen, S. N., Kao, C. M., & Buttner, M. J. (2003). The chaplins: a family of hydrophobic cell-surface proteins involved in aerial mycelium formation in *Streptomyces coelicolor*. *Genes Dev.*, 17(14), 1727-1740. <https://doi.org/10.1101/gad.264403>
- Elliot, M. A., & Talbot, N. J. (2004). Building filaments in the air: aerial morphogenesis in bacteria and fungi. *Curr Opin Microbiol.*, 7(6), 594-601. <https://doi.org/10.1016/j.mib.2004.10.013>
- Farkas, K., Varsani, A., & Pang, L. (2015). Adsorption of Rotavirus, MS2 Bacteriophage and Surface-Modified Silica Nanoparticles to Hydrophobic Matter. *Food Environ Virol.*, 7(3), 261-268. <https://doi.org/10.1007/s12560-014-9171-3>
- Flårdh, K., & Buttner, M. J. (2009). *Streptomyces* morphogenetics: dissecting differentiation in a filamentous bacterium. *Nat Rev Microbiol.*, 7(1), 36-49. <https://doi.org/10.1038/nrmicro1968>
- Forster, B., Ville, D. V. D., Bererit, J., Sage, D., & Unser, M. (2004). Extended depth-of-focus for multi-channel microscopy images: a complex wavelet approach. *2004 2nd IEEE International Symposium on Biomedical Imaging: Nano to Macro (IEEE Cat No. 04EX821)*, Arlington, VA, USA, 1, 660-663. <https://doi.org/10.1109/ISBI.2004.1398624>
- Fröjd, M. J., & Flårdh, K. (2019). Extrusion of extracellular membrane vesicles from hyphal tips of *Streptomyces venezuelae* coupled to cell-wall stress. *Microbiology*, 165(12), 1295-1305. <https://doi.org/10.1099/mic.0.000836>
- Geiser, E., Wiebach, V., Wierckx, N., & Blank, L. M. (2014). Prospecting the biodiversity of the fungal family Ustilaginaceae for the production of value-added chemicals. *Fungal Biol. Biotechnol.*, 1(2). <https://doi.org/10.1186/s40694-014-0002-y>

- Ghanem, N., Stanley, C. E., Harms, H., Chatzinotas, A., & Wick, L. Y. (2019). Mycelial Effects on Phage Retention during Transport in a Microfluidic Platform. *Environ Sci Technol*, 53(20), 11755-11763. <https://doi.org/10.1021/acs.est.9b03502>
- Gibson, D. G. (2011). Enzymatic assembly of overlapping DNA fragments. *Methods in Enzymology*, 498, 349-361. <https://doi.org/10.1016/B978-0-12-385120-8.00015-2>
- Glazebrook, M. A., Doull, J. L., Stuttard, C., & Vining, L. C. (1990). Sporulation of *Streptomyces venezuelae* in submerged cultures. *J Gen Microbiol*, 136(3), 581-588. <https://doi.org/10.1099/00221287-136-3-581>
- Hardy, A., Sharma, V., Kever, L., & Frunzke, J. (2020). Genome sequence and characterization of five bacteriophages infecting *Streptomyces coelicolor* and *Streptomyces venezuelae*: Alderaan, Coruscant, Dagobah, Endor1 and Endor2. *Viruses*, 12(10), 1065. <https://doi.org/10.3390/v12101065>
- Hatfull, G. F. (2020). Actinobacteriophages: Genomics, Dynamics, and Applications. *Annu Rev Virol*, 7(1), 37-61. <https://doi.org/10.1146/annurev-virology-122019-070009>
- Hopwood, D. A. (1999). Forty years of genetics with *Streptomyces*: from *in vivo* through *in vitro* to *in silico*. *Microbiology*, 145(9), 2183-2202. <https://doi.org/10.1099/00221287-145-9-2183>
- Hünnefeld, M., Viets, U., Sharma, V., Wirtz, A., Hardy, A., & Frunzke, J. (2021). Genome Sequence of the Bacteriophage CL31 and Interaction with the Host Strain *Corynebacterium glutamicum* ATCC 13032. *Viruses*, 13(3), 495. <https://doi.org/10.3390/v13030495>
- Kensy, F., Zang, E., Faulhammer, C., Tan, R. K., & Buchs, J. (2009). Validation of a high-throughput fermentation system based on online monitoring of biomass and fluorescence in continuously shaken microtiter plates. *Microb Cell Fact*, 8, 31. <https://doi.org/10.1186/1475-2859-8-31>
- Kever, L., Hardy, A., Luthe, T., Hünnefeld, M., Gätgens, C., Milke, L., Wiechert, J., Wittmann, J., Moraru, C., Marienhagen, J., & Frunzke, J. (2022). Aminoglycoside Antibiotics Inhibit Phage Infection by Blocking an Early Step of the Infection Cycle. *mBio*, 13(3). <https://doi.org/10.1128/mbio.00783-22>
- Kronheim, S., Daniel-Ivad, M., Duan, Z., Hwang, S., Wong, A. I., Mantel, I., Nodwell, J. R., & Maxwell, K. L. (2018). A chemical defence against phage infection. *Nature*, 564(7735), 283-286. <https://doi.org/10.1038/s41586-018-0767-x>
- Luthe, T., Kever, L., Hänsch, S., Hardy, A., Tschwori, N., Weidtkamp Peters, S., & Frunzke, J. (2023). *Streptomyces* development is involved in the efficient containment of viral infections. *Microlife*, 4(uqad002). <https://doi.org/10.1093/temsmi/uqad002>
- Madden, T., & Ison, J. M. W. A. P. (1996). Organic acid excretion by *Streptomyces lividans* TK24 during growth on defined carbon and nitrogen sources. *Microbiology*, 142(Pt11), 3181-3185. <https://doi.org/10.1099/13500872-142-11-3181>
- Manteca, A., Alvarez, R., Salazar, N., Yagüe, P., & Sanchez, J. (2008). Mycelium differentiation and antibiotic production in submerged cultures of *Streptomyces coelicolor*. *Appl Environ Microbiol*, 74(12), 3877-3886. <https://doi.org/10.1128/AEM.02715-07>
- Manteca, A., Claessen, D., Lopez-Iglesias, C., & Sanchez, J. (2007). Aerial hyphae in surface cultures of *Streptomyces lividans* and *Streptomyces coelicolor* originate from viable segments surviving an early programmed cell death event. *FEMS Microbiol Lett*, 274(1), 118-125. <https://doi.org/10.1111/j.1574-6968.2007.00825.x>
- Marsh, P., & Wellington, E. M. H. (1992). Interactions between Actinophage and their Streptomyces Hosts in Soil and the Fate of Phage Borne Genes. In M. J. Gauthier (Ed.), *Gene Transfers and Environment* (pp. 135-142). Springer Berlin Heidelberg. [https://doi.org/10.1007/978-3-642-77450-8\\_15](https://doi.org/10.1007/978-3-642-77450-8_15)
- McCormick, J. R., & Flärdh, K. (2012). Signals and regulators that govern *Streptomyces* development. *FEMS Microbiol. Rev.*, 36(1), 206-231. <https://doi.org/10.1111/j.1574-6976.2011.00317.x>
- Miguelé, E., Hardisson, C., & Manzanal, M. (1999). Hyphal Death during Colony Development in *Streptomyces antibioticus*: Morphological Evidence for the Existence of a Process of Cell Deletion in a Multicellular Prokaryote. *The Journal of Cell Biology*, 145(3), 515-525. <https://doi.org/10.1083/jcb.145.3.515>
- Rosner, A., & Gutstein, R. (1981). Adsorption of actinophage Pal6 to developing mycelium of *Streptomyces albus*. *Can. J. Microbiol.*, 27(2), 254-257. <https://doi.org/10.1139/m81-039>
- Sambrook, J., & Russell, D. W. (2001). *Molecular Cloning: A Laboratory Manual* (3rd ed.). Cold Spring Harbor Laboratory Press, NY.
- Schneider, C. A., Rasband, W. S., & Eliceiri, K. W. (2012). NIH Image to ImageJ: 25 years of image analysis. *Nat Methods*, 9(7), 671-675. <https://doi.org/10.1038/nmeth.2089>
- Schrempf, H., Koebsch, I., Walter, S., Engelhardt, H., & Meschke, H. (2011). Extracellular *Streptomyces* vesicles: amphorae for survival and defence. *Microb Biotechnol*, 4(2), 286-299. <https://doi.org/10.1111/j.1751-7915.2011.00251.x>
- Teertstra, W. R., Deelstra, H. J., Vranes, M., Bohlmann, R., Kahmann, R., Kämper, J., & Wösten, H. A. B. (2006). Repellents have functionally replaced hydrophobins in mediating attachment to a hydrophobic surface and in formation of hydrophobic aerial hyphae in *Ustilago maydis*. *Microbiology*, 152(12), 3607-3612. <https://doi.org/10.1099/mic.0.29034-0>
- Teertstra, W. R., van der Velden, G. J., de Jong, J. F., Kruijtz, J. A., Liskamp, R. M., Kroon-Batenburg, L. M., Muller, W. H., Gebbink, M. F., & Wösten, H. A. (2009). The filament-specific Rep1-1 repellent of the

- phytopathogen *Ustilago maydis* forms functional surface-active amyloid-like fibrils. *J Biol Chem*, 284(14), 9153-9159. <https://doi.org/10.1074/jbc.M900095200>
- Tschowri, N., Schumacher, M. A., Schlimpert, S., Chinnam, N. B., Findlay, K. C., Brennan, R. G., & Buttner, M. J. (2014). Tetrameric c-di-GMP mediates effective transcription factor dimerization to control *Streptomyces* development. *Cell*, 158(5), 1136-1147. <https://doi.org/10.1016/j.cell.2014.07.022>
- Vidakovic, L., Singh, P. K., Hartmann, R., Nadell, C. D., & Drescher, K. (2018). Dynamic biofilm architecture confers individual and collective mechanisms of viral protection. *Nat Microbiol*, 3(1), 26-31. <https://doi.org/10.1038/s41564-017-0050-1>
- Vining, L. C., & Stuttard, C. (1995). CHAPTER 18 - Chloramphenicol. In L. C. Vining & C. Stuttard (Eds.), *Genetics and Biochemistry of Antibiotic Production* (pp. 505-530). Butterworth-Heinemann. <https://doi.org/10.1016/B978-0-7506-9095-9.50028-9>
- Watve, M. G., Tickoo, R., Jog, M. M., & Bhole, B. D. (2001). How many antibiotics are produced by the genus *Streptomyces*? *Arch Microbiol*, 176(5), 386-390. <https://doi.org/10.1007/s002030100345>
- Willey, J. M., Willems, A., Kodani, S., & Nodwell, J. R. (2006). Morphogenetic surfactants and their role in the formation of aerial hyphae in *Streptomyces coelicolor*. *Mol Microbiol*, 59(3), 731-742. <https://doi.org/10.1111/j.1365-2958.2005.05018.x>
- Wosten, H. A. B. (2001). Hydrophobins: Multipurpose Proteins. *Mol Microbiol*, 55, 625-646. <https://doi.org/10.1146/annurev.micro.55.1.625>

**Acknowledgements** | We thank the Deutsche Forschungsgemeinschaft (SPP 2330, project 464434020) and the European Research Council (ERC Starting Grant 757563) for financial support. We would like to thank Dr. Mathias Mücken from the ZEIM department (Central Facility for Microscopy) at the Helmholtz Centre for Infection Research (HZI, Braunschweig, Germany) for conducting scanning electron microscopy.

**Author contributions** | Conceptualization: L.K., J.F. | Data curation: L.K. | Formal analysis: L.K. | Funding acquisition: J.F. | Investigation: L.K. | Methodology: L.K., J.F. | Project administration: L.K., J.F. | Supervision: L.K., J.F. | Validation: L.K., J.F. | Visualization: L.K. | Writing – original draft: L.K., J.F. | Writing – review and editing: L.K., J.F.

**Competing interest statement** | The authors declare no conflict of interest.

### 3.4. Genome sequence and characterization of five bacteriophages infecting *Streptomyces coelicolor* and *Streptomyces venezuelae*: Alderaan, Coruscant, Dagobah, Endor1 and Endor2

Hardy, A., Sharma, V., Kever, L. and Frunzke, J.

Published in Viruses, 2020

Contributor role	Contributor
Conceptualization	AH (50%), JF (30%), VS (10%), LK (10%)
Data curation	VS (55%), AH (30%), LK (10%), JF (5%)
Formal analysis	VS (80%), AH (15%), LK (5%)
Funding acquisition	JF (100%)
Investigation	AH (85%), LK (10%), VS (5%)
Methodology	AH (55%), VK (25%), JF (10%), LK (10%)
Project administration	JF (60%), AH (40%)
Resources	-
Software	VS (95%), AH (5%)
Supervision	JF (60%), AH (40%)
Validation	AH (35%), LK (35%), VS (30%)
Visualization	AH (55%), VS (40%), LK (5%)
Writing – original draft	AH (70%), VS (15%), JF (10%), LK (5%)
Writing – review and editing	AH (40%), JF (40%), LK (10%), VS (10%)

#### Overall contribution: 10%

LK conducted the experimental work and data analysis shown in Figure 2B. Visualization of the Figure 2A and B was done by LK. To a minor extent, LK was involved in writing the original draft as well as in the review and editing process.



Article

# Genome Sequence and Characterization of Five Bacteriophages Infecting *Streptomyces coelicolor* and *Streptomyces venezuelae*: Alderaan, Coruscant, Dagobah, Endor1 and Endor2

Aël Hardy , Vikas Sharma, Larissa Kever and Julia Frunzke \*

Institute of Bio- and Geosciences, IBG-1: Biotechnology, Forschungszentrum Jülich, 52425 Jülich, Germany; a.hardy@fz-juelich.de (A.H.); v.sharma@fz-juelich.de (V.S.); l.kever@fz-juelich.de (L.K.)

\* Correspondence: j.frunzke@fz-juelich.de; Tel.: +49-2461-615430

Received: 17 August 2020; Accepted: 21 September 2020; Published: 23 September 2020



**Abstract:** *Streptomyces* are well-known antibiotic producers, also characterized by a complex morphological differentiation. *Streptomyces*, like all bacteria, are confronted with the constant threat of phage predation, which in turn shapes bacterial evolution. However, despite significant sequencing efforts recently, relatively few phages infecting *Streptomyces* have been characterized compared to other genera. Here, we present the isolation and characterization of five novel *Streptomyces* phages. All five phages belong to the *Siphoviridae* family, based on their morphology as determined by transmission electron microscopy. Genome sequencing and life style predictions suggested that four of them were temperate phages, while one had a lytic lifestyle. Moreover, one of the newly sequenced phages shows very little homology to already described phages, highlighting the still largely untapped viral diversity. Altogether, this study expands the number of characterized phages of *Streptomyces* and sheds light on phage evolution and phage-host dynamics in *Streptomyces*.

**Keywords:** phage isolation; phage genomics; *Streptomyces*; *Siphoviridae*; actinobacteriophages; actinorhodin

## 1. Introduction

*Streptomyces* is a genus of Gram-positive bacteria belonging to the order of Actinobacteria that exhibit a high GC-content (on average about 73 mol% G + C). *Streptomyces* are prolific producers of natural products with a wide range of biological activities. This repertoire of bioactive molecules has been harnessed for medical and agricultural purposes, as for example 2/3 of known antibiotics of microbial origin are produced by *Streptomyces* [1–3].

Another distinctive feature of *Streptomyces* is their complex developmental cycle. Unlike most bacteria—that divide by binary fission, *Streptomyces* development is instead centered on the formation of spores. Germinating spores first form a network of interconnected cells, called vegetative mycelium. The vegetative mycelium later serves as a basis for the coordinated erection of an aerial mycelium. This is followed by the segmentation of these aerial filaments into spores, which can then start a new cycle [3–5].

Phages infecting *Streptomyces* were described at a quick pace in the 1970–1980s, but most of them were not sequenced later [6–8]. The phage phiC31 represents a notable exception to this trend, as it was used to develop crucial genetic tools for *Streptomyces* before being sequenced in 1999 [9–11]. Phages R4, SV1, VP5 were also the subject of numerous studies, but the latter was not sequenced [12,13].

*Streptomyces* peculiarities were studied in the context of phage infection. For example, adsorption to mycelium of phage Pal6 was shown to differ depending on the stage of development of

*Streptomyces albus* [14]. In this instance, phage adsorption was found to be maximal for germinating spores. Combined with the observation that germinating spores showed an intense average metabolic activity, this suggests that spore germination represents the most sensitive development stage for phage infection.

Conversely, the recent years have seen a sustained effort into the isolation and sequencing of *Streptomyces* phages, notably by the Science Education Alliance-Phage Hunters Advancing Genomics and Evolutionary Science (SEA-PHAGES; <https://seaphages.org/>) program in the USA [15]. However, few of these phages were extensively characterized.

Here, we report the isolation, characterization and genome analysis of five novel *Streptomyces* phages. Two of them (Alderaan and Coruscant) were isolated using *S. venezuelae*, the remaining three (Dagobah, Endor1 and Endor2) were isolated using *S. coelicolor*. Observation with transmission electron microscopy showed that all five phages belong to the *Siphoviridae* family. Lifestyle prediction with the complete nucleotide sequences revealed that four (Alderaan, Dagobah, Endor1 and Endor2) are probably temperate, while Coruscant was predicted to be a virulent phage. Alderaan, Coruscant, Endor1 and Endor2 show close relatedness to already described *Streptomyces* phages—Endor1 and Endor2 being highly homologous to each other. In contrast, Dagobah showed very little relatedness to any sequenced phage, highlighting the still massively untapped viral diversity.

## 2. Materials and Methods

### 2.1. Bacterial Strains and Growth Conditions

*Streptomyces venezuelae* ATCC 10712 [16] and *Streptomyces coelicolor* M600 [17] and strain M145 [18] were used as main host strains in this study. Cultures were started by inoculating spores from spore stocks stored in 20% glycerol at  $-20\text{ }^{\circ}\text{C}$  [19]. *S. venezuelae* was grown in liquid Glucose Yeast Malt extract (GYM) medium, while *S. coelicolor* was grown in liquid Yeast Extract Malt Extract (YEME) medium. Unless otherwise stated, cultivation was carried out at  $30\text{ }^{\circ}\text{C}$ . For double agar overlays, GYM agar was used for both species, with 0.5% and 1.5% agar for the top and bottom layers, respectively.

### 2.2. Phage Isolation and Propagation

Phages were isolated from soil samples taken near the Forschungszentrum Jülich (Jülich, Germany). Phages contained in soil samples were resuspended by incubation in sodium chloride/magnesium sulfate (SM) buffer (10 mM Tris-HCl pH 7.3, 100 mM NaCl, 10 mM  $\text{MgSO}_4$ , 2mM  $\text{CaCl}_2$ ) for 2 h. The samples were centrifuged at  $5000\times g$  for 10 min to remove solid impurities. The supernatants were filtered through a  $0.22\text{-}\mu\text{m}$  pore-size membrane filter to remove bacteria. For each sample, 1 mL of filtered supernatant was mixed with 3 mL of liquid medium inoculated with  $10^7$  *Streptomyces* spores.

After overnight incubation, the culture supernatant was collected by centrifugation at  $5000\times g$  for 10 min and filtered through a  $0.22\text{-}\mu\text{m}$  pore-size membrane filter. Serial dilutions of the filtrate were then spotted on a bacterial lawn propagated by mixing 200  $\mu\text{L}$  of *Streptomyces* overnight culture with 4 mL top agar, according to a modified version of the double agar overlay method [20]. Plaques were visualized after overnight incubation at  $30\text{ }^{\circ}\text{C}$ .

Purification of the phage samples was carried out by restreaking single plaques twice [20]. Phage amplification was achieved by mixing 100  $\mu\text{L}$  of the purified phage lysate into top agar to obtain confluent lysis on the plate. After overnight incubation, 5 mL of SM buffer were used to soak the plates and resuspend phages. The resulting phage lysate was centrifuged, and the supernatant was filtered to obtain the high-titer phage solution used for downstream processes.

To assess presence of actinorhodin, the plates were inverted and exposed to ammonia fumes for 15 min by placing 5 mL of 20% ammonium hydroxide solution on the inner surface of the lid.



### 2.3. Electron Microscopy Observation of Phage Virions

For electron microscopy, 5  $\mu$ L of purified phage suspension were deposited on a glow-discharged formvar carbon-coated nickel grids (200 mesh; Maxtaform; Plano, Wetzlar, Germany) and stained with 0.5% (*w/vol*) uranyl acetate. After air drying, the sample was observed with a TEM LEO 906 (Carl Zeiss, Oberkochen, Germany) at an acceleration voltage of 60 kV.

### 2.4. Phage Infection Curves

Growth experiments were performed in the BioLector® microcultivation system of m2p-labs (Aachen, Germany). Cultivation was performed as biological triplicates in 48-well FlowerPlates (m2plabs) at 30 °C and a shaking frequency of 1200 rpm [21]. Backscatter was measured by scattered light with an excitation wavelength of 620 nm (filter module:  $\lambda_{Ex}/\lambda_{Em}$ : 620 nm/620 nm, gain: 25) every 15 min. Each well contained 1 mL YEME or GYM medium and was inoculated using an overnight culture of *S. coelicolor* or *S. venezuelae*, respectively, to an initial OD<sub>450</sub> of 0.1. Phages were directly added to an initial titer of 10<sup>5</sup>, 10<sup>6</sup> or 10<sup>7</sup> PFU/mL, and sampling was performed at the indicated time points. Subsequently, 2  $\mu$ L of the supernatants were spotted on a lawn of *S. coelicolor* or *S. venezuelae* propagated on a double overlay of GYM agar inoculated at an initial OD<sub>450</sub> = 0.5.

### 2.5. Host Range Determination

The host range of our phages was determined for the following *Streptomyces* species: *S. rimosus* (DSM 40260), *S. scabiei* (DSM 41658), *S. griseus* (DSM 40236), *S. platensis* (DSM 40041), *S. xanthochromogenes* (DSM 40111), *S. mirabilis* (DSM 40553), *S. lividans* TK24 [22], *S. olivaceus* (DSM 41536) and *S. cyaneofuscatus* (DSM 40148). The different *Streptomyces* species were grown in GYM medium, to which glass beads were added to favor dispersed growth.

The host range was determined by spotting serial dilutions of phage solution on lawns of the different *Streptomyces* species, in duplicates. A species was considered sensitive to a given phage only if single plaques could be detected; we further indicated if the phages are able to lyse a species (Table 1).

### 2.6. DNA Isolation

For isolation of phage DNA, 1  $\mu$ L of 20 mg/mL RNase A and 1 U/ $\mu$ L DNase (Invitrogen, Carlsbad, CA, USA) were added to 1 mL of the filtered lysates to limit contamination by host nucleic acids. The suspension was incubated at 37 °C for 30 min. Then, EDTA, proteinase K and SDS were added to the mixture at final concentrations of 50  $\mu$ g/mL (EDTA and proteinase K) and 1% SDS (*w/v*), respectively. The digestion mixture was incubated for 1 h at 56 °C, before adding 250  $\mu$ L of phenol:chloroform:isopropanol. The content was thoroughly mixed before centrifugation at 16,000 $\times$  g for 4 min.

The upper phase containing the DNA was carefully transferred to a clean microcentrifuge tube and 2 volumes of 100% ethanol were added as well as sodium acetate to a final concentration of 0.3 M. After centrifugation at 16,000 $\times$  g for 10 min, the supernatant was discarded, and the pellet washed with 1 mL 70% ethanol. Finally, the dried pellet was resuspended in 30  $\mu$ L DNase-free water and stored at 4 °C until analyzed.

### 2.7. DNA Sequencing and Genome Assembly

The DNA library was prepared using the NEBNext Ultra II DNA Library Prep Kit for Illumina according to the manufacturer's instructions and shotgun-sequenced using the Illumina MiSeq platform with a read length of 2  $\times$  150 bp (Illumina). In total, 100,000 reads were subsampled for each phage sample, and de novo assembly was performed with Newbler (GS De novo assembler; 454 Life Sciences, Branford, CT, USA). Finally, contigs were manually curated with Consed version 29.0 [23].



## 2.8. Gene Prediction and Functional Annotation

Open reading frames (ORFs) in the phage genomes were identified with Prodigal v2.6.3 [24] and functionally annotated using an automatic pipeline using Prokka 1.11 [25]. The functional annotation was automatically improved and curated with hidden Markov models (HMMs), and Blastp [26] searches against different databases (Prokaryotic Virus Orthologous Groups (pVOGs) [27], viral proteins and Conserved Domain Database CDD [28]), with the e-value cutoff  $10^{-10}$ .

The annotated genomes were deposited in GenBank under the following accession numbers: MT711975 (Alderaan), MT711976 (Coruscant), MT711977 (Dagobah), MT711978 (Endor1) and MT711979 (Endor2). The ends of the phage genomes were determined with PhageTerm [29] using default parameters. Phage lifecycle was predicted with PhageAI [30] using default parameters.

## 2.9. Genome Comparison and Classification

To classify the unknown phage genomes at the nucleotide level, 31 complete reference actinophage genomes belonging to different known clusters were downloaded from the Actinobacteriophage Database [31]. Pairwise average nucleotide identities (ANI) were calculated with the five unknown *Streptomyces* phages and the 31 reference genomes using the python program pyani 0.2.9 [32] with ANIb method. The output average percentage identity matrix file generated from pyani was used for clustering and displayed using the ComplexHeatmap package in R [33]. Phage genome map with functional annotation was displayed using the gggenes package in R.

## 2.10. Protein Domain-Based Classification

An alternative approach was used to classify newly sequenced phages based on conserved protein domains [28]. RPS-BLAST (Reverse PSI-BLAST) searches were performed with e-value cutoff 0.001 against the Conserved Domain Database [28] using the 2486 complete reference actinophages [31], including the newly sequenced phage genomes. Identified Pfam protein domains output files from each phage genome were merged and converted into a numerical presence-absence matrix. The hierarchical clustering dendrogram was constructed with the help of the ward.2 method using the R platform. The resulting dendrogram was visualized using ggtree [34].

# 3. Results

## 3.1. Phage Isolation and Virion Morphology

Five novel phages infecting *Streptomyces* were isolated from soil samples close to the Forschungszentrum Jülich in Germany. The phages Alderaan and Coruscant were isolated using *Streptomyces venezuelae* ATCC 10712. Alderaan formed small, transparent, and round plaques of approximately 2 mm of diameter, while the plaques formed Coruscant were very small (<1 mm) and were fully visible only after 2 days of incubation (Figure 1A).

The phages Dagobah, Endor1 and Endor2 were isolated using *Streptomyces coelicolor* M600 as a host strain. Dagobah's plaques were very small (<1 mm) and were completely formed only after 2 days of incubation. Endor1 and Endor2 formed plaques of 2 mm in diameter with a distinct turbid zone in the center. Additionally, colored halos circling the plaques appeared after 3 days of incubation (Figure 1B). These halos were mostly brownish in the case of Dagobah, and reddish for Endor1 and Endor2. Exposure to ammonia fume resulted in a pronounced blue coloration around plaques, confirming that the halos surrounding plaques contained actinorhodin (Figure S1) [35].

TEM observation of the phage particles revealed that all five phages exhibit an icosahedral capsid and a non-contractile tail (Figure 1C). Based on the morphology, the phages were classified as members of the *Siphoviridae* family.

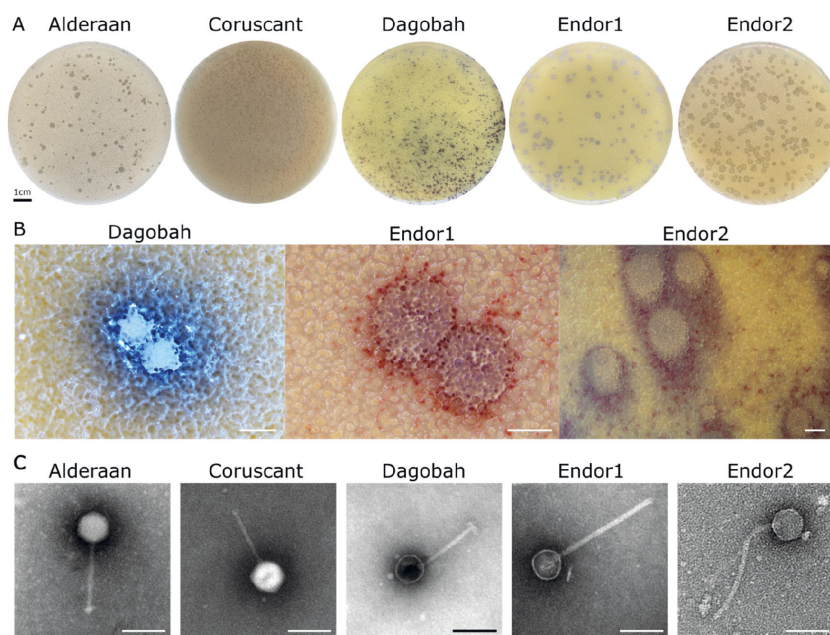


**Figure 1.** Morphology observation of five novel *Streptomyces* phages. **(A)** Plaque morphologies of the five phages. Double agar overlays were performed to infect *S. venezuelae* ATCC 10712 with the phages Alderaan and Coruscant, and *S. coelicolor* M600 with the phages Dagobah, Endor1, and Endor2. Plates were incubated overnight at 30 °C and another day (3 days in the case of Dagobah) at room temperature to reach full maturity of the bacterial lawn. **(B)** Close-ups of phage plaques imaged using a stereomicroscope Nikon SMZ18. *S. coelicolor* M145 was infected by phages using GYM double agar overlays. The plates were incubated at 30 °C overnight and then kept at room temperature for two (Endor1 and Endor2) or three days (Dagobah). Scale bar: 1 mm. **(C)** Transmission electron microscopy (TEM) of phage isolates. The phage virions were stained with uranyl acetate. Scale bar: 150 nm.

### 3.2. Infection Curves and Host-Range Determination

Phage infection in liquid cultures was performed to assess infection dynamics. Due to the complex developmental cycle of *Streptomyces*, standard one-step growth curves could not be performed. Instead, we cultivated *S. coelicolor* and *S. venezuelae* in microtiter plates in presence of phage challenge, and cell growth was monitored over a 24 h time period using continuous backscatter measurements. In both cases, phage titer was measured over time to estimate the production of phage progeny.

Infection of *S. venezuelae* with Alderaan showed a marked culture collapse at the highest initial phage load ( $10^7$  PFU/mL), and a plateauing of cell biomass at a significantly reduced level for the intermediate phage challenge ( $10^6$  PFU/mL). In contrast, addition of Coruscant causes only a mild but initial titer-dependent growth delay of the cultures (Figure 2A). For both phages, phage titers peaked at 6 h at the higher initial phage titer ( $10^7$  PFU/mL), and at the intermediate phage challenge, phage amplification was delayed or very weak for Alderaan and Coruscant, respectively.

As for the *S. coelicolor* phages (Figure 2B), infection with Dagobah caused a mild growth delay, visible especially when  $10^7$  PFU/mL was initially added. In parallel, the phage titers either declined over time or grew moderately (10-fold increase between 0 and 8 h) for initially intermediate ( $10^6$  PFU/mL) or high ( $10^7$  PFU/mL) phage challenge, respectively. Infection with Endor1 and Endor2 showed a similar behavior and caused a stronger growth delay than Dagobah, even for the intermediate initial

phage burden ( $10^6$  PFU/mL). The phage titers showed concordant behavior, with a strong increase in titers for both Endor1 and Endor2 until 10 h, followed by a marked decline up to 24 h.

Altogether, infection curves revealed that all five phages can successfully propagate in liquid cultures at the expense of their host. Surprisingly, the titers of all phages dropped after an initial increase, which needs further investigation.

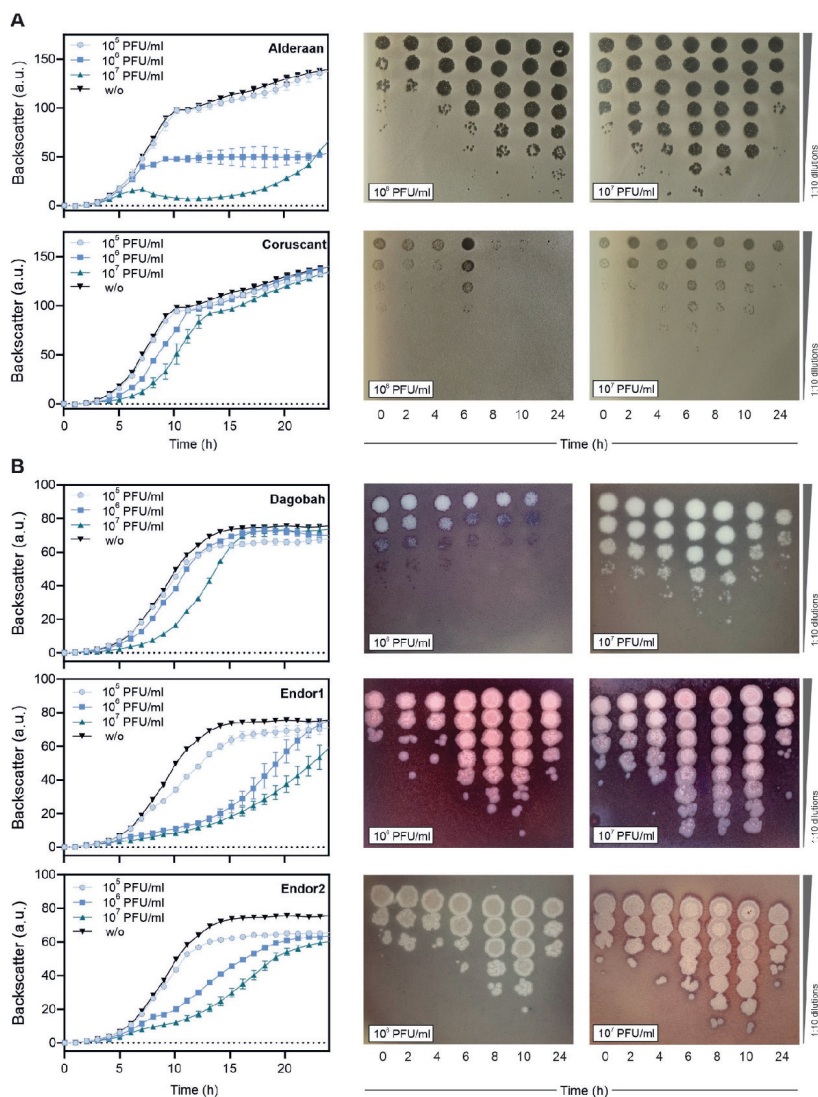


**Figure 2.** Infection curves of the five phages infecting *S. venezuelae* (A) and *S. coelicolor* (B). *S. venezuelae* or *S. coelicolor* were inoculated to GYM or YEME medium, respectively, and grown in microtiter plates, to which phages were added at the indicated initial phage titers. Backscatter was measured over time (left panels), in parallel to phage titers (right panels).

While phages usually have a relatively narrow host range, some phages can sometimes infect many strains of the same species and even distinct species. We assessed the host-range of our phages by spotting them on lawns of different *Streptomyces* species (Table 1).

**Table 1.** The host range of the five phages was assessed by spotting serial dilutions of these phages on lawns of different *Streptomyces* species propagated on GYM medium. The outcome of the spot assays is reported as follows: plaque formation (green), clearance of the bacterial lawn without visible plaques (yellow), no plaque or lysis visible (no color). The efficiency of plating (EOP) of a phage on a given strain relative to the host used for isolation is indicated, when plaques are countable.

	Alderaan	Coruscant	Dagobah	Endor1	Endor2
<i>S. venezuelae</i>					
<i>S. coelicolor</i> M600					
<i>S. coelicolor</i> M145			1	1	1
<i>S. rimosus</i> subsp. <i>rimosus</i>					
<i>S. scabiei</i>					
<i>S. griseus</i>					
<i>S. platensis</i>					
<i>S. xanthochromogenes</i>					
<i>S. lividans</i>			0.2		
<i>S. olivaceus</i>					4
<i>S. cyaneofuscatus</i>				0.08	0.4

*S. coelicolor* M145 showed the same sensitivity pattern than the M600 strain. M145 and M600 are both plasmid-free derivatives of A3(2) and mainly differ from each other in the length of their direct terminal repeats [17].

Beside *S. venezuelae* and *S. coelicolor*, *S. lividans* showed plaque formation by phage Dagobah. Endor1 and Endor2 also formed plaques on *S. olivaceus* and *S. cyaneofuscatus*. Alderaan, Endor1 and Endor2 caused indefinite clearance of the bacterial lawn of several species, but higher dilutions did not reveal distinct, single plaques. For these species, the phage lysates could have inhibitory effects on growth or cause non-productive infection [36,37].

In summary, Endor1 and Endor2 showed the broadest host range, but overall, the five phages we isolated feature a relatively modest host range, as they are only able to infect few other *Streptomyces* species.

### 3.3. Genome Sequencing and Genome Features

All phages were sequenced using short-read technology (Illumina Mi-Seq). Each genome could be assembled to a single contig, to which >80% of the reads could be mapped confirming the purity of the samples.

The genome features of the five phages are summed up in Table 2. Briefly, they show diverse genome sizes (39 to 133 kb), GC-contents (48 to 72%) and ORFs numbers (51 to 290). The phage Coruscant differed from other phages, in that its genome is significantly larger than the other phages and exhibits a markedly low GC content (48%), in comparison to the one of its host (72%). The genomic ends were predicted using PhageTerm, which detects biases in the number of reads to determine DNA termini and phage packaging mechanisms [29]. Alderaan, Endor1 and Endor2 showed a headful packaging mechanism where the phage genomes have a fixed start at the *pac* site, but the end of the genome is variable. In contrast, phages Coruscant and Dagobah have direct terminal repeats (DTR). These DTR were identified in the initial assembly by an approximately 2-fold increase in

coverage clearly delimited at single base positions. Phage lifecycle was predicted using PhageAI, which developed a lifecycle classifier based on machine learning and natural language processing [30].

**Table 2.** Basic genome features of the five phages. Open reading frames (ORFs) were predicted using Prokka [25] and were later manually curated. Protein domains encoded in ORFs were identified using RPS-BLAST against the Conserved Domain Database (CDD). The type of genome ends was determined using Phage Term [29]. The lifestyle of each phage was predicted by the machine-learning based program PhageAI [30].

Phage Name	Accession Number	Reference Host	Genome Size (kb)	GC Content (%)	ORF Number	Genome Termini Class	Lifestyle Prediction
Alderaan	MT711975	<i>Streptomyces venezuelae</i> ATCC 10712	39	72.1	51	Headful ( <i>pac</i> )	Temperate
Coruscant	MT711976	<i>Streptomyces venezuelae</i> ATCC 10712	133 (12 kb DTR)	48.4	290	DTR (long)	Virulent
Dagobah	MT711977	<i>Streptomyces coelicolor</i> M600	47 kb (1 kb DTR)	68.9	93	DTR (short)	Temperate
Endor1	MT711978	<i>Streptomyces coelicolor</i> M600	49	65.8	75	Headful ( <i>pac</i> )	Temperate
Endor2	MT711979	<i>Streptomyces coelicolor</i> M600	48	65.1	75	Headful ( <i>pac</i> )	Temperate

Phage genes involved in the same function are usually clustered together, forming functional modules (Figure 3) [38,39]. These modules fulfil the basic functions necessary for production of progeny phages, including DNA/RNA metabolism, DNA replication and repair, DNA packaging, virion structure and assembly (tail and capsid), regulation, lysogeny (in the case of temperate phages) and lysis.

Interestingly, Coruscant's large genomes is paralleled by a high genome complexity. It contains no less than 41 copies of tRNAs, covering 19 different amino acids—all standard amino acids except valine. Coruscant has also a relatively high fraction of coding sequences for which no function could be predicted (155 hypothetical proteins out 290 CDS compared to 16/51 for Alderaan).

The phages were also found to encode homologs of bacterial regulators that are typically used by *Streptomyces* to control sporulation and overall development. For example, *whiB* (found in Alderaan, and Coruscant) and *ssgA* (found in Dagobah) are both essential for sporulation of *Streptomyces* [40,41]. Three phages (Coruscant, Endor1 and Endor2) also encode Lsr2-like proteins, which are nucleoid-associated proteins functioning as xenogeneic silencing proteins and are conserved throughout Actinobacteria [42].

Additionally, despite overall high synteny and homology, the phages Endor1 and Endor2 showed sequence variations in the tail fiber proteins, tapemeasure and endolysin. In particular, the region encoding distal elements of the tail (ORF\_00022 to ORF\_00025 in Endor1, ORF\_00023 to ORF\_00026 in Endor2) displays reduced similarity at the nucleotide level (Supplementary Table S1). The resulting differences at the protein level could potentially account for the differences in host range between these two phages, e.g., infectivity on *S. olivaceus* (Table 1).



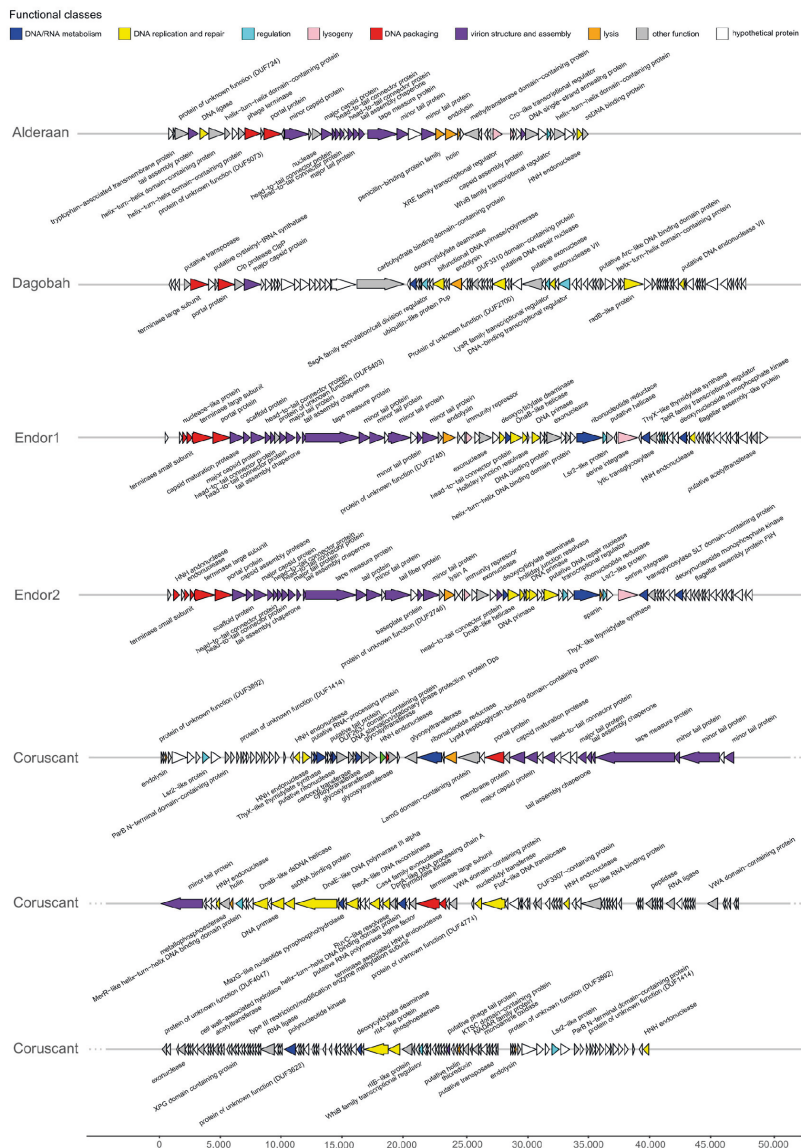


**Figure 3.** Genome map of the five *Streptomyces* phages. Open reading frames (ORFs) were identified with Prodigal and functionally annotated using an automatic pipeline based on Prokka [25]. The functional annotation was automatically improved and curated using hidden Markov models (HMMs), and Blastp searches [26] against different databases (Prokaryotic Virus Orthologous Groups (pVOGs) [27], viral proteins and Conserved Domain Database (CDD) [28]. Genome maps were created using the R package gggenes.

### 3.4. Average Nucleotide Identity (ANI) Analysis

We established the sequence relationship between the newly sequenced *Streptomyces* phages and the selected genomes from the representative group members of actinophages.

The Average nucleotide identity (ANI) based clustering dendrogram analysis showed that four (Endor1, Endor2, Alderaan, and Coruscant) out of five phage genomes clustered confidently with the members of already known clusters (Endor1/Endor2: BD, Coruscant: BE, and Alderaan: BC) (Figure 4). However, one of the phage genomes (Dagobah) does not share sufficient similarity and was therefore clustered as an unresolved group. Calculation of virus intergenomic similarities using VIRIDIC [43] showed congruent results to the ANI-based clustering (Figure S2), providing further support to the clustering shown in Figure 4. Altogether, the overall analysis showed that except Dagobah, all four phages show close relatedness to *Streptomyces* phages.

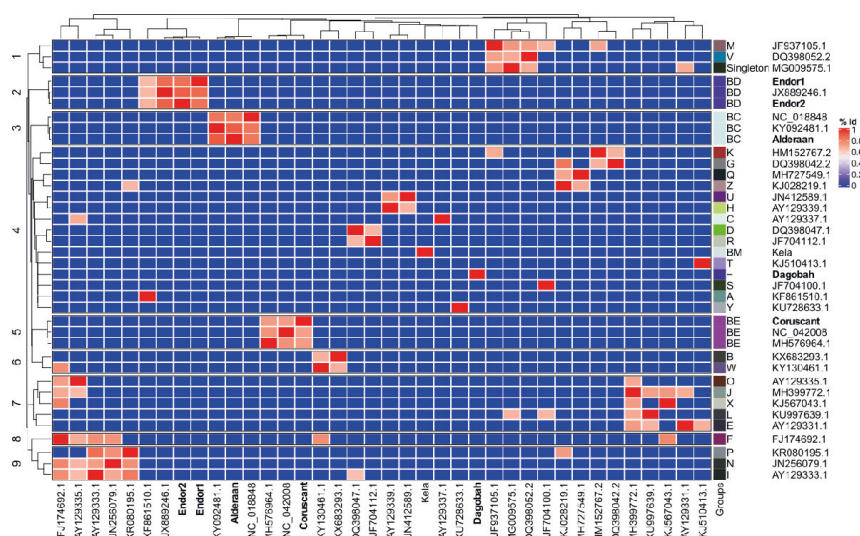


**Figure 4.** Average nucleotide-based dendrogram analysis using 38 actinophage genomes. These 38 genomes include 31 genomes downloaded from the Actinophage Database (<https://phagesdb.org/>), two genomes from NCBI based on close relatedness, and the five newly sequenced phages. The group of each phage, as defined by the Actinophage Database, is indicated.

### 3.5. Protein Domain-Based Analysis

Sequence relationship between the phage genomes is most commonly determined with the help of genome-wide similarity or average nucleotide identity-based analysis. However, a traditional method such as phylogeny with single genes is challenging because of the high variability and lack of universal genes across the phage genomes. Thus, we used additional phyletic-based analysis to establish a sequence relationship between the phage genomes. The hierarchical clustering dendrogram based on the identified 703 Pfam domains presence-absence matrix confidently clusters newly sequenced phages with known actinophages (Figure 5).

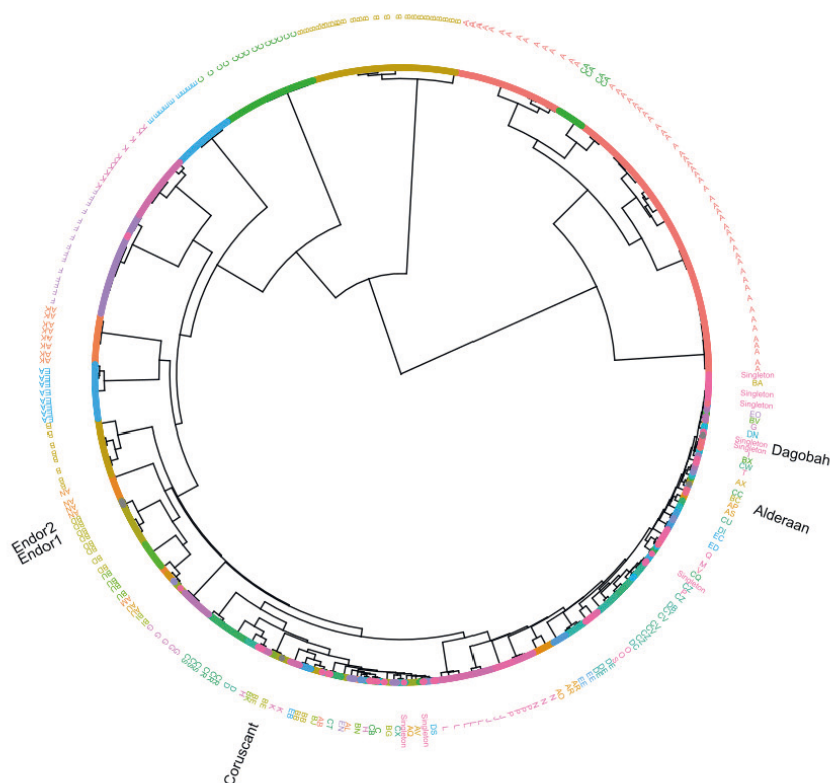


**Figure 5.** Protein domain-based hierarchical clustering. The dendrogram was constructed based on the presence-absence matrix of the >700 Pfam protein domains identified from 2486 actinophage genomes. Phages are color-coded according to known groups from the Actinobacteriophage Database (<https://phagesdb.org/>) [31]. The overlapping labels of the outer ring were merged to improve the figure's readability. The position of the five new phage genomes is indicated as black text.

In comparison to ANI-based analysis, hierarchical clustering showed congruent topology for the four newly sequenced *Streptomyces* phage genomes (Endor1 and Endor2: BD cluster, Alderaan: BC cluster, and Coruscant: BE cluster) (Supplementary Figures S3–S6). It also resolved polytomy between the unresolved groups and showed that Dagobah comes under the singleton group, consisting of highly divergent phages. Moreover, a high level of congruence was observed between already known groups and the groups identified by our hierarchical clustering. Thus, our results strongly suggest domain-based phyletic or hierarchical clustering analysis as an alternate way of classification of newly sequenced phage genomes.

#### 4. Discussion

In this study, we report the isolation and characterization of five novel *Streptomyces* phages. Alderaan and Coruscant were isolated using *S. venezuelae*, while *S. coelicolor* was the host used for isolation of Dagobah, Endor1 and Endor2.

The machine-learning based lifestyle prediction tool PhageAI suggested a temperate lifestyle for four of the phages (Alderaan, Dagobah, Endor1 and Endor2) and a virulent lifestyle for Coruscant.



These results were congruent with the lifestyle indicated by PhagesDB of phages belonging to the same cluster, as shown by the protein domain-based hierarchical clustering (Supplementary Figures S3–S6). However, unlike the other members of the BC cluster, Alderaan does not seem to have any integrase domain or gene. Together with the clear plaques it forms, this suggests that this phage potentially lost its integrase and therefore adopted a lytic lifestyle. Such events alter only slightly the overall genome landscape, be it at the nucleotide or protein level, and could thereby explain why whole-genome based predictions like PhageAI or protein domain-based clustering still predict Alderaan as temperate. These incongruencies, however, highlight the requirement of further experimental validation.

In contrast to the other four phages, Coruscant exhibits a large genome (superior to 130 kb) with massive direct terminal repeats (12 kb) and a low GC content (48%), in comparison to the 72% of its *Streptomyces* host. Coruscant also encodes 41 copies of tRNA genes, spanning 19 of the 20 standard amino acids. This large tRNA gene repertoire could be used to optimize gene expression in hosts that have differing codon usage patterns or to counteract potential tRNA-based degradation defense systems [44]. Altogether, the combination of a low GC content and a substantial tRNA equipment suggests a recent adaptation of the phage Coruscant to *Streptomyces*.

ANI and hierarchical clustering analysis revealed that Alderaan, Coruscant and Endor1/Endor2 belong to clusters BC, BE and BD defined by PhagesDB [31], respectively. In contrast, Dagobah showed very little homology with described phages, and was thus considered as a singleton. This finding highlights the largely untapped phage diversity, making the isolation of entirely “novel” phages still possible.

*Streptomyces* are characterized by their complex lifestyle and cellular differentiation. Interestingly, the isolated actinophages also encode homologs of SsgA, WhiB and Lsr2 proteins—regulatory proteins typically encoded by their hosts. The *ssgA* gene product was previously shown to be necessary for proper sporulation of *Streptomyces coelicolor* [41]; *whiB* is also essential for sporulation of *Streptomyces* and was already reported to be found in several actinophages [45–47]. Interestingly, the WhiB-like protein of mycobacteriophage TM4, WhiB<sub>TM4</sub>, was shown to inhibit the transcription of *Mycobacterium tuberculosis* WhiB2. Expression of WhiB<sub>TM4</sub> in *M. smegmatis* led to hindered septation resembling a WhiB2 knockout phenotype, highlighting how phage can interfere with their host’s development [46].

Lsr2-like proteins are nucleoproteins conserved in Actinobacteria. In *Streptomyces*, they were recently shown to silence cryptic specialized metabolic clusters [48]. The first example of a phage-encoded Lsr2-like protein is the prophage-encoded Lsr2-like protein CgpS in *Corynebacterium glutamicum* [49]. CgpS was shown to maintain the lysogenic state of the prophage on which it resides. Further bioinformatic searches revealed that Lsr2-like proteins are abundant in actinophages, with almost 20% of *Streptomyces* phages encoding such proteins [42]. However, their role in the coordination of the phage life cycle still remains unclear. Altogether, these observations suggest that phages manipulate their host development, by interfering with central processes such as sporulation and antibiotic production.

More generally, the specificities of *Streptomyces*—especially its morphological complexity—impact the phage isolation and characterization process. For example, the mycelial nature of streptomycetes complicates quantitative studies. The notion of MOI loses a lot of its significance once mycelium has formed, as the network structure originating from one spore has greatly increased phage adsorption but would still be counted as one CFU [14,50]. Furthermore, the formation of clumps, although mitigated by the addition of glass beads or increase of osmotic pressure [51], makes accurate monitoring of cell growth (based on optical density or backscatter) difficult.

*S. coelicolor* was established as a model system for the *Streptomyces* genus partly because of its prolific pigment production [52]. Interestingly, we observed colored halos around the plaques formed by the *S. coelicolor* phages. Exposure to ammonia fume confirmed that these colored halos contain actinorhodin. This observation suggests that *Streptomyces* release metabolites in reaction to phage predation, some of which may potentially have anti-phage properties as it was shown recently with anthracyclines in *Streptomyces peucetius* [53].

Understanding the processes governing phage infection has the potential to illuminate the basic physiology of their hosts. Therefore, phages can serve as a basis to study *Streptomyces*' specific traits—its complex reproduction cycle and abundant production of secondary metabolites—in the context of phage infection.

**Supplementary Materials:** The following are available online at <http://www.mdpi.com/1999-4915/12/10/1065/s1>, Figure S1: Close-ups of phage plaques imaged using a Nikon SMZ18 stereomicroscope, before (upper row) and after (lower row) exposure to ammonia fumes. Figure S2: VIRIDIC generated heatmap showing the intergenomic similarities of the newly sequenced phages with reference phages. Figure S3: Subclade dendrogram with *Streptomyces* phage Alderaan and its closely related actinophages. Figure S4: Subclade dendrogram with *Streptomyces* phage Coruscant and its closely related actinophages. Figure S5: Subclade dendrogram with *Streptomyces* phage Dagobah and its closely related actinophages. Figure S6: Subclade dendrogram with *Streptomyces* phages Endor1 and Endor2 and their closely related actinophages. Supplementary Table S1: List of the functional annotation of proteins ORFs within phage genomes.

**Author Contributions:** Conceptualization, A.H., and J.F.; methodology, All; validation, All; formal analysis, All; investigation, A.H. and L.K.; resources, V.S. and J.F.; data curation, A.H. and V.S.; writing—original draft preparation, A.H. and V.S.; writing—review and editing, All; visualization, A.H., V.S. and L.K.; supervision, J.F.; project administration, J.F.; funding acquisition, J.F. All authors have read and agreed to the published version of the manuscript.

**Funding:** We thank the European Research Council (ERC Starting Grant, grant number 757563) for financial support. A.H. was supported by a fellowship from the Ecole Normale Supérieure (Paris, France).

**Acknowledgments:** We thank David Brandt (Center for Biotechnology, University of Bielefeld) for his help with genome assembly and Julio Ortiz (Forschungszentrum Jülich) for his assistance during electron microscopy. The *S. cyaneofuscatus* and *S. olivaceus* strains were kindly provided by the German Collection of Microorganisms and Cell Cultures (DSMZ). We are also grateful to the entire Frunzke lab for fruitful discussions.

**Conflicts of Interest:** The authors declare no conflict of interest.

## References

1. Bibb, M.J. Understanding and manipulating antibiotic production in actinomycetes. *Biochem. Soc. Trans.* **2013**, *41*, 1355–1364. [CrossRef] [PubMed]
2. Hopwood, D.A. *Streptomyces in Nature and Medicine: The Antibiotic Makers*; Oxford University Press: Oxford, NY, USA, 2007; ISBN 978-0-19-515066-7.
3. Keiser, T.; Bibb, M.J.; Buttner, M.J.; Chater, K.F.; Hopwood, D.A. *Practical Streptomyces Genetics*; The John Innes Foundation: Norwich, UK, 2000; ISBN 0-7084-0623-8.
4. Elliot, M.A.; Buttner, M.J.; Nodwell, J.R. 24 Multicellular Development in *Streptomyces*. *Myxobacteria* **2008**, 419–438. [CrossRef]
5. McCormick, J.R.; Flärdh, K. Signals and regulators that govern *Streptomyces* development. *FEMS Microbiol. Rev.* **2012**, *36*, 206–231. [CrossRef] [PubMed]
6. Anne, J.; Wohlleben, W.; Burkhardt, H.J.; Springer, R.; Pohler, A. Morphological and Molecular Characterization of Several Actinophages Isolated from Soil Which Lyse *Streptomyces cattleya* or *S. venezuelae*. *Microbiology* **1984**, *130*, 2639–2649. [CrossRef] [PubMed]
7. Donadio, S.; Paladino, R.; Costanzi, I.; Sparapani, P.; Schreil, W.; Iaccarino, M. Characterization of bacteriophages infecting *Streptomyces erythraeus* and properties of phage-resistant mutants. *J. Bacteriol.* **1986**, *166*, 1055–1060. [CrossRef] [PubMed]
8. Dowding, J.E. Characterization of a Bacteriophage Virulent for *Streptomyces coelicolor* A3 (2) | Microbiology Society. *J. Gen. Microbiol.* **1973**, *76*, 163–176. [CrossRef]
9. Smith, M.C.M.; Hendrix, R.W.; Dedrick, R.; Mitchell, K.; Ko, C.-C.; Russell, D.; Bell, E.; Gregory, M.; Bibb, M.J.; Pethick, F.; et al. Evolutionary Relationships among Actinophages and a Putative Adaptation for Growth in *Streptomyces* spp. *J. Bacteriol.* **2013**, *195*, 4924–4935. [CrossRef]
10. Smith, M.C.M.; Burns, R.N.; Wilson, S.E.; Gregory, M.A. The complete genome sequence of the *Streptomyces* temperate phage  $\phi$ C31: Evolutionary relationships to other viruses. *Nucleic Acids Res.* **1999**, *27*, 2145–2155. [CrossRef]
11. Lomovskaya, N.D.; Mkrtumian, N.M.; Gostimskaya, N.L.; Danilenko, V.N. Characterization of Temperate Actinophage  $\phi$ C31 Isolated from *Streptomyces coelicolor* A3(2). *J. Virol.* **1972**, *9*, 5. [CrossRef]

12. Lomovskaya, N.D.; Chater, K.F.; Mkrtumian, N.M. Genetics and molecular biology of *Streptomyces* bacteriophages. *Microbiol. Mol. Biol. Rev.* **1980**, *44*, 206–229. [\[CrossRef\]](#)
13. Burke, J.; Schneider, D.; Westpheling, J. Generalized transduction in *Streptomyces coelicolor*. *Proc. Natl. Acad. Sci. USA* **2001**, *98*, 6289–6294. [\[CrossRef\]](#) [\[PubMed\]](#)
14. Rosner, A.; Gustein, R. Adsorption of actinophage Pal 6 to developing mycelium of *Streptomyces*. *Can. J. Microbiol.* **1981**, *27*, 254–257. [\[CrossRef\]](#) [\[PubMed\]](#)
15. Jordan, T.C.; Burnett, S.H.; Carson, S.; Caruso, S.M.; Clase, K.; DeJong, R.J.; Dennehy, J.J.; Denver, D.R.; Dunbar, D.; Elgin, S.C.R.; et al. A Broadly Implementable Research Course in Phage Discovery and Genomics for First-Year Undergraduate Students. *mBio* **2014**, *5*. [\[CrossRef\]](#) [\[PubMed\]](#)
16. Pullan, S.T.; Chandra, G.; Bibb, M.J.; Merrick, M. Genome-wide analysis of the role of GlnR in *Streptomyces venezuelae* provides new insights into global nitrogen regulation in actinomycetes. *BMC Genom.* **2011**, *12*, 175. [\[CrossRef\]](#) [\[PubMed\]](#)
17. Weaver, D.; Karoonuthaisiri, N.; Tsai, H.-H.; Huang, C.-H.; Ho, M.-L.; Gai, S.; Patel, K.G.; Huang, J.; Cohen, S.N.; Hopwood, D.A.; et al. Genome plasticity in *Streptomyces*: Identification of 1 Mb TIRs in the *S. coelicolor* A3(2) chromosome: Identification of 1 Mb TIRs in *S. coelicolor* A3(2). *Mol. Microbiol.* **2004**, *51*, 1535–1550. [\[CrossRef\]](#)
18. Bentley, S.D.; Chater, K.F.; Cerdeño-Tárraga, A.-M.; Challis, G.L.; Thomson, N.R.; James, K.D.; Harris, D.E.; Quail, M.A.; Kieser, H.; Harper, D.; et al. Complete genome sequence of the model actinomycete *Streptomyces coelicolor* A3(2). *Nature* **2002**, *417*, 141–147. [\[CrossRef\]](#)
19. Shepherd, M.D.; Kharel, M.K.; Bosserman, M.A.; Rohr, J. Laboratory Maintenance of *Streptomyces* species. *Curr. Protoc. Microbiol.* **2010**, *18*, 10E.1.1–10E.1.8. [\[CrossRef\]](#)
20. Kauffman, K.M.; Polz, M.F. Streamlining standard bacteriophage methods for higher throughput. *MethodsX* **2018**, *5*, 159–172. [\[CrossRef\]](#)
21. Kensy, F.; Zang, E.; Faulhammer, C.; Tan, R.-K.; Büchs, J. Validation of a high-throughput fermentation system based on online monitoring of biomass and fluorescence in continuously shaken microtiter plates. *Microb. Cell Fact.* **2009**, *8*, 31. [\[CrossRef\]](#)
22. Rückert, C.; Albersmeier, A.; Busche, T.; Jaenicke, S.; Winkler, A.; Friðjónsson, Ó.H.; Hreggviðsson, G.Ó.; Lambert, C.; Badcock, D.; Bernaerts, K.; et al. Complete genome sequence of *Streptomyces lividans* TK24. *J. Biotechnol.* **2015**, *199*, 21–22. [\[CrossRef\]](#)
23. Gordon, D.; Green, P. Consed: A graphical editor for next-generation sequencing. *Bioinformatics* **2013**, *29*, 2936–2937. [\[CrossRef\]](#) [\[PubMed\]](#)
24. Hyatt, D.; Chen, G.-L.; LoCascio, P.F.; Land, M.L.; Larimer, F.W.; Hauser, L.J. Prodigal: Prokaryotic gene recognition and translation initiation site identification. *BMC Bioinform.* **2010**, *11*, 119. [\[CrossRef\]](#) [\[PubMed\]](#)
25. Seemann, T. Prokka: Rapid prokaryotic genome annotation. *Bioinformatics* **2014**, *30*, 2068–2069. [\[CrossRef\]](#) [\[PubMed\]](#)
26. Altschul, S.F.; Gish, W.; Miller, W.; Myers, E.W.; Lipman, D.J. Basic local alignment search tool. *J. Mol. Biol.* **1990**, *215*, 403–410. [\[CrossRef\]](#)
27. Grazziotin, A.L.; Koonin, E.V.; Kristensen, D.M. Prokaryotic Virus Orthologous Groups (pVOGs): A resource for comparative genomics and protein family annotation. *Nucleic Acids Res.* **2017**, *45*, D491–D498. [\[CrossRef\]](#)
28. Marchler-Bauer, A.; Derbyshire, M.K.; Gonzales, N.R.; Lu, S.; Chitsaz, F.; Geer, L.Y.; Geer, R.C.; He, J.; Gwadz, M.; Hurwitz, D.L.; et al. CDD: NCBI's conserved domain database. *Nucleic Acids Res.* **2015**, *43*, D222–D226. [\[CrossRef\]](#)
29. Gameau, J.R.; Depardieu, F.; Fortier, L.-C.; Bikard, D.; Monot, M. PhageTerm: A tool for fast and accurate determination of phage termini and packaging mechanism using next-generation sequencing data. *Sci. Rep.* **2017**, *7*, 8292. [\[CrossRef\]](#)
30. Tynecki, P.; Guziński, A.; Kazimierzczak, J.; Jadczyk, M.; Dastyk, J.; Onisko, A. PhageAI—Bacteriophage Life Cycle Recognition with Machine Learning and Natural Language Processing. *Bioinformatics* **2020**. [\[CrossRef\]](#)
31. Russell, D.A.; Hatfull, G.F. PhagesDB: The actinobacteriophage database. *Bioinformatics* **2017**, *33*, 784–786. [\[CrossRef\]](#)
32. Pritchard, L. Widdowquinn/pyani. 2020. Available online: <https://github.com/widdowquinn> (accessed on 21 September 2020).
33. Gu, Z.; Eils, R.; Schlesner, M. Complex heatmaps reveal patterns and correlations in multidimensional genomic data. *Bioinformatics* **2016**, *32*, 2847–2849. [\[CrossRef\]](#)

34. Yu, G.; Smith, D.K.; Zhu, H.; Guan, Y.; Lam, T.T.-Y. Ggtree: An R package for visualization and annotation of phylogenetic trees with their covariates and other associated data. *Methods Ecol. Evol.* **2017**, *8*, 28–36. [\[CrossRef\]](#)
35. Rudd, B.A.M.; Hopwood, D.A. Genetics of Actinorhodin Biosynthesis by *Streptomyces coelicolor* A3(2). *Microbiology* **1979**, *114*, 35–43. [\[CrossRef\]](#)
36. Abedon, S.T. Lysis from without. *Bacteriophage* **2011**, *1*, 46–49. [\[CrossRef\]](#)
37. Abedon, S.T. Detection of Bacteriophages: Phage Plaques. In *Bacteriophages: Biology, Technology, Therapy*; Harper, D.R., Abedon, S.T., Burrowes, B.H., McConville, M.L., Eds.; Springer International Publishing: Cham, Switzerland, 2018; pp. 1–32. ISBN 978-3-319-40598-8.
38. Botstein, D. A Theory of Modular Evolution for Bacteriophages. *Ann. N. Y. Acad. Sci.* **1980**, *354*, 484–491. [\[CrossRef\]](#) [\[PubMed\]](#)
39. Brüssow, H.; Desiere, F. Comparative phage genomics and the evolution of *Siphoviridae*: Insights from dairy phages. *Mol. Microbiol.* **2001**, *39*, 213–223. [\[CrossRef\]](#) [\[PubMed\]](#)
40. Molle, V.; Palframan, W.J.; Findlay, K.C.; Buttner, M.J. WhiD and WhiB, homologous proteins required for different stages of sporulation in *Streptomyces coelicolor* A3(2). *J. Bacteriol.* **2000**, *182*, 1286–1295. [\[CrossRef\]](#)
41. van Wezel, G.P.; van der Meulen, J.; Kawamoto, S.; Luiten, R.G.M.; Koerten, H.K.; Kraal, B. *ssgA* Is Essential for Sporulation of *Streptomyces coelicolor* A3(2) and Affects Hyphal Development by Stimulating Septum Formation. *J. Bacteriol.* **2000**, *182*, 5653–5662. [\[CrossRef\]](#)
42. Pfeifer, E.; Hünnefeld, M.; Popa, O.; Frunzke, J. Impact of Xenogeneic Silencing on Phage–Host Interactions. *J. Mol. Biol.* **2019**. [\[CrossRef\]](#) [\[PubMed\]](#)
43. Moraru, C.; Varsani, A.; Kropinski, A.M. VIRIDIC—A novel tool to calculate the intergenomic similarities of prokaryote-infecting viruses. *bioRxiv* **2020**. [\[CrossRef\]](#)
44. Hyman, P.; Abedon, S.T. Chapter 7—Bacteriophage Host Range and Bacterial Resistance. In *Advances in Applied Microbiology*; Academic Press: Cambridge, MA, USA, 2010; Volume 70, pp. 217–248.
45. Morris, P.; Marinelli, L.J.; Jacobs-Sera, D.; Hendrix, R.W.; Hatfull, G.F. Genomic Characterization of Mycobacteriophage Giles: Evidence for Phage Acquisition of Host DNA by Illegitimate Recombination. *J. Bacteriol.* **2008**, *190*, 2172–2182. [\[CrossRef\]](#)
46. Rybníček, J.; Nowag, A.; van Gumpel, E.; Nissen, N.; Robinson, N.; Plum, G.; Hartmann, P. Insights into the function of the WhiB-like protein of mycobacteriophage TM4—A transcriptional inhibitor of WhiB2. *Mol. Microbiol.* **2010**, *77*, 642–657. [\[CrossRef\]](#)
47. Van Dessel, W.; Van Mellaert, L.; Liesegang, H.; Raasch, C.; DeKeersmaecker, S.; Geukens, N.; Lammertyn, E.; Streit, W.; Anné, J. Complete genomic nucleotide sequence and analysis of the temperate bacteriophage VWB. *Virology* **2005**, *331*, 325–337. [\[CrossRef\]](#) [\[PubMed\]](#)
48. Gehrke, E.J.; Zhang, X.; Pimentel-Elardo, S.M.; Johnson, A.R.; Rees, C.A.; Jones, S.E.; Gehrke, S.S.; Turvey, S.; Boursalie, S.; Hill, J.E.; et al. Silencing cryptic specialized metabolism in *Streptomyces* by the nucleoid-associated protein Lsr2. *eLife* **2019**, *8*, e47691. [\[CrossRef\]](#)
49. Pfeifer, E.; Hünnefeld, M.; Popa, O.; Polen, T.; Kohlheyer, D.; Baumgart, M.; Frunzke, J. Silencing of cryptic prophages in *Corynebacterium glutamicum*. *Nucleic Acids Res.* **2016**, *44*, 10117–10131. [\[CrossRef\]](#) [\[PubMed\]](#)
50. Gilmour, C.M.; Noller, E.C.; Watkins, B. Studies on *Streptomyces* Phage: I. Growth Characteristics of the *Streptomyces griseus* Host-Phage System. *J. Bacteriol.* **1959**, *78*, 186–192. [\[CrossRef\]](#) [\[PubMed\]](#)
51. Nguyen, L.D.; Kalachová, L.; Novotná, J.; Holub, M.; Kofroňová, O.; Benada, O.; Thompson, C.J.; Weiser, J. Cultivation System Using Glass Beads Immersed in Liquid Medium Facilitates Studies of *Streptomyces* Differentiation. *Appl. Environ. Microbiol.* **2005**, *71*, 2848–2852. [\[CrossRef\]](#) [\[PubMed\]](#)
52. Chater, K. David Hopwood and the emergence of *Streptomyces* genetics. *Int. Microbiol.* **1999**, *2*, 61–68.
53. Kronheim, S.; Daniel-Ivad, M.; Duan, Z.; Hwang, S.; Wong, A.I.; Mantel, I.; Nodwell, J.R.; Maxwell, K.L. A chemical defence against phage infection. *Nature* **2018**, *564*, 283. [\[CrossRef\]](#)



3.5. Antiphage small molecules produced by bacteria – beyond protein-mediated defenses

Hardy A., **Keuer L.** and Frunzke J.

Published in Trends in Microbiology, 2023

Contributor role	Contributor
Conceptualization	AH (60%), JF (30%), LK (10%)
Data curation	AH (95%), LK (5%)
Formal analysis	-
Funding acquisition	JF (100%)
Investigation	AH (90%), LK (5%), JF (5%)
Methodology	AH (65%), JF (30%), LK (5%)
Project administration	AH (90%), JF (10%)
Resources	-
Software	-
Supervision	AH (60%), JF (40%)
Validation	AH (70%), LK (20%), JF (10%)
Visualization	LK (80%), AH (15%), JF (5%)
Writing – original draft	AH (95%), JF (5%)
Writing – review and editing	JF (60%), AH (30%), LK (10%)

Overall contribution: 7.5%

Design of the review figures was mainly done by LK and optimized in cooperation with JF and AH. LK was further involved in the conceptualization as well as review and editing process.

## Review

## Antiphage small molecules produced by bacteria – beyond protein-mediated defenses

Aël Hardy,<sup>1</sup> Larissa Kever,<sup>1</sup> and Julia Frunzke<sup>1,\*</sup>

**Bacterial populations face the constant threat of viral predation exerted by bacteriophages ('phages'). In response, bacteria have evolved a wide range of defense mechanisms against phage challenges. Yet the vast majority of antiphage defense systems described until now are mediated by proteins or RNA complexes acting at the single-cell level. Here, we review small molecule-based defense strategies against phage infection, with a focus on the antiphage molecules described recently. Importantly, inhibition of phage infection by excreted small molecules has the potential to protect entire bacterial communities, highlighting the ecological significance of these antiphage strategies. Considering the immense repertoire of bacterial metabolites, we envision that the list of antiphage small molecules will be further expanded in the future.**

## Highlights

Bacteria are prolific metabolite producers, but the role of this metabolite diversity in protection against phages has been only recently appreciated.

Anthracyclines, aminoglycosides, and chain terminators produced by prokaryotic viperins represent the main classes of antiphage small molecules known to date.

Aminoglycosides have both antibacterial and antiphage properties, this dual function making them an interesting example of molecular multitasking.

Secreted antiphage metabolites have the potential to protect bacterial communities, serving as a multicellular defense strategy.

Bacteriophages (or phages for short) are viruses preying on bacteria and are considered to be titans in the biosphere [1]. They represent a ubiquitous feature of bacterial existence as there is virtually no ecosystem where bacteria do not coexist with phages infecting them [1]. The strong evolutionary pressure imposed by phage predation has led to a sophisticated arsenal of antiphage strategies, which have been extensively reviewed elsewhere [2–5]. The repertoire of known defense systems has been significantly expanded through large-scale bioinformatics screenings followed by experimental validation [6,7]. In addition to the already known defense systems, such as restriction-modification systems, CRISPR-Cas, or abortive infection (Abi), antiviral strategies now include the use of cyclic nucleotides as signaling molecules (CBASS [8], Pycsar [9]) and NAD<sup>+</sup> depletion as a widespread response to viral infection [10–13]. Scrutiny of these novel antiphage defense systems revealed striking similarities to eukaryotic immune systems, suggesting that a previously underappreciated fraction of eukaryotic immunity evolved from prokaryotic antiphage defenses [8,10,14–16]. With the accelerating pace of discovery of new antiphage systems, keeping an overview of the currently known antiviral prokaryotic arsenal has become increasingly difficult but has been facilitated by the development of tools aimed at systematic and comprehensive identification of defense systems in prokaryotic genomes [17,18]. The notion of a bacterial pan-immune system has been recently proposed to recognize phage defense as a community resource distributed between closely related bacteria via horizontal gene transfer (HGT) [19].

In nature, bacteria live in complex, spatially structured and multispecies communities [20], which highlights the need to consider antiphage strategies at the community level. These mechanisms include the release of extracellular vesicles [21,22], formation of protective biofilm structures [23,24], or quorum sensing [25–27]. Chemical inhibition of phages using small molecules secreted in the extracellular space represents another effective multicellular strategy against phage infection, which, unlike most defense systems described until now, does not rely on proteins or RNA.

<sup>1</sup>Institute of Bio- und Geosciences, IBG-1: Biotechnology, Forschungszentrum Jülich, 52425 Jülich, Germany

\*Correspondence: j.frunzke@fz-juelich.de (J. Frunzke).

The direct inhibition of phage infection by bacterial small molecules was an intense research field in the 1950s and 1960s and has recently regained significant attention. Here, we aim at summarizing the extensive but largely overlooked body of research in the field of antiphage molecules and present the latest developments in this emerging research area. Furthermore, we outline future perspectives for the discovery of novel antiphage metabolites and discuss the ecological significance of this defense strategy.

The present review aims at presenting small molecules, other than RNAs and proteins, that are produced by bacteria and confer protection against phage infection. As a result, antibiotics preventing phage infection by a primary action on the bacterium are not included.

### Chemical defense against phage infection

Overall, the study of antiphage molecules has known two distinct periods of interest – the first one spanning the third quarter of the 20th century while the second started only a few years ago. The interest to find new compounds active against phages was very strong in the 1950s [28–30], with, in some cases, heroic screening efforts such as those performed by Schatz and Jones or Asheshov and colleagues – who assessed the antiphage activity of more than 170 and 1000 strains of actinomycetes, respectively [28,29]. In these screenings, the supernatants of 29% (49/176) and 17% (144/1000) of the tested actinomycete isolates caused an inhibition of plaque formation, suggesting that the release of antiphage metabolites is not uncommon in actinobacteria. These two screenings led to the description in follow-up studies of four antiphage compounds (chrysomycin, phagolessin A58, nybomycin, and aklavin), the latter being shown to be a close congener of the **anthracycline** (see **Glossary**) aclacinomycin A [31]. The primary goal of these screenings was, however, not to understand how bacteria defend themselves against phages but rather to find new antiviral drugs usable in a clinical or agricultural setting [30]. An additional focus was put on substances able to specifically prevent phages from infecting ***Streptomyces griseus*** because of the risk phages posed to industrial production of streptomycin by this important production host [32].

Over the decades, a significant number of molecules were described to have antiphage properties. We listed these antiphage compounds in **Table 1**, which includes the phages inhibited and their bacterial hosts. In the following, we focus on the three main classes of antiphage small molecules described to date: anthracyclines, **aminoglycosides**, and modified nucleotides produced by prokaryotic **viperins**.

#### Anthracyclines

Anthracyclines are secondary metabolites naturally produced by *Streptomyces* – a common genus of soil-dwelling bacteria. Chemically speaking, anthracyclines belong to the family of type II aromatic polyketides and feature an aglycone scaffold decorated by a sugar residue [58]. Soon after their discovery, anthracyclines were shown to possess potent antitumor activity and have since been used to treat a wide range of cancers [59]. They are still among the most effective anticancer treatments ever developed [60–62]. The precise mechanism behind their cytotoxic effect in eukaryotic cells is still subject to debate. However, their antitumor activity can be broadly attributed to their ability to intercalate into the DNA helix and/or bind covalently to proteins involved in DNA replication and transcription [63]. The DNA-damaging properties of anthracyclines also affect their producer, which, as a result, evolved several self-resistance mechanisms. In the case of *Streptomyces peucetius*, the toxic effects of daunorubicin and doxorubicin are mitigated by a combination of active efflux by DrrA and DrrB, extracellular sequestration to prevent reimport, and dislodgement of intercalated anthracyclines by DrrC [64–66].

### Glossary

**Aminoglycosides:** antibacterials naturally produced by *Streptomyces* and *Micromonosporas* species. They target bacterial translation by binding to the 30S ribosomal subunit. Besides their antibacterial action, additional antiphage properties were recently discovered.

**Anthracyclines:** DNA-intercalating antibiotics produced by *Streptomyces* having antitumor as well as antiphage properties.

**Bioactivity-guided fractionation:** chromatographic separation of extracts aiming at the isolation of a pure biologically active compound.

**Chemical defense:** protection against phage infection via bacterial small molecules.

**Streptomyces:** a genus of Gram-positive bacteria of the phylum Actinobacteria. *Streptomyces* species are found mainly in the soil and are characterized by mycelial development as well as by their complex secondary metabolism. *Streptomyces* is one of the most important producers of bioactive molecules.

**Viperins:** virus-inhibitory proteins in eukaryotes which convert ribonucleotides into chain terminators, thereby preventing transcription of viral genes. Viperin homologs are found in prokaryotes and are known as prokaryotic viperins (pVips). pVips inhibit phage infection by a mode of action similar to that of their eukaryotic counterparts.



Table 1. Small molecules with known antiphage properties<sup>a</sup>

Class	Compound	Phages affected	Bacterial host	Phage family	Genome	Refs
DNA-intercalating agents						
Alkaloid	Ellipticine	λ	<i>Escherichia coli</i>	<i>Siphoviridae</i>	Linear dsDNA	[33]
Fluorochrome	Acridine family compounds	Propidium iodide	<i>E. coli</i>	<i>Siphoviridae</i>	Linear dsDNA	[33]
		↑Scoe2	<i>Streptomyces coelicolor</i>	<i>Siphoviridae</i>	Linear dsDNA	
		↑Scoe25	<i>S. coelicolor</i>	<i>Siphoviridae</i>	Linear dsDNA	
		λ	<i>E. coli</i>	<i>Siphoviridae</i>	Linear dsDNA	
		↑Scoe2	<i>S. coelicolor</i>	<i>Siphoviridae</i>	Linear dsDNA	
		↑Scoe25	<i>S. coelicolor</i>	<i>Siphoviridae</i>	Linear dsDNA	
	Ethacridine lactate	λ	<i>E. coli</i>	<i>Siphoviridae</i>	Linear dsDNA	[43]
Polypeptide antibiotic	Actinomycin D	T2r	<i>E. coli</i>	<i>Myoviridae</i>	Linear dsDNA	[34]
		T4	<i>E. coli</i>	<i>Myoviridae</i>	Linear dsDNA	[35]
Anthracyclines	Rutlantin	Various phages infecting both Gram + and Gram –				[29]
	Aclacinomycin (aklavin) A and analogs	K174	<i>E. coli</i>	<i>Microviridae</i>	Circular ssDNA	[36]
		λ	<i>E. coli</i>	<i>Siphoviridae</i>	Linear dsDNA	[37]
		Various phages infecting both Gram + and Gram –				[38]
	Daunorubicin (daunomycin)	K174	<i>E. coli</i>	<i>Microviridae</i>	Circular ssDNA	[36]
		λ	<i>E. coli</i>	<i>Siphoviridae</i>	Linear dsDNA	[33]
		T1	<i>E. coli</i>	<i>Siphoviridae</i>	Linear dsDNA	[39]
		T3	<i>E. coli</i>	<i>Autographiviridae</i>	Linear dsDNA	[39]
		T4	<i>E. coli</i>	<i>Myoviridae</i>	Linear dsDNA	[39]
		T5	<i>E. coli</i>	<i>Siphoviridae</i>	Linear dsDNA	[33]
		T6	<i>E. coli</i>	<i>Myoviridae</i>	Linear dsDNA	[33,39]
		T7	<i>E. coli</i>	<i>Autographiviridae</i>	Linear dsDNA	[33]
		JBD26	<i>Pseudomonas aeruginosa</i>	<i>Siphoviridae</i>	Linear dsDNA	[33]
		JBD30	<i>P. aeruginosa</i>	<i>Siphoviridae</i>	Linear dsDNA	[33]
		↑Scoe2	<i>S. coelicolor</i>	<i>Siphoviridae</i>	Linear dsDNA	[33]
		↑Scoe25	<i>S. coelicolor</i>	<i>Siphoviridae</i>	Linear dsDNA	[33]
	Doxorubicin (Adriamycin)	K174	<i>E. coli</i>	<i>Microviridae</i>	Circular ssDNA	[36]
		λ	<i>E. coli</i>	<i>Siphoviridae</i>	Linear dsDNA	[33]
		↑Scoe2	<i>S. coelicolor</i>	<i>Siphoviridae</i>	Linear dsDNA	[33]
		↑Scoe25	<i>S. coelicolor</i>	<i>Siphoviridae</i>	Linear dsDNA	[33]
		PBS1	<i>Bacillus subtilis</i>	<i>Myoviridae</i>	Linear dsDNA	[40]
		SP10	<i>B. subtilis</i>	<i>Myoviridae</i>	Linear dsDNA	[40]
		↑Scoe2	<i>S. coelicolor</i>	<i>Siphoviridae</i>	Linear dsDNA	[33]
		↑Scoe25	<i>S. coelicolor</i>	<i>Siphoviridae</i>	Linear dsDNA	[33]
	Cosmomycin D	↑Scoe2	<i>S. coelicolor</i>	<i>Siphoviridae</i>	Linear dsDNA	[33]
		↑Scoe25	<i>S. coelicolor</i>	<i>Siphoviridae</i>	Linear dsDNA	[33]
	Epirubicin	λ	<i>E. coli</i>	<i>Siphoviridae</i>	Linear dsDNA	[33]
	Idarubicin	λ	<i>E. coli</i>	<i>Siphoviridae</i>	Linear dsDNA	[33]
	Mitoxantrone	λ	<i>E. coli</i>	<i>Siphoviridae</i>	Linear dsDNA	[33]

(continued on next page)



Table 1. (continued)

Class	Compound	Phages affected	Bacterial host	Phage family	Genome	Refs
Protein biosynthesis inhibitors <sup>a</sup>						
Aminoglycosides	Streptomycin	MS-2	<i>E. coli</i>	<i>Leviviridae</i>	Linear ssRNA	[41]
		P9	<i>Streptococcus faecium</i>	<i>Siphoviridae</i>	Linear dsDNA	[42,43]
		f2	<i>E. coli</i>	<i>Leviviridae</i>	Linear ssRNA	[44]
		μ2	<i>E. coli</i>	<i>Leviviridae</i>	Linear ssRNA	[44]
		fd	<i>E. coli</i>	<i>Inoviridae</i>	Circular ssDNA	[44]
		F-WJ-I	–	–	–	[45]
		Legendre	<i>Mycobacterium smegmatis</i>	<i>Siphoviridae</i>	Linear dsDNA	[45]
		Clark	<i>M. smegmatis</i>	<i>Siphoviridae</i>	Linear dsDNA	[45]
		D29	<i>M. smegmatis</i>	<i>Siphoviridae</i>	Linear dsDNA	[45,46]
		phAE159	<i>M. smegmatis</i>	Phasmid (derived from TM4 phage)	Circular dsDNA	[46]
	Kanamycin	D29	<i>M. smegmatis</i>	<i>Siphoviridae</i>	Linear dsDNA	[46]
		phAE159	<i>M. smegmatis</i>	Phasmid (derived from TM4 phage)	Circular dsDNA	[46]
		Spe2	<i>Corynebacterium glutamicum</i>	<i>Siphoviridae</i>	Linear dsDNA	[47]
		λ	<i>E. coli</i>	<i>Siphoviridae</i>	Linear dsDNA	[46]
		T3	<i>E. coli</i>	<i>Autographiviridae</i>	Linear dsDNA	[48]
		WSP	<i>E. coli</i>	–	–	[48]
		BSP	<i>Bacillus cereus</i>	–	–	[48]
	Hygromycin	D29	<i>M. smegmatis</i>	<i>Siphoviridae</i>	Linear dsDNA	[46]
		phAE159	<i>M. smegmatis</i>	Phasmid (derived from TM4 phage)	Circular dsDNA	[46]
		Alderaan	<i>Streptomyces venezuelae</i>	<i>Siphoviridae</i>	Linear dsDNA	[47]
	Apramycin	Alderaan	<i>S. venezuelae</i>	<i>Siphoviridae</i>	Linear dsDNA	[47]
		λ	<i>E. coli</i>	<i>Siphoviridae</i>	Linear dsDNA	[47]
	Neomycin	80	<i>Staphylococcus aureus</i>	<i>Siphoviridae</i>	Linear dsDNA	[49]
		T3	<i>E. coli</i>	<i>Autographiviridae</i>	Linear dsDNA	[48]
		WSP	<i>E. coli</i>	–	–	[48]
		BSP	<i>B. cereus</i>	–	–	[48]
Others						
Di-benzimidazole	Ro 90-7501	λ	<i>E. coli</i>	<i>Siphoviridae</i>	Linear dsDNA	[33]
Quaternary ammonium	Dequalinium chloride	λ	<i>E. coli</i>	<i>Siphoviridae</i>	Linear dsDNA	[33]
λ	'Phagostatin'	T3	<i>E. coli</i>	<i>Autographiviridae</i>	Linear dsDNA	[50]
Cyclopentenone	Sarkomycin	f2	<i>E. coli</i>	<i>Leviviridae</i>	Linear ssRNA	[51]
Naphthocoumarin	Chrysomycin	Diverse phages				[52]
λ	'Phagocidin'	T3	<i>E. coli</i>	<i>Autographiviridae</i>	Linear dsDNA	[53,54]
Pyrrolobenzodiazepine	Tomaymycin	T1	<i>E. coli</i>	<i>Siphoviridae</i>	Linear dsDNA	[55]
		T3	<i>E. coli</i>	<i>Autographiviridae</i>	Linear dsDNA	

Table 1. (continued)

Class	Compound	Phages affected	Bacterial host	Phage family	Genome	Refs
		M2	<i>B. subtilis</i>	<i>Podoviridae</i>	Linear dsDNA	
		SP10	<i>B. subtilis</i>	<i>Myoviridae</i>	Linear dsDNA	
Heterocyclic anthracene	Nyboromycin	15/60 phages tested				[56]
λ	'Phagolessin A58'	T1	<i>E. coli</i>	<i>Siphoviridae</i>	Linear dsDNA	[57]
		T3	<i>E. coli</i>	<i>Autographiviridae</i>	Linear dsDNA	
		T7	<i>E. coli</i>	<i>Autographiviridae</i>	Linear dsDNA	
Modified ribonucleotides produced by prokaryotic viperins	ddhCTP, ddhGTP, ddhUTP	T7	<i>E. coli</i>	<i>Autographiviridae</i>	Linear dsDNA	[14]
		P1	<i>E. coli</i>	<i>Myoviridae</i>	Linear dsDNA	
		λ	<i>E. coli</i>	<i>Siphoviridae</i>	Linear dsDNA	

<sup>a</sup>The classification of aminoglycosides as protein synthesis inhibitors is based on their antibacterial action.

Multiple reports described the inhibition of phage infection by anthracyclines such as daunorubicin, doxorubicin, or cosmomycin (Table 1). Parisi and Soller assessed the impact of daunomycin on the steps of the lytic cycle and showed a strong impairment of phage DNA synthesis during phage infection, suggesting a blockage occurring during replication or between injection and replication [39].

A major step forward in the understanding of both the mechanism and biological significance of the antiphage properties of anthracyclines was made more than 40 years later by Kronheim and colleagues [33]. In this study, the authors show that daunorubicin inhibits phage λ in *Escherichia coli* as well as several double-stranded DNA (dsDNA) phages infecting *E. coli*, *Streptomyces coelicolor*, or *Pseudomonas aeruginosa* and encompassing the three main families of tailed phages (*Siphoviridae*, *Podoviridae*, and *Myoviridae*). The exact mechanism of action remains unclear, but inhibition by daunorubicin takes place at an early stage of the infection cycle, namely, after injection of the phage genome but before phage replication (Figure 1). All dsDNA phages tested – whose incoming genome is linear – are inhibited by daunorubicin. In contrast, the filamentous M13 phage, whose single-stranded DNA (ssDNA) genome enters as a circular molecule, is not, suggesting that the circularization of incoming linear dsDNA could be the step blocked by daunorubicin. The anthracyclines doxorubicin and cosmomycin D were also shown to have antiphage properties. Importantly, the inhibition of phage infection could be reproduced with supernatants from natural producers of these anthracyclines (*S. peucetius* for daunorubicin and doxorubicin; strains of the WAC collection [67] for cosmomycin D, respectively). This observation suggests that phage inhibition by anthracyclines is physiologically relevant in the natural environment.

Kronheim and colleagues also reported the antiphage properties of synthetic DNA-intercalating agents such as propidium iodide or acridine derivatives [33]. Further, the inhibition of *E. coli* phage T2 by actinomycin D – another DNA-intercalating agent produced by *Streptomyces* – was already described in 1961 [34]. Altogether, this suggests that intercalation into phage DNA is probably a widespread antiphage strategy (Table 1).

Aminoglycosides

Aminoglycosides are bactericidal antibiotics that are active against Gram-negative and Gram-positive organisms [68,69]. As their name suggests, aminoglycosides are pseudosaccharides that possess several amino and hydroxy functionalities and most of them share a core 2-deoxystreptamine ring [70]. Since the amine groups are typically protonated under physiologically relevant conditions, these antibiotics can be considered as polycationic species featuring a

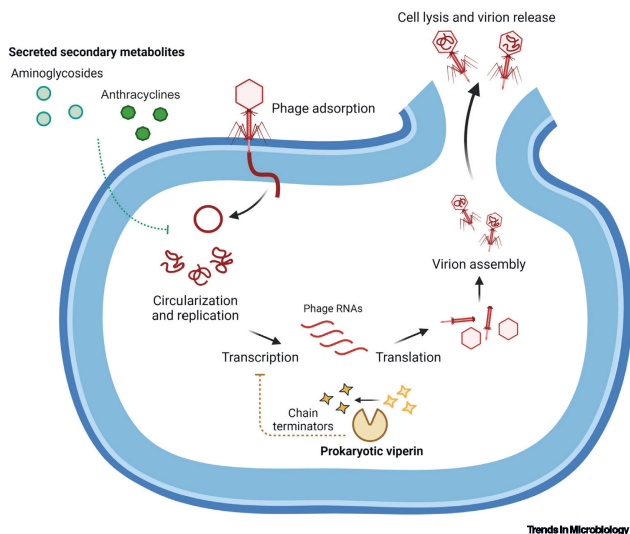


**Figure 1.** Mechanism of action of antiphage molecules anthracyclines, aminoglycosides, and modified nucleotides produced by prokaryotic viperin homologs (pVips). The phage replication cycle comprises several steps, some of which are targeted by antiphage molecules. Unlike the modified ribonucleotides produced by pVips, anthracyclines and aminoglycosides are secreted by producer cells and can be taken up by neighboring cells.

binding affinity for nucleic acids. In bacteria, they disrupt protein biosynthesis by targeting the 30S subunit of the ribosomes, which, in turn, leads to complete blockage of translation or promotes mistranslation [71]. Aminoglycosides were originally isolated from actinomycetes belonging to the genera *Streptomyces* and *Micromonospora* [72]. In nature, aminoglycoside producers are resistant to these molecules, which is a feature important to keep in mind when screening aminoglycosides – and small molecules in general – for antiviral properties.

Using bacterial hosts expressing plasmid-borne aminoglycoside-resistance cassettes, aminoglycosides were recently shown to inhibit phages infecting the Gram-negative bacterium *E. coli* as well as Gram-positive bacteria such as *Corynebacterium glutamicum* and *Streptomyces venezuelae* [47]. Experiments aiming at shedding light on the molecular mechanism of phage infection inhibition revealed that phage DNA was present inside cells in the presence of aminoglycosides. Together with the observation that amplification of phage DNA was strongly impaired, these results suggest that the blockage exerted by aminoglycosides occurs mostly after DNA injection but before genome replication (Figure 1). These results are in line with those obtained by Jiang and colleagues, who reported the inhibition of the two mycobacteriophages phAE159 and D29 by kanamycin, hygromycin, and streptomycin [46]. Following the impact of streptomycin on phage adsorption and amplification of phage DNA, the authors propose that the blockage caused by aminoglycosides occurs between genome circularization and replication.

One important question is whether this inhibition of phage infection by aminoglycosides is relevant in a physiological context. In the case of apramycin, inhibition of the *Streptomyces* phage Alderaan could be reproduced with supernatants of the natural producer of apramycin [47], *Streptoalloteichus tenebrarius* (formerly known as *Streptomyces tenebrarius* [73]). Appearance of the antiphage effect of supernatants coincided with the detection of apramycin in the culture supernatants. In combination with the antiphage effect of purified apramycin, these data strongly suggest that the main molecule behind the antiphage properties of the supernatants of *S. tenebrarius* is apramycin [47]. Additionally, it indicates that aminoglycosides are secreted by producers at levels which prevent infection in neighboring bacteria, opening the door to community-wide protection.

In a natural context, most bacteria do not possess aminoglycoside-resistance genes, and residual concentrations of antibiotics are pervasive across man-shaped and natural environments alike. Zuo and colleagues studied the impact of sublethal concentrations of aminoglycosides on phage infection in aminoglycoside-sensitive hosts [48]. Phage amplification was strongly impeded by concentrations as low as 3 mg/l. Interestingly, tetracycline, another antibiotic which blocks protein synthesis by binding to the 30S ribosomal subunit, had a significantly reduced impact on phage proliferation. These results suggest that blockade of translation alone is not sufficient to efficiently prevent phage replication. Alternatively, the mechanism of translation inhibition may be of importance, and the mistranslation caused by tetracycline could participate in the difference of impact observed with aminoglycosides [48].

Although the action of aminoglycosides on the phage life cycle *in vivo* is not fully understood yet, independent *in vitro* studies provide further hints about the basis of aminoglycosides' antiphage properties. Exposure of purified phage  $\lambda$  DNA to aminoglycosides leads to condensation of DNA, presumably coated by aminoglycoside fibers [74]. The same authors later proposed that aminoglycosides form a clamp around the DNA double helix, causing a bend responsible for the formation of structural deformations such as toroids [75].

*In vivo* mechanistic studies about the inhibition of phage infection by aminoglycosides are scarce, but Brock and his collaborators contributed work worthy of attention. Using *Streptococcus faecium* and its phage P9, Brock and Wooley investigated the inhibition of phage infection by streptomycin [42]. The authors used resistance to shearing forces as an indicator for DNA injection, under the assumption that the formation of a plaque from an initially infected cell subjected to shearing implies a successful delivery of the phage genome. Using this technique, they proposed that streptomycin inhibits phage infection at an early stage of the phage infection cycle, namely, the DNA injection step. They further hypothesized that streptomycin exerts its inhibition by binding phage DNA in the capsid, thus preventing its unfolding necessary for infection. It is, however, important to note that, although phage infection could already be inhibited by a concentration of 100  $\mu\text{g/ml}$ , high concentrations of streptomycin were used (1 mg/ml) in most experiments. Such high concentrations could cause nonspecific effects such as phage precipitation potentially not present at lower concentrations. Moreover, the streptomycin-resistant bacterial host was reported to bind very low amounts of streptomycin, which suggests modifications of the cell surface that could, in turn, influence the antiphage properties of streptomycin. In another study, Brock demonstrated the inhibitory effect of streptomycin on the *E. coli* RNA phage MS-2 [41]. Streptomycin inhibited the formation of phage progeny very early in the replication cycle (5–10 min after infection), and no impact of streptomycin was noticed when added shortly after injection had occurred.

The fact that aminoglycosides have both antibacterial and antiviral properties raises the question of the interplay between these two facets. In the case of apramycin, acetylation of one of its amino

groups by the well-studied apramycin acetyltransferase AAC(3)IV abolished its impact on bacterial growth, while fully retaining its protective effect against phages [47]. This observation suggests that the antibacterial and antiviral actions of apramycin, and potentially further aminoglycosides, could be decoupled from one another and that the respective molecular targets are distinct.

Taken together, these studies suggest that aminoglycosides are used by their producers not only as toxic molecules against bacterial competitors but also as a protection against the threat of phage predation at the community level.

#### Modified ribonucleotides produced by prokaryotic viperins

Viperins are important players of the innate antiviral response in eukaryotes [76]. They produce ddhCTP, a modified ribonucleoside lacking the 3'-hydroxyl group necessary for elongation of the nascent viral mRNA; hence, they act as chain terminators [77].

Viperin-like genes were known to be present in prokaryotes too, but the function of these prokaryotic viperin homologs (pVips) remained unknown. Recently, they were shown to protect archaea and bacteria from viral infection and displayed a remarkable conservation between the eukaryotic and prokaryotic kingdoms [14]. Indeed, pVips use a mode of action similar to that of their eukaryotic homologs to inhibit viral transcription (Figure 1) – except that pVips produce a wider range of modified ribonucleotides (ddhCTP, but also ddhGTP and ddhUTP) [14]. Strikingly, the human viperin, when expressed in *E. coli*, conferred resistance to phage infection, which underlines inhibition of viral transcription as a broad antiviral strategy. Interestingly, inhibition of phage infection was also observed with phages like P1 and  $\lambda$  which do not encode their own RNA polymerases and rely instead on the host polymerase to complete transcription. This raises the possibility that pVips also exert their antiviral activity independently of premature termination of viral transcripts, via mechanisms which remain to be elucidated.

Mirroring the absence of toxic effects caused by human viperin in human cells, expression of pVips in *E. coli* had no effect on host transcription and did not cause toxicity. This observation hints that the bacterial RNA polymerase may be less sensitive than the phage RNA polymerase to ddh-ribonucleotides, as self-resistance to the ddh-ribonucleotides would be favored during coevolution of bacterial RNA polymerase and pVips. In contrast to anthracyclines and aminoglycosides, the modified nucleotides synthesized by viperins do not show antibacterial activity. Additionally, they are not secreted, and protection is thus conferred only to producer cells.

### Perspectives

#### Discovery of novel antiphage small molecules

Until now, the antiphage effects of most molecules were either discovered empirically or based on earlier reports describing antiphage properties of the same or closely related molecules. However, recent progress in the fields of genomics, metabolomics, and automation has the potential to greatly accelerate the discovery of new antiviral molecules.

Automated screening allows high-throughput testing of the antiphage properties of molecule libraries (Figure 2). To this end, bacteria are cultivated in microtiter plates, either alone, in the presence of phages, or together with both phages and the compounds to be tested. If the addition of a given compound suppresses the phage-mediated lysis of the culture, this hit indicates a probable inhibition of phage infection by this molecule, warranting further investigation. This strategy was successfully used with *E. coli* and phage  $\lambda$  to reveal the antiphage activity of anthracyclines and other DNA-intercalating agents [33]. One major limitation of this approach is

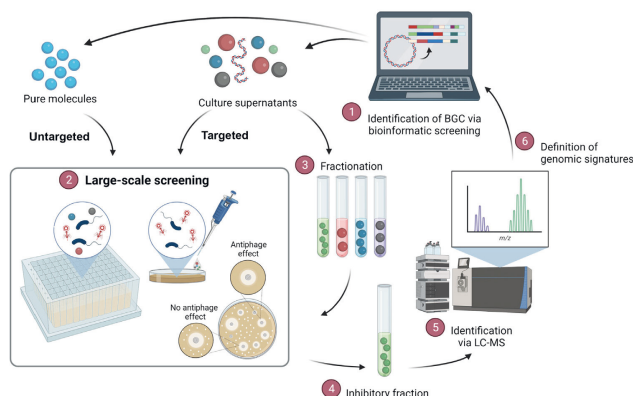


**Figure 2. Discovery strategies for the identification of new antiphage molecules.** Bioinformatic prediction of candidate biosynthetic gene clusters (BGCs) whose products may act against phages (1) inform large-scale testing of small molecule libraries as well as complex supernatants (2). The elucidation of the antiphage compounds can be achieved by bioactivity-guided fractionation (3,4) followed by analytic techniques such as liquid chromatography–mass spectrometry (LC-MS) (5). Results of the screening efforts can then be fed back to the bioinformatic screening to help define genomic features of antiphage BGCs (6).

that the compounds tested need to not interfere with the growth of the bacterium, since strong growth defects would prevent the detection of antiphage effects.

Alternatively, spotting the molecules of interest on a phage-infected bacterial lawn represents another screening strategy with potential for automation and upscaling (Figure 2). This technique has been used for decades to assess antibacterial activity of antibiotics and has been harnessed by phage researchers too [56,78,79]. It enables the appreciation of antiphage effects (or, on the contrary, phage–antibiotic synergy) despite inhibition of bacterial growth, as shown by rings devoid of plaque formation – or displaying larger plaques, respectively – around the zone of growth inhibition caused by the candidate molecule.

These two strategies are not restricted to pure compounds and can also be used with complex supernatants from bacterial hosts, enabling the exploration of a vaster metabolic landscape as well as of potential synergistic interactions between candidate molecules. In the case where a supernatant inhibits phage infection, **bioactivity-guided fractionation** followed by liquid chromatography–mass spectrometry (LC-MS) can narrow the antiphage properties of the supernatant down to one or a few compounds [33].

These screening approaches are likely to have a low discovery rate due to their untargeted nature. Screening can be narrowed down by testing in priority metabolites released in reaction to phage infection. For example, phage infection in *S. coelicolor* leads to the formation of colored halos around phage plaques. The presence of pigmented compounds at the infection interface suggests that *Streptomyces* reacts to phage infection by releasing these molecules, making them interesting candidates for further analysis [80].

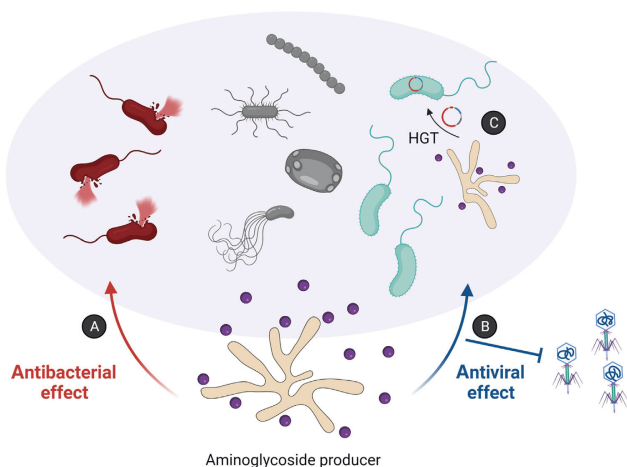
*In silico* prediction of gene clusters involved in chemical antiphage defense would allow rational identification and validation of candidate molecules. However, antiphage biosynthetic gene clusters (BGCs) such as the ones encoding aminoglycosides and anthracyclines are not detected using the now well-established 'guilty-by-association' approach. This discovery strategy is based on the observation that defense systems are clustered in genomic 'defense islands'. Genes markedly enriched in the vicinity of known defense genes are therefore assumed to be also involved in antiphage defense [6]. The use of this concept has led in recent years to a considerable expansion of the known repertoire of antiphage defense systems [6,7,14]. It is, however, biased towards small and very well-conserved genes, explaining why this approach did not detect large and genus- or sometimes even species-specific BGCs as putative novel antiphage defense systems. Now that tools systematically screening for known defense systems are available [17,18], combining detection of phage defense systems and prediction of BGCs could reveal interesting patterns of co-occurrence and help to define genomic features of antiphage BGCs. In the case of antiphage metabolites fulfilling several roles (e.g., antibacterial and antiviral), such as aminoglycosides, these supplementary functions likely impose further genomic and evolutionary constraints, hindering the establishment of genomic signatures for gene clusters encoding multifunctional molecules.

Importantly, empirical approaches and *in silico* screening are not mutually exclusive; uncovering more antiphage secondary metabolites will help to define genomic signatures for antiphage molecules. *Streptomyces* species are considered to encode the largest biosynthetic diversity across bacterial genera, and actinobacteria at large show remarkable diversity in their secondary metabolism [81]. Yet these findings are presumably biased by the extensive knowledge we already have about actinobacteria. Less-well-studied bacterial phyla, such as myxobacteria [82,83] or planctomycetes [84,85], to name only a few, also have elaborate BGC arsenals which represent promising sources for the discovery of novel antiviral molecules.

#### Ecological relevance

The ecological significance of antiphage molecules was mostly ignored in the first wave of research focusing on antiphage molecules and has only been recently appreciated. When considering the ecological relevance of antiphage molecules, one key question is: is the antiphage molecule secreted? If yes, are the concentrations reached high enough to block phage amplification? With the evidence currently available, we can answer in the affirmative to these two questions regarding both anthracyclines and aminoglycosides. Indeed, anthracyclines and aminoglycosides are typically exported from producer cells by ABC-type transporters [66,86], and culture supernatants of producers were shown to inhibit phage replication [33,47].

Contrary to most protein-based defense systems, antiphage molecules described so far display rather broad inhibitory abilities. Anthracyclines and aminoglycosides inhibit seemingly very disparate phages infecting diverse bacteria, Gram-positive and -negative alike. So far, the rules behind the sensitivity of a given phage to these two classes of compounds remain unclear, the only common feature of the inhibited phages being their dsDNA genome and tailed morphology. This broad range of inhibition has important ecological implications: depending on their local concentrations and diffusion, these antiphage compounds could serve as 'public goods' and protect not only producer cells but also neighboring, unrelated cells – provided they are resistant to these compounds (Figure 3). The fact that nonrelatives could benefit from antiphage molecules is debatable under the light of sociomicrobiology. We can imagine that spatial structure and biofilms play a key role in restricting the access to these molecules primarily to genetic kin. Alternatively, the substantial metabolic costs associated with the production of complex compounds like aminoglycosides and anthracyclines, combined with the genomic instability in *Streptomyces*



Trends in Microbiology

**Figure 3. Ecological significance of the dual properties of aminoglycosides in a bacterial community.** Aminoglycoside producers release aminoglycosides (purple) in their environment. Aminoglycosides kill sensitive bacteria (antibacterial effect, A) while they may protect neighboring bacteria from phage infection (antiviral effect, B), provided they are resistant to these molecules, for example, via prior horizontal gene transfer (HGT) of resistance genes from producer cells (C). Bystander microorganisms not affected by aminoglycosides are shown in gray.

[87], may lead to a partial or complete loss of the corresponding BGCs in certain subpopulations, following a division of labor strategy. This loss of BGCs following genetic instability could be offset by the gene flow from related bacteria. For instance, actinobacteria like *Salinispora* maintain a pool of BGCs at the population level which are shuffled between strains through HGT, following a 'plug-and-play' strategy [88].

The dual function of certain antiphage molecules adds another layer of complexity. For instance, aminoglycosides represent a remarkable example of molecular multitasking, with the same molecules exerting two seemingly unrelated effects – inhibition of bacterial translation and of phage replication.

Furthermore, acquisition of resistance to aminoglycosides by initially sensitive cells is highly beneficial for two reasons: not suffering from their antibacterial effect anymore while benefiting from the inhibition of phage infection. Naturally, the mode of resistance to these antibiotics is of particular importance. Considering that aminoglycosides are thought to act intracellularly to block phage infection, resistance mechanisms based on decreased aminoglycoside intracellular concentration – such as decreasing uptake or expressing efflux pumps – would confer resistance to the antibiotic at the expense of the loss of its protective antiphage effect. Conversely, resistance to aminoglycosides mediated by aminoglycoside-modifying enzymes has the potential to inactivate aminoglycosides' antibacterial activity without reducing intracellular concentrations. With the aminoglycoside apramycin, it was shown that acetylation of one of its amino groups suppresses its antibacterial



effect while retaining its antiphage properties [47]. Whether this example is a unique case or is a general feature of aminoglycoside modifications remains to be determined. However, this observation could potentially be one factor contributing to the wide distribution of aminoglycoside-modifying enzymes catalyzing, for example, the acetylation, phosphorylation, or adenylation of amino or hydroxyl groups at various positions of the aminoglycoside scaffold [89].

While secreted antiphage metabolites raise important ecological questions, keeping antiphage compounds strictly intracellularly also provides the producer with special advantages. From a metabolic point of view, this obviously suppresses the costs associated with exporting the molecules and the problematics of re-entry in neighboring cells. Privatizing the antiviral molecules also prevents nonrelated bacteria occupying the same niche from benefiting from this resource. Moreover, the modified ribonucleotides produced by pVips necessitate a single enzyme, which greatly facilitates the spread of this antiviral strategy by HGT as reflected by the scattered phylogenetic distribution of pVips across the main bacterial clades [14]. Lastly, the substrates of viperins (ribonucleotides) are so pervasive across life-forms that this antiviral mechanism is applicable against a wide range of viruses, prokaryotic and eukaryotic alike [14]. We anticipate that bacteria have evolved further defense mechanisms acting as molecular ‘grains of sand’ jamming key steps of the viral machinery such as replication or translation.

To fully appreciate the ecological significance of **chemical defense** against phages, moving away from the traditional ‘one phage – one bacterium’ approach represents a key step. Building simplified, synthetic communities by increasing phage and/or bacterial diversity can provide decisive insights into the physiology of antiphage defense strategies, as shown, for example, with the importance of CRISPR-mediated phage resistance over modifications of the phage receptor in complex microbial communities [90]. Yet, additional mechanistic insights are required to understand the impact of antiphage molecules on community interactions.

Finally, one further direction worthy of investigation is the study of the interplay between the different defense systems – small molecule- and protein-based. Producers of antiphage molecules also encode other defense systems, and certain secondary metabolites could serve as a trigger for other defense strategies. For instance, it was recently shown that the transcription-inhibiting antibiotic rifampicin activates nucleotide-depletion defense, even in the absence of phages [91]. Our current knowledge about how prokaryotes coordinate these diverse antiphage strategies to mount efficient antiviral responses is still in its infancy and needs to be advanced to provide an integrated view of the prokaryotic immune system.

### Concluding remarks

Phage defense systems are often considered at the level of the individual cell, where it is mechanistically described how they protect a bacterium from being infected by an incoming phage. By acting at the single-cell level, antiphage strategies prevent the spread of the infection and thereby protect the broader bacterial community. However, some mechanisms specifically protect several cells or the entire population simultaneously. One of these consists in the release of small molecules into the extracellular environment. The antiphage metabolites described until now predominantly correspond to anthracyclines and aminoglycosides, both inhibiting the early steps of the phage infection cycle. Interestingly, aminoglycosides are well-known antibacterial agents, but were also shown to be potent inhibitors of phage infection, suggesting that evolutionary constraints allowed the development of two seemingly very distinct functions.

From a therapeutic standpoint, antiviral metabolites in bacteria have the potential to fuel the discovery pipeline for novel antiviral drugs in humans. For example, synthetic nucleoside chain

### Outstanding questions

What is the molecular mechanism of action underlying the antiviral activity of anthracyclines and aminoglycosides?

How did the dual antibacterial and antiviral functions of aminoglycosides shape the evolution of these molecules?

To what extent do secreted antiphage molecules confer protection at the community level?

Can genomic signatures be determined for antiphage biosynthetic gene clusters?

Is chemical defense against phages a conserved defense strategy across bacteria?

Are there strategies involved in the conditional privatization of secreted antiviral molecules?

How does the production of antiphage molecules interact with other antiviral defenses in prokaryotic immune systems?

terminators are widely used in conditions such as HIV [92,93] or infection with herpes viruses [94], and chain terminators produced by pVips could represent new avenues for treatments of viral infections in humans [14]. Knowledge gained about small molecule-mediated inhibition of phage infection is also relevant for phage therapy, for example, to avoid antagonistic effects when administering phage–antibiotic combination treatments.

The repertoire of bacterial secondary metabolites is extremely large, and the physiological function of many of these compounds remains unclear. We can thus hypothesize that the number of described antiphage molecules will keep growing in the future (see [Outstanding questions](#)). For example, molecules triggering death of parts of the bacterial population represent promising candidates as their release in reaction to phage predation would mimic the effect of protein-mediated Abi systems.

Phages have developed ways to circumvent most bacterial defense strategies, as part of the arms race in which they are engaged with their bacterial hosts. It is therefore plausible that phages have evolved means to overcome this metabolite-based defense system. Elucidating these adaptations could illuminate phage biology by attributing a function to certain already known phage features and further our understanding of the intricate relationships between phages and their bacterial hosts in the context of chemical defense.

#### Acknowledgments

Research in the Frunzke laboratory is supported by the European Research Council (ERC Starting Grant 757563) and the Deutsche Forschungsgemeinschaft (SPP 2330, project 464434020). We thank Aude Bernheim for critical reading of the manuscript. Figures were created using [BioRender.com](#).

#### Declaration of interests

No interests are declared.

#### References

- Crickle, M.R. *et al.* (2011) Phages in nature. *Bacteriophage* 1, 31–45.
- Rostol, J.T. and Maraffini, L. (2019) (P)highting phages: how bacteria resist their parasites. *Cell Host Microbe* 25, 184–194.
- Sten, A. and Sorek, R. (2011) The phage-host arms race: shaping the evolution of microbes. *BioEssays* 33, 43–51.
- Hampton, H.G. *et al.* (2020) The arms race between bacteria and their phage foes. *Nature* 577, 327–336.
- Dy, R.L. *et al.* (2014) Remarkable mechanisms in microbes to resist phage infections. *Annu. Rev. Virol.* 1, 307–331.
- Doron, S. *et al.* (2018) Systematic discovery of antiphage defense systems in the microbial pangenome. *Science* 359, eaar4120.
- Gao, L. *et al.* (2020) Diverse enzymatic activities mediate antiviral immunity in prokaryotes. *Science* 369, 1077–1084.
- Cohen, D. *et al.* (2019) Cyclic GMP–AMP signaling protects bacteria against viral infection. *Nature* 574, 691–695.
- Tal, N. *et al.* (2021) Cyclic CMP and cyclic UMP mediate bacterial immunity against phages. *Cell* 184, 5728–5739.e16.
- Off, G. *et al.* (2021) Antiviral activity of bacterial TIR domains via immune signalling molecules. *Nature* 600, 116–120.
- Gierb, J. *et al.* (2021) Multiple phage resistance systems inhibit infection via SFR2-dependent NAD<sup>+</sup> depletion. *bioRxiv* Published online December 14, 2021. <https://doi.org/10.1101/2021.12.14.472415>.
- Zarembka, M. *et al.* (2021) Sir2-domain associated short prokaryotic Argonautes provide defence against invading mobile genetic elements through NAD<sup>+</sup> depletion. *bioRxiv* Published online December 14, 2021. <https://doi.org/10.1101/2021.12.14.472599>.
- Tal, N. and Sorek, R. (2022) SnapShot: bacterial immunity. *Cell* 185, 578–578.e1.
- Bernheim, A. *et al.* (2021) Prokaryotic vipsins produce diverse antiviral molecules. *Nature* 589, 120–124.
- Monhouse, B.F. *et al.* (2020) STING cyclic dinucleotide sensing originated in bacteria. *Nature* 586, 429–433.
- Wein, T. and Sorek, R. (2022) Bacterial origins of human cell-autonomous innate immune mechanisms. *Nat. Rev. Immunol.* Published online April 8, 2022. <https://doi.org/10.1038/s41577-022-x0705-4>.
- Payne, L.J. *et al.* (2021) Identification and classification of antiviral defence systems in bacteria and archaea with PADLOC reveals new system types. *Nucleic Acids Res.* 49, 10668–10678.
- Tesson, F. *et al.* (2022) Systematic and quantitative view of the antiviral arsenal of prokaryotes. *Nat. Commun.* 13, 2561.
- Bernheim, A. and Sorek, R. (2020) The pan-immune system of bacteria: antiviral defence as a community resource. *Nat. Rev. Microbiol.* 18, 115–119.
- Stubbendieck, R.M. *et al.* (2016) Bacterial communities: interactions to scold. *Front. Microbiol.* 7, 1234.
- Manning, A.J. and Kuehn, M.J. (2011) Contribution of bacterial outer membrane vesicles to innate bacterial defense. *BMC Microbiol.* 11, 258.
- Reyes-Robles, T. *et al.* (2018) *Vibrio cholerae* outer membrane vesicles inhibit bacteriophage infection. *J. Bacteriol.* 200, e00792–17.
- Vidakovic, L. *et al.* (2018) Dynamic biofilm architecture confers individual and collective mechanisms of viral protection. *Nat. Microbiol.* 3, 26–31.
- Simmons, M. *et al.* (2018) Phage mobility is a core determinant of phage–bacteria coexistence in biofilms. *ISME J.* 12, 531–543.
- Hayland-Kroghsbo, N.M. *et al.* (2013) A quantum-sensing-induced bacteriophage defense mechanism. *mBio* 4, e00362–00312.

26. Slipe, J.E. and Bassler, B.L. (2019) A host-produced quorum-sensing autoinducer controls a phage lysis-lysogeny decision. *Cell* 176, 268–280.e13
27. León-Félix, J. and Vilcaña, C. (2021) The impact of quorum sensing on the modulation of phage-host interactions. *J. Bacteriol.* 203, 60087–20
28. Schatz, A. and Jones, D. (1947) The production of antiphage agents by actinomycetes. *Bull. Torrey Bot. Club* 74, 9
29. Asheshov, I.N. et al. (1954) A survey of actinomycetes for antiphage activity. *Antibiot. Chemother.* 4, 380–394
30. Bydzovský, V. and Šimek, A. (1960) Antiphage activity of some actinomycetes. *Folia Microbiol.* 5, 46–49
31. Kumar, V. et al. (1977) The structure of akavins. *J. Antibiot.* 30, 861–882
32. Portman, D. et al. (1951) Observations on the chemical inhibition of *Streptomyces griseus* bacteriophage multiplication. *J. Bacteriol.* 61, 135–143
33. Kronheim, S. et al. (2018) A chemical defence against phage infection. *Nature* 564, 283
34. Nakata, A. et al. (1991) Inhibition of multiplication of bacteriophage by actinomycin. *Nature* 186, 246–247
35. Korn, D. et al. (1983) A novel effect of actinomycin D in preventing bacteriophage T4 maturation in *Escherichia coli*. *Biochem. Biophys. Res. Commun.* 19, 473–481
36. Morita, J. et al. (1979) Inactivation of phage  $\phi$ X174 by anthracycline antibiotics, actinomycin A, doxorubicin and daunorubicin. *Agric. Biol. Chem.* 43, 2629–2631
37. Tanaka, A. et al. (1983) Phage inactivation by actinomycin A and its analogues. *J. Antibiot.* 36, 1242–1244
38. Streitz, F. et al. (1956) Akavins, an antibiotic substance with antiphage activity. *J. Bacteriol.* 72, 90–94
39. Paris, B. and Solier, A. (1964) Studies on antiphage activity of daunomycin. *G. Microbiol.* 12, 183–194
40. Pitkin, W.B. and Reiter, H. (1969) Abortive infection of *Bacillus subtilis* bacteriophage PB51 in the presence of actinomycin D. *J. Virol.* 3, 578–585
41. Brock, T.D. (1962) The inhibition of an RNA bacteriophage by streptomycin, using host bacteria resistant to the antibiotic. *Biochem. Biophys. Res. Commun.* 9, 184–187
42. Brock, T.D. and Woolly, S.C. (1963) Streptomycin as an antiviral agent: mode of action. *Science* 141, 1066–1067
43. Brock, T.D. et al. (1963) The inhibition by streptomycin of certain *Streptococcus* bacteriophages, using host bacteria resistant to the antibiotic. *J. Gen. Microbiol.* 33, 9–22
44. Schindler, J. (1964) Inhibition of reproduction of the f2 bacteriophage by streptomycin. *Folia Microbiol.* 9, 269–276
45. Jones, W.D. and Greenberg, J. (1978) Resistance relationships in *Mycobacterium smegmatis* ATCC 607 to phages sensitive or resistant to both diuronolom and streptomycin sulphate. *J. Gen. Virol.* 39, 555–557
46. Jiang, Z. et al. (2020) Aminoglycoside antibiotics inhibit mycobacteriophage infection. *Antibiotics* 9, 714
47. Kever, J. et al. Aminoglycoside antibiotics inhibit phage infection by blocking an early step of the infection cycle. *mBio*, 13, e0078322
48. Zuo, P. et al. (2021) Aminoglycosides antagonize bacteriophage proliferation, attenuating phage suppression of bacterial growth, biofilm formation, and antibiotic resistance. *Appl. Environ. Microbiol.* 87, e0046821
49. Joy, Henson, K. et al. (1959) The effect of neomycin on phage-typing of staphylococci. *Lancet* 273, 908–910
50. Higo, N. (1958) Studies on antiviral antibiotics produced by *Streptomyces* XI. Effect of phagostin on the multiplication of bacteriophage T3. *Jap. J. Microbiol.* 2, 203–215
51. Koenuma, M. et al. (1974) An improved screening method for antiphage antibiotics and isolation of sarkomycin and its relatives. *J. Antibiot.* 27, 801–804
52. Streitz, F. et al. (1955) Chrysomycin: a new antibiotic substance for bacterial viruses. *J. Bacteriol.* 69, 280–283
53. Higo, N. (1956) Studies on antiviral antibiotics from *Streptomyces*. II. Phagodin, a new antiviral antibiotic. *J. Antibiot. (Tokyo)* 9, 152–156
54. Higo, N. and Hinuma, Y. (1956) Studies on antiviral antibiotics from *Streptomyces*. III. Mode of action of phagodin on bacterial virus. *J. Antibiot. (Tokyo)* 9, 157–163
55. Arima, K. et al. (1972) Studies on tomaymycin, a new antibiotic. I. Isolation and properties of tomaymycin. *J. Antibiot.* 25, 437–444
56. Streitz, F. et al. (1955) Nybomycin, a new antibiotic with antiphage and antibacterial properties. *Proc. Natl. Acad. Sci. U. S. A.* 41, 620–624
57. Hail, E.A. and Asheshov, I.N. (1953) A study of the action of phageostin A58 on the T phages. *J. Gen. Physiol.* 37, 217–230
58. Laatsch, H. and Fdso, S. (2008) Naturally occurring anthracyclines. In *Anthracycline Chemistry and Biology* (Frohn, K., ed.), pp. 4–74. Springer
59. Fujiwara, A. et al. (1985) Anthracycline antibiotics. *Crit. Rev. Biotechnol.* 3, 133–157
60. Minetti, G. et al. (2008) Anthracyclines: molecular advances and pharmacologic developments in antitumor activity and cardiotoxicity. *Pharmacol. Rev.* 56, 185–229
61. Weiss, R.B. (1992) The anthracyclines: will we ever find a better doxorubicin? *Semin. Oncol.* 19, 670–686
62. Peng, X. et al. (2005) The cardiotoxicology of anthracycline chemotherapeutics: translating molecular mechanism into preventative medicine. *Mol. Interv.* 5, 163–171
63. Cavalitto, C. et al. (2008) Doxorubicin: the good, the bad and the ugly effect. *Curr. Med. Chem.* 15, 3267–3285
64. Tenconi, E. and Rigali, S. (2018) Self-resistance mechanisms to DNA-damaging antitumor antibiotics in actinobacteria. *Curr. Opin. Microbiol.* 45, 100–108
65. Priya, F. and Prasad, R. (2017) DnC protein of *Streptomyces peuceletii* removes daunorubicin from intercalated *chrI* promoter. *Microbiol. Res.* 202, 30–35
66. Li, W. et al. (2014) The DmAB efflux system of *Streptomyces peuceletii* is a multidrug transporter of broad substrate specificity. *J. Biol. Chem.* 289, 12633–12646
67. Thaker, M.N. et al. (2013) Identifying producers of antibacterial compounds by screening for antibiotic resistance. *Nat. Biotechnol.* 31, 922–927
68. Mingot-Leciercq, M.-P. et al. (1999) Aminoglycosides: activity and resistance. *Antimicrob. Agents Chemother.* 43, 771–787
69. Krause, K.M. et al. (2016) Aminoglycosides: an overview. *Cold Spring Harb. Perspect. Med.* 6, a027029
70. Busscher, G.F. et al. (2006) 2-Deoxystreptamine: central scaffold of aminoglycoside antibiotics. *Chem. Rev.* 106, 775–792
71. Houghton, J.L. et al. (2010) The future of aminoglycosides: the end or renaissance? *ChemBioChem* 11, 880–902
72. Sano, A.W. et al. (2018) Aminoglycoside revisited: review of a historically important class of antimicrobials undergoing rejuvenation. *EcoSal Plus* 8, 1–20
73. Tamura, T. et al. (2008) Classification of 'Streptomyces tenebrarius' Higgins and Kastner as *Streptolobos tenebrarius* nom. rev., comb. nov., and amended description of the genus *Streptolobos*. *Int. J. Syst. Evol. Microbiol.* 58, 688–691
74. Kopaczynska, M. et al. (2004) Aminoglycoside antibiotics aggregate to form starch-like fibers on negatively charged surfaces and on phage  $\lambda$ -DNA. *Langmuir* 20, 9270–9275
75. Kopaczynska, M. et al. (2016) Selective condensation of DNA by aminoglycoside antibiotics. *Eur. Biophys. J.* 45, 287–299
76. Rivera-Semano, E.E. et al. (2020) Vipin reveals its true function. *Annu. Rev. Virol.* 7, 421–448
77. Gizi, A.S. et al. (2018) A naturally occurring antiviral ribonucleotide encoded by the human genome. *Nature* 558, 610–614
78. Comeau, A.M. et al. (2007) Phage-antibiotic synergy (PAS):  $\beta$ -lactam and quinolone antibiotics stimulate virulent phage growth. *PLoS One* 2, e799
79. Stachurska, X. et al. (2021) Double-layer agar (DLA) modifications for the first step of the phage-antibiotic synergy (PAS) identification. *Antibiotics* 10, 1306
80. Hardy, A. et al. (2020) Genome sequence and characterization of five bacteriophages infecting *Streptomyces coelicolor* and *Streptomyces venezuelae*: Alderaan, Corsucant, Dagobah, Endori and Endor2. *Virus* 12, 1065
81. Gavrilidou, A. et al. (2022) Compendium of specialized metabolite biosynthetic diversity encoded in bacterial genomes. *Nat. Microbiol.* 7, 726–735

82. Amin Moghaddam, J. *et al.* (2018) Analysis of the genome and metabolome of marine myxobacteria reveals high potential for biosynthesis of novel specialized metabolites. *Sci. Rep.* 8, 16600
83. Gregory, K. *et al.* (2019) Survey of biosynthetic gene clusters from sequenced myxobacteria reveals unexplored biosynthetic potential. *Microorganisms* 7, 161
84. Kalscheuer, N. and Jogler, C. (2021) The bacterial phylum Planctomycetes as novel source for bioactive small molecules. *Biotechnol. Adv.* 53, 107818
85. Wiegand, S. *et al.* (2020) Cultivation and functional characterization of 79 planctomycetes uncovers their unique biology. *Nat. Microbiol.* 5, 126–140
86. Kudo, F. and Eguchi, T. (2009) Biosynthetic genes for aminoglycoside antibiotics. *J. Antibiot.* 62, 471–481
87. Zhang, Z. *et al.* (2020) Antibiotic production in *Streptomyces* is organized by a division of labor through terminal genomic differentiation. *Sci. Adv.* 6, essay5781
88. Ziemert, N. *et al.* (2014) Diversity and evolution of secondary metabolism in the marine actinomycete genus *Salinispora*. *Proc. Natl. Acad. Sci. U. S. A.* 111, E1130–E1139
89. Ramirez, M.S. and Tolmasky, M.E. (2010) Aminoglycoside modifying enzymes. *Drug Resist. Updates* 13, 151–171
90. Assef, E.D. *et al.* (2019) Bacterial biodiversity drives the evolution of CRISPR-based phage resistance. *Nature* 574, 549–552
91. Tai, N. *et al.* (2022) Bacteria deplete deoxynucleotides to defend against bacteriophage infection. *Nat. Microbiol.* 7, 1200–1209
92. Donno, B. (2019) Key principles of antiretroviral pharmacology. *Infect. Dis. Clinics North Am.* 33, 787–805
93. Simon, V. *et al.* (2006) HIV/AIDS epidemiology, pathogenesis, prevention, and treatment. *Lancet* 368, 489–504
94. Shiraki, K. (2018) Antiviral drugs against alphaherpesvirus. *Adv. Exp. Med. Biol.* 1045, 103–122

## 4. Appendix

### 4.1. Appendix to 3.1. Identification of Gip as a novel phage-encoded gyrase inhibitor protein of *Corynebacterium glutamicum*

Supplemental information to:

#### **Identification of Gip as a novel phage-encoded gyrase inhibitor protein of *Corynebacterium glutamicum***

Running title: CGP3-encoded Gip inhibits C.g. DNA gyrase

Larissa Kever<sup>1</sup>, Max Hünnefeld<sup>1</sup>, Jannis Brehm<sup>2</sup>, Ralf Heermann<sup>2</sup> and Julia Frunzke<sup>1\*</sup>

<sup>1</sup>Institute of Bio- und Geosciences, IBG-1: Biotechnology, Forschungszentrum Jülich, 52425 Jülich, Germany

<sup>2</sup>Institut für Molekulare Physiologie, Biozentrum II, Mikrobiologie und Weinforschung, Johannes-Gutenberg-Universität Mainz, 55128 Mainz, Germany

\*Corresponding authors:

Julia Frunzke; Email: [j.frunzke@fz-juelich.de](mailto:j.frunzke@fz-juelich.de); Phone: +49 2461 615430

## Content

**Figure S1:** Screening of small phagic proteins regarding their impact on cellular growth and CGP3 induction in *C. glutamicum*.

**Figure S2:** Cell growth and prophage inducibility in the  $\Delta cg1914$  or  $\Delta cg1978$  mutant strain.

**Figure S3:** Purification of proteins for surface plasmon resonance spectroscopy of protein-protein interaction.

**Figure S4:** Sequence alignment of the DNA gyrase subunit A from *C. glutamicum*, *M. tuberculosis* and *E. coli*.

**Figure S5:** Sequence alignment of the DNA gyrase subunit B from *C. glutamicum*, *M. tuberculosis* and *E. coli*.

**Figure S6:** Gyrase activity and supercoiling assays.

**Table S1:** Bacterial strains used in this study.

**Table S2:** Plasmids used in this study.

**Table S3:** Oligonucleotides used in this study.

**Table S4:** Impact of *gip* (*cg1978*) overexpression on global expression levels.

**Video S1:** Time-lapse video of a *C. glutamicum* microcolony of the prophage reporter strain under *cg1978* overexpression (50  $\mu$ M IPTG).

**Video S2:** Time-lapse video of a *C. glutamicum* microcolony of the prophage reporter strain under standard conditions (0  $\mu$ M IPTG).

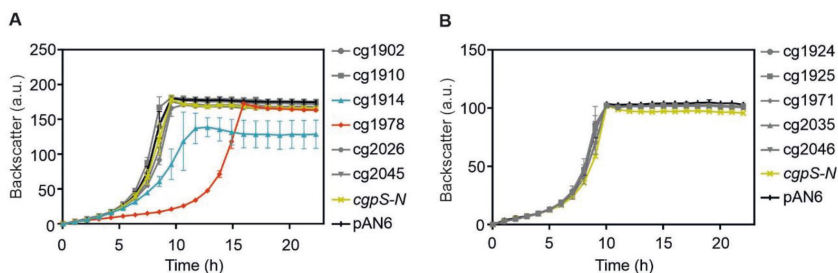


**Figure S1: Screening of small phagic proteins regarding their impact on cellular growth and CGP3 induction in *C. glutamicum*.** The cultivation of *C. glutamicum* ATCC 13032::P<sub>lys</sub><sup>-</sup> *eyfp* strains carrying the corresponding gene sequences of the small proteins on the pAN6 vector (under control of P<sub>tac</sub>) was performed in CGXII minimal medium with 2 % (w/v) glucose and 50 μM IPTG for 24 h. **(A,B)** Growth curves upon small protein overproduction are based on the backscatter measurements in the BioLector® microcultivation system. All data represent mean values with standard deviations from three independent biological replicates (n=3). As the backscatter values were measured with two different BioLector® devices, data are represented in two separated graphs.

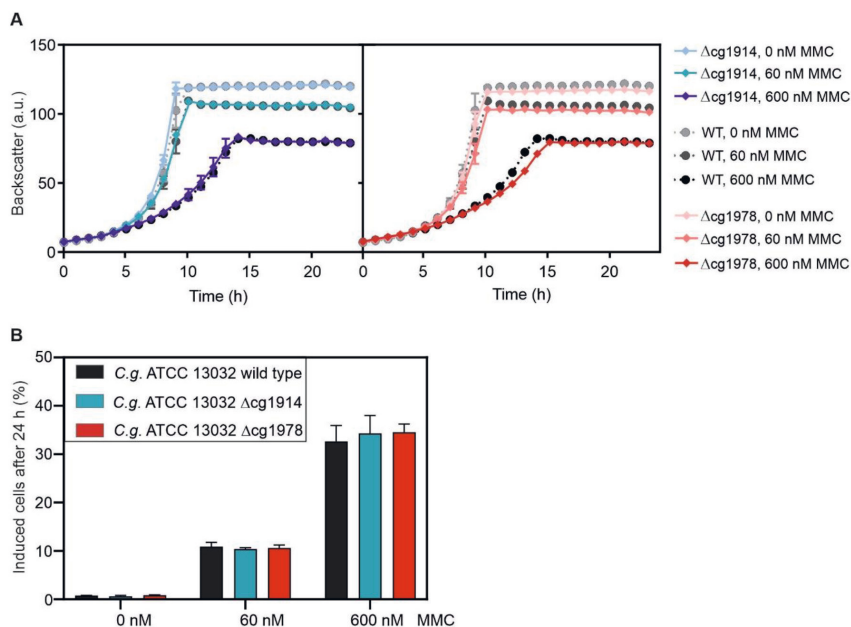


**Figure S2: Cell growth and prophage inducibility in the  $\Delta cg1914$  or  $\Delta cg1978$  mutant strain.** Cultivation of the *C. glutamicum* ATCC 13032  $\Delta cg1914$  strain, the *C. glutamicum* ATCC 13032  $\Delta cg1978$  strain and the *C. glutamicum* ATCC 13032 wild type strain carrying the plasmid-based prophage reporter pJC1- $P_{lys^-lys'}$ -*venus* was performed in the BioLector® microcultivation system in CGXII minimal medium with 2 % (w/v) glucose. All data represent mean values with standard deviations from three independent biological replicates (n=3). **(A)** Growth curves based on the backscatter measurements in the BioLector® microcultivation system. **(B)** Percentage of induced cells after 24 h cultivation based on the flow cytometric measurements of the plasmid-based prophage reporter.



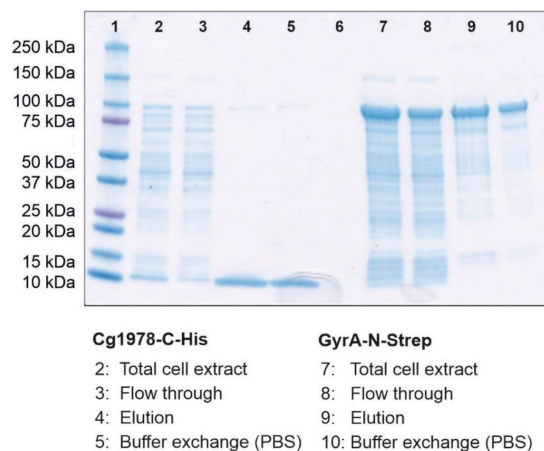


**Figure S3: Purification of proteins for surface plasmon resonance analysis of protein-protein interaction.** Cg1978 containing a C-terminal His-tag and GyrA containing a N-terminal Strep-tag were overproduced in *E. coli* BL21 (DE3) and purified via affinity purification. The gel electrophoresis was performed with 4-20 % gradient gels at 120 V for 60 min using the Precision Plus Protein™ Dual protein marker as a standard.

Sequence alignment GyrA (E: *E. coli*, C: *C. glutamicum*, M: *M. tuberculosis*)

```

E.      1  -----MSDLAREITPVNIEELKSSYDYAMSVIVGRALPEVRDGLKPVHRRVLYAMN
C.      1  ---MSDDNTGQFDRNPIDINEEMQSSYIDYAMSVIVGRALPEVRDGLKPVHRRVLYAMF
M.      1  MTDITLPPDPSLDRIEFPVDIEQEMQSSYIDYAMSVIVGRALPEVRDGLKPVHRRVLYAMF

E.      54  VLGNOWNKMKKSARVVDVIGKYHPHGDSAYDTIVRMAQPFSLRYMLVDGGQGNFGSID
C.      58  DNGVRPDRSYVKSAPVADTMGNFHPHGDIAIYDTLVRMAQPWSLRYPLVDGGQGNFGSRG
M.      61  DSCVRPDRSHAKSARSVAETMGNYHPHGDAIYDSLVRMAQFWSLRYPLVDGGQGNFGSPG

E.      114  GDSAAAMRYTEIRLAKIAHELMADLEKETVDFVDNYDCTEKTIDVNFPTKIPNLLVNGSSG
C.      118  NDGPAAMRYTECRITPLAMEMVRDIRENTVNFSPNYDGKTLPEVDLPSRVPNLLVNGSGG
M.      121  NDEPAAMRYTEARLTPLAMEMIRLIEETVDFIPNYDGRVQETPLPSRVPNLLVNGSGG

E.      174  IAVGMATNIPPHNLTEVINGCLAYID---EISIEGLMPEHIPGPDFPTAATINGREGI
C.      178  IAVGMATNIPPHNLDELADAFWLLNPDAFESDALEACMKFVKGPDFPTAGLIIGDNGI
M.      181  IAVGMATNIPPHNLRELADAFWALENHDAFEEETLAAMGVKVGPDFPTAGLIVGSQGT

E.      230  EDAYRTGRGKYIRRAEVEVDAKTGRETIIVHEIPYQVNARLIEKIABLVKEKRVEGI
C.      238  HDAYTTGRGSIRMRGVTSIEEFG--NRTVIVITELPYQVNPDLISNIAEQVRDGKLVGI
M.      241  ADAYKTGRGSIRMRGVVEEDS--RGRTSIVITELPYQVNHDFIISIAEQVRDGKLAGI

E.      290  SAIRDESDKDMRIVIEVKRDAVGQVVLNNLYSQTLQVSEGINMVAHHGQPKIINLK
C.      296  SKIEDESSDRVGMRIVVTIKRDAVAVVLNNLKHSQLQANFGANMISTVDGVPRTLRLD
M.      300  SNIEDOSSDRVGLRIVIEIKRDAVAVVLNNLYKHTQLQTSFGANMLAIVDGVPTLRLD

E.      349  DIIAAVVRHREVTIRRTIEELRKARIRAHILEALVALANIDPIELIRHAPTPAEAKT
C.      356  QMIRYYVAHQEIVVRRTOYRLDKAPERAHILRGLVKALDMLDEVIALIRASPTPEART
M.      360  QIRYYVDHQLDVIVRRTTYRLKANERAHILRGLVKALDALDEVIALIRASPTVDIARA

E.      409  ALIANPQQLGNVAAMLERAGDDAARPEWLEPEFGVRDGLYYITEQQAQAILDRLOKITG
C.      416  GLIS-----LLDVDEAQADAILAMQLRLAA
M.      420  GLIE-----LLDVDEIQQAAILDMQLRLAA

E.      469  LEHEKLIDEYKEILLDQIAELLRLILGSADRLMEVIREIEELVREQGDKRRTEITANSADI
C.      442  LERQKIIDEIAEIEIADLKAILASPERQRTIVRDEITEIVEKYGDERRSQIIAAAGDV
M.      446  LERQRIIDDLAKIEAEIADLEDILARPERQRGIVRDEIAEIVDRHGDRRTRIIAAGDV

E.      529  NLEDLITQEDVVVTLSHQGYVKYQPISEYEACRRGGKCKSARIKEDFTDRLIVANTHD
C.      502  SEEDLIARENVVITITSTGYAKRTKIDAYISQKRGKGKVGRAELKQDDIVRHFVCSSTD
M.      506  SEDLIARENVVITITSTGYAKRTKIDLYISQKRGKGKVGQAGLQKDDIVAHFVCSSTD

E.      589  HII CFSSRGRVYSMKVYOLPEATRGARGPIVNLPLEQDERITAILPTEEBEGVKVFM
C.      562  WILFFTNVYGRVYRLKAFELPEASRTARGQHVANLLEFQPGQIAQVIQIESYNLFPPYLV
M.      566  LILFFTNVGRVYRAKAYLPEASRTARGQHVANLLAFQPFERIAQVIQIRGYIDAPYLV

E.      649  ATANGTVKKIVLTENRRLRTACKVAIKLVGDELIGVDLTSDEDEVMLFSAEKKVVRKE
C.      622  ATAHGRVKKSLLDVESARSGGLIATNLNEDDLIGALCGEDDLLLVSEFGQSIRFTA
M.      626  ATNGLVKKSKLTDFFSNRSGGIVANLNRNDELNGAVLCSAGDDLLLVANGQSIRFSA

```

```

E.      709  --SSVRAMGCNTIGVVGIRLGEGDKVVSLLVPRGDGAILTATQNGYGKRTAAEYPTKSR
C.      682  DDEQLRPMGRATAGVKGMRFRINDQLLSVSVVRDGEFLLVATSGGYGKRTPLEIYSTQGR
M.      686  TDEALRPMGRATSGVQGMRFNIDDFLLSLNVVRGTYLLVATSGGYAKRTALEEYFVQGR

E.      767  ATKGVISIKVTERNGLVGAVOVDDCDQIMMITDAGTVRTRVSEISIVGRNTQGVILIR
C.      742  GGLGVITFKYTPKRGRIVSAIAVEEDDEIFAITSAGGVVRTEVVKQIRPSSRAIMGVRLVN
M.      746  GGKGVITVMYDRRRGRIVGALIVDDSELYAVTSGGGVIRTAARQVRKAGROTKGVRLMN

E.      827  TLEDENVVGIQFVAEPVDEEDLDTDCSAAEGDDEIAPEV--D-VLDEPEE---E
C.      802  LEEGVELLAIIDRNVEDQGEASAPAAKGAVEGPAASKTAAEETDSVDNGSDENGEE
M.      806  LEEGETLLAIARNAEESGDDNAVDANGADQTCN-----

```

**Figure S4: Sequence alignment of the DNA gyrase subunit A from *C. glutamicum* (C), *M. tuberculosis* (M) and *E. coli* (E).** The multiple sequence alignment was conducted by using the Clustal Omega platform (Sievers et al., 2011). The output file was further transformed using Boxshade ([https://embnet.vital-it.ch/software/BOX\\_form.html](https://embnet.vital-it.ch/software/BOX_form.html)). The sequence similarity of the DNA gyrase subunit A between *C. glutamicum* (UniProtKB - Q8NUC6) and *M. tuberculosis* (UniProtKB - P9WG47) is 71.34 %, the one between *C. glutamicum* and *E. coli* (UniProtKB - P0AES4) is 45.17 %.

Sequence alignment GyrB (E: *E. coli*, C: *C. glutamicum*, M: *M. tuberculosis*)

```

E.      1  -----MSNSYDSSSIKVLKGLAVRKRPGMYIGTDDGTGLHHMVFEVVDNAIDEALA
C.      1  ----MANTEHNYDASSITILEGLEAVRKRPGMYIGSTG-PRGLHHLIWEVVDN|SVDEAMA
M.      1  MAAQKKKAQDEYGAASITILEGLEAVRKRPGMYIGSTG-ERGLHHLIWEVVDNAVDEAMA

E.     54  GHCKEIVTVTHADNSVSVQDDGRGIPTGTHPEEGVSAAEVIMTVLHAGGKFDDNSYKVS
C.     56  GHATKVEVTLLLEDGGVQVVDGRGIPVDMHPS-CAPTQVVMVMTQLHAGGKFDSDSYAVSG
M.     60  GYATTVNVVLLLEDGGVEVADDGRGIPVATHAS-GIPTVDVVMVMTQLHAGGKFDSLAYASG

E.    114  GLHGVGVSVVNALSOKLEIVIOREGKIHROIYEHGVFOPLAVTGETEKTGTMVRFWESL
C.    115  GLHGVGLSVVNALSTRVPAIDIKLHGKHVWYCNTEKSVPDE-LIEGGNARCTGTTIRFWPDA
M.    119  GLHGVGVSVVNALSTRLEVEIKRQGYEWSQYKSEPLG-LKQGFPTKKTGSTVRFWADP

E.    174  EITTNVTEFEYEILAKRLREISFLNSGVSIPLRLDKRD-----
C.    174  EITFE-TTEFDFETISRRLOEMAFLNKGLTITLTDNRATDEFELEAALQCEETATELSLD
M.    178  AVFE-TTEYDFETIARRLOEMAFLNKGLTINLTDERTVQDEIVDEVSVVEAPKSAS--

E.    211  -----GKEDHFHYEGGKAFVEYLNKNTPIHENIFYFSTEKD
C.    233  EIDNETELVEETTDAPKKPKKKEKKIIFHYPNGLEDVHYLNRSKTNIHPSIVSFEAKGD
M.    235  -----E-RAAESTAPHKVKSRTHYPPGGIVDFVKHINRIKNAIHSSIVDFSCKGT

E.    249  GIGVEVALQWNDGQENYCFINNTIPQGGTHLAGFRAMTRTINAYMDKEGYSRKAKV
C.    293  DHEVEVAMQWNSSYKESVHTFANTINTREGGTHEEGFRSALTSMLNRYAREHLLKKKEA
M.    284  GHEVEIAMQWNAGYSESVHTFANTINTHEGGTHEEGFRSALTSVNVKYAKDRLLKKKDP

E.    309  SATGDDAREGLIAVSVKVPDPKFSSTQTKKLVSSEVKSAMVEQQMELLAEYLLNPTDA
C.    353  NLTGDDCREGLISAVISVVGDPQFEGQTKKLGNTEIKSFVORMANEHTGHWLEANPAEA
M.    344  NLTGDDTREGLAAVISVKVSELPQFEGQTKKLGNTEVKS FVQKVQNEQITHWFEANPTDA

E.    369  KIVVGKILDAARAREAAAREVTRRGALDLGLPGKLADQERDPAISELYIVEGDSA
C.    413  KVLINKAVGSAQARLAARKARILVRRKSATDLGGLPGKLADCRSDPEKSELYIVEGDSA
M.    404  KVVVNKAVSSAQARLAARKARELVRRKSATDLGGLPGKLADCRSDPRKSELYIVEGDSA

E.    429  GGSAKQGRNRKNQAILPLRGKILNVEKAREDKMISSECVATITALGCGIGRDEYNPDKL
C.    473  GGSAKSGRDSMFQAILPLRGKILNVEKARDKVLKNAEVQAIITALGTGIH-DEFDINKL
M.    464  GGSAKSGRDSMFQAILPLRGKILNVEKARDKVLKNTEVQAIITALGTGIH-DEFDIGKL

E.    489  RYHSIIIMTDADVDGSHIRLLLLLFFYRQMPETVERGHVYLAQPPPLYKWKGRQEQYIKD
C.    532  RYHKIVLMADADVDGQHIATLLLLLTLFRFMEDLVAEGHVYLAQPPPLYKWKQRFEGFAY
M.    523  RYHKIVLMADADVDGQHISTLLLLLTLFRFMRLTENGHVLAQPPPLYKWKQRSDFEFAY

E.    549  DEAMDQYQISIALDGATLHTNASAPALAGEALEKLVSEYNATQKMINRMERRYPKAMLKE
C.    592  S-----
M.    583  S-----

E.    609  LIYQPTLTEADLSDEQTVTRWVNALVSELNDKEQHSQWKFDVHTNAEQNLFEPIVRVRT
C.    593  -----DE-----ERD-----
M.    584  -----DR-----ERD-----

```

E.	669	HGVDDTDYPLDHEFITGGEYRRICITLGEKLRGLLEEDAFIERGERQPVASFQALDWLVK
C.	598	-----EQLN-----EGLA-----AGR
M.	589	-----GLLE-----AGLK-----AGK
E.	729	ESRFGLSIQRYKGLGEMNPEQLWETTMDESRRLRVTKDAIAADQLFTILMGDAVTPR
C.	609	KINKDDGIQRYKGLGEMNASELWETTMDEPVRLLRRVDIADAQRADELFSLMGDDVVAR
M.	600	KINKEDGIQRYKGLGEMDAKELWETTMDEPVRVLRQVTDDAAADELFSILMGEDVTAR
E.	789	RFETEEENALKAAANDI
C.	669	RSFITRNAKDVRFLDI
M.	660	RSFITRNAKDVRFLDV

**Figure S5: Sequence alignment of the DNA gyrase subunit B from *C. glutamicum* (C), *M. tuberculosis* (M) and *E. coli* (E).** The multiple sequence alignment was conducted by using the Clustal Omega platform (Sievers et al., 2011). The output file was further transformed using Boxshade ([https://embnet.vital-it.ch/software/BOX\\_form.html](https://embnet.vital-it.ch/software/BOX_form.html)). The sequence similarity of the DNA gyrase subunit B between *C. glutamicum* (UniProtKB - A0A6L2RK64) and *M. tuberculosis* (UniProtKB - P9WG45) is 73.92 %, the one between *C. glutamicum* and *E. coli* (UniProtKB - P0AES6) is 53.77 %.

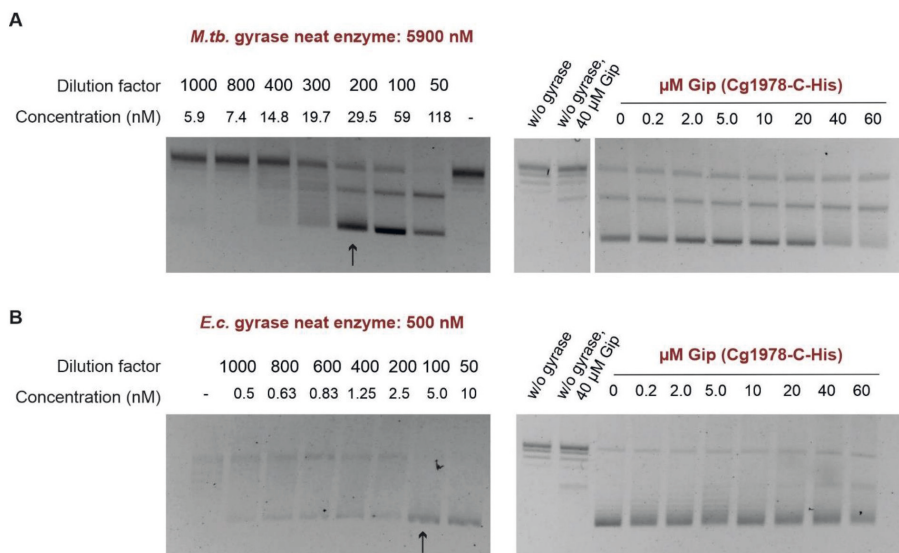


**Figure S6: Gyrase activity and supercoiling assays.** (A) Different gyrase concentrations of the *M. tuberculosis* (*M.tb.*) gyrase and (B) the *E. coli* (*E.c.*) gyrase were tested to determine the concentration required for maximal supercoiling of 0.5  $\mu$ g relaxed plasmid DNA. The assay was conducted according to the manual of the Gyrase Supercoiling Inhibition Assay Kit from Inspiralis (Norwich, UK). Subsequently, 1 U of the respective gyrases were used to investigate a potential inhibitory activity of Gip on the supercoiling activity. Different agarose gels were compiled as indicated by the boundaries.

**Table S1: Bacterial strains used in this study**

Strain	Genotype and relevant characteristics	Reference
<i>E. coli</i> BL21 (DE3)	F <sup>-</sup> <i>ompT hsdSB(rB<sup>-</sup> mB<sup>-</sup>) gal dcm λ</i> (DE3)	(Studier & Moffatt, 1986)
<i>E. coli</i> DH5α	<i>supE44 ΔlacU169 (ϕ80lacZDM15) hsdR17 recA1 endA1 gyrA96 thi-1 relA1</i>	Invitrogen
<i>C. glutamicum</i> ATCC 13032	Biotin-auxotrophic wild type (NC_003450.3)	(Ikeda & Nakagawa, 2003)
ATCC 13032::P <sub>lys</sub> - <i>eyfp</i>	ATCC 13032 with promoter fusion P <sub>lys</sub> - <i>eyfp</i> integrated into the intergenic region of cg1121 and cg1122	(Helfrich et al., 2015)
ATCC 13032 Δ <i>recA</i> ::P <sub>lys</sub> - <i>eyfp</i>	ATCC 13032::P <sub>lys</sub> - <i>eyfp</i> with in-frame deletion of ATPase domain of <i>recA</i> (cg2141)	(Helfrich et al., 2015)
ATCC 13032::P <sub>recA</sub> - <i>venus</i>	ATCC 13032 with promoter fusion P <sub>recA</sub> - <i>venus</i> integrated into the intergenic region of cg1121 and cg1122	(Helfrich et al., 2015)
MB001	ATCC 13032 ΔCGP1 (cg1507-cg1524), ΔCGP2 (cg1746-cg1752) and ΔCGP3 (cg1890-cg2071) (BA strain)	(Baumgart et al., 2013)
ATCC 13032 Δcg1914	ATCC 13032 with partial in-frame deletion of cg1914	This work
ATCC 13032 Δcg1978	ATCC 13032 with in-frame deletion of cg1978	This work

**Table S2: Plasmids used in this study.** Numbers represent oligonucleotides used for amplification of the insert DNA (Table S3) using the *C. glutamicum* genome as template. The vectors were linearized with the indicated restriction enzyme and plasmids were constructed using Gibson assembly. Sequencing was performed using the listed oligonucleotides.

Plasmids	Template	Primer	Vector	Restriction enzymes	Sequencing primer
<b>Plasmids for overproduction of small proteins in <i>C. glutamicum</i></b>					
pAN6	Kan <sup>R</sup> ; <i>C. glutamicum</i> / <i>E. coli</i> shuttle vector for regulated gene expression; derivative of pEKEx2 ( <i>P</i> <sub>tac</sub> , <i>lacI</i> <sup>q</sup> , pBL1 oriV <sub>C.g.</sub> , pUC18 oriV <sub>E.c.</sub> ) (Frunzke et al., 2008)				
pAN6- <i>cgpS-N</i>	Kan <sup>R</sup> ; pAN6 derivative containing a truncated variant of the <i>cgpS</i> gene under control of <i>P</i> <sub>tac</sub> (Pfeifer et al., 2016)				
pAN6-cg1902	<i>C. glutamicum</i> chromosome	1 + 2	pAN6	NdeI + EcoRI	45 + 46
pAN6-cg1910	<i>C. glutamicum</i> chromosome	3 + 4	pAN6	NdeI + EcoRI	45 + 46
pAN6-cg1914	<i>C. glutamicum</i> chromosome	5 + 6	pAN6	NdeI + EcoRI	45 + 46
pAN6-cg1924	<i>C. glutamicum</i> chromosome	7 + 8	pAN6	NdeI + EcoRI	45 + 46
pAN6-cg1925	<i>C. glutamicum</i> chromosome	9 + 10	pAN6	NdeI + EcoRI	45 + 46
pAN6-cg1971	<i>C. glutamicum</i> chromosome	11 + 12	pAN6	NdeI + EcoRI	45 + 46
pAN6-cg1978 / pAN6- <i>gip</i>	<i>C. glutamicum</i> chromosome	13 + 14	pAN6	NdeI + EcoRI	45 + 46
pAN6-cg2026	<i>C. glutamicum</i> chromosome	15 + 16	pAN6	NdeI + EcoRI	45 + 46
pAN6-cg2035	<i>C. glutamicum</i> chromosome	17 + 18	pAN6	NdeI + EcoRI	45 + 46
pAN6-cg2045	<i>C. glutamicum</i> chromosome	19 + 20	pAN6	NdeI + EcoRI	45 + 46
pAN6-cg2046	<i>C. glutamicum</i> chromosome	21 + 22	pAN6	NdeI + EcoRI	45 + 46
<b>Plasmids for overproduction of proteins with affinity tags in <i>E. coli</i></b>					
pET24b	Kan <sup>R</sup> ; <i>E. coli</i> vector for regulated gene expression; derivative of pBR322 ( <i>P</i> <sub>T7</sub> , <i>lacI</i> , f1 ori, pBR322 ori, T7 terminator) (Novagen)				
pET2b- <i>Cstrep</i>	pET24b derivative with TEV cleavage site and C-terminal Strep-tag (Davoudi, unpublished)				
pET2b- <i>Nstrep</i>	pET24b derivative with TEV cleavage site and N-terminal Strep-tag (Davoudi, unpublished)				



pET2b- <i>Chis</i>	pET24b derivative with TEV cleavage site and C-terminal His-tag (Davoudi, unpublished)				
pET24b-cg1978-C- <i>strep</i>	<i>C. glutamicum</i> chromosome	23 + 24	pET24b- <i>Cstrep</i>	NdeI + NheI	47 + 48
pET24b-cg1978-C- <i>his</i>	<i>C. glutamicum</i> chromosome	25 + 26	pET24b- <i>Chis</i>	NdeI + NheI	47 + 48
pET24b- <i>gyrA</i> -C- <i>strep</i>	<i>C. glutamicum</i> chromosome	27 + 28	pET24b- <i>Cstrep</i>	NdeI + NheI	47 + 48 49 + 50
pET24b- <i>gyrA</i> -N- <i>strep</i>	<i>C. glutamicum</i> chromosome	29 + 30	pET24b- <i>Nstrep</i>	BlnI + NheI	47 + 48 49 + 50
pET24b- <i>gyrB</i> -N- <i>strep</i>	<i>C. glutamicum</i> chromosome	31 + 32	pET24b- <i>Nstrep</i>	BlnI + NheI	47 + 48 51 + 52

#### Plasmids for construction of deletion mutants

pK19 <i>mobsacB</i>	Plasmid containing a negative ( <i>sacB</i> ) as well as a positive selection marker ( <i>kan<sup>R</sup></i> ) for allelic exchange in <i>C. glutamicum</i> (pK18 ori <sub>VE.c</sub> , <i>sacB</i> , <i>lacZα</i> ) (Schäfer et al., 1994)				
pK19 <i>mobsacB</i> - $\Delta$ cg1914	<i>C. glutamicum</i> chromosome	33 + 34 35 + 36	pK19 <i>mobsacB</i>	EcoRI + HindIII	41 + 42 53 + 54
pK19 <i>mobsacB</i> - $\Delta$ cg1978	<i>C. glutamicum</i> chromosome	37 + 38 39 + 40	pK19 <i>mobsacB</i>	EcoRI + HindIII	43 + 44 53 + 54

#### Reporter plasmids

pJC1	Kan <sup>R</sup> , Amp <sup>R</sup> , <i>C. glutamicum</i> shuttle vector (Cremer et al., 1990)				
pJC1-P <sub>lys</sub> - <i>lys</i> '-venus	Prophage reporter plasmid carrying the gene coding for the fluorescent protein Venus under control of the P <sub>lys</sub> promoter (Hünnefeld et al., 2019)				

Table S3: Oligonucleotides used in this study

Primer No.	Oligonucleotide name	Sequence (5' → 3')
<b>Construction of plasmids for overproduction of small proteins in <i>C. glutamicum</i></b>		
1	pAN6_cg1902_fw	CAGAAGGAGATATACATATGATGATTAAGAGACTGGCTGCAGG
2	pAN6_cg1902_rv	AAACGACGGCCAGTGAATTCCTTACAACCTGAATAGCCGTACCTG
3	pAN6_cg1910_fw	CAGAAGGAGATATACATATGTTGGAGTTATTTTATTTTTCGACTT
4	pAN6_cg1910_rv	AAACGACGGCCAGTGAATTCCTATTTTCCAACCTTGTCGCTCTTAC
5	pAN6_cg1914_fw	CAGAAGGAGATATACATATGATGAAGTGCCTCAAACTGCTC
6	pAN6_cg1914_rv	AAACGACGGCCAGTGAATTCCTACAGTACTTCGATATATCCGACGTC
7	pAN6_cg1924_fw	CTGCAGAAGGAGATATACATATGCTACTCGACATCATCATTTACC
8	pAN6_cg1924_rv	AAACGACGGCCAGTGAATTCCTACTGCTCATTATGAGGTGCC
9	pAN6_cg1925_fw	CTGCAGAAGGAGATATACATATGGTGGTGTGCGGC
10	pAN6_cg1925_rv	AAACGACGGCCAGTGAATTCCTACGGCTGTGCGAGCTG
11	pAN6_cg1971_fw	CTGCAGAAGGAGATATACATATGTCTAATCTCGGCACATACTATG
12	pAN6_cg1971_rv	AAACGACGGCCAGTGAATTCCTCAGAAACAGGCTGTTGAGAC
13	pAN6_cg1978_fw	CAGAAGGAGATATACATATGATGGCTAAAGAATTCGAATTCACC
14	pAN6_cg1978_rv	AAACGACGGCCAGTGAATTCCTACTCGACGATGACGTAGGG
15	pAN6_cg2026_fw	CAGAAGGAGATATACATATGATGACCAAGCGAAATATCACTACTGT
16	pAN6_cg2026_rv	AAACGACGGCCAGTGAATTCCTAGCCCTTAGGTGGGTG
17	pAN6_cg2035_fw	CTGCAGAAGGAGATATACATATGTCAATCAATGCGTTCTGG
18	pAN6_cg2035_rv	AAACGACGGCCAGTGAATTCCTAGGCACCTAGATATGTGATTAC
19	pAN6_cg2045_fw	CAGAAGGAGATATACATATGATGCCTCAACGCGAAAGC
20	pAN6_cg2045_rv	AAACGACGGCCAGTGAATTCCTAGCTGTCCACAGAAGATGCC
21	pAN6_cg2046_fw	CTGCAGAAGGAGATATACATATGGGTACCTGGGAATTGATAG
22	pAN6_cg2046_rv	AAACGACGGCCAGTGAATTCCTAGATATCGACTCCTAGCGCTC
<b>Construction of plasmids for overproduction of proteins with affinity tags in <i>E. coli</i></b>		
23	cg1978_C-Strep_pET_fw	AAGAAGGAGATATACATATGATGGCTAAAGAATTCGAATTCACCATC
24	cg1978_C-Strep_pET_rv	AAATACAGTTCTCGCTAGCCTCGACGATGACGTAGGG
25	cg1978_C-His_pET_fw	AAGAAGGAGATATACATATGATGGCTAAAGAATTCGAATTCACCATC
26	cg1978_C-His_pET_rv	AAATACAGTTCTCGCTAGCCTCGACGATGACGTAGGG
27	gyrA_C-Strep_pET_fw	AAGAAGGAGATATACATATGGTGAGCGACACAATACCGGAC
28	gyrA_C-Strep_pET_rv	AAATACAGTTCTCGCTAGCTTCTCGCCGTTTTCTGTCG
29	gyrA_N-Strep_pET_fw	TGTATTTTCAGGGCGCTAGCGTGAGCGACGACAATACC
30	gyrA_N-Strep_pET_rv	TATGCTAGTTATTGCTCAGCTTATTCCTCGCCGTTTTCTGTCG
31	gyrB_N-Strep_pET_fw	TGTATTTTCAGGGCGCTAGCGTGGCAAACACTGAACACAATTATG
32	gyrB_N-Strep_pET_rv	TATGCTAGTTATTGCTCAGCTTAGATATCGAGGAAACGAACATCCTTG
<b>Construction of plasmids for genomic deletion in <i>C. glutamicum</i></b>		
33	LF_fw_cg1914	CCATGATTACGCCAAGCTTGTCTGTGGACATCATGAAAAACG
34	LF_rv_cg1914	GTCTGTAACCGAGCATCTCTCGATGATCTCCTTTTAAGGGATTGAGGTG
35	RF_fw_cg1914	GAGAGATGCTCGGTTACAGACCACGCTCTGCAGCGACTG
36	RF_rv_cg1914	AACGACGGCCAGTGAATTCGGACCATGAGCGGCCGGTT
37	LF_fw_cg1978	ACCATGATTACGCCAAGCTTGACCAAATCGGCGATGTGTTTG
38	LF_rv_cg1978	GTCTGTAACCGAGCATCTCTCAATAAGTGTTCTTTCTTATGCGAGGTG

39	RF_fw_cg1978	GAGAGATGCTCGGTTACAGACAGGCGTTTCTTTTCTCCCC
40	RF_rv_cg1978	AAACGACGGCCAGTGAATTGCCCGTGAGGTCACCCCTTAT

## Sequencing primer

41	$\Delta$ cg1914_fw_seq	AGGTGTGTATAACACCCGACAAG
42	$\Delta$ cg1914_rv_seq	ATGCGACGCAAATTTGGACC
43	$\Delta$ cg1978_fw_seq	TCCGACATCATTACATGACTGAC
44	$\Delta$ cg1978_rv_seq	TCGTCAAGGTAGAGAGACATAAGTTATGTAG
45	pAN6_fw_seq	GATATGACCATGATTACGCCAAGC
46	pAN6_rv_seq	CGGCGTTTCACTTCTGAGTTCGGC
47	pET24b_fw_seq	CGATATAGGCGCCAGCAACC
48	pET24b_rv_seq	CCTCAAGACCCGTTTAGAGG
49	<i>gyrA</i> -C/N-strep_fw_seq	GGCTGACGCAATTCTGGCAATG
50	<i>gyrA</i> -C/N-strep_rv_seq	CAGCTCATCGCGAACGATGG
51	<i>gyrB</i> -N-strep_fw_seq	CGAGGAAGGTTTCCGCTCTG
52	<i>gyrB</i> -N-strep_rv_seq	GGAATAACCGCGGACAGGC
53	pK19mobSacB_fw_seq	AGCGGATAACAATTCACACAGGA
54	pK19mobSacB_rv_seq	CGCCAGGGTTTTCCCAGTCACGAC

**Table S4: Impact of *gip* (cg1978) overexpression on global expression levels.** A genome-wide comparison of mRNA levels the *C. glutamicum* ATCC 13032 strain overexpressing *gip* and the wild type strain carrying the empty vector control was performed. The shown mRNA ratios indicated mean values from three independent biological replicates (n=3). The strains were cultivated in CGXII minimal medium with 2 % (w/v) glucose and mRNA was prepared from cells at an OD<sub>600</sub> of 6. The mRNA ratios were calculated by dividing the mRNA levels of the *gip* overexpressing strain by the mRNA levels of the strain carrying the empty vector control. The table includes all genes which showed a changed mRNA level in all experiments (mRNA ratio > 2.0: upregulation (red) or < 0.5: downregulation (green), p-value < 0.05).

The table is provided in a separate file (Table S4\_Complete Microarray Data).

**Table S4: Impact of *gip* (cg1978) overexpression on global expression levels.** A genome-wide comparison of mRNA levels the *C. glutamicum* ATCC 13032 strain overexpressing *gip* and the wildtype strain carrying the empty vector control was performed. The shown mRNA ratios indicated mean values from three independent biological replicates (n=3). The strains were cultivated in CGXII minimal medium with 2 % (w/v) glucose and mRNA was prepared from cells at an OD<sub>600</sub> of 6. The mRNA ratios were calculated by dividing the mRNA levels of the *gip* overexpressing strain by the mRNA levels of the strain carrying the empty vector control. The table includes all genes which showed a changed mRNA level in all experiments (mRNA ratio > 2.0: upregulation (red) or < 0.5: downregulation (green), p-value < 0.05).

Gene	mRNA ratio	P-value	Gene name	Annotation	Categorization
cg0001	0,60	0,02	<i>dnaA</i>	dnaA, chromosomal replication initiation protein	DNA replication, recombination, repair, and degradation
cg0004	0,70	0,02	<i>dnaN</i>	dnaN, DNA polymerase III subunit beta	DNA replication, recombination, repair, and degradation
cg0007	4,44	0,01	<i>gyrB</i>	gyrB, DNA topoisomerase IV subunit B	DNA replication, recombination, repair, and degradation
cg0008	0,59	0,01		hypothetical protein cg0008   hypothetical protein cg0008	General function prediction only
cg0009	0,77	0,01		uncharacterized membrane protein	Unknown function
cg0010	1,64	0,04		hypothetical protein cg0010	Unknown function
cg0012	6,95	0,00	<i>ssuR</i>	ssuR, sulphate sulphur utilization transcriptional regulator SsuR	Signal transduction mechanisms
cg0013	1,16	0,00		bacterial regulatory proteins, TetR family	Signal transduction mechanisms
cg0015	6,23	0,00	<i>gyrA</i>	gyrA, DNA gyrase subunit A	DNA replication, recombination, repair, and degradation
cg0016	2,41	0,00		putative integral membrane protein	Unknown function
cg0018	9,84	0,00		hypothetical membrane protein	Unknown function
cg0025	1,18	0,04	<i>ccdA2</i>	putative integral membrane cytochrome biogenesis protein	Protein turnover and chaperones
cg0033	0,65	0,04		putative secreted protein	Unknown function
cg0038	0,44	0,00	<i>ohr</i>	organic hydroperoxide resistance protein   organic hydroperoxide resistance protein	General function prediction only
cg0040	0,57	0,02		putative secreted protein	Inorganic ion transport, metabolism, and storage
cg0044	0,32	0,00	<i>rbsB</i>	rbsB, ABC transporter/periplasmic D-ribose-binding protein   rbsB, ABC transporter/periplasmic D-ribose-binding protein	Carbon source transport and metabolism
cg0045	0,38	0,00		probable ABC transport protein, membrane component	Carbon source transport and metabolism
cg0046	0,81	0,01		probable ABC transport protein, ATP-binding component	Carbon source transport and metabolism
cg0047	0,67	0,02		hypothetical protein cg0047	Unknown function
cg0054	0,42	0,04		cytoplasmic siderophore-interacting protein	Inorganic ion transport, metabolism, and storage
cg0055	0,82	0,01	<i>crgA</i>	crgA, ortholog of Rv0011c, member of the cell division complex in mycobacteria	Cell division, chromosome partitioning
cg0057	0,62	0,00	<i>pknB</i>	pknB, eukaryotic-type serine/threonine kinase	Post-translational modification; Signal transduction mechanisms
cg0059	0,77	0,03	<i>pknA</i>	pknA, serine/threonine protein kinase	Post-translational modification; Signal transduction mechanisms
cg0060	0,54	0,00	<i>pbp2b</i> ( <i>pbpA</i> )	pbpA, D-alanyl-D-alanine carboxypeptidase   pbpA, D-alanyl-D-alanine carboxypeptidase	Cell wall/membrane/envelope biogenesis
cg0061	0,58	0,00	<i>rodA</i>	rodA, putative FTSW/RODA/SPOVE family cell cycle protein	Cell division, chromosome partitioning
cg0062	0,62	0,02	<i>ppp</i>	ppp, protein phosphatase	Post-translational modification; Signal transduction mechanisms
cg0063	0,61	0,00	<i>fhaB</i>	secreted protein	General function prediction only
cg0064	0,66	0,05	<i>fhaA</i>	hypothetical protein cg0064   hypothetical protein cg0064	General function prediction only
cg0065	0,78	0,04		haem peroxidase superfamily	General function prediction only
cg0067	0,54	0,00	<i>gabD3</i>	gabD3, succinate-semialdehyde dehydrogenase (NADP+)	Amino acid transport and metabolism
cg0071	0,58	0,02		metallo-beta-lactamase superfamily	General function prediction only
cg0072	0,57	0,03		hypothetical protein cg0072	Unknown function
cg0073	0,44	0,02		sulfurtransferase	General function prediction only
cg0075	0,92	0,03		hypothetical protein cg0075	Unknown function
cg0076	0,37	0,04		hypothetical protein cg0076	Unknown function

cg0080	0,82	0,01		CorA-like Mg2+ transporter protein   CorA-like Mg2+ transporter protein	Inorganic ion transport, metabolism, and storage
cg0081	1,77	0,03		putative tautomerase	Carbon source transport and metabolism
cg0082	0,74	0,04		voltage gated chloride channel	Inorganic ion transport, metabolism, and storage
cg0088	0,53	0,00	<i>citH (citP, citM)</i>	citH, citrate transporter	Carbon source transport and metabolism
cg0090	0,55	0,01	<i>citB</i>	citB, two-component response regulator CitB	Signal transduction mechanisms
cg0095	0,56	0,03	<i>bioB</i>	bioB, biotin synthase	Coenzyme transport and metabolism
cg0097	0,72	0,04		hypothetical protein cg0097   hypothetical protein cg0097   hypothetical protein cg0097	Unknown function
cg0104	1,87	0,00	<i>codA</i>	codA, creatinine deaminase	Amino acid transport and metabolism
cg0107	0,65	0,00		secreted protein	Unknown function
cg0109	4,16	0,00	<i>lip1</i>	triacylglycerol lipase precursor	Lipid transport and metabolism
cg0111	0,82	0,02		hypothetical protein cg0111	Unknown function
cg0112	1,51	0,03	<i>ureR</i>	ureR, bacterial regulatory protein, MarR family	Signal transduction mechanisms
cg0113	1,35	0,01	<i>ureA</i>	ureA, probable urease gamma subunit	Transport and metabolism of further metabolites
cg0117	1,45	0,02	<i>ureF</i>	ureF, urease accessory protein	Transport and metabolism of further metabolites
cg0122	1,51	0,01		putative glycerol 3-phosphate dehydrogenase	Lipid transport and metabolism
cg0123	0,45	0,00	<i>htpG</i>	putative heat shock protein (HSP90-family)	Protein turnover and chaperones
cg0128	0,71	0,01		secreted protein, signal peptide	Unknown function
cg0131	0,70	0,03		putative oxidoreductase   putative oxidoreductase	General function prediction only
cg0133	0,21	0,00	<i>abgT</i>	p-aminobenzoyl-glutamate transporter	Amino acid transport and metabolism
cg0134	0,25	0,00	<i>abgB</i>	hydrolase, AMA/HIPO/HYUC family	Amino acid transport and metabolism
cg0135	0,41	0,00		putative inner membrane protein	Unknown function
cg0136	0,48	0,01		hypothetical protein cg0136	Unknown function
cg0138	1,81	0,01		ATP/GTP-binding protein	Unknown function
cg0144	0,62	0,04	<i>rbtT</i>	rbtT, putative ribitol transporter	Carbon source transport and metabolism
cg0148	0,41	0,00	<i>panC</i>	panC, pantoate--beta-alanine ligase protein	Coenzyme transport and metabolism
cg0149	0,51	0,03	<i>panB</i>	panB, 3-methyl-2-oxobutanoate hydroxymethyltransferase	Coenzyme transport and metabolism
cg0150	0,68	0,01		bacterial regulatory protein	Signal transduction mechanisms
cg0156	2,39	0,00	<i>cysR</i>	cysR, transcriptional regulator involved in sulphonate utilisation	Signal transduction mechanisms
cg0158	0,51	0,00		putative membrane transport protein	General function prediction only
cg0159	0,42	0,02		hypothetical protein cg0159   hypothetical protein cg0159	Unknown function
cg0161	0,60	0,00		putative secreted or membrane protein	Unknown function
cg0162	0,53	0,00		membrane spanning protein	Unknown function
cg0163	0,64	0,00		N-acetylglucosaminyltransferase	General function prediction only
cg0165	0,72	0,05		ABC-2 type transporter	General function prediction only
cg0170	1,36	0,02		probable transmembrane protein	Unknown function
cg0171	1,39	0,00		secreted protein	Unknown function
cg0172	1,76	0,03	<i>panD</i>	panD, aspartate 1-decarboxylase precursor	Amino acid transport and metabolism; Coenzyme transport and metabolism
cg0174	0,49	0,00		putative transport protein	Unknown function
cg0176	0,69	0,02		permease	Unknown function
cg0180	0,38	0,00	<i>maa</i>	maa, maltose O-acetyltransferase	Carbon source transport and metabolism
cg0182	0,44	0,02	<i>tagA2</i>	tagA2, probable DNA-3-methyladenine glycosylase I protein	DNA replication, recombination, repair, and degradation
cg0183	0,42	0,01		putative lyse type translocator	Amino acid transport and metabolism
cg0184	1,65	0,01		hypothetical protein cg0184	Unknown function
cg0185	1,79	0,01		glyoxalase/bleomycin resistance protein/dioxygenase	General function prediction only
cg0186	0,67	0,02		methylated-DNA--protein-cysteine methyltransferase	DNA replication, recombination, repair, and degradation
cg0191	0,36	0,00		translation initiation inhibitor	General function prediction only
cg0193	0,50	0,01	<i>pepO</i>	pepO, endopeptidase O	Protein turnover and chaperones
cg0197	1,22	0,02	<i>iolC</i>	iolC, myo-Inositol catabolism, carbohydrate kinase	Carbon source transport and metabolism
cg0198	0,82	0,03		hypothetical protein cg0198	Carbon source transport and metabolism
cg0199	0,68	0,02	<i>iolA</i>	iolA, myo-Inositol catabolism, aldehyde dehydrogenase	Carbon source transport and metabolism
cg0201	0,49	0,01	<i>iolB</i>	iolB, enzyme involved in inositol metabolism	Carbon source transport and metabolism
cg0202	0,50	0,00	<i>iolD</i>	iolD, putative acetolactate synthase protein	Carbon source transport and metabolism

cg0203	0,50	0,00	<i>iolE</i>	iolE, 2-Keto-myo-inositol dehydratase	Carbon source transport and metabolism
cg0205	0,63	0,00	<i>iolH</i>	iolH, myo-inositol catabolism protein	Carbon source transport and metabolism
cg0207	0,54	0,03	<i>oxiA</i>	oxi1, myo-Inositol dehydrogenase, oxidoreductase	Carbon source transport and metabolism
cg0208	1,75	0,02		hypothetical protein cg0208	Unknown function
cg0209	1,73	0,01		hypothetical protein cg0209	Unknown function
cg0211	0,54	0,00	<i>oxiB</i>	putative oxidoreductase	General function prediction only
cg0212	0,67	0,03		phosphate isomerase/epimerase	General function prediction only
cg0214	0,70	0,04		hypothetical protein cg0214	Unknown function
cg0215	0,28	0,01	<i>cspA</i>	cspA, cold-shock protein CSPA   cspA, cold-shock protein CSPA	Transcription including sigma factors, RNA processing and modification
cg0217	0,68	0,02		bacterial regulatory protein, ArsR family	Signal transduction mechanisms
cg0218	1,71	0,00		O-methyl transferase (N-terminal fragment)	General function prediction only
cg0219	2,18	0,00		O-methyl transferase (C-terminal fragment)	General function prediction only
cg0220	0,65	0,01		acetyltransferase, GNAT family	General function prediction only
cg0222	0,65	0,03		membrane protein	Unknown function
cg0223	0,34	0,01	<i>iolT1</i>	iolT1, myo-Inositol transporter   iolT1, myo-Inositol transporter	Carbon source transport and metabolism
cg0228	0,26	0,00	<i>hkm</i>	sensor histidine kinase of two-component system, fragment	Post-translational modification; Signal transduction mechanisms
cg0229	0,37	0,02	<i>gltB</i>	gltB, glutamine 2-oxoglutarate aminotransferase large SU	Amino acid transport and metabolism
cg0230	0,31	0,01	<i>gltD</i>	gltD, glutamine 2-oxoglutarate aminotransferase small SU	Amino acid transport and metabolism
cg0232	0,54	0,00		hypothetical secreted protein	Unknown function
cg0233	0,61	0,01		hypothetical protein cg0233	Unknown function
cg0236	0,73	0,00	<i>aftA</i>	aftA, arabinofuranosyltransferase   aftA, arabinofuranosyltransferase	Cell wall/membrane/envelope biogenesis
cg0241	1,35	0,01		hypothetical protein cg0241	Unknown function
cg0243	0,73	0,01		membrane protein	Unknown function
cg0244	0,73	0,01		membrane protein	Unknown function
cg0245	0,70	0,05		hypothetical protein cg0245   hypothetical protein cg0245	Unknown function
cg0246	0,63	0,02		glycosyl transferase	General function prediction only
cg0247	0,76	0,03		hypothetical protein cg0247	Unknown function
cg0249	1,57	0,01		polysaccharide/polyol phosphate export systems, permease component	General function prediction only
cg0250	1,34	0,01		aminotransferase	General function prediction only
cg0252	0,55	0,01		membrane protein	Unknown function
cg0254	0,43	0,01		amino acid carrier protein (sodium/alanine symporter)	Amino acid transport and metabolism
cg0255	0,51	0,00		hypothetical protein cg0255	Unknown function
cg0256	0,45	0,02		hypothetical protein cg0256	Unknown function
cg0257	1,60	0,01	<i>moeB</i>	molybdopterin biosynthesis protein MoeB	Coenzyme transport and metabolism
cg0259	1,72	0,02	<i>moaB</i>	moaB, molybdenum cofactor biosynthesis protein	Coenzyme transport and metabolism
cg0260	0,73	0,02	<i>moaC</i>	moaC, molybdenum cofactor biosynthesis protein C	Coenzyme transport and metabolism
cg0262	1,30	0,03	<i>modB</i>	modB, sulfate/molybdate transport system, permease component	Coenzyme transport and metabolism
cg0264	0,57	0,01		putative molybdopterin converting factor	Coenzyme transport and metabolism
cg0266	0,84	0,02		membrane protein	Unknown function
cg0272	1,41	0,02		bacterial regulatory protein, LysR family	Signal transduction mechanisms
cg0273	0,57	0,03		probable alcohol dehydrogenase	General function prediction only
cg0274	0,54	0,01	<i>maoA</i>	putative oxidoreductase protein	Carbon source transport and metabolism
cg0275	0,62	0,01	<i>mgfE2</i>	mgfE2, mg2+ transporter	Inorganic ion transport, metabolism, and storage
cg0277	0,29	0,00	<i>dccT (dcsT)</i>	dccT, dicarboxylate uptake system (succinate, fumarate or L-malate)   dccT, dicarboxylate uptake system (succinate, fumarate or L-malate)   dccT, dicarboxylate uptake system (succinate, fumarate or L-malate)	Carbon source transport and metabolism
cg0279	1,21	0,03	<i>tyrA</i>	tyrA, prephenate dehydrogenase	Amino acid transport and metabolism
cg0283	0,55	0,02		membrane protein	Unknown function
cg0285	0,69	0,01	<i>tgt</i>	tgt, putative trna-guanine transglycosylase	Transcription including sigma factors, RNA processing and modification
cg0286	0,63	0,02		hypothetical protein cg0286	Unknown function
cg0287	0,43	0,02		similar to malic enzyme	General function prediction only
cg0291	1,65	0,01		3,4-dioxygenase beta subunit   3,4-dioxygenase beta subunit	General function prediction only

cg0292	0,63	0,03	<i>tnp16a</i>	tnp16a(ISCg16a), transposase	DNA replication, recombination, repair, and degradation
cg0293	0,49	0,00		hypothetical protein cg0293	Unknown function
cg0294	0,87	0,01	<i>aspT (aspB)</i>	aspT, aspartate aminotransferase	Amino acid transport and metabolism
cg0295	0,80	0,03		hypothetical protein cg0295	Unknown function
cg0297	3,71	0,03		hypothetical protein cg0297	Unknown function
cg0298	3,51	0,00	<i>recR</i>	recR, recombination protein RecR   recR, recombination protein RecR   recR, recombination protein RecR	DNA replication, recombination, repair, and degradation
cg0300	1,38	0,02		hypothetical tripeptide synthase involved in murein formation	Cell wall/membrane/envelope biogenesis
cg0303	0,80	0,05	<i>leuA</i>	leuA, 2-isopropylmalate synthase   leuA, 2-isopropylmalate synthase	Amino acid transport and metabolism
cg0304	2,53	0,00		membrane protein   membrane protein	Unknown function
cg0305	0,85	0,01	#NV	hypothetical protein cg0305	#NV
cg0306	2,53	0,00	<i>lysC</i>	lysC, aspartate kinase	Amino acid transport and metabolism
cg0307	2,66	0,01	<i>asd</i>	asd, aspartate-semialdehyde dehydrogenase	Amino acid transport and metabolism
cg0308	2,39	0,00		hypothetical protein cg0308	Unknown function
cg0310	2,15	0,01	<i>katA</i>	katA, catalase   katA, catalase	Inorganic ion transport, metabolism, and storage
cg0314	8,35	0,01	<i>brnF</i>	brnF, branched chain amino acid exporter, large subunit   brnF, branched chain amino acid exporter, large subunit	Amino acid transport and metabolism
cg0315	5,93	0,00	<i>brnE</i>	brnE, branched chain amino acid exporter, small subunit	Amino acid transport and metabolism
cg0317	2,48	0,02	<i>arsR2</i>	arsR2, arsenate/arsenite regulatory protein	Signal transduction mechanisms
cg0318	0,77	0,04	<i>arsC1 (arsB2)</i>	arsB2, arsenite permease	Inorganic ion transport, metabolism, and storage
cg0321	0,52	0,02	<i>mrpG1 (mnhG)</i>	Na <sup>+</sup> /H <sup>+</sup> antiporter subunit	Inorganic ion transport, metabolism, and storage
cg0322	0,42	0,01	<i>mrpF1 (mnhF)</i>	predicted conserved membrane protein	Inorganic ion transport, metabolism, and storage
cg0323	0,58	0,01	<i>mrpE1 (mnhE)</i>	conserved hypothetical secreted protein	Inorganic ion transport, metabolism, and storage
cg0324	0,42	0,00	<i>mrpD1 (mnhD)</i>	mnhD, NADH dehydrogenase subunit N	Inorganic ion transport, metabolism, and storage
cg0325	0,40	0,01	<i>mrpC1 (mnhC)</i>	hypothetical protein cg0325	Inorganic ion transport, metabolism, and storage
cg0326	0,43	0,01	<i>mrpA1 (mnhAB)</i>	nuoL, NADH-quinone oxidoreductase chain 5	Inorganic ion transport, metabolism, and storage
cg0327	0,36	0,04		membrane protein   membrane protein	Unknown function
cg0332	0,76	0,00		secreted protein	Unknown function
cg0333	1,07	0,02		possible membrane protein	Unknown function
cg0334	0,75	0,02		secreted phosphohydrolase	General function prediction only
cg0335	0,46	0,00		conserved hypothetical protein, GatB/Yqey domain	Unknown function
cg0336	2,23	0,00	<i>pbp1a</i>	ponA, penicillin-binding protein 1B	Cell wall/membrane/envelope biogenesis
cg0337	0,88	0,01	<i>whcA (whiB4)</i>	whcA, negative role in SigH-mediated (oxidative) stress response	Cell wall/membrane/envelope biogenesis
cg0338	1,78	0,03		hypothetical protein cg0338   hypothetical protein cg0338	Unknown function
cg0339	2,74	0,02		translation initiation inhibitor	General function prediction only
cg0340	0,51	0,01	<i>phdT</i>	putative integral membrane transport protein	Carbon source transport and metabolism
cg0343	0,50	0,02	<i>phdR</i>	putative transcription regulator protein, MarR fam	Signal transduction mechanisms
cg0344	0,62	0,00	<i>phdB (fabG1)</i>	fabG1, 3-oxoacyl-(acyl-carrier protein) reductase   fabG1, 3-oxoacyl-(acyl-carrier protein) reductase   fabG1, 3-oxoacyl-(acyl-carrier protein) reductase	Carbon source transport and metabolism
cg0345	0,47	0,02	<i>phdC</i>	metal-dependent hydrolase of the TIM-barrel fold	Carbon source transport and metabolism
cg0346	0,47	0,01	<i>phdD (fadE)</i>	fadE, glutaryl-CoA dehydrogenase	Carbon source transport and metabolism
cg0347	0,57	0,01	<i>phdE (hdtZ)</i>	hdtZ, 3-hydroxyacyl-thioester dehydratase	Carbon source transport and metabolism
cg0350	0,59	0,01	<i>glxR</i>	glxR, cAMP-dependent transcriptional regulator   glxR, cAMP-dependent transcriptional regulator	Signal transduction mechanisms
cg0352	0,69	0,05		putative secreted protein	Unknown function
cg0353	0,62	0,00	<i>nth</i>	nth, probable endonuclease III protein	General function prediction only



cg0354	0,49	0,01		thioredoxin-related protein, secreted	Inorganic ion transport, metabolism, and storage
cg0355	0,51	0,00		pyrophosphohydrolase	General function prediction only
cg0356	0,50	0,02		putative serine protease, membrane protein	General function prediction only
cg0358	0,76	0,01		hydrolase or acyltransferase	General function prediction only
cg0360	1,62	0,02		putative phosphatase	General function prediction only
cg0365	1,71	0,01		membrane protein	Unknown function
cg0370	1,18	0,01		DEAD/DEAH box helicase   DEAD/DEAH box helicase	Transcription including sigma factors, RNA processing and modification
cg0371	0,56	0,01	<i>cspA2</i>	cspA2, cold-shock protein CSP A	Transcription including sigma factors, RNA processing and modification
cg0372	0,50	0,03		hypothetical protein cg0372	Unknown function
cg0373	0,40	0,00	<i>topA</i>	topA, DNA topoisomerase I   topA, DNA topoisomerase I	DNA replication, recombination, repair, and degradation
cg0374	0,48	0,03		hypothetical protein cg0374   hypothetical protein cg0374	Unknown function
cg0376	0,72	0,02	<i>dnaX</i>	dnaX, putative DNA polymerase III, delta subunit	DNA replication, recombination, repair, and degradation
cg0378	0,64	0,02		putative phage-associated protein	General function prediction only
cg0384	0,37	0,00	<i>rluC1</i>	rluC1, ribosomal large subunit pseudouridine synthase C	Translation, ribosomal structure and biogenesis
cg0386	0,38	0,05	<i>bglS</i>	bglS, beta-glucosidase-C-terminal domain	Carbon source transport and metabolism
cg0388	0,61	0,04		Zn-dependent hydrolase	General function prediction only
cg0389	0,89	0,01		short chain dehydrogenase	General function prediction only
cg0390	0,44	0,00		permease, major facilitator family	General function prediction only
cg0393	0,75	0,02		hypothetical protein cg0393	Unknown function
cg0394	0,71	0,00		glycosyl transferase	General function prediction only
cg0395	0,61	0,00		hypothetical protein cg0395	Transcription including sigma factors, RNA processing and modification
cg0396	0,57	0,02		glycosyl transferase	General function prediction only
cg0398	4,30	0,00		hypothetical protein predicted by Glimmer	Unknown function
cg0399	4,61	0,00		hypothetical protein cg0399	Unknown function
cg0400	4,14	0,00	<i>adhC</i>	adhC, alcohol dehydrogenase, class C   adhC, alcohol dehydrogenase, class C	Carbon source transport and metabolism
cg0402	1,28	0,04	<i>rmlCD</i>	rmlCD, dTDP-4-dehydrorhamnose 3,5-epimerase, dTDP-dehydrorhamnose reductase	Nucleotide transport and metabolism
cg0403	1,72	0,02	<i>rmlB1</i>	rmlB1, dTDP-glucose 4,6-dehydratase	Nucleotide transport and metabolism
cg0404	1,70	0,05		nitroreductase family	General function prediction only
cg0407	0,48	0,01		secreted protein	Unknown function
cg0408	0,59	0,02		membrane protein	Unknown function
cg0410	0,54	0,00		putative prolyl endopeptidase	Protein turnover and chaperones
cg0411	0,53	0,01		hypothetical protein cg0411	Unknown function
cg0413	1,55	0,02	<i>cmt1</i>	cmt1, trehalose corynomycolyl transferase	Cell wall/membrane/envelope biogenesis
cg0418	0,67	0,04		putative aminotransferase	Cell wall/membrane/envelope biogenesis
cg0422	0,68	0,05	<i>murA</i>	murA, UDP-N-acetylglucosamine 1-carboxyvinyltransferase	Cell wall/membrane/envelope biogenesis
cg0424	0,69	0,03		putative glycosyltransferase	General function prediction only
cg0426	1,87	0,00	<i>tnp17a</i>	tnp17a(ISCg17a), transposase-fragment   tnp17a(ISCg17a), transposase-fragment	DNA replication, recombination, repair, and degradation
cg0431	3,23	0,01		hypothetical protein cg0431	General function prediction only
cg0432	1,83	0,01		putative acyltransferase, expression is under the control of autoinducers	Cell wall/membrane/envelope biogenesis
cg0435	2,46	0,01	<i>udgA1</i>	udgA1, UDP-glucose 6-dehydrogenase   udgA1, UDP-glucose 6-dehydrogenase	Nucleotide transport and metabolism
cg0436	1,50	0,04		hypothetical protein cg0436	Unknown function
cg0445	0,27	0,01	<i>sdhC sdhCD</i>	sdhC, succinate dehydrogenase	Central carbon metabolism; Anaerobic metabolism; Respiration and oxidative phosphorylation
cg0446	0,18	0,00	<i>sdhA</i>	sdhA, succinate dehydrogenase	Central carbon metabolism; Anaerobic metabolism; Respiration and oxidative phosphorylation
cg0447	0,21	0,00	<i>sdhB</i>	sdhB, succinate dehydrogenase   sdhB, succinate dehydrogenase	Central carbon metabolism; Anaerobic metabolism; Respiration and oxidative phosphorylation
cg0448	0,35	0,00		hypothetical protein cg0448   hypothetical protein cg0448	Central carbon metabolism; Anaerobic metabolism; Respiration and oxidative phosphorylation
cg0450	2,40	0,00		hypothetical protein cg0450	Unknown function
cg0452	1,35	0,03		hypothetical protein cg0452	Unknown function

cg0453	1,76	0,00		predicted membrane protein	Unknown function
cg0455	1,36	0,03		permease, major facilitator superfamily	General function prediction only
cg0456	1,66	0,01		permease, major facilitator superfamily	General function prediction only
cg0457	1,49	0,03	<i>purU</i>	purU, formyltetrahydrofolate deformylase	Coenzyme transport and metabolism; Nucleotide transport and metabolism; Carbon source transport and metabolism
cg0458	1,46	0,01	<i>deoC</i>	deoC, deoxyribose-phosphate aldolase	Central carbon metabolism; Nucleotide transport and metabolism
cg0462	0,87	0,01		hypothetical protein cg0462	Unknown function
cg0463	5,77	0,00	<i>csaR</i>	hypothetical protein cg0463	Signal transduction mechanisms; Inorganic ion transport, metabolism, and storage
cg0464	7,03	0,00	<i>copA (ctpA, ctpV)</i>	ctpA, copper-transporting ATPase   ctpA, copper-transporting ATPase	Inorganic ion transport, metabolism, and storage
cg0466	0,55	0,00	<i>htaA</i>	htaA, secreted heme-transport associated protein	Transport and metabolism of further metabolites
cg0467	0,57	0,03	<i>hmuT</i>	hmuT, hemin-binding periplasmic protein precursor	Transport and metabolism of further metabolites
cg0468	0,66	0,00	<i>hmuU</i>	hmuU, hemin transport system, permease protein	Transport and metabolism of further metabolites
cg0469	0,86	0,04	<i>hmuV</i>	hmuV, hemin transport system, ATP-binding protein	Transport and metabolism of further metabolites
cg0470	4,41	0,04	<i>htaB</i>	htaB, secreted heme transport-associated protein	Transport and metabolism of further metabolites
cg0472	2,25	0,00		hypothetical protein cg0472   hypothetical protein cg0472   hypothetical protein cg0472	Unknown function
cg0474	0,53	0,01		hypothetical protein cg0474	Unknown function
cg0476	1,55	0,02	<i>murB2</i>	murB, UDP-N-acetylenolpyruvoylglucosamine reductase	Cell wall/membrane/envelope biogenesis
cg0480	2,20	0,02	<i>fadD5 (fcs)</i>	fadD5, acyl-coA synthase	Carbon source transport and metabolism
cg0481	1,55	0,00	<i>mshA</i>	mshA, glycosyltransferase	Transport and metabolism of further metabolites
cg0482	0,74	0,02	<i>gpmA</i>	gpmA, phosphoglyceromutase	Central carbon metabolism
cg0488	0,49	0,02	<i>ppx1</i>	ppx1, exopolyphosphatase	Inorganic ion transport, metabolism, and storage
cg0489	0,41	0,00		hypothetical membrane protein	Unknown function
cg0490	0,38	0,01	<i>proC</i>	proC, pyrroline-5-carboxylate reductase	Amino acid transport and metabolism
cg0491	0,47	0,03		hypothetical protein cg0491	Unknown function
cg0492	0,38	0,00		extremely conserved possible DNA-binding protein   extremely conserved possible DNA-binding protein	DNA replication, recombination, repair, and degradation
cg0493	0,48	0,02		hypothetical protein predicted by Glimmer	Unknown function
cg0494	0,61	0,01		extremely conserved hypothetical protein	Unknown function
cg0499	1,95	0,00		hypothetical protein cg0499	Unknown function
cg0500	0,55	0,00	<i>qsuR</i>	bacterial regulatory protein, LysR family	Signal transduction mechanisms
cg0501	0,51	0,00	<i>qsuA</i>	putative integral membrane transport protein	Amino acid transport and metabolism
cg0502	0,54	0,00	<i>qsuB</i>	phosphate isomerase/epimerase   phosphate isomerase/epimerase	Amino acid transport and metabolism
cg0504	0,65	0,01	<i>qsuD (aroE)</i>	an NAD-dependent quinate dehydrogenase	Amino acid transport and metabolism
cg0505	0,85	0,04		putative ribosomal protein L7/L12 family	Translation, ribosomal structure and biogenesis
cg0506	0,22	0,02		ATP-binding protein of ABC transporter	General function prediction only
cg0507	0,18	0,00		permease of ABC transporter	General function prediction only
cg0508	0,19	0,00		secreted substrate-binding lipoprotein	General function prediction only
cg0510	0,46	0,01	<i>hemD</i>	hemD, uroporphyrinogen III synthase/methyltransferase	Transport and metabolism of further metabolites
cg0512	0,62	0,01	<i>hemB</i>	hemB, delta-aminolevulinic acid dehydratase	Transport and metabolism of further metabolites
cg0513	0,63	0,01		hypothetical membrane protein	Unknown function
cg0514	0,55	0,01		hypothetical membrane protein	Unknown function
cg0522	1,42	0,01	<i>ccsA</i>	ccsA, cytochrome c biogenesis protein, membrane protein	Transport and metabolism of further metabolites
cg0523	1,45	0,03		membrane protein required for cytochrome c biosynthesis	Transport and metabolism of further metabolites
cg0530	1,35	0,03		hypothetical protein cg0530	Unknown function
cg0532	0,64	0,05		putative glycosyltransferase	General function prediction only
cg0535	1,31	0,04		probable ketoglutarate semialdehyde dehydrogenase	Carbon source transport and metabolism
cg0536	1,87	0,04		putative 5-dehydro-4-deoxyglucarate dehydratase	Carbon source transport and metabolism

cg0537	2,61	0,01		putative transcriptional regulator lysr-type	signal transduction mechanisms
cg0550	1,47	0,03	<i>pepE2</i>	putative peptidase E   putative peptidase E	Protein turnover and chaperones
cg0551	0,64	0,01	<i>menC</i>	menC, O-succinylbenzoate synthase	Coenzyme transport and metabolism
cg0552	0,59	0,02	<i>menD</i>	menD, 2-oxoglutarate decarboxylase	Coenzyme transport and metabolism
cg0553	0,63	0,00		hypothetical protein cg0553	Unknown function
cg0554	0,84	0,05	<i>mgtA</i>	mgtA, alpha-mannosyltransferase (add mannose to GlcAGroAc2)	Cell wall/membrane/envelope biogenesis
cg0555	0,53	0,03		amino acid permease	Amino acid transport and metabolism
cg0559	0,60	0,02	<i>ispB</i>	ispB, putative octaprenyl-diphosphate synthase protein	Transport and metabolism of further metabolites
cg0563	0,37	0,01	<i>rplK</i>	rplK, 50S ribosomal protein L11	Translation, ribosomal structure and biogenesis
cg0564	0,41	0,00	<i>rplA</i>	rplA, 50S ribosomal protein L1	Translation, ribosomal structure and biogenesis
cg0569	29,82	0,00		cation-transporting ATPase	Carbon source transport and metabolism; Inorganic ion transport, metabolism, and storage
cg0570	8,16	0,00		putative dehydrogenase	General function prediction only
cg0571	12,37	0,00		hypothetical protein cg0571   hypothetical protein cg0571	Unknown function
cg0573	0,61	0,03	<i>rplL</i>	rplL, 50S ribosomal protein L7/L12	Translation, ribosomal structure and biogenesis
cg0579	1,47	0,02		transcriptional regulator	signal transduction mechanisms
cg0581	0,59	0,05	<i>rpsL</i>	rpsL, 30S ribosomal protein S12	Translation, ribosomal structure and biogenesis
cg0582	0,59	0,04	<i>rpsG</i>	rpsG, 30S ribosomal protein S7	Translation, ribosomal structure and biogenesis
cg0583	0,67	0,00	<i>fusA</i>	fusA, elongation factor EF-2	Translation, ribosomal structure and biogenesis
cg0587	0,59	0,00	<i>tuf</i>	tuf, elongation factor Tu	Translation, ribosomal structure and biogenesis
cg0588	0,92	0,04		hypothetical protein cg0588	Unknown function
cg0592	0,59	0,02		putative butyryl-CoA:acetate coenzyme A transferase	Carbon source transport and metabolism
cg0594	0,45	0,04	<i>rplC</i>	rplC, 50S ribosomal protein L3	Translation, ribosomal structure and biogenesis
cg0596	0,40	0,00	<i>rplD</i>	rplD, 50S ribosomal protein L4   rplD, 50S ribosomal protein L4	Translation, ribosomal structure and biogenesis
cg0597	0,50	0,00	<i>rplW</i>	rplW, 50S ribosomal protein L23	Translation, ribosomal structure and biogenesis
cg0598	0,55	0,03	<i>rplB</i>	rplB, 50S ribosomal protein L2	Translation, ribosomal structure and biogenesis
cg0599	0,50	0,01	<i>rpsS</i>	rpsS, 30S ribosomal protein S19	Translation, ribosomal structure and biogenesis
cg0600	0,42	0,01	<i>rplV</i>	rplV, 50S ribosomal protein L22	Translation, ribosomal structure and biogenesis
cg0601	0,50	0,00	<i>rpsC</i>	rpsC, 30S ribosomal protein S3	Translation, ribosomal structure and biogenesis
cg0602	0,60	0,01	<i>rplP</i>	rplP, 50S ribosomal protein L16	Translation, ribosomal structure and biogenesis
cg0603	0,46	0,00	<i>rpmC</i>	rpmC, 50S ribosomal protein L29	Translation, ribosomal structure and biogenesis
cg0604	0,51	0,04	<i>rpsQ</i>	rpsQ, 30S ribosomal protein S17	Translation, ribosomal structure and biogenesis
cg0606	2,40	0,00		hypothetical membrane protein	Unknown function
cg0607	3,88	0,00		hypothetical secreted protein	Unknown function
cg0608	0,43	0,01	<i>rplN</i>	rplN, 50S ribosomal protein L14	Translation, ribosomal structure and biogenesis
cg0609	0,42	0,01	<i>rplX</i>	rplX, 50S ribosomal protein L24	Translation, ribosomal structure and biogenesis
cg0610	0,41	0,01	<i>rplE</i>	rplE, 50S ribosomal protein L5	Translation, ribosomal structure and biogenesis
cg0611	0,62	0,00		secreted protein	Unknown function
cg0617	0,84	0,02		putative molybdopterin-guanine dinucleotide biosyn	Carbon source transport and metabolism
cg0620	0,49	0,01		secreted protein	Unknown function
cg0621	0,49	0,03	<i>cbrT</i>	substrate-specific component SCO2325 of predicted cobalamin ECF transporter	Coenzyme transport and metabolism

cg0622	0,36	0,00	<i>cbrU</i>	duplicated ATPase component SCO2324 of energizing module of predicted cobalamin ECF transporter	Coenzyme transport and metabolism
cg0623	0,29	0,00	<i>cbrV</i>	transmembrane component SCO2323 of energizing module of predicted cobalamin ECF transporter	Coenzyme transport and metabolism
cg0624	0,29	0,00		secreted oxidoreductase	General function prediction only
cg0625	0,37	0,00		secreted protein	Unknown function
cg0628	0,35	0,01	<i>rpsH</i>	rpsH, 30S ribosomal protein S8	Translation, ribosomal structure and biogenesis
cg0629	0,32	0,02	<i>rplF</i>	rplF, 50S ribosomal protein L6	Translation, ribosomal structure and biogenesis
cg0630	0,29	0,01	<i>rplR</i>	rplR, 50S ribosomal protein L18	Translation, ribosomal structure and biogenesis
cg0631	0,29	0,01	<i>rpsE</i>	rpsE, 30S ribosomal protein S5	Translation, ribosomal structure and biogenesis
cg0632	0,28	0,00	<i>rpmD</i>	rpmD, 50S ribosomal protein L30	Translation, ribosomal structure and biogenesis
cg0634	0,51	0,01	<i>rplO</i>	rplO, 50S ribosomal protein L15	Translation, ribosomal structure and biogenesis
cg0637	0,89	0,01	<i>creC (betB)</i>	betB, putative betaine aldehyde dehydrogenase (BADH) oxidoreductase	Carbon source transport and metabolism
cg0638	0,86	0,00	<i>creD</i>	HD superfamily hydrolase	Carbon source transport and metabolism
cg0639	0,80	0,04	<i>creE</i>	ferredoxin reductase	Carbon source transport and metabolism
cg0640	0,65	0,01	<i>creF (fdxB)</i>	fdxB, ferredoxin	Carbon source transport and metabolism
cg0641	0,69	0,02	<i>creG (fabG2)</i>	fabG2, probable short-chain dehydrogenase, secreted	Carbon source transport and metabolism
cg0644	0,68	0,01	<i>creI</i>	pyruvate phosphate dikinase, PEP/pyruvate binding	Carbon source transport and metabolism
cg0647	2,83	0,00	<i>secY</i>	secY, preprotein translocase SecY	Protein secretion
cg0648	1,78	0,01	<i>adk</i>	adk, adenylate kinase	Nucleotide transport and metabolism
cg0650	0,73	0,01		secreted protein	Unknown function
cg0651	0,67	0,02	<i>infA</i>	infA, translation initiation factor IF-1	Translation, ribosomal structure and biogenesis
cg0653	0,55	0,04	<i>rpsK</i>	rpsK, 30S ribosomal protein S11	Translation, ribosomal structure and biogenesis
cg0654	0,57	0,03	<i>rpsD</i>	rpsD, 30S ribosomal protein S4	Translation, ribosomal structure and biogenesis
cg0655	0,45	0,02	<i>rpoA</i>	rpoA, DNA-directed RNA polymerase alpha subunit	Transcription including sigma factors, RNA processing and modification
cg0656	0,51	0,03	<i>rplQ</i>	rplQ, 50S ribosomal protein L17	Translation, ribosomal structure and biogenesis
cg0658	0,60	0,01	<i>rptA</i>	rptA, terminal Rhannopyranosyltransferase	Cell wall/membrane/envelope biogenesis
cg0659	0,77	0,02		acetyltransferase, GNAT family	General function prediction only
cg0661	0,38	0,03		hypothetical protein cg0661	Unknown function
cg0662	2,07	0,01		FAD/FMN-containing dehydrogenase	General function prediction only
cg0672	0,70	0,03		hypothetical protein cg0672	Unknown function
cg0673	0,35	0,01	<i>rplM</i>	rplM, 50S ribosomal protein L13	Translation, ribosomal structure and biogenesis
cg0674	0,34	0,01	<i>rpsI</i>	rpsI, 30S ribosomal protein S9	Translation, ribosomal structure and biogenesis
cg0675	0,43	0,00	<i>mrsA</i>	mrsA, phosphoglucosamine mutase / phosphoacetylglucosami	Cell wall/membrane/envelope biogenesis
cg0678	0,46	0,03		hypothetical protein cg0678   hypothetical protein cg0678	Unknown function
cg0679	0,57	0,03		hypothetical protein cg0679	Unknown function
cg0681	0,78	0,01	<i>alr</i>	alr, alanine racemase	Amino acid transport and metabolism; Cell wall/membrane/envelope biogenesis
cg0682	0,55	0,00		ATPase or kinase	General function prediction only
cg0683	0,50	0,03		permease	General function prediction only
cg0684	0,48	0,00	<i>papA</i>	papA, prolyl aminopeptidase A	Protein turnover and chaperones
cg0685	0,41	0,00		homolog of metal-dependent protease, putative molecular chaperone	Protein turnover and chaperones
cg0686	0,40	0,00		acetyltransferase, GNAT family	General function prediction only
cg0687	0,64	0,00	<i>gcp</i>	gcp, probable O-sialoglycoprotein endopeptidase	Carbon source transport and metabolism; Amino acid transport and metabolism
cg0688	0,61	0,02		hypothetical protein cg0688	Unknown function
cg0689	0,41	0,00		hypothetical protein cg0689	Unknown function
cg0690	2,82	0,01	<i>groES</i>	groES, chaperonin 10 Kd subunit	Protein turnover and chaperones

cg0691	2,58	0,03	<i>groEL</i>	groEL, 60 KDA chaperonin (protein CPN60) (HSP60)-N-terminal fragment	Protein turnover and chaperones
cg0692	0,81	0,02	<i>tnp1c</i>	tnp1c(ISCg1c), transposase	DNA replication, recombination, repair, and degradation
cg0693	2,44	0,02	<i>groEL</i>	groEL, 60 KDA chaperonin (protein CPN60) (groEL protein) C-terminal fragment   groEL, 60 KDA chaperonin (protein CPN60) (groEL protein) C-terminal fragment   groEL, 60 KDA chaperonin (protein CPN60) (groEL protein) C-terminal fragment	Protein turnover and chaperones
cg0696	1,85	0,02	<i>sigD</i>	sigD, RNA polymerase sigma-70 factor	Transcription including sigma factors, RNA processing and modification
cg0697	1,23	0,05		hypothetical protein cg0697	Unknown function
cg0699	0,61	0,03	<i>guaB2</i>	guaB2, inositol-5-monophosphate dehydrogenase	Carbon source transport and metabolism
cg0700	0,60	0,01	<i>guaB3</i>	guaB3, inositol-5-monophosphate dehydrogenase	Carbon source transport and metabolism
cg0704	2,04	0,00		hypothetical protein cg0704	Unknown function
cg0705	1,34	0,03		hypothetical protein predicted by Glimmer	Unknown function
cg0706	2,84	0,00		conserved hypothetical membrane protein	Unknown function
cg0710	0,72	0,03		membrane protein	Unknown function
cg0711	0,54	0,02		membrane protein	Unknown function
cg0712	0,41	0,00		secreted protein	Unknown function
cg0713	2,13	0,00		hypothetical protein cg0713	Unknown function
cg0715	0,46	0,02		secreted protein	Unknown function
cg0717	1,46	0,04	<i>crtEb (ubiA)</i>	crtEb, hypothetical protein cg0717	Transport and metabolism of further metabolites
cg0719	2,08	0,04	<i>crtYe</i>	crtYe, C50 carotenoid epsilon cyclase	Transport and metabolism of further metabolites
cg0720	2,38	0,01	<i>crtI</i>	crtI2, phytoene dehydrogenase (desaturase)	Transport and metabolism of further metabolites
cg0721	2,92	0,01	<i>crtB</i>	crtB2, phytoene synthetase   crtB2, phytoene synthetase	Transport and metabolism of further metabolites
cg0722	3,29	0,00		drug exporter, RND superfamily	Transport and metabolism of further metabolites
cg0723	3,65	0,01	<i>crtE</i>	crtE, geranylgeranyl-pyrophosphate synthase	Transport and metabolism of further metabolites
cg0726	1,66	0,02		secreted lipoprotein	Unknown function
cg0728	0,38	0,00	<i>phr</i>	phr, deoxyribodipyrimidine photolyase	DNA replication, recombination, repair, and degradation
cg0730	0,65	0,03		glycosyl transferase	General function prediction only
cg0733	0,70	0,03		putative ABC transporter ATP-binding protein	General function prediction only
cg0735	0,76	0,04	<i>metI</i>	ABC transporter, transmembrane component	Amino acid transport and metabolism
cg0737	0,63	0,01	<i>metQ</i>	ABC-type transport system, secreted lipoprotein component	Amino acid transport and metabolism
cg0738	3,11	0,02	<i>dnaE2</i>	dnaE2, DNA polymerase III subunit alpha   dnaE2, DNA polymerase III subunit alpha	DNA replication, recombination, repair, and degradation
cgU/39	1,32	0,02		putative integral membrane protein	Unknown function
cg0741	1,35	0,02	<i>mntR</i>	sirR, iron repressor protein	signal transduction mechanisms
cg0742	0,60	0,00		putative integral membrane protein	Unknown function
cg0745	0,60	0,00		NAD-dependent deacetylase	General function prediction only
cg0747	0,58	0,01		cytidine and deoxycytidylate deaminase	Nucleotide transport and metabolism
cg0749	0,62	0,01	<i>spoU</i>	spoU, putative tRNA/rRNA methyltransferase protein	Translation, ribosomal structure and biogenesis
cg0751	0,69	0,02		membrane protein	Unknown function
cg0752	1,89	0,02		putative secreted or membrane protein   putative secreted or membrane protein	Unknown function
cg0753	4,29	0,00		secreted protein	Unknown function
cg0754	4,88	0,00	<i>metA (metX)</i>	metA, homoserine O-acetyltransferase	Amino acid transport and metabolism
cg0755	2,63	0,01	<i>metY</i>	metY, O-acetylhomoserine sulphydrylase	Amino acid transport and metabolism
cg0758	0,50	0,01		hypothetical protein predicted by Glimmer	Unknown function
cg0759	0,28	0,01	<i>prpD2</i>	prpD2, 2-methylcitrate dehydratase	Carbon source transport and metabolism
cg0760	0,25	0,01	<i>prpB2</i>	prpB2, 2-methylisocitrate lyase	Carbon source transport and metabolism
cg0762	0,26	0,02	<i>prpC2</i>	prpC2, 2-methylcitrate synthase	Carbon source transport and metabolism
cg0764	1,62	0,02		putative GntR-family transcriptional regulator	signal transduction mechanisms
cg0765	2,45	0,00		secreted protein	Unknown function
cg0766	1,58	0,02	<i>icd</i>	icd, isocitrate dehydrogenase	Central carbon metabolism
cg0772	1,50	0,01		sugar efflux permease	Carbon source transport and metabolism

cg0773	1,09	0,04		putative exodeoxyribonuclease	DNA replication, recombination, repair, and degradation
cg0774	0,65	0,01		membrane protein	Unknown function
cg0776	0,59	0,03		secreted siderophore-binding lipoprotein	Inorganic ion transport, metabolism, and storage; Transport and metabolism of further metabolites
cg0777	0,87	0,04		siderophore ABC transporter, ATP-binding protein	Inorganic ion transport, metabolism, and storage; Transport and metabolism of further metabolites
cg0779	0,58	0,03	<i>trpS</i>	trpS, tryptophanyl-tRNA synthetase   trpS, tryptophanyl-tRNA synthetase	Translation, ribosomal structure and biogenesis
cg0780	1,63	0,02		membrane protein ribonuclease BN-like family	General function prediction only
cg0782	0,63	0,01	<i>pbp4 (dac)</i>	dac, D-alanyl-D-alanine carboxypeptidase	Cell wall/membrane/envelope biogenesis
cg0783	0,59	0,00		hypothetical protein cg0783	Unknown function
cg0786	0,47	0,02	<i>upp</i>	upp, uracil phosphoribosyltransferase	Nucleotide transport and metabolism
cg0787	0,37	0,00		transcriptional regulator	signal transduction mechanisms
cg0788	1,77	0,01	<i>pmmB</i>	pmmB, phosphoglucomutase/phosphomannomutase	Carbon source transport and metabolism
cg0791	0,31	0,00	<i>pyc</i>	pyc, pyruvate carboxylase	Central carbon metabolism
cg0792	0,34	0,00		thioredoxin domain-containing protein	Unknown function
cg0795	0,52	0,01		FAD-dependent pyridine nucleotide-disulphide oxidoreductase	Inorganic ion transport, metabolism, and storage
cg0797	0,53	0,03	<i>prpB1</i>	prpB1, 2-methylisocitrate lyase	Carbon source transport and metabolism
cg0798	0,70	0,01	<i>prpC1</i>	prpC1, 2-methylcitrate synthase	Carbon source transport and metabolism
cg0800	2,00	0,00	<i>prpR</i>	transcriptional regulator, MerR family	signal transduction mechanisms
cg0801	0,72	0,01		hypothetical protein cg0801	Unknown function
cg0803	0,50	0,01	<i>thtR</i>	thtR, thiosulfate sulfurtransferase	Inorganic ion transport, metabolism, and storage
cg0808	0,51	0,01	<i>wbpC</i>	wbpC, lipopolysaccharide biosynthesis acyltransferase, m	Cell wall/membrane/envelope biogenesis
cg0809	0,75	0,03	<i>maf</i>	maf, Maf-like protein   maf, Maf-like protein   maf, Maf-like protein	Cell division, chromosome partitioning
cg0810	0,55	0,03	<i>accE</i>	hypothetical protein cg0810	Lipid transport and metabolism
cg0811	0,55	0,02	<i>dtsR2 (accD2)</i>	dtsR2, acetyl/propionyl CoA carboxylase, beta subunit   dtsR2, acetyl/propionyl CoA carboxylase, beta subunit	Cell wall/membrane/envelope biogenesis
cg0814	1,53	0,01	<i>birA</i>	birA, biotin--protein ligase	Coenzyme transport and metabolism
cg0815	0,67	0,00		membrane protein	Unknown function
cg0821	0,66	0,01		hypothetical protein cg0821	Unknown function
cg0822	0,75	0,02		hypothetical protein cg0822	Unknown function
cg0824	0,73	0,04	<i>tnp5a</i>	tnp5a(ISCg5a), transposase	DNA replication, recombination, repair, and degradation
cg0828	1,48	0,00		putative dihydrofolate reductase	Coenzyme transport and metabolism
cg0829	1,42	0,00		lactoylglutathione lyase or related lyase	General function prediction only
cg0830	0,79	0,01		membrane protein	Unknown function
cg0831	0,56	0,02	<i>tusG</i>	tusG, sugar ABC transporter, permease protein	Carbon source transport and metabolism
cg0832	0,48	0,00	<i>tusF</i>	tusF, ABC transporter, membrane spanning protein, trehalose uptake system	Carbon source transport and metabolism
cg0833	0,42	0,00		putative membrane protein, involved in trehalose uptake system	Carbon source transport and metabolism
cg0834	0,34	0,02	<i>tusE</i>	tusE, bacterial extracellular solute-binding protein, trehalose uptake system	Carbon source transport and metabolism
cg0835	0,65	0,00	<i>tusK (msiK2)</i>	tusK, ABC-type sugar transport systems, trehalose uptake system	Carbon source transport and metabolism
cg0837	0,36	0,03		hypothetical protein cg0837	Unknown function
cg0838	0,22	0,01		putative helicase	DNA replication, recombination, repair, and degradation
cg0839	0,30	0,01		hypothetical protein cg0839	Unknown function
cg0841	0,31	0,02		hypothetical protein cg0841	Unknown function
cg0842	0,39	0,01		putative DNA helicase	DNA replication, recombination, repair, and degradation
cg0843	0,45	0,02		putative helicase	DNA replication, recombination, repair, and degradation
cg0844	0,45	0,01		type II restriction enzyme, methylase subunit   type II restriction enzyme, methylase subunit	DNA replication, recombination, repair, and degradation
cg0845	0,49	0,00		putative superfamily II DNA/RNA helicase, SNF2 family	DNA replication, recombination, repair, and degradation

cg0847	0,74	0,03	<i>lcpA</i>	putative transcriptional regulator	Cell wall/membrane/envelope biogenesis
cg0848	0,74	0,04	<i>wbbL</i>	wbbL, putative rhamnosyl transferase WbbL	Cell wall/membrane/envelope biogenesis
cg0849	0,59	0,04	<i>manC (rmlA2)</i>	rmlA2, GDP-mannose pyrophosphorylase	Cell wall/membrane/envelope biogenesis
cg0850	0,59	0,00	<i>whcD (whiB2)</i>	whiB2, transcription factor whiB	signal transduction mechanisms
cg0851	0,77	0,01		hypothetical protein cg0851	Unknown function
cg0853	0,63	0,02		hypothetical protein cg0853	Unknown function
cg0854	1,48	0,05	<i>manB (pmmA)</i>	pmmA, phosphomannomutase	Carbon source transport and metabolism
cg0859	0,40	0,00		hypothetical protein cg0859	Unknown function
cg0860	0,45	0,01	<i>sahH</i>	sahH, S-adenosyl-L-homocysteine hydrolase	Amino acid transport and metabolism
cg0861	0,35	0,00	<i>tmk</i>	tmk, thymidylate kinase	Nucleotide transport and metabolism
cg0862	0,76	0,04	<i>mtrA</i>	mtrA, response regulator	Signal transduction mechanisms; Cell wall/membrane/envelope biogenesis
cg0864	0,76	0,01	<i>mtrB</i>	mtrB, signal transduction histidine kinase	Signal transduction mechanisms; Cell wall/membrane/envelope biogenesis
cg0871	0,87	0,01		hypothetical protein cg0871	Unknown function
cg0876	1,91	0,01	<i>sigH</i>	sigH, RNA polymerase sigma-70 factor	Transcription including sigma factors, RNA processing and modification
cg0877	2,03	0,00	<i>rshA</i>	putative anti-sigma factor	Transcription including sigma factors, RNA processing and modification
cg0878	4,17	0,01	<i>whcE (whiB1)</i>	whcE, positive role in survival under (heat and oxidative) stress	Signal transduction mechanisms
cg0879	2,73	0,00		membrane protein	Unknown function
cg0880	1,55	0,01		secreted protein	Unknown function
cg0881	1,57	0,02	<i>rhIE</i>	rhIE, probable ATP-dependent RNA helicase protein	Transcription including sigma factors, RNA processing and modification
cg0882	1,13	0,00		hypothetical protein cg0882	Unknown function
cg0885	0,40	0,02		helicase, UvrD/Rep family	General function prediction only
cg0886	0,39	0,00		probable DNA helicase II protein   probable DNA helicase II protein	General function prediction only
cg0887	0,41	0,01	<i>cgIK</i>	cgIK, major potassium uptake system	Inorganic ion transport, metabolism, and storage
cg0888	0,51	0,02		NTP pyrophosphohydrolase	General function prediction only
cg0889	0,48	0,00		putative DNA helicase RecQ	DNA replication, recombination, repair, and degradation
cg0892	3,30	0,01		hypothetical protein cg0892	Unknown function
cg0894	0,73	0,01		conserved hypothetical protein, possibly secreted	Unknown function
cg0895	0,63	0,02		hypothetical protein cg0895	Unknown function
cg0896	1,24	0,05		hypothetical protein cg0896	Unknown function
cg0897	1,74	0,01	<i>pdxR</i>	pdxR, pyridoxine biosynthesis transcriptional regulator, aminotransferase	Signal transduction mechanisms
cg0898	0,85	0,01	<i>pdxS</i>	pdxS, pyridoxine biosynthesis enzyme	Coenzyme transport and metabolism
cg0899	0,52	0,00	<i>pdxT</i>	pdxT, pyridoxine biosynthesis enzyme	Coenzyme transport and metabolism
cg0903	0,79	0,01		hypothetical protein cg0903   hypothetical protein cg0903	Unknown function
cg0905	0,77	0,03	<i>psp2</i>	psp2, putative secreted protein	Unknown function
cg0906	1,80	0,00		hypothetical protein cg0906   hypothetical protein cg0906	Unknown function
cg0907	3,02	0,01		hypothetical protein cg0907	Unknown function
cg0908	3,05	0,00		putative secreted protein	Unknown function
cg0909	3,39	0,00		hypothetical protein cg0909   hypothetical protein cg0909	Unknown function
cg0911	1,42	0,02		inositol monophosphatase	Carbon source transport and metabolism
cg0913	1,63	0,04	<i>prfB</i>	prfB, peptide chain release factor 2	Translation, ribosomal structure and biogenesis
cg0918	0,75	0,02		putative uroporphyrin-III C-methyltransferase	Transport and metabolism of further metabolites
cg0924	0,29	0,01		secreted siderophore-binding lipoprotein	Inorganic ion transport, metabolism, and storage; Transport and metabolism of further metabolites
cg0926	0,45	0,02		siderophore ABC transporter, permease protein	Inorganic ion transport, metabolism, and storage; Transport and metabolism of further metabolites
cg0927	0,38	0,01		siderophore ABC transporter, permease protein	Inorganic ion transport, metabolism, and storage; Transport and metabolism of further metabolites
cg0928	0,53	0,02		siderophore ABC transporter, ATP-binding protein	Inorganic ion transport, metabolism, and storage; Transport and metabolism of further metabolites
cg0932	3,34	0,01		membrane protein	Unknown function



cg0933	2,65	0,02		DNA or RNA helicase of superfamily II   DNA or RNA helicase of superfamily II	General function prediction only
cg0936	0,54	0,04	<i>rpf1</i>	rpf1, resuscitation promoting factor	Cell wall/membrane/envelope biogenesis
cg0939	0,67	0,05		secreted protein	Unknown function
cg0944	0,67	0,01		xanthine/uracil permeases family	Nucleotide transport and metabolism
cg0949	0,47	0,00	<i>gltA</i>	gltA, citrate synthase	Central carbon metabolism
cg0950	0,79	0,03	<i>fkpA</i>	fkpA, probable FKBP-type peptidyl-prolyl cis-trans isomerase	Protein turnover and chaperones
cg0952	0,37	0,00	<i>mctB</i>	putative integral membrane protein	Unknown function
cg0953	0,35	0,00	<i>mctC</i>	mctC, monocarboxylic acid transporter	Carbon source transport and metabolism
cg0957	1,40	0,01	<i>fas-IB</i>	fas-IB, fatty acid synthase   fas-IB, fatty acid synthase	Lipid transport and metabolism
cg0958	0,35	0,00		secreted protein	Unknown function
cg0960	0,44	0,00		hypothetical protein predicted by Glimmer	Unknown function
cg0961	0,39	0,01		homoserine O-acetyltransferase	Amino acid transport and metabolism
cg0962	3,08	0,01		secreted protein	Unknown function
cg0964	2,04	0,01	<i>mrx1</i>	glutaredoxin or related protein	Transport and metabolism of further metabolites
cg0965	2,33	0,00	<i>folA</i>	folA, dihydrofolate reductase	Coenzyme transport and metabolism
cg0966	2,78	0,00	<i>thyA</i>	thyA, thymidylate synthase	Nucleotide transport and metabolism
cg0967	2,35	0,00	<i>cysQ</i>	cysQ, 3-phosphoadenosine 5-phosphosulfate (PAPS) 3-phosphatase	Amino acid transport and metabolism; Inorganic ion transport, metabolism, and storage
cg0968	0,66	0,01		putative ATP-dependent helicase	General function prediction only
cg0970	2,78	0,01		membrane protein	Unknown function
cg0972	0,74	0,02	<i>cynX</i>	cyanate permease	Inorganic ion transport, metabolism, and storage
cg0973	0,51	0,00	<i>pgi</i>	pgi, glucose-6-phosphate isomerase	Central carbon metabolism
cg0974	0,76	0,03		hypothetical protein cg0974	Unknown function
cg0975	1,47	0,05		chorismate mutase	Amino acid transport and metabolism
cg0976	0,57	0,01	<i>pcrA</i>	pcrA, ATP-dependent helicase PCRA	General function prediction only
cg0977	0,76	0,03		ABC-type transport system, involved in lipoprotein release, permease component   ABC-type transport system, involved in lipoprotein release, permease component	Protein secretion
cg0979	1,38	0,00		transcriptional regulator PadR-like family	Signal transduction mechanisms
cg0982	0,49	0,00		membrane protein	Unknown function
cg0983	0,51	0,00	<i>purN</i>	purN, phosphoribosylglycinamide formyltransferase	Nucleotide transport and metabolism
cg0985	0,61	0,01	<i>citE</i>	citE, citryl-CoA lyase beta subunit homolog	Carbon source transport and metabolism
cg0986	0,62	0,00	<i>amtR</i>	amtR, master regulator of nitrogen control	Signal transduction mechanisms
cg0987	0,57	0,03		hypothetical protein cg0987	Unknown function
cg0988	0,47	0,02	<i>rpsR</i>	rpsR, 30S ribosomal protein S18	Translation, ribosomal structure and biogenesis
cg0989	0,47	0,00	<i>rpsN</i>	rpsN, 30S ribosomal protein S14   rpsN, 30S ribosomal protein S14	Translation, ribosomal structure and biogenesis
cg0990	0,44	0,00	<i>rpmG</i>	rpmG, 50S ribosomal protein L33	Translation, ribosomal structure and biogenesis
cg0991	0,66	0,04	<i>rpmB</i>	rpmB, 50S ribosomal protein L28	Translation, ribosomal structure and biogenesis
cg0992	0,65	0,02	<i>sutP</i>	sulfate permease or related transporter (MFS superfamily)	Inorganic ion transport, metabolism, and storage
cg0994	0,61	0,01	<i>rpmE</i>	rpmE, 50S ribosomal protein L31	Translation, ribosomal structure and biogenesis
cg0995	0,61	0,00	<i>rpmF</i>	rpmF, 50S ribosomal protein L32	Translation, ribosomal structure and biogenesis
cg0996	1,29	0,01	<i>cgtR2</i>	cgtR2, putative two component response regulator	Signal transduction mechanisms
cg0998	2,24	0,00	<i>pepD</i>	trypsin-like serine protease	Protein turnover and chaperones
cg1000	1,48	0,04		hypothetical protein cg1000	Unknown function
cg1001	0,33	0,03	<i>mscL</i>	mscL, large conductance mechanosensitive channel	Carbon source transport and metabolism; Inorganic ion transport, metabolism, and storage
cg1005	1,21	0,04	<i>moeA2</i>	moeA2, molybdenum cofactor biosynthesis protein	Coenzyme transport and metabolism
cg1006	1,06	0,01	<i>act1</i>	acetyltransferase	General function prediction only
cg1007	0,64	0,00		hypothetical protein cg1007	Unknown function
cg1009	0,72	0,02		putative integral membrane transporter	Inorganic ion transport, metabolism, and storage
cg1010	1,31	0,04		hypothetical protein cg1010	Unknown function



cg1012	2,28	0,03	<i>cdaS</i>	cyclomaltodextrinase   cyclomaltodextrinase	Carbon source transport and metabolism
cg1014	0,88	0,00	<i>pmt</i>	pmt, glycosyltransferase	Cell wall/membrane/envelope biogenesis
cg1016	0,25	0,00	<i>betP</i>	betP, glycine betaine transporter	Transport and metabolism of further metabolites
cg1018	0,33	0,00		probable ATP-dependent DNA helicase protein   probable ATP-dependent DNA helicase protein	General function prediction only
cg1019	0,80	0,00		predicted metal-dependent hydrolase	General function prediction only
cg1022	1,67	0,04	<i>tnp6a</i>	tnp6a(ISCg6a), transposase	DNA replication, recombination, repair, and degradation
cg1027	1,69	0,02	<i>dld</i>	dld, D-lactate dehydrogenase	Carbon source transport and metabolism; Respiration and oxidative phosphorylation
cg1032	1,24	0,04	<i>cadR</i>	bacterial regulatory protein, ArsR family	Signal transduction mechanisms
cg1037	0,27	0,00	<i>rfp2</i>	rfp2, resuscitation promoting factor	Cell wall/membrane/envelope biogenesis
cg1044	1,28	0,04		hypothetical protein cg1044	Unknown function
cg1046	0,38	0,00	<i>ppk2A (ppk2)</i>	ppk2A, polyphosphate kinase	Inorganic ion transport, metabolism, and storage
cg1048	0,69	0,01		haloacid dehalogenase/epoxide hydrolase family	Carbon source transport and metabolism
cg1049	0,42	0,02		enoyl-CoA hydratase	Carbon source transport and metabolism
cg1051	1,40	0,03		hypothetical protein cg1051   hypothetical protein cg1051	Unknown function
cg1055	0,39	0,01	<i>rraA (menG is cg0556)</i>	menG, ribonuclease activity regulator protein RraA   menG, ribonuclease activity regulator protein RraA	Transcription including sigma factors, RNA processing and modification
cg1056	0,60	0,04		hypothetical protein cg1056	Unknown function
cg1062	0,48	0,02	<i>urtB</i>	urtB, ABC-type urea uptake system, permease subunit	Transport and metabolism of further metabolites
cg1064	0,67	0,03	<i>urtC</i>	urtC, ABC-type urea uptake system, permease subunit	Transport and metabolism of further metabolites
cg1065	0,34	0,03	<i>urtD</i>	urtD, ABC-type urea uptake system	Transport and metabolism of further metabolites
cg1067	0,85	0,05	<i>pth2</i>	pth2, peptidyl-tRNA hydrolase	Translation, ribosomal structure and biogenesis
cg1068	1,31	0,05		probable oxidoreductase	General function prediction only
cg1069	0,49	0,01	<i>gapB (gapX)</i>	gapX, glyceraldehyde-3-phosphate dehydrogenase	Central carbon metabolism
cg1070	0,69	0,00		hypothetical protein cg1070	Unknown function
cg1072	0,58	0,02	<i>rplY</i>	rplY, 50S ribosomal protein L25	Translation, ribosomal structure and biogenesis
cg1073	5,40	0,00		predicted lactoylglutathione lyase   predicted lactoylglutathione lyase	Transport and metabolism of further metabolites
cg1074	0,60	0,00		hypothetical protein cg1074	Unknown function
cg1075	0,54	0,02	<i>prsA</i>	prsA, ribose-phosphate pyrophosphokinase	Amino acid transport and metabolism; Nucleotide transport and metabolism; Coenzyme transport and metabolism
cg1080	2,67	0,01		putative multicopper oxidase   putative multicopper oxidase	General function prediction only
cg1081	3,90	0,00		ABC-type multidrug transport system, ATPase component	General function prediction only
cg1082	3,56	0,00		hypothetical protein cg1082	Unknown function
cg1083	3,39	0,00	<i>cgtS10</i>	cgtS10, probable two component sensor kinase	Post-translational modification; Signal transduction mechanisms
cg1084	2,34	0,01	<i>cgtR10</i>	cgtR10, putative two component response regulator	Signal transduction mechanisms
cg1085	0,58	0,01		hypothetical protein cg1085	Unknown function
cg1087	0,72	0,01		hypothetical protein cg1087	Unknown function
cg1088	0,66	0,01		ABC-type multidrug/protein/lipid transport system, ATPase component	General function prediction only
cg1089	0,74	0,01		ABC-type multidrug/protein/lipid transport system, ATPase component	General function prediction only
cg1090	0,32	0,00	<i>ggtB</i>	ggtB, probable gamma-glutamyltranspeptidase precursor PR	Transport and metabolism of further metabolites
cg1094	1,40	0,01	<i>tnp3a</i>	tnp3a(ISCg3a), transposase	DNA replication, recombination, repair, and degradation
cg1095	1,86	0,03		hypothetical protein cg1095   hypothetical protein cg1095   hypothetical protein cg1095   hypothetical protein cg1095	Unknown function
cg1096	1,97	0,00		hypothetical protein cg1096	Unknown function

cg1097	0,82	0,04		hypothetical protein cg1097	Unknown function
cg1098	1,66	0,00		bacterial regulatory proteins, TetR family	Signal transduction mechanisms
cg1099	1,34	0,00	<i>mfd</i>	mfd, putative transcription-repair coupling factor	Transcription including sigma factors, RNA processing and modification
cg1100	2,13	0,00		ABC transporter transmembrane component	General function prediction only
cg1101	2,73	0,02		ABC-type multidrug/protein/lipid transport system, membrane component	General function prediction only
cg1103	2,33	0,00		hypothetical protein cg1103	Unknown function
cg1104	3,23	0,00		predicted esterase, membrane protein	General function prediction only
cg1105	1,56	0,02	<i>lysI</i>	lysI, L-lysine permease	Amino acid transport and metabolism
cg1107	0,66	0,05		predicted pyrophosphatase	General function prediction only
cg1108	0,44	0,01	<i>porC</i>	porC, putative secreted protein   porC, putative secreted protein	Unknown function
cg1109	0,46	0,01	<i>porB</i>	porB, anion-specific porin precursor	Inorganic ion transport, metabolism, and storage
cg1112	0,61	0,04		septum formation initiator, secreted protein	Cell division, chromosome partitioning
cg1117	0,89	0,04		hypothetical protein cg1117	Unknown function
cg1121	4,64	0,00		permease of the major facilitator superfamily	General function prediction only
cg1122	1,53	0,02		putative secreted protein	Unknown function
cg1123	1,92	0,03	<i>greA</i>	greA, transcription elongation factor GreA	Transcription including sigma factors, RNA processing and modification
cg1125	4,05	0,00		hypothetical protein cg1125	Unknown function
cg1127	1,40	0,02	<i>mca</i>	uncharacterized proteins, LmbE homolog	Transport and metabolism of further metabolites
cg1128	0,77	0,00		similar to ribosomal protein S2	Unknown function
cg1129	1,45	0,03	<i>aroF</i>	aroF, 3-deoxy-7-phosphoheptulonate synthase	Amino acid transport and metabolism
cg1132	0,65	0,05	<i>coaA</i>	coaA, pantothenate kinase	Coenzyme transport and metabolism
cg1135	0,80	0,03	<i>pabC</i>	branched-chain amino acid aminotransferase/4-amino-4-deoxychorismate lyase	Amino acid transport and metabolism
cg1136	0,55	0,01		hypothetical protein cg1136   hypothetical protein cg1136	Unknown function
cg1139	0,51	0,00		allophanate hydrolase subunit 2	Transport and metabolism of further metabolites
cg1140	0,53	0,00		allophanate hydrolase subunit 1	Transport and metabolism of further metabolites
cg1141	0,61	0,00		hypothetical protein cg1141	Carbon source transport and metabolism
cg1142	0,48	0,00		Na <sup>+</sup> /proline, Na <sup>+</sup> /panthothenate symporter   Na <sup>+</sup> /proline, Na <sup>+</sup> /panthothenate symporter	Amino acid transport and metabolism; Coenzyme transport and metabolism
cg1143	0,76	0,04		putative GntR-family transcriptional regulator	Signal transduction mechanisms
cg1145	5,29	0,00	<i>fumC (fum)</i>	fumC, fumarate hydratase	Central carbon metabolism
cg1147	7,00	0,00	<i>ssuI</i>	ssuI, FMN-binding protein required for sulfonate and sulfonate ester utilization   ssuI, FMN-binding protein required for sulfonate and sulfonate ester utilization	Transport and metabolism of further metabolites
cg1150	2,63	0,01		NADPH-dependent FMN reductase   NADPH-dependent FMN reductase	General function prediction only
cg1151	4,50	0,00	<i>seuA</i>	seuA, monooxygenase for sulfonate ester utilization	Transport and metabolism of further metabolites
cg1152	3,20	0,02	<i>seuB</i>	seuB, monooxygenase for sulfonate ester utilization	Transport and metabolism of further metabolites
cg1153	3,66	0,00	<i>seuC</i>	seuC, monooxygenase for sulfonate ester utilization	Transport and metabolism of further metabolites
cg1156	6,64	0,00	<i>ssuD2</i>	ssuD2, monooxygenase for sulfonate utilization	Transport and metabolism of further metabolites
cg1157	3,08	0,00	<i>fbp</i>	fbp, class II, essential for gluconeogenesis	Central carbon metabolism
cg1158	1,22	0,00		putative secreted protein	Unknown function
cg1160	3,27	0,00		similar to arabinose efflux permease	Unknown function
cg1162	2,41	0,00	<i>xseB</i>	xseB, exodeoxyribonuclease VII small subunit	DNA replication, recombination, repair, and degradation
cg1163	2,81	0,01	<i>xseA</i>	xseA, exodeoxyribonuclease VII large subunit	DNA replication, recombination, repair, and degradation
cg1166	1,27	0,00		hypothetical protein cg1166	Unknown function
cg1167	0,29	0,01	<i>metS</i>	putative secreted protein	Amino acid transport and metabolism

cg1169	0,32	0,01	<i>metP</i>	Na <sup>+</sup> -dependent transporters of the SNF family   Na <sup>+</sup> -dependent transporters of the SNF family	Amino acid transport and metabolism
cg1170	0,54	0,01	<i>cmt5</i>	cmt5, corynomycyl transferase   cmt5, corynomycyl transferase	Cell wall/membrane/envelope biogenesis
cg1172	0,78	0,05		hypothetical protein cg1172	General function prediction only
cg1174	1,40	0,01	<i>arcB</i>	arcB, probable ornithine carbamoyltransferase protein   arcB, probable ornithine carbamoyltransferase protein	Amino acid transport and metabolism
cg1178	0,58	0,03	<i>tnp9a</i>	tnp9a(ISCg9a), transposase	DNA replication, recombination, repair, and degradation
cg1182	1,78	0,02		hypothetical protein cg1182	Unknown function
cg1183	1,55	0,02		predicted dinucleotide-utilizing enzyme	Unknown function
cg1184	1,40	0,02	<i>tnp10c</i>	tnp10c(ISCg10a), transposase-fragment	DNA replication, recombination, repair, and degradation
cg1185	1,55	0,04	<i>tnp10b</i>	tnp10b(ISCg10a), transposase-fragment	DNA replication, recombination, repair, and degradation
cg1187	5,59	0,00	<i>tnp10a</i>	tnp10a(ISCg10a), transposase-fragment	DNA replication, recombination, repair, and degradation
cg1189	1,91	0,03		hypothetical protein cg1189	Unknown function
cg1190	4,28	0,00		hypothetical protein cg1190	Unknown function
cg1191	0,77	0,01		hypothetical protein cg1191	Unknown function
cg1193	0,54	0,02		carboxymuconolactone decarboxylase	Carbon source transport and metabolism
cg1195	1,90	0,01		sulfate permease or related transporter (MFS superfamily)	General function prediction only
cg1197	0,46	0,00		ABC-type transport systems, involved in lipoprotein release, ATPase component	Cell wall/membrane/envelope biogenesis
cg1203	1,90	0,01		Mg-chelatase subunit ChII	Inorganic ion transport, metabolism, and storage
cg1205	2,02	0,00		hypothetical protein cg1205	Unknown function
cg1206	1,86	0,00		PEP phosphonmutase or related enzyme   PEP phosphonmutase or related enzyme	Transport and metabolism of further metabolites
cg1208	1,28	0,01		hypothetical protein cg1208	Unknown function
cg1211	1,74	0,02		putative MarR-family transcriptional regulator	Signal transduction mechanisms
cg1213	0,78	0,05	<i>tnp1a</i>	tnp1a(ISCg1a), transposase	DNA replication, recombination, repair, and degradation
cg1215	1,52	0,00	<i>nadC</i>	nadC, quinolinate phosphoribosyltransferase	Coenzyme transport and metabolism
cg1216	1,86	0,01	<i>nadA</i>	nadA, quinolinate synthetase	Coenzyme transport and metabolism
cg1218	4,35	0,01	<i>ndnR</i>	ndnR, transcriptional repressor of NAD de novo biosynthesis genes	Signal transduction mechanisms
cg1219	1,39	0,04		hypothetical protein cg1219	Unknown function
cg1220	2,77	0,00		predicted Zn-dependent hydrolase of the beta-lactamase fold	General function prediction only
cg1221	1,35	0,02		hypothetical protein cg1221	Unknown function
cg1222	1,67	0,00	<i>lplA</i>	lplA, lipote-protein ligase	Coenzyme transport and metabolism
cg1224	6,69	0,00	<i>phnB2</i>	phnB2, similarity to alkylphosphonate uptake operon protein PhnB-Escherichia coli	Transport and metabolism of further metabolites
cg1225	1,80	0,00	<i>benK3 (pcaK)</i>	benK3, putative benzoate transport transmembrane protein	Carbon source transport and metabolism
cg1226	0,36	0,00	<i>pobB (pobA)</i>	pobB, 4-hydroxybenzoate 3-monoxygenase   pobB, 4-hydroxybenzoate 3-monoxygenase	Carbon source transport and metabolism
cg1227	3,12	0,00	<i>ykoE</i>	ykoE, substrate-specific component YkoE of thiamin-regulated ECF transporter for hydroxymethylpyrimidine	Coenzyme transport and metabolism
cg1228	1,51	0,00	<i>ykoD</i>	ykoD, duplicated ATPase component YkoD of energizing module of thiamin-regulated ECF transporter for hydroxymethyl   ykoD, duplicated ATPase component YkoD of energizing module of thiamin-regulated ECF transporter for hydroxymethyl	Coenzyme transport and metabolism
cg1231	1,76	0,01	<i>chaA</i>	chaA, Ca <sup>2+</sup> /H <sup>+</sup> antiporter	Inorganic ion transport, metabolism, and storage
cg1232	2,20	0,00		hypothetical protein cg1232	Unknown function
cg1233	1,82	0,01		hypothetical protein cg1233	Unknown function
cg1234	1,81	0,02		putative excinuclease ATPase subunit-UvrA-like protein	DNA replication, recombination, repair, and degradation
cg1236	1,26	0,01	<i>tpx (prx)</i>	tpx, thiol peroxidase	Transport and metabolism of further metabolites

cg1237	0,39	0,03		hypothetical protein cg1237	Unknown function
cg1239	0,71	0,03		2-dehydropantoate 2-reductase	Coenzyme transport and metabolism
cg1241	1,24	0,05		hypothetical protein cg1241	Unknown function
cg1242	1,77	0,05		hypothetical protein cg1242	Unknown function
cg1243	2,97	0,00		secreted trypsin-like serine protease, contain C-terminal PDZ domain	General function prediction only
cg1244	2,65	0,02	<i>arsC4</i>	arsC4, arsenate reductase	Inorganic ion transport, metabolism, and storage
cg1245	2,33	0,04		hypothetical protein cg1245	Unknown function
cg1246	3,94	0,01		hypothetical protein cg1246	Unknown function
cg1247	3,95	0,00		putative secreted protein	Unknown function
cg1248	1,52	0,04		GTPase involved in stress response	General function prediction only
cg1249	1,67	0,00	<i>lpqW</i>	lpqW, homologue to Rv1166 lipoprotein required to channel PIM4 into LAM synthesis, cell envelope	Cell wall/membrane/envelope biogenesis
cg1250	1,36	0,04	<i>mshB</i>	mshB, deacetylase	Cell wall/membrane/envelope biogenesis
cg1251	1,44	0,00		hypothetical protein cg1251	Unknown function
cg1252	0,53	0,02	<i>fdxC</i>	fdxC, ferredoxin	Transport and metabolism of further metabolites
cg1253	0,56	0,00	<i>dapC</i>	dapC, N-succinyl-2,6-diaminopimelate aminotransferase	Amino acid transport and metabolism
cg1254	0,63	0,03		hypothetical protein cg1254	Unknown function
cg1255	5,11	0,01		putative HNH endonuclease, conserved	General function prediction only
cg1259	2,34	0,00	<i>dapD2</i>	dapD2, similar to tetrahydridipicolinate N-succinyltransferase	Amino acid transport and metabolism
cg1261	0,82	0,03		lysine decarboxylase family protein	Amino acid transport and metabolism
cg1264	4,08	0,00		hypothetical protein cg1264	Unknown function
cg1265	5,41	0,00		hypothetical protein cg1265	Unknown function
cg1266	5,75	0,00	<i>rrmA</i>	rrmA, rRNA guanine-N1-methyltransferase	Translation, ribosomal structure and biogenesis
cg1268	0,54	0,00	<i>glgA</i>	glgA, glycogen synthase   glgA, glycogen synthase	Carbon source transport and metabolism
cg1269	0,43	0,00	<i>glgC</i>	glgC, ADP-glucose pyrophosphorylase	Carbon source transport and metabolism
cg1271	3,26	0,00	<i>sigE</i>	sigE, RNA polymerase sigma-70 factor   sigE, RNA polymerase sigma-70 factor	Transcription including sigma factors, RNA processing and modification
cg1272	4,85	0,01	<i>cseE</i>	hypothetical protein cg1272	Transcription including sigma factors, RNA processing and modification
cg1273	5,24	0,00	<i>tatB</i>	tatB, sec-independent translocase	Protein secretion
cg1274	1,27	0,02	<i>mrp</i>	mrp, ATPase involved in chromosome partitioning	Cell division, chromosome partitioning
cg1275	2,16	0,01		hypothetical protein cg1275	Unknown function
cg1276	2,89	0,00	<i>mgtE1</i>	mgtE1, Mg/Co/Ni transporter MgtE (contains CBS domain) intracellular	Inorganic ion transport, metabolism, and storage
cg1277	6,31	0,00		hypothetical protein cg1277	Unknown function
cg1278	3,60	0,00		conserved hypothetical secreted protein	Unknown function
cg1280	0,70	0,04	<i>odhA</i>	odhA, 2-oxoglutarate dehydrogenase	Central carbon metabolism
cg1284	2,26	0,00	<i>lipT</i>	lipT, type B carboxylesterase	Lipid transport and metabolism
cg1285	1,40	0,02		hypothetical protein cg1285	Unknown function
cg1286	3,09	0,00		hypothetical protein cg1286	Unknown function
cg1287	0,42	0,01		hypothetical protein cg1287	Unknown function
cg1288	2,83	0,00		putative multidrug efflux permease of the major facilitator superfamily	General function prediction only
cg1290	0,19	0,02	<i>metE</i>	metE, 5-methyltetrahydropteroylglutamate--homocysteine methyltransferase	Amino acid transport and metabolism
cg1291	8,05	0,00		hypothetical protein cg1291   hypothetical protein cg1291	Unknown function
cg1292	0,34	0,01		flavin-containing monooxygenase 3	General function prediction only
cg1293	0,53	0,01		putative secreted protein	Unknown function
cg1295	2,35	0,01		predicted hydrolase or acyltransferase (alpha/beta hydrolase superfamily)	General function prediction only
cg1300	0,73	0,02	<i>cydB</i>	cydB, cytochrome D terminal oxidase polypeptide subunit	Respiration and oxidative phosphorylation
cg1304	0,49	0,02		putative secreted protein	Unknown function
cg1305	0,70	0,04	<i>pheP</i>	L-phenylalanine transporter	Amino acid transport and metabolism
cg1307	2,31	0,00		superfamily II DNA and RNA helicase   superfamily II DNA and RNA helicase   superfamily II DNA and RNA helicase	DNA replication, recombination, repair, and degradation; Transcription including sigma factors, RNA processing and modification
cg1310	0,76	0,02	<i>rolM (tfdF)</i>	tfdF, maleylacetate reductase	Carbon source transport and metabolism

cg1311	0,56	0,01	<i>rolD (catA2)</i>	catA2, catechol 1,2-dioxygenase   catA2, catechol 1,2-dioxygenase	Carbon source transport and metabolism
cg1313	0,41	0,02		putative secreted lipoprotein	Unknown function
cg1314	0,30	0,00	<i>putP</i>	putP, proline transport system	Amino acid transport and metabolism
cg1316	1,42	0,03		superfamily II DNA/RNA helicases, SNF2 family	DNA replication, recombination, repair, and degradation; Transcription including sigma factors, RNA processing and modification
cg1317	1,25	0,04		putative 2-oxo acid dehydrogenase	General function prediction only
cg1319	0,56	0,02		ATPase involved in DNA repair	DNA replication, recombination, repair, and degradation
cg1320	0,66	0,01	<i>lipP</i>	lipP, lipase	Lipid transport and metabolism
cg1325	1,64	0,00		putative stress-responsive transcriptional regulator	Signal transduction mechanisms
cg1328	1,97	0,02		putative copper chaperone	Protein turnover and chaperones
cg1329	2,28	0,04	<i>ctpC</i>	ctpC, cation transport ATPase	Inorganic ion transport, metabolism, and storage
cg1333	0,44	0,01	<i>argS</i>	argS, arginyl-tRNA synthetase	Translation, ribosomal structure and biogenesis
cg1334	0,36	0,00	<i>lysA</i>	lysA, diaminopimelate decarboxylase	Amino acid transport and metabolism
cg1335	0,62	0,02		hypothetical protein cg1335	Unknown function
cg1337	3,08	0,01	<i>hom</i>	hom, homoserine dehydrogenase	Amino acid transport and metabolism
cg1338	3,19	0,02	<i>thrB</i>	thrB, homoserine kinase	Amino acid transport and metabolism
cg1341	0,42	0,00	<i>narI</i>	narI, respiratory nitrate reductase 2 gamma chain	Respiration and oxidative phosphorylation
cg1342	0,38	0,00	<i>narJ</i>	narJ, nitrate reductase delta chain	Respiration and oxidative phosphorylation
cg1343	0,48	0,00	<i>narH</i>	narH, probable respiratory nitrate reductase oxidoreduct	Respiration and oxidative phosphorylation
cg1344	0,31	0,01	<i>narG</i>	narG, nitrate reductase 2, alpha subunit	Respiration and oxidative phosphorylation
cg1345	0,55	0,01	<i>narK</i>	narK, putative nitrate/nitrite transporter   narK, putative nitrate/nitrite transporter	Inorganic ion transport, metabolism, and storage
cg1346	0,53	0,03	<i>mog</i>	mog, putative molybdopterin biosynthesis MOG protein	Coenzyme transport and metabolism
cg1347	0,66	0,02		secreted phospholipid phosphatase	Cell wall/membrane/envelope biogenesis
cg1349	1,32	0,02		membrane protein containing CBS domain	Unknown function
cg1351	0,71	0,03	<i>moeA3</i>	moeA3, molybdopterin biosynthesis protein	Coenzyme transport and metabolism
cg1352	2,98	0,01	<i>moaA</i>	moaA, molybdenum cofactor biosynthesis protein A	Coenzyme transport and metabolism
cg1354	0,66	0,02	<i>rho</i>	rho, transcription termination factor Rho	Transcription including sigma factors, RNA processing and modification
cg1355	0,58	0,00	<i>prfA</i>	prfA, peptide chain release factor 1	Translation, ribosomal structure and biogenesis
cg1359	0,80	0,01		membrane protein, UDP-N-acetyl(muramyl) pentapeptide phosphotransferase/UDP-N-acetylglucosamine-1-pho	Cell wall/membrane/envelope biogenesis
cg1360	0,63	0,03		hypothetical protein cg1360	Unknown function
cg1361	1,52	0,01	<i>atpI</i>	hypothetical protein cg1361	Inorganic ion transport, metabolism, and storage
cg1362	0,88	0,00	<i>atpB</i>	atpB, ATP synthase subunit A	Respiration and oxidative phosphorylation
cg1368	0,70	0,03	<i>atpD</i>	atpD, ATP synthase subunit B	Respiration and oxidative phosphorylation
cg1372	0,55	0,02		hypothetical protein cg1372	Unknown function
cg1373	0,34	0,01		glyoxalase/bleomycin resistance/dioxygenase superfamily protein	General function prediction only
cg1375	0,83	0,03		putative thioredoxin	General function prediction only
cg1376	2,20	0,01	<i>ssuD1</i>	ssuD1, alkanesulfonate monooxygenase	Transport and metabolism of further metabolites
cg1377	3,12	0,00	<i>ssuC</i>	ssuC, aliphatic sulfonates transmembrane ABC transporterprotein	Transport and metabolism of further metabolites
cg1379	2,97	0,00	<i>ssuB</i>	ssuB, aliphatic sulfonates ATP-binding ABC transporterprotein	Transport and metabolism of further metabolites
cg1380	2,35	0,01	<i>ssuA</i>	ssuA, aliphatic sulfonate binding protein	Transport and metabolism of further metabolites
cg1381	0,80	0,04	<i>glgB</i>	glgB, glycogen branching enzyme	Carbon source transport and metabolism
cg1383	0,57	0,01		ABC-type molybdenum transport system, ATPase component	Coenzyme transport and metabolism
cg1384	1,63	0,02		putative NUDIX hydrolase	General function prediction only
cg1385	0,77	0,01		SAM-dependent methyltransferase	General function prediction only
cg1386	2,53	0,01	<i>etfB (fixA)</i>	fixA, putative electron transfer flavoprotein, beta subunit   fixA, putative electron transfer flavoprotein, beta subunit	Respiration and oxidative phosphorylation

cg1387	2,16	0,02	<i>etfA (fixB)</i>	fixB, putative electron transfer flavoprotein, alpha subunit	Respiration and oxidative phosphorylation
cg1388	1,48	0,03	<i>nifS1</i>	nifS1, probable pyridoxal-phosphate-dependent aminotransferase/cysteine desulfurase	Amino acid transport and metabolism
cg1391	1,28	0,02		uncharacterized protein related to capsule biosynthesis enzyme	General function prediction only
cg1394	1,61	0,01	<i>speE2</i>	putative spermidine synthase   putative spermidine synthase	Transport and metabolism of further metabolites
cg1395	1,93	0,01		hypothetical protein cg1395   hypothetical protein cg1395	Unknown function
cg1396	3,37	0,00		hypothetical protein cg1396	Unknown function
cg1397	1,71	0,02	<i>trmU</i>	tRNA (5-methylaminomethyl-2-thiouridylate)-methyltransferase	Translation, ribosomal structure and biogenesis
cg1398	1,27	0,02		hypothetical protein cg1398	Unknown function
cg1399	0,71	0,01		permease of the major facilitator superfamily	General function prediction only
cg1400	0,33	0,00		DNA polymerase III subunit epsilon	DNA replication, recombination, repair, and degradation
cg1404	0,86	0,04	<i>gatA</i>	gatA, glutamyl-tRNA amidotransferase subunit A	Translation, ribosomal structure and biogenesis
cg1409	1,24	0,04	<i>pfkA (pfk)</i>	pfkA, 6-phosphofructokinase	Central carbon metabolism
cg1410	0,68	0,02	<i>rbsR</i>	rbsR, transcriptional repressor of ribose transport	Signal transduction mechanisms
cg1411	0,40	0,01	<i>rbsA</i>	ABC-type sugar (aldose) transport system, ATPase component	Carbon source transport and metabolism
cg1412	0,52	0,01	<i>rbsC</i>	ribose/xylose/arabinose/galactoside ABC-type transport system, permease component	Carbon source transport and metabolism
cg1413	0,43	0,01	<i>rbsB</i>	secreted sugar-binding protein	Carbon source transport and metabolism
cg1414	0,41	0,00	<i>rbsD</i>	uncharacterized component of ribose/xylose transport systems	Carbon source transport and metabolism
cg1417	2,67	0,00	<i>act2</i>	acetyltransferase	General function prediction only
cg1420	1,54	0,00	<i>gatB</i>	gatB, aspartyl/glutamyl-tRNA amidotransferase subunit B	Translation, ribosomal structure and biogenesis
cg1421	2,00	0,00		putative dinucleotide-binding enzyme	General function prediction only
cg1423	2,57	0,00		putative oxidoreductase (related to aryl-alcohol dehydrogenase)   putative oxidoreductase (related to aryl-alcohol dehydrogenase)	General function prediction only
cg1426	1,74	0,01	<i>gst</i>	putative glutathione S-transferase   putative glutathione S-transferase	Transport and metabolism of further metabolites
cg1434	2,22	0,02	<i>yggB (mscCG)</i>	yggB, small-conductance mechanosensitive channel   yggB, small-conductance mechanosensitive channel   yggB, small-conductance mechanosensitive channel	Amino acid transport and metabolism
cg1444	0,48	0,00		putative flavoprotein oxygenase	General function prediction only
cg1452	1,34	0,00		hypothetical protein cg1452	Unknown function
cg1456	0,77	0,04		predicted signal-transduction protein containing cAMP-binding and CBS domain	Signal transduction mechanisms
cg1457	0,34	0,01	<i>dnaQ2</i>	dnaQ2, DNA polymerase III, epsilon subunit, putative	DNA replication, recombination, repair, and degradation
cg1458	0,49	0,00	<i>odx</i>	odx, oxaloacetate decarboxylase	Central carbon metabolism
cg1459	0,61	0,03		SAM-dependent methyltransferase   SAM-dependent methyltransferase   SAM-dependent methyltransferase	General function prediction only
cg1464	1,87	0,00		putative transcriptional regulatory protein	Signal transduction mechanisms
cg1465	2,34	0,00		hypothetical protein cg1465	Unknown function
cg1468	0,77	0,02		hypothetical protein cg1468	Unknown function
cg1476	1,56	0,02	<i>thiC</i>	thiC, thiamine biosynthesis protein ThiC	Coenzyme transport and metabolism
cg1478	2,15	0,01		hypothetical protein cg1478   hypothetical protein cg1478	Unknown function
cg1479	0,59	0,00	<i>malP (glgP1)</i>	malP, maltodextrin phosphorylase   malP, maltodextrin phosphorylase   malP, maltodextrin phosphorylase	Carbon source transport and metabolism
cg1481	2,00	0,01		hypothetical protein cg1481	Unknown function
cg1482	3,39	0,00		Zn-dependent hydrolase, including glyoxylases	General function prediction only
cg1483	2,60	0,01		hypothetical protein cg1483   hypothetical protein cg1483	Unknown function
cg1487	1,50	0,05	<i>leuC</i>	leuC, isopropylmalate isomerase large subunit	Amino acid transport and metabolism
cg1491	0,67	0,03		hypothetical protein cg1491	Unknown function

cg1492	0,46	0,02	<i>gpsA</i>	gpsA, NAD(P)H-dependent glycerol-3-phosphate dehydrogenase	Central carbon metabolism
cg1493	0,71	0,04	<i>ddl</i>	ddl, D-alanylalanine synthetase	Cell wall/membrane/envelope biogenesis
cg1497	0,83	0,01		predicted kinase related to dihydroxyacetone kinase	General function prediction only
cg1498	0,43	0,02		putative RecG-like helicase	DNA replication, recombination, repair, and degradation
cg1502	0,90	0,02		ABC-type polar amino acid transport system, ATPase component	Amino acid transport and metabolism
cg1505	1,34	0,02		putative secreted protein	Unknown function
cg1508	0,67	0,04		hypothetical protein predicted by Glimmer	Prophage genes
cg1511	2,40	0,01		hypothetical protein cg1511	Prophage genes
cg1512	2,61	0,00		hypothetical protein cg1512	Prophage genes
cg1515	0,67	0,01	<i>tnp24a</i>	tnp24a(ISCg24a), transposase-fragment	Prophage genes, DNA replication, recombination and repair
cg1516	0,67	0,04		hypothetical protein cg1516   hypothetical protein cg1516	Prophage genes
cg1517	0,59	0,03		putative secreted protein	Prophage genes
cg1519	1,33	0,02		hypothetical protein cg1519	Prophage genes
cg1520	0,70	0,02		putative secreted protein   putative secreted protein	Prophage genes
cg1524	0,79	0,04		hypothetical protein cg1524	Prophage genes
cg1525	1,45	0,00	<i>polA</i>	polA, DNA polymerase I	DNA replication, recombination, repair, and degradation
cg1527	1,20	0,02		hypothetical protein cg1527	Signal transduction mechanisms
cg1531	0,62	0,02	<i>rpsA</i>	rpsA, 30S ribosomal protein S1	Translation, ribosomal structure and biogenesis
cg1537	0,32	0,00	<i>ptsG</i>	ptsG, glucose-specific enzyme II BC component of PTS   ptsG, glucose-specific enzyme II BC component of PTS	Carbon source transport and metabolism; signal transduction mechanisms
cg1540	0,56	0,04		putative secreted protein	Unknown function
cg1542	1,30	0,04		hypothetical protein cg1542	Unknown function
cg1546	1,16	0,04	<i>rbkK1</i>	rbkK1, putative ribokinase protein	Nucleotide transport and metabolism
cg1548	0,55	0,01		hypothetical protein cg1548	Unknown function
cg1549	0,61	0,00		hypothetical protein cg1549	Unknown function
cg1550	2,58	0,00	<i>uvrB</i>	uvrB, excinuclease ABC subunit B	DNA replication, recombination, repair, and degradation
cg1551	1,49	0,00	<i>uspA1</i>	uspA1, universal stress protein UspA and related nucleotide-binding proteins	DNA replication, recombination, repair, and degradation
cg1555	2,45	0,00		superfamily I DNA or RNA helicase	DNA replication, recombination, repair, and degradation; Transcription including sigma factors, RNA processing and modification
cg1556	2,32	0,01		hypothetical protein cg1556	Unknown function
cg1560	1,99	0,00	<i>uvrA</i>	uvrA, excinuclease ABC subunit A	DNA replication, recombination, repair, and degradation
cg1563	0,52	0,05	<i>infC</i>	infC, translation initiation factor IF3 protein	Translation, ribosomal structure and biogenesis
cg1564	0,46	0,04	<i>rpmI</i>	rpmI, 50S ribosomal protein L35	Translation, ribosomal structure and biogenesis
cg1565	0,37	0,02	<i>rplT</i>	rplT, 50S ribosomal protein L20	Translation, ribosomal structure and biogenesis
cg1567	1,66	0,01		hypothetical protein cg1567	Unknown function
cg1568	2,04	0,01	<i>ugpA</i>	ugpA, sn-glycerol-3-phosphate transport system permease protein	Carbon source transport and metabolism
cg1570	2,13	0,00	<i>ugpB</i>	ugpB, secreted sn-glycerol-3-phosphate-binding protein	Carbon source transport and metabolism
cg1572	0,54	0,03	<i>glpQ2</i>	glpQ2, putative glycerophosphoryl diester phosphodiesterase	Carbon source transport and metabolism
cg1574	2,77	0,02	<i>pheS</i>	pheS, phenylalanyl-tRNA synthetase alpha subunit	Translation, ribosomal structure and biogenesis
cg1577	0,53	0,05		putative secreted hydrolase	General function prediction only
cg1578	0,40	0,00		acyltransferase family, membrane protein	General function prediction only
cg1579	0,62	0,02		putative secreted protein   putative secreted protein	Unknown function
cg1580	4,17	0,02	<i>argC</i>	argC, N-acetyl-gamma-glutamyl-phosphate reductase	Amino acid transport and metabolism
cg1589	1,65	0,04		putative secreted protein	Unknown function
cg1590	2,05	0,00		secreted Mg-chelatase subunit	Inorganic ion transport, metabolism, and storage



cg1591	2,27	0,01		putative secreted protein	Unknown function
cg1592	3,15	0,03		hypothetical protein cg1592	Unknown function
cg1594	2,54	0,01	<i>tyrS</i>	tyrS, tyrosyl-tRNA synthetase	Translation, ribosomal structure and biogenesis
cg1597	1,50	0,01		hypothetical protein cg1597	Unknown function
cg1598	1,24	0,03		sugar phosphatase of the HAD superfamily	General function prediction only
cg1602	10,96	0,00	<i>recN</i>	recN, DNA repair protein RecN	DNA replication, recombination, repair, and degradation
cg1603	0,49	0,00		hypothetical protein cg1603	Unknown function
cg1604	0,61	0,00		Ortholog of M, tub, outer membrane protein, porin	General function prediction only
cg1606	3,66	0,00	<i>pyrG</i>	pyrG, CTP synthetase	Nucleotide transport and metabolism
cg1607	1,27	0,03		NTP pyrophosphohydrolase including oxidative damage repair enzyme	DNA replication, recombination, repair, and degradation
cg1612	0,15	0,01		acetyltransferase   acetyltransferase	General function prediction only
cg1615	0,55	0,02	<i>rluA</i>	16S rRNA uridine-516 pseudouridylate synthase or related pseudouridylate synthase	Translation, ribosomal structure and biogenesis
cg1616	0,49	0,01	<i>cmk</i>	cmk, cytidylate kinase	Nucleotide transport and metabolism
cg1617	0,64	0,01		GTP-binding protein EngA   GTP-binding protein EngA	General function prediction only
cg1618	3,55	0,00		hypothetical protein cg1618	Unknown function
cg1619	2,93	0,00		putative DNA gyrase inhibitor	Transcription including sigma factors, RNA processing and modification
cg1621	0,57	0,03		ABC-type multidrug/protein/lipid transport system, ATPase component	General function prediction only
cg1622	0,56	0,01		ABC-type multidrug/protein/lipid transport system, ATPase component	General function prediction only
cg1626	8,48	0,00		hypothetical protein cg1626	Unknown function
cg1628	15,59	0,00		hydrolase of the alpha/beta superfamily	General function prediction only
cg1632	1,54	0,00		hypothetical protein cg1632	Unknown function
cg1633	0,57	0,01		predicted transcriptional regulator	Signal transduction mechanisms
cg1638	0,67	0,01		hypothetical protein cg1638	Unknown function
cg1639	0,72	0,02		membrane protein containing CBS domain	Unknown function
cg1643	2,76	0,00	<i>gnd</i>	gnd, 6-phosphogluconate dehydrogenase	Central carbon metabolism
cg1645	0,67	0,01		SAM-dependent methyltransferase	General function prediction only
cg1646	3,05	0,00		ABC-type multidrug transport system, ATPase component	General function prediction only
cg1647	4,37	0,00		ABC-type multidrug transport system, permease component	General function prediction only
cg1653	0,62	0,01	<i>pctH (pgp1)</i>	pgp1, putative phosphoglycolate phosphatase	Transport and metabolism of further metabolites
cg1655	0,67	0,00	<i>thiM</i>	thiM, hydroxyethylthiazole kinase   thiM, hydroxyethylthiazole kinase	Coenzyme transport and metabolism
cg1656	0,67	0,01	<i>ndh</i>	ndh, NADH dehydrogenase   ndh, NADH dehydrogenase	Respiration and oxidative phosphorylation
cg1657	0,73	0,03	<i>ufaA</i>	ufaA, putative cyclopropane fatty acid synthase (cyclopropane-fatty-acyl-phospholipid synthase)   ufaA, putative cyclopropane fatty acid synthase (cyclopropane-fatty-acyl-phospholipid synthase)	Cell wall/membrane/envelope biogenesis
cg1658	1,60	0,01		permease of the major facilitator superfamily   permease of the major facilitator superfamily	General function prediction only
cg1659	2,65	0,01	<i>gpt</i>	gpt, purine phosphoribosyltransferase   gpt, purine phosphoribosyltransferase   gpt, purine phosphoribosyltransferase	Nucleotide transport and metabolism
cg1662	3,11	0,00		putative secreted protein	Unknown function
cg1665	0,47	0,00		putative secreted protein   putative secreted protein	Unknown function
cg1668	1,93	0,02		hypothetical protein cg1668	Unknown function
cg1669	2,78	0,00		putative secreted protein	Unknown function
cg1670	2,24	0,00		hypothetical protein cg1670	Unknown function
cg1671	3,58	0,00		putative membrane-associated GTPase	Unknown function
cg1672	0,74	0,01	<i>ppmC (ppm1)</i>	ppm1, polyprenyl monophosphomannose synthase	Cell wall/membrane/envelope biogenesis
cg1673	2,54	0,01	<i>ppmN (ppm2)</i>	apolipoprotein N-acyltransferase, ortholog of mycobacterium MSMEG_3860	Cell wall/membrane/envelope biogenesis
cg1675	2,74	0,00		hypothetical protein cg1675	Unknown function
cg1676	2,17	0,00	<i>lip3</i>	lip, putative lipase	Lipid transport and metabolism



cg1678	2,08	0,02	<i>cobL</i>	cobL, precorrin-6Y C5,15-methyltransferase (decarboxylating)	Coenzyme transport and metabolism
cg1680	0,53	0,00		hypothetical protein cg1680	General function prediction only
cg1681	0,50	0,00	<i>pepE (pepQ?)</i>	pepE, proline dipeptidase	Protein turnover and chaperones
cg1682	1,57	0,04		trypsin-like serine protease	Protein turnover and chaperones
cg1683	1,38	0,03		superfamily II DNA and RNA helicase	General function prediction only
cg1685	1,88	0,05	<i>tatA</i>	tatA, twin arginine translocase protein A	Protein secretion
cg1688	0,68	0,02	<i>pafA (pafA2)</i>	pafA, proteasome accessory factor A, pupylation machinery	Post-translational modification
cg1691	1,45	0,01	<i>arc (mpa)</i>	arc, AAA+ ATPase ARC, pupylation machinery	Post-translational modification; Protein turnover and chaperones
cg1693	2,12	0,01	<i>pepC</i>	pepC, putative aminopeptidase 2	Protein turnover and chaperones
cg1694	0,46	0,01	<i>recB</i>	recB, RecB family exonuclease	DNA replication, recombination, repair, and degradation
cg1695	0,49	0,00		putative plasmid maintenance system antidote protein	General function prediction only
cg1696	2,68	0,02		permease of the major facilitator superfamily   permease of the major facilitator superfamily	General function prediction only
cg1697	3,25	0,00	<i>aspA</i>	aspA, aspartate ammonia-lyase (aspartase)	Amino acid transport and metabolism
cg1698	6,21	0,00	<i>hisG</i>	hisG, ATP phosphoribosyltransferase	Amino acid transport and metabolism
cg1699	6,41	0,00	<i>hisE</i>	hisE, phosphoribosyl-ATP pyrophosphatase	Amino acid transport and metabolism
cg1700	1,97	0,02		putative phosphatase/phosphohexomutase	General function prediction only
cg1701	3,56	0,01	<i>metH</i>	metH, homocysteine methyltransferase	Amino acid transport and metabolism
cg1702	2,15	0,02		hypothetical protein cg1702	Unknown function
cg1706	0,77	0,02	<i>arsC1</i>	arsC1, arsenate reductase	Inorganic ion transport, metabolism, and storage
cg1709	1,97	0,01	<i>mshC</i>	mshC, ligase, cysteinyl-tRNA synthetase   mshC, ligase, cysteinyl-tRNA synthetase	Transport and metabolism of further metabolites
cg1710	1,71	0,01	<i>uppP (bacA)</i>	uppP, undecaprenyl pyrophosphate phosphatase	Cell wall/membrane/envelope biogenesis
cg1712	2,70	0,00	<i>lppL</i>	lppL, secreted lipoprotein	Cell wall/membrane/envelope biogenesis
cg1713	1,99	0,00	<i>pyrD</i>	pyrD, dihydroorotate dehydrogenase	Nucleotide transport and metabolism
cg1715	0,55	0,03		hypothetical protein cg1715   hypothetical protein cg1715	Unknown function
cg1716	0,51	0,03	<i>tnp16b</i>	tnp16b(ISCg16b), transposase   tnp16b(ISCg16b), transposase	DNA replication, recombination, repair, and degradation
cg1717	0,73	0,00		hypothetical protein cg1717	Unknown function
cg1719	1,23	0,02	<i>tetB</i>	tetB, ABC-type multidrug/protein/lipid transport system, ATPase component	Transport and metabolism of further metabolites
cg1722	7,23	0,00	<i>act3</i>	N-acetylglutamate synthase activity, complements arginine-auxotrophic argJ strain	Amino acid transport and metabolism
cg1724	0,31	0,00	<i>meaB</i>	meaB, accessory protein of methylmalonyl-CoA mutase	Amino acid transport and metabolism; Lipid transport and metabolism
cg1725	0,26	0,00	<i>mutA (mcmB)</i>	mutA, methylmalonyl-CoA mutase, subunit	Amino acid transport and metabolism; Lipid transport and metabolism
cg1726	0,27	0,01	<i>mutB (mcmA)</i>	mutB, methylmalonyl-CoA mutase, small subunit	Amino acid transport and metabolism; Lipid transport and metabolism
cg1728	0,87	0,03		hypothetical protein cg1728	Unknown function
cg1730	3,83	0,01		secreted protease subunit, stomatin/prohibitin homolog	Protein turnover and chaperones
cg1731	2,68	0,00		membrane protein implicated in regulation of membrane protease activity	Protein turnover and chaperones
cg1732	1,48	0,02		hypothetical protein cg1732	Unknown function
cg1734	3,36	0,00	<i>hemH</i>	hemH, ferrochelatase precursor	Transport and metabolism of further metabolites
cg1735	0,29	0,01		secreted cell wall-associated hydrolase (invasion-associated protein)	Cell wall/membrane/envelope biogenesis
cg1736	0,63	0,00		hypothetical protein cg1736   hypothetical protein cg1736	Unknown function
cg1737	0,52	0,01	<i>acn</i>	acn, aconitate hydratase	Central carbon metabolism
cg1738	0,82	0,04	<i>acnR</i>	acnR, transcriptional regulator, represses aconitase	Signal transduction mechanisms
cg1739	2,55	0,02	<i>gat</i>	glutamine amidotransferase	Amino acid transport and metabolism; Nucleotide transport and metabolism; Coenzyme transport and metabolism
cg1740	1,28	0,02		putative nucleoside-diphosphate-sugar epimerase	Nucleotide transport and metabolism
cg1741	2,01	0,04		hypothetical protein cg1741	Unknown function

cg1742	0,66	0,01		hypothetical protein cg1742	Unknown function
cg1743	0,45	0,00		hypothetical protein cg1743	Unknown function
cg1744	1,61	0,00	<i>pacL</i>	pacL, cation-transporting ATPase	Inorganic ion transport, metabolism, and storage
cg1750	0,66	0,02		hypothetical protein cg1750	Prophage genes
cg1753	2,25	0,00		ATPase component of ABC transporters with duplicated ATPase domains	General function prediction only
cg1758	1,98	0,00		hypothetical protein cg1758	Unknown function
cg1762	1,52	0,05	<i>sufC</i>	sufC, Fe-S cluster assembly ATPase	Coenzyme transport and metabolism
cg1763	1,82	0,04	<i>sufD</i>	sufD, Fe-S cluster assembly membrane protein	Coenzyme transport and metabolism
cg1765	1,91	0,02	<i>sufR</i>	sufR, transcriptional regulator of suf operon	Signal transduction mechanisms
cg1766	1,88	0,01	<i>mptB</i>	mptB, Mannosyltransferase	Cell wall/membrane/envelope biogenesis
cg1767	1,23	0,05		ABC-type multidrug transport system, ATPase component	General function prediction only
cg1768	1,67	0,01		ABC-type multidrug transport system, permease component	General function prediction only
cg1769	6,28	0,01	<i>ctaA</i>	ctaA, cytochrome oxidase assembly protein	Protein turnover and chaperones
cg1773	2,82	0,00	<i>ctaB</i>	ctaB, hypothetical protein cg1773   ctaB, hypothetical protein cg1773	Protein turnover and chaperones
cg1779	0,73	0,02	<i>opcA</i>	opcA, putative subunit of glucose-6-P dehydrogenase	Central carbon metabolism
cg1780	0,74	0,02	<i>pgl (devB)</i>	devB, 6-phosphogluconolactonase	Central carbon metabolism
cg1781	0,63	0,05	<i>soxA</i>	soxA, sarcosine oxidase-fragment	Carbon source transport and metabolism
cg1782	0,26	0,00	<i>tnp13b</i>	tnp13b(ISCg13b), transposase	DNA replication, recombination, repair, and degradation
cg1783	0,70	0,05	<i>soxA</i>	soxA, sarcosine oxidase-N-terminal fragment	Carbon source transport and metabolism
cg1785	1,67	0,03	<i>amtA (amt)</i>	amt, high-affinity ammonia permease	Inorganic ion transport, metabolism, and storage
cg1786	3,14	0,00	<i>secG</i>	secG, protein-export membrane protein	Protein secretion
cg1790	1,36	0,02	<i>pgk</i>	pgk, phosphoglycerate kinase	Central carbon metabolism
cg1792	2,61	0,01		putative transcriptional regulator-WhiA homolog	Signal transduction mechanisms
cg1793	2,65	0,01		hypothetical protein cg1793	Unknown function
cg1794	2,31	0,00		hypothetical protein cg1794	General function prediction only
cg1795	1,57	0,00	<i>uvrC</i>	uvrC, excinuclease ABC subunit C	DNA replication, recombination, repair, and degradation
cg1799	1,60	0,03	<i>ribC</i>	ribC, riboflavin synthase subunit alpha	Coenzyme transport and metabolism
cg1800	1,53	0,02	<i>ribG</i>	ribG, putative bifunctional riboflavin-specific deaminase/reductase	Coenzyme transport and metabolism
cg1801	1,37	0,02	<i>rpe</i>	rpe, ribulose-phosphate 3-epimerase	Central carbon metabolism
cg1802	1,46	0,00	<i>fmu</i>	fmu, putative 16S rRNA m(5)C 967 methyltransferase	Translation, ribosomal structure and biogenesis
cg1803	1,33	0,00	<i>fmt</i>	fmt, methionyl-tRNA formyltransferase	Translation, ribosomal structure and biogenesis
cg1804	2,01	0,00	<i>def2</i>	def, peptide deformylase	Post-translational modification
cg1805	0,89	0,04	<i>priA</i>	priA, primosome assembly protein PriA	Transcription including sigma factors, RNA processing and modification
cg1806	1,66	0,04	<i>metK</i>	metK, S-adenosylmethionine synthetase	Amino acid transport and metabolism
cg1807	0,74	0,01	<i>dfp</i>	dfp, phosphopantothenoylcysteine synthase/decarboxylase	Coenzyme transport and metabolism
cg1808	1,21	0,02	<i>#NV</i>	hypothetical protein predicted by Glimmer	#NV
cg1809	1,69	0,05		DNA-directed RNA polymerase omega subunit	Transcription including sigma factors, RNA processing and modification
cg1812	0,42	0,00	<i>pyrF</i>	pyrF, orotidine 5-phosphate decarboxylase	Nucleotide transport and metabolism
cg1813	0,52	0,04	<i>carB</i>	carB, carbamoyl-phosphate synthase large subunit	Amino acid transport and metabolism; Nucleotide transport and metabolism; Coenzyme transport and metabolism
cg1819	1,57	0,00		nucleoside-diphosphate sugar epimerase (SulA family)	Nucleotide transport and metabolism
cg1821	1,56	0,02		hypothetical protein cg1821	Unknown function
cg1822	1,56	0,01		hypothetical protein cg1822	Unknown function
cg1823	1,25	0,05		hypothetical protein cg1823	Unknown function
cg1824	0,60	0,02	<i>nusB</i>	nusB, transcription antitermination protein NusB   nusB, transcription antitermination protein NusB	Transcription including sigma factors, RNA processing and modification
cg1825	0,55	0,00	<i>efp</i>	efp, elongation factor p	Translation, ribosomal structure and biogenesis
cg1826	0,81	0,04	<i>pepQ</i>	pepQ, XAA-pro aminopeptidase	Protein turnover and chaperones

cg1829	1,57	0,01	<i>aroC</i>	aroC, chorismate synthase	Amino acid transport and metabolism
cg1831	1,06	0,05		bacterial regulatory protein, ArsR family	Signal transduction mechanisms
cg1833	1,21	0,04		secreted substrate-binding lipoprotein	Inorganic ion transport, metabolism, and storage; Transport and metabolism of further metabolites
cg1834	0,48	0,02		ATP-binding protein of ABC transporter	Inorganic ion transport, metabolism, and storage; Transport and metabolism of further metabolites
cg1835	0,34	0,02	<i>aroE3</i>	aroE3, shikimate 5-dehydrogenase	Amino acid transport and metabolism
cg1836	0,34	0,00		secreted solute-binding protein, aminodeoxychorismate lyase-like	General function prediction only
cg1837	0,55	0,04		holliday junction resolvase-like protein	DNA replication, recombination, repair, and degradation
cg1838	0,60	0,00	<i>alaS</i>	alaS, alanyl-tRNA synthetase	Translation, ribosomal structure and biogenesis
cg1839	1,18	0,04		uncharacterized ATPase related to the helicase subunit of the holliday junction resolvase	DNA replication, recombination, repair, and degradation
cg1841	1,48	0,00	<i>aspS</i>	aspS, aspartyl-tRNA synthetase   aspS, aspartyl-tRNA synthetase	Translation, ribosomal structure and biogenesis
cg1844	0,49	0,00		membrane protein	Unknown function
cg1848	1,63	0,00		coenzyme F420-dependent N5,N10-methylene tetrahydromethanopterin reductase or related flavin-depende   coenzyme F420-dependent N5,N10-methylene tetrahydromethanopterin reductase or related flavin-depende	Coenzyme transport and metabolism
cg1849	1,50	0,03		hypothetical protein cg1849	Unknown function
cg1852	2,66	0,01	<i>sdaA</i>	sdaA, serine deaminase   sdaA, serine deaminase	Amino acid transport and metabolism
cg1855	1,35	0,02	<i>hisS</i>	hisS, histidyl-tRNA synthetase	Translation, ribosomal structure and biogenesis
cg1856	2,55	0,00		Zn-dependent hydrolase   Zn-dependent hydrolase	General function prediction only
cg1857	0,65	0,02	<i>ppiB</i>	ppiB, peptidyl-prolyl cis-trans isomerase   ppiB, peptidyl-prolyl cis-trans isomerase	Protein turnover and chaperones
cg1859	1,44	0,01		putative secreted protein	Unknown function
cg1860	2,24	0,00		hypothetical protein cg1860	Unknown function
cg1861	0,54	0,03	<i>rel</i>	rel, ppGpp synthetase, ppGpp pyrophosphorylase	Signal transduction mechanisms
cg1862	0,69	0,05	<i>apt</i>	apt, adenine phosphoribosyltransferase	Nucleotide transport and metabolism
cg1865	0,70	0,00	<i>secF</i>	secF, protein export protein SecF   secF, protein export protein SecF	Protein secretion
cg1867	0,64	0,03	<i>secD</i>	secD, protein export protein SecD   secD, protein export protein SecD	Protein secretion
cg1869	0,74	0,00	<i>ruvB</i>	ruvB, holliday junction DNA helicase RuvB	DNA replication, recombination, repair, and degradation
cg1870	0,64	0,01	<i>ruvA</i>	ruvA, holliday junction DNA helicase motor protein	DNA replication, recombination, repair, and degradation
cg1872	0,94	0,04		hypothetical protein cg1872	Unknown function
cg1876	1,13	0,02		glycosyl transferase   glycosyl transferase	General function prediction only
cg1878	0,81	0,03	<i>pgsA1</i>	pgsA1, phosphatidylglycerophosphate synthase   pgsA1, phosphatidylglycerophosphate synthase   pgsA1, phosphatidylglycerophosphate synthase   pgsA1, phosphatidylglycerophosphate synthase	Cell wall/membrane/envelope biogenesis
cg1891	2,12	0,02	<i>alpA</i>	hypothetical protein cg1891	Prophage genes
cg1893	4,49	0,00	<i>act4</i>	acetyltransferase	Prophage genes
cg1894	0,49	0,01		hypothetical protein cg1894	Prophage genes
cg1896	1,79	0,00		putative secreted protein	Prophage genes
cg1897	2,90	0,00		putative secreted protein	Prophage genes
cg1898	1,53	0,02		hypothetical protein cg1898	Prophage genes
cg1899	2,92	0,01		hypothetical protein cg1899	Prophage genes
cg1900	1,60	0,03		hypothetical protein cg1900	Prophage genes
cg1901	3,62	0,00		hypothetical protein cg1901	Prophage genes
cg1902	4,13	0,01		putative secreted protein	Prophage genes
cg1903	1,67	0,01		ABC-type multidrug transport system, ATPase component	Prophage genes

cg1904	1,96	0,01		hypothetical protein cg1904	Prophage genes
cg1905	0,68	0,02		hypothetical protein cg1905   hypothetical protein cg1905	Prophage genes
cg1909	1,52	0,00		hypothetical protein cg1909	Prophage genes
cg1912	1,53	0,00		hypothetical protein cg1912	Prophage genes
cg1913	1,48	0,01		hypothetical protein cg1913   hypothetical protein cg1913   hypothetical protein cg1913	Prophage genes
cg1914	3,51	0,03		hypothetical protein predicted by Glimmer	Prophage genes
cg1915	2,85	0,02		hypothetical protein cg1915	Prophage genes
cg1916	2,24	0,02		hypothetical protein cg1916	Prophage genes
cg1918	1,70	0,04		putative secreted protein	Prophage genes
cg1919	2,94	0,02		hypothetical protein cg1919	Prophage genes
cg1920	3,09	0,02		hypothetical protein cg1920	Prophage genes
cg1921	3,15	0,01		hypothetical protein cg1921	Prophage genes
cg1922	4,47	0,01		hypothetical protein cg1922	Prophage genes
cg1923	3,25	0,01		hypothetical protein cg1923	Prophage genes
cg1924	2,55	0,01		hypothetical protein cg1924	Prophage genes
cg1928	1,80	0,05		hypothetical protein cg1928	Prophage genes
cg1931	1,26	0,01		putative secreted protein	Prophage genes
cg1934	4,49	0,01		hypothetical protein cg1934	Prophage genes
cg1937	2,31	0,01		putative secreted protein	Prophage genes
cg1940	2,97	0,02		putative secreted protein	Prophage genes
cg1941	2,65	0,00		putative secreted protein	Prophage genes
cg1942	0,59	0,02		putative secreted protein   putative secreted protein	Prophage genes
cg1943	0,63	0,01		hypothetical protein cg1943	Prophage genes
cg1944	1,58	0,02		hypothetical protein cg1944	Prophage genes
cg1947	0,68	0,02		hypothetical protein cg1947	Prophage genes
cg1949	1,73	0,01		hypothetical protein cg1949   hypothetical protein cg1949	Prophage genes
cg1950	1,79	0,03	<i>tnp14b</i>	tnp14b(ISCg14a), transposase	Prophage genes
cg1951	2,10	0,02	<i>tnp14a</i>	tnp14a(ISCg14a), transposase	Prophage genes
cg1954	0,46	0,02		hypothetical protein cg1954	Prophage genes
cg1956	10,31	0,00	<i>recJ</i>	recJ, single-stranded-DNA-specific exonuclease	Prophage genes
cg1957	1,77	0,00		hypothetical protein cg1957   hypothetical protein cg1957	Prophage genes
cg1959	3,85	0,01	<i>priP</i>	priP, prophage DNA primase	Prophage genes
cg1960	3,09	0,00		hypothetical protein cg1960	Prophage genes
cg1961	4,40	0,00		hypothetical protein predicted by Glimmer	Prophage genes
cg1962	0,13	0,00		hypothetical protein cg1962	Prophage genes
cg1963	4,51	0,00		superfamily II DNA/RNA helicase	Prophage genes
cg1964	4,02	0,00		hypothetical protein cg1964	Prophage genes
cg1965	2,46	0,01		similarity to hypothetical protein gp57-phage N15	Prophage genes
cg1966	1,52	0,02	<i>cgpS</i>	hypothetical protein cg1966	Prophage genes
cg1967	2,70	0,00		hypothetical protein cg1967	Prophage genes
cg1968	2,56	0,00		hypothetical protein cg1968	Prophage genes
cg1969	2,24	0,00		hypothetical protein cg1969	Prophage genes
cg1970	2,92	0,00		hypothetical protein cg1970	Prophage genes
cg1971	2,13	0,01		hypothetical protein predicted by Glimmer	Prophage genes
cg1972	0,75	0,04		putative translation elongation factor (GTPase)	Prophage genes
cg1974	1,41	0,05		putative lysin	Prophage genes
cg1975	2,67	0,01		hypothetical protein cg1975	Prophage genes
cg1976	2,87	0,01		hypothetical protein cg1976	Prophage genes
cg1977	4,52	0,00		putative secreted protein	Prophage genes
cg1978	135,36	0,00		hypothetical protein cg1978	Prophage genes
cg1980	4,28	0,00		MaxR-like ATPase	Prophage genes
cg1981	3,46	0,01		hypothetical protein cg1981	Prophage genes
cg1982	4,36	0,00		ATPase with chaperone activity, ATP-binding subunit	Prophage genes
cg1983	2,87	0,00		hypothetical protein cg1983	Prophage genes
cg1984	4,47	0,00		hypothetical protein cg1984	Prophage genes
cg1985	1,98	0,02		superfamily I DNA or RNA helicase	Prophage genes
cg1986	2,35	0,01		hypothetical protein cg1986   hypothetical protein cg1986	Prophage genes
cg1987	2,68	0,01		hypothetical protein cg1987	Prophage genes
cg1988	2,20	0,01		hypothetical protein cg1988	Prophage genes
cg1989	2,24	0,00		hypothetical protein cg1989	Prophage genes

cg1990	1,59	0,04		NUDIX hydrolase	Prophage genes
cg1991	2,51	0,02		similar to gp52-bacteriophage PHIC31	Prophage genes
cg1992	2,53	0,01		hypothetical protein predicted by Glimmer	Prophage genes
cg1993	3,08	0,00		hypothetical protein cg1993   hypothetical protein cg1993	Prophage genes
cg1994	4,80	0,01		hypothetical protein cg1994	Prophage genes
cg1996	0,34	0,01	<i>cglIM</i>	cglIM, modification methylase	Prophage genes
cg1997	0,41	0,01	<i>cglIR</i>	cglIR, type II restriction endonuclease	Prophage genes
cg1998	0,58	0,02	<i>cglIR</i>	cglIR, restriction endonuclease CGLIR protein	Prophage genes
cg1999	1,79	0,04		hypothetical protein cg1999   hypothetical protein cg1999	Prophage genes
cg2001	2,11	0,03		hypothetical protein cg2001   hypothetical protein cg2001	Prophage genes
cg2002	1,80	0,00		hypothetical protein cg2002	Prophage genes
cg2003	1,46	0,04		hypothetical protein cg2003	Prophage genes
cg2004	3,19	0,04		similar to 232 protein-lactobacillus bacteriophage g1e	Prophage genes
cg2005	0,73	0,01		conserved hypothetical protein-plasmid encoded	Prophage genes
cg2008	1,31	0,04		hypothetical protein cg2008	Prophage genes
cg2009	1,47	0,01		putative CLP-family ATP-binding protease	Prophage genes
cg2010	1,29	0,02		permease of the major facilitator superfamily	Prophage genes
cg2011	1,47	0,04		hypothetical protein cg2011   hypothetical protein cg2011	Prophage genes
cg2014	2,77	0,00		hypothetical protein cg2014	Prophage genes
cg2015	1,50	0,02		hypothetical protein cg2015   hypothetical protein cg2015	Prophage genes
cg2017	1,41	0,05		hypothetical protein cg2017	Prophage genes
cg2020	1,92	0,03		hypothetical protein cg2020	Prophage genes
cg2023	1,92	0,02		hypothetical protein cg2023	Prophage genes
cg2024	1,60	0,03		putative nuclease subunit of the excinuclease complex	Prophage genes
cg2026	0,58	0,01		hypothetical protein predicted by Glimmer	Prophage genes
cg2028	3,39	0,00		hypothetical protein cg2028	Prophage genes
cg2029	4,66	0,00		hypothetical protein predicted by Glimmer	Prophage genes
cg2030	3,03	0,02		hypothetical protein predicted by Glimmer	Prophage genes
cg2031	2,76	0,00		hypothetical protein cg2031	Prophage genes
cg2032	1,60	0,01		hypothetical protein cg2032   hypothetical protein cg2032	Prophage genes
cg2033	1,41	0,02		putative secreted protein	Prophage genes
cg2035	2,03	0,03		putative methyltransferase	Prophage genes
cg2037	2,30	0,01		hypothetical protein cg2037	Prophage genes
cg2038	2,91	0,00		hypothetical protein predicted by Glimmer	Prophage genes
cg2039	1,84	0,01		hypothetical protein cg2039	Prophage genes
cg2040	1,85	0,00		putative transcriptional regulator	Prophage genes
cg2041	1,43	0,04		hypothetical protein predicted by Glimmer	Prophage genes
cg2042	0,84	0,03		putative secreted protein	Prophage genes
cg2046	3,21	0,00		hypothetical protein cg2046	Prophage genes
cg2047	1,66	0,04		putative secreted protein	Prophage genes
cg2051	1,68	0,00		hypothetical protein cg2051	Prophage genes
cg2052	0,65	0,01		putative secreted protein	Prophage genes
cg2053	4,51	0,00		hypothetical protein cg2053	Prophage genes
cg2054	16,97	0,00		hypothetical protein cg2054	Prophage genes
cg2055	19,69	0,00		hypothetical protein cg2055	Prophage genes
cg2056	3,52	0,01		hypothetical protein cg2056	Prophage genes
cg2057	3,31	0,00		putative secreted protein	Prophage genes
cg2058	3,63	0,00		hypothetical protein predicted by Glimmer and Critica	Prophage genes
cg2059	2,74	0,01		putative secreted protein   putative secreted protein	Prophage genes
cg2060	1,75	0,01		hypothetical protein cg2060   hypothetical protein cg2060	Prophage genes
cg2061	0,38	0,00	<i>psp3</i>	psp3, putative secreted protein	Prophage genes
cg2062	1,57	0,04		similar to plasmid-encoded protein PXO2,09	Prophage genes
cg2063	1,26	0,00		hypothetical protein cg2063	Prophage genes
cg2064	1,89	0,04		DNA topoisomerase I (omega-protein)   DNA topoisomerase I (omega-protein)	Prophage genes
cg2065	0,75	0,03		superfamily II DNA or RNA helicase   superfamily II DNA or RNA helicase	Prophage genes

cg2070	4,49	0,00	<i>int2</i>	int2, putative phage integrase (C-terminal fragment)	Prophage genes
cg2071	3,05	0,00	<i>int2</i>	int2, putative phage integrase (N-terminal fragment)	Prophage genes
cg2074	0,60	0,01		hypothetical protein cg2074   hypothetical protein cg2074   hypothetical protein cg2074   hypothetical protein cg2074   hypothetical protein cg2074	Unknown function
cg2075	0,44	0,03		hypothetical protein cg2075   hypothetical protein cg2075   hypothetical protein cg2075   hypothetical protein cg2075	Unknown function
cg2076	1,67	0,04	<i>ribD</i>	ribD, hypothetical protein cg2076	Transport and metabolism of further metabolites
cg2078	1,62	0,01	<i>msrB</i>	peptide methionine sulfoxide reductase-related protein	Amino acid transport and metabolism
cg2079	2,03	0,01		hypothetical protein cg2079	Inorganic ion transport and metabolism
cg2080	0,42	0,00		hypothetical protein cg2080	Unknown function
cg2081	1,90	0,00	<i>rnd</i>	rnd, probable ribonuclease D protein   rnd, probable ribonuclease D protein	Transcription including sigma factors, RNA processing and modification
cg2084	0,77	0,04		putative RNA methyltransferase	Transcription including sigma factors, RNA processing and modification
cg2086	0,59	0,00	<i>dut</i>	dut, deoxyuridine 5-triphosphate nucleotidohydrolase	Nucleotide transport and metabolism
cg2087	2,46	0,02		hypothetical protein cg2087	Unknown function
cg2088	0,77	0,02		hypothetical protein cg2088	Unknown function
cg2095	1,79	0,00		hypothetical protein cg2095   hypothetical protein cg2095	Unknown function
cg2096	1,75	0,01		hypothetical protein cg2096	Unknown function
cg2098	0,97	0,01		hypothetical protein cg2098	Unknown function
cg2101	0,72	0,03		D-tyrosyl-tRNA deacylase	Translation, ribosomal structure and biogenesis
cg2102	3,65	0,01	<i>sigB</i>	sigB, RNA polymerase sigma factor	Transcription including sigma factors, RNA processing and modification
cg2103	4,54	0,01	<i>dtxR</i>	dtxR, diphtheria toxin repressor	Signal transduction mechanisms
cg2104	2,56	0,01	<i>galE</i>	galE, UDP-glucose 4-epimerase	Carbon source transport and metabolism
cg2105	1,58	0,02		hypothetical protein cg2105   hypothetical protein cg2105	Unknown function
cg2106	3,13	0,00		hypothetical protein cg2106	Unknown function
cg2107	0,56	0,04		superfamily II DNA or RNA helicase	General function prediction only
cg2110	1,82	0,00		hypothetical protein cg2110	Unknown function
cg2111	1,73	0,01	<i>hrpA</i>	hrpA, probable ATP-dependent RNA helicase protein	Transcription including sigma factors, RNA processing and modification
cg2112	1,59	0,05	<i>nrdR</i>	nrdR, transcriptional regulator of deoxyribonucleotide biosynthesis	Signal transduction mechanisms
cg2113	1,32	0,05	<i>divS</i>	divS, suppressor of cell division	Signal transduction mechanisms
cg2114	2,09	0,01	<i>lexA</i>	transcriptional repressor/regulator, involved in SOS/stress response, LexA-family	Signal transduction mechanisms
cg2116	0,76	0,00		putative phosphofructokinase	Central carbon metabolism
cg2117	0,58	0,00	<i>ptsI</i>	ptsI, phosphoenolpyruvate:sugar phosphotransferase system enzyme	Carbon source transport and metabolism
cg2118	0,40	0,03	<i>fruR</i>	transcriptional regulator of sugar metabolism, DeoR family	Signal transduction mechanisms
cg2119	0,29	0,00	<i>pfkB (fruK)</i>	pfkB, 1-phosphofructokinase protein	Central carbon metabolism
cg2120	0,30	0,00	<i>ptsF</i>	ptsF, sugar specific PTS system, fructose/mannitol-specific transport protein	Carbon source transport and metabolism
cg2125	1,36	0,02	<i>uraA</i>	uraA, putative uracyl permease	Nucleotide transport and metabolism
cg2126	3,19	0,00	<i>hflX</i>	GTPase	Translation, ribosomal structure and biogenesis
cg2127	3,20	0,02		hypothetical protein cg2127	Unknown function
cg2128	0,60	0,05		putative secreted or membrane protein	Unknown function
cg2129	1,65	0,00	<i>dapF</i>	dapF, diaminopimelate epimerase	Amino acid transport and metabolism
cg2131	0,43	0,01		hypothetical protein cg2131	Unknown function
cg2132	0,78	0,04		hypothetical protein cg2132	Unknown function
cg2133	0,69	0,02		acetyltransferase, GNAT family	General function prediction only
cg2134	1,46	0,01		hypothetical protein cg2134	Unknown function
cg2135	1,37	0,02	<i>miaB</i>	miaB, tRNA methyltransferase	Translation, ribosomal structure and biogenesis
cg2136	0,31	0,01	<i>gluA</i>	gluA, glutamate uptake system ATP-binding protein	Amino acid transport and metabolism
cg2137	0,30	0,00	<i>gluB</i>	gluB, glutamate secreted binding protein	Amino acid transport and metabolism
cg2138	0,33	0,00	<i>gluC</i>	gluC, glutamate permease	Amino acid transport and metabolism

cg2139	0,35	0,01	<i>gluD</i>	gluD, glutamate permease	Amino acid transport and metabolism
cg2141	0,73	0,04	<i>recA</i>	recA, recombinase A	DNA replication, recombination, repair, and degradation
cg2145	3,55	0,01		hypothetical protein cg2145	Unknown function
cg2146	1,23	0,02		hypothetical protein cg2146	Unknown function
cg2147	2,47	0,00	<i>bioY</i>	bioY, substrate-specific component BioY of biotin ECF transporter	Coenzyme transport and metabolism
cg2148	1,51	0,00	<i>bioM</i>	bioM, ATPase component BioM of energizing module of biotin ECF transporter	Coenzyme transport and metabolism
cg2149	1,55	0,03	<i>bioN</i>	bioN, transmembrane component BioN of energizing module of biotin ECF transporter	Coenzyme transport and metabolism
cg2151	2,91	0,02		similar to phage shock protein A   similar to phage shock protein A	General function prediction only
cg2152	2,99	0,01	<i>clgR</i>	clgR, transcriptional regulator	Signal transduction mechanisms
cg2153	2,03	0,00		similar to competence-and mitomycin-induced protein	General function prediction only
cg2154	2,00	0,01	<i>pgsA2</i>	pgsA2, CDP-diacylglycerol--glycerol-3-phosphate 3-phosphatidyltransferase   pgsA2, CDP-diacylglycerol--glycerol-3-phosphate 3-phosphatidyltransferase	Cell wall/membrane/envelope biogenesis
cg2155	0,64	0,01		hypothetical protein cg2155	Unknown function
cg2157	1,50	0,01	<i>terC</i>	terC, tellurium resistance membrane protein	Inorganic ion transport and metabolism
cg2158	2,46	0,01	<i>ftsK</i>	ftsK, cell division protein, required for cell division and chromosome partitioning	Cell division, chromosome partitioning
cg2159	1,34	0,04		hypothetical protein cg2159	Unknown function
cg2163	2,12	0,04	<i>dapB</i>	dapB, dihydrodipicolinate reductase	Amino acid transport and metabolism
cg2165	3,23	0,02		putative secreted protein	Unknown function
cg2167	0,41	0,01	<i>rpsO</i>	rpsO, 30S ribosomal protein S15	Translation, ribosomal structure and biogenesis
cg2169	1,32	0,02	<i>ribF</i>	ribF, hypothetical protein cg2169	Coenzyme transport and metabolism
cg2170	0,71	0,04	<i>truB</i>	truB, tRNA pseudouridine synthase B   truB, tRNA pseudouridine synthase B	Translation, ribosomal structure and biogenesis
cg2175	1,22	0,03	<i>rbfA</i>	rbfA, ribosome-binding factor A	Translation, ribosomal structure and biogenesis
cg2178	0,27	0,02	<i>nusA</i>	nusA, transcription elongation factor NusA   nusA, transcription elongation factor NusA   nusA, transcription elongation factor NusA	Transcription including sigma factors, RNA processing and modification
cg2179	0,54	0,01		hypothetical protein cg2179	Unknown function
cg2181	0,30	0,03	<i>oppA</i>	ABC-type peptide transport system, secreted component   ABC-type peptide transport system, secreted component	Transport and metabolism of further metabolites
cg2182	0,35	0,01	<i>oppB</i>	ABC-type peptide transport system, permease component	Transport and metabolism of further metabolites
cg2184	0,61	0,00	<i>oppD</i>	ATPase component of peptide ABC-type transport system, contains duplicated ATPase domains   ATPase component of peptide ABC-type transport system, contains duplicated ATPase domains	Transport and metabolism of further metabolites
cg2185	1,75	0,01	<i>proS</i>	proS, prolyl-tRNA synthetase	Translation, ribosomal structure and biogenesis
cg2186	1,23	0,03		hypothetical protein cg2186   hypothetical protein cg2186	Unknown function
cg2189	0,71	0,03	<i>cobA (cysG)</i>	cobA, uroporphyrinogen III synthase/methyltransferase	Transport and metabolism of further metabolites
cg2190	0,81	0,02		hypothetical protein cg2190	Unknown function
cg2192	2,47	0,02	<i>mgo</i>	mgo, malate:quinone oxidoreductase	Central carbon metabolism; Respiration and oxidative phosphorylation
cg2193	0,60	0,02		putative lysophospholipase	Cell wall/membrane/envelope biogenesis
cg2195	1,79	0,01		putative secreted or membrane protein	Unknown function
cg2196	1,54	0,03		putative secreted or membrane protein	Unknown function
cg2197	1,40	0,04		hypothetical protein cg2197	Unknown function
cg2198	2,52	0,00	<i>map2</i>	map2, methionine aminopeptidase	Protein turnover and chaperones
cg2199	0,55	0,01	<i>pbp2a</i>	pbp, penicillin-binding protein, putative D-alanyl-D-alanine carboxypeptidase	Cell wall/membrane/envelope biogenesis
cg2200	0,71	0,02	<i>chrA (cgtR8)</i>	cgtR8, two-component system, response regulator	Signal transduction mechanisms
cg2201	0,79	0,03	<i>chrS (cgtS8)</i>	cgtS8, two-component system, signal transduction histidine kinase	Post-translational modification; Signal transduction mechanisms
cg2202	0,61	0,04	<i>hrtB</i>	hrtB, ABC-type transport system, permease component	Transport and metabolism of further metabolites



cg2204	0,68	0,04	<i>hrtA</i>	hrtA, ABC-type transport system, ATPase component	Transport and metabolism of further metabolites
cg2206	1,64	0,03	<i>ispG</i>	ispG, 4-hydroxy-3-methylbut-2-en-1-yl diphosphate synthase	Transport and metabolism of further metabolites
cg2208	1,40	0,01	<i>dxr</i>	dxr, 1-deoxy-D-xylulose 5-phosphate reductoisomerase	Transport and metabolism of further metabolites
cg2213	0,82	0,01		ABC-type multidrug transport system, ATPase component	General function prediction only
cg2214	1,52	0,04		predicted Fe-S-cluster redox enzyme	General function prediction only
cg2215	3,48	0,00		hypothetical protein cg2215	General function prediction only
cg2221	0,72	0,01	<i>tsf</i>	tsf, elongation factor Ts	Translation, ribosomal structure and biogenesis
cg2222	0,54	0,01	<i>rpsB</i>	rpsB, 30S ribosomal protein S2	Translation, ribosomal structure and biogenesis
cg2230	2,77	0,00	<i>rnhB</i>	rnhB, ribonuclease HII	Transcription including sigma factors, RNA processing and modification
cg2232	2,00	0,00	<i>lepB</i>	lepB, probable signal peptidase I (spase I)	Protein secretion
cg2237	0,69	0,01	<i>thiO</i>	thiO, putative D-amino acid oxidase flavoprotein oxidoreductase	Coenzyme transport and metabolism
cg2238	0,71	0,05	<i>thiS</i>	thiS, sulfur transfer protein involved in thiamine biosynthesis	Coenzyme transport and metabolism
cg2239	0,71	0,01	<i>thiG</i>	thiG, thiazole synthase	Coenzyme transport and metabolism
cg2240	0,65	0,04	<i>thiF</i>	thiF, molybdopterin biosynthesis protein MoeB   thiF, molybdopterin biosynthesis protein MoeB	Coenzyme transport and metabolism
cg2241	1,19	0,01	<i>tex</i>	putative transcriptional accessory protein, RNA binding	Transcription including sigma factors, RNA processing and modification
cg2242	0,41	0,01		putative transcription regulation repressor, LacI family   putative transcription regulation repressor, LacI family	Signal transduction mechanisms
cg2248	0,86	0,04		hypothetical protein cg2248	Unknown function
cg2249	1,15	0,03	<i>trmD</i>	trmD, tRNA (guanine-N(1)-)-methyltransferase	Translation, ribosomal structure and biogenesis
cg2250	1,56	0,00		putative secreted lipoprotein	Unknown function
cg2251	0,56	0,00	<i>rimM</i>	rimM, 16S rRNA-processing protein	Translation, ribosomal structure and biogenesis
cg2252	4,03	0,01		double-stranded beta-helix domain	Unknown function
cg2253	0,50	0,02	<i>rpsP</i>	rpsP, 30S ribosomal protein S16   rpsP, 30S ribosomal protein S16	Translation, ribosomal structure and biogenesis
cg2257	1,19	0,05	<i>srp</i>	srp, signal recognition particle GTPase	Translation, ribosomal structure and biogenesis
cg2258	0,61	0,01	<i>glnD</i>	glnD, PII uridylyl-transferase	Signal transduction mechanisms
cg2261	1,88	0,01	<i>amtB</i>	amtB, low affinity ammonium uptake protein	Inorganic ion transport and metabolism
cg2262	0,51	0,01	<i>ftsY</i>	ftsY, signal recognition particle GTPase   ftsY, signal recognition particle GTPase   ftsY, signal recognition particle GTPase   ftsY, signal recognition particle GTPase	Translation, ribosomal structure and biogenesis
cg2263	1,41	0,02		hypothetical protein cg2263   hypothetical protein cg2263   hypothetical protein cg2263	Unknown function
cg2265	0,54	0,02	<i>smc</i>	smc, chromosome segregation ATPase   smc, chromosome segregation ATPase	Cell division, chromosome partitioning
cg2267	2,13	0,01		hypothetical protein cg2267   hypothetical protein cg2267	Unknown function
cg2272	1,54	0,02	<i>mutM1</i>	mutM1, formamidopyrimidine-DNA glycosylase	DNA replication, recombination, repair, and degradation
cg2275	1,97	0,02		putative F0F1-type ATP synthase b subunit	Cell division, chromosome partitioning
cg2277	0,64	0,02		ABC-type multidrug/protein/lipid transport system, transmembrane ATPase component   ABC-type multidrug/protein/lipid transport system, transmembrane ATPase component	General function prediction only
cg2279	0,56	0,03		ABC-type multidrug/protein/lipid transport system, transmembrane ATPase component   ABC-type multidrug/protein/lipid transport system, transmembrane ATPase component	General function prediction only
cg2280	0,71	0,01	<i>gdh</i>	gdh, glutamate dehydrogenase	Amino acid transport and metabolism
cg2282	1,21	0,01	<i>glxK</i>	glxK, putative glycerate kinase	Amino acid transport and metabolism; Lipid transport and metabolism
cg2284	0,44	0,01	<i>galT</i>	galactose-1-phosphate uridylyltransferase	Carbon source transport and metabolism
cg2285	0,78	0,02	<i>hipO</i>	hipO, putative hippurate hydrolase protein	Amino acid transport and metabolism
cg2286	0,60	0,02		hypothetical protein cg2286	General function prediction only
cg2287	0,72	0,02		hypothetical protein cg2287	Unknown function



cg2289	1,98	0,01	<i>glgP</i>	glgP2, alpha-glucan phosphorylase, glycogen phosphorylase   glgP2, alpha-glucan phosphorylase, glycogen phosphorylase	Carbon source transport and metabolism
cg2290	1,78	0,03		glyoxalase/bleomycin resistance/dioxygenase superfamily protein	General function prediction only
cg2293	0,75	0,01		putative indole-3-glycerol phosphate synthase	Amino acid transport and metabolism
cg2294	1,48	0,01		hypothetical protein cg2294	Unknown function
cg2296	1,51	0,03	<i>hisI</i>	hisI, phosphoribosyl-AMP cyclohydrolase	Amino acid transport and metabolism
cg2298	1,43	0,02	<i>impA</i>	impA, myo-inositol-1(or 4)-monophosphatase family protein	Cell wall/membrane/envelope biogenesis
cg2299	1,44	0,02	<i>hisA</i>	hisA, 1-(5-phosphoribosyl)-5-	Amino acid transport and metabolism
cg2300	2,62	0,00	<i>hisH</i>	hisH, imidazole glycerol phosphate synthase subunit HisH	Amino acid transport and metabolism
cg2302	0,73	0,01		hypothetical protein cg2302	Unknown function
cg2303	0,67	0,01	<i>hisB</i>	hisB, imidazoleglycerol-phosphate dehydratase	Amino acid transport and metabolism
cg2304	0,75	0,03	<i>hisC</i>	hisC, histidinol-phosphate aminotransferase	Amino acid transport and metabolism
cg2308	1,82	0,02		putative secreted protein	Unknown function
cg2309	0,67	0,04	<i>bioQ</i>	bacterial regulatory proteins, TetR family   bacterial regulatory proteins, TetR family	Signal transduction mechanisms
cg2310	0,50	0,00	<i>glgX</i>	glgX, glycogen debranching enzyme	Carbon source transport and metabolism
cg2311	3,08	0,01		SAM-dependent methyltransferase	General function prediction only
cg2313	1,87	0,02	<i>idhA3</i>	idhA3, myo-inositol 2-dehydrogenase	Cell wall/membrane/envelope biogenesis
cg2315	1,21	0,02		ATP-binding protein of ABC transporter	Carbon source transport and metabolism; Inorganic ion transport and metabolism
cg2317	1,62	0,00		permease of ABC transporter	Carbon source transport and metabolism; Inorganic ion transport and metabolism
cg2318	1,76	0,01		putative secreted vitamin B12-binding lipoprotein	Carbon source transport and metabolism; Inorganic ion transport and metabolism
cg2320	2,54	0,00		predicted transcriptional regulator	Signal transduction mechanisms
cg2321	0,72	0,05		DNA polymerase III epsilon subunit or related 3-5 exonuclease	DNA replication, recombination, repair, and degradation
cg2323	1,86	0,01	<i>treY</i>	treY, maltotigosyl trehalose synthase	Carbon source transport and metabolism; Cell wall/membrane/envelope biogenesis
cg2324	1,55	0,02		hypothetical protein cg2324	Unknown function
cg2329	1,33	0,01		coenzyme F420-dependent N5,N10-methylene tetrahydromethanopterin reductase or related flavin-dependent	Coenzyme transport and metabolism
cg2330	2,89	0,00		ribosome-associated heat shock protein implicated in the recycling of the 50S subunit (S4 paralog)	Translation, ribosomal structure and biogenesis
cg2331	2,63	0,01		hypothetical protein cg2331	Unknown function
cg2333	2,14	0,00	<i>treZ</i>	treZ, malto-oligosyltrehalose trehalohydrolase	Carbon source transport and metabolism; Cell wall/membrane/envelope biogenesis
cg2334	1,87	0,00	<i>ilvA</i>	ilvA, threonine dehydratase	Amino acid transport and metabolism; Coenzyme transport and metabolism
cg2338	3,58	0,00	<i>dnaE1</i>	dnaE1, DNA polymerase III subunit alpha	DNA replication, recombination, repair, and degradation
cg2339	2,92	0,01		predicted permease	General function prediction only
cg2341	1,81	0,03		predicted Co/Zn/Cd cation transporter   predicted Co/Zn/Cd cation transporter	Inorganic ion transport and metabolism
cg2342	3,12	0,00		dehydrogenase	General function prediction only
cg2348	0,60	0,00		putative secreted protein	Unknown function
cg2349	2,34	0,02		ATPase component of ABC transporters with duplicated ATPase domains	General function prediction only
cg2352	1,30	0,01	<i>ansA</i>	ansA, L-asparaginase   ansA, L-asparaginase	Amino acid transport and metabolism
cg2353	1,24	0,02		hypothetical protein disrupted by insertion of ISCG2e	Unknown function
cg2356	0,57	0,02		permease of the drug/metabolite transporter (DMT) superfamily	General function prediction only
cg2357	0,76	0,04		bacterial regulatory proteins, MerR family	Signal transduction mechanisms
cg2358	0,79	0,01		hypothetical protein cg2358	Unknown function
cg2359	0,84	0,02	<i>ileS</i>	ileS, isoleucyl-tRNA synthetase	Translation, ribosomal structure and biogenesis
cg2362	1,67	0,04		hypothetical protein cg2362	Unknown function
cg2363	0,48	0,00		hypothetical protein cg2363   hypothetical protein cg2363	Cell division, chromosome partitioning
cg2366	1,24	0,04	<i>ftsZ</i>	ftsZ, cell division protein FtsZ   ftsZ, cell division protein FtsZ	Cell division, chromosome partitioning

cg2368	1,49	0,00	<i>murC</i>	murC, UDP-N-acetylmuramate--L-alanine ligase	Cell wall/membrane/envelope biogenesis
cg2369	1,50	0,03	<i>murG</i>	murG, N-acetylglucosaminyl transferase	Cell wall/membrane/envelope biogenesis
cg2370	1,54	0,02	<i>ftsW</i>	ftsW, bacterial cell division membrane protein	Cell division, chromosome partitioning
cg2372	1,18	0,05	<i>mraY</i>	mraY, phospho-N-acetylmuramoyl-pentapeptide-transferase	Cell wall/membrane/envelope biogenesis
cg2374	1,51	0,01	<i>murE</i>	murE, UDP-N-acetylmuramoylalanine-D-glutamate--2,6-diaminopimelate ligase	Cell wall/membrane/envelope biogenesis
cg2378	0,50	0,00	<i>mraZ</i>	mraZ, hypothetical protein cg2378	Signal transduction mechanisms
cg2380	2,43	0,00		hypothetical protein cg2380	Unknown function
cg2381	0,47	0,02		hypothetical protein cg2381	Unknown function
cg2382	1,55	0,00	<i>act5</i>	GCN5-related N-acetyltransferase	General function prediction only
cg2383	0,51	0,01	<i>metF</i>	metF, 5,10-methylenetetrahydrofolate reductase	Amino acid transport and metabolism
cg2384	1,65	0,00	<i>idsA</i>	idsA, putative geranylgeranyl pyrophosphate synthase	Transport and metabolism of further metabolites
cg2385	1,24	0,00	<i>mptA</i>	mptA, alpha-1,6-mannopyranosyltransferase	Cell wall/membrane/envelope biogenesis
cg2390	4,52	0,00		hypothetical protein cg2390	Unknown function
cg2391	0,40	0,01	<i>aroG</i>	aroG, phospho-2-dehydro-3-deoxyheptonate aldolase	Amino acid transport and metabolism
cg2393	1,70	0,04		hypothetical protein cg2393	Unknown function
cg2394	0,69	0,03	<i>cmt4</i>	cmt4, corynomycolyl transferase	Cell wall/membrane/envelope biogenesis
cg2397	0,89	0,04		hypothetical protein cg2397	Unknown function
cg2400	1,30	0,00		pimB, Ac1PIM1 mannosyltransferase	General function prediction only
cg2402	0,63	0,01	<i>nlpC</i>	nlpC, putative secreted cell wall peptidase   nlpC, putative secreted cell wall peptidase	Cell wall/membrane/envelope biogenesis
cg2407	0,61	0,03	<i>#NV</i>	hypothetical protein cg2407	#NV
cg2408	0,51	0,01	<i>ctaF</i>	ctaF, cytochrome aa3 oxidase SU IV	Respiration and oxidative phosphorylation
cg2409	0,52	0,01	<i>ctaC</i>	ctaC, cytochrome C oxidase chain II   ctaC, cytochrome C oxidase chain II	Respiration and oxidative phosphorylation
cg2410	0,44	0,03	<i>ltsA</i>	ltsA, glutamine-dependent amidotransferase involved in formation of cell wall and L-glutamate biosynthesis   ltsA, glutamine-dependent amidotransferase involved in formation of cell wall and L-glutamate biosynthesis	Amino acid transport and metabolism; Cell wall/membrane/envelope biogenesis
cg2411	1,87	0,02		hypothetical protein HesB/YadR/YfhF family	Unknown function
cg2413	0,66	0,04	<i>cobU</i>	cobU, cobinamide kinase / cobinamide phosphate guanylyltransferase   cobU, cobinamide kinase / cobinamide phosphate guanylyltransferase	Coenzyme transport and metabolism
cg2414	0,47	0,00	<i>cobT</i>	cobT, nicotinate-nucleotide--dimethylbenzimidazole phosphoribosyltransferase   cobT, nicotinate-nucleotide--dimethylbenzimidazole phosphoribosyltransferase	Coenzyme transport and metabolism
cg2415	0,72	0,04	<i>cobS</i>	cobS, cobalamin synthase   cobS, cobalamin synthase	Coenzyme transport and metabolism
cg2417	2,20	0,00		short chain dehydrogenase   short chain dehydrogenase	General function prediction only
cg2418	0,56	0,01	<i>ilvE</i>	ilvE, branched-chain amino acid aminotransferase   ilvE, branched-chain amino acid aminotransferase	Amino acid transport and metabolism
cg2419	0,57	0,05	<i>pepB</i>	pepB, leucyl aminopeptidase   pepB, leucyl aminopeptidase   pepB, leucyl aminopeptidase	Protein turnover and chaperones
cg2420	2,15	0,00		hypothetical protein cg2420	Unknown function
cg2423	1,41	0,01	<i>lipA</i>	lipA, lipoyl synthase	Coenzyme transport and metabolism
cg2424	0,70	0,02		hypothetical protein cg2424	Unknown function
cg2428	2,04	0,01		hypothetical protein cg2428   hypothetical protein cg2428	Unknown function
cg2429	2,99	0,00	<i>glnA</i>	glnA, glutamine synthetase I	Amino acid transport and metabolism
cg2430	0,47	0,00		hypothetical protein cg2430	Unknown function
cg2431	0,73	0,04		putative transcriptional regulator	Signal transduction mechanisms
cg2437	1,72	0,03	<i>thrC</i>	thrC, threonine synthase   thrC, threonine synthase	Amino acid transport and metabolism
cg2438	0,50	0,02		hypothetical protein predicted by Glimmer	Unknown function
cg2440	0,83	0,04		permease of the major facilitator superfamily	General function prediction only

cg2444	1,16	0,03		hypothetical protein cg2444   hypothetical protein cg2444	Unknown function
cg2445	0,64	0,01	<i>hmuO</i>	hmuO, heme oxygenase   hmuO, heme oxygenase	Transport and metabolism of further metabolites
cg2446	0,52	0,01	<i>glnE</i>	glnE, glutamate-ammonia-ligase adenyl/transferase	Post-translational modification
cg2447	0,61	0,01	<i>glnA2</i>	glnA2, glutamine synthetase 2	Amino acid transport and metabolism
cg2449	0,66	0,04		hypothetical protein cg2449   hypothetical protein cg2449	General function prediction only
cg2450	1,46	0,02		putative pyridoxine biosynthesis enzyme	Coenzyme transport and metabolism
cg2451	3,43	0,00		hypothetical protein cg2451	Unknown function
cg2453	1,44	0,01		putative exoribonuclease   putative exoribonuclease	DNA replication, recombination, repair, and degradation
cg2454	0,61	0,01	<i>#NV</i>	hypothetical protein cg2454	#NV
cg2458	0,48	0,01	<i>pgp2</i>	pgp2, predicted phosphatase, HAD family	Carbon source transport and metabolism
cg2461	0,41	0,01	<i>tnp4a</i>	tnp4a(ISCg4a), transposase	DNA replication, recombination, repair, and degradation
cg2464	0,53	0,00		hypothetical protein cg2464	Unknown function
cg2466	0,73	0,04	<i>aceE</i>	aceE, pyruvate dehydrogenase subunit E1	Central carbon metabolism
cg2467	0,27	0,01		ABC transporter ATP-binding protein	Amino acid transport and metabolism
cg2468	0,33	0,01		branched-chain amino acid ABC-type transport system, permease component	Amino acid transport and metabolism
cg2470	0,27	0,00		secreted ABC transporter substrate-binding protein	Amino acid transport and metabolism
cg2471	2,45	0,00		weakly conserved hypothetical protein	Unknown function
cg2475	1,76	0,00		ATPase component of ABC transporters with duplicated ATPase domains	General function prediction only
cg2478	0,64	0,01	<i>pbp6</i>	putative penicillin binding protein	General function prediction only
cg2482	1,57	0,03		hypothetical protein cg2482	Unknown function
cg2483	0,61	0,04		hypothetical protein cg2483	Unknown function
cg2484	0,63	0,05		hypothetical protein cg2484	Unknown function
cg2485	0,57	0,01	<i>phoD</i>	phoD, secreted alkaline phosphatase precursor	Post-translational modification; Signal transduction mechanisms
cg2487	0,85	0,01		hypothetical protein cg2487	Unknown function
cg2490	1,62	0,00		secreted guanine-specific ribonuclease	Transcription including sigma factors, RNA processing and modification
cg2495	1,16	0,03		hypothetical protein cg2495	Unknown function
cg2497	1,22	0,01		hypothetical protein cg2497	Unknown function
cg2499	1,33	0,02	<i>glyS</i>	glyS, glycyl-tRNA synthetase	Translation, ribosomal structure and biogenesis
cg2502	2,14	0,02	<i>zur (fur)</i>	zur, zinc-dependent transcriptional regulator	Signal transduction mechanisms
cg2507	0,80	0,00		hypothetical protein cg2507	Unknown function
cg2509	0,70	0,02	<i>recO</i>	recO, DNA repair protein RecO	DNA replication, recombination, repair, and degradation
cg2510	0,61	0,01	<i>era (bex)</i>	era, GTP-binding protein Era	Cell division, chromosome partitioning
cg2516	1,60	0,03	<i>hrcA</i>	hrcA, heat-inducible transcription repressor	Signal transduction mechanisms
cg2519	0,53	0,00		hypothetical protein cg2519	Unknown function
cg2520	0,71	0,01		hypothetical protein cg2520	Unknown function
cg2523	1,88	0,00	<i>malQ</i>	malQ, 4-alpha-glucanotransferase	Carbon source transport and metabolism
cg2524	2,04	0,02		putative beta (1-->2) glucan export composite transmembrane/ATP-binding protein	Carbon source transport and metabolism
cg2527	0,72	0,00	<i>dcp</i>	dcp, probable peptidyl-dipeptidase A protein	Protein turnover and chaperones
cg2529	1,93	0,00	<i>treS</i>	treS, trehalose synthase (maltose alpha-D-glucosyltransferase)	Carbon source transport and metabolism; Cell wall/membrane/envelope biogenesis
cg2530	2,16	0,00	<i>treX</i>	treX, probable trehalose synthase	Carbon source transport and metabolism; Cell wall/membrane/envelope biogenesis
cg2536	0,57	0,00	<i>metC (aceD)</i>	metC, cystathionine beta-lyase   metC, cystathionine beta-lyase	Amino acid transport and metabolism
cg2537	0,48	0,01	<i>brnQ</i>	brnQ, branched-chain amino acid uptake carrier	Amino acid transport and metabolism
cg2538	1,41	0,02		alkanal monooxygenase alpha chain	General function prediction only
cg2539	0,45	0,00	<i>ectP</i>	ectP, ectoine/proline/glycine betaine carrier EctP   ectP, ectoine/proline/glycine betaine carrier EctP	Amino acid transport and metabolism
cg2542	0,71	0,04		predicted permease	Carbon source transport and metabolism
cg2545	0,64	0,01		putative secreted or membrane protein	Unknown function
cg2546	0,51	0,01		hypothetical protein cg2546	Carbon source transport and metabolism
cg2548	1,91	0,00	<i>#NV</i>	putative secreted protein	#NV

cg2549	0,58	0,00		ABC-type dipeptide/oligopeptide/nickel transport system, secreted component	General function prediction only
cg2550	0,42	0,00		ABC-type dipeptide/oligopeptide/nickel transport system, permease component	General function prediction only
cg2551	0,51	0,01		ABC-type dipeptide/oligopeptide/nickel transport system, permease component	General function prediction only
cg2552	0,48	0,00		ATPase component of ABC-type transport system, contains duplicated ATPase domain   ATPase component of ABC-type transport system, contains duplicated ATPase domain	General function prediction only
cg2553	2,07	0,01		2-5 RNA ligase	Transcription including sigma factors, RNA processing and modification
cg2554	3,62	0,00	<i>rbsK2</i>	rbsK2, probable ribokinase protein	Nucleotide transport and metabolism
cg2556	2,95	0,00		uncharacterized iron-regulated membrane protein	Unknown function
cg2557	0,26	0,00		predicted Na <sup>+</sup> -dependent transporter	General function prediction only
cg2558	1,16	0,02		related to aldose 1-epimerase	General function prediction only
cg2559	0,55	0,02	<i>aceB</i>	aceB, malate synthase	Central carbon metabolism
cg2560	0,20	0,00	<i>aceA</i>	aceA, isocitrate lyase	Central carbon metabolism
cg2563	1,44	0,01	<i>lcoP</i>	lcoP, ectoine betaine transporter   lcoP, ectoine betaine transporter   lcoP, ectoine betaine transporter	Transport and metabolism of further metabolites
cg2564	3,33	0,01		hypothetical protein cg2564	Unknown function
cg2565	0,66	0,01		hypothetical protein cg2565	Unknown function
cg2572	3,02	0,00		hypothetical protein cg2572	Unknown function
cg2573	0,39	0,00	<i>rpsT</i>	rpsT, 30S ribosomal protein S20	Translation, ribosomal structure and biogenesis
cg2574	1,50	0,00		lyse type translocator	Amino acid transport and metabolism
cg2576	0,74	0,01		DNA polymerase III subunit delta	DNA replication, recombination, repair, and degradation
cg2578	0,69	0,05		secreted DNA uptake protein or related DNA-binding protein	DNA replication, recombination, repair, and degradation
cg2579	0,46	0,01		protein DegV family	Unknown function
cg2581	0,47	0,00		putative fructose-2,6-bisphosphatase	Central carbon metabolism
cg2582	0,47	0,03		hypothetical protein cg2582	Unknown function
cg2584	0,79	0,04	<i>nadD</i>	nadD, nicotinic acid mononucleotide adenyltransferase	Coenzyme transport and metabolism
cg2585	0,68	0,03		putative secreted protein	Unknown function
cg2586	1,54	0,01	<i>proA</i>	proA, gamma-glutamyl phosphate reductase	Amino acid transport and metabolism
cg2587	1,44	0,02		phosphoglycerate dehydrogenase or related dehydrogenase	General function prediction only
cg2588	1,49	0,01	<i>proB</i>	proB, gamma-glutamyl kinase	Amino acid transport and metabolism
cg2589	1,67	0,03		predicted GTPase	General function prediction only
cg2591	2,26	0,01	<i>dkgA</i>	dkgA, 2,5-diketo-D-gluconic acid reductase	Coenzyme transport and metabolism
cg2594	0,64	0,01	<i>rpmA</i>	rpmA, 50S ribosomal protein L27	Translation, ribosomal structure and biogenesis
cg2595	0,57	0,04	<i>rplU</i>	rplU, 50S ribosomal protein L21	Translation, ribosomal structure and biogenesis
cg2597	0,66	0,01	<i>rneG</i>	rne, probable ribonuclease E (RNase E) protein   rne, probable ribonuclease E (RNase E) protein	Transcription including sigma factors, RNA processing and modification
cg2598	0,59	0,00		hypothetical protein cg2598   hypothetical protein cg2598	Unknown function
cg2599	1,32	0,03		pirin-related protein-fragment	General function prediction only
cg2600	0,80	0,03	<i>tnp1d</i>	tnp1d(ISCg1d), transposase   tnp1d(ISCg1d), transposase   tnp1d(ISCg1d), transposase   tnp1d(ISCg1d), transposase   tnp1d(ISCg1d), transposase	DNA replication, recombination, repair, and degradation
cg2602	0,59	0,05		hypothetical protein cg2602	Unknown function
cg2604	1,56	0,01		putative secreted or membrane protein	Unknown function
cg2605	1,28	0,04		predicted acetyltransferase	General function prediction only
cg2609	1,29	0,05	<i>valS</i>	valS, valyl-tRNA synthetase	Translation, ribosomal structure and biogenesis
cg2610	0,49	0,01		ABC-type dipeptide/oligopeptide/nickel transport system, secreted component   ABC-type dipeptide/oligopeptide/nickel transport system, secreted component	General function prediction only
cg2612	1,06	0,02		predicted rosmann fold nucleotide-binding protein	General function prediction only

cg2613	1,20	0,04	<i>mdh</i>	mdh, malate dehydrogenase   mdh, malate dehydrogenase	Anaerobic metabolism
cg2616	0,66	0,01	<i>vanA</i>	vanA, vanillate demethylase, oxygenase subunit   vanA, vanillate demethylase, oxygenase subunit	Carbon source transport and metabolism
cg2617	0,31	0,01	<i>vanB</i>	vanB, vanillate demethylase	Carbon source transport and metabolism
cg2618	0,39	0,00	<i>vanK</i>	vanK, transporter (vanillate/protocatechuate)   vanK, transporter (vanillate/protocatechuate)	Carbon source transport and metabolism
cg2619	4,73	0,00		predicted permease	General function prediction only
cg2620	2,92	0,00	<i>clpX</i>	clpX, ATP-dependent protease ATP-binding subunit   clpX, ATP-dependent protease ATP-binding subunit	Protein turnover and chaperones
cg2622	0,86	0,01	<i>pcaJ</i>	pcaJ, 7-ketoadipate succinyl-CoA transferase subunit   pcaJ, 7-ketoadipate succinyl-CoA transferase subunit	Carbon source transport and metabolism
cg2624	1,28	0,02	<i>pcaR</i>	pcaR, transcriptional regulator of 4-hydroxybenzoate, protocatechuate, p-cresol pathway	Signal transduction mechanisms
cg2628	0,46	0,01	<i>pcaC</i>	pcaC, 7-carboxymuconolactone decarboxylase	Carbon source transport and metabolism
cg2629	0,48	0,01	<i>pcaB</i>	pcaB, 7-carboxy-cis,cis-muconate cycloisomerase   pcaB, 7-carboxy-cis,cis-muconate cycloisomerase	Carbon source transport and metabolism
cg2630	0,38	0,00	<i>pcaG</i>	pcaG, protocatechuate dioxygenase alpha subunit   pcaG, protocatechuate dioxygenase alpha subunit	Carbon source transport and metabolism
cg2631	0,35	0,00	<i>pcaH</i>	pcaH, protocatechuate dioxygenase beta subunit	Carbon source transport and metabolism
cg2633	3,31	0,02		putative restriction endonuclease	DNA replication, recombination, repair, and degradation
cg2634	0,62	0,01	<i>catC</i>	catC, muconolactone isomerase	Carbon source transport and metabolism
cg2635	0,44	0,01	<i>catB</i>	catB, chloromuconate cycloisomerase	Carbon source transport and metabolism
cg2636	0,28	0,00	<i>catA1 (catA)</i>	catA1, catechol 1,2-dioxygenase   catA1, catechol 1,2-dioxygenase	Carbon source transport and metabolism
cg2637	0,29	0,00	<i>benA</i>	benA, benzoate 1,2-dioxygenase alpha subunit (aromatic ring hydroxylation dioxygenase A)   benA, benzoate 1,2-dioxygenase alpha subunit (aromatic ring hydroxylation dioxygenase A)	Carbon source transport and metabolism
cg2638	0,30	0,01	<i>benB</i>	benB, benzoate dioxygenase small subunit	Carbon source transport and metabolism
cg2639	0,41	0,02	<i>benC</i>	benC, benzoate 1,2-dioxygenase ferredoxin reductase subunit	Carbon source transport and metabolism
cg2640	0,40	0,03	<i>benD</i>	benD, cis-diol dehydrogenase	Carbon source transport and metabolism
cg2641	5,40	0,00	<i>benR</i>	benR, bacterial regulatory protein, LuxR family   benR, bacterial regulatory protein, LuxR family	Signal transduction mechanisms
cg2642	2,06	0,01	<i>benK1 (benK)</i>	benK1, putative benzoate transport protein   benK1, putative benzoate transport protein	Carbon source transport and metabolism
cg2643	1,72	0,04	<i>benE</i>	benE, benzoate membrane transport protein	Carbon source transport and metabolism
cg2644	4,81	0,00	<i>clpP2</i>	clpP2, ATP-dependent Clp protease proteolytic subunit	Protein turnover and chaperones
cg2645	5,29	0,00	<i>clpP1</i>	clpP1, ATP-dependent Clp protease proteolytic subunit	Protein turnover and chaperones
cg2648	0,68	0,02		bacterial regulatory protein, ArsR family	Signal transduction mechanisms
cg2649	0,70	0,04	<i>pbp5</i>	secreted penicillin binding protein	Transport and metabolism of further metabolites
cg2650	0,83	0,01		hypothetical protein cg2650	Unknown function
cg2651	2,47	0,00		conserved hypothetical protein-fragment	Unknown function
cg2652	0,50	0,02	<i>tnp12a</i>	tnp12a(ISC12a), transposase-fragment	DNA replication, recombination, repair, and degradation
cg2657	2,09	0,00		putative membrane protein-fragment	Unknown function
cg2658	2,14	0,03	<i>rpi</i>	rpi, ribose-5-phosphate isomerase B   rpi, ribose-5-phosphate isomerase B	Central carbon metabolism
cg2662	0,76	0,01	<i>pepN</i>	pepN, aminopeptidase N	Protein turnover and chaperones
cg2667	2,22	0,01		hypothetical protein predicted by Glimmer	Unknown function
cg2668	1,08	0,03	<i>crtI2-2</i>	crtI, phytoene desaturase (C-terminal fragment)	Transport and metabolism of further metabolites
cg2679	2,74	0,01		hypothetical protein cg2679	Unknown function
cg2685	1,70	0,01		short chain dehydrogenase	General function prediction only
cg2687	3,03	0,00	<i>metB</i>	metB, cystathionine gamma-synthase	Amino acid transport and metabolism

cg2688	0,73	0,03		ABC-type molybdenum transport system, ATPase component/photorepair protein PhrA	Inorganic ion transport and metabolism
cg2691	1,24	0,00		hypothetical protein cg2691	Unknown function
cg2694	0,58	0,02		hypothetical protein cg2694	Unknown function
cg2695	0,70	0,00		ABC-type transport system, ATPase component	General function prediction only
cg2699	2,87	0,02		hypothetical protein cg2699	Inorganic ion transport and metabolism
cg2700	0,38	0,02	<i>phoB</i>	phoB, alkaline phosphatase precursor	Post-translational modification; Signal transduction mechanisms
cg2701	0,40	0,02	<i>musI</i>	hypothetical protein cg2701	Carbon source transport and metabolism
cg2703	0,44	0,01	<i>musG</i>	sugar permease	Carbon source transport and metabolism
cg2704	0,52	0,04	<i>musF</i>	ABC-type sugar transport system, permease component	Carbon source transport and metabolism
cg2705	0,27	0,00	<i>musE (amyE/malE1)</i>	amyE, maltose-binding protein precursor	Carbon source transport and metabolism
cg2707	0,43	0,01		hypothetical protein cg2707	Unknown function
cg2708	0,47	0,02	<i>musK (msiK1)</i>	msiK1, ABC-type sugar transport system, ATPase component	Carbon source transport and metabolism
cg2710	0,43	0,02	<i>int3</i>	int3, integrase	DNA replication, recombination, repair, and degradation
cg2712	0,86	0,02		AraC-type regulator   AraC-type regulator	Signal transduction mechanisms
cg2714	0,59	0,05		Zn-dependent alcohol dehydrogenase, class III	General function prediction only
cg2715	0,69	0,03		hypothetical protein cg2715	Unknown function
cg2716	1,62	0,00	<i>hyi</i>	hyi, hydroxypyruvate isomerase	Carbon source transport and metabolism
cg2720	0,71	0,02	<i>lppS</i>	lppS, secreted lipoprotein Erk/YbiS/YcfS/YnhG family   lppS, secreted lipoprotein Erk/YbiS/YcfS/YnhG family	General function prediction only
cg2723	0,38	0,00		hypothetical protein cg2723	Unknown function
cg2727	1,24	0,05		putative secreted protein   putative secreted protein	Unknown function
cg2728	1,99	0,01	<i>glsK</i>	glsK, glutaminase	Amino acid transport and metabolism
cg2729	0,72	0,02		transcriptional repressor, LacI family, N-terminus	Signal transduction mechanisms
cg2732	1,69	0,01	<i>gntV (gntK)</i>	gntV, putative gluconokinase	Central carbon metabolism
cg2734	1,29	0,01	<i>pncA</i>	pncA, nicotinamidase/ pyrazinamidase	Coenzyme transport and metabolism
cg2735	1,95	0,00		hypothetical protein cg2735	Unknown function
cg2736	2,37	0,00	<i>bcp</i>	bcp, probable bacterioferritin comigratory oxidoreductase	Inorganic ion transport and metabolism
cg2737	1,82	0,03	<i>fasR</i>	fasR, regulator involved in control of cellular fatty acid synthesis	Signal transduction mechanisms
cg2738	1,24	0,04	<i>acpS (ppt1)</i>	acpS, 4-phosphopantetheinyl transferase   acpS, 4-phosphopantetheinyl transferase	Lipid transport and metabolism
cg2745	1,37	0,02		hypothetical protein cg2745	Unknown function
cg2746	0,65	0,01		putative sugar diacid utilization regulator	Signal transduction mechanisms
cg2748	2,55	0,02		hypothetical protein cg2748	Unknown function
cg2750	4,18	0,00		hypothetical protein cg2750	Unknown function
cg2751	0,69	0,01		putative deoxyribonucleotide triphosphate pyrophosphatase	Nucleotide transport and metabolism
cg2753	1,53	0,01	<i>rph</i>	rph, ribonuclease PH	Transcription including sigma factors, RNA processing and modification
cg2755	0,57	0,01		hypothetical protein cg2755	Unknown function
cg2761	0,71	0,03	<i>cpdA</i>	metal-dependent hydrolase of the beta-lactamase superfamily III	Signal transduction mechanisms
cg2765	0,58	0,01		putative secreted protein	Unknown function
cg2766	0,76	0,01		bacterial regulatory protein, MarR family	Signal transduction mechanisms
cg2768	1,35	0,02		L-aminopeptidase/D-esterase	General function prediction only
cg2770	1,49	0,02		hypothetical protein cg2770	Unknown function
cg2772	1,49	0,03	<i>clpS</i>	clpS, ATP-dependent Clp protease adaptor protein ClpS	Protein turnover and chaperones
cg2774	1,58	0,02		nicotinate phosphoribosyltransferase	Coenzyme transport and metabolism
cg2775	1,99	0,00		hypothetical protein cg2775	Unknown function
cg2778	1,12	0,04		hypothetical protein cg2778	Unknown function
cg2779	1,20	0,03	<i>serB</i>	serB, phosphoserine phosphatase	Amino acid transport and metabolism
cg2780	0,57	0,02	<i>ctaD</i>	ctaD, cytochrome aa3 oxidase, subunit 1   ctaD, cytochrome aa3 oxidase, subunit 1   ctaD, cytochrome aa3 oxidase, subunit 1	Respiration and oxidative phosphorylation
cg2781	3,48	0,01	<i>nrdF</i>	nrdF, ribonucleotide-diphosphate reductase beta subunit	Nucleotide transport and metabolism

cg2782	5,67	0,05	<i>ftn</i>	ftn, ferritin-like protein	Inorganic ion transport, metabolism, and storage
cg2783	0,88	0,01	<i>gntR1</i>	gntR1, gluconate-responsive repressors of genes involved in gluconate catabolism and the pentose phosphate pathway	Signal transduction mechanisms
cg2786	9,79	0,00	<i>nrdE</i>	nrdE, ribonucleotide-diphosphate reductase alpha subunit	Nucleotide transport and metabolism
cg2787	10,16	0,00	<i>nrdI</i>	nrdI, hypothetical protein cg2787	Nucleotide transport and metabolism
cg2789	7,12	0,00	<i>nrdH (mrX2)</i>	nrdH, putative glutaredoxin NRDH	0
cg2793	1,98	0,01		hypothetical protein cg2793	Unknown function
cg2795	2,62	0,00		NADPH quinone reductase or related Zn-dependent oxidoreductase	General function prediction only
cg2797	0,39	0,01		hypothetical protein cg2797	Unknown function
cg2799	0,50	0,00	<i>pknE</i>	pknE, putative secreted protein	Post-translational modification
cg2800	0,44	0,00	<i>pgm</i>	pgm, phosphoglucomutase	Central carbon metabolism
cg2801	0,86	0,00	<i>ccrB</i>	ccrB, camphor resistance protein CrcB	Inorganic ion transport, metabolism, and storage
cg2803	5,13	0,00		hypothetical protein cg2803	Unknown function
cg2805	0,66	0,02	<i>psp4</i>	psp4, putative secreted protein	Unknown function
cg2806	0,56	0,01		hypothetical protein cg2806	Unknown function
cg2809	0,72	0,01		hypothetical protein cg2809	Unknown function
cg2811	2,90	0,00		ABC-type transport system, involved in lipoprotein release, permease component	General function prediction only
cg2812	3,71	0,00		ABC-type transport system, involved in lipoprotein release, ATPase component	General function prediction only
cg2824	1,66	0,00		SAM-dependent methyltransferase	General function prediction only
cg2828	0,61	0,05		hypothetical protein cg2828   hypothetical protein cg2828	Unknown function
cg2829	3,11	0,00	<i>murA2</i>	murA2, UDP-N-acetylglucosamine 1-carboxyvinyltransferase	Cell wall/membrane/envelope biogenesis
cg2830	1,67	0,02	<i>pduO</i>	pduO, adenosylcobalamin-dependent diol dehydratase gamma	Coenzyme transport and metabolism
cg2831	0,91	0,05	<i>ramA</i>	ramA, transcriptional regulator, acetate metabolism	Signal transduction mechanisms
cg2833	3,25	0,00	<i>cysK</i>	cysK, O-acetylserine (thiol)-lyase	Amino acid transport and metabolism
cg2834	1,67	0,01	<i>cysE</i>	cysE, serine O-acetyltransferase	Amino acid transport and metabolism
cg2835	1,41	0,04		predicted acetyltransferase	General function prediction only
cg2836	0,23	0,01	<i>sucD</i>	sucD, succinyl-CoA synthetase alpha subunit	Central carbon metabolism
cg2837	0,23	0,00	<i>sucC</i>	sucC, succinyl-CoA synthetase subunit beta	Central carbon metabolism
cg2840	0,62	0,03	<i>actA (ctfA)</i>	actA, CoA transferase (acetate, propionate, succinate)	Central carbon metabolism
cg2842	3,19	0,00	<i>phoU</i>	phoU, putative phosphate uptake regulator	Inorganic ion transport, metabolism, and storage
cg2845	2,03	0,02	<i>pstC</i>	pstC, ABC-type phosphate transport system, permease component	Inorganic ion transport, metabolism, and storage
cg2848	0,51	0,01		putative secreted protein	Unknown function
cg2849	0,79	0,03		predicted kinase related to diacylglycerol kinase	General function prediction only
cg2850	0,68	0,00		hypothetical protein cg2850	Unknown function
cg2852	2,62	0,00		putative aminomethyltransferase, GCVT homolog   putative aminomethyltransferase, GCVT homolog	General function prediction only
cg2853	2,09	0,02		conserved hypothetical protein-fragment	Unknown function
cg2856	1,28	0,00	<i>purM</i>	purM, phosphoribosylaminoimidazole synthetase	Nucleotide transport and metabolism
cg2857	2,63	0,00	<i>purF</i>	purF, amidophosphoribosyltransferase	Nucleotide transport and metabolism
cg2860	0,48	0,01		putative acyl-CoA thioester hydrolase protein	General function prediction only
cg2862	0,56	0,00	<i>purL</i>	purL, phosphoribosylformylglycinamide synthase subunit II	Nucleotide transport and metabolism
cg2863	0,78	0,03	<i>purQ</i>	purQ, phosphoribosylformylglycinamide synthase subunit I	Nucleotide transport and metabolism
cg2867	0,43	0,00	<i>mpx</i>	gpx, glutathione peroxidase	Transport and metabolism of further metabolites
cg2868	0,70	0,00	<i>nuc (nucH)</i>	nuc, predicted extracellular nuclease	DNA replication, recombination, repair, and degradation
cg2869	1,67	0,04		predicted deacetylase	General function prediction only
cg2870	0,46	0,00	<i>dctA</i>	dctA, Na <sup>+</sup> /H <sup>+</sup> -dicarboxylate symporter	Carbon source transport and metabolism; Inorganic ion transport, metabolism, and storage
cg2873	3,30	0,00	<i>ptrB</i>	ptrB, prolyl oligopeptidase	Protein turnover and chaperones



cg2877	0,68	0,00	<i>avtA</i>	avtA, aminotransferase, uses alanine, keto-isovalerate and ketobutyrate	Amino acid transport and metabolism
cg2878	0,46	0,00	<i>purD</i>	purD, phosphoribosylamine-glycine ligase   purD, phosphoribosylamine-glycine ligase	Nucleotide transport and metabolism
cg2883	0,70	0,04		SAM-dependent methyltransferase	General function prediction only
cg2884	0,59	0,01		dipeptide/tripeptide permease	General function prediction only
cg2886	0,70	0,03	<i>bioD</i>	bioD, dithiobiotin synthetase   bioD, dithiobiotin synthetase	Coenzyme transport and metabolism
cg2887	1,53	0,04	<i>phoS (cgtS3)</i>	phoS, two component sensor kinase	Post-translational modification; Signal transduction mechanisms
cg2888	2,55	0,02	<i>phoR (cgtR3)</i>	phoR, two component response regulator	Signal transduction mechanisms
cg2890	1,28	0,01		putative amino acid processing enzyme	General function prediction only
cg2893	2,73	0,02		putative cadaverine transporter	Carbon source transport and metabolism
cg2896	0,34	0,00		putative secreted protein, hypothetical endoglucanase	General function prediction only
cg2898	1,78	0,00		putative 3-ketosteroid dehydrogenase	Carbon source transport and metabolism
cg2900	1,37	0,00	<i>ddh</i>	ddh, meso-diaminopimelate dehydrogenase	Amino acid transport and metabolism
cg2902	1,29	0,03		predicted hydrolase of the HAD superfamily	General function prediction only
cg2905	1,41	0,03	<i>thrE</i>	thrE, threonine export carrier	Amino acid transport and metabolism
cg2907	1,67	0,02	<i>otsA</i>	otsA, trehalose-6-phosphate synthase   otsA, trehalose-6-phosphate synthase	Carbon source transport and metabolism; Cell wall/membrane/envelope biogenesis
cg2909	1,75	0,05	<i>otsB</i>	otsB, trehalose phosphatase	Carbon source transport and metabolism; Cell wall/membrane/envelope biogenesis
cg2910	0,83	0,03	<i>ipsA</i>	transcriptional regulator, LacI family	Signal transduction mechanisms
cg2911	0,58	0,00	<i>znuA1</i>	ABC-type Mn/Zn transport system, secreted Mn/Zn-binding (lipo)protein (surface adhesion)	Inorganic ion transport, metabolism, and storage
cg2912	0,75	0,01	<i>znuC1</i>	ABC-type cobalamin/Fe3+-siderophores transport system, ATPase component	Inorganic ion transport, metabolism, and storage
cg2913	0,58	0,02	<i>znuB1</i>	ABC-type Mn2+/Zn2+ transport system, permease component	Inorganic ion transport, metabolism, and storage
cg2915	0,35	0,03		hypothetical protein cg2915	Unknown function
cg2925	0,33	0,01	<i>ptsS</i>	ptsS, enzyme II sucrose protein   ptsS, enzyme II sucrose protein	Carbon source transport and metabolism
cg2927	0,43	0,00	<i>scrB</i>	scrB, putative sucrose-6-phosphate hydrolase   scrB, putative sucrose-6-phosphate hydrolase	Carbon source transport and metabolism
cg2929	2,35	0,01	<i>nagA</i>	nagA1, probable N-acetylglucosamine-6-phosphate deacetylase   nagA1, probable N-acetylglucosamine-6-phosphate deacetylase	Carbon source transport and metabolism
cg2931	4,67	0,01	<i>nanA</i>	nanA, N-acetylneuraminase lyase (aldolase)   nanA, N-acetylneuraminase lyase (aldolase)	Carbon source transport and metabolism
cg2932	3,58	0,01	<i>nanK</i>	transcriptional regulator ROK family, putative sugar kinase	Carbon source transport and metabolism
cg2933	3,99	0,01	<i>nanE</i>	nanE, N-acetylmannosamine-6-phosphate 2-epimerase / N-AC   nanE, N-acetylmannosamine-6-phosphate 2-epimerase / N-AC	Carbon source transport and metabolism
cg2935	0,45	0,01	<i>nanP</i>	nanP, neuraminidase NANP   nanP, neuraminidase NANP	Carbon source transport and metabolism
cg2936	0,49	0,00	<i>nanR</i>	bacterial regulatory proteins, GntR family	Signal transduction mechanisms
cg2937	0,55	0,02	<i>siaE</i>	ABC-type dipeptide/oligopeptide/nickel transport system, secreted component   ABC-type dipeptide/oligopeptide/nickel transport system, secreted component   ABC-type dipeptide/oligopeptide/nickel transport system, secreted component	Carbon source transport and metabolism
cg2938	0,50	0,02	<i>siaF</i>	ABC-type dipeptide/oligopeptide/nickel transport system, permease component   ABC-type dipeptide/oligopeptide/nickel transport system, permease component	Carbon source transport and metabolism
cg2939	0,70	0,00	<i>siaG</i>	ABC-type dipeptide/oligopeptide/nickel transport system, fused permease and ATPase components	Carbon source transport and metabolism
cg2940	0,56	0,01	<i>siaI</i>	ATPase components of ABC-type transport system, contain duplicated ATPase domains	Carbon source transport and metabolism
cg2941	0,48	0,02		lyse type translocator	Amino acid transport and metabolism
cg2943	1,63	0,00		hypothetical protein cg2943	Unknown function
cg2944	1,55	0,00	<i>ispF</i>	ispF, 2-C-methyl-D-erythritol 2,4-cyclodiphosphate synthase   ispF, 2-C-	Transport and metabolism of further metabolites



				methyl-D-erythritol 2,4-cyclodiphosphate synthase	
cg2945	1,96	0,02	<i>ispD</i>	ispD, 2-C-methyl-D-erythritol 4-phosphate cytidyltransferase   ispD, 2-C-methyl-D-erythritol 4-phosphate cytidyltransferase	Transport and metabolism of further metabolites
cg2946	3,38	0,01		CarD-like transcriptional regulator   CarD-like transcriptional regulator	Signal transduction mechanisms
cg2947	0,60	0,03	<i>cgtR5</i>	cgtR5, putative two component response regulator	Signal transduction mechanisms
cg2948	0,48	0,02	<i>cgtS5</i>	cgtS5, probable two component sensor kinase	Post-translational modification; Signal transduction mechanisms
cg2949	0,54	0,05		putative secreted protein	Unknown function
cg2950	0,48	0,03	<i>radA</i>	putative ATP-dependent protease, DNA repair	DNA replication, recombination, repair, and degradation
cg2951	0,77	0,04		predicted nucleic-acid-binding protein (contains the HHH domain)	General function prediction only
cg2952	0,33	0,00		putative secreted protein	Unknown function
cg2953	0,62	0,01	<i>vdh</i>	xylC, benzaldehyde dehydrogenase   xylC, benzaldehyde dehydrogenase	Carbon source transport and metabolism
cg2954	0,69	0,01	<i>bca (cynT)</i>	cynT, carbonic anhydrase	Inorganic ion transport, metabolism, and storage
cg2955	0,82	0,02	<i>mutY</i>	mutY, A/g-specific adenine glycosylase	DNA replication, recombination, repair, and degradation
cg2959	0,54	0,01		putative secreted protein	Unknown function
cg2962	3,70	0,03		uncharacterized enzyme involved in biosynthesis of extracellular polysaccharides	Cell wall/membrane/envelope biogenesis
cg2965	0,67	0,05		AraC-type transcriptional regulator	Signal transduction mechanisms
cg2966	0,52	0,01		phenol 2-monooxygenase	Carbon source transport and metabolism
cg2975	1,52	0,00	<i>panC2</i>	panC2, pantoate-beta-alanine ligase	Coenzyme transport and metabolism
cg2976	1,93	0,01		hypothetical protein cg2976	Unknown function
cg2977	1,43	0,00		hypothetical protein cg2977	Unknown function
cg2982	0,78	0,04	<i>folP1</i>	folP1, dihydropteroate synthase	Coenzyme transport and metabolism
cg2983	0,65	0,01	<i>folE</i>	folE, GTP cyclohydrolase I	Coenzyme transport and metabolism
cg2985	0,69	0,04	<i>hpt</i>	hpt, hypoxanthine-guanine phosphoribosyltransferase	Nucleotide transport and metabolism
cg2986	0,43	0,01	<i>mesJ</i>	mesJ, ATPase of the PP-loop superfamily implicated in cell cycle control	Cell division, chromosome partitioning
cg2987	0,47	0,02	<i>pbp4b (dacB)</i>	dacB, penicillin-binding protein, D-Ala-D-Ala carboxypeptidase   dacB, penicillin-binding protein, D-Ala-D-Ala carboxypeptidase	Cell wall/membrane/envelope biogenesis
cg2988	0,74	0,01	<i>ppa</i>	ppa, inorganic pyrophosphatase	Inorganic ion transport, metabolism, and storage
cg2990	1,20	0,01	<i>speE</i>	speE, spermidine synthase	Transport and metabolism of further metabolites
cg2991	0,90	0,02		hypothetical protein cg2991	Unknown function
cg2993	1,10	0,03		hypothetical protein cg2993   hypothetical protein cg2993	Unknown function
cg2994	1,21	0,02		putative secreted or membrane protein	Unknown function
cg2999	1,98	0,01		putative ferredoxin reductase	General function prediction only
cg3001	0,75	0,03		hypothetical protein cg3001	Signal transduction mechanisms
cg3003	0,71	0,03	<i>cps</i>	cps, non-ribosomal peptide synthetase   cps, non-ribosomal peptide synthetase	Amino acid transport and metabolism
cg3004	0,61	0,01	<i>gabD1</i>	gabD2, succinic semialdehyde dehydrogenase	Transport and metabolism of further metabolites
cg3008	0,62	0,03	<i>porA</i>	porA, main cell wall channel protein	Inorganic ion transport, metabolism, and storage Transport and metabolism of further metabolites
cg3013	0,60	0,02		hypothetical protein cg3013	Unknown function
cg3014	0,56	0,01		hypothetical protein cg3014	Unknown function
cg3015	0,46	0,01		hypothetical protein cg3015	Unknown function
cg3016	0,38	0,00		hypothetical protein cg3016	Unknown function
cg3017	0,44	0,03		hypothetical protein cg3017   hypothetical protein cg3017   hypothetical protein cg3017	Unknown function
cg3018	0,52	0,01		hypothetical protein cg3018	Unknown function
cg3019	0,55	0,01		putative secreted protein	Unknown function
cg3021	0,74	0,03	<i>tpdA</i>	hypothetical protein cg3021   hypothetical protein cg3021	Protein turnover and chaperones
cg3022	2,17	0,00		acetyl-CoA acetyltransferase	General function prediction only

cg3024	1,46	0,00	<i>mrpA2 (mrpA)</i>	mrpA, NADH ubiquinone oxidoreductase subunit 5 (chain L)/multisubunit Na <sup>+</sup> /H <sup>+</sup> antiporter, A subunit	Inorganic ion transport, metabolism, and storage
cg3025	1,62	0,01	<i>mrpC2 (mrpC)</i>	mrpC, hypothetical protein cg3025   mrpC, hypothetical protein cg3025	Inorganic ion transport, metabolism, and storage
cg3026	2,27	0,01	<i>mrpD2 (mrpD)</i>	mrpD, NADH-ubiquinone oxidoreductase/multisubunit Na <sup>+</sup> /H <sup>+</sup> antiporter, D subunit	Inorganic ion transport, metabolism, and storage
cg3027	2,18	0,01	<i>mrpE2 (mrpE)</i>	mrpE, hypothetical protein cg3027	Inorganic ion transport, metabolism, and storage
cg3028	2,60	0,02	<i>mrpF2 (mrpF)</i>	mrpF, hypothetical protein cg3028	Inorganic ion transport, metabolism, and storage
cg3029	2,48	0,01	<i>mrpG2 (mrpG)</i>	mrpG, multisubunit Na <sup>+</sup> /H <sup>+</sup> antiporter, g subunit	Inorganic ion transport, metabolism, and storage
cg3031	0,73	0,05		hypothetical protein cg3031	Unknown function
cg3033	0,51	0,02		hypothetical protein cg3033	Unknown function
cg3034	0,45	0,00	<i>def1 (def)</i>	def, peptide deformylase	Post-translational modification
cg3035	0,46	0,00	<i>nagS?</i>	acetyltransferase	Amino acid transport and metabolism
cg3036	0,60	0,03	<i>xthA</i>	xthA, exodeoxyribonuclease III	DNA replication, recombination, repair, and degradation
cg3040	0,85	0,03		predicted epimerase, PhzC/PhzF homolog	General function prediction only
cg3041	0,82	0,04		ABC-type multidrug transport system, permease component	General function prediction only
cg3046	2,00	0,01	<i>pknG</i>	pknG, serine/threonine protein kinase	Post-translational modification
cg3047	0,28	0,00	<i>ackA</i>	ackA, acetate/propionate kinase	Anaerobic metabolism
cg3048	0,28	0,00	<i>pta</i>	pta, phosphate acetyltransferase	Anaerobic metabolism
cg3049	3,45	0,00	<i>fprA (fpr1)</i>	fprA, putative ferredoxin/ferredoxin-NADP reductase	Transport and metabolism of further metabolites
cg3050	1,24	0,02		acyltransferase	General function prediction only
cg3051	0,70	0,03		putative secreted protein	Unknown function
cg3053	0,49	0,01		permease of the major facilitator superfamily	General function prediction only
cg3054	0,51	0,02	<i>purT</i>	purT, 5-phosphoribosylglycinamide transformylase   purT, 5-phosphoribosylglycinamide transformylase	Nucleotide transport and metabolism
cg3057	0,75	0,04		putative secreted protein	Unknown function
cg3058	2,72	0,02	<i>tnp8b</i>	tnp8b(ISCg8a), transposase	DNA replication, recombination, repair, and degradation
cg3059	2,41	0,01	<i>tnp8a</i>	tnp8a(ISCg8a), transposase	DNA replication, recombination, repair, and degradation
cg3060	1,65	0,03	<i>cgtS6</i>	cgtS6, probable two component sensor kinase	Post-translational modification; Signal transduction mechanisms
cg3061	2,33	0,01	<i>cgtR6</i>	cgtR6, putative two component response regulator	Signal transduction mechanisms
cg3063	0,72	0,00	<i>purA</i>	purA, adenylosuccinate synthetase	Nucleotide transport and metabolism
cg3065	1,31	0,02		hypothetical protein cg3065	Unknown function
cg3068	1,34	0,03	<i>fda</i>	fda, fructose-bisphosphate aldolase	Central carbon metabolism
cg3070	0,55	0,00		SpoU rRNA methylase family protein	Translation, ribosomal structure and biogenesis
cg3071	0,59	0,02	<i>pyrE</i>	pyrE, orotate phosphoribosyltransferase	Nucleotide transport and metabolism
cg3072	1,92	0,03		putative secreted or membrane protein	Unknown function
cg3074	0,61	0,00		predicted transcriptional regulator	Signal transduction mechanisms
cg3075	0,63	0,00	<i>cmr</i>	cmr, multidrug resistance protein	Transport and metabolism of further metabolites
cg3077	1,91	0,00		hypothetical protein cg3077	Unknown function
cg3078	1,63	0,04		hypothetical protein cg3078	Unknown function
cg3079	2,05	0,01	<i>clpB</i>	clpB, probable ATP-dependent protease (heat shock protein)	Protein turnover and chaperones
cg3080	0,61	0,04	<i>gltS</i>	Na <sup>+</sup> /glutamate symporter	Inorganic ion transport, metabolism, and storage
cg3084	1,92	0,03		predicted flavoprotein involved in K <sup>+</sup> transport	Inorganic ion transport, metabolism, and storage
cg3086	0,63	0,01		putative L,L-cystathionine gamma-lyase	Transport and metabolism of further metabolites
cg3096	0,35	0,02	<i>ald (padaA)</i>	ald, alcohol dehydrogenase	Carbon source transport and metabolism
cg3097	1,79	0,00	<i>hspR</i>	hspR, transcriptional regulator MerR family   hspR, transcriptional regulator MerR family	Signal transduction mechanisms
cg3099	2,04	0,04	<i>grpE</i>	grpE, molecular chaperone GrpE (heat shock protein)	Protein turnover and chaperones
cg3102	0,53	0,04		nucleosidase	Nucleotide transport and metabolism
cg3103	0,38	0,01		hypothetical protein cg3103	Unknown function

cg3104	0,47	0,01		ATPase involved in DNA repair   ATPase involved in DNA repair	DNA replication, recombination, repair, and degradation
cg3105	0,37	0,01		hypothetical protein cg3105	Unknown function
cg3106	0,47	0,01		hypothetical protein cg3106   hypothetical protein cg3106	Unknown function
cg3107	0,21	0,01	<i>adhA</i>	<i>adhA</i> , Zn-dependent alcohol dehydrogenase	Carbon source transport and metabolism
cg3112	4,78	0,00	<i>cysZ</i>	predicted permease	Amino acid transport and metabolism; Inorganic ion transport, metabolism, and storage
cg3113	3,92	0,00	<i>cysY</i>	hypothetical protein cg3113	Amino acid transport and metabolism; Inorganic ion transport, metabolism, and storage
cg3114	4,56	0,00	<i>cysN</i>	<i>cysN</i> , sulfate adenylyltransferase subunit 1	Amino acid transport and metabolism; Inorganic ion transport, metabolism, and storage
cg3115	4,86	0,00	<i>cysD</i>	<i>cysD</i> , sulfate adenylyltransferase subunit 2	Amino acid transport and metabolism; Inorganic ion transport, metabolism, and storage
cg3116	4,38	0,01	<i>cysH</i>	<i>cysH</i> , phosphoadenosine-phosphosulfate reductase	Amino acid transport and metabolism; Inorganic ion transport, metabolism, and storage
cg3117	3,62	0,02	<i>cysX</i>	hypothetical protein cg3117	Amino acid transport and metabolism; Inorganic ion transport, metabolism, and storage
cg3118	4,32	0,01	<i>cysI</i>	<i>cysI</i> , sulfite reductase (hemoprotein)   <i>cysI</i> , sulfite reductase (hemoprotein)	Amino acid transport and metabolism; Inorganic ion transport, metabolism, and storage
cg3119	5,29	0,00	<i>cysJ (fpr2)</i>	<i>cysJ</i> , probable sulfite reductase (flavoprotein)	Amino acid transport and metabolism; Inorganic ion transport, metabolism, and storage
cg3120	1,47	0,01		hypothetical protein cg3120	Unknown function
cg3122	0,55	0,03	<i>phnB1</i>	<i>phnB1</i> , uncharacterized protein, homolog of PhnB E.coli	Inorganic ion transport, metabolism, and storage
cg3125	0,46	0,02	<i>tctA</i>	<i>tctA</i> , tricarboxylate transport membrane protein	Carbon source transport and metabolism
cg3126	0,38	0,00	<i>tctB</i>	<i>tctB</i> , tricarboxylate transport membrane protein	Carbon source transport and metabolism
cg3127	0,46	0,00	<i>tctC</i>	<i>tctC</i> , tricarboxylate-binding protein	Carbon source transport and metabolism
cg3128	0,75	0,02		ABC-type transport system, ATPase component	General function prediction only
cg3129	0,80	0,04		ABC-type transport system, ATPase component	General function prediction only
cg3130	0,43	0,01		permease of the major facilitator superfamily	General function prediction only
cg3131	1,67	0,01		acetylornithine deacetylase or related deacetylase	General function prediction only
cg3133	0,47	0,01		ATPase component STY3232 of energizing module of queuosine-regulated ECF transporter / ATPase component STY3233 of	Carbon source transporter and metabolism; Inorganic ion transport, metabolism, and storage
cg3134	0,54	0,02		transmembrane component STY3231 of energizing module of queuosine-regulated ECF transporter	Carbon source transporter and metabolism; Inorganic ion transport, metabolism, and storage
cg3135	0,56	0,01		substrate-specific component STY3230 of queuosine-regulated ECF transporter	Carbon source transporter and metabolism; Inorganic ion transport, metabolism, and storage
cg3137	0,54	0,00	<i>iunH1</i>	<i>iunH1</i> , inosine-uridine preferring nucleoside hydrolase   <i>iunH1</i> , inosine-uridine preferring nucleoside hydrolase	Nucleotide transport and metabolism
cg3138	0,82	0,01	<i>ppmA</i>	<i>ppmA</i> , putative membrane-bound protease modulator	Protein turnover and chaperones
cg3141	3,36	0,02	<i>hmp</i>	<i>hmp</i> , flavohemoprotein	Inorganic ion transport, metabolism, and storage
cg3142	1,37	0,04		hypothetical protein cg3142	Unknown function
cg3143	2,01	0,04		putative secreted protein	Unknown function
cg3148	0,77	0,02	<i>fepC</i>	ABC-type cobalamin/Fe3+-siderophores transport system, ATPase component	General function prediction only
cg3149	0,62	0,01	<i>alaT</i>	<i>alaT</i> , aminotransferase, uses alanine, glutamate, 2-aminobutyrate ad aspartate	Amino acid transport and metabolism
cg3154	1,83	0,02	<i>udgA2</i>	<i>udgA2</i> , UDP-glucose 6-dehydrogenase	Nucleotide transport and metabolism
cg3155	1,85	0,03	<i>dcd</i>	<i>dcd</i> , deoxycytidine triphosphate deaminase	Nucleotide transport and metabolism
cg3157	1,94	0,04		putative secreted protein   putative secreted protein	Unknown function

cg3158	0,56	0,00	<i>nagA2</i>	nagA2, beta-N-acetylglucosaminidase precursor	Cell wall/membrane/envelope biogenesis
cg3160	0,68	0,00		putative secreted protein	Unknown function
cg3162	0,38	0,04		hypothetical protein cg3162	Unknown function
cg3164	0,59	0,01		putative secreted or membrane protein	Cell wall/membrane/envelope biogenesis
cg3165	0,69	0,01		hypothetical protein cg3165   hypothetical protein cg3165	Cell wall/membrane/envelope biogenesis
cg3170	0,76	0,01		tellurite resistance protein or related permease   tellurite resistance protein or related permease	General function prediction only
cg3172	1,52	0,02	<i>trmB</i>	trmB, tRNA (guanine-N(7)-)-methyltransferase	Translation, ribosomal structure and biogenesis
cg3174	1,60	0,00	<i>mmpL1</i>	mmpL1, exporter of the MMPL family	Cell wall/membrane/envelope biogenesis
cg3176	0,60	0,02		hypothetical protein cg3176	Unknown function
cg3177	0,57	0,02	<i>pccB (accD4)</i>	pccB, propionyl-CoA carboxylase beta chain	Cell wall/membrane/envelope biogenesis
cg3179	0,65	0,00	<i>fadD2</i>	fadD2, acyl-CoA synthase	Cell wall/membrane/envelope biogenesis
cg3180	0,61	0,01		putative secreted protein, lipase-associated function	General function prediction only
cg3181	0,40	0,01		putative secreted protein	Unknown function
cg3182	0,45	0,01	<i>cop1</i>	cop1, trehalose corynomycyl transferase	Cell wall/membrane/envelope biogenesis
cg3185	0,49	0,00		hypothetical protein cg3185	Unknown function
cg3186	0,45	0,01	<i>cmt2</i>	cmt2, trehalose corynomycyl transferase	Cell wall/membrane/envelope biogenesis
cg3187	0,44	0,03	<i>aftB</i>	aftB, arabinofuranosyltransferase	Cell wall/membrane/envelope biogenesis
cg3189	0,44	0,00	<i>ubiA</i>	hypothetical protein cg3189	Transport and metabolism of further metabolites; Cell wall/membrane/envelope biogenesis
cg3190	0,51	0,01		membrane-associated phospholipid phosphatase   membrane-associated phospholipid phosphatase	Unknown function
cg3192	2,37	0,01		putative secreted or membrane protein	Unknown function
cg3194	0,80	0,05		membrane-associated PA-phosphatase related phosphoesterase	Cell wall/membrane/envelope biogenesis
cg3195	0,21	0,01		flavin-containing monooxygenase (FMO)	General function prediction only
cg3196	0,55	0,00	<i>glf</i>	glf, UDP-galactopyranose mutase	Cell wall/membrane/envelope biogenesis
cg3199	1,76	0,00		predicted hydrolase of the HAD superfamily	General function prediction only
cg3200	1,36	0,03		acyltransferase family protein	General function prediction only
cg3201	1,53	0,01	<i>serS</i>	serS, seryl-tRNA synthetase	Translation, ribosomal structure and biogenesis
cg3203	1,33	0,03		hypothetical protein cg3203	Unknown function
cg3204	0,64	0,02		hypothetical protein cg3204	Unknown function
cg3205	0,50	0,04		hypothetical protein cg3205	Unknown function
cg3206	0,46	0,01		phosphoglycerate mutase family protein	General function prediction only
cg3207	0,64	0,00	<i>pheA</i>	pheA, prephenate dehydratase	Amino acid transport and metabolism
cg3208	0,71	0,04		Asp-tRNAAsn/Glu-tRNAIle amidotransferase A subunit or related amidase	Translation, ribosomal structure and biogenesis
cg3209	0,58	0,00		predicted metal-dependent membrane protease	Protein turnover and chaperones
cg3210	0,43	0,00	<i>lcpB</i>	cell envelope-related transcriptional regulator	Cell wall/membrane/envelope biogenesis
cg3211	1,80	0,01		putative secreted protein	Unknown function
cg3213	2,03	0,01		putative secreted protein	Unknown function
cg3214	0,59	0,01		hypothetical protein cg3214	Unknown function
cg3216	0,33	0,02	<i>gntP</i>	gntP, gluconate permease	Carbon source transport and metabolism
cg3218	1,32	0,04		pyruvate kinase	General function prediction only
cg3220	0,39	0,03		hypothetical protein cg3220	Unknown function
cg3221	0,72	0,03		predicted hydrolase of the HAD superfamily	General function prediction only
cg3223	1,52	0,03		NADPH-dependent FMN reductase	Coenzyme transport and metabolism
cg3225	1,45	0,04		putative serine/threonine-specific protein phosphatase	Post-translational modification; Signal transduction mechanisms
cg3226	0,03	0,00		putative L-lactate permease	Carbon source transport and metabolism
cg3227	0,09	0,00	<i>lldD</i>	lldD, quinone-dependent L-lactate dehydrogenase LldD	Carbon source transport and metabolism; Respiration and oxidative phosphorylation
cg3228	0,35	0,01		hypothetical protein cg3228	Unknown function
cg3232	1,91	0,00		secreted phosphohydrolase, ICC family	General function prediction only
cg3233	3,52	0,01		hypothetical protein cg3233	Unknown function
cg3234	1,85	0,03		metal-dependent amidase/aminoacylase/carboxypeptidase   metal-dependent amidase/aminoacylase/carboxypeptidase	Protein turnover and chaperones

cg3235	2,13	0,00	#NV	hypothetical protein cg3235   hypothetical protein cg3235	#NV
cg3236	3,41	0,00	<i>msrA</i>	<i>msrA</i> , peptide methionine sulfoxide reductase	Transport and metabolism of further metabolites
cg3238	0,70	0,01		hypothetical protein cg3238	Unknown function
cg3243	0,30	0,01		predicted RecB family nuclease	DNA replication, recombination, repair, and degradation
cg3246	0,66	0,03		bacterial regulatory protein, MarR family	Signal transduction mechanisms
cg3248	0,75	0,02	<i>hrrS (cgtS11)</i>	<i>cgtS11</i> , probable two component sensor kinase   <i>cgtS11</i> , probable two component sensor kinase	Post-translational modification; Signal transduction mechanisms
cg3249	0,85	0,03		putative secreted protein	Unknown function
cg3252	1,83	0,00		putative inner membrane protein translocase component VidC	Protein secretion
cg3253	1,54	0,02	<i>mcbR</i>	<i>mcbR</i> , TetR-type transcriptional regulator of sulfur metabolism	Signal transduction mechanisms
cg3254	1,64	0,02		hypothetical protein cg3254   hypothetical protein cg3254	Unknown function
cg3256	1,72	0,00		alkanal monooxygenase alpha chain	General function prediction only
cg3257	1,56	0,03		hypothetical protein cg3257	Unknown function
cg3258	1,63	0,04	<i>rluC2</i>	<i>rluC2</i> , putative ribosomal pseudouridine synthase	Translation, ribosomal structure and biogenesis
cg3260	0,51	0,04	#NV	hypothetical protein cg3260   hypothetical protein cg3260   hypothetical protein cg3260	#NV
cg3263	0,64	0,03		hypothetical protein cg3263	Unknown function
cg3264	1,62	0,01	<i>rsmP</i>	<i>rsmP</i> , cytoskeletal protein RsmP, regulates rod-shape morphology	Cell division, chromosome partitioning
cg3267	0,53	0,02		hypothetical protein cg3267	Unknown function
cg3273	2,75	0,03		hypothetical protein predicted by Glimmer	Unknown function
cg3274	4,40	0,01		site-specific recombinases, DNA invertase Pin homolog-fragment   site-specific recombinases, DNA invertase Pin homolog-fragment	DNA replication, recombination, repair, and degradation
cg3275	3,50	0,00	<i>fdxA</i>	<i>fdxA</i> , ferredoxin	General function prediction only
cg3276	1,32	0,03	#NV	hypothetical protein cg3276	#NV
cg3277	2,58	0,02		uncharacterized ACR, double-stranded beta-helix domain	General function prediction only
cg3279	2,75	0,01		putative dehydrogenase-fragment	General function prediction only
cg3280	4,98	0,00		putative secreted protein   putative secreted protein	Unknown function
cg3281	6,89	0,00	<i>copB</i>	probable cation-transporting ATPase transmembrane protein	Inorganic ion transport, metabolism, and storage
cg3282	6,22	0,00		cation transport ATPase	Inorganic ion transport, metabolism, and storage
cg3283	7,40	0,01		hypothetical protein predicted by Glimmer	Unknown function
cg3284	0,33	0,02	<i>copS (cgtS9)</i>	<i>cgtS9</i> , probable two component sensor kinase	Post-translational modification; Signal transduction mechanisms
cg3285	0,57	0,04	<i>copR (cgtR9)</i>	<i>cgtR9</i> , putative two component response regulator	Signal transduction mechanisms
cg3286	0,46	0,03		putative secreted protein	Unknown function
cg3287	0,49	0,01	<i>copO</i>	secreted multicopper oxidase	Inorganic ion transport, metabolism, and storage
cg3288	0,35	0,00		hypothetical protein predicted by Glimmer	Unknown function
cg3291	0,33	0,04		bacterial regulatory protein, Crp family   bacterial regulatory protein, Crp family	Signal transduction mechanisms
cg3294	0,49	0,02		hypothetical protein cg3294	Unknown function
cg3295	0,67	0,02		cation transport ATPase	Inorganic ion transport, metabolism, and storage
cg3297	1,21	0,03	<i>tnp19b</i>	<i>tnp19b</i> (ISCG19a), transposase-fragment   <i>tnp19b</i> (ISCG19a), transposase-fragment	DNA replication, recombination, repair, and degradation
cg3299	0,55	0,03	<i>trxB1</i>	<i>trxB1</i> , thioredoxin	Transport and metabolism of further metabolites
cg3300	0,40	0,00		cation transport ATPase	Inorganic ion transport, metabolism, and storage
cg3303	2,92	0,02		transcriptional regulator PadR-like family	Signal transduction mechanisms
cg3306	0,54	0,02	<i>rplI</i>	<i>rplI</i> , 50S ribosomal protein L9	Translation, ribosomal structure and biogenesis
cg3308	0,52	0,03	<i>rpsF</i>	<i>rpsF</i> , 30S ribosomal protein S6	Translation, ribosomal structure and biogenesis
cg3309	2,16	0,02		putative secreted protein	Unknown function

cg3311	0,67	0,04		hypothetical protein cg3311	Unknown function
cg3313	1,17	0,03	<i>pbp1b (mcrB)</i>	mrcB, membrane carboxypeptidase, penicillin-binding protein	Cell wall/membrane/envelope biogenesis
cg3314	2,02	0,01		hypothetical protein cg3314	Unknown function
cg3315	1,81	0,04	<i>malR</i>	bacterial regulatory protein, MarR family	Signal transduction mechanisms
cg3316	2,06	0,00		universal stress protein UspA or related nucleotide-binding protein	Transcription including sigma factors, RNA processing and modification
cg3318	2,89	0,00		uncharacterized enzyme involved in biosynthesis of extracellular polysaccharides	Cell wall/membrane/envelope biogenesis
cg3320	0,75	0,02		ABC-type transport system, involved in lipoprotein release, permease component	Protein secretion
cg3321	0,78	0,04		ABC-type transport system, involved in lipoprotein release, ATPase component	Protein secretion
cg3323	0,46	0,03	<i>ino1</i>	myo-inositol-1-phosphate synthase	Cell wall/membrane/envelope biogenesis
cg3324	0,47	0,01		putative secreted protein	Unknown function
cg3325	0,65	0,01		hypothetical protein cg3325   hypothetical protein cg3325	Unknown function
cg3327	4,38	0,04	<i>dps</i>	dps, starvation-induced DNA protecting protein	Inorganic ion transport, metabolism, and storage
cg3328	0,86	0,04	<i>mutM2</i>	mutM2, probable formamidopyrimidine-DNA glycosylase protein	DNA replication, recombination, repair, and degradation
cg3329	3,25	0,01		hypothetical protein cg3329	Unknown function
cg3330	1,84	0,01		putative secreted protein	Unknown function
cg3331	1,41	0,00	<i>ogt</i>	ogt, methylated-DNA--protein-cysteine methyltransferase	DNA replication, recombination, repair, and degradation
cg3332	1,57	0,01	<i>qor3</i>	putative quinone oxidoreductase	Respiration and oxidative phosphorylation
cg3335	0,21	0,00	<i>malE (mez)</i>	malE, malic enzyme	Central carbon metabolism
cg3336	2,16	0,02	<i>gntK</i>	gntK, putative gluconate kinase   gntK, putative gluconate kinase	Central carbon metabolism
cg3337	3,34	0,00		hypothetical protein cg3337	Unknown function
cg3338	4,83	0,00		hypothetical protein cg3338	Unknown function
cg3339	1,62	0,01	<i>merA</i>	merA, putative FAD-dependent pyridine nucleotide-disulphideoxidoreductase, similar to mercuric reductases	DNA replication, recombination, repair, and degradation
cg3341	0,48	0,00		hypothetical protein cg3341	Unknown function
cg3342	0,56	0,00		putative secreted protein	Unknown function
cg3345	0,24	0,00		hypothetical protein cg3345   hypothetical protein cg3345	Unknown function
cg3346	0,68	0,04	<i>leuS</i>	leuS, leucyl-tRNA synthetase	Translation, ribosomal structure and biogenesis
cg3348	0,53	0,01		putative plasmid maintenance system antidote protein, HigA homolog	General function prediction only
cg3352	0,64	0,00	<i>nagR (genR)</i>	nagR, transcriptional regulator of gentisate pathway	Signal transduction mechanisms
cg3353	0,49	0,04	<i>nagT (genK)</i>	nagT, gentisate transporter	Amino acid transport and metabolism
cg3354	0,37	0,01	<i>genH (nahG)</i>	3-hydroxybenzoate 6-hydroxylase	Transport and metabolism of further metabolites
cg3356	0,36	0,01		Na <sup>+</sup> /H <sup>+</sup> -dicarboxylate symporter	Carbon source transport and metabolism; Inorganic ion transport, metabolism, and storage
cg3358	0,67	0,05	<i>#NV</i>	hypothetical protein predicted by Glimmer	#NV
cg3359	0,89	0,04	<i>trpE</i>	trpE, anthranilate synthase component I	Amino acid transport and metabolism
cg3360	0,77	0,00	<i>trpG</i>	trpG, anthranilate synthase component II	Amino acid transport and metabolism
cg3364	0,61	0,00	<i>trpA</i>	trpA, tryptophan synthase subunit alpha	Amino acid transport and metabolism
cg3365	0,40	0,00	<i>ptsA1 (ulaA, rmpC)</i>	ulaA, ascorbate-specific PTS system enzyme IIC	Carbon source transport and metabolism; Signal transduction mechanisms
cg3366	0,46	0,01	<i>ptsA2 (sgCA, rmpA)</i>	rmpA, putative ribitol-specific enzyme II of PTS system	Carbon source transport and metabolism; Signal transduction mechanisms
cg3368	2,65	0,01		ABC-transporter permease protein   ABC-transporter permease protein	General function prediction only
cg3369	2,53	0,04		Rieske-type iron-sulfur protein	General function prediction only
cg3370	2,05	0,01		putative NADH-dependent flavin oxidoreductase   putative NADH-dependent flavin oxidoreductase	General function prediction only
cg3371	1,36	0,00		Na <sup>+</sup> -dependent transporter	General function prediction only
cg3372	2,39	0,00		hypothetical protein cg3372	Unknown function
cg3373	1,77	0,00	<i>cyeR</i>	bacterial regulatory proteins, ArsR family	Signal transduction mechanisms
cg3374	3,74	0,01	<i>cye1</i>	putative NADH-dependent flavin oxidoreductase   putative NADH-dependent flavin oxidoreductase	General function prediction only

cg3375	1,49	0,03		predicted nucleoside-diphosphate-sugar epimerase	Nucleotide transport and metabolism
cg3378	0,63	0,02		hypothetical protein cg3378	Unknown function
cg3384	0,77	0,03		bacterial regulatory protein, TetR family	Signal transduction mechanisms
cg3387	0,64	0,04	<i>iolT2</i>	<i>iolT2</i> , myo-Inositol transporter	Carbon source transport and metabolism
cg3388	0,56	0,03		bacterial regulatory proteins, IclR family	Signal transduction mechanisms
cg3390	0,96	0,05		myo-Inositol catabolism, sugar phosphate isomerase/epimerase	Carbon source transport and metabolism
cg3393	0,65	0,05	<i>phoC</i>	putative secreted phosphoesterase	Inorganic ion transport, metabolism, and storage
cg3395	0,31	0,01	<i>proP</i>	<i>proP</i> , proline/ectoine carrier	Amino acid transport and metabolism
cg3397	0,70	0,01		hypothetical protein cg3397	Unknown function
cg3398	0,53	0,01		DNA or RNA helicase of superfamily II	General function prediction only
cg3399	7,88	0,00		permease of the major facilitator superfamily	General function prediction only
cg3402	3,54	0,00		copper chaperone   copper chaperone	Inorganic ion transport, metabolism, and storage
cg3404	4,35	0,00		secreted siderophore-binding lipoprotein	Carbon source transport and metabolism; Inorganic ion transport, metabolism, and storage
cg3405	0,70	0,04		NADPH quinone reductase or Zn-dependent oxidoreductase	General function prediction only
cg3407	0,90	0,03		hypothetical protein cg3407	Unknown function
cg3408	2,47	0,02		hypothetical protein predicted by Glimmer	Unknown function
cg3409	0,73	0,04	<i>thiD2</i>	<i>thiD2</i> , phosphomethylpyrimidine kinase	Coenzyme transport and metabolism
cg3410	0,63	0,02		hypothetical protein cg3410	Unknown function
cg3411	2,62	0,00		copper chaperone	Inorganic ion transport, metabolism, and storage
cg3412	0,52	0,01	<i>azlD</i>	<i>azlD</i> , predicted branched-chain amino acid permease (azaleucine resistance)	Amino acid transport and metabolism
cg3415	0,65	0,04	<i>pcnA</i>	<i>pcnA</i> , poly-A polymerase	DNA replication, recombination, repair, and degradation
cg3417	0,53	0,03		NTP pyrophosphohydrolase   NTP pyrophosphohydrolase	Nucleotide transport and metabolism
cg3418	0,51	0,00		putative secreted protein	Unknown function
cg3419	0,36	0,00		uncharacterized membrane protein, virulence factor homolog	General function prediction only
cg3420	0,56	0,00	<i>sigM</i>	<i>sigM</i> , RNA polymerase sigma-70 factor, ECF subfamily	Transcription including sigma factors, RNA processing and modification
cg3422	0,67	0,03	<i>trxB</i>	<i>trxB</i> , thioredoxin reductase	General function prediction only
cg3423	0,61	0,03	<i>trxC</i>	<i>trxC</i> , thioredoxin	General function prediction only
cg3428	0,41	0,00	<i>gidB</i>	<i>gidB</i> , glucose-inhibited division protein B	Cell division, chromosome partitioning
cg3429	0,50	0,01		putative inner membrane protein translocase component YidC	Protein secretion
cg3431	0,45	0,03	<i>rnpA</i>	<i>rnpA</i> , ribonuclease p	Transcription including sigma factors, RNA processing and modification
cg3433	0,62	0,03		hypothetical protein cg3433	Unknown function
cg4000	2,00	0,01	<i>#NV</i>	hypothetical protein cg4000	<i>#NV</i>
cg4001	0,49	0,02		hypothetical protein cg4001	Unknown function
cg4003	1,36	0,03	<i>#NV</i>	hypothetical protein cg4003	<i>#NV</i>
cg4004	1,11	0,02		hypothetical protein cg4004   hypothetical protein cg4004	Unknown function
cg4007	2,89	0,00		hypothetical protein cg4007	Prophage genes
cgr01	1,69	0,01		16S ribosomal RNA	Translation, ribosomal structure and biogenesis
cgr04	1,79	0,01		16S ribosomal RNA   geneID:3345599	Translation, ribosomal structure and biogenesis
cgr05	1,86	0,03		23S ribosomal RNA   geneID:3345511	Translation, ribosomal structure and biogenesis
cgr07	1,74	0,01		16S ribosomal RNA   geneID:3345547	Translation, ribosomal structure and biogenesis
cgr12	1,80	0,00		16S ribosomal RNA   geneID:3344357	Translation, ribosomal structure and biogenesis
cgr18	1,76	0,05		16S ribosomal RNA   geneID:3344358	Translation, ribosomal structure and biogenesis
cgs01	0,43	0,04	<i>ssrA (cgb_09185)</i>	<i>tmRNA</i>   geneID:3343963	Translation, ribosomal structure and biogenesis; Protein turnover and chaperones
cgtRNA_3528	1,52	0,01			Translation, ribosomal structure and biogenesis

cgtRNA_3529	0,80	0,01			Translation, ribosomal structure and biogenesis
cgtRNA_3533	0,48	0,03			Translation, ribosomal structure and biogenesis
cgtRNA_3534	0,42	0,03			Translation, ribosomal structure and biogenesis
cgtRNA_3535	0,58	0,01			Translation, ribosomal structure and biogenesis
cgtRNA_3536	0,25	0,00			Translation, ribosomal structure and biogenesis
cgtRNA_3537	0,48	0,02			Translation, ribosomal structure and biogenesis
cgtRNA_3542	0,31	0,01			Translation, ribosomal structure and biogenesis
cgtRNA_3545	0,64	0,02			Translation, ribosomal structure and biogenesis
cgtRNA_3560	0,82	0,01			Translation, ribosomal structure and biogenesis
cgtRNA_3561	0,70	0,04			Translation, ribosomal structure and biogenesis
cgtRNA_3570	0,57	0,01			Translation, ribosomal structure and biogenesis
cgtRNA_3572	0,31	0,05			Translation, ribosomal structure and biogenesis
cgtRNA_3577	0,53	0,03			Translation, ribosomal structure and biogenesis
cgtRNA_3586	0,62	0,03			Translation, ribosomal structure and biogenesis
cgtRNA_3587	0,57	0,04			Translation, ribosomal structure and biogenesis



**Video S1: Time-lapse video of a *C. glutamicum* microcolony of the prophage reporter strain under cg1978 overexpression (50  $\mu$ M IPTG).** Cells of the prophage reporter strain ATCC 13032::P<sub>lys</sub>-*eyfp* carrying the overexpression plasmid pAN6-cg1978 were cultivated in microfluidic chambers (Grünberger et al., 2015) using CGXII minimal medium with 2% (w/v) glucose and 25  $\mu$ g ml<sup>-1</sup> kanamycin for 18 h. Overexpression was induced using 50  $\mu$ M IPTG.

**Video S2: Time-lapse video of a *C. glutamicum* microcolony of the prophage reporter strain under standard conditions (0  $\mu$ M IPTG).** The same reporter strain (Video S1) carrying the overexpression plasmid pAN6-cg1978 was grown in the absence of IPTG serving as a control for normal cell growth.

**The videos are provided as separate files:**

- Video S1\_cg1978 overexpression\_prophage reporter\_50  $\mu$ M IPTG
- Video S2\_cg1978 overexpression\_prophage reporter\_0  $\mu$ M IPTG

## References

- Baumgart, M., Unthan, S., Ruckert, C., Sivalingam, J., Grünberger, A., Kalinowski, J., . . . Frunzke, J. (2013). Construction of a prophage-free variant of *Corynebacterium glutamicum* ATCC 13032 for use as a platform strain for basic research and industrial biotechnology. *Applied and Environmental Microbiology*, 79(19), 6006-6015. doi:10.1128/AEM.01634-13
- Cremer, J., Eggeling, L., & Sahm, H. (1990). Cloning the *dapA dapB* cluster of the lysine-secreting bacterium *Corynebacterium glutamicum*. *Molecular and General Genetics*, 220, 478-480. doi:10.1007/BF00391757
- Frunzke, J., Engels, V., Hasenbein, S., Gätgens, C., & Bott, M. (2008). Co-ordinated regulation of gluconate catabolism and glucose uptake in *Corynebacterium glutamicum* by two functionally equivalent transcriptional regulators, GntR1 and GntR2. *Molecular Microbiology*, 67(2), 305-322. doi:10.1111/j.1365-2958.2007.06020.x
- Grünberger, A., Probst, C., Helfrich, S., Nanda, A., Stute, B., Wiechert, W., . . . Kohlheyer, D. (2015). Spatiotemporal microbial single-cell analysis using a high-throughput microfluidics cultivation platform. *Cytometry Part A*, 87(12), 1101-1115. doi:10.1002/cyto.a.22779
- Helfrich, S., Pfeifer, E., Krämer, C., Sachs, C. C., Wiechert, W., Kohlheyer, D., . . . Frunzke, J. (2015). Live cell imaging of SOS and prophage dynamics in isogenic bacterial populations. *Molecular Microbiology*, 98(4), 636-650. doi:10.1111/mmi.13147
- Hünnefeld, M., Persicke, M., Kalinowski, J., & Frunzke, J. (2019). The MarR-Type Regulator MalR Is Involved in Stress-Responsive Cell Envelope Remodeling in *Corynebacterium glutamicum*. *Frontiers in Microbiology*, 10, 1039. doi:10.3389/fmicb.2019.01039
- Ikeda, M., & Nakagawa, S. (2003). The *Corynebacterium glutamicum* genome: features and impacts on biotechnological processes. *Applied Microbiology and Biotechnology*, 62(2-3), 99-109. doi:10.1007/s00253-003-1328-1
- Pfeifer, E., Hünnefeld, M., Popa, O., Polen, T., Kohlheyer, D., Baumgart, M., & Frunzke, J. (2016). Silencing of cryptic prophages in *Corynebacterium glutamicum*. *Nucleic acids research*, 44(21), 10117-10131. doi:10.1093/nar/gkw692
- Schäfer, A., Tauch, A., Jäger, W., Kalinowski, J., Thierbach, G., & Pühler, A. (1994). Small mobilizable multi-purpose cloning vectors derived from the *Escherichia coli* plasmids pK18 and pK19: selection of defined deletions in the chromosome of *Corynebacterium glutamicum*. *Gene*, 145(1), 69-73. doi:10.1016/0378-1119(94)90324-7
- Sievers, F., Wilm, A., Dineen, D., Gibson, T. J., Karplus, K., Li, W., . . . Higgins, D. G. (2011). Fast, scalable generation of high-quality protein multiple sequence alignments using Clustal Omega. *Molecular Systems Biology*, 7, 539. doi:10.1038/msb.2011.75
- Studier, F. W., & Moffatt, B. A. (1986). Use of bacteriophage T7 RNA polymerase to direct selective high-level expression of cloned genes. *Journal of Molecular Biology*, 189(1), 113-130. doi:10.1016/0022-2836(86)90385-2

## 4.2. Appendix to 3.2: Aminoglycoside antibiotics inhibit phage infection by blocking an early step of the infection cycle

Part A: Supplementary material to the published manuscript

**Supplementary information to**

### **Aminoglycoside antibiotics inhibit phage infection by blocking an early step of the infection cycle**

Running title: Aminoglycosides inhibit phage infection

Larissa Kever<sup>1#</sup>, Aël Hardy<sup>1#</sup>, Tom Luthe<sup>1</sup>, Max Hünnefeld<sup>1</sup>, Cornelia Gätgens<sup>1</sup>, Lars Milke<sup>1</sup>, Johanna Wiechert<sup>1</sup>, Johannes Wittmann<sup>2</sup>, Cristina Moraru<sup>3</sup>, Jan Marienhagen<sup>1,4</sup> and Julia Frunzke<sup>1\*</sup>

<sup>1</sup>Institute of Bio- und Geosciences, IBG-1: Biotechnology, Forschungszentrum Jülich, 52425 Jülich, Germany

<sup>2</sup>Leibniz Institute DSMZ—German Collection of Microorganisms and Cell Cultures, Inhoffenstraße 7B, 38124 Braunschweig, Germany

<sup>3</sup>Institute for Chemistry and Biology of the Marine Environment (ICBM), Carl-von-Ossietzky-University Oldenburg, Oldenburg, Germany

<sup>4</sup>Institute of Biotechnology, RWTH Aachen University, Aachen, Germany

<sup>#</sup> Authors contributed equally to this work.

\*Corresponding author:

Julia Frunzke; Email: [j.frunzke@fz-juelich.de](mailto:j.frunzke@fz-juelich.de); Phone: +49 2461 615430

**Tables**

Supplementary Table S1 | Aminoglycoside-modifying enzymes used in this study

Supplementary Table S2A | Bacterial strains used in this study.

Supplementary Table S2B | Phages used in this study

Supplementary Table S2C | Plasmids used in this study.

Supplementary Table S2D | Oligonucleotides used in this study

Supplementary Table S3 | Polynucleotides used for phage targeting direct-geneFISH

**Figures**

Supplementary Figure S1 | Dose-dependent effect of apramycin on the *Streptomyces* phage Alderaan.

Supplementary Figure S2 | Effect of aminoglycosides on *E. coli* phage  $\lambda$ .

Supplementary Figure S3 | Synchronized infection of *Streptomyces venezuelae* with phage Alderaan under apramycin pressure.

Supplementary Figure S4 | Investigations of the mechanism of action of apramycin.

Supplementary Figure S5 | Pre-incubation of phage Alderaan with apramycin.

Supplementary Figure S6 | Distribution of fluorescence intensities from phage targeting direct-geneFISH.

**Videos**

Supplementary Video S1 | Apramycin prevents cell lysis during infection of *S. venezuelae* with phage Alderaan.

Supplementary Table S1: Aminoglycoside-modifying enzymes used in this study

Antibiotic	Gene	Annotation	Protein sequence	Modification
<b>Apramycin</b>	<i>aac(3)IV' (apr)</i>	Aminoglycoside N(3)-acetyltransferase	VQYEWKRAELIGQLNLGVTPGGV LLVHSSFRSVRPLEDGPLGLIEALRA ALGPGGTLVMPWSWGLDDEPFDPA TSPVTPDLGVVSDTFWRLPNVKRS AHPFAFAAAGPQAEQIISDPLPLPH SPASPVARVHELDDGQVLLGVGH ANTTLHLAELMAKVYPYGVPRHCTI LQDGKLVVRVDYLENDHCCERFALA DRWLKEKSLQKEGPVGHAFARLIR SRDIVATALGQLGRDPLIFLHPPEA GCEECDAARQSIG	Acetylation of 3-amino group of the deoxystreptamine ring
<b>Hygromycin</b>	<i>aph(7'')-Ia</i>	Aminoglycoside O-phosphotransferase APH(7'')-Ia,	VTQESLLLLDRIDSDDSYASLRNDQ EFWEPLARRALEELGLPVPPVLRVP GESTNPVLVGEPPVVKLFGEHWCG PESLASESEAYAVLADAPVPVPRLL GRGELRPGTGAWPWPYLVMSRMT GTTWRSAMDGTTRNALLALARE LGRVLGRLHRVPLTGNTVLTPHSE VFPELLRERRAATVEDHRGWGYLS PRLLDRLDOWLDPDVTLLAGREPR FVHGDLHGNTNIFVDLAATEVTGIVD FTDVYAGDSRYSLVQLHLNAFRGD REILAAALDGAQWKRTEDFARELL AFTFLHDFEVFEETPLDLSGFTDPEE LAQFLWGPPDTAPGA	Phosphorylation of hydroxyl group at position 7''
<b>Kanamycin</b>	<i>aph(3'')-Ia</i>	Aminoglycoside 3'-phosphotransferase	MSHIQRETSCSRPRLNSNMDADLY GYKWARDNVGQSGATTYRLYGKP DAPELFLKHGKGSVANDVTDEM RLNWLTEFMPLPTIKHFIRTPDDAW LLTTAIPGKTAQVLEEYDSDGENIV DALAVFLRRLHSIPVNCNCPNSDRV FRLAQASRMNNGLVASDFDDER NGWPVEQVWKEMHKLLPSPDSV VTHGDFSLDNLFDEGLIGCIDVVG RVGLADRYQDLAILWNCLEGFSPSL QKRLFQKYGIDNPD MNKLQFHLML DEFF	Phosphorylation of hydroxyl group at position 3'
<b>Spectinomycin/ Streptomycin</b>	<i>aadA</i>	Aminoglycoside (3'') (9) adenylyltransferase	MREAVIAEVSTQLSEVVGVIERHLE PTLLAVHLYGSVDGGLKPHSDIDL LVTVTVRLDETTRRALINDLLETS SPGESEILRAVEVTIVVHDDIIPWRY PAKRELQFGEWQRNDILAGIFEPAT IDIDLAILLTKAREHSVALVGPAEE LFDVPVEQDLFEALNETLTLWNSPP DWAGDERNVVLTLSRIWYSAVTG KIAPKDVAAADWAMERLPAQYQPV LEARQAYLGQEEEDRLASRADQLEE FVHYVKGEITKVVVGK	O-adenylation at positions 3'' and 9

**Supplementary Table S2A: Bacterial strains used in this study**

Strains	Genotype	Reference
<i>C. glutamicum</i> MB001	ATCC 13032 strain with deletion of prophages ΔCGP1 (cg1507-cg1524), ΔCGP2 (cg1746-cg1752) und ΔCGP3 (cg1890-cg2071)	<sup>1</sup>
<i>C. glutamicum</i> MB001 – pEKEx2a	MB001 carrying the plasmid pEKEx2a, Kan <sup>R</sup>	This study
<i>C. glutamicum</i> MB001 – pEKEx2b	MB001 carrying the plasmid pEKEx2b, Hyg <sup>R</sup>	This study
<i>C. glutamicum</i> MB001 – pEKEx2d	MB001 carrying the plasmid pEKEx2d, Apr <sup>R</sup>	This study
<i>C. glutamicum</i> MB001 – pEKEx2e	MB001 carrying the plasmid pEKEx2e, Sp <sup>R</sup> /Sm <sup>R</sup>	This study
<i>Escherichia coli</i> DH5α	<i>supE44 lacU169 (ΔlacZDM15) hsdR17 recA1 endA1 gyrA96 thi-1 relA1</i>	Invitrogen
<i>Escherichia coli</i> ET12567/pUZ8002	<i>dam-13::Tn9 dcm-6 hsdM hsdR</i> , carrying plasmid pUZ8002	<sup>2</sup>
<i>Escherichia coli</i> BL21 (DE3)	F <sup>-</sup> <i>ompT hsdS<sub>B</sub>(r<sub>B</sub><sup>-</sup> m<sub>B</sub><sup>-</sup>) gal dcm λ(DE3)</i>	<sup>3</sup>
<i>Escherichia coli</i> DSM 613	Wild-type strain	<sup>4</sup>
<i>E. coli</i> DSM 613 – pEKEx2a	<i>E. coli</i> DSM 613 carrying the plasmid pEKEx2a, Kan <sup>R</sup>	This study
<i>E. coli</i> DSM 613 – pEKEx2b	<i>E. coli</i> DSM 613 carrying the plasmid pEKEx2b, Hyg <sup>R</sup>	This study
<i>E. coli</i> DSM 613 – pEKEx2d	<i>E. coli</i> DSM 613 carrying the plasmid pEKEx2d, Apr <sup>R</sup>	This study
<i>E. coli</i> DSM 613 – pEKEx2e	<i>E. coli</i> DSM 613 carrying the plasmid pEKEx2e, Sp <sup>R</sup> /Sm <sup>R</sup>	This study
<i>Escherichia coli</i> DSM 5695	F <sup>+</sup> <i>met str T1<sup>s</sup> T6<sup>s</sup> lambda</i>	<sup>5</sup>
<i>E. coli</i> DSM 5695 – pEKEx2a	<i>E. coli</i> DSM 5695 carrying the plasmid pEKEx2a, Kan <sup>R</sup>	This study
<i>E. coli</i> DSM 5695 – pEKEx2b	<i>E. coli</i> DSM 5695 carrying the plasmid pEKEx2b, Hyg <sup>R</sup>	This study
<i>E. coli</i> DSM 5695 – pEKEx2d	<i>E. coli</i> DSM 5695 carrying the plasmid pEKEx2d, Apr <sup>R</sup>	This study
<i>E. coli</i> DSM 5695 – pEKEx2e	<i>E. coli</i> DSM 5695 carrying the plasmid pEKEx2e, Sp <sup>R</sup> /Sm <sup>R</sup>	This study
<i>Escherichia coli</i> DSM 4230	F <sup>-</sup> <i>hsdR514 (rk mk<sup>-</sup>) supE44 supF58 Δ(lacIZY)6 galK2 galT22 metB1 trpR55 lambda</i>	<sup>6</sup>
<i>E. coli</i> DSM 4230 – pEKEx2a	<i>E. coli</i> DSM 4230 carrying the plasmid pEKEx2a, Kan <sup>R</sup>	This study
<i>E. coli</i> DSM 4230 – pEKEx2b	<i>E. coli</i> DSM 4230 carrying the plasmid pEKEx2b, Hyg <sup>R</sup>	This study
<i>E. coli</i> DSM 4230 – pEKEx2d	<i>E. coli</i> DSM 4230 carrying the plasmid pEKEx2d, Apr <sup>R</sup>	This study

<i>E. coli</i> DSM 4230 – pEKEx2e	<i>E. coli</i> DSM 4230 carrying the plasmid pEKEx2e, Sp <sup>R</sup> /Sm <sup>R</sup>	This study
<i>Escherichia coli</i> JW3996	<i>E. coli</i> BW25113 $\Delta lamB$	7
<i>Streptomyces venezuelae</i> ATCC 10712	Wild-type strain	8
<i>S. venezuelae</i> ATCC 10712 – pJLK01	<i>S. venezuelae</i> ATCC 10712 carrying the integrative plasmid pJLK01, Hyg <sup>R</sup>	This study
<i>S. venezuelae</i> ATCC 10712 – pJLK04	<i>S. venezuelae</i> ATCC 10712 carrying the integrative plasmid pJLK04, Apr <sup>R</sup>	This study
<i>S. venezuelae</i> ATCC 10712 – pJLK05	<i>S. venezuelae</i> ATCC 10712 carrying the integrative plasmid pJLK05, Sp <sup>R</sup> /Sm <sup>R</sup>	This study
<i>Streptomyces coelicolor</i> M145	<i>S. coelicolor</i> A3(2) lacking plasmids SCP1 and SCP2	9
<i>S. coelicolor</i> M145– pJLK01	<i>S. coelicolor</i> M145 carrying the integrative plasmid pJLK01, Hyg <sup>R</sup>	This study
<i>S. coelicolor</i> M145– pJLK04	<i>S. coelicolor</i> M145 carrying the integrative plasmid pJLK04, Apr <sup>R</sup>	This study
<i>S. coelicolor</i> M145– pJLK05	<i>S. coelicolor</i> M145 carrying the integrative plasmid pJLK05, Sp <sup>R</sup> /Sm <sup>R</sup>	This study

Supplementary Table S2B: Phages used in this study

Phage	Host organism	Lifestyle	Family	Genome	State of injected genome <sup>13,14</sup>	Reference
<b>Alderaan</b>	<i>S. venezuelae</i> ATCC 10712	Virulent	<i>Siphoviridae</i>	dsDNA	Linear with terminal redundancy	15
<b>Coruscant</b>	<i>S. venezuelae</i> ATCC 10712	Virulent	<i>Siphoviridae</i>	dsDNA	Linear with terminal repeats	15
<b>Dagobah</b>	<i>S. coelicolor</i> M145	Temperate	<i>Siphoviridae</i>	dsDNA	Linear with terminal repeats	15
<b>Endor1</b>	<i>S. coelicolor</i> M145	Temperate	<i>Siphoviridae</i>	dsDNA	Linear with terminal redundancy	15
<b>Endor2</b>	<i>S. coelicolor</i> M145	Temperate	<i>Siphoviridae</i>	dsDNA	Linear with terminal redundancy	15
<b>CL31</b>	<i>C. glutamicum</i> MB001	Temperate	<i>Siphoviridae</i>	dsDNA	Linear with cohesive ends	16
<b>Spe2</b>	<i>C. glutamicum</i> ATCC 13032	Virulent	<i>Siphoviridae</i>	dsDNA	Unknown	This study, DSM110582
<b>T4</b>	<i>E. coli</i> B (DSM613)	Virulent	<i>Myoviridae</i>	dsDNA	Linear with terminal redundancy	DSM4505
<b>T5</b>	<i>E. coli</i> B (DSM613)	Virulent	<i>Siphoviridae</i>	dsDNA	Linear with terminal redundancy	DSM16353
<b>T6</b>	<i>E. coli</i> B (DSM613)	Virulent	<i>Myoviridae</i>	dsDNA	Linear with terminal repeats	DSM4622
<b>T7</b>	<i>E. coli</i> B (DSM613)	Virulent	<i>Podoviridae</i>	dsDNA	Linear with terminal repeats	DSM4623
<b>M13</b>	<i>E. coli</i> W1485 (DSM5695)	Chronic infection	<i>Inoviridae</i>	ssDNA	Circular (+) strand	DSM13976
<b>fd</b>	<i>E. coli</i> W1485 (DSM5695)	Chronic infection	<i>Inoviridae</i>	ssDNA	Circular (+) strand	DSM4498
<b>MS2</b>	<i>E. coli</i> W1485 (DSM5695)	Virulent	<i>Leviviridae</i>	ssRNA	Linear, bound to the maturation protein <sup>17</sup>	DSM13767
<b>Lambda (λ)</b>	<i>E. coli</i> LE392 (DSM4230)	Temperate	<i>Siphoviridae</i>	dsDNA	Linear with cohesive ends	DSM4499



**Supplementary Table S2C: Plasmids used in this study.** Insert DNA was amplified using the listed oligonucleotides (compare Supplementary File 5). Linearization of vector DNA was conducted with the indicated restriction enzyme and plasmids were constructed using Gibson assembly. Sequencing was performed by Eurofins Genomics (Ebersberg, Germany) with the sequencing oligonucleotides listed.

Plasmids	Characteristics						Reference
pIJ10257	Hyg <sup>R</sup> , Cloning vector for the conjugal transfer of DNA from <i>E. coli</i> to <i>Streptomyces spp.</i> ; (constitutive promoter <i>ermE</i> <sup>*</sup> ; Integration at the ΦBT1 attachment site)						18
pEKEx2	Kan <sup>R</sup> , <i>C. glutamicum</i> / <i>E. coli</i> shuttle vector for regulated gene expression; <i>P</i> <sub>tac</sub> , <i>lacI</i> <sup>q</sup> , pBL1 <i>oriV</i> <sub>C.g.</sub> , pUC18 <i>oriV</i> <sub>E.c.</sub>						19
pIJ773	pBluescript II SK(+)-based plasmid containing the apramycin resistance cassette flanked by FRT (FLP recognition target) recombination sites						20
pCDFduet-1	Sp <sup>R</sup> /Sm <sup>R</sup> ; <i>E. coli</i> vector for coexpression of two target genes; Pr <sub>7</sub> , <i>lacI</i> , CloDF13 ori, T7 terminator						Novagen
pUZ8002	Kan <sup>R</sup> , RK2 derivative with nontransmissible oriT						21
pAN6	Kan <sup>R</sup> ; <i>E. coli</i> vector for regulated gene expression; derivative of pEKEx2 ( <i>P</i> <sub>tac</sub> , <i>lacI</i> <sup>q</sup> , pBL1 <i>oriV</i> <sub>C.g.</sub> , pUC18 <i>oriV</i> <sub>E.c.</sub> )						22
Plasmids	Characteristics	Template	Primer	Vector	Restriction enzyme	Sequencing primer	Reference
pIJLK01	Hyg <sup>R</sup> , Derivative of pIJ10257 with additional restrictions sites Bst1107I (upstream) and StuI (downstream) of the <i>aph(7'')-Ia</i> gene allowing exchanging of the antibiotic cassette	pIJ10257	1 + 2 3 + 4 5 + 6	pIJ10257	KpnI; PvuII	25 - 28	This study
pIJLK04	Apr <sup>R</sup> ; Derivative of pIJLK01 with <i>aph(7'')-Ia</i> exchanged for <i>aac(3)IV</i> (apramycin resistance gene)	pIJ773	7 + 8	pIJLK01	Bst1107I; StuI	28	This study

<b>pIJLK05</b>	Sp <sup>R</sup> /Sm <sup>R</sup> ; Derivative of pIJLK01 with <i>aph(7'')-la</i> exchanged for <i>aadA</i> (spectinomycin/streptomycin resistance gene)	pCDFduet-1	9 + 10	pIJLK01	Bst1107I; StuI	28	This study
<b>pEKEEx2a</b>	Kan <sup>R</sup> ; Derivative of pEKEEx2 with additional restrictions sites Bst1107I (upstream) and NotI (downstream) of the <i>aphA1</i> gene allowing exchanging of the antibiotic cassette	pEKEEx2	11 + 12 13 + 14 15 + 16	pEKEEx2	SapI; StuI	29 - 32	This study
<b>pEKEEx2b</b>	Hyg <sup>R</sup> ; Derivative of pEKEEx2a with <i>aphA1</i> exchanged for <i>aph(7'')-la</i> (hygromycin resistance gene)	pIJ10257	17 + 18	pEKEEx2a	Bst1107I; NotI	31 + 32	This study
<b>pEKEEx2d</b>	Apr <sup>R</sup> ; Derivative of pEKEEx2a with <i>aphA1</i> exchanged for <i>aac(3)IV</i> (apramycin resistance gene)	pIJ773	19 + 20	pEKEEx2a	Bst1107I; NotI	31 + 32	This study
<b>pEKEEx2e</b>	Sp <sup>R</sup> /Sm <sup>R</sup> ; Derivative of pEKEEx2a with <i>aphA1</i> exchanged for <i>aadA</i> (spectinomycin/streptomycin resistance gene)	pCDFduet-1	21 + 22	pEKEEx2a	Bst1107I; NotI	31 + 32	This study
<b>pAN6_aac(3)IV_Cstrep</b>	Kan <sup>R</sup> ; Derivative of pAN6 with <i>aac(3)IV</i> fused to a C-terminal Strep-tag	pIJ773	23 + 24	pAN6_CStrep	NdeI; NheI	33 + 34	This study

**Supplementary Table S2D: Oligonucleotides used in this study**

No.	Oligonucleotide name	Sequence (5' - 3')
<b>Construction of plasmids</b>		
1	pIJ10257_RE1_1_fw	TGCTCGGGTCGGGCTGGTACCAGTGAGCGTTTTTCAACCTCAG
2	pIJ10257_RE1_1_rv	GATTCTTGTCACGTATACAGCGGACCTCTATTACAGGG
3	pIJ10257_RE1_2_fw	AATAGAGGTCCGCTGTATACGTGACACAAGAATCCCTGTTACTTCTCG
4	pIJ10257_RE2_2_rv	CGGGCGGCCCGGGCGAGGCCTTCAGGCGCCGGGGG
5	pIJ10257_RE2_3_fw	CCCCGGCGCCTGAAGGCCTCGCCCGGGCCGC
6	pIJ10257_RE2_3_rv	GAAACCTGTCGTGCCAGCTGCATTAATGAATCGGCCAACGCGC
7	pIJLK04_aac(3)IV_fw	TGAATAGAGGTCCGCTGTATACGTGCAATACGAATGGCGAAAAAG
8	pIJLK04_aac(3)IV_rv	GGCGGCCCGGGGCGAGGCCTTCAGCCAATCGACTGGCG
9	pIJLK05_aadA_fw	TGAATAGAGGTCCGCTGTATACATGAGGGAAGCGGTGATCG
10	pIJLK05_aadA_rv	GCGGCCCGGGGCGAGGCCTTTATTGCGGACTACCTTGGTGAT
11	pEKEx2_RE1_1_fw	GCGGTTTGCGTATTGGGCGCTCT
12	pEKEx2_RE1_1_rv	ATGGCTCATGTATACAACACCCCTTGTATTACTGTTTATGTAAGCAGAC
13	pEKEx2_RE1_2_fw	GGGGTGTGTATACATGAGCCATATTCAACGGGAAACGTCT
14	pEKEx2_RE2_2_rv	TTCTGAGCGGCCGCTTAGAAAACTCATCGAGCATCAAAATGAAAC
15	pEKEx2_RE2_3_fw	TTTCTAAGCGGCCGCTCAGAATTGGTTAATTGGTTGTAACA
16	pEKEx2_RE2_3_rv	CGTGAAGAAGGTGTTGCTGACTC
17	pEKEx2b_hygR_fw	ATACAAGGGTGTGTGTATACGTGACACAAGAATCCCTGTTACTTCTC
18	pEKEx2b_hygR_rv	AATTAACCAATTCTGAGCGGCCGCTCAGGCGCCGGGGGC
19	pEKEx2d_aac(3)IV_fw	ATACAAGGGTGTGTGTATACGTGCAATACGAATGGCGAAAAAG
20	pEKEx2d_aac(3)IV_rv	ACCAATTCTGAGCGGCCGCTCAGCCAATCGACTGGCGAG
21	pEKEx2e_aadA_fw	ACAAGGGTGTGTGTATACATGAGGGAAGCGGTGATCG
22	pEKEx2e_aadA_rv	ACCAATTCTGAGCGGCCGCTTATTTCGGGACTACCTTGGTGATC
23	pAN6_aac(3)IV_Cstrep_fw	CCTGCAGAAGGAGATATACATATGATGTCATCAGCGGTGGAG
24	pAN6_aac(3)IV_Cstrep_rv	TGTGGGTGGGACCAGCTAGCGCCAATCGACTGGCGAGC
<b>Sequencing primer</b>		
25	pIJLK01_seq_fw_1	GATCAACCGCGACTAGCATC
26	pIJLK01_seq_fw_2	CCGGTGATCAAGCTGTTTC
27	pIJLK01_seq_fw_3	TTTCTGCGCGTAATCTGCTG
28	pIJLK0x_seq_fw_4	CGTAGAGATTGGCGATCCC
29	pEKEx2a_seq_fw	TTCCAGTCGGGAAACCTGTC
30	pEKEx2a_seq_rv	TCGCGAGCCCAATTATACCC
31	pEKEx2x_seq_fw	GGAAAGCCACGTTGTGTCTC
32	pEKEx2x_seq_rv	GCCTCGTGAAGAAGGTGTTG
33	pAN6_seq_Cstrep_fw	CGGCGTTTCACTTCTGAGTTCCGGC
34	pAN6_seq_Cstrep_rv	GATATGACCATGATTACGCC
<b>qPCR primer</b>		
35	qPCR_atpD_Sv_fw	TGTTTCGAGACCGGCCTGAAG
36	qPCR_atpD_Sv_rv	AGACACCGTCGTGCAGCTTG
37	qPCR_Alderaan_HQ601_00028_fw	CTCGGCTATCCGATCATCC
38	qPCR_Alderaan_HQ601_00028_rv	TTGGTTGCGGTTGATGGAC

**Supplementary Table S3: Polynucleotides used for phage targeting direct-geneFISH**

No	Sequence (5' - 3')
<b>Gene probes for phage targeting direct-geneFISH with Alderaan infecting <i>S. venezuelae</i></b>	
1	ACGGCGATCAGCACCCAGGACAGGACGACGCTTTGTGTGCGACCCACCATGGCGGTCTCGGTCTCGGCTCTTCCATCAACTTCCCCAGTTCCGGCAACAGTCGACATCGTATGGAGAGAGGGGGTGAGCCCGTGCCCATTCACCCCGCATGGTGCAGCCCTCGCCGAACGACCCGCGATCTCTACGCCGCCGCCG
2	TACCGGGACGCCGAGGACGCTGTAACGGCTACCTCCTGAACAAGAAGGCCAAGGCGGACGCGCATCAACCCGGCCGCTGTTCAGCGGCCAGCCCGTATCGCGTACGCCCGAGCGTCGGACGAGCTGAAAGAGTGGTGGGCCGAACACGGTCGCCTAACGACGGCGGAGTTATCGAGCAGGTACCCGCAAGGCTCA
3	CGCCGACAGCAACGGCCGTACAGGACGTCACCAACTACGACGTGCGCACGGCCTCCCCACCAACCCCGTAAAGAGGTCCGCCATGGCGGGTAACAGCAGGTCCATCGACGCGCGCGGATGGCTCTTCGAGGTCAAGGACACCGACGCCAGCACCGAGACGTGGTCCCGATCGCCGGTCTCAACTCCTGGTGTACT
4	CGGCGGTACGAGGAGGACGTCATGCAGCGCGGCCCTCCATCACCTGGAGGGTCAGTACCGCATCGACAAGACGACCAAGGCCCGCGAGCTGGGACAGGCGTACATCGATGAGGAATGGACGCCGCTCTCGGCATCGACTCGACAACAGATCCGCTACCGGCACGAGACGCAGTCCGCATGGGCGATCTGGGACG
5	CGTAGACGTGCGCGAAGACCTCTTGGACACGTTGCGCGAGTATCCGACGGAGTTCGGTCAGCTCGGCTCGACGCGAGACGGCGATGGGGCTGCTCTCCAGGGACTCCAAGCGGGTGCGCGCGACGCCGATACGGTTCGCCGACGCGTTGAAGGAATTACGCTCATGGCTCAGGGCATGGGCGAGTCAACTGCGGAGT
6	GCCGTGTGGGCCGGGGCCATCGTCGTGGTTCAGTGGGTCTCATGGCCACACAGGCCCTCATGCAGGCCGCCCGCATGGCCGCGCGTGGTCTATCGGCATGGGCCGATTGGCTGTCTATCGTCCCGTGGTTCGGTCTCGTCTCCTGATCATCAAGTATTGGGATGACATCGTCGAGCCACCACGAAGGCGTGGGA
7	GGCCGCCGGCGACTACGTGAGATGACCATTTTCAGCGGCGCCGCTGTCCGGCATTCCGTCCAGCTACAGCCGGCGTCGTTGGTCTGGCAGGGCCCGGTGAGCGGCATGTACCGCTCGTTCTGTGCGACCTGCGATCCGACCAAGTCTCGACATCCTTCCCGCGAGGGCATCAAGTGCGACGACTACATCGG
8	CCGCGACGTTGCGACTCGTACCTCGCGCACCGGCTACTCAAGGACGGGTGGACCGGGAACGGGGTCGACCACTCGACATCGCCCGTCAGATCGTACGATGGGTCCAGTCGACCGAGGGCGGCAACATCGGCATCGAACTGGACTGGTTCGACAGATCCGGAGTGTCCGCGACCGGGCGTACTCCCGTACGACCTGTAC
9	GTCGTGCGCGACGTGCTCGACCAACTCGCCAACGTCGAGAACGGGTTTCAGTGGCGCGTACGTACGTACCGCGATGCGTCCGGCCGCCGCTGAAGAGCTTGCAGCTCGGCTATCCGATCATCCGAGACGCCGTACCGAGTTGGTTCTCTCTCCCCGGGCCCGTATCGACTACCGGATGCCGAGGACGGCACCTC
10	GCGCCACCGCGCAGCTTCAGTTCCGCGTGAACGGAACCATCGTGGCGACCGGCACGGCGGGTCAACCGCTCTTGCCACCTTCGCCATCCCGTCGTACGCGTTCGGCATGAACGCCGAGTTCGAGCTACAGGCCCGCGTGTCCA GCGGCACCGGAACCGCTACGCCAGACCCGCTACCTGTACGGCTTCCAGTCTAA
11	GGCGCGGTGCTCGGCGCGGTGCTCGGCACGGTCGTCGTGGCGCTCATCGGCTGCTCTCCTTCCTTGGGGGCGTGCTCCGGAATGGCTCCACCTTGACACCCCGTCCGGACGTATCTGCCCCAAAGCGAGGACAGTTGAGACGTCTCTCGCTAGGGTCAATAAGGCCCAAAAGTCCGGGCGAGGGGGTTGACAGTGA
12	AACCGCGCGGACGCTGCACGGGCGTGGGAGTGGATGAGGAAATGATCTGGCCGAAGGCGGTGCAGGACCGCGTAAAGGTCCGGCGGACCGGGAGATCCTCCGCACCTACCCATACCGCTCGGCGTGCCCTCCAACGTGTGGCGGACCTCGTGC CGGCGCCGAGCAGGAGCTGTTCTCGCCGGGTATACGAACTA
13	GCGAGGTGACCCGGCAGCGGAGGTAATCGAAGGCGTTCCGCTGTGGTTCACGCGCATTCGGATCACGCTCGATGAGTTGGCGCGGCTCGGGTCGGTCGAGGGTGTGAGGCCCCGGCTGAGCGCTGCCGAGGATGCCGTA AATACGTTGAGCTGTGGTATTCGATTGACGAGGAGGCCCTCGTAACGCTCAT

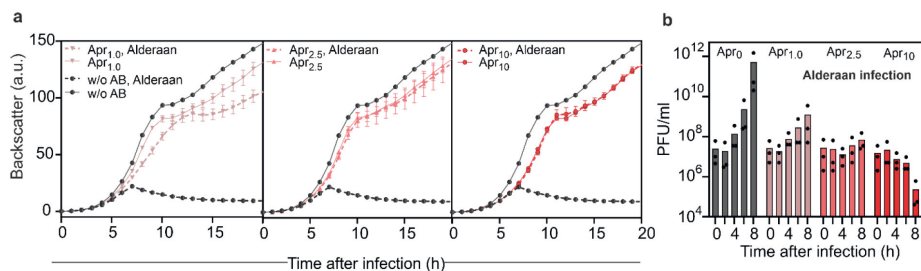
14	TGCGGCGGCACGTTGACGGCGGGATGTTGACCGCTTCGCAGAGCACGCCGAAGAGCTGTGGGAGCGGGCCGTGCCCCGTGACGTGCTAGACGACGAAACGGCCCCGCTCCACAGACAGGGAACGGGGCCGTGCGTTCCGCAGGTCAAGCAACCATTCGGTATCGTCCCCCTTAGGTCCACTGTCGTGGGGTGTGGA
15	GACGCGAGTGTCTGTGACTGCTTCGCCCCCTGAGGAGCCGGCCGACGGTCGAGGCGCTGATGCCGCTATCTGCGCAAAAGCGGGAGCGCCCCCGCTGCGTAGGCCGGTGACGTGCTATCCGCGTCTCACGAGTTCTCTGGGAGAGCCATGCGGCGAACGCCGAGCGCTGCGTCGGTCTTGTTTCTGCCATGCGAGAAA
16	CCGCGCGGCGAGAAGGGCACGCACACCGTGCTCCGGATGCTGTACCGCATCTACGGCCCGCGCGGCGACTGCCTGCGCGTCACCATCCCGGGCGAGGCCATGGACACGGCCGACAAGAGCACCAACAAGGCGATGTCGGCCGCGCTCAAGTACATGCTCTTACAGTGTTTCATGATCCCCGTGGACGCCCGCAGCATCGA
17	GGTGATCCCGCCCGCGTTACCCCGGAGGACGGCACCTAGCCCCCTCGATAAGGGGAGCGGGATCAGCCCCACATCCGCTATCTTTCTGTCTCGACAGATACATGCTGTGACAGACAACCGCGAGCGCGCGCTCAGCACGTAGAGCAGGAGGACCGCCCCGTGAACACCCCGAGCGCTTCGCCGCCAAGGTCGA
<b>Gene probes for phage targeting direct-geneFISH with <math>\lambda</math> infecting <i>E. coli</i></b>	
1	AGCAGTATCTTAAATTTGGCGACAAAGAGACGCCGTTTGGCCTCAAATGGACGCCGGATGACCCCTCCAGCGTGTTTTATCTCTGCGAGCATAATGCTGCGTCATCCGCCAGCAGGAGCTGGACTTTACTGATGCCGTTATATCTGCGAAAAGACCGGGATCTGGACCCGTGATGGCATTCTCTGGTTCGTCATCCGGTGAAGAGATTGAGCCACCTGACAGTGTGACCTTTCACATCTGGACAGCGTACAGCCCGTTCACCACCTGGGTGCGAGATTGTCAAAGA CTGGATGAAAA
2	GCAGGACAACGTATTCGATGTGTTATCTGAAAGTACTGATGAACGGTGCGGTGATTATGATGGCGCGGCGAACGAGGCGGTACAGGTGTTCTCCCGTATTGTTGACATGCCAGCGGGTCGGGGAACCGTGATCCTGACGTTCA CGTTACGTCCACACGGCATTGCGCAGATATTCCGCCGTATACGTTTGCCAGCGATGTGCAGGTATATGGTGATTAAGAAACAGGCGCTGGGCATCAGCGTGCTGAGTGTGTTACAGAGGTTTCGTCGGGAACGGGCGTTTAT TATAAACAGT
3	AGATTATTATGGGCCGCCACGACGATGAACAGACGCTGCTGCGTGTGGATGAGGCCATCAATAAACCTATA CCCGCCGGAATGGTGCGAAATGTCGATATCCCGTATCTGCTGGGATACTGGCGGGATTGACCCGACCATTTG TATGAACGCTCGAAAAAACATGGGCTGTTCCGGGTGATCCCCATTAAAGGGGCATCCGCTCTACGGAAGC CGGTGGCCAGCATGCCACGTAAGCGAAACAAAAACGGGGTTACCTTACCGAAATCGGTACGGATACCGCG AAAGAGCAGATTT
4	CAATTTTGTCCCACTCCCTGCTCTGTCATCAGGATACTGTGATGCCATGGTGTCCGACTTATGCCCGAGAAG ATGTTGAGCAAACCTATCGCTTATCTGCTTCTCATAGAGTCTTGACAGACAACTGCGCAACTCGTGAAAGGT AGGCGGATCCCCCTCGAAGGAAAGACCTGATGCTTTTCGTGCGCGCATAAAATACCTTGATACTGTGCCGGA TGAAGACGGTTCGCGACGAGTAGATGCAATTATGGTTTCTCCGCCAAGAATCTCTTTGCATTTATCAAGTGT TCCCTCATTTG
5	TGCTCGACATAAAGATATCCATCTACGATATCAGACCACTTCATTTGCGATAAATCACCAACTCGTTGCCCG TAACAACAGCCAGTTCATTGCAAGTCTGAGCCAACATGGTGATGATTCTGCTGCTTGATAAATTTTACGGTA TTCGTGACCGGTAAGTCTTGATCTCCTTACCTCTGATTTTGTGCGCGAGTGGCAGCGACATGGTTTGTGTT ATATGGCCCTTCAGCTATTGCCCTCTCGGAATGCATCGCTCAGTGTGTGATCTGATTAACCTTGCTGACGCCGCT TGCCTCG
6	AACTCAATGTTGGCCTGTATAGCTTCAGTGATTGCGATTGCGCTGTCTCTGCCTAATCCAAACTCTTTACCCG TCCTTGGGTCCTGTAGCAGTAATATCCATTGTTCTTATATAAAGGTTAGGGGGTAAATCCCGCGCTCATG ACTTCGCTTCTTCCCATTTCTGATCCTCTTCAAAAGGCCACCTGTTACTGGTCGATTTAAGTCAACCTTTACC GCTGATTGCTGGAACAGATACTCTCTTCCATCCTTAACCGGAGGTGGGAATATCTGCATTCCCGAACCCATC GACGAAC
7	TGTTTCAAGGCTTCTTGGACGTGCTGCGGTGCGTTCCTACTCCTGAAGTGTCAAGTACATCGAAAAGTCTCCG CAATTACACGCAAGAAAAAACCGCCATCAGCGCGCTTGGTGTCTTTTCAGTTCTCAATTGCAATATTGGTTA CGTCTGCATGTGCTATCTGCGCCCATATCATCCAGTGGTTCGTAGCAGTCGTGATGTTCTCCGCTTCGATAAC TCTGTTGAATGGCTCTCCATTCCATTCTCTGTGACTCGGAAGTGCAATTTATCATCTCCATAAAACAAAACCC GCCGTAGC
8	ACTCAACCCGATGTTTGAGTACGGTTCATCTGACACTACAGACTCTGGCATCGCTGTGAAGACGACGCGGA AATTCAGCATTTTCAACAAGCTTATCTTTTCAAAAACCGATCTCACTCTCCTTTGATGCCAATGCCAGCGTCA GATCATATGACGATACTACCTGCATCCTGAACCATTGACCTCAACCCCGTAATAGCCAGTCGTAATG ATGTCGATAGTTACTAACGGGCTTGTTCGATTAACCTGCCGAGAACTCTCCAGGTCACCAAGTGCAGTGC TGTGATAACAGG

9	GTTTATCCAGCAGTTCCAGCACAAATCGATGGTGTACCAATTTCATGGAAAAGGTCTGCGTCAAATCCCCAGT CGTCATGCATTGCCTGCTCTGCCGCTTACGCGAGTGCCTGAGAGTTAAATTCGCTCACTTCGAACCTCTCTGTT TACTGATAAGTTCAGATCCTCCTGGCAACTTGCACAAGTCCGACAACCCCTGAACGACACAGGCGTCTCGTT CATCTATCGGATCGCCACACTCACAACAATGAGTGGCAGATATAGCCTGGTGGTTACGGCGGCGCATTTTTA TTGCTGTGTT
10	TGAGGGTGAATGCGAATAATAAAAAAGGAGCCTGTAGCTCCCTGATGATTTTGTCTTTTCATGTTTCATCGTTCC TTAAAGACGCGGTTTAAACATGCCGATTGCCAGGCTTAAATGAGTCGGTGTGAATCCCATCAGCGTTACCGTTT CGCGGTGCTTCTTCAGTACGCTACGGCAAATGTCATCGACGTTTTATCCGGAACCTGCTGTCTGGCTTTTTT GATTTCAGAATTAGCCTGACGGGCAATGCTGCGAAGGGCGTTTTCTGCTGAGGTGTCATTGAACAAGTCCC ATGTCGGC
11	AGGTAACCGGGCATTTTCAGTTCAAGGCCGTTGCCGTCACTGCATAAACCATCGGGAGAGCAGGCGGTACGC ATACTTTCGTCGCGATAGATGATCGGGGATTTCAGTAACATTCACGCCGGAAGTGAATCAAACAGGGTCTCG GCGTCGTCTCTGACTGTTTTCCCGAGGCCAGTGTCTTAGCGTTAACTCCCGAGGCCACACCGGTGCAACCT CAGCAAGCAGGGTGTGGAAGTAGGACATTTTCATGTCAGGCCACTTCTTCCGGAGCGGGGTTTTGCTATCA CGTTGTGAACCT
12	TGATGACGCCGAGCCGTAATTTGTGCCACGCATCATCCCTGTTTCGACAGCTCTCACATCGATCCCGTACG CTGCAGGATAATGTCCGGTGTCTATGCTGCCACCTTCTGCTCTGCGGCTTTCTGTTTCAGGAATCCAAGAGCTT TTACTGCTTCGGCTGTGTCACTGCTGACGATGCACGAATGTCGCGGCGAAAATATCTGGGAACAGAGCGGCA ATAAGTCGTATCCCATGTTTTATCCAGGGCGATCAGCAGAGTGTTAATCTCCTGCATGGTTTCATCGTTAAC CGGAGTGAT
13	TCGCGTTCGGCTGACGTTCTGCGAGTGTATGCAGTATTTTCGACAATGCGCTCGGCTTCATCCTTGTCTATAGA TACCAGCAAAATCCGAAGGCCAGACGGGCACACTGAATCATGGCTTTATGACGTAAACATCCGTTTGGGATGCG ACTGCCACGGCCCCGTGATTTCTCTGCCCTTCGCGAGTTTTGAATGGTTCGCGGCGGCATTATCCATCCATT GGTAACGAGATCGGATGATTACGGTCTTTCGCGTAAATCCGGCATGTACAGGATTCATTGTCTGCTCAAA GTCCATGCCA
14	TCAAACCTGCTGGTTTTTCATTGATGATGCGGGACCAGCCATCAACGCCACCACCAGGAACGATGCCATTCTGC TTATCAGGAAAGGCGTAAATTTCTTTCGTCACGGATTAAAGGCCGTACTGGTTGGCAACGATCAGTAATGCG ATGAACTGCGCATCGCTGGCATCACCTTTAAATGCCGTCTGGCGAAGAGTGGTGATCAGTTCTCTGTGGGTGCG ACAGAATCCATGCCGACACGTTTCAGCCAGCTTCCAGCCAGCGTTGCGAGTGCAGTACTCATTCTGTTTATAC CTCTGAATCAA
15	TATCAACCTGGTGGTGAGCAATGGTTTCAACCATGTACCGGATGTGTTCTGCCATGCGCTCCTGAAACTCAAC ATCGTCATCAAACGCACGGGTAATGGATTTTTGCTGGCCCCGTGGCGTTGCAAAATGATCGATGCATAGCGA TTCAAACAGGTGCTGGGGCAGGCCTTTTCCATGTCGTCTGCCAGTCTGCTCTCTTCTTCACGGGCGAGC TGCTGGTAGTGACGCGCCAGCTCTGAGCCTCAAGACGATCCTGAATGTAATAAGCGGTTTCATGGCTGAACTC CTGAAATAGC
16	GATAAAGCCAAGGCCAATATCTAAGTAACTAGATAAGAGGAATCGATTTTCCCTTAATTTTCTGCGCTCCAC TGCATGTTATGCCGCTTCGCCAGGCTTGCTGTACCATGTGCGCTGATTTCTGCGCTCAATACGTTGACAGTT GCTTCAACTGTTTGTGGTATTTCAGCCAGCACTGTAAGGTCATATCGGATTTAGTGCGCTTTTACTCTGGATT TCGGTTTGGGATTACGCGAGAGAAATAGGGCGGTTAACTGGTTTTGCGCTTACCCCAACCAACAGGGGATTG CTGCTTCC
17	AGCCTGTTTCTCTGCGCGACGTTTCGCGGCGGCGTGTGTTGTCATCCATCTGGATTCTCTGTCACTAGCTTTG GTGGTGTGTGGCAGTTGTAGTCTGAACGAAAAACCCCGCGATTGGCACATTGGCAGCTAAATCCGGAATCG CACTTACGGCCAATGCTTCGTTTTCGATCACACACCCCAAGGCTTCTGCTTTGAATGCTGCCCTTCTCAGG GCTTAATTTTAAAGCGTCACCTTCATGGTGGTCAGTGCCTCTGCTGATGTGCTCAGTATCACCGCCAGTG GTATTTAT
18	TACTATGTTATGTTCTGAGGGGAGTGAAAAATCCCTAATTCGATGAAGATTCTTGCTCAATTGTTATCAGCT ATGCGCCGACCAGAACACCTTGCCGATCAGCCAAACGCTCTCTCAGGCCACTGACTAGCGATAACTTCCCC ACAACGGAACAACCTCTCATTGTCATGGGATCATGGGTACTGTGGGTTTGTGGTTGTAAGGTTGAAAAACCTGACCG CTATCCCTGATCAGTTTCTTGAAGGTAACTCATACCCCCAAGTCTGGCTATGCAGAAATCACTGGCTCAA CAGCTGTCTC
19	TATTTGCATACATTCAATCAATTGTTATCTAAGGAAATACTTACATATGGTTTCGTGCAAAACAAACGCAACGA GGCTCTACGAATCGAGATGCGTGTCTTAAACAAAATCGCAATGCTTGAAGTGAAGACAGCGGAAGCTG TGGCGCTTGATAAGTCGAGATCAGCAGGTGGAAGAGGGACTGGATTCCAAAGTTCTCAATGCTGTCTGCTG TTCTTGAATGGGGGTCGTTGACGACGACATGGCTCGATTGGCGCGACAAGTTGCTGCGATTCTCACCATA AAAAACGCCCCGC
20	TCAAGCAGCAAGGCGGCATGTTTGGACCAATAAAAAACATCTCAGAATGGTGCATCCCTCAAACAGAGGGA AAATCCCTAAAACGAGGGATAAAACATCCCTCAAATTGGGGGATTGCTATCCCTCAAACAGGGGACAC AAAAGACACTATTACAAAAGAAAAAGAAAGATTATCGTCAGAGAAATCTGGCGAATCTCTGACCAAGC CAGAAAACGACCTTTCTGTGGTGAACCGGATGCTGCAATTACAGAGCGGCAGCAAGTGGGGACAGCAGAA GACCTGACCGCCGAG

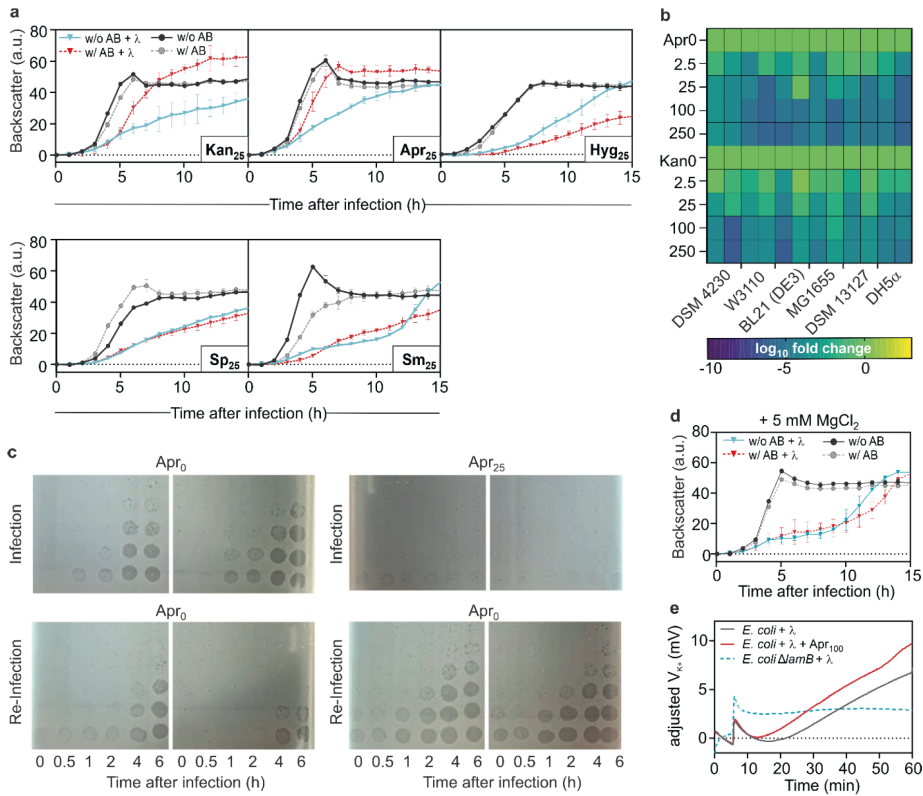
21	ATAAGTGGACCCAACTCGAAATCAACCGTAACAAGCAACAGGCAGGCGTGACAGCCAGCAAACCAAACTC GACCTGACAAACACAGACTGGATTACGGGGTGGATCTATGAAAAACATCGCCGCACAGATGGTTAACTTTG ACCGTGAGCAGATGCGTCGGATCGCCAAACAATGCGCGGAACAGTACGACGAAAAGCCGAGGTACAGCAG GTAGCGCAGATCATCAACGGTGTGTTACGCCAGTTACTGGCAACTTTCCCGCGAGCCTGGCTAACCGTGAC CAGAACGAAGTGAA
22	TGGCGGTATATGGAGTTAAAGATGACCATCTACATTACTGAGCTAATAACAGGCCCTGCTGGTAATCGCAGG CCTTTTTATTGGGGGAGAGGGAAGTCATGAAAAAACTAACCTTTGAAATTTCGATCTCCAGCAGCATCAGCAA AACGCTATTACGCGAGTACAGCAAATCCTTCAGACCCAACCAACCAATCGTAGTAACCAATTCAGGAACGC AACCGCAGCTTAGACAAAACAGGAAGCTATGGGCCTGCTTAGGTGACGCTCTCTCGTCAGGTTGAATGGCAT GGTCGCTGGCTG
23	GATGCAGAAAGCTGGAAGTGTGTTTTACCGCAGCATTAAAGCAGCAGGATGTTGTTCTTAACCTTGCCGGG ATGGCTTTGTGGTAATAGGCCAGTCAACCAGCAGGATGCGTGTAGGCCAAATTGCGGAGCTATTAGAGCTT ATACAGGCATTTCGGTACAGAGCGTGGCGTTAAGTGGTCAGACGAAGCGGAGACTGGCTCTGGAGTGAAAGC GAGATGGGGAGACAGGGCTGCATGATAAATGTCGTTAGTTTCTCCGGTGGCAGGACGTCAGCATATTTGCTC TGGCTAATGGAGC
24	CCATTTCGGGCGAGGGAATTACACCAGTGGATTGGCATCAGAGCTGATGAACCGAAGCGGCTAAAGCCAA AGCCTGGAATCAGATATCTTGCTGAATGTCAGACTTTGAGAAGGAAGATATCCTCGCATGGTGGAAGCAAC AACCATTTCGATTTGCAAAATACCGGAACATCTCGGTAACTGCATATTCGCAATTAATAAATCAACGCAAAAAA TCGGACTTGCCTGCAAAAGATGAGGAGGGATTGACGCGTGTITTTAATGAGGTATCACGGGATCCCATGTGC GTGACGGACATCG
25	GGAAACGCCAAAGGAGATTATGTACCGAGGAAGAATGTCGCTGGACGGTATCGCGAAAAATGTATTCAGAAA ATGATTATCAAGCCCTGTATCAGGACATGGTACGAGCTAAAGATTTCGATACCGGCTCTGTGTTCTGAGTCAT GCGAAATATTTGGAGGGCAGCTTGATTTTCGACTTCGGGAGGGAAGCTGCATGATGCGATGTTATCGGTGCGG TGAATGCAAAAGATAAACCGCTTCCGACCAAAATCAACCTTACTGGAATCGATGGTGTCTCCGGTGTGAAAG AACACCAACAGGG
26	GTGTTACCACTACCGCAGGAAAAGGAGGACGTGTGGCGAGACAGCGACGAAGTATCACCGACATAATCTGC GAAAACCTGCAAAATACCTTCCAACGAAAACGCACCAAGAAAATAAACCCAAAGCCAATCCCAAAAGAATCTGACGT AAAAACCTTCAACTACACGGCTCACCTGTGGGATATCCGGTGGCTAAGACGTCGTGCGAGGAAAAACAAGGT GATTGACCAAAATCGAAGTTACGAACAAGAAAGCGTCGAGCGAGCTTTAACGTGCGCTAACTGCGGTGAGA AGTGCATGTGCTGGA
27	GCGCAGAACTGATGAGCGATCCGAATAGTTCGATGCACGAGGAAGAAGATGATGGCTAAACCAGCGCGAAG ACGATGTAAAAACGATGAATGCCGGGAATGGTTTACCCTGCATTTCGTAATCAGTGGTGGTGTCTTCCAGA GTGTGGAACCAAGATAGCACTCGAACGACGAAGTAAAGAACGCGAAAAAGCGGAAAAAGCAGCAGAGAAG AAACGACGACGAGGAGGAGCAAAAAAGATAAACTTAAGATTGCAAAACTCGCCTTAAAGCCCGCGCA GTTACTGGATTAAACAA
28	CCAACAAGCCGTAAACGCCTTCATCAGAGAAAAGAGACCGGACTTACCATGTATCTCGTGGGAACGCTCAC GTCTGTCTCAGTGGGATGCCGGACATTACCGGACAACCTGCTGCGGCACCTCAACTCCGATTTAATGAACGCAA TATTCACAAGCAATGCGTGGTGTGCAACCGACGCAAAAAAGCGGAAATCTCGTCCGATGCGCTGCAACTGAT TAGCCGCATCGGGCAGGAAGCAGTAGACGAAATCGAATCAAACCATAACCGCCATCGCTGGACTATCGAAG AGTGCAAGGCGAT
29	TGTTATCTGCCACGCCGATTATCCCTTTGACGAATACGAGTTTGAAAGCCAGTTGATCATCAGCAGGTAATC TGGAAACCGGAACGAATCAGCAACTCACAAAACGGGATCGTGAAGAATAACAAAGCGCGGACACGTTTCAT CTTTGGTCATACGCCAGCAGTGAAACCACTCAAGTTTGCCAACCAAAATGTATATCGATACCGGCGCAGTGTT CTGCGAAAACCTAACATTGATTCAGGTACAGGAGAAGGCGCATGAGACTCGAAAGCGTAGCTAAATTTCA TTCCGCAAAAAAGC
30	CAGAGATTGCCATGGTACAGGCCGTGCGGTTGATATTGCCAAAACAGAGCTGTGGGGAGAGAGTTGTCGAGA AAGAGTGCAGGAAGATGCAAAAGGCGTCGGCTATTCAAGGATGCCAGCAAGCGCAGCATATCGCGCTGTGACG ATGCTAATCCCAAACCTTACCAACCCACCTGGTCACGCACTGTTAAGCCGCTGTATGACGCTCTGGTGGTGC AATGCCACAAAGAAGAGTCAATCGCAGACACAATTTGAATGCGGTACACGTTAGCAGCATGATTGCCAC GGATGGCAACATAT
31	TGAATAAAATTGGGTAATTTGACTCAACGATGGGTTAATTCGCTCGTTGTGGTAGTGAGATGAAAAGAGGC GAGGCTTACTACCGATTCCCGCTAGTTGGTCACTTCGACGTATCGTCTGGAAGCTCAACCATCGCAGGCAGA GAGGTCTGCAAAATGCAATCCCGAAACAGTTCGAGGTAATAGTTAGAGCCTCATACCGGTTTCGGGGATT TTTATATCTGCACAACAGGTAAGAGCATTGAGTCGATAATCGTGAAGAGTTCGCGAGCCTGGTTAGCCAGTG CTCTTTCCGTTG
32	TGCTGAATTAAGCGAATACCGGAAGCAGAACCGGATCACCAAATGCGTACAGGCGTCATCGCCGCCAGCA ACAGCACAAACCAAACTGAGCCGTAGCCACTGTCTGTCTGAATTCATTAGTAATAGTTACGCTGCGGCCCTT TACACATGACCTTCGTGAAAGCGGGTGGCAGGAGGTCGCGCTAACCAACCTCCTGCCGCTTTGCCCCGTGATA TCGGTCACGAACCAATCTGATTACTAAACACAGTAGCCTGGATTGTTCTATCAGTAATCGACCTTATTCCTA ATTAATAGAG

33	CAAATCCCCTTATTGGGGGTAAGACATGAAGATGCCAGAAAAACATGACCTGTTGGCCGCCATTCTCGCGGC AAAGGAACAAGGCATCGGGGCAATCCTTGCGTTTGCAATGGCGTACCTTCGCGGCAGATATAATGGCGGTGC GTTTACAAAAACAGTAATCGACGCAACGATGTGCGCCATTATCGCCTGGTTCATTCTGTGACCTTCTCGACTTC GCCGGACTAAGTAGCAATCTCGCTTATATAACGAGCGTGTTTATCGGCTACATCGGTACTGACTCGATTGGTT CGCTTATCAA
34	ATCATGGTTATGACGTCATTGTAGGCGGAGAGCTATTTACTGATTACTCCGATCACCTCGAAAATTGTAC GCTAAACCCAAAACCTCAAAATCAACAGGCGCCGGACGCTACCAGCTTCTTTCCCGTTGGTGGGATGCCACCG CAAGCAGCTTGGCCTGAAAGACTTCTCTCCGAAAAGTCAGGACGCTGTGGCATTGCAGCAGATTAAGGAGC GTGGCGCTTTACCTATGATTGATCGTGGTGATATCCGTCAGGCAATCGACCGTTGCAGCAATATCTGGGCTTC ACTGCCGGGCG
35	GATAAAACAAAAGCCACCGTGTGCGGTACGTGGTATGACCATCACCGTGAACGGCGTTGCTGCAGGCAAGGT CAACATTCCGGTTGTATCCGGTAATGGTGAGTTTGTGCGGTTGCAGAAATTACCGTCACCGCCAGTTAATCC GGAGAGTCAGCGATGTCTGAAAACCGAATCATTGAACATAACGGTGTGACCGTCACGCTTCTGAACTG TCAGCCCTGCAGCGCATTGAGCATCTCGCCCTGATGAAACGGCAGGCAGAACAGGCGGAGTCAGACAGCAA CCGGAAGTTACT

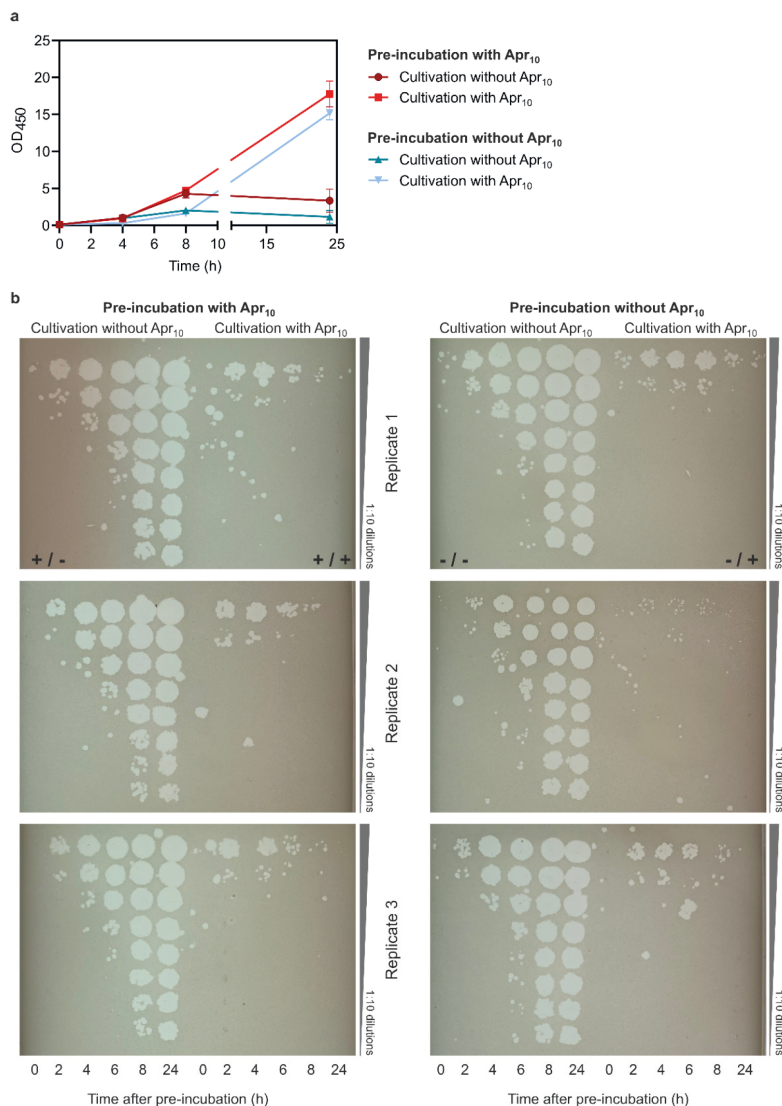




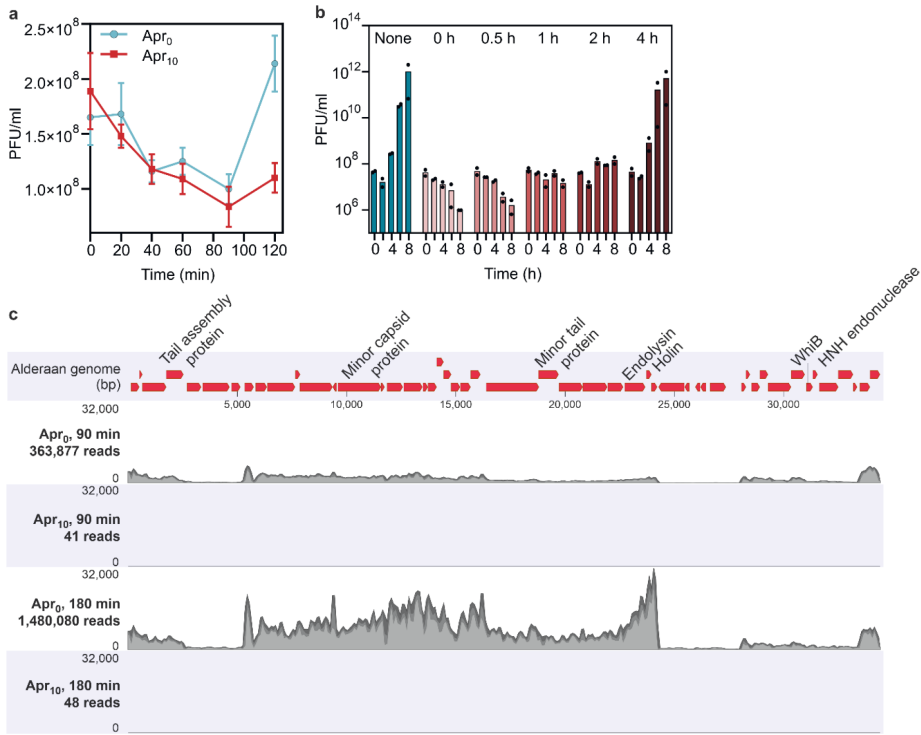
**Supplementary Figure S1 | Dose-dependent effect of apramycin on the *Streptomyces* phage Alderaan.** (a) Growth of *Streptomyces venezuelae* ATCC 10712 pIJLK04 infected with the phage Alderaan showing the dose-dependent effects of apramycin on infection (n = 3 independent biological replicates; error bars represent standard deviations [SD]) (AB; antibiotic). (b) Corresponding phage titers over time in presence of increasing concentrations of apramycin (0, 1, 2.5, and 10  $\mu\text{g}/\text{mL}$ ). Data are averages for three independent biological replicates.



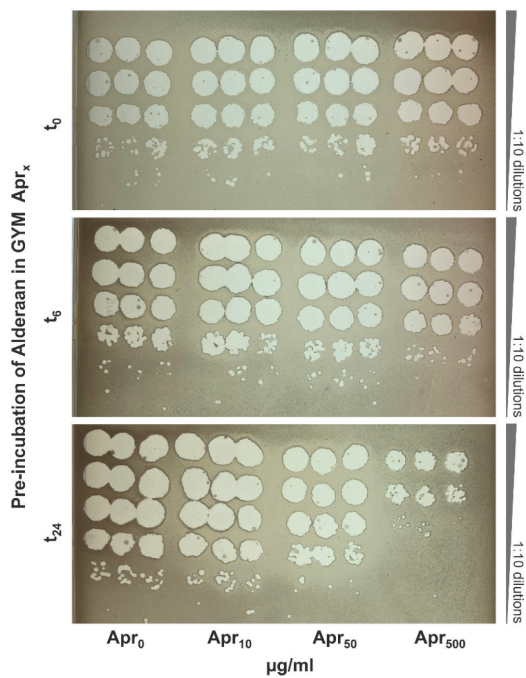
**Supplementary Figure S2 | Effect of aminoglycosides on *E. coli* phage  $\lambda$ .** (a) Infection curves of *E. coli* DSM 4230 infected with phage  $\lambda$  in presence of different aminoglycosides ( $n = 3$  independent biological replicates; error bars represent SD). (b) Heat map showing the  $\log_{10}$  fold change in plaque formation by  $\lambda$  on different *E. coli* strains in the presence of aminoglycosides relative to the aminoglycoside-free control. (c) Re-infection of cultures previously treated with apramycin (Apr<sub>25</sub>, top row, right), shows efficient infection of *E. coli* DSM 4230 by phage  $\lambda$  in the absence of apramycin (Apr<sub>25</sub>, bottom row, right). (d) Addition of MgCl<sub>2</sub> counteracts the effect of apramycin on infection of *E. coli* DSM 4230 by  $\lambda$ . (e) Potassium efflux assays performed with *E. coli* DSM 4230 wild type and the *E. coli* JW3996  $\Delta lamB$  strain (lacking the  $\lambda$  receptor).  $\lambda$  was added after 5.5 min.



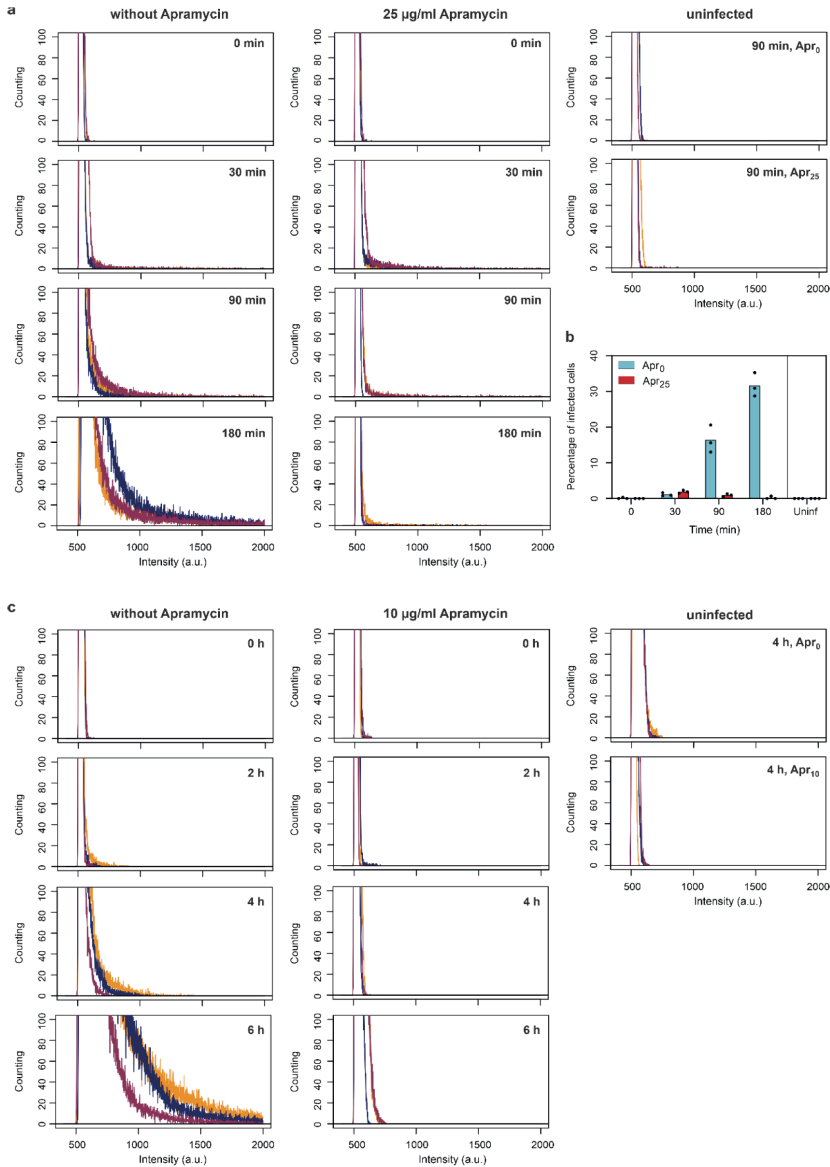
**Supplementary Figure S3 | Synchronized infection of *Streptomyces venezuelae* with phage Alderaan under apramycin pressure.** *Streptomyces venezuelae* ATCC 10712 pIJLK04 was inoculated to an OD<sub>450</sub> of 1 and preincubated with 10<sup>8</sup> PFU/mL for 15 min at room temperature with gentle shaking. After four washing steps with GYM medium to remove unadsorbed phages, cultures were diluted to a final starting OD<sub>450</sub> of 0.1. Preincubation with phages and further cultivation was performed with and without apramycin (10 µg/mL) as indicated. (a) Growth of *Streptomyces venezuelae* infected with phage Alderaan (n=3 independent biological replicates). (b) Corresponding plaque assays showing comparable phage amplification during the main cultivations performed in absence of apramycin, independent of the presence of apramycin in the preincubation step.



**Supplementary Figure S4 | Investigations of the mechanism of action of apramycin.** (a) Effect of apramycin on phage adsorption of phage Alderaan to *S. venezuelae* ATCC 10712 pJLK04. Shown is the time-resolved quantification of extracellular Alderaan DNA via qPCR using a gene coding for the minor tail protein (HQ601\_00028, oligonucleotide sequences are provided in Table S2D). Culture supernatants were pretreated with 100 U/mL DNase to exclusively quantify phage DNA deriving from intact phage particles. A DNase-treated phage stock with known phage titer was used to infer phage titers (in PFU/mL) from DNA quantification. Data are means for two independent biological replicates measured as technical duplicates. (b) Impact of apramycin (10  $\mu$ g/mL) when added at the different indicated time points after phage infection. For each sample, phage titers were measured over time. Data are averages for two independent biological replicates. (c) Enlargement of Fig. 4c showing the RNA-seq coverage of the Alderaan genome in presence or absence of apramycin. Genome organization of Alderaan is displayed at the top.



**Supplementary Figure S5 | Preincubation of phage Alderaan with apramycin.** Alderaan phages were preincubated in GYM medium containing the indicated apramycin concentrations at 30°C and 900 rpm before spotting on a bacterial lawn of *Streptomyces venezuelae* ATCC 10712 pIJLK04.



**Supplementary Figure S6 | Distribution of fluorescence intensities from phage targeting direct-geneFISH.** (a and c) Quantification of Alexa647 fluorescence in (a) *E. coli* cells infected with  $\lambda$  and (c) *S. venezuelae* cells infected with Alderaan, shown as density plots of pixel counts relative to their fluorescence intensity. For each panel, profiles of the three biological replicates are shown. (b) Determination of the percentage of *E. coli* cells infected with  $\lambda$  over time ( $n = 3$  independent biological replicates) (Uninf, uninfected). A cell was considered infected if Alexa647 (red) fluorescence was detected within the cell.

**Supplementary Video S1 | Apramycin prevents cell lysis during infection of *S. venezuelae* with phage Alderaan.** Time-lapse video of *S. venezuelae* ATCC 10712 carrying the plasmid pJLK04, which was cultivated in a microfluidics system and challenged with Alderaan ( $10^8$  PFU/mL; flow rate, 200 nL/min) in presence and absence of 5 or 10  $\mu$ g/mL apramycin.

## References

- 1 Baumgart, M. *et al.* Construction of a prophage-free variant of *Corynebacterium glutamicum* ATCC 13032 for use as a platform strain for basic research and industrial biotechnology. *Appl Environ Microbiol* **79**, 6006-6015, doi:10.1128/AEM.01634-13 (2013).
- 2 MacNeil, D. J. *et al.* Analysis of *Streptomyces avermitilis* genes required for avermectin biosynthesis utilizing a novel integration vector. *Gene* **111**, 61-68, doi:10.1016/0378-1119(92)90603-M (1992).
- 3 Studier, F. W. & Moffatt, B. A. Use of Bacteriophage T7 RNA Polymerase to Direct Selective High-level Expression of Cloned Genes *J Mol Biol* **189**, 113-130, doi:10.1016/0022-2836(86)90385-2 (1986).
- 4 Luria, S. E., Delbrück, M. & Anderson, T. F. Electron microscope studies of bacterial viruses. *Journal of Bacteriology* **46**, 57-77, doi:10.1128/JB.46.1.57-77.1943 (1943).
- 5 Lederberg, E. M. & Lederberg, J. Genetic Studies of Lysogenicity in *Escherichia Coli*. *Genetics* **38**, 51-64 (1953).
- 6 Murray, N. E., Brammar, W. J. & Murray, K. Lambdoid Phages that Simplify the Recovery of in vitro Recombinants. *Mol Gen Genet.* **150**, 53-61, doi:10.1007/BF02425325. (1977).
- 7 Baba, T. *et al.* Construction of *Escherichia coli* K-12 in-frame, single-gene knockout mutants: the Keio collection. *Mol Syst Biol* **2**, 2006 0008, doi:10.1038/msb4100050 (2006).
- 8 Ehrlich, J., Gottlieb, D., Burkholder, P. R., Anderson, L. E. & Pridham, T. G. *Streptomyces venezuelae*, n. sp., the source of chloromycetin. *Journal of Bacteriology* **56**, 467-477, doi:10.1128/jb.56.4.467-477.1948 (1948).
- 9 Bentley, S. D. *et al.* Complete genome sequence of the model actinomycete *Streptomyces coelicolor* A3(2). *Nature* **417**, 141-147, doi:10.1038/417141a (2002).
- 10 Higgins, C. E. & Kastner, R. E. Nebramycin, a new broad-spectrum antibiotic complex. II. Description of *Streptomyces tenebrarius*. *Antimicrobial agents and chemotherapy* **7**, 324-331 (1967).
- 11 Lv, M. *et al.* Characterization of a C3 Deoxygenation Pathway Reveals a Key Branch Point in Aminoglycoside Biosynthesis. *Journal of the American Chemical Society* **138**, 6427-6435, doi:10.1021/jacs.6b02221 (2016).
- 12 Zhang, Q., Chi, H. T., Wu, L., Deng, Z. & Yu, Y. Two Cryptic Self-Resistance Mechanisms in *Streptomyces tenebrarius* Reveal Insights into the Biosynthesis of Apramycin. *Angewandte Chemie (International ed. in English)* **60**, 8990-8996, doi:10.1002/anie.202100687 (2021).
- 13 Kronheim, S. *et al.* A chemical defence against phage infection. *Nature* **564**, 283-286, doi:10.1038/s41586-018-0767-x (2018).
- 14 Casjens, S. R. & Gilcrease, E. B. Determining DNA packaging strategy by analysis of the termini of the chromosomes in tailed-bacteriophage virions. *Methods in molecular biology (Clifton, N.J.)* **502**, 91-111, doi:10.1007/978-1-60327-565-1\_7 (2009).
- 15 Hardy, A., Sharma, V., Kever, L. & Frunzke, J. Genome sequence and characterization of five bacteriophages infecting *Streptomyces coelicolor* and *Streptomyces venezuelae*: Alderaan, Coruscant, Dagobah, Endor1 and Endor2. *Viruses* **12**, 1065, doi:10.3390/v12101065 (2020).
- 16 Hünnefeld, M. *et al.* Genome Sequence of the Bacteriophage CL31 and Interaction with the Host Strain *Corynebacterium glutamicum* ATCC 13032. *Viruses* **13**, 495, doi:10.3390/v13030495 (2021).
- 17 Harb, L. *et al.* ssRNA phage penetration triggers detachment of the F-pilus. *Proc Natl Acad Sci U S A* **117**, 25751-25758, doi:10.1073/pnas.2011901117 (2020).
- 18 Hong, H. J., Hutchings, M. I., Hill, L. M. & Buttner, M. J. The role of the novel Fem protein VanK in vancomycin resistance in *Streptomyces coelicolor*. *J Biol Chem* **280**, 13055-13061, doi:10.1074/jbc.M413801200 (2005).
- 19 Eikmanns, B. J., Kleinertz, E., Liehl, W. & Sahm, H. A family of *Corynebacterium glutamicum*/*Escherichia coli* shuttle vectors for cloning, controlled gene expression, and promoter probing. *Gene* **102**, 93-98, doi:10.1016/0378-1119(91)90545-M (1991).
- 20 Gust, B., Challis, G. L., Fowler, K., Kieser, T. & Chater, K. F. PCR-targeted *Streptomyces* gene replacement identifies a protein domain needed for biosynthesis of the sesquiterpene soil odor geosmin. *PNAS* **100**, 1541-1546, doi:10.1073/pnas.0337542100 (2003).



- 21 Paget, M. S. B., Chamberlin, L., Atrih, A., Foster, S. J. & Buttner, M. J. Evidence that the Extracytoplasmic Function Sigma Factor  $\sigma^E$  Is Required for Normal Cell Wall Structure in *Streptomyces coelicolor* A3(2). *Journal of Bacteriology* **181**, 204-211, doi:10.1128/JB.181.1.204-211.1999 (1999).
- 22 Frunzke, J., Engels, V., Hasenbein, S., Gätgens, C. & Bott, M. Co-ordinated regulation of gluconate catabolism and glucose uptake in *Corynebacterium glutamicum* by two functionally equivalent transcriptional regulators, GntR1 and GntR2. *Mol Microbiol* **67**, 305-322, doi:10.1111/j.1365-2958.2007.06020.x (2008).

## Part B: Supplementary information about aminoglycoside resistance via methyltransferase KamB (Figure 10 in “Scientific context and key results”)

(Data set is not part of the published manuscript)

Table S1: Microbial strains

Strain and phages	Characteristics	Reference
<i>Escherichia coli</i> DH5α	<i>supE44ΔlacU169 (φ80lacZDM15) hsdR17 recA1 endA1 gyrA96 thi-1 relA1</i>	Invitrogen
<i>Escherichia coli</i> ET12567/pUZ8002	<i>dam-13::Tn9 dcm-6 hsdM hsdR</i> , carrying plasmid pUZ8002	(MacNeil et al., 1992)
<i>Streptomyces venezuelae</i> NRRL B-65442	Wild-type strain	(Gomez-Escribano et al., 2021)

Table S2: Construction of pIJ10257-*kamB*

Plasmids & primer	Characteristics/Sequence 5'-3'	Reference
Plasmids		
pIJ10257	Hyg <sup>R</sup> ; Cloning vector for the conjugal transfer of DNA from <i>E. coli</i> to <i>Streptomyces</i> spp. (Constitutive promoter <i>ermE</i> *; Integration at the ΦBT1 attachment site)	(Hong et al., 2005)
pIJ10257- <i>kamB</i>	Hyg <sup>R</sup> ; Derivative of pIJ10257 containing the gene sequence <i>kamB</i> under control of the constitutive promoter <i>ermE</i> * <ul style="list-style-type: none"> <li>constructed via Gibson assembly with Primer 1 + 2 for insert amplification using gDNA of <i>S. tenebrarius</i> DSM 40477 as template</li> <li>digestion of vector pIJ10257 via NdeI and HindIII</li> </ul>	This study
Oligonucleotides for plasmid construction		
1_pIJ10257 <i>kamB</i> fw	TAGAACAGGAGGCCCATATGATGCGCCGCGTGGTGGCAA	This study
2_pIJ10257- <i>kamB</i> -rv	TCATGAGAACCTAGGATCCAAGCTTTCACGGACTGATCGTCCGGTGAG	This study
Oligonucleotides for sequencing		
3_pIJ10257-seq-fw	AGATGGTTACCTCGCCTCTG	This study
4_pIJ10257-seq-rv	TCAGCGAGCTGAAGAAAGAC	This study

Plasmid construction, conjugation and infection assays were performed as described in Kever et al. (2022).

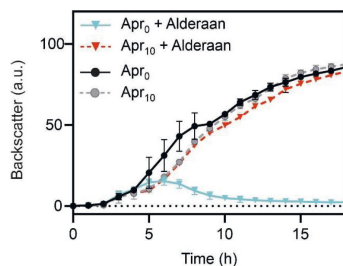


Figure S1: Alderaan infection assays of the apramycin-resistant strain *S. venezuelae* encoding the 16S rRNA methyltransferase KamB as resistance mechanism. Infection of *S. venezuelae* NRRL B-65442 carrying the integrative plasmid pIJ10257-kamB was performed in the BioLector microcultivation system (Beckman Coulter Life Sciences, Krefeld, Germany) in presence and absence of 10 µg/ml apramycin as described in Kever et al. (2022) (n = 3 independent biological replicates).

## References

- Gomez-Escribano, J. P., Holmes, N. A., Schlimpert, S., Bibb, M. J., Chandra, G., Wilkinson, B., Buttner, M. J., & Bibb, M. J. (2021). *Streptomyces venezuelae* NRRL B-65442: genome sequence of a model strain used to study morphological differentiation in filamentous actinobacteria. *J Ind Microbiol Biotechnol*, 48(9-10). <https://doi.org/10.1093/jimb/kuab035>
- Hong, H. J., Hutchings, M. I., Hill, L. M., & Buttner, M. J. (2005). The role of the novel Fem protein VanK in vancomycin resistance in *Streptomyces coelicolor*. *J Biol Chem*, 280(13), 13055-13061. <https://doi.org/10.1074/jbc.M413801200>
- Kever, L., Hardy, A., Luthe, T., Hünnefeld, M., Gätgens, C., Milke, L., Wiechert, J., Wittmann, J., Moraru, C., Marienhagen, J., & Frunzke, J. (2022). Aminoglycoside Antibiotics Inhibit Phage Infection by Blocking an Early Step of the Infection Cycle. *mBio*, 13(3). <https://doi.org/10.1128/mbio.00783-22>
- MacNeil, D. J., Gewain, K. M., Ruby, C. L., Dezeny, G., Gibbons, P. H., & MacNeil, T. (1992). Analysis of *Streptomyces avermitilis* genes required for avermectin biosynthesis utilizing a novel integration vector. *Gene*, 111(1), 61-68. [https://doi.org/10.1016/0378-1119\(92\)90603-M](https://doi.org/10.1016/0378-1119(92)90603-M)

#### 4.3. Appendix to 3.3: Inactivation of phage particles in the extracellular space of *Streptomyces* populations

Supplementary information to:

##### Inactivation of phage particles in the extracellular space of *Streptomyces* populations

Larissa Kever<sup>1</sup> and Julia Frunzke<sup>1\*</sup>

<sup>1</sup>Institute of Bio- und Geosciences, IBG-1: Biotechnology, Forschungszentrum Jülich, 52425 Jülich, Germany

\*Corresponding author: Julia Frunzke; Email: j.frunzke@fz-juelich.de

### Tables

Table S1: Microbial strains used in this study

Table S2: Phages used in this study

Table S3: Plasmids and oligonucleotides used in this study

### Figures

Figure S1: Influence of re-growing *S. venezuelae* NRRL B-65442 mycelium on phage Alderaan

Figure S2: Time course of Alderaan titers during infection of different developmental stages of *Streptomyces*

Figure S3: Influence of *S. venezuelae* NRRL B-65442 mycelium on extracellular titers of different phages

Figure S4: Failed visualization of CL31 phages on *S. venezuelae* mycelium

Table S1: Microbial strains used in this study

Strain and phages	Characteristics	Reference
<i>Escherichia coli</i> DH5 $\alpha$	<i>supE44</i> $\Delta$ <i>lacU169</i> ( $\phi$ 80 <i>lacZ</i> M15) <i>hsdR17 recA1 endA1 gyrA96 thi-1 relA1</i>	Invitrogen
<i>Escherichia coli</i> ET12567/pUZ8002	<i>dam-13::Tn9 dcm-6 hsdM hsdR</i> , carrying plasmid pUZ8002	(MacNeil et al., 1992)
<i>Escherichia coli</i> LE392	<i>F hsdR514 (rk<sup>-</sup> mk<sup>-</sup>) supE44 supF58 <math>\Delta</math>(<i>lacIZY</i>)6 galK2 galT22 metB1 trpR55 lambda<sup>-</sup></i>	(Murray et al., 1977)
<i>Escherichia coli</i> W1485	<i>F<sup>+</sup> met str T1<sup>s</sup> T6<sup>s</sup> lambda<sup>-</sup></i>	(Lederberg & Lederberg, 1953)
<i>Escherichia coli</i> B	Wild-type strain	(Luria et al., 1943)
<i>Corynebacterium glutamicum</i> ATCC 13032	Biotin-auxotrophic wild type (Accession: BX927147)	(Ikeda & Nakagawa, 2003)
<i>Corynebacterium glutamicum</i> MB001	ATCC 13032 with in-frame deletion of prophages CGP1 (cg1507-cg1524), CGP2 (cg1746-cg1752), and CGP3 (cg1890-cg2071)	(Baumgart et al., 2013)
<i>Pseudomonas putida</i> KT2440	Wild-type strain	(Nelson et al., 2002)
<i>Pseudomonas syringae</i> pv. <i>lapse</i> ATCC 10859	Wild-type strain, plant pathogen	(Kong et al., 2016)
<i>Bacillus subtilis</i> EC1524	Bioassay strain	(Widdick et al., 2003)
<i>Ustilago cynodontis</i> NBRC 9727	Wild-type strain, haploid	(Geiser et al., 2014)
<i>Xanthomonas translucens</i> pv. <i>translucens</i>	Wild-type strain, plant pathogen	(Sapkota et al., 2020)
<i>Streptomyces venezuelae</i> NRRL B-65442	Wild-type strain	(Gomez-Escribano et al., 2021)
<i>Streptomyces venezuelae</i> NRRL B-65442 $\Delta$ <i>bldD::apr</i>	NRRL B-65442 with <i>bldD::apr</i> mutant allele	(Tschowri et al., 2014)
<i>Streptomyces venezuelae</i> NRRL B-65442 $\Delta$ <i>bldN::apr</i>	NRRL B-65442 with <i>bldN::apr</i> mutant allele	(Bibb et al., 2012)

<i>Streptomyces venezuelae</i> NRRL B-65442 – pIJ10257- <i>bldN</i>	NRRL B-65442 containing integrative vector pIJ10257 for <i>bldN</i> overexpression	This study
<i>Streptomyces coelicolor</i> M145	<i>S. coelicolor</i> A3(2) lacking plasmids SCP1 and SCP2	(Bentley et al., 2002)
<i>Streptomyces olivaceus</i> BU 16	Wild-type strain	DSM1536

Table S2: Phages used in this study

Phages	Characteristics	Reference
Alderaan	<i>Caudoviricetes</i> (morphotype: siphovirus), virulent, infecting <i>S. venezuelae</i> NRRL B-65442	(Hardy et al., 2020)
Endor1	<i>Caudoviricetes</i> (morphotype: siphovirus), temperate, infecting <i>S. coelicolor</i> M145	(Hardy et al., 2020)
Lambda	<i>Caudoviricetes</i> (morphotype: siphovirus), temperate, infecting <i>E. coli</i> LE392	DSM4499
I4	<i>Caudoviricetes</i> (morphotype: myovirus), virulent, infecting <i>E. coli</i> B	DSM4505
T5	<i>Caudoviricetes</i> (morphotype: siphovirus), virulent, infecting <i>E. coli</i> B	DSM16353
T6	<i>Caudoviricetes</i> (morphotype: myovirus), virulent, infecting <i>E. coli</i> B	DSM4622
T7	<i>Caudoviricetes</i> (morphotype: podovirus), virulent, infecting <i>E. coli</i> B	DSM4623
M13	<i>Faserviricetes</i> (morphotype: inovirus), chronic infection, infecting <i>E. coli</i> W1485	DSM13976
MS2	<i>Leviviricetes</i> , (morphotype: levivirus), virulent, infecting <i>E. coli</i> W1485	DSM13767
Langgrundblatt 1	<i>Caudoviricetes</i> (morphotype: siphovirus), virulent, infecting <i>Xanthomonas translucens</i> pv. <i>translucens</i>	(Erdrich et al., 2022)
Pfeifenkraut	<i>Caudoviricetes</i> (morphotype: siphovirus), virulent, infecting <i>Xanthomonas translucens</i> pv. <i>translucens</i>	(Erdrich et al., 2022)
Athelas	<i>Caudoviricetes</i> (morphotype: podovirus), virulent, infecting <i>Pseudomonas syringae</i> pv. <i>lapsea</i>	Isolated by S. Erdrich (unpublished)
CL31	<i>Caudoviricetes</i> (morphotype: siphovirus), virulent, infecting <i>C. glutamicum</i> MB001	(Hünnefeld et al., 2021)



Table S3: Plasmids and oligonucleotides used in this study

Plasmids and primer	Characteristics/Sequence 5'-3'	Reference
Plasmids		
pIJ10257	Hyg <sup>R</sup> ; Cloning vector for the conjugal transfer of DNA from <i>E. coli</i> to <i>Streptomyces</i> spp. (Constitutive promoter <i>ermE</i> <sup>*</sup> ; Integration at the $\Phi$ BT1 attachment site)	(Hong et al., 2005)
pIJ10257- <i>bldN</i>	<p>Hyg<sup>R</sup>; Derivative of pIJ10257 containing the gene sequence encoding the mature BldN<sup>1</sup> under control of the constitutive promoter <i>ermE</i><sup>*</sup></p> <ul style="list-style-type: none"> <li>constructed via Gibson assembly with Primer 1 and 2 for insert amplification using gDNA of <i>S. venezuelae</i> NRRL B-65442 as template</li> <li>digestion of vector pIJ10257 via NdeI and HindIII</li> </ul> <p><sup>1</sup>mature BldN: lacking 84 aa N-terminal extension of the proprotein (Bibb &amp; Buttner, 2003; Bibb et al., 2012)</p>	This study
Oligonucleotides for plasmid construction		
1_pIJ10257- <i>bldN</i> -fw	C TAGAACAGGAGGCCCA TATGATGGACCTGGTCGAGCG	This study
2_pIJ10257- <i>bldN</i> -rv	TCATGAGAACCTAGGATCCAAGCTTTCAGCGGCGTCGTC	This study
Oligonucleotides for sequencing		
3_pIJ10257-seq-fw	AGATGGTTACCTCGCCTCTG	This study
4_pIJ10257-seq-rv	TCAGCGAGCTGAAGAAAGAC	This study
Oligonucleotides for qPCR		
5_cgl56-qPCR-fw	TTGCGGAAGGTCTCGGCA	This study
6_cgl56-qPCR-rv	AAGTTGGAGCAAGGTCACCG	This study
7_HQ601_00028-fw	CTCGGCTATCCGATCATCC	(Kever et al., 2022)
8_HQ601_00028-rv	TTGGTTCGGTTGATGGAC	(Kever et al., 2022)

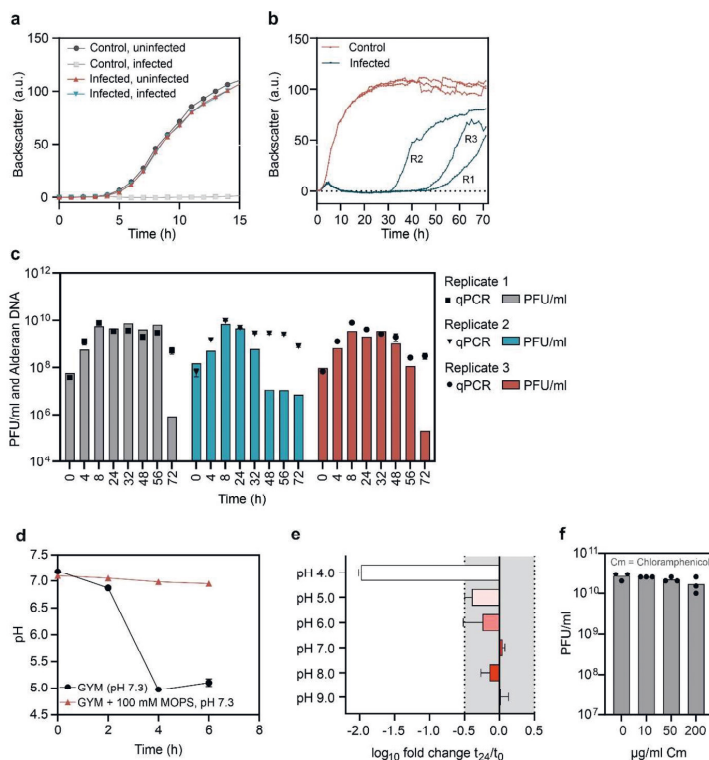


Figure S1: Influence of re-growing *S. venezuelae* NRRL B-65442 mycelium on phage Alderaan. a) Re-infection of *S. venezuelae* mycelium, which was re-grown during an infection experiment. Infection of re-grown mycelium with Alderaan revealed high phage resistance in comparison to naive infection (control). b) Growth curves of *S. venezuelae* infected with phage Alderaan showing re-growth of mycelium (R1-3 = biological triplicates). For a) and b), cultivations were conducted in the Biolector microcultivation systems (Beckman Coulter Life Sciences, Krefeld, Germany) using an initial phage titer of  $10^8$  PFU/ml ( $n=3$  independent biological replicates). c) Quantification of extracellular Alderaan titers via qPCR ( $n=9$ , three independent biological replicates measured as technical triplicates) and double-agar overlays ( $n=3$  independent biological replicates) during long-term infection and bacterial re-growth shown in b). d) Time course of pH during cultivation of *S. venezuelae* under normal cultivation conditions (GYM, 50 % tap water, pH 7.3) and buffered conditions (GYM supplemented with 100 mM MOPS, pH 7.3) ( $n=2$  independent biological replicates). e) Stability of infectious Alderaan particles in GYM medium (50% tap water) adjusted to different pH values quantified over 24 h via double-agar overlays ( $n=3$  independent biological replicates). Incubation was performed under cultivation conditions at 30 °C and 900 rpm in DeepWell plates. f) Plaque formation in presence of different chloramphenicol (Cm) concentrations calculated via double-agar overlay assays ( $n=3$  independent biological replicates).

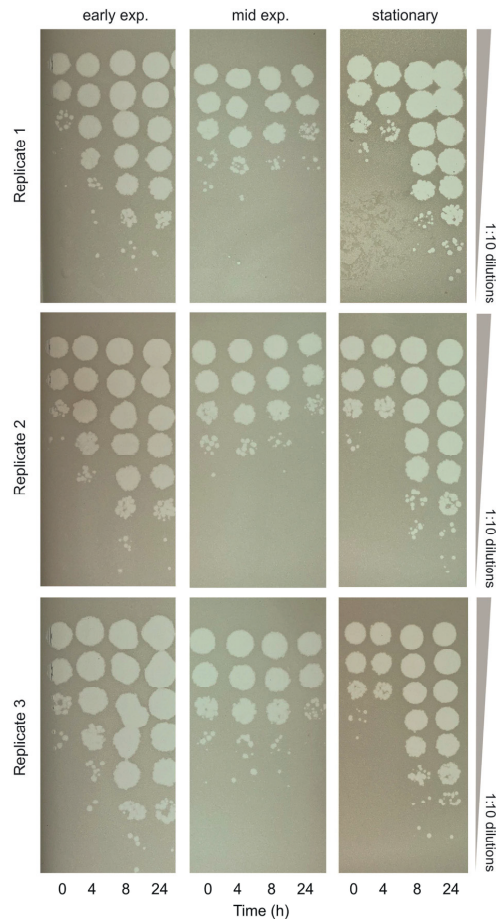


Figure S2: Time course of Alderaan titers during infection of different developmental stages of *Streptomyces*. Phage quantification via double-agar overlay assays showing the phage amplification during infection of different developmental stages of *Streptomyces venezuelae* mycelium. These assays were used to quantify the  $\log_{10}$  fold change ( $t_{24}/t_0$ ) shown in Figure 3.

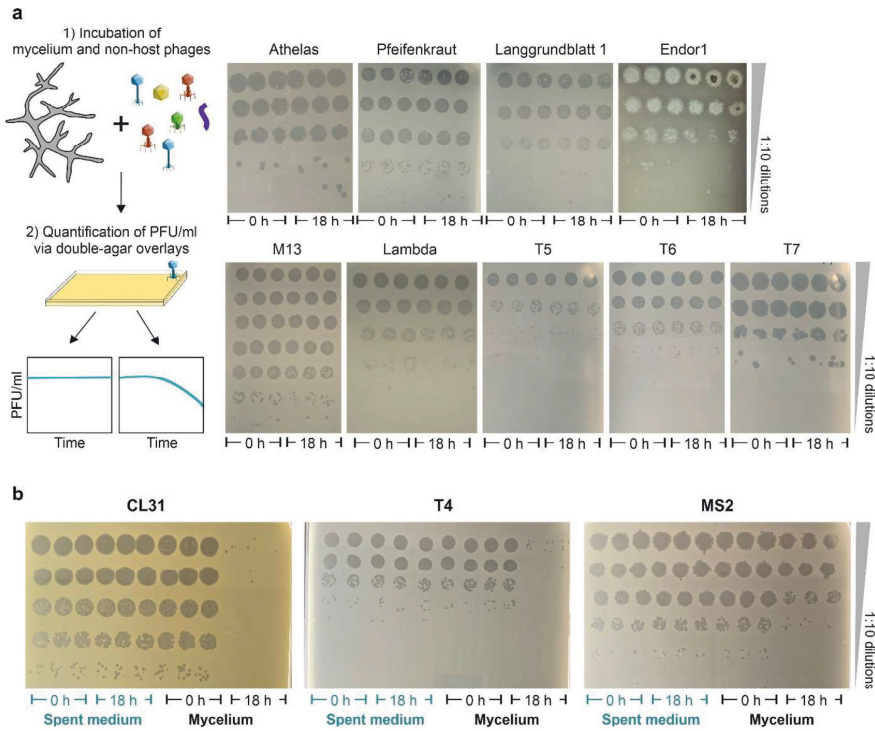


Figure S3: Influence of *S. venezuelae* NRRL B-65442 mycelium on extracellular titers of different phages. a) Schematic representation of experimental set-up composed of 1) incubation of non-host phages with *S. venezuelae* mycelium and 2) subsequent quantification of infectious phage particles via double-agar overlay assays using the corresponding host strains. b) Phages showing constant extracellular phage titers during incubation with *S. venezuelae* mycelium over 18 h. c) Phages showing a decline in extracellular titers over 18 h of cultivation with *S. venezuelae* mycelium. Incubation with corresponding *S. venezuelae* spent medium taken after 18 h exhibited no influence on infectious phage particles ( $n = 3$  independent biological replicates).

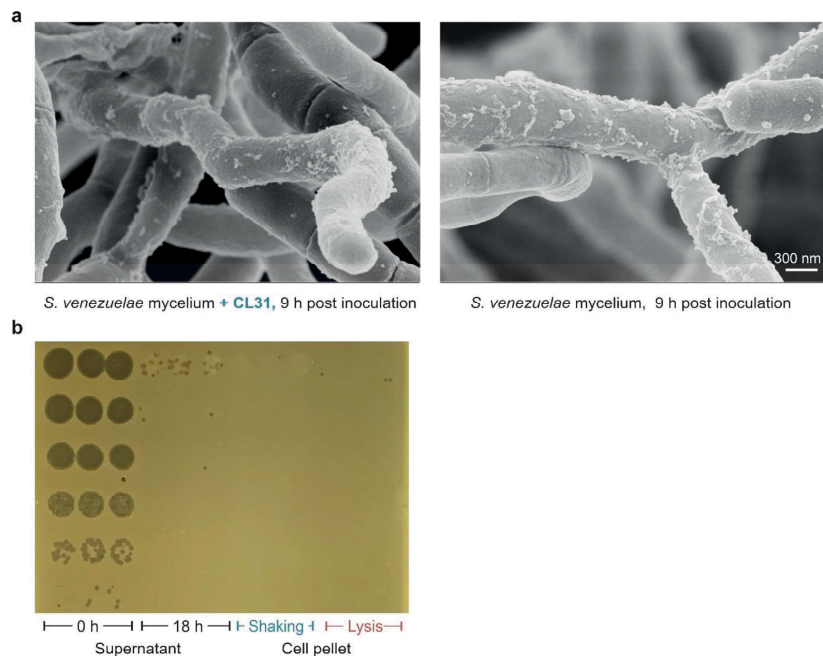


Figure S4: Failed visualization of CL31 phages on *S. venezuelae* mycelium. a) SEM images of *S. venezuelae* mycelium during the decrease in extracellular infectious CL31 titers in comparison to an uninfected control (scale bar = 300 nm) allowing no detection of phage particles on cell surface. b) Decrease in extracellular infectious CL31 phages over 18 h of cultivation and failed re-covering of the phages from mycelial fraction via intensive shaking or mechanical cell disruption.

## References

- Baumgart, M., Unthan, S., Ruckert, C., Sivalingam, J., Grunberger, A., Kalinowski, J., Bott, M., Noack, S., & Frunzke, J. (2013). Construction of a prophage-free variant of *Corynebacterium glutamicum* ATCC 13032 for use as a platform strain for basic research and industrial biotechnology. *Appl Environ Microbiol*, 79(19), 6006-6015. <https://doi.org/10.1128/AEM.01634-13>
- Bentley, S. D., Chater, K. F., Cerdeño-Tárraga, A. M., Challis, G. L., Thomson, N. R., James, K. D., Harris, D. E., Quail, M. A., Kieser, H., Harper, D., Bateman, A., Brown, S., Chandra, G., Chen, C. W., Collins, M., Cronin, A., Fraser, A., Goble, A., Hidalgo, J., Hornsby, T., Howarth, S., Huang, C. H., Kieser, T., Larke, L., Murphy, L., Oliver, K., O'Neill, S., Rabinowitsch, E., Rajadream, M. A., Rutherford, K., Rutter, S., Seeger, K., Saunders, D., Sharp, S., Squares, R., Squares, S., Taylor, K., Warren, T., Wietzorrek, A., Woodward, J., Barrell, B. G., Parkhill, J., & Hopwood, D. A. (2002). Complete genome sequence of the model actinomycete *Streptomyces coelicolor* A3(2). *Nature*, 417(6885), 141-147. <https://doi.org/10.1038/417141a>
- Bibb, M. J., & Buttner, M. J. (2003). The *Streptomyces coelicolor* developmental transcription factor  $\sigma^{BldN}$  is synthesized as a proprotein. *J Bacteriol*, 185(7), 2338-2345. <https://doi.org/10.1128/JB.185.7.2338-2345.2003>
- Bibb, M. J., Domonkos, A., Chandra, G., & Buttner, M. J. (2012). Expression of the chaplin and rodlin hydrophobic sheath proteins in *Streptomyces venezuelae* is controlled by  $\sigma^{BldN}$  and a cognate anti-sigma factor, RsbN. *Mol Microbiol*, 84(6), 1033-1049. <https://doi.org/10.1111/j.1365-2958.2012.08070.x>
- Erdrich, S. H., Sharma, V., Schurr, U., Arsova, B., & Frunzke, J. (2022). Isolation of Novel *Xanthomonas* Phages Infecting the Plant Pathogens *X. translucens* and *X. campestris*. *Viruses*, 14(7). <https://doi.org/10.3390/v14071449>
- Geiser, E., Wiebach, V., Wierckx, N., & Blank, L. M. (2014). Prospecting the biodiversity of the fungal family Ustilaginaceae for the production of value-added chemicals. *Fungal Biol. Biotechnol.*, 1(2). <https://doi.org/10.1186/s40694-014-0002-y>
- Gomez-Escribano, J. P., Holmes, N. A., Schlimpert, S., Bibb, M. J., Chandra, G., Wilkinson, B., Buttner, M. J., & Bibb, M. J. (2021). *Streptomyces venezuelae* NRRL B-65442: genome sequence of a model strain used to study morphological differentiation in filamentous actinobacteria. *J Ind Microbiol Biotechnol*, 48(9-10). <https://doi.org/10.1093/jimb/kuab035>
- Hardy, A., Sharma, V., Kever, L., & Frunzke, J. (2020). Genome sequence and characterization of five bacteriophages infecting *Streptomyces coelicolor* and *Streptomyces venezuelae*: Alderaan, Coruscant, Dagobah, Endor1 and Endor2. *Viruses*, 12(10), 1065. <https://doi.org/10.3390/v12101065>
- Hong, H. J., Hutchings, M. I., Hill, L. M., & Buttner, M. J. (2005). The role of the novel Fem protein VanK in vancomycin resistance in *Streptomyces coelicolor*. *J Biol Chem*, 280(13), 13055-13061. <https://doi.org/10.1074/jbc.M413801200>
- Hünnefeld, M., Viets, U., Sharma, V., Wirtz, A., Hardy, A., & Frunzke, J. (2021). Genome Sequence of the Bacteriophage CL31 and Interaction with the Host Strain *Corynebacterium glutamicum* ATCC 13032. *Viruses*, 13(3), 495. <https://doi.org/10.3390/v13030495>
- Ikeda, M., & Nakagawa, S. (2003). The *Corynebacterium glutamicum* genome: features and impacts on biotechnological processes. *Appl. Microbiol. Biotechnol.*, 62(2-3), 99-109. <https://doi.org/10.1007/s00253-003-1328-1>
- Kever, L., Hardy, A., Luthe, T., Hünnefeld, M., Gätgens, C., Milke, L., Wiechert, J., Wittmann, J., Moraru, C., Marienhagen, J., & Frunzke, J. (2022). Aminoglycoside Antibiotics Inhibit Phage Infection by Blocking an Early Step of the Infection Cycle. *mBio*, 13(3). <https://doi.org/10.1128/mbio.00783-22>
- Kong, J., Jiang, H., Li, B., Zhao, W., Li, Z., & Zhu, S. (2016). Complete Genome Sequence of *Pseudomonas syringae* pv. *lapsa* Strain ATCC 10859, Isolated from Infected Wheat. *Genome Announc*, 4(2). <https://doi.org/10.1128/genomeA.00024-16>
- Lederberg, E. M., & Lederberg, J. (1953). Genetic Studies of Lysogenicity in *Escherichia Coli*. *Genetics*, 38(1), 51-64. <https://doi.org/10.1093/genetics/38.1.51>

- Luria, S. E., Delbrück, M., & Anderson, T. F. (1943). Electron microscope studies of bacterial viruses. *J Bacteriol*, 46(1), 57-77. <https://doi.org/10.1128/JB.46.1.57-77.1943>
- MacNeil, D. J., Gewain, K. M., Ruby, C. L., Dezeny, G., Gibbons, P. H., & MacNeil, T. (1992). Analysis of *Streptomyces avermitilis* genes required for avermectin biosynthesis utilizing a novel integration vector. *Gene*, 111(1), 61-68. [https://doi.org/10.1016/0378-1119\(92\)90603-M](https://doi.org/10.1016/0378-1119(92)90603-M)
- Murray, N. E., Brammar, W. J., & Murray, K. (1977). Lambdoid Phages that Simplify the Recovery of in vitro Recombinants. *Mol Gen Genet.*, 150(1), 53-61. <https://doi.org/10.1007/BF02425325>.
- Nelson, K. E., Hilbert, H., Gill, S. R., Beanan, M., Madupu, R., Khouri, H., Scanlan, D., Rizzo, M., Lauber, J., Heim, S., Weinell, C., DeBoy, R. T., Nelson, W., Hance, I., Tran, K., Lee, K., Düsterhöft, A., Paulsen, I. T., Holmes, M., Santos, V. A. P. M. d., Pop, M., Lee, P. C., Moazzes, A., Kosack, D., Tümmeler, B., Eisen, J., Dodson, R. J., Fouts, D. E., Brinkac, L., Daugherty, S., White, O., Kolonay, J., Peterson, J., Holtzapple, E., Utterback, T., Moestl, D., Wedler, H., Stjepandic, D., Hoheisel, J., Straetz, M., Kiewitz, C., Timmis, K. N., & Fraser, C. M. (2002). Complete genome sequence and comparative analysis of the metabolically versatile *Pseudomonas putida* KT2440. *Environ. Microbiol.*, 4(12), 799-808. <https://doi.org/10.1046/j.1462-2920.2002.00366.x>.
- Sapkota, S., Mergoum, M., & Liu, Z. (2020). The translucens group of *Xanthomonas translucens*: Complicated and important pathogens causing bacterial leaf streak on cereals. *Mol Plant Pathol*, 21(3), 291-302. <https://doi.org/10.1111/mpp.12909>
- Tschowri, N., Schumacher, M. A., Schlimpert, S., Chinnam, N. B., Findlay, K. C., Brennan, R. G., & Buttner, M. J. (2014). Tetrameric c-di-GMP mediates effective transcription factor dimerization to control *Streptomyces* development. *Cell*, 158(5), 1136-1147. <https://doi.org/10.1016/j.cell.2014.07.022>
- Widdick, D. A., Dodd, H. M., Barraille, P., White, J., Stein, T. H., Chater, K. F., Gasson, M. J., & Bibb, M. J. (2003). Cloning and engineering of the cinnamycin biosynthetic gene cluster from *Streptomyces cinnamomeus cinnamomeus* DSM 40005. *PNAS*, 100(7), 4310-4321 <https://doi.org/10.1073/pnas.0230516100>

#### 4.4. Appendix to 3.4: Genome sequence and characterization of five bacteriophages infecting *Streptomyces coelicolor* and *Streptomyces venezuelae*: Alderaan, Coruscant, Dagobah, Endor1 and Endor2



Article

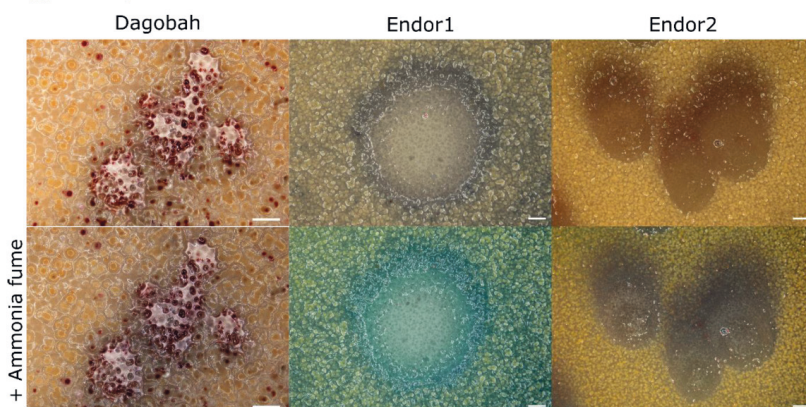
### Genome sequence and characterization of five bacteriophages infecting *Streptomyces coelicolor* and *Streptomyces venezuelae*: Alderaan, Coruscant, Dagobah, Endor1 and Endor2

Aël Hardy, Vikas Sharma, Larissa Kever and Julia Frunzke\*

Institute of Bio- und Geosciences, IBG-1: Biotechnology, Forschungszentrum Jülich, 52425 Jülich, Germany

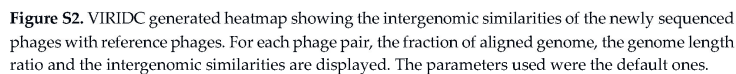
\* Correspondence: j.frunzke@fz-juelich.de; Tel.: +49 2461 615430

#### Supplementary data



**Figure S1.** Close-ups of phage plaques imaged using a Nikon SMZ18 stereomicroscope, before (upper row) and after (lower row) exposure to ammonia fumes. *S. coelicolor* M145 was infected by phages using GYM double agar overlays. The plates were incubated at 30°C overnight and then kept at room temperature for two (Dagobah and Endor2) or three days (Endor1). The ammonia fume test was performed as follows: the plates were inverted and exposed to ammonia fumes for 15 min by placing 5 ml of 20% ammonium hydroxide solution on the inner surface of the lid. Scale bar: 1 mm.





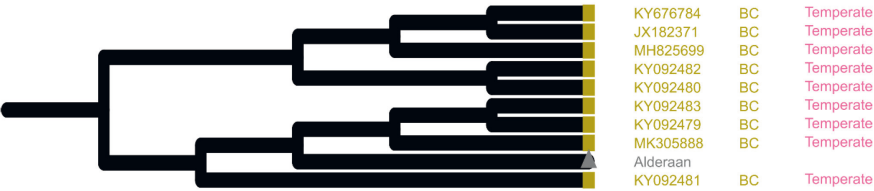


**Figure S3.** Subclade dendrogram with *Streptomyces* phage Alderaan and its closely related actinophages(enlargement from Figure 5). The phage lifestyles shown are those indicated on PhagesDB.

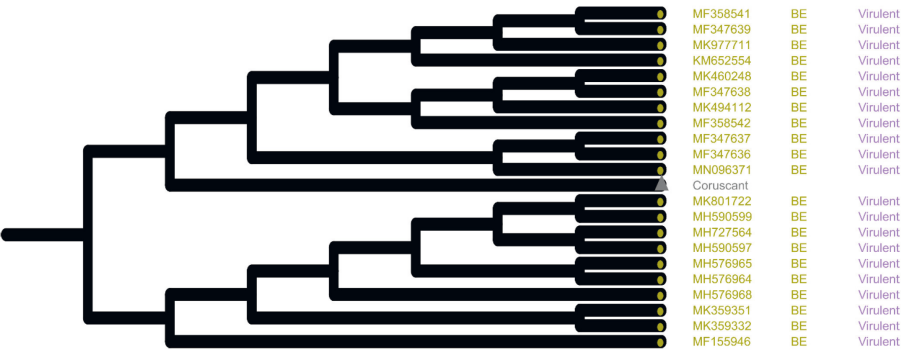


**Figure S4.** Subclade dendrogram with *Streptomyces* phage Coruscant and its closely related actinophages (enlargement from Figure 5). The phage lifestyles shown are those indicated on PhagesDB.

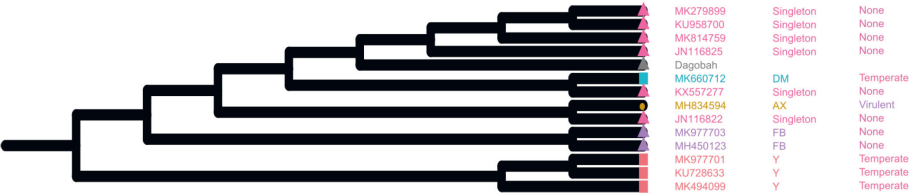


**Figure S5.** Subclade dendrogram with *Streptomyces* phage Dagobah and its closely related actinophages (enlargement from Figure 5). The phage lifestyles shown are those indicated on PhagesDB. “None” corresponds to phages with no lifestyle prediction on PhagesDB.

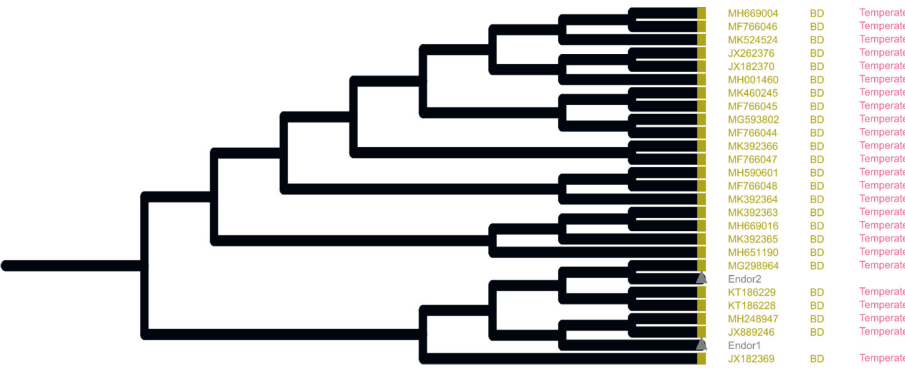


**Figure S6.** Subclade dendrogram with *Streptomyces* phages Endor1 and Endor2 and their closely related actinophages (enlargement from Figure 5). The phage lifestyles shown are those indicated on PhagesDB.

**Table S1:** List of the functional annotation of protein ORFs within phage genomes is available under the following hyperlink: <https://doi.org/10.3390/v12101065>

## Acknowledgements

An erster Stelle möchte ich mich bei Frau Prof. Dr. Julia Frunzke bedanken, die mir die Möglichkeit gegeben hat, an diesen faszinierenden Projekten zu arbeiten sowie für ihr Vertrauen, ihre Hilfe und viele fachliche Ratschläge und motivierende Worte. Darüber hinaus möchte ich mich bei Prof. Dr. Ilka Maria Axmann als Co-Betreuerin bedanken.

Mein besonderer Dank gilt natürlich auch den ehemaligen und jetzigen Mitgliedern der AG Frunzke für die tolle Zusammenarbeit, eine fantastische Arbeitsatmosphäre und unzählige lustige Mittagspausen. Dabei möchte ich mich besonders bei Dr. Max Hünnefeld bedanken, der mich seit meiner Masterarbeit begleitet hat, mir immer hilfsbereit zur Seite stand und viele anregende Diskussionen mit mir geführt hat. Des Weiteren möchte ich Aileen Krüger dafür danken, dass sie von Beginn an nicht nur eine Kollegin, sondern vielmehr eine gute Freundin war, mit der man über alles reden kann. Mit ihr waren auch die schwierigeren Zeiten nur halb so schlimm, weil sie immer die richtigen, ermutigenden Worte gefunden hat. Vielen Dank auch an Cornelia Gätgens für ihren unermüdlichen Einsatz im Labor und viele hilfreiche Gespräche, sowohl im privaten wie auch im beruflichen Bereich. Ein spezieller Dank geht auch an Dr. Aël Hardy und Tom Luthe für die tolle Zusammenarbeit an diesen spannenden Projekten sowie an mein Proofreading-Team.

Von ganzem Herzen möchte ich auch meiner Familie, insbesondere meinen Eltern danken. Ohne ihre dauerhafte Unterstützung, ihre ermutigenden Worte und ihr Verständnis wäre ich heute nicht da, wo ich jetzt bin. Ein großes Dankeschön geht auch an meine Großeltern, die keine Sekunde an mir gezweifelt haben und mich unterstützt haben, wo immer sie konnten. Zu guter Letzt danke ich vor allem auch meinem Partner Philipp, der mir immer mit Rat und Tat zur Seite stand und mir auch in schwierigen Zeiten immer ein Lächeln ins Gesicht zaubern konnte.



## Erklärung

Hiermit versichere ich an Eides Statt, dass die Dissertation von mir selbständig und ohne unzulässige fremde Hilfe unter Beachtung der „Grundsätze zur Sicherung guter wissenschaftlicher Praxis an der Heinrich-Heine-Universität Düsseldorf“ erstellt worden ist. Die Dissertation wurde in der vorgelegten oder in ähnlicher Form noch bei keiner anderen Institution eingereicht. Ich habe bisher keine erfolglosen Promotionsversuche unternommen.

A handwritten signature in black ink, appearing to read 'd. Kever', written over a horizontal line.

Larissa Kever



Band / Volume 263

**9<sup>th</sup> Georgian-German School and Workshop in Basic Science  
September 12 – 16, 2022 | Kutaisi, Tbilisi | Georgia**

A. Kacharava, E. Portius, N. J. Shah, H. Ströher (2022)

ISBN: 978-3-95806-664-9

Band / Volume 264

**Self-assembly of Au-Fe<sub>3</sub>O<sub>4</sub> dumbbell nanoparticles**

N. Nandakumaran (2022), xiv, 234 pp

ISBN: 978-3-95806-666-3

Band / Volume 265

**Time-resolved and three-dimensional characterisation of magnetic states  
in nanoscale materials in the transmission electron microscope**

T. Weßels (2023), xx, 211 pp

ISBN: 978-3-95806-685-4

Band / Volume 266

**Dissecting iron and heme regulatory networks and adaptation  
to heme stress in *Corynebacterium glutamicum***

A. Krüger (2023), IV, 274 pp

ISBN: 978-3-95806-686-1

Band / Volume 267

**Morphological and functional characterization of layer 5 neurons in rat  
medial prefrontal cortex, their synaptic microcircuitry and serotonin  
modulation**

R. Rama (2023), 116 pp

ISBN: 978-3-95806-688-5

Band / Volume 268

**Magnetic and transport studies of the parent and  
Fe doped Hexagonal-Mn<sub>3</sub>Ge Weyl semimetal**

V. Rai (2023), xviii, 156 pp

ISBN: 978-3-95806-695-3

Band / Volume 269

**The complex inositol metabolism of *Corynebacterium glutamicum* and its  
application for the production of rare inositols**

P. Ramp (2023), VI, 161 pp

ISBN: 978-3-95806-699-1

Band / Volume 270

**Spin- and orbital-dependent band structure of  
unconventional topological semimetals**

K. Hagiwara (2023), v, 115 pp

ISBN: 978-3-95806-701-1



Band / Volume 271

**Neutron scattering**

Experimental Manuals of the JCNS Laboratory Course held at  
Forschungszentrum Jülich and at the Heinz-Maier-Leibnitz Zentrum Garching  
edited by T. Brückel, S. Förster, K. Frieze, M. Kruteva, M. Zobel and R. Zorn  
(2023), ca 150 pp  
ISBN: 978-3-95806-705-9

Band / Volume 272

**Ab-initio investigation of the interplay between the hyperfine  
interaction and complex magnetism at the nanoscale**

S. R. S. Shehada (2023), ix, xi, 119 pp  
ISBN: 978-3-95806-718-9

Band / Volume 273

**Analysis of the signal transduction cascade tuning the 2-oxoglutarate  
dehydrogenase activity in *Corynebacterium glutamicum***

L. Sundermeyer (2023), VI, 119 pp  
ISBN: 978-3-95806-722-6

Band / Volume 274

**Multicellular defense against phage infection in *Streptomyces* – impact of  
secondary metabolites and mycelial development**

L. Kever (2023), iv, 246 pp  
ISBN: 978-3-95806-724-0

Weitere **Schriften des Verlags im Forschungszentrum Jülich** unter  
<http://www.zb1.fz-juelich.de/verlagextern1/index.asp>



Schlüsseltechnologien / Key Technologies  
Band / Volume 274  
ISBN 978-3-95806-724-0